Medical Radiology · Diagnostic Imaging
Series Editors: Hans-Ulrich Kauczor · Paul M. Parizel · Wilfred C. G. Peh

Mohamed Fethi Ladeb
Wilfred C. G. Peh *Editors*

Imaging of Spinal Infection

Springer

Medical Radiology

Diagnostic Imaging

Series Editors

Hans-Ulrich Kauczor
Paul M. Parizel
Wilfred C. G. Peh

The book series Medical Radiology – Diagnostic Imaging provides accurate and up-to-date overviews about the latest advances in the rapidly evolving field of diagnostic imaging and interventional radiology. Each volume is conceived as a practical and clinically useful reference book and is developed under the direction of an experienced editor, who is a world-renowned specialist in the field. Book chapters are written by expert authors in the field and are richly illustrated with high quality figures, tables and graphs. Editors and authors are committed to provide detailed and coherent information in a readily accessible and easy-to-understand format, directly applicable to daily practice.

Medical Radiology – Diagnostic Imaging covers all organs systems and addresses all modern imaging techniques and image-guided treatment modalities, as well as hot topics in management, workflow, and quality and safety issues in radiology and imaging. The judicious choice of relevant topics, the careful selection of expert editors and authors, and the emphasis on providing practically useful information, contribute to the wide appeal and ongoing success of the series. The series is indexed in Scopus.

For further volumes: http://www.springer.com/series/4354

Mohamed Fethi Ladeb
Wilfred C. G. Peh
Editors

Imaging of Spinal Infection

Springer

Editors
Mohamed Fethi Ladeb
Department of Radiology
Mohamed Kassab Orthopedic Institute
Tunis, Tunisia

Wilfred C. G. Peh
Department of Diagnostic Radiology
Khoo Teck Puat Hospital
Singapore, Singapore

ISSN 0942-5373 ISSN 2197-4187 (electronic)
Medical Radiology
ISBN 978-3-030-70458-2 ISBN 978-3-030-70459-9 (eBook)
https://doi.org/10.1007/978-3-030-70459-9

© The Editor(s) (if applicable) and The Author(s), under exclusive license to Springer Nature Switzerland AG 2021, corrected publication 2021
This work is subject to copyright. All rights are solely and exclusively licensed by the Publisher, whether the whole or part of the material is concerned, specifically the rights of translation, reprinting, reuse of illustrations, recitation, broadcasting, reproduction on microfilms or in any other physical way, and transmission or information storage and retrieval, electronic adaptation, computer software, or by similar or dissimilar methodology now known or hereafter developed. The use of general descriptive names, registered names, trademarks, service marks, etc. in this publication does not imply, even in the absence of a specific statement, that such names are exempt from the relevant protective laws and regulations and therefore free for general use.
The publisher, the authors, and the editors are safe to assume that the advice and information in this book are believed to be true and accurate at the date of publication. Neither the publisher nor the authors or the editors give a warranty, expressed or implied, with respect to the material contained herein or for any errors or omissions that may have been made. The publisher remains neutral with regard to jurisdictional claims in published maps and institutional affiliations.

This Springer imprint is published by the registered company Springer Nature Switzerland AG
The registered company address is: Gewerbestrasse 11, 6330 Cham, Switzerland

‘This book is dedicated to our students and juniors - the future of Radiology’.

Foreword

The discovery of antibiotics and anti-tuberculosis drugs in the mid-twentieth century raised the hope of complete control of human infection. However, despite fantastic improvements in diagnosis and treatment, infections remain a major concern in a context of intensive circulation of people, which increases the diffusion of microorganisms. In addition, the huge increase in the number of surgical and interventional procedures has resulted in a large rise in opportunistic infections, and globalization has been accompanied by a revival of skeletal tuberculosis—even in developed countries. Therefore, the diagnosis of skeletal infection, and more specifically spinal infection, remains one of the major concerns in our daily practice.

This book, *Imaging of Spinal Infection*, is authored by the teams of Professors Ladeb, Bouaziz, and Peh, who originate from two areas of the world at the crossroads of several continents, sites of intensive exchanges, and population circulation. Both teams have therefore an extensive experience of spinal infection imaging, including those due to atypical microorganisms, such as hydatidosis and fungal infection.

The first part of this book, which covers all the facets of spinal infection imaging, is devoted to its epidemiology, pathophysiology, clinical and imaging findings, including the most recent imaging and nuclear medicine modalities and techniques, and is illustrated by an abundant number of figures and explanatory drawings. Specific chapters are dedicated to the distinct aspects of the main types of spinal infection: pyogenic infection, brucellosis, salmonella spondylodiscitis, tuberculosis, hydatidosis, and fungal infection. The last chapter is original and practical: it provides an algorithm defining the management steps of spinal infection imaging diagnosis—both in cases of clinically suspected spinal infection as well as in cases of incidental finding of typical imaging features of spinal infection.

Overall, *Imaging of Spinal Infection* achieves a remarkable challenge covering the whole topic supported by an extensive literature review, in a very concise and readable format, accessible to specialists as well as residents.

November 2020

Jean-Denis Laredo
Professeur émérite de l'Université de Paris
Paris, France
Membre de l'Académie Nationale de Médecine
Paris, France

Preface

Spinal infection is a serious medical condition that can result in neurological complications, with potentially high morbidity and mortality. This disease has a global distribution, is caused by many different organisms, and manifests in a variety of clinical patterns. The numbers are variable among different studies but the following figures are generally accepted: spinal infection comprises 2–7% of musculoskeletal infections; incidence of spinal infection varies from 1:20,000 to 1:25,000 population, with mortality in the range of 2–20%.

The incidence of spinal infection is on an upward trend, even in developed countries, as it is related to increased use of vascular devices and other forms of instrumentation, a rise in intravenous drug abuse, and early detection due to advances in modern imaging. Risk factors for developing spinal infection include conditions that compromise the immune system, such as advanced age, human immunodeficiency virus (HIV) infection, long-term systemic steroids, diabetes mellitus, organ transplantation, malnutrition, and cancer; as well as a host of surgical risk factors. Infections such as tuberculosis and brucellosis remain prevalent in many developing countries.

Early clinical features of spinal infection are usually nonspecific and insidious, which is why the interval between symptom onset and diagnosis is often long and complications manifest. Rapid and effective diagnosis and management help prevent irreversible neurological and bony complications. Therefore, imaging has an important role to play in the overall management of spinal infection and ideally should be highly sensitive in order to detect the disease at an early stage.

We believe that *Imaging of Spinal Infection* fulfills a niche area in imaging that, to our knowledge, has not previously been comprehensively dealt with. This volume comprises 15 chapters. The first six chapters deal with the epidemiology and pathophysiology of, and various imaging techniques useful in diagnosing spinal infection. The next chapters are devoted to the different etiologies of spinal infection, with an emphasis on imaging features, and including iatrogenic factors and the various specific causative organisms. The last chapter presents decision algorithms relating to diagnosis and management.

This book is authored mainly by the most unique combination of contributors from Tunisia and Singapore. There is a chapter from an eminent group from Belgium and the Foreword has been kindly written by our mutual friend Professor Jean-Denis Laredo from France. Besides musculoskeletal

radiologists, other authors include experts in neuroradiology, nuclear medicine, parasitology, laboratory medicine, pathology, and infectious disease. We gratefully acknowledge Professor Filip Vanhoenacker for introducing us. We both know Filip as a good friend and collaborator of long standing.

Imaging of Spinal Infection aims to be useful and practical reference for all specialists who deal with spinal infection. Targeted readers include clinical practitioners in radiology, orthopedic and spine surgery, rheumatology, infectious disease, and pathology. Residents and trainees in these specialties should also benefit from this textbook.

November 2020
Tunis, Tunisia — Mohamed Fethi Ladeb
Singapore, Singapore — Wilfred C. G. Peh

The original version of this book was revised. The incorrect author affiliation has been corrected. The correction to this book can be found at https://doi.org/10.1007/978-3-030-70459-9_16

Contents

Epidemiology of Spinal Infection

Aida Berriche, Lamia Ammari, Hend Riahi, and Mouna Chelli Bouaziz

Contents

A. Berriche (✉) · L. Ammari
Department of Infectious Diseases, Rabta Hospital, Tunis, Tunisia

Faculty of Medicine of Tunis, Tunis-El Manar University, Tunis, Tunisia
e-mail: aida.berricheg@gmail.com; lamia_ammarib@yahoo.fr

H. Riahi · M. Chelli Bouaziz
Department of Radiology, MT Kassab Institute of Orthopaedics, Tunis, Tunisia

Faculty of Medicine of Tunis, Tunis-El Manar University, Tunis, Tunisia
e-mail: hend.riahi@gmail.com; bouaziz_mouna@yahoo.fr

© The Author(s), under exclusive license to Springer Nature Switzerland AG 2021

M. F. Ladeb, W. C. G. Peh (eds.), *Imaging of Spinal Infection*, Medical Radiology Diagnostic Imaging, https://doi.org/10.1007/978-3-030-70459-9_1

Abstract

Spinal infection is a serious disease which can result in neurological complications, with potentially high morbidity and mortality. Spondylodiscitis can be due to various pyogenic organisms, granulomatous organisms such as tuberculosis and brucellosis, and rarely, parasitic or fungal organisms. The incidence of spondylodiscitis varies from region to region, with the incidence of pyogenic spondylodiscitis being more frequent in developed countries. Tuberculosis and brucellar infections are more frequent in developing countries. There are also variations in risk factors for the different organisms and locations. The symptoms of spondylodiscitis are typically nonspecific, with a delay between symptom onset and diagnosis usually being long. Rapid and effective diagnosis and management help prevent irreversible neurological and bony complications.

Abbreviations

BSD	Brucellar spondylodiscitis
PSD	Pyogenic spondylodiscitis
SD	Spondylodiscitis
TB	Tuberculosis
TSD	Tuberculous spondylodiscitis

1 Introduction

Spinal infection is an important clinical problem. Spondylodiscitis (SD) can be classified as pyogenic, granulomatous such as tuberculosis (TB) and brucellosis, or rarely, parasitic or fungal. Symptoms of SD may be nonspecific, including fever, back pain, local tenderness, and neurological signs. The disease course may be acute or chronic. The lack of specific symptoms usually results in delayed diagnosis, leading to neurological complications and potentially high morbidity and mortality. In most cases the affected patients have one or more predisposing underlying conditions, such as diabetes mellitus, alcoholism, human immunodeficiency virus (HIV) infection, renal failure, intravenous drug abuse, spinal abnormality or intervention, or a potential local or systemic source of infection (Kapsalaki et al. 2009). TB is the most common cause (around 50% of worldwide cases), followed by pyogenic agents, whereas parasitic and fungal cases are rare (Castilla et al. 2002; Zimmerli 2010; Duarte and Vaccaro 2013; Lee 2014). The incidence of pyogenic spondylodiscitis (PSD) is more frequent in developed countries, while TB and brucellar infections are more frequent and endemic in North Africa, Asia, and the Middle East (Ben Taarit et al. 2002; Menon and Sorour 2016).

2 Epidemiology of Spinal Brucellosis

Brucellosis is one of the most common zoonoses globally (Kursun et al. 2013; Kazak et al. 2016). It is currently still a major public health problem, mainly in the Mediterranean region, the Middle East and parts of Central and South America (Maurin 2005). The disease usually affects young and middle-aged adults, with infants and elderly patients being less vulnerable (Aubry 2017). Brucellosis is a zoonosis caused by *Brucella* spp. that can involve various tissues and systems in humans and leads to different clinical

presentations. The incidence of brucellosis has however shown a mild decrease in some countries in the recent years.

Brucellosis is usually transmitted to humans by direct contact with infected animals, through damaged skin and nasal or conjunctival mucosa. It can also occur through the consumption of unpasteurized milk and milk products from infected animals (Kursun et al. 2013; Kazak et al. 2016) or via airborne transmission from contaminated aerosols in laboratories and meat-packing plants (Aubry 2017). It is more frequently transmitted by occupational exposure in developed countries. Farmers and veterinary surgery operators are the main affected occupational group. Laboratory workers processing specimens are also vulnerable (Aubry 2017). Epidemiological studies conducted in Turkey have demonstrated that 62.6–94.6% of affected patients have a history of consuming unpasteurized dairy products (Kursun et al. 2013).

The disease appears in three forms according to the symptom duration, namely, acute, subacute, and chronic (Kursun et al. 2013; Kazak et al. 2016). In various studies, the acute form is reported to be observed in 25–77% of cases, the subacute form in 12.5–59% of cases, and the chronic form in 5–27.5% of cases (Kursun et al. 2013; Kazak et al. 2016). These differences are attributed to economic and cultural differences among patients, as well as differences in diagnostic approaches.

2.1 **Frequency** (Table 1)

The World Health Organization (WHO) has reported the global incidence of human brucellosis at 500,000 reported cases per year. However, due to the underestimated reporting, which is not yet systematic in some countries, its actual impact remains unknown (Maurin 2005; Ministry of Health Tunisia 2020). The prevalence varies from country to country. As a result, it has practically been eradicated from Japan, Australia, New Zealand, some northern European countries, and North America. However, it remains endemic in the Mediterranean basin, West Asia, the Middle East, South America, Central America, and sub-Saharan Africa (Papadimitriou et al. 2006). Of all the countries reporting their statistics to WHO, Syria has the highest incidence with 1603.4 cases/1,000,000 inhabitants, followed by Mongolia (818.5/1,000,000), Iraq (268.8/1,000,000), Tajikistan (211.9/1,000,000), Saudi Arabia (149.5/1,000,000), and finally Iran (141.6/1,000,000) (Kursun et al. 2013; Kazak et al. 2016; Menon and Sorour 2016). The disease incidence has declined in some countries such as Turkey (49.5/1,000,000) and Kyrgyzstan (88.0/1,000,000) (WHO 2015).

Table 1 Incidence of brucellosis in different countries

Countries	Incidence
Syria	1603.4 cases/1,000,000 inhabitants
Mongolia	818.5 cases/1,000,000 inhabitants
Iraq	268.8 cases/1,000,000 inhabitants
Tajikistan	211.9 cases/1,000,000 inhabitants
Saudi Arabia	149 cases/1,000,000 inhabitants
Iran	141.6 cases/1,000,000 inhabitants
Turkey	49.5 cases/1,000,000 inhabitants
Kyrgyzstan	88.0 cases/1,000,000 inhabitants
Algeria	28 cases/100,000 inhabitants
Libya	22 cases/100,000 inhabitants
Morocco	131 cases/100,000 inhabitants

Eight European countries have been declared free from brucellosis by the European Union. In contrast, Greece, Italy, Portugal, and Spain have the highest incidences, ranging from 0.14 to 0.87 confirmed cases/100,000 persons (Crump et al. 2003; Welburn et al. 2015; Hull and Schumaker 2018). The cases reported were mainly people who had stayed in an endemic country or immigrants from endemic countries (Zhang et al. 2010; Rubach et al. 2013).

In the United States of America, the Institute of Health classifies human brucellosis as a rare disease with 80–120 cases reported per year. Most of the cases are located in the south and southwest and are secondary either to exposure in known endemic regions or to the consumption of cheese illegally imported from Mexico (Bechtol et al. 2011; Ducrotoy et al. 2014; Negrón et al. 2019). Indeed, brucellosis remains endemic in countries of Central and South America such as Mexico (Guzmán et al. 2016), Argentina (Aznar

et al. 2014), and Brazil (Tuon et al. 2017). The incidence of brucellosis remains as high in Asian countries, such as Kyrgyzstan (Mirnejad et al. 2017) and Azerbaijan (Dean et al. 2012) and also in China (European Surveillance System 2020).

Few studies have been done in sub-Saharan Africa. The highest incidences are noted in Niger (European Centre for Disease Prevention and Control 2020), Chad (Pelerito et al. 2017), Ethiopia (Georgi et al. 2017), and Tanzania (Norman et al. 2016). The Maghreb (Northwest Africa) as a whole is still considered an endemic region. In Algeria, the incidence was estimated at 28 cases/100,000 inhabitants in 2010 (Abdullayev et al. 2012). In Libya, the incidence was found to be 22 cases/100,000 inhabitants in 2009 (Lai et al. 2017). In Morocco, this disease is rife with the enzootic state in different regions of the country with varying prevalence. In 2017, an epidemic was notified in the Laayoune region with 131 cases (Abdou 2013).

Brucellosis is a multisystem disease, and patients may present with a broad spectrum of clinical manifestations and develop various complications. Almost every organ can be affected. Musculoskeletal complications are the leading complications of brucellosis, with various prevalence rates reported. Musculoskeletal complications may have a genetic predisposition, as recent data suggest an association with HLA-B39 (Chakroun and Bouzouaia 2007). In brucellosis, any region in the musculoskeletal system may be affected (Zribi et al. 2009; Zhang et al. 2010; WHO 2020). The most important clinical forms of osteoarticular involvement are arthritis, spondylodiscitis (SD), bursitis, tenosynovitis, and osteomyelitis. Arthritis is usually observed in large joints and especially in the sacroiliac joint (Turan et al. 2011). The frequency of osteoarticular complications is in the range of 10–85% in various studies (Turan et al. 2011; Koubaa et al. 2014).

In a Turkish study, musculoskeletal involvement represented 30.6% of subacute brucellosis. SD was the most prevalent complication of musculoskeletal system involvement (19%) in this study (Kursun et al. 2013). In France, brucellar spondylodiscitis (BSD) is very rare, comprising only 0.4% of all cases of SD (Sans et al. 2012). In Turkey, its frequency varied from 19 to 73.6% of all musculoskeletal complications (Sans et al. 2012; Kursun et al. 2013; ErenGok et al. 2014; Kazak et al. 2016). ErenGok et al. (2014) found that out of 214 patients with SD, 96 (45%) had BSD, 63 (29%) had tuberculous spondylodiscitis (TSD), and 55 (26%) had PSD. In a Tunisian study, the frequency of BSD was 19.5% (Koubaa et al. 2014).

2.2 Microbiology

The agent of brucellosis is a small, gram-negative, unencapsulated, and non-sporulating coccobacilli from the *Brucella* genus. This genus is divided into six major animal species based on natural host preference and cultural, metabolic, and antigenic characteristics. Four of these are known to produce disease in humans, namely, *Brucella abortus*, *B. melitensis*, *B. suis*, and *B. canis* (KaragozGuzey et al. 2007). *B. melitensis* accounts for the majority of the human brucellosis (Kazak et al. 2016) and is the most virulent and invasive (Akakpo et al. 2020; WHO 2020). *B. canis* is an infrequent cause of human infection (Maurin 2005). The typical reservoirs of *B. melitensis* are goats and sheep, while *B. abortus* are found principally in cattle, *B. suis* in swine, and *B. canis* in canines. *Brucella* organisms are shed in the excreta (urine, stool, milk, and products of conception) of infected animals (Papadimitriou et al. 2006; Ducrotoy et al. 2014; Ministry of Health Tunisia 2020).

2.3 Age and Gender

BSD is detected in the older age group, while brucellar sacroiliitis affects the young (Sans et al. 2012). In Turkish studies, the mean age varied from 53 to 58.4 years (Sans et al. 2012; Kazak et al. 2016). The mean age was 55 years in a multinational, multicenter study, which included patients from 35 different centers in four countries (Turkey, Egypt, Albania, and Greece) (Erdem et al. 2015). The mean age was 54.8 years

Table 2 Mean ages of patients with spinal brucellosis

Study	Country	Mean age (years)
Kazak et al. (2016)	Turkey	53
Sans et al. (2012)	France	58.4
Erdem et al. (2015)	Multinational and multicenter	55
Lebre et al. (2014)	Greece	54.8
Koubaa et al. (2014)	Tunisia	51

in a Portuguese study (Lebre et al. 2014), 68 years in another Turkish study (Turunc et al. 2007), and 51 (range 19–74) years in a Tunisian study (Koubaa et al. 2014) (Table 2). There was no significant difference between the mean ages of the patients with and without osteoarticular involvement (Turan et al. 2011).

In a comparative Turkish study, the mean age of the patients with TSD was lower than that of the patients with BSD and PSD: 43 years versus 53 years and 53 years, respectively ($p < 0.001$) (ErenGok et al. 2014). In another comparative study, patients with BSD were younger than patients with TSD or PSD (59 years versus 68 years versus 65.5 years, respectively) (Turunc et al. 2007). A male predominance was noted in the majority of studies. Men represented 52.6% in a multinational and multicenter study (Erdem et al. 2015), 55.6% in a Portuguese study (Lebre et al. 2014), 58–64.3% in Turkish studies (Turgut et al. 2006; Turunc et al. 2007; ErenGok et al. 2014), and 72% in a Tunisian study (Koubaa et al. 2014).

2.4 Risk Factors

The risk factors for BSD are the same for all forms of brucellosis. Brucellosis is transmitted to humans either by direct contact with infected animals or by consumption of unpasteurized milk obtained from infected animals or dairy products produced from such milk (Turan et al. 2011). It is encountered as an "occupational disease" in countries where pasteurized dairy products are consumed; this is especially the case if the infection is found among veterinarians, slaughterhouse workers, farmers, and laboratory workers (Kazak et al. 2016). Even though there are studies showing that occupational brucellosis is more common in men, other studies have reported that men and women are affected equally (Turan et al. 2011).

In a Turkish study including 202 patients, 94 had osteoarticular involvement. A possible source of infection could be identified in 70 cases (74.5%). Fifty-three patients (75.7%) had a history of farming and/or consumption of unpasteurized milk and dairy products (especially fresh cheese). Apart from that, 15 (21.4%) of these patients with osteoarticular involvement had only a history of consumption of unpasteurized milk and dairy products. In addition, two (2.9%) patients were exposed to the disease occupationally (veterinarian, laboratory worker, etc.). Sixty-one percent of patients lived in a rural area (Turan et al. 2011).

In another Turkish study comprising 164 patients, 109 (66.5%) resided in urban areas and 55 (33.5%) in rural areas. Evaluation of patient histories revealed that 83 (50.6%) patients consumed unpasteurized cheese, 61 (37.2%) had animal contact, and 30 (18.3%) both consumed unpasteurized cheese and had animal contact. The transmission route in 48 (29.3%) patients was unknown. Laboratory transmission occurred in one patient (0.6%) (Kazak et al. 2016). In a Tunisian study, 37.5% of patients had occupational exposure, and 87.5% lived in rural areas. The ingestion of unpasteurized milk or milk products of infected cows (96.9%) and contact with infected animals (90.6%) were the main risk factors for human brucellosis (Koubaa et al. 2014).

2.5 Location

The lumbar spine is the most affected (60%), particularly at the L4–L5 level (Turgut et al. 2006; Kursun et al. 2013), followed by thoracic (19%) and cervical spine (12%). More than one level is affected in 6–14% of cases (Papadimitriou et al. 2006; Zribi et al. 2009; Ducrotoy et al. 2014; WHO 2020; Ministry of Health Tunisia 2020). Involvement of the spine may be either focal or

diffuse (Papadimitriou et al. 2006; Zribi et al. 2009; Ducrotoy et al. 2014; WHO 2020; Ministry of Health Tunisia 2020). In a Tunisian study, the lumbar spine was the most frequently involved region with the rate of 78%, particularly at the level of the L4–L5 vertebra, followed by thoracic (21.8%), cervical (6.3%), lumbosacral (6.3%), and thoracolumbar segments (3.1%) (Koubaa et al. 2014).

The focal form is confined to the anterior portion of the vertebral body end plate. This typically occurs in the anterior superior end plate of a lumbar vertebra at the discovertebral junction because of its rich blood supply (Zribi et al. 2009; Ducrotoy et al. 2014). The diffuse form may involve the entire vertebral body and extend to the adjacent disk, vertebrae, and epidural space. Infection diffuses via the ligaments and vascular communications. Posterior elements are rarely involved, but facet joint arthritis may occur (Zribi et al. 2009; Ducrotoy et al. 2014; WHO 2015; Ministry of Health Tunisia 2020). Among the patients with BSD, lumbar involvement is significantly more common than in TSD and PSD ($p < 0.001$) (ErenGok et al. 2014).

2.6 Clinical Signs

Clinical signs and symptoms of brucellosis are usually not specific, with none being characteristic of brucellosis (Kazak et al. 2016). Clinical symptoms of BSD may include moderate fever and spinal pain of variable intensity and of mixed type (Papadimitriou et al. 2006). In a Portuguese study, the most common signs and symptoms of BSD were back pain (98.1%), fever (46.3%), and neurological deficits (25.9%) (Lebre et al. 2014). In a Tunisian study, back or neck pain (100% of patients), fever (78%), and sweats (68.6%) were the most common symptoms (Koubaa et al. 2014). Fever was significantly more frequent in BSD patients than in TSD and PSD ($p < 0.017$) in comparative studies (Turunc et al. 2007; Skaf et al. 2010a, b). Another comparative Turkish study found no statistically difference for the frequency of fever among the three groups; however, sweating was more common (81%) among the patients with BSD ($p < 0.001$), and the history of upper back pain and cervical pain was more common in patients with TSD ($p = 0.016$ and $p = 0.014$, respectively) than in those with BSD and PSD (ErenGok et al. 2014).

Neurological symptoms were more common in patients with TSD (61.5%), followed by pyogenic (50%) and BSD (31.2%), but with no significant differences (Turunc et al. 2007). Physical examination usually shows a "spinal syndrome," with segmental spinal rigidity and paravertebral muscle contracture. Pressure applied to the spinous process of the involved vertebra elicits pain. It is uncommon for BSD to present with spinal cord or nerve root compression. The long latent stage between the onset of symptoms and the appearance of radiological changes (ranging from 2 to 8 weeks) may prevent early diagnosis (Papadimitriou et al. 2006).

3 Epidemiology of Spinal Tuberculosis

Tuberculosis (TB) remains one of the most widespread infectious diseases in the world, mostly found in developing countries. It is still a major health problem globally (Chen et al. 2016). TB infects one-third of the world's population, with 8.7 million new cases annually. Worldwide rates of TB have increased in parallel with acquired immunodeficiency syndrome (AIDS) incidence (Batirel et al. 2015). In addition, TB ranks second, just after HIV infection, among infectious causes of mortality (Batirel et al. 2015). Pulmonary TB is the most frequent manifestation; however, extrapulmonary TB is common among people from TB high-endemic countries (Kristensen et al. 2017). TSD, also known as Pott disease, is a chronic disease that is slowly progressive, and diagnosing it is relatively difficult (Liu et al. 2019). If undiagnosed, it often leads to irreversible neurological injury, including paralysis, with resultant spinal cord compression causing severe and disabling neurological sequelae (Kristensen et al. 2017; Liu et al. 2019; Pu et al. 2019).

Table 3 Frequency of spinal tuberculosis among cases of spinal infection

Study	Country	Frequency (%)
Javed et al. (2018)	Spain	14–45.2
Cebrián Parra et al. (2012)	Spain	19.6
Venugopal Menon and Moawad Sorour (2016)	Oman	17

3.1 Frequency (Table 3)

Worldwide, 80% of patients with TSD are found in developing countries and poverty-stricken areas (Liu et al. 2019). TSD is the most common form of extrapulmonary TB and accounts for less than 5% of all TB cases (Zimmerli 2010; Duarte and Vaccaro 2013; Lee 2014; Kristensen et al. 2017; Javed et al. 2018; Pu et al. 2019) and for half of the bone and joint TB (Kristensen et al. 2017; Tom et al. 2018; Pu et al. 2019). TSD represents 10–35% of the cases of SD (Javed et al. 2018; Tom et al. 2018; Liu et al. 2019).

In Taiwan, TSD accounts for around 2% of all cases of TB and around 15% of extrapulmonary TB (Chen et al. 2016). In a Spanish study, an increase in cases of TSD from 14 to 45.2% among foreign-born residents in Barcelona over a period of 10 years was reported (Javed et al. 2018). In another Spanish study comprising 108 patients, TB was the second most common etiology of SD after *Staphylococcus* spp. (11 cases from 56 positive cultures) (Cebrián Parra et al. 2012). In 2013, TSD represented only 2.3% of all US TB cases (Sans et al. 2012). In a study conducted in Oman, which included 62 cases of SD, the frequency of TSD was 17% (Venugopal Menon and Moawad Sorour 2016).

3.2 Microbiology

Mycobacterium tuberculosis is the most frequent microorganism responsible for TSD. In a multinational, multicenter study consisting of 314 patients, *M. tuberculosis* was identified in 110 cases (Batirel et al. 2015). In France, *M. tuberculosis* is responsible for 21% of all SD in France, with more than 75% of cases of TSD being found in the immigrant population (Sans et al. 2012). In a Tunisian study, among 23 patients with bacteriologically confirmed TSD occurring between January 2014 and May 2018, 19 were caused by *M. tuberculosis* and four by *M. bovis* (Chebbi et al. 2019).

3.3 Age and Gender

This disease is most commonly seen in patients older than 50 years (Batirel et al. 2015). In a multinational, multicenter study (35 centers in Turkey, Egypt, Albania, and Greece) consisting of 314 patients, the mean age was 51 ± 18 years (Batirel et al. 2015). In another retrospective multinational (Turkey, Egypt, Albania, and Greece), and multicenter study (35 centers) of 641 patients (314 TSD and 327 BSD), the median age was similar (53 years versus 55 years, $p = 0.344$) (Erdem et al. 2015). In a comparative study, patients with TSD were older than patients having BSD or PSD (mean ages were 68 years, 59 years, and 65.5 years, respectively), without significant difference (Turunc et al. 2007). In a Chinese study comprising 1378 cases of TSD, patients were younger with a mean age of 43.7 years. A total of 561 patients (40.7%) were aged 18–45 years, followed by those 46–60 years old (27.2%) (Pu et al. 2019). A male predominance has been reported in many studies. In two multinational (Turkey, Egypt, Albania, and Greece), multicenter (35 centers) studies, men represent 51.2% and 51.9%, respectively, of cases (Batirel et al. 2015; Erdem et al. 2015). In a Chinese study comprising 1378 cases of TSD, 805 were men (58.4%) and 573 women (Liu et al. 2019). In a comparative study, there was no significant difference in gender between TSD, BSD, and PSD (Turunc et al. 2007).

3.4 Risk Factors (Table 4)

The risk factors of TSD are diabetes mellitus (12%) (Batirel et al. 2015; Liu et al. 2019; Pu et al. 2019), chronic renal failure (5%) (Turunc et al. 2007; Batirel et al. 2015), malignancy (2%) (Batirel et al. 2015), immunosuppression due to

Table 4 Risk factors of spinal tuberculosis (Batirel et al. 2015)

Risk factors	Frequency (%)
Diabetes mellitus	12
Chronic renal failure	5
Malignancy	2
Others (e.g., pulmonary diseases, coronary diseases)	19

treatment with antineoplastic chemotherapy (Batirel et al. 2015; Chen et al. 2016), HIV (Chen et al. 2016), glucocorticoids, TNF-alpha blockers (2%) (Batirel et al. 2015), recent contact with patients with TB (Chen et al. 2016), long-term physical labor (Liu et al. 2019), and others (e.g., hypertension, coronary artery disease, chronic obstructive pulmonary disease, asthma, nephrolithiasis) (19%) (Batirel et al. 2015). The prevalence of TB is three to six times higher in patients with diabetes mellitus, compared to those without diabetes mellitus. Additionally, the incidence of TB is three times higher in patients with poorly controlled diabetes mellitus than in those with ideally controlled diabetes mellitus (Liu et al. 2019). It has been also reported that the incidence of TB increases by 6.9–52.5 times in dialysis patients, compared to the general population (Turunc et al. 2007).

3.5 Location

TSD often affects the thoracic and lumbar spine (Tom et al. 2018). In a multinational, multicenter study, the lumbar spine (56%) was the most commonly involved region of the spinal column, followed by the thoracic spine (49%) (Chen et al. 2016). The same results were found in a Chinese study, where the lumbar segment (38.2%) was the most frequently affected, followed by the thoracic spine (35.7%) (Liu et al. 2019). In another multinational, multicenter study, thoracic and thoracolumbar involvement was the favored site in TSD, while lumbar involvement was more frequent in BSD ($p < 0.001$ for all comparisons) (Erdem et al. 2015). In a Turkish study, the thoracic location was more frequent in TSD (53.8%), while the lumbar spine was more frequent in BSD (65.6%), but the difference was not significant (Turunc et al. 2007).

3.6 Clinical Signs

The clinical pattern of SD is quite nonspecific. Typically, the onset of symptoms is insidious, and disease progression is slow (Chen et al. 2016; Pu et al. 2019). Early clinical manifestations of TSD are also atypical and insidious (Pu et al. 2019). The median duration of symptoms before the diagnosis has been reported to be between 2.5 and 16 months (Batirel et al. 2015; Liu et al. 2019; Varo et al. 2019). Moreover, despite advanced diagnostic methods, diagnosis of TSD is usually delayed. The clinical presentation and physical examination findings depend on the site and stage of the disease, presence of complications, and constitutional symptoms (Chen et al. 2016). The early clinical manifestations of TSD are insidious, usually manifesting first as back pain (83–92.5%) (Batirel et al. 2015; Javed et al. 2018; Liu et al. 2019; Pu et al. 2019) and local tenderness (Batirel et al. 2015; Pu et al. 2019).

The most commonly reported symptoms in a Chinese study were back pain (1438/2040, 70.4%), fever (667/2040, 32.7%), body weight loss (620/2040, 30.3%), neurological abnormalities (315/2040, 15.4%), and night sweats (390/2040, 19.1%) (Chen et al. 2016). In a comparative study, fever (139/314, 44.3%), back pain (176/314, 56%), loss of appetite (154/314, 49%), and weight (132/314, 42%) were more common on TSD than on BSD ($p < 0.001$) (Erdem et al. 2015). In another comparative study, fever was significantly more common in patients with BSD ($p < 0.017$) (KaragozGuzey et al. 2007), and the history of upper back pain and cervical pain were more common in patients with TSD ($p = 0.016$ and $p = 0.014$, respectively) than in those with BSD and PSD (ErenGok et al. 2014). In a comparative Turkish study, neurological symptoms were more common in TSD patients (61.5%), followed by PSD (50%) and BSD patients (31.2%), but there was no significant difference. Likewise, neurological deficit was more common in TSD patients (61.5%), followed by PSD

(46.6%) and BSD patients (25.8%), but with no significant difference (Turunc et al. 2007).

3.7 Complications

In a Chinese study, abscesses were detected by computed tomography (CT) or magnetic resonance imaging (MRI) in 903 of 1378 patients (65.5%), including paravertebral and psoas abscesses (Liu et al. 2019). They were detected in 30% of cases in a Tunisian study (Tarzi Brahem 1983). The incidence of neurological deficit varies from 23 to 76% (Turunc et al. 2007; Chen et al. 2016). In a multinational, multicenter study, 69% of patients had abscesses (with the majority being paravertebral at 39%), 40% had neurologic deficits, 21% had spinal instability, and 16% had spinal deformity (Batirel et al. 2015). Complications were more frequent in patients with an unfavorable outcome: abscesses in 74%, neurological deficits in 56%, spinal instability in 36%, and spinal deformity in 61%, with significant differences ($p < 0.05$). Complications can occur during the course of treatment, namely, neurological deficits (6%) and spinal deformities (4%) (Batirel et al. 2015). In a comparative study, prevertebral, paravertebral, epidural, and psoas abscesses were more frequently observed in TSD than in BSD ($p < 0.01$) (Erdem et al. 2015). Neurological complications ($p < 0.001$), spinal instability ($p < 0.001$), and spinal deformity ($p < 0.002$) were also more frequent with TSD than with BSD ($p < 0.001$) (Erdem et al. 2015).

3.8 Associated Sites

Pulmonary TB is the most commonly associated location. Concomitant pulmonary TB, including a previous history of pulmonary TB, was present in 366/1378 Chinese patients (26.6%) (Liu et al. 2019). In a retrospective multinational (Turkey, Egypt, Albania, and Greece), and multicenter (35 centers) study including 641 patients (314 TSD and 327 BSD), 51 patients who had TSD also had another location of TB (pulmonary 29 and meningitis 13) (Erdem et al. 2015).

4 Epidemiology of Spinal Pyogenic Infection

Pyogenic spondylodiscitis (PSD) was first described by Lannelongue in 1879, and the first series of pyogenic cases was published by Kulowski in 1936 (Kulowski 1936). Spontaneous PSD represents 2–7% of all cases of osteomyelitis (Gouliouris et al. 2010). The incidence of PSD appears to be on rise, with the increasing incidence seemingly related to the high number of chronic debilitating diseases, rise of intravenous drug abuse (IVDA), and rising numbers of patients undergoing spinal surgery (Kapsalaki et al. 2009).

4.1 Frequency

The incidence of PSD is more frequent in developed countries. Nevertheless, tuberculous and brucellar infections are more frequent and endemic in North Africa, Asia, and the Middle East (Ben Taarit et al. 2002; Menon and Sorour 2016). The incidence of PSD is estimated to be 5–5.3 per million patients per year. In Europe, the annual incidence of this infection ranges from 0.5 to 2.4 cases per 100,000 inhabitants (Krogsgaard et al. 1998; Hopkinson and Patel 2016). A French study has reported an annual incidence of spinal infection of 2.4 per 100,000 person-years, with the mean age being 59 (1–98) years (Sans et al. 2012). On the other hand, a Danish study has reported an annual incidence of PSD increasing from 2.2 to 5.8/100,000 inhabitants over a 14-year period (Kehrer et al. 2014), while a Japanese study showed an increase in the incidence of approximately 140% from 2007 to 2010 (Akiyama et al. 2013).

4.2 Microbiology

The causative agent of PSD is variable, depending on the initial contamination route. The main microorganism responsible for pyogenic spinal infections is *Staphylococcus aureus* (Chong et al. 2018). According to the series of Koutsoumbelis

et al. (2011), methicillin-resistant *Staphylococcus aureus* (MRSA) was reported in 34% of cases of PSD. Chronic dialysis patients have a higher proportion of MRSA (Kuo et al. 2018). Coagulase-negative staphylococci have been reported in 5–16% of cases. *Staphylococcus epidermidis* is often related to postoperative spinal infection (Fantoni et al. 2012). Staphylococci are followed by gram-negative aerobic bacilli, *Streptococcus pyogenes* and *Enterococcus* spp., in terms of frequency. Gram-negative agents are causative agents in 7–33% of cases of PSD. *Escherichia coli*, *Proteus* spp., *Enterobacter cloacae*, and *Pseudomonas aeruginosa* are are often reported in patients with comorbidities such as diabetes mellitus, IVDA, immunodeficiency, and following procedures or infections involving the genitourinary and gastrointestinal tracts (Skaf et al. 2010a, b; Koutsoumbelis et al. 2011).

There is an increasing proportion of *Streptococcus* spp., coagulase-negative *Staphylococcus*, and other fastidious bacteria compared with gram-negative bacilli. Indeed, coagulase-negative *Staphylococcus* more frequently occurs in postoperative implant-associated spinal infection compared to hematogeneous native PSD (Doutchi et al. 2015). Anaerobic agents are observed in 3% of cases. Among anaerobic bacteria, *Bacteroides* spp., *Peptococcus* spp., and *Propionibacterium acnes* are more common in patients with diabetes mellitus (Bontoux et al. 1992; Hadjipavlou et al. 2000; Kourbeti et al. 2008; Chong et al. 2018). *Bacteroides fragilis* has been reported in patients with diabetes mellitus or intra-abdominal infection. For IVDA patients, *Staphylococcus aureus* was the predominant microorganism detected in 61.7% of cases. *Pseudomonas aeruginosa* were isolated in four cases from the culture of bone biopsy (Ziu et al. 2014).

4.3 Age and Gender

PSD is more frequent in adults older than 50 years of age and in childhood (Petkova et al. 2017). Two peaks of pyogenic spinal infection, in patients under 20 years and in the age range of 50–70 years, have been reported. PSD is more common among men, with a sex ratio of 1.6–2.0:1, which further increases in the elderly population (Skaf et al. 2010a, b).

4.4 Risk Factors

The risk factors known to increase the risk of pyogenic spinal infection include diabetes mellitus, smoking, obesity, distant infection site, advanced age, IVDA, immunosuppression, steroid therapy, HIV infection, chronic kidney disease, alcoholism, malnutrition, malignancy, and liver cirrhosis (Cottle and Riordan 2008; Mylona et al. 2009; Meredith et al. 2012; Chong et al. 2018). The incidence of pyogenic spinal infection is rising, according to an increase in the rate of nosocomial infections associated with vascular devices and other forms of instrumentation and to an increasing prevalence of IVDA (Torda et al. 1995; Skaf et al. 2010a, b).

Pyogenic spinal infection results from hematogeneous infection (60–80% of cases), direct inoculation (15–40% of cases), or contiguous contamination (3% of cases). It is often the result of hematogeneous spread from either the skin, respiratory tract, genitourinary tract, gastrointestinal tract, or the oral cavity giving rise to bacteremia (Govender 2005). The urinary tract has been reported as the predominant source of infection in 17–30% of cases (Mylona et al. 2009; Doutchi et al. 2015). Approximately 37% of PSD does not have an identifiable source (Lestini and Bell 1999).

The increase in IVDA has led to the increase of the incidence of PSD. An American study reported 102 cases in patients with a history of IVDA. The mean age was 45.4 years and majority of patients were men. Other comorbidities were associated to IVDA, such as HIV infection, hepatitis C, endocarditis, and alcohol abuse (Ziu et al. 2014). Chronic dialysis patients, particularly those under hemodialysis, may present with PSD as a result of bacteremia which comes from punctures of the water pipeline or from the vascular contamination by intravenous catheters (Cervan et al. 2012). Hemodialysis vascular access is one of the most routes of bacterial entry

(Kuo et al. 2018). In most cases, patients under hemodialysis are elderly, have other underlying diseases, and are immunocompromised. Hence, morbidity and mortality are higher in this population. A Taiwanese study reported 106 cases of PSD in patients under hemodialysis. The average age was 66.7 years, and diabetes mellitus was reported in 48.6% of cases (Kuo et al. 2018).

For iatrogenic PSD, the incidence of postoperative spondylodiscitis (POSD) after lumbar discectomy has been reported to be between 0.7 and 2.8% of operated cases. Spinal instrumentation adds further complicating factors, with infection rates averaging 7% (range 1.3–12%) (Gepstein and Eistmont 1990). POSD is the most common complication following a spinal operation. The incidence of POSD is affected by three types of risk factors, namely, the nature of the spinal pathology, the surgical procedure, and the patient-related risk factors. On the one hand, the incidence of POSD depends on the complexity of the index surgical procedure and its duration. The risk of infection has been found to be higher after arthrodesis with posterior instrumentation (Meredith et al. 2012). In the literature, rates of POSD after thoracic or lumbar spinal arthrodesis range from 1.9 to 4.4% (Meredith et al. 2012). In a systematic review of literature, the rate of POSD was found to be decreased significantly after minimally invasive transforaminal interbody fusion, compared to open transforaminal interbody fusion (0.6% versus 4%) (Parker et al. 2011). Some factors have been cited to increase the rate of infection following a spinal procedure, such as prolonged preoperative hospitalization, suboptimal sterile techniques, prolonged procedures, and increased operating room traffic (Parker et al. 2011).

4.5 Location

The most common level of involvement of PSD is the lumbar spine, followed by the thoracic, cervical, and sacral levels (Wisneski 1991). The literature on cervical PSD is scarce. However, these infections can lead to severe neurological complications compared to other locations (Urrutia et al. 2013). For PSD in patients with a history of IVDA, the most commonly affected level is the lumbar spine (57.8% of cases), followed by the thoracic and cervical spine (Ziu et al. 2014). The lumbar vertebra is also the most affected in patients on chronic dialysis (84.8%) (Cervan et al. 2012; Kuo et al. 2018).

4.6 Clinical Signs

The clinical presentation of PSD is not specific. The delay in diagnosis of PSD varies between 1 and 6 months (Petkova et al. 2017). It is much longer in TSD than in PSD (Batirel et al. 2015; Liu et al. 2019; Varo et al. 2019). In immunocompromised patients, such as patients undergoing hemodialysis, the delay is greater and can range from 5 to 183 days (Cervan et al. 2012). The main symptom is back and/or neck pain, depending on the level of the disease. Unremitting back pain, particularly worsening during the night, is the most common presenting symptom, followed by fever. Fever (>38 °C) is present in about one-half of the cases (Skaf et al. 2010a, b; Fantoni et al. 2012).

For POSD, clinical signs are complex, difficult to interpret, and poorly characterized. The interval between symptom onset and diagnosis is longer for POSD (16 weeks) than for spontaneous PSD (3–4 weeks) (Dufour et al. 2005). Neurological complications, such as spinal cord or nerve root compression, occur more frequently in PSD. They are present in approximately 12% of patients (Skaf et al. 2010a, b). Eismont et al. (1983) found that sensory involvement is rare, whereas motor and long-tract signs are more common because of mainly anterior cord compression. Epidural abscesses are detected in the majority of patients with pronounced neurological symptoms (Petkova et al. 2017).

5 Epidemiology of Spinal Fungal Infection

Fungal SD is uncommon (0.5–1.6%) and is usually due to *Candida albicans*. The immunocompromised population that is susceptible to fungal

infections is ever increasing. Risk factors of fungal infection include prior use of broad-spectrum antibiotics, central venous access devices, immunosuppression, neutropenia, chronic granulomatous disease, and intravenous drug use (Gouliouris et al. 2010; Berbari Elie et al. 2015). A wide variety of fungal organisms can cause spinal infection. The most common fungal organisms causing SD include *Aspergillus* spp., *Candida* spp., and *C. neoformans*. *Candida albicans* is the commonest *Candida* species in the literature (Kim et al. 2006). Whereas *Cryptococcus*, *Candida*, and *Aspergillus* have a worldwide distribution, other fungi such as *Coccidioides immitis* and *Blastomyces dermatitidis* are limited to specific geographical areas. Therefore, residence in or travel to endemic areas should be taken into consideration when evaluating patients with prolonged evolution of SD.

5.1 Candida Spondylodiscitis

Candida spondylitis accounts for approximately 1% of infectious SD (Richaud et al. 2017). It was previously considered a complication of intravenous drug use but is now mostly a healthcare-associated infection, such as most invasive Candida infections. With the increase in invasive Candida infections, the incidence of *Candida* spondylitis is increasing, and this trend will likely continue in the future (Cornely et al. 2012; Pappas et al. 2016). Although there are ten species of Candida that are pathogenic to humans, 62% of cases of vertebral osteomyelitis are caused by *Candida albicans*, 19% by *Candida tropicalis*, and 14% by *Candida glabrata* (Kim et al. 2006). Infection caused by *Candida glabrata* is becoming more common.

5.2 Aspergillus Spondylodiscitis

Aspergilli are opportunistic mycelial organisms. They are abundant in the environment. They live as saprophytes, and their concentration in the air undergoes seasonal variation (higher during autumn and winter). Nosocomial aspergillosis is due to infiltration of conidia into ward air from outside. Aspergillus is the most common cause of infection and death in patients with chronic granulomatous disease (Heinrich et al. 1991). Aspergillosis is also the second most common invasive fungal infection in cancer patients and most of them were or had been neutropenic. Bone marrow transplant recipients may be at risk of invasive aspergillosis, especially during profound neutropenia (Govender et al. 1991). Aspergillus is the most common cause of skeletal mycosis, and the vertebrae are the most commonly involved structures in fungal osteomyelitis. The most common causative species is *Aspergillus fumigatus*. In fewer instances, *Aspergillus flavus*, *Aspergillus niger*, *Aspergillus nodulans*, and *Aspergillus terreus* have been isolated (Govender et al. 1991).

5.3 Cryptococcal Spondylodiscitis

Cryptococcosis is a systemic mycosis that often involves the lungs and the central nervous system. It is caused by *Cryptococcus neoformans*, which is found in fruits, milk, soil, and feces of some birds. The disease has a worldwide distribution. Immunosuppression related to altered T-cell function is the most common predisposing factor. In non-HIV-infected patients, predisposing factors for cryptococcosis include malignancy, solid organ transplantation, connective tissue diseases, and immunosuppressive therapy. Estimates of the annual incidence of cryptococcosis in non-HIV individuals are 1.3–8 per 100,000 (Legarth et al. 2014). The disease is generally acquired by the respiratory route through inhalation of aerosolized spores. Pulmonary infection with cryptococcus may be asymptomatic or symptomatic. It may regress, progress, or remain stable for years. Extrapulmonary infection usually results from a hematogeneous spread and can involve any organ. There is a predilection for central nervous system involvement, which is the most common extrapulmonary manifestation (Kim et al. 2006). Osseous involvement is a manifestation of disseminated cryptococcosis in 5–10% of cases.

The most commonly involved skeletal sites are the spine, pelvis, ribs, skull, tibia, and knee (Chhem et al. 2001).

5.4 Coccidioidal Spondylodiscitis

Coccidioidomycosisis endemic in South Africa, South America, and the United States (Dalinka et al. 1971). Coccidioidomycosis results from inhalation of spores of the fungus, which causes a variable pulmonary response in affected individuals. Extrapulmonary dissemination occurs in approximately 0.5% of affected patients. Spinal involvement develops in approximately 25% of patients with disseminated disease (Huntington et al. 1967; Galgiani 1993).

5.5 Blastomycotic Spondylodiscitis

Blastomyces dermatitidis is a dimorphic fungus endemic in the Southeastern and South Central United States of America. *Blastomyces dermatitidis* is considered to be an inhabitant of soil, and infection occurs by inhalation of conidia. For blastomycosis, the hematogeneous dissemination of infection to almost any organ can occur months to years after the initial pulmonary involvement (Kuzo and Goodman 1996). The skin is the most common extrapulmonary site (40–80% incidence). Skeletal blastomycosis is seen in 14–60% of disseminated cases (Riegler et al. 1974; Hadjipavlou et al. 1998). The spine is the most common site of skeletal involvement, followed by the skull, ribs, tibia, and the bones of the foot and wrist.

5.6 Mycetoma Spondylodiscitis

Mycetoma is a neglected tropical disease that is endemic in many tropical and subtropical areas. Mycetoma is a chronic mutilating disease of the skin and the underlying tissues caused by fungi (eumycetomas) or bacteria (actinomycetomas). The most frequent organisms causing actinomycetoma are *Streptomyces somaliensis*, *Actinomadura madurae*, and *A. pelletieri*, while the most common pathogens reported in eumycetoma are *M. mycetomatis*, *M. grisea*, *Pseudallescheria boydii*, and *Leptosphaeria senegalensis*. It follows implantation of infectious organisms into subcutaneous tissue, from where the infection spreads to the skin and bone. The organisms form small microcolonies that are discharged onto the skin surface via sinus tracts or that can burrow into other adjacent tissues including bone (Zijlstra et al. 2016). Mycetoma occurs in all age groups but is rarely seen in children. It commonly occurs in field laborers and cultivators whose occupation involves direct contact with the soil (Lichon and Khachemoune 2006). The foot is the commonest site affected by mycetoma and accounts for 70% of cases, followed by the hand (12%). Spinal cord involvement is rare, and only a few cases have been reported (Fahal 2004, 2011; Cascio et al. 2011).

6 Conclusion

Spinal infection is a serious disease which can induce neurological complications, with potentially high morbidity and mortality. The incidence of PSD is more frequent in developed countries. Many risk factors have been identified for PSD, and it is rising, including an increased rate of nosocomial infections associated with vascular devices and other forms of instrumentation and to an increasing prevalence of IVDA. Tuberculous and brucellar infections are more frequent in developing countries. Worldwide, 80% of patients with TSD are found in developing countries and poverty-stricken areas. TSD accounts for half of the bone and joint TB and is the most common form of extrapulmonary TB. Fungal PSD is uncommon and is usually due to *Candida albicans*, occurring essentially in immunocompromised patients. Early clinical manifestations of spinal infection are usually insidious, leading to a long mean interval between symptom onset and diagnosis; hence complications are frequent. Rapid and effective diagnosis and management help prevent irreversible neurological and bony complications.

References

Abdou R (2013) Epidémiologie de la brucellose et de la tuberculose animales dans les milieux urbain, périurbain et rural au Niger [Thèse]. Medecine, Liège, 212 p

Abdullayev R, Kracalik I, Ismayilova R et al (2012) Analyzing the spatial and temporal distribution of human brucellosis in Azerbaijan (1995-2009) using spatial and spatio-temporal statistics. BMC Infect Dis 12:185

Akakpo AJ, Têko-Agbo A, Koné P (2020) L'impact de la brucellose sur l'economie et la santé publique en afrique [En ligne]. EISMV [cité le 3 février 2020]; [environ 28 écrans]. Disponible à l'URL: https://www.oie.int/doc/ged/D9761.PDF

Akiyama T, Chikuda H, Yasunaga H et al (2013) Incidence and risk factors for mortality of vertebral osteomyelitis: a retrospective analysis using the Japanese diagnosis procedure combination database. BMJ Open 3:e002412

Aubry PP (2017) Brucellose actualités. Med Trop 47:1–3

Aznar MN, Samartino LE, Humblet MF et al (2014) Bovine brucellosis in Argentina and bordering countries: update. Transbound Emerg Dis 61:121–133

Batirel A, Erdem H, Sengoz G et al (2015) The course of spinal tuberculosis (Pott disease): results of the multinational, multicenter Backbone-2 study. Clin Microbiol Infect 21:1008.e9–1008.e18

Bechtol D, Carpenter LR, Mosites E et al (2011) Brucella melitensis infection following military duty in Iraq: brucella melitensis infection following military duty in Iraq. Zoonoses Public Health 58:489–492

Ben Taarit C, Turki S, Ben Maiz H (2002) Infectious spondylitis: a review of 151 cases. Acta Orthop Belg 68:381–387

Berbari Elie F, KaniSouha S, Kowalski Todd J et al (2015) Infectious Disease Society of America (IDSA) clinical practice guidelines for the diagnosis and treatment of native vertebral osteomyelitis in adults. Clin Infect Dis 61:e26–e46

Bontoux D, Codello L, Debiais F et al (1992) Infectious spondylodiscitis. Analysis of series of 105 cases. Rev Rhum Mal Osteoartic 59:709–715

Cascio A, Mandraffino G, Cinquegrani M et al (2011) Actinomadura pelletieri mycetoma—an atypical case with spine and abdominal wall involvement. J Med Microbiol 60:673–676

Castilla JM, Martin V, Rodriguez-Salazar A (2002) Surgical treatment of patients with spinal infection. Neurocirugia (Astur) 13:101–109

Cebrián Parra JL, Martín ASA, Urda Martínez-Aedo AL et al (2012) Management of infectious discitis. Outcome in one hundred and eight patients in a University Hospital. Int Orthop 36:239–244

Cervan AM, Colmenero JD, Del Arco A et al (2012) Spondylodiscitis in patients under haemodialysis. Int Orthop 36:421–426

Chakroun M, Bouzouaia N (2007) La brucellose: une zoonose toujours d'actualité brucellosis: atopical zoonosis. Rev Tun Infectiol 1(2):1–10

Chebbi Y, Riahi H, Bouaziz M et al (2019) Mycobacterium bovis spondylodiscitis: report of 4 cases. J Clin Rheumatol 10:1097

Chen CH, Chen YM, Lee CW et al (2016) Early diagnosis of spinal tuberculosis. J Formos Med Assoc 115:825–836

Chhem RK, Wang S, Jaovisidha S et al (2001) Imaging of fungal, viral, and parasitic musculoskeletal and spinal diseases. Radiol Clin North Am 39:357–378

Chong BSW, Brereton CJ, Gordon A et al (2018) Epidemiology, microbiological diagnosis, and clinical outcomes in pyogenic vertebral osteomyelitis: a 10-year retrospective cohort study. Open Forum Infect Dis 5(3):ofy037

Cornely OA, Bassetti M, Calandra T et al (2012) ESCMID∗ guideline for the diagnosis and management of Candida diseases 2012: non-neutropenic adult patients. Clin Microbiol Infect 18(Suppl 7):19–37

Cottle L, Riordan T (2008) Infectious spondylodiscitis. J Infect 56:401–412

Crump JA, Youssef FG, Luby SP et al (2003) Estimating the incidence of typhoid fever and other febrile illnesses in developing countries. Emerg Infect Dis 9:539–544

Dalinka MK, Dinnenberg S, Greendyk WH et al (1971) Genographic features of osseous coccidioidomycosis and differential diagnosis. J Bone Joint Surg Am 53:1157–1164

Dean AS, Crump L, Greter H et al (2012) Global burden of human brucellosis: a systematic review of disease frequency. PLoS Negl Trop Dis 6:1–10

Doutchi M, Seng P, Menard A et al (2015) Changing trends in the epidemiology of vertebral osteomyelitis in Marseille, France. New Microbes New Infect 7:1–7

Duarte RM, Vaccaro AR (2013) Spinal infection: state of the art and management algorithm. Eur Spine J 22:2787–2799

Ducrotoy MJ, Bertu WJ, Ocholi RA et al (2014) Brucellosis as an emerging threat in developing economies: lessons from Nigeria. PLoS Negl Trop Dis 8:1–19

Dufour V, Feydy A, Rillardon L et al (2005) Comparative study of postoperative and spontaneous pyogenic spondylodiscitis. Semin Arthritis Rheum 34:766–771

Eismont FJ, Bohlman HH, Soni PL et al (1983) Pyogenic and fungal vertebral osteomyelitis with paralysis. J Bone Joint Surg Am 65:19–29

Erdem H, Elaldi N, Batirel A et al (2015) Comparison of brucellar and tuberculous spondylodiscitis patients: results of the multicenter "Backbone-1 Study". Spine J 15:2509–2517

ErenGok S, Kaptanoglu E, Elikbas AC et al (2014) Vertebral osteomyelitis: clinical features and diagnosis. Clin Microbiol Infect 20(10):1055–1060. https://doi.org/10.1111/1469-0691.12653

European Centre for Disease Prevention and Control (2017) Brucellosis—annual epidemiological report for 2017 [En ligne]. ECDC [cité le 3 février 2020]; [environ 5 écrans]. Disponible à l'URL: http://ecdc.europa.eu/en/publications-data/brucellosis-annual-epidemiological-report-2017

European Surveillance System (2016) Brucellosis—annual epidemiological report for 2016 [En ligne]. ECDC [cité le 3 février 2020]; [environ 7 écrans]. Disponible à l'URL: https://www.ecdc.europa.eu/en/publications-data/brucellosis-annual-epidemiological-report-2016

Fahal AH (2004) Mycetoma: a thorn in the flesh. Trans R Soc Trop Med Hyg 98:3–11

Fahal AH (2011) Mycetoma. Khartoum Med J 4:514–523

Fantoni M, Trecarichi EM, Rossi B et al (2012) Epidemiological and clinical features of pyogenic spondylodiscitis. Eur Rev Med Pharmacol Sci 16(Suppl 2):2–7

Galgiani JN (1993) Coccidioidomycosis. West J Med 159:154–171

Georgi E, Walter MC, Pfalzgraf MT et al (2017) Whole genome sequencing of brucella melitensis isolated from 57 patients in Germany reveals high diversity in strains from middle east. PLoS One 12:1–15

Gepstein R, Eistmont FI (1990) Post-operative spine infections. In: Weinstein JN, Wiesel SW (eds) The lumbar spine. WB Saunders, Philadelphia

Gouliouris T, Aliyu SH, Brown NM (2010) Spondylodiscitis: update on diagnosis and management. J Antimicrob Chemother 65(Suppl 3):iiii11–iiii24

Govender S (2005) Spinal infections. J Bone Joint Surg Br 87:1454–1458

Govender S, Rajoo R, Goga IE et al (1991) Aspergillus osteomyelitis of the spine. Spine 16:746–749

Guzmán HL, Contreras RA, Ávila CD et al (2016) Brucelosis: zoonosis de importancia en méxico. Rev Chil Infectol 33:656–662

Hadjipavlou AG, Mader JT, Nauta HJ et al (1998) Blastomycosis of the lumbar spine: case report and review of the literature, with emphasis on diagnostic laboratory tools and management. Eur Spine J 7:416–421

Hadjipavlou AG, Mader JT, Necessary JT et al (2000) Hematogenous pyogenic infections and their surgical management. Spine 25:1668–1679

Heinrich SD, Finney T, Craver R et al (1991) Aspergillus osteomyelitis in patients who have chronic granulomatous disease. J Bone Joint Surg Am 73: 456–460

Hopkinson N, Patel K (2016) Clinical features of septic discitis in the UK: a retrospective case ascertainment study and review of management recommendations. Rheumatol Int 36:1319–1326

Hull NC, Schumaker BA (2018) Comparisons of brucellosis between human and veterinary medicine. Infect Ecol Epidemiol 8:1–13

Huntington RW, Waldmann WJ, Sargent JA et al (1967) Pathologic and clinical observations on 142 cases of fatal coccidioidomycosis. In: Ajello L (ed) Coccidioidomycosis. University of Arizona Press, Tucson, pp 221–222

Javed G, Laghari AA, Ahmed SL et al (2018) Development of criteria highly suggestive of spinal tuberculosis. World Neurosurg 116:e1002–e1006

Kapsalaki E, Gatselis N, Stefos A et al (2009) Spontaneous spondylodiscitis: presentation, risk factors, diagnosis, management, and outcome. Int J Infect Dis 13:564–569

KaragozGuzey F, Emel E, Sel B et al (2007) Cervical spinal brucellosis causing epidural and prevertebral abscesses and spinal cord compression: a case report. Spine J 7:240–244

Kazak E, Akalın H, Yılmaz E et al (2016) Brucellosis: a retrospective evaluation of 164 cases. Singapore Med J 57:624–629

Kehrer M, Pedersen C, Jensen TG et al (2014) Increasing incidence of pyogenic spondylodiscitis: a 14-year population-based study. J Infect 68:313–320

Kim CW, Perry A, Currier B et al (2006) Fungal infections of the spine. Clin Orthop Relat Res 444:92–99

Koubaa M, Maaloul I, Marrakchi C et al (2014) Spinal brucellosis in South of Tunisia: review of 32 cases. Spine J 14:1538–1544

Kourbeti IS, Tsiodras S, Boumpas DT (2008) Spinal infections: evolving concepts. Curr Opin Rheumatol 20:471–479

Koutsoumbelis S, Hughes AP, Girardi FP et al (2011) Risk factors for postoperative infection following posterior lumbar instrumented arthrodesis. J Bone Joint Surg Am 93:1627–1633

Kristensen KL, Podlekareva D, Ravn P (2017) Delayed diagnosis of severe tuberculous spondylodiscitis in an asylum seeker; patient or doctors delay? Respir Med Case Rep 21:145–146

Krogsgaard MR, Wagn P, Bengtsson J (1998) Epidemiology of acute vertebral osteomyelitis in Denmark: 137 cases in Denmark 1978-1982, compared to cases reported to the National Patient Register 1991-1993. Acta Orthop Scand 69:513–517

Kulowski J (1936) Pyogenic osteomyelitis of the spine: an analysis and discussion of 102 cases. J Bone Joint Surg Am 18:343–364

Kuo G, Sun WC, Lu YA et al (2018) Chronic dialysis patients with infectious spondylodiscitis have poorer outcomes than non-dialysis populations. Ther Clin Risk Manag 14:257–263

Kursun E, Turunc T, Demiroglu Y, Arslanand H (2013) Evaluation of four hundred and forty seven brucellosis cases. Intern Med 52:745–750

Kuzo RS, Goodman LR (1996) Blastomycosis. Semin Roentgenol 31:45–51

Lai S, Zhou H, Xiong W et al (2017) Changing epidemiology of human brucellosis, China, 1955-2014. Emerg Infect Dis 23:184–194

Lebre A, Velez J, Seixas D et al (2014) Brucellar spondylodiscitis: case series of the last 25 years. Acta Med Port 27:204–210

Lee KY (2014) Comparison of pyogenic spondylitis and tuberculous spondylitis. Asian Spine J 8:216–223

Legarth RA, Christensen M, Calum H et al (2014) Cryptococcal rib osteomyelitis as primary and only symptom of idiopathic CD4 penia. Med Mycol Case Rep 4:16–18

Lestini WF, Bell GR (1999) Spinal infections: patient evaluation. Semin Spine Surg 2:244–256

Lichon V, Khachemoune A (2006) Mycetoma: a review. Am J Clin Dermatol 7:315–321

Liu Z, Wang J, Chen GZ et al (2019) Clinical characteristics of 1378 in patients with spinal tuberculosis in general hospitals in South-Central China. BioMed Res Int 2019:9765253

Maurin M (2005) La brucellose à l'aube du 21e siècle. Med Mal Infect 35:6–16

Menon KV, Sorour TMM (2016) Epidemiologic and demographic attributes of primary spondylodiscitis in a Middle Eastern population sample. World Neurosurg 95:31–39

Meredith DS, Kepler CK, Huang RC et al (2012) Postoperative infections of the lumbar spine: presentation and management. Int Orthop 36:439–444

Ministry of Health Tunisia (2020). http://www.santetunisie.rns.tn

Mirnejad R, Jazi FM, Mostafaei S et al (2017) Epidemiology of brucellosis in Iran: a comprehensive systematic review and meta-analysis study. Microb Pathog 109:239–247

Mylona E, Samarkos M, Kakalou E et al (2009) Pyogenic vertebral osteomyelitis: a systematic review of clinical characteristics. Semin Arthritis Rheum 39:10–17

Negrón ME, Kharod GA, Bower WA et al (2019) Notes from the field: human *Brucella abortus* rb51 infections caused by consumption of unpasteurized domestic dairy products—United States, 2017–2019. Morb Mortal Wkly Rep 68:185

Norman FF, Monge MB, Chamorro TS et al (2016) Imported brucellosis: a case series and literature review. Travel Med Infect Dis 14:182–199

Papadimitriou P, Akritidis N, Christou L et al (2006) The new global map of human brucellosis. Lancet Infect Dis 6:91–99

Pappas PG, Kauffman CA, Andes DR et al (2016) Clinical Practice Guideline for the Management of Candidiasis: 2016 update by the Infectious Diseases Society of America. Clin Infect Dis 62:e1–e50

Parker SL, Adogwa O, Witham TF et al (2011) Postoperative infection after minimally invasive versus open transforaminal lumbar interbody fusion (TLIF): literature review and cost analysis. Minim Invasive Neurosurg 54:33–37

Pelerito A, Cordeiro R, Matos R et al (2017) Human brucellosis in Portugal: retrospective analysis of suspected clinical cases of infection from 2009 to 2016. PLoS One 12:1–7

Petkova AS, Zhelyazkov CB, Kitov BD (2017) Spontaneous spondylodiscitis—epidemiology, clinical features, diagnosis and treatment. Folia Med 59:254–260

Pu F, Feng J, Yang L et al (2019) Misdiagnosed and mismanaged atypical spinal tuberculosis: a case series report. Exp Ther Med 18:3723–3728

Richaud C, De Lastours V, Panhard X et al (2017) Candida vertebral osteomyelitis (CVO) 28 cases from a 10-year retrospective study in France. Medicine (Baltimore) 96(31):e7525

Riegler HF, Goldstein LA, Betts RF (1974) Blastomycosis osteomyelitis. Clin Orthop Relat Res 100: 225–231

Rubach MP, Halliday JEB, Cleaveland S et al (2013) Brucellosis in low-income and middle-income countries. Curr Opin Infect Dis 26:404–412

Sans N, Faruch M, Lapègue F et al (2012) Infections of the spinal column—spondylodiscitis. Diagn Interv Imaging 93:520–529

Skaf GS, Domloj NT, Fehlings MG et al (2010a) Pyogenic spondylodiscitis: an overview. J Infect Public Health 3:5–16

Skaf GS, Kanafani ZA, Araj GF et al (2010b) Non-pyogenic infections of the spine. Int J Antimicrob Agents 36:99–105

Tarzi Brahem H (1983) Les spondylodiscites infectieuses en médecine interne. Thèse médecine, Tunis

Tom J, Hines A, Lazarescu R (2018) Pott's disease: a rare but critical diagnosis. Chest Annual Meeting 2018. https://doi.org/10.1016/j.chest.2018.08.122

Torda AJ, Gottlieb T, Bardbury R (1995) Pyogenic vertebral osteomyelitis: analysis of 20 cases and review. Clin Infect Dis 20:320–328

Tuon FF, Cerchiari N, Cequinel JC et al (2017) Guidelines for the management of human brucellosis in the state of Paraná, Brazil. Rev Soc Bras Med Trop 50: 458–464

Turan H, Serefhanoglu K, Karadeli E et al (2011) Osteoarticular involvement among 202 brucellosis cases identified in Central Anatolia Region of Turkey. Intern Med 50:421–428

Turgut M, Turgut AT, Kosar U et al (2006) Spinal brucellosis: Turkish experience based on 452 cases published during the last century. Acta Neurochir (Wien) 148:1033–1044

Turunc T, Demiroglu YZ, Uncu H et al (2007) A comparative analysis of tuberculous, brucellar and pyogenic spontaneous spondylodiscitis patients. J Infect 55:158–163

Urrutia J, Zamora T, Campos M (2013) Cervical pyogenic spinal infections: are they more severe diseases than infections in other vertebral locations? Eur Spine J 22:2815–2820

Varo R, Bila R, Saavedra B et al (2019) Paraplegia and spinal deformity in a Mozambican child with Pott's disease and tuberculous scrofula. Lancet 394(10209):1651

Venugopal Menon K, Moawad Sorour TM (2016) Epidemiologic and demographic attributes of primary

spondylodiscitis in a Middle Eastern Population sample. World Neurosurg 95:31–39

Welburn SC, Beange I, Ducrotoy MJ et al (2015) The neglected zoonoses the case for integrated control and advocacy. Clin Microbiol Infect 21:433–443

Wisneski RJ (1991) Infectious disease of the spine. Diagnostic and treatment considerations. Orthop Clin North Am 22:491–501

World Health Organization (2015) International Meeting on neglected zoonotic diseases, World Health Organization, Food and Agriculture Organization of the United Nations, International Office of Epizootics. The control of neglected zoonotic diseases: from advocacy to action: report of the fourth International Meeting held at WHO headquarters; 19–20 November 2014; Geneva. WHO, Geneva, pp 1–40

World Health Organization (2020) Brucellosis in humans and animals. FAO [cité le 3 février 2020]; [environ 90 écrans]. https://www.who.int/csr/resources/publications/Brucellosis.pdf

Zhang WY, Guo WD, Sun SH et al (2010) Human brucellosis, Inner Mongolia, China. Emerg Infect Dis 16:2001–2003

Zijlstra EE, van de Sande WW, Welsh O et al (2016) Mycetoma: a unique neglected tropical disease. Lancet Infect Dis 16:100–112

Zimmerli W (2010) Clinical practice. Vertebral osteomyelitis. N Engl J Med 362:1022–1029

Ziu M, Dengler B, Cordell D et al (2014) Neurosurg Focus 37:1–8

Zribi M, Ammari L, Masmoudi A et al (2009) Aspects cliniques, microbiologiques et thérapeutiques de la brucellose: étude de 45 cas. Pathol Biol 57:349–352

Pathophysiology of Spinal Infection

Nadia Hammami

Contents

Abstract

Although rare, spondylodiscitis is the main manifestation of hematogeneous osteomyelitis in patients aged more than 50 years. In this chapter, we discuss the pathophysiology of spinal infections. We review the vascular supply of the spine and its development with age, which is important in understanding the typical patterns of infection in adults and children. Routes of pathogen spread are detailed, with a review of the literature. We identify specificities of pathophysiology in the most common causes of spinal infection, namely, pyogenic and tuberculous spondylodiscitis.

N. Hammami (✉)
Department of Neuroradiology, National Institute of Neurology Mongi Ben Hamida, Tunis, Tunisia

Faculty of Medicine of Tunis, Tunis-El Manar University, Tunis, Tunisia
e-mail: nadiahamaied@hotmail.com

1 Introduction

Spinal infection is defined as an infectious disease that affects the vertebral body, intervertebral disk, or the adjacent paravertebral tissue. There are two main infection routes that can contribute to the development of spinal infection. Infectious spread may be hematogeneous or non-hematogeneous; the latter can be either the result of direct external inoculation or extension from a contiguous infection site (Gouliouris et al. 2010; Mavrogenis et al. 2017).

© The Author(s), under exclusive license to Springer Nature Switzerland AG 2021
M. F. Ladeb, W. C. G. Peh (eds.), *Imaging of Spinal Infection*,
Medical Radiology Diagnostic Imaging, https://doi.org/10.1007/978-3-030-70459-9_2

2 Routes of Pathogenic Spread

2.1 Hematogeneous Route

Two hematogenous routes have been described, namely, arterial and venous routes. Recent studies have concluded that hematogeneous arterial spread is the most common route, allowing bacteria from distant sites to contaminate the spine in the setting of bacteremia. The origin of infection in these patients may be the oral cavity, skin, any infected implanted device and the respiratory, urinary, or gastrointestinal tracts (Gouliouris et al. 2010; Sundaram and Doshi 2016; Mavrogenis et al. 2017). Rarely, the propagation of organisms can occur via the venous circulation (Moraru 2012). An understanding of the vascular supply of the spine and its development with age is important in understanding the typical patterns of infection within the spinal column in adults and children (Gouliouris et al. 2010; Sundaram and Doshi 2016).

The arterial supply to each vertebral body consists of paired segmental arteries that arise, depending on the location, from the vertebral arteries, aorta, or iliac arteries (Fig. 1). The segmental arteries run in the equatorial plane around their respective vertebral body, toward the transverse processes, and give off multiple extraosseous anastomotic channels (Sundaram and Doshi 2016). Ratcliffe (1980) demonstrated that on the anterolateral surface of the spine, there is a longitudinal ladder-like anastomosis of arteries in the periosteum. The horizontal components consist of the segmental arteries in the equatorial plane of the vertebra and two horizontal metaphyseal anastomoses, one at each metaphysis. The vertical components of the anastomosis consist of primary periosteal arteries, which join the segmental arteries to the metaphyseal anastomoses and transdiscal arteries, that travel in the adventitia of the disk and connect the metaphyseal anastomosis of one vertebral body to the metaphyseal anastomosis of the adjacent vertebral body (Ratcliffe 1980) (Fig. 2).

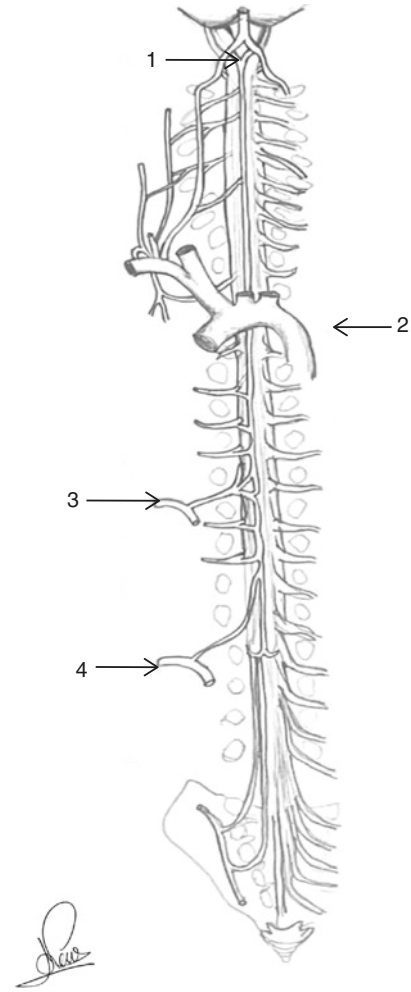

Fig. 1 Diagram shows arterial supply of the spine. Key: *1* vertebral artery, *2* aorta, *3* intercostal artery, *4* lumbar artery. [Adapted from: Kamina P (2008). Anatomie clinique; Tome 5 Neuroanatomie. 2008.197]

The intraosseous arteries arise from the periosteal arteries of this longitudinal anastomosis and its branches in the spinal canal. From each metaphyseal anastomosis, there arise 15–30 metaphyseal arteries which have long straight stems and terminate in a leash of centrifugal branches (Fig. 3). The stems of all these arteries lie more or less in a horizontal metaphyseal plane parallel to the disk surface (Ratcliffe 1980). In the equatorial zone, one or two anterolateral

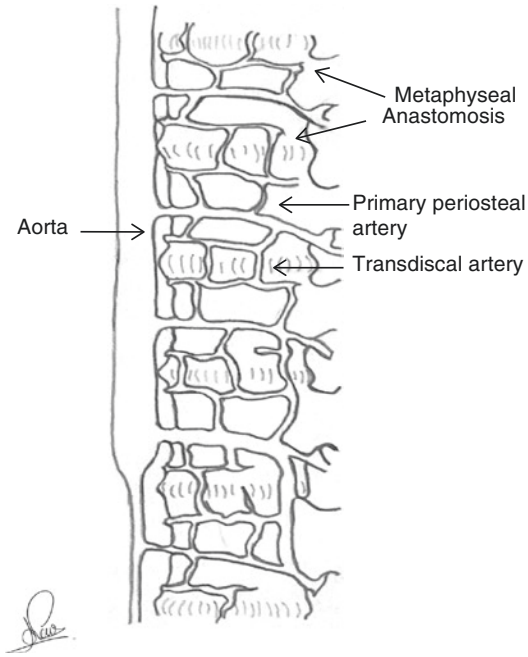

Fig. 2 Diagram shows the longitudinal anastomosis with horizontal and vertical components. [Adapted from: Ratcliffe JF (1985) Anatomic basis for the pathogenesis and radiologic features of vertebral osteomyelitis and its differentiation from childhood discitis. A microarteriographic investigation. Acta Radiologica Diagnosis 26: Fasc 2]

equatorial arteries on each side arise directly from the segmental artery; and on the posterior surface, the nutrient artery also lies in the equatorial plane and arises from the spinal branch of the segmental artery (Ratcliffe 1980) (Fig. 3).

In childhood, there is widespread intraosseous arterial anastomoses; this arterial network extends to the level of the intervertebral disk and provides a rich capillary network that is considered to be end vessels and are typically the final location for septic emboli. In adults, however, the rich capillary network regresses, and the arterial end vessels terminate at the superior and inferior end plates of the vertebral bodies, resulting in a different typical initial location for spinal infection compared to pediatric patients (Ratcliffe 1982; Sundaram and Doshi 2016). In adolescents and adults, the metaphyseal arteries are end arteries, and septic embolism forms a septic infarct of the subdiscal area of bone. The thrombus extends proximally in the metaphyseal artery to its origin from the metaphyseal anastomosis. The thrombus then extends circumferentially around the metaphyseal anastomosis and obstructs the origins of the other metaphyseal arteries sequentially (Ratcliffe 1980) (Fig. 4).

The area of vertebral metaphysis supplied by each artery will undergo sequential septic infarction. The thrombotic process can thus spread around the metaphysis of the same vertebral body. The spreading septic thrombosis in small arteries may cross the disk space in the adventitial arteries to involve the metaphyseal anastomosis of the adjacent vertebral body. Transdiscal metaphyseal spread is characteristic of vertebral osteomyelitis in adults. The equatorial region is supplied by arteries which arise from the main segmental artery in which there is a sufficiently fast flow of blood to wash away septic thrombus. The equatorial region of the vertebral body is thus relatively protected (Ratcliffe 1980) (Fig. 5).

Extensive vascular bone infarcts and spread of infection to adjacent structures lead to the classic appearance of spondylodiscitis on imaging, namely, destruction of vertebral end plates, osteolytic lesions, and compression fractures, which can lead to spine instability, deformity, and risk of spinal cord compression (Cheung and Luk 2012; Duarte and Vaccaro 2013). Neurological deficit during pyogenic osteomyelitis may have several mechanisms which can be isolated or associated: epidural abscess with narrowing of the spinal canal, septic embolization of the vertebral artery with spinal cord ischemia, and septic vertebral fracture with mechanical compression (Lemaignen et al. 2017). On the other hand, tuberculous osteomyelitis may cause a vasculitis that leads to ischemia in the spinal cord and that even with decompression, neurological recovery may not be as significant as expected (Finger et al. 2019). In childhood, a septic embolus in a metaphyseal artery will cause the death of cells in only a very small area of bone because the

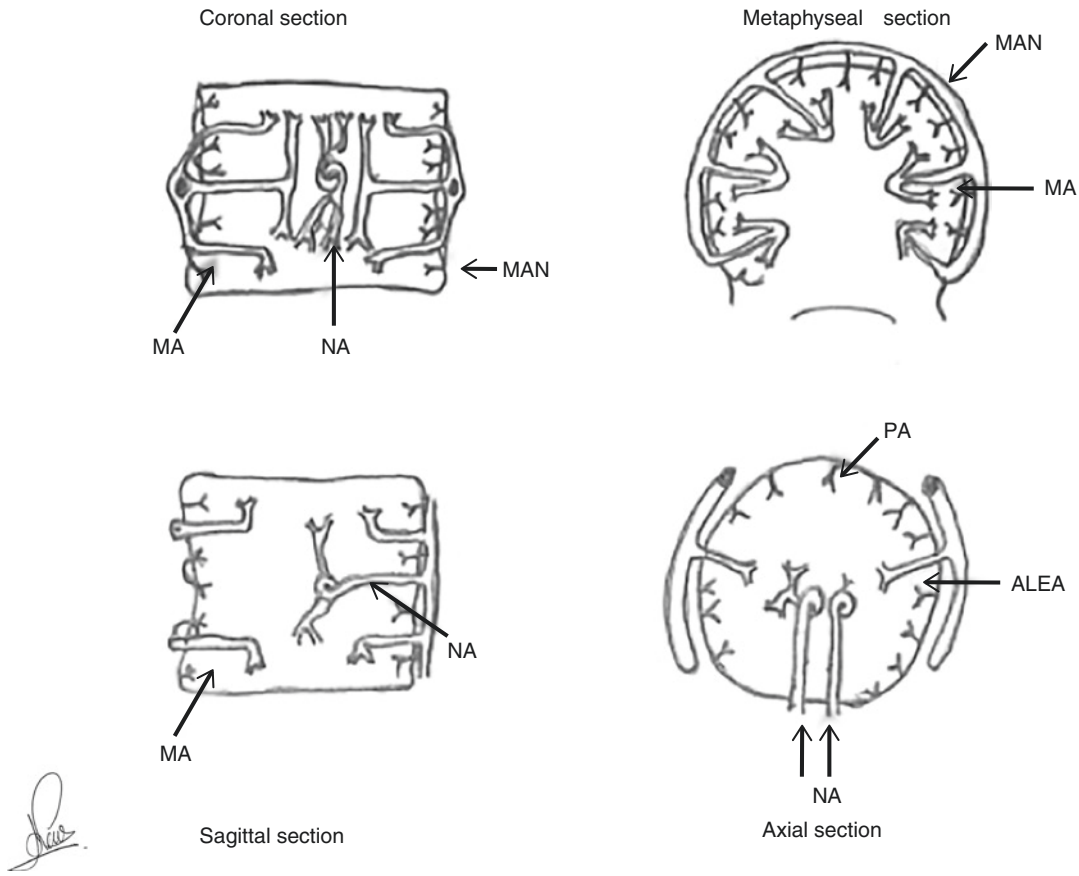

Fig. 3 Diagram shows the intra-osseous arteries of the adult lumbar vertebral body. Key: *ALEA* anterolateral equatorial artery, *LA* lumbar artery, *MA* metaphyseal artery, *MAN* metaphyseal anastomosis, *NA* nutrient artery, *PA* periosteal artery, *PPA* primary periosteal artery. [Adapted from: Ratcliffe JF (1980) The arterial anatomy of the adult human lumbar vertebral body: a microarteriographic study. J Anat 131:57–79]

Fig. 4 Schematic diagram shows the mode of spread of septic thrombosis. The thrombus (brown dot) extends circumferentially around the metaphyseal anastomosis (arrows) and obstructs the origins of the other metaphyseal arteries (crosses)

intraosseous anastomoses prevent infarction and the infection is located essentially within the disk. The clinical disease is mild and radiographic changes are often minimal in juveniles (including infants and small children) compared with adults (Ratcliffe 1980).

The venous route in the pathogenesis of spondylodiscitis has often been considered a common route, with retrograde spread of infection from abdominal and pelvic organs, such as in urinary tract infection. Batson (1940) discovered that the vertebral veins are a large-capacity longitudinal valveless venous plexus that lies outside the thoracoabdominal cavity and anastomoses with the pelvic venous plexus caudally, and postulated its role in the spread of metastases. He concluded that, when intra-abdominal pressure rises as a

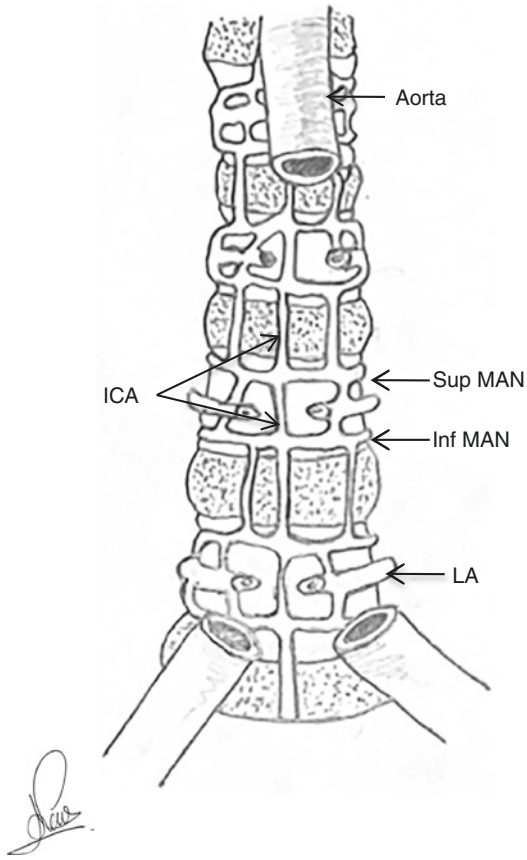

Fig. 5 Diagram shows the spread of septic thrombosis from one metaphysis to the other in a single vertebral body and in the adjacent vertebral metaphysis via intermetaphyseal communicating arteries without destruction of the equator of the vertebral body. Key: *ICA* intermetaphyseal communicating artery, *inf* inferior, *LA* lumbar artery, *MAN* metaphyseal anastomosis, *sup* superior. [Adapted from: Ratcliffe JF (1985) Anatomic basis for the pathogenesis and radiologic features of vertebral osteomyelitis and its differentiation from childhood discitis. A microarteriographic investigation. Acta Radiologica Diagnosis 26: Fasc 2]

result of coughing or straining, pelvic infection could spread via the vertebral collateral venous system to cause spinal lesions (Gouliouris et al. 2011; Sundaram and Doshi 2016).

However, since 1959, Wiley and Trueta, using anatomical contrast studies to demonstrate that the veins of the vertebral bodies could only be filled retrogradely utilizing high pressures, postulated that the vertebral veins form predominantly a drainage system. Furthermore, the radiological findings in cases of spondylodiscitis displayed the characteristic anterior metaphyseal vertebral lesions, which are rich in arterial but not venous supply (Wiley and Trueta 1959; Gouliouris et al. 2011). The involvement of adjacent vertebrae is also suggestive of arterial spread, in view of the bifurcation of the feeding arteries. Finally, in clinical cases of spondylodiscitis arising from a pelvic source, preceding symptoms of bacteremia such as fever and rigors are commonly documented, suggesting systemic spread (Gouliouris et al. 2011).

2.2 Non-hematogeneous Route

Direct bacterial inoculation is mainly iatrogenic, following spinal surgery, lumbar puncture, or epidural procedures. This infectious route accounts for 14–26% of spinal infections (Mavrogenis et al. 2017). Multiple factors increase the rates of infection following spinal surgery. These include the staging of surgery (multiple sequential operations), long operative time (>5 h), blood transfusions, use of allograft, and a greater number of operated levels. A higher infection rate is also related to the introduction of posterior spinal instrumentation and is mainly attributed to increased wound exposure to air and greater posterior soft tissue dissection (Kasliwal et al. 2013).

The risk of infection varies with the type of implant, due to an increased susceptibility to the development of biofilm which is a microbial agglomeration characterized by cells that are embedded in a matrix of extracellular polymeric substances, which they produce (Kasliwal et al. 2013). Within biofilm, bacterial cells become irreversibly attached to the implant. Implants vary in their susceptibility to the development of biofilm. Soultanis et al. (2008) found that titanium had a lower infection rate than stainless steel. Contiguous spread is extremely rare. Infection in these cases may spread from adjacent infected tissues such as a ruptured esophagus or an infected aortic graft (Gouliouris et al. 2010; Mavrogenis et al. 2017).

3 Pyogenic Spondylodiscitis

Based on the typical adult arterial anatomy, hematogeneous pyogenic spondylodiscitis often first affects the subchondral region of the vertebral body end plates and spreads in an anterior to posterior direction. Over time, bacteria with more virulent and proteolytic properties, such as *Staphylococcus aureus*, cause cortical destruction and invade beyond the end plates and into the intervertebral disks. They can also spread along the arterial anastomotic networks to multiple, sometimes noncontiguous, vertebral bodies, or into the epidural space (Sundaram and Doshi 2016). Pyogenic facet involvement also exists as an independent entity but is extremely rare (Hadjipavlou 2000). The pathogenesis of this posterior involvement can be explained either as a primary hematogeneous osteomyelitis with extension into the facet joint or as a primary paravertebral soft tissue infection with direct spread into the facet joint and subsequent osteomyelitis (Ehara et al. 1989).

4 Tuberculous Spondylodiscitis

The pathophysiology of tuberculous spondylodiscitis still remains a subject of controversy. Tuberculous osteomyelitis and arthritis are generally believed to arise from foci of bacilli lodged in the bone during the original mycobacteremia of primary infection (Agrawal et al. 2010). The primary focus may be active or quiescent, apparent or latent, either in the lungs or in the lymph glands of the mediastinum, mesentery, kidney, or other viscera (Agrawal et al. 2010). Tuberculous bacilli may travel from the lung to the spine by Batson paravertebral venous plexus or by lymphatic drainage to the para-aortic lymph nodes (Agrawal et al. 2010). However, according to Trecarichi et al. (2012), tuberculous spondylodiscitis can result from arterial hematogeneous seeding of *Mycobacterium tuberculosis* starting from a quiescent or active pulmonary focus or can be due to contiguous or lymphatic spread from pleural disease (Trecarichi et al. 2012). The predominant localization of tuberculosis in the thoracic segment would be related to the frequent involvement of mediastinal lymph nodes and the pleura in pulmonary tuberculosis, from where microorganisms can reach the vertebral bone through the lymphatic route (Trecarichi et al. 2012).

Since the intervertebral disk does not have a direct blood supply in adults, most hematogeneous infections of the disk space are the result of the dissemination from the adjacent bone. The natural evolution of the infection is the formation of a granuloma, whose center tends to caseate and become necrotic. The infection can then progress to destroy the bone, causing pain and leading to the collapse of the vertebral body (Trecarichi et al. 2012). The bacilli may then spread beneath the anterior spinal ligament and involve the anterosuperior aspect of the adjacent inferior vertebra, giving rise to the typical "wedge-shaped" deformity. Further spread may result in adjacent abscesses. The infection may spread cranially and caudally, stripping the anterior and posterior longitudinal ligaments and the periosteum from the front and the sides of the vertebral bodies (Agrawal et al. 2010). Disk space narrowing occurs secondarily and usually is limited relative to the degree of bone destruction. A lack of proteolytic enzymes in the mycobacterium as compared with pyogenic infection has been proposed as the cause of relative preservation of the intervertebral disk (Smith et al. 1989).

5 Conclusion

Hematogeneous arterial spread is the most common route of spinal infection. In childhood, discitis is common due to the intra-osseous arterial anastomoses extending to the level of the intervertebral disk. In adults, as the disk is avascular, the infection is located initially at the superior or the inferior end plate of the vertebral body, and then extensive vascular bone infarcts and spread of infection to adjacent structures leads to the classic spondylodiscitis. Iatrogenic direct bacterial inoculation has increased in frequency

because spinal instrumentation became an integral component in the treatment of multiple spinal pathologies. The understanding of the pathogenesis of this pathology has evolved with the improved knowledge of the role of biofilm and the development of newer spinal implants.

References

Agrawal V, Patgaonkar R, Nagariya SP (2010) Tuberculosis of spine. J Craniovertebr Junction Spine 1:74–85

Batson OV (1940) The function of the vertebral veins and their role in the spread of metastasis. Ann Surg 112:138–149

Cheung WY, Luk KDK (2012) Pyogenic spondylitis. Int Orthop 36:397–404

Duarte RM, Vaccaro AR (2013) Spinal infection: state of the art and management algorithm. Eur Spine J 22:2787–2799

Ehara S, Khurana JS, Kattapuram SV (1989) Pyogenic vertebral osteomyelitis of the posterior elements. Skeletal Radiol 18:175–178

Finger G, Lima Cecchini AM, Sreddo E et al (2019) Spondylodiscitis investigation and therapeutic protocol: neurosurgery service results. Coluna/Columna 18:138–143

Gouliouris T, Aliyu SH, Brown NM (2010) Spondylodiscitis: update on diagnosis and management. J Antimicrob Chemother 65:11–24

Gouliouris T, Aliyu SH, Brown NM (2011) Spondylodiscitis: update on diagnosis and management—authors' responses. J Antimicrob Chemother 66:1200–1202

Hadjipavlou AG (2000) Hematogenous pyogenic spinal infections and their surgical management. Spine 25:1668–1679

Kasliwal MK, Tan LA, Traynelis VC (2013) Infection with spinal instrumentation: review of pathogenesis, diagnosis, prevention, and management. Surg Neurol Int 4(Suppl 5):S392–S403

Lemaignen A, Ghout I, Dinh A et al (2017) Characteristics of and risk factors for severe neurological deficit in patients with pyogenic vertebral osteomyelitis: a case–control study. Medicine (Baltimore) 96:e6387

Mavrogenis AF, Megaloikonomos PD, Igoumenou VG et al (2017) Spondylodiscitis revisited. EFFORT Open Rev 2:447–461

Moraru I (2012) Neurological point of view. Bacterial spondylodiscitis: diagnostic challenges and therapeutic strategies. Rom Neurosurg 19:299–308

Ratcliffe JF (1980) The arterial anatomy of the adult human lumbar vertebral body: a microarteriographic study. J Anat 131:57–79

Ratcliffe JF (1982) An evaluation of the intra-osseous arterial anastomoses in the human vertebral body at different ages. A microarteriographic study. J Anat 134:373–382

Smith AS, Weinstein MA, Mizushima A et al (1989) MR imaging characteristics of tuberculous spondylitis vs vertebral osteomyelitis. AJR Am J Roentgenol 153:399–405

Soultanis KC, Pyrovolou N, Zahos KA et al (2008) Late postoperative infection following spinal instrumentation: stainless steel versus titanium implants. J Surg Orthop Adv 17:193–109

Sundaram VK, Doshi A (2016) Infections of the spine: a review of clinical and imaging findings. Appl Radiol 45:10–20

Trecarichi EM, Di Meco E, Mazzotta V, Fantoni M (2012) Tuberculous spondylodiscitis: epidemiology, clinical features, treatment, and outcome. Eur Rev Med Pharmacol Sci 16(Suppl 2):58–72

Wiley AM, Trueta J (1959) The vascular anatomy of the spine and its relationship to pyogenic vertebral osteomyelitis. J Bone Joint Surg Br 41:796–809

Radiography and Computed Tomography of Spinal Infection

Sravanthi Mantripragada, Niraj Dubey, and Wilfred C. G. Peh

Contents

Abstract

As clinical features of spinal infection are usually nonspecific, imaging has a major role in facilitating prompt diagnosis. It is also an essential investigative tool to help avoid delayed or improper treatment that may result in increased morbidity and mortality. This chapter reviews the role of radiographs and computed tomography (CT) in the investigation and management of spinal infection by outlining the techniques, key imaging features, and the advantages and limitations of these two modalities. Radiographs remain the preliminary screening imaging investigation, and the radiologist must not forget to assess the spine radiograph prior to magnetic resonance imaging (MRI). Although CT is not the primary investigation, its strength lies in its ability to depict fine bony details and its role in guiding percutaneous biopsy.

S. Mantripragada (✉) · N. Dubey · W. C. G. Peh
Department of Diagnostic Radiology, Khoo Teck Puat Hospital, Singapore, Republic of Singapore
e-mail: sravanti.mantripragada@gmail.com; dubey.niraj@ktph.com.sg; Wilfred.peh@gmail.com.sg

© The Author(s), under exclusive license to Springer Nature Switzerland AG 2021, corrected publication 2021

M. F. Ladeb, W. C. G. Peh (eds.), *Imaging of Spinal Infection*,
Medical Radiology Diagnostic Imaging, https://doi.org/10.1007/978-3-030-70459-9_3

Abbreviations

AP Anteroposterior
CT Computed tomography
MRI Magnetic resonance imaging

1 Introduction

Manifestations of spinal infection include spondylitis, discitis, spondylodiscitis, facet joint infective arthropathy, epidural infection, meningitis, polyradiculopathy, and myelitis (Tali and Gültekin 2005). The spine is affected in 2–7% of skeletal infections and can broadly be divided into pyogenic, granulomatous, fungal, parasitic, and iatrogenic causes (Tyrrell et al. 1999; Hong et al. 2009; Cheung and Luk 2012). The clinical features of spinal infection are nonspecific, subtle, and often misleading; hence they are frequently a diagnostic challenge. Imaging of the spine facilitates prompt diagnosis and is an essential investigative tool to help avoid delayed or improper treatment that may result in increased morbidity and mortality (Tali and Gültekin 2005; Diehn 2012). This chapter reviews the role of radiographs and computed tomography (CT) in the investigation and management of spinal infection. We aim to outline the techniques and imaging features and discuss the advantages and limitations of radiographs and CT. Armed with the clinical information of each individual patient and knowing the roles of radiographs, CT, and other modalities such as magnetic resonance imaging (MRI) and nuclear medicine imaging (the latter two to be discussed in subsequent chapters), radiologists should be able to offer early and relevant guidance in the imaging workup of patients with suspected spinal infection.

2 Overview of Spinal Infection

It is essential to know about the various types of spinal infection and their pathophysiology, in order to be able to optimally interpret imaging findings on radiographs and CT. The most common route for the spread of spinal infection is hematogeneous from a distant septic focus. *Staphylococcus aureus* is the most common infective organism. Granulomatous infections include *Mycobacterium tuberculosis*, *Brucella*, fungi, and parasites (Hong et al. 2009). Pyogenic bacterial infection commonly affects the lumbar spine, followed by the thoracic and cervical spine. The most widely accepted pathophysiologic mechanism is that an infected embolus causes septic infarction, typically in the anterior metaphysis of the vertebral body. This subsequently spreads to the rest of the vertebral body, end plate, and the adjacent avascular disk. Contiguous spread may occur into the paraspinal and/or epidural spaces. Overall, pyogenic infections are characterized by the early loss of disk height (due to disk destruction by proteolytic enzymes produced by pyogenic bacteria), preserved vertebral height, increased healing responses in the form of sclerosis and bony ankylosis, paucity of posterior spinal involvement, and smaller paraspinal abscesses. Multilevel spinal involvement and skip lesions are uncommon (Tali and Gültekin 2005; Hong et al. 2009; Diehn 2012).

Tuberculous involvement of the spine favors the thoracolumbar junction. Spinal tuberculosis also begins in the anterior vertebral body and typically spreads in a sub-ligamentous fashion, deep to the anterior longitudinal ligament, and traverses multiple vertebral levels. *Mycobacterium tuberculosis* lacks proteolytic enzymes to lyse the disk and typically spares the disk till late. There is an increased incidence of vertebral body destruction and collapse. Paravertebral soft tissue abscesses are larger and more common. There is paucity of bony sclerosis and increased spinal deformity/kyphoscoliosis in the chronic healed stage (Tali and Gültekin 2005; Diehn 2012). Fungal spondylodiscitis typically involves the lumbar spine, resembles tuberculous infection, and should be suspected in the presence of background immunosuppression (Hong et al. 2009; Diehn 2012). Brucellar spondylitis is due to a gram-negative bacillus causing granulomatous infection in the lower lumbar levels. The anterosuperior vertebral body and disk are the initial foci of infection, with preservation of the height of the involved

vertebra. Simultaneous bony healing at the site of infection is a unique feature of this disease (Tali and Gültekin 2005).

Details of the pathophysiology and imaging features of the various etiologic types of spinal infection (such as pyogenic, brucellosis, salmonellosis, tuberculosis, hydatidosis, fungal and iatrogenic) will be addressed in subsequent individual chapters of this book. In general, the roles of imaging in spinal infections (Sans et al. 2012) are:

- Early diagnosis at the affected area, as well as the spread of the disease into the vertebra, disk, and adjacent soft tissues
- To characterize specific infections (e.g., pyogenic, tuberculous), identify the infective agent, and guide percutaneous interventions
- Early detection of complications (e.g., neurological compromise, abscesses) that could benefit from surgical or percutaneous interventions

The roles of radiographs and CT will be discussed in this chapter.

3 Role of Radiographs

3.1 Views and Techniques

Radiographic assessment typically consists of standard anteroposterior (AP) and lateral views of the painful segment of the spine (Sans et al. 2012) (Fig. 1). In the lumbar spine, these

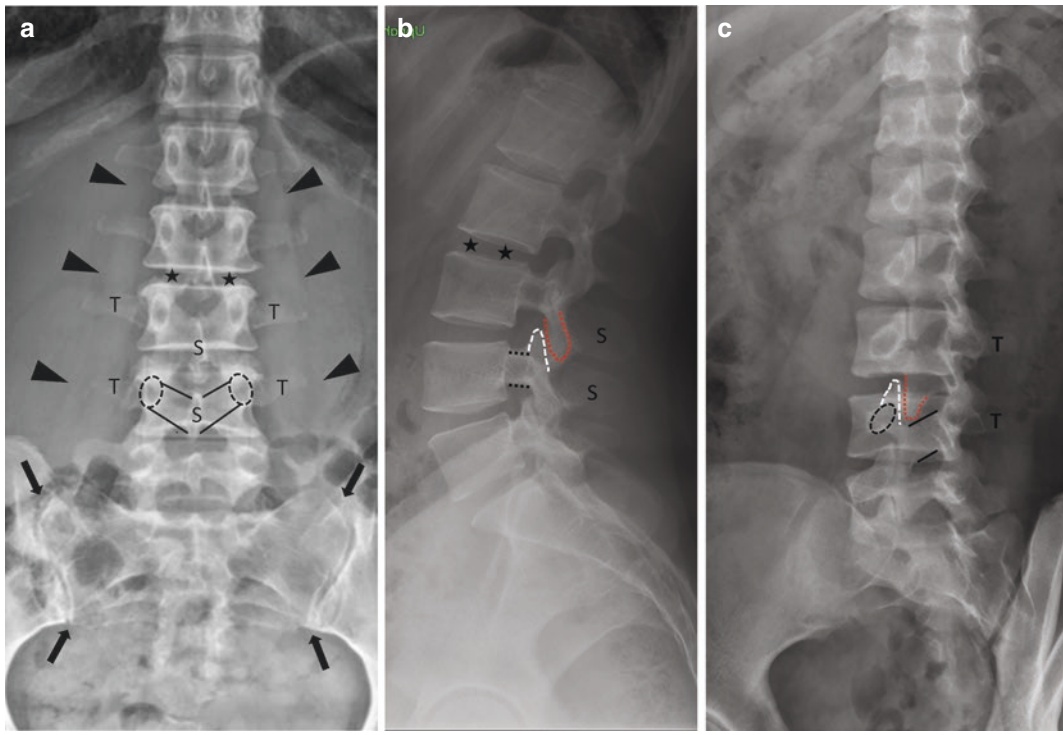

Fig. 1 (**a**) Anteroposterior (AP), (**b**) lateral, and (**c**) oblique radiographs of the lumbar spine show key normal anatomical structures. Note the well-delineated bilaterally symmetrical outline of the lateral psoas muscle margins on the AP radiograph (black arrowheads). The vertebral bodies, their cortical end plates, and the intervertebral disk spaces (black asterisks show L2/3 disk space) are well seen. The L4 superior articular process (outlined in dotted white line) and L3 inferior articular process (outlined in dotted red line) and the intervening L3/4 facet joint are best seen on lateral and oblique views. The pedicles can be seen on all 3 views (L4 pedicle outlined in black dotted circles/lines). The transverse processes (T) are best seen on the AP view and the spinous processes (S) on the lateral view. The L4 laminae are outlined in solid black lines in the AP and oblique views. The sacroiliac joints are well seen on the AP view (black arrows)

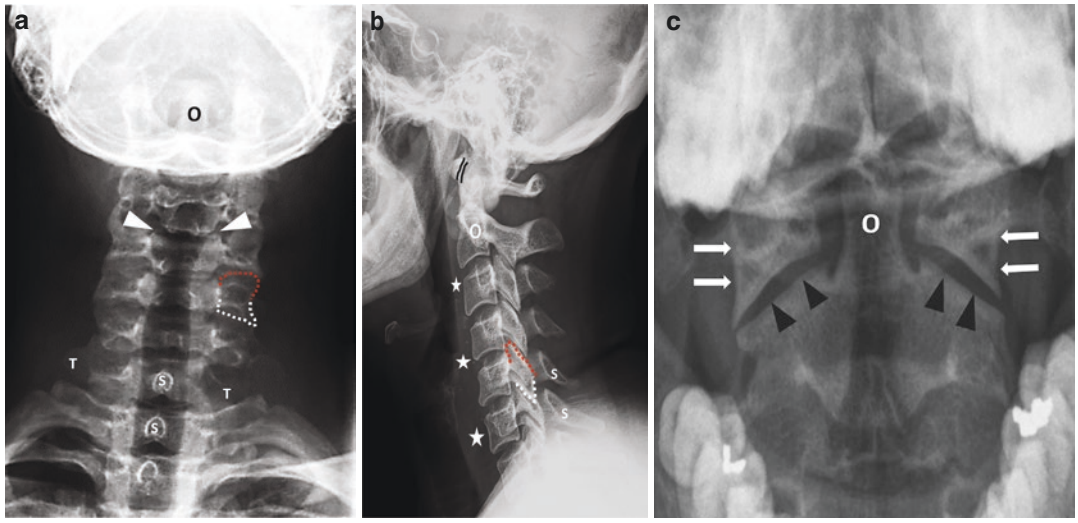

Fig. 2 (**a**) AP, (**b**) lateral, and (**c**) open-mouth radiographs of the normal cervical spine show key normal anatomical structures. Uncovertebral joints unique to the cervical spine (white arrowheads) and transverse processes (T) are best seen on the AP view. The C2 odontoid peg (O), C5 superior articular process (outlined in red dotted line), and C5 inferior articular process (outlined in white dotted line) are shown on AP and lateral views. The cortical end plates of the cervical vertebral bodies, intervertebral disk spaces, prevertebral soft tissue (white asterisks), spinous processes (S), and the anterior C1/C2 articulation (between black lines) are best evaluated on the lateral view. The lateral masses of C1 vertebra (white arrows), the odontoid process (O), and the body of the C2 vertebra, together with the intervening lateral atlanto-axial joints (black arrowheads) are best evaluated on the open-mouth view

standard views should be taken in expiration (to minimize superimposition of the diaphragm over the upper lumbar vertebrae) with the centering point at L3 vertebral level for the AP view and at the iliac crest level for the lateral view. Ideal exposure factors are 70–80 kVp and 60–80 mAs. Additional coned, oblique, and flexion/extension views can be useful for a clearer delineation of the L5/S1 junction, facet joint destruction, and instability, respectively (Fig. 1). Standard AP and lateral projections of the thoracic spine require a higher exposure (80 kVp or more), are obtained at the end of inspiration (to minimize diaphragmatic overlap), and cover the spine from C7 to L1 vertebral levels. The overlapping mediastinal soft tissue structures require a higher kVp to optimize visualization of the thoracic spine and paraspinal soft tissues.

In the cervical spine, AP (covering C3 to C7/T1 levels) and lateral (covering occiput to C7/T1 levels) projections and open-mouth views of the C1/C2 junction are useful preliminary radiographs (Fig. 2). The anterior atlanto-axial articulation is best seen on the lateral view and the lateral atlanto-axial articulations on the open-mouth views (Alsop 2005). The cervical spine swimmer lateral radiograph is a modified coned lateral projection of the cervical spine for visualizing the C7/T1 junction. CT has largely replaced this projection, but in many centers located in rural areas where CT is not readily available, this special radiograph still has a role.

3.2 Radiographic Findings in Spinal Infection

The initial radiographs may be completely normal, with radiographic findings typically lagging 2–3 weeks behind clinical symptoms. Hence, a normal radiograph does not exclude the presence of infection (Fig. 3a). Radiographic signs are usually seen earlier in nontuberculous compared to tuberculous spondylodiscitis, typically manifesting only after more than 35–40% bony destruction. It is recommended to view digital

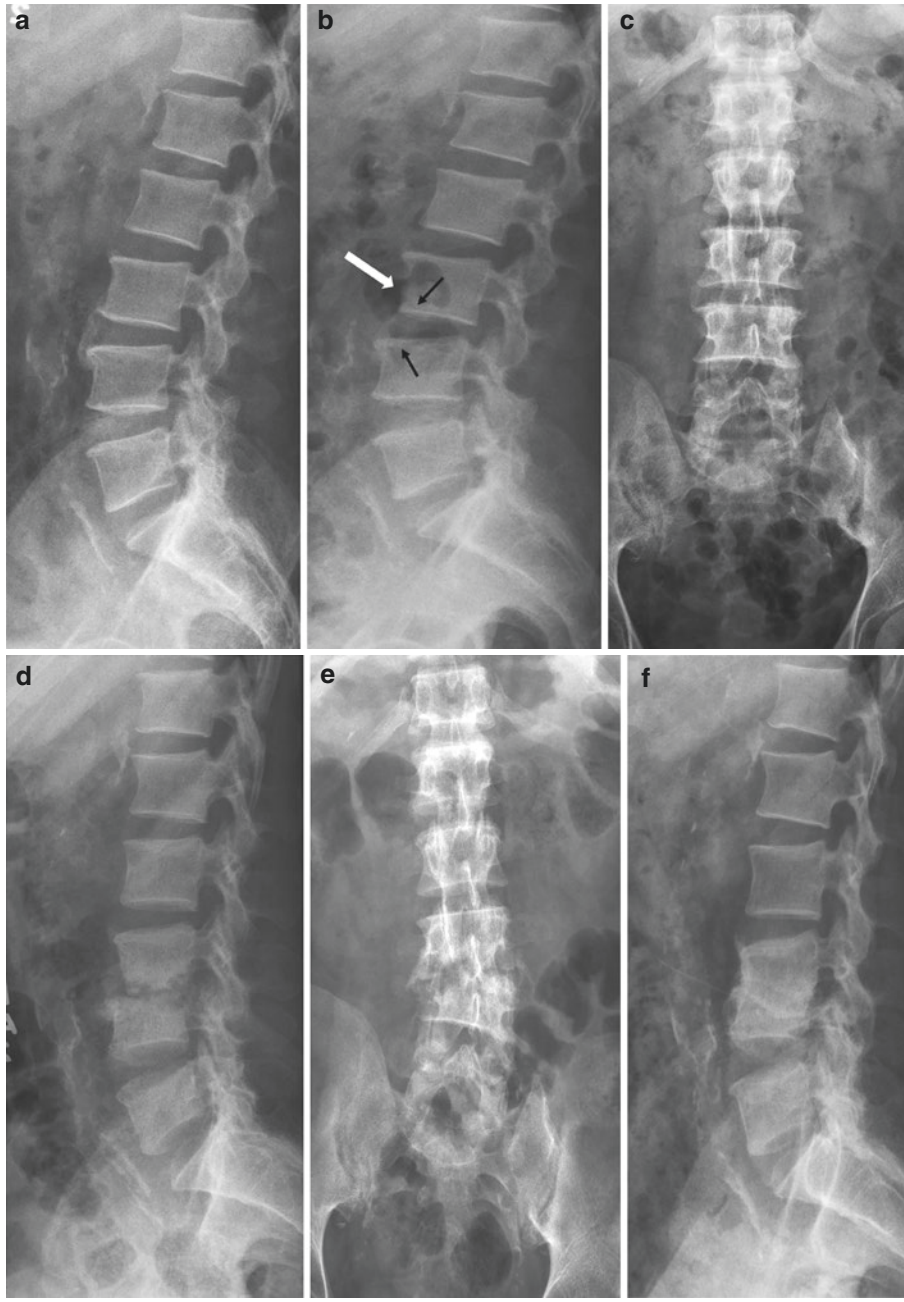

Fig. 3 Sequential lumbar spine radiographic changes in a 45-year-old man presenting with low back pain. (**a**) Initial lateral radiograph shows mild degenerative spondylosis with no apparent bone destruction. (**b**) Lateral and (**c**) AP radiographs taken 1 month later show indistinct cortices and subtle blurring of the adjacent end plates of L3 and L4 vertebral bodies (thin black arrows), partial cortical destruction at the anterior and anteroinferior aspect of L3 vertebral body (white arrow), mild disk space reduction, and mild retrolisthesis of L3 over L4 vertebral bodies. At this stage, MRI of the lumbar spine (not shown) confirmed infective spondylodiscitis and cultures revealed *E. coli* sepsis. (**d**) Lateral and (**e**) AP radiographs taken 4 months later show contiguous L3/4 vertebral end plate and disk destruction with mild kyphoscoliosis. (**f**) Lateral radiograph taken at 6 months shows healing evident in the form of L3/4 bony sclerosis and ankylosis with obliteration of the disk space. The sclerosed end plates and bony ankylosis are signs of ongoing healing, especially with pyogenic infections

radiographs in both bone and soft tissue windows, to achieve greater detection accuracy and hence avoid diagnostic delay (Stäbler and Reiser 2001; Diehn 2012; Sans et al. 2012).

Radiographs are used mainly to screen for abnormalities at the vertebral end plates, intervening disks, and the adjacent soft tissue planes. The earliest radiographic sign is a loss of definition/blurring and irregularity of the anterosuperior vertebral end plate; usually detected at 2–8 weeks after infection onset (Fig. 3b, c). Sequential changes are initial disk space increase (evident only rarely), followed by a decrease of the disk height. Gradually increasing osteolysis causes full-fledged end-plate erosions and vertebral body medullary bone destruction. Cortical end-plate erosions of two contiguous vertebrae with reduction of the intervening disk space and associated paraspinal soft tissue prominence are the hallmarks of pyogenic infection. The reduction of the intervening disk space typically progresses quickly, usually less than a month, in pyogenic infections (Varma et al. 2001; Tali and Gültekin 2005; Diehn 2012; Sans et al. 2012; Lee 2014) (Fig. 3d, e).

Paraspinal soft tissue extension of the infection frequently affects the psoas muscle in the lumbar region and the posterior mediastinum in the thoracic region. These changes are more difficult to visualize on radiographs in the lumbar region, albeit the earliest soft tissue changes include blurring of the edge of the psoas muscle with effacement of its normal fat plane and a convex paraspinal soft tissue bulge. In the thoracic spine, soft tissue changes/abscesses are usually seen as fusiform soft tissue bulges on AP radiographs (Fig. 4). Tracheal and pharyngoesophageal displacement and narrowing by prevertebral cervical or posterior mediastinal abscesses are better seen on lateral views of the cervical and AP views of the thoracic spine (Varma et al. 2001; Tali and Gültekin 2005;

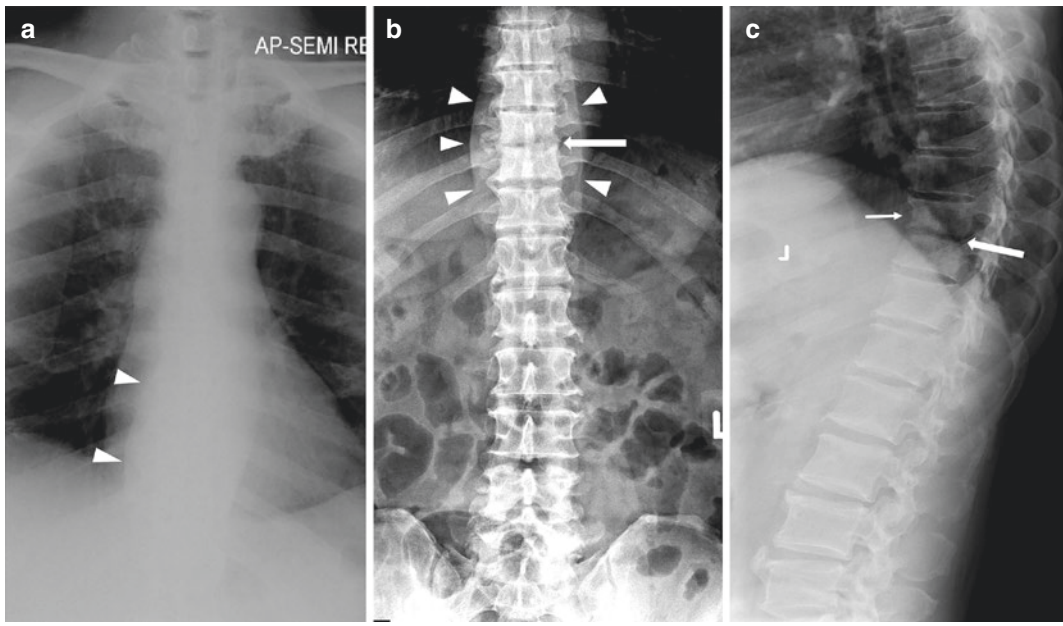

Fig. 4 (**a**) Frontal chest, and (**b**) AP, and (**c**) lateral thoracic spine radiographs of a 50-year-old man with tuberculous spondylodiscitis show the classic radiographic findings of spondylodiscitis at T9/T10 level. There is abnormal paraspinal soft tissue widening on AP view of the thoracic spine (arrowheads), subtly appreciable on the chest radiograph. Both AP and lateral views of the thoracic spine show partial cortical destruction at the T9/T10 vertebral body end plates, evident in the form of blurring and irregularity, and reduction of the intervening T9/10 disk height (large thick arrows). Lateral view of the spine also shows mild anterior scalloping due to cortical destruction of the T9 vertebral body (small thin arrow) which was confirmed on MRI as abnormal subligamentous phlegmonous soft tissue

Diehn 2012; Sans et al. 2012; Lee 2014). The imaging hallmarks and differentiating features among spinal infections caused by various causative microorganisms are discussed in subsequent chapters.

In the chronic stages of spinal infection, there are usually general signs of bony healing and remodeling. The degree of spinal deformity depends on the amount of disk and vertebral body destruction. Radiographic findings comprise reactive bony sclerosis, osteophytosis, and vertebral body ankylosis with a fusion of the disk space (Fig. 3e). Progressive kyphoscoliosis may be the eventual result of a chronic infection of 4–6 months of duration (Fig. 3). At this burnt-out stage, it may be difficult on radiographs to differentiate among chronic infection, degenerative changes (primary or secondary which may be sequelae of healed infection/trauma), and congenital segmentation anomalies. A feature strongly in favor of previous tuberculous infection is calcification of large soft tissue abscesses in the lumbar and thoracic paraspinal soft tissues (Moore and Rafii 2001; Varma et al. 2001; Tali and Gültekin 2005; Acharya and Gibbs 2016). Radiographs are frequently used to follow-up and monitor spinal deformities, including the stability of kyphoscoliosis, vertebral collapse, and spinal canal compromise due to posterior vertebral retropulsion and gibbus deformity (Sans et al. 2012).

3.3 Advantages of Radiographs

Radiographs remain the primary and preliminary imaging investigation in musculoskeletal back pain. The advantages of radiographs and their significance in imaging of spinal infection (Peh 2002) are:

1. Easy availability and cost-efficiency make radiographs the primary investigation, especially in healthcare centers with limited resources.
2. Quick global screening tool for assessment of the entire spine with less radiation exposure compared to CT.
3. Whenever visible, identification and localization of the lesion(s) in infective spondylodiscitis serve as a guide for further imaging with CT or MRI.
4. Good screening modality to assess multifocal skip lesions, anterior vertebral body defects, and gibbus deformity in tuberculosis.
5. If visible, an initial clue to paraspinal soft tissue abscesses may be provided by radiographs, e.g., obliteration of psoas margin, mediastinal fusiform paraspinal soft tissue bulge, prevertebral soft tissue thickening at the cervical spinal region, and mass effect on the trachea and the esophagus. The extensive calcification of tuberculous psoas abscesses makes them easily visible on radiographs.
6. Simple initial investigation for follow-up of chronic healed infections for assessment and monitoring of the degree of kyphoscoliosis and vertebral body height in cases of partial collapse.
7. Easy screening tool for postoperative follow-up and assessment of any surgical spinal fixation devices for stabilizing the partially destroyed spinal segments (Fig. 5).
8. Current state-of-the-art digital radiography allows contrast/window adjustments for assessment of soft tissues and bones, without the need for multiple exposures.

3.4 Disadvantages and Pitfalls of Radiographs

Radiographs generally lack the ability to show the early findings of spinal infection (Figs. 6 and 7). They may be normal in a majority of the cases, and this should not prevent further investigation with advanced modalities such as CT and MRI, if there is strong clinical suspicion. Pitfalls of conventional radiographs in the context of spinal infection (Tali and Gültekin 2005; Sans et al. 2012; Low and Peh 2017) are:

1. Inherent limitations of radiographs. Early erosive changes at the discovertebral junction are appreciable only late in the course of the disease (after 2–8 weeks in pyogenic infection,

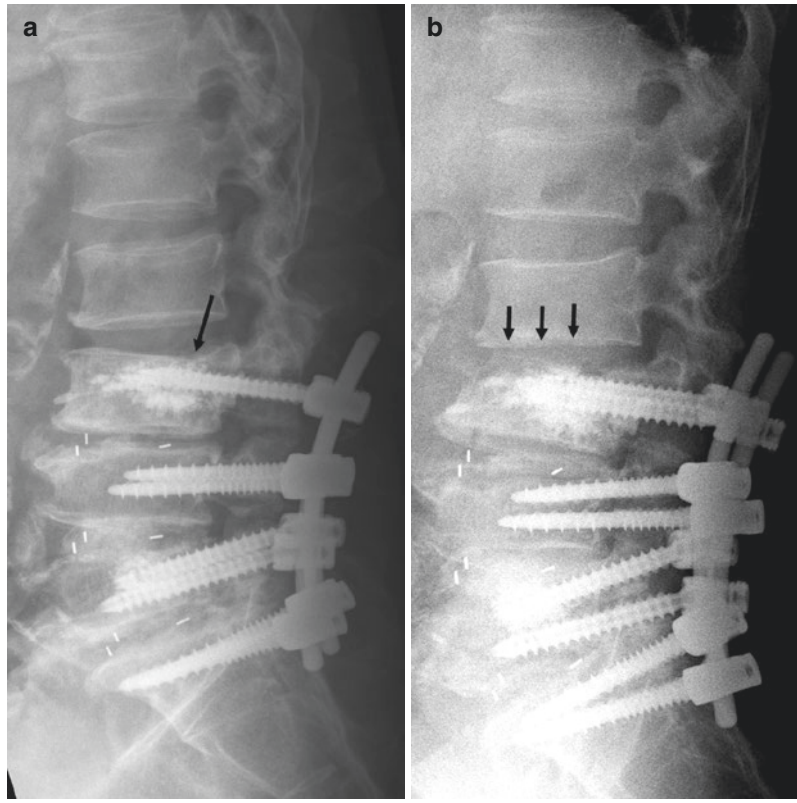

Fig. 5 A 56-year-old man presenting with back pain and previous operative history of posterior spinal fixation. (**a**) Lateral lumbar spine radiograph shows well-aligned transpedicular prosthesis and mild superior end-plate collapse of the L3 vertebral body (black arrow). (**b**) Follow-up radiograph performed 1 month later, done because of persistent and increased back pain, shows interval collapse of L3 vertebral body with destruction of the superior end plate and blurring of the inferior L2 vertebral body end plate (small arrows). CT performed a day later confirmed partial destruction of L3 vertebral body and early osteolysis of the inferior L2 vertebral end plate. The spinal prosthesis was eventually removed, and the patient was treated for the L2/3 pyogenic spondylodiscitis. Radiographs are especially useful in imaging of the postoperative spine and spinal devices. MRI may be suboptimal due to extensive susceptibility artifacts obscuring the adjacent bony details

and sometimes as late as 6 months in tuberculosis). This causes a false sense of security and allows further temporal bony destruction due to delay in diagnosis (Fig. 3).

2. Intrinsically poor soft tissue contrast, making it difficult or impossible to depict any direct evidence of discitis and ligamentous abnormalities.
3. Unreliable modality for identifying early paraspinal soft tissue abnormalities such as small psoas abscesses and mild mediastinal infection.
4. Spinal canal and cord abnormalities responsible for neurological compression in spinal infections (such as epidural abscess, leptomeningitis, intrinsic cord swelling) are undetectable on radiographs (Fig. 7).
5. Poor depiction of posterior element involvement such as facet joint, and transverse and spinous process lesions.

An outline of the normal radiological findings in the spine with emphasis on specific findings in the clinical context of spinal infection is

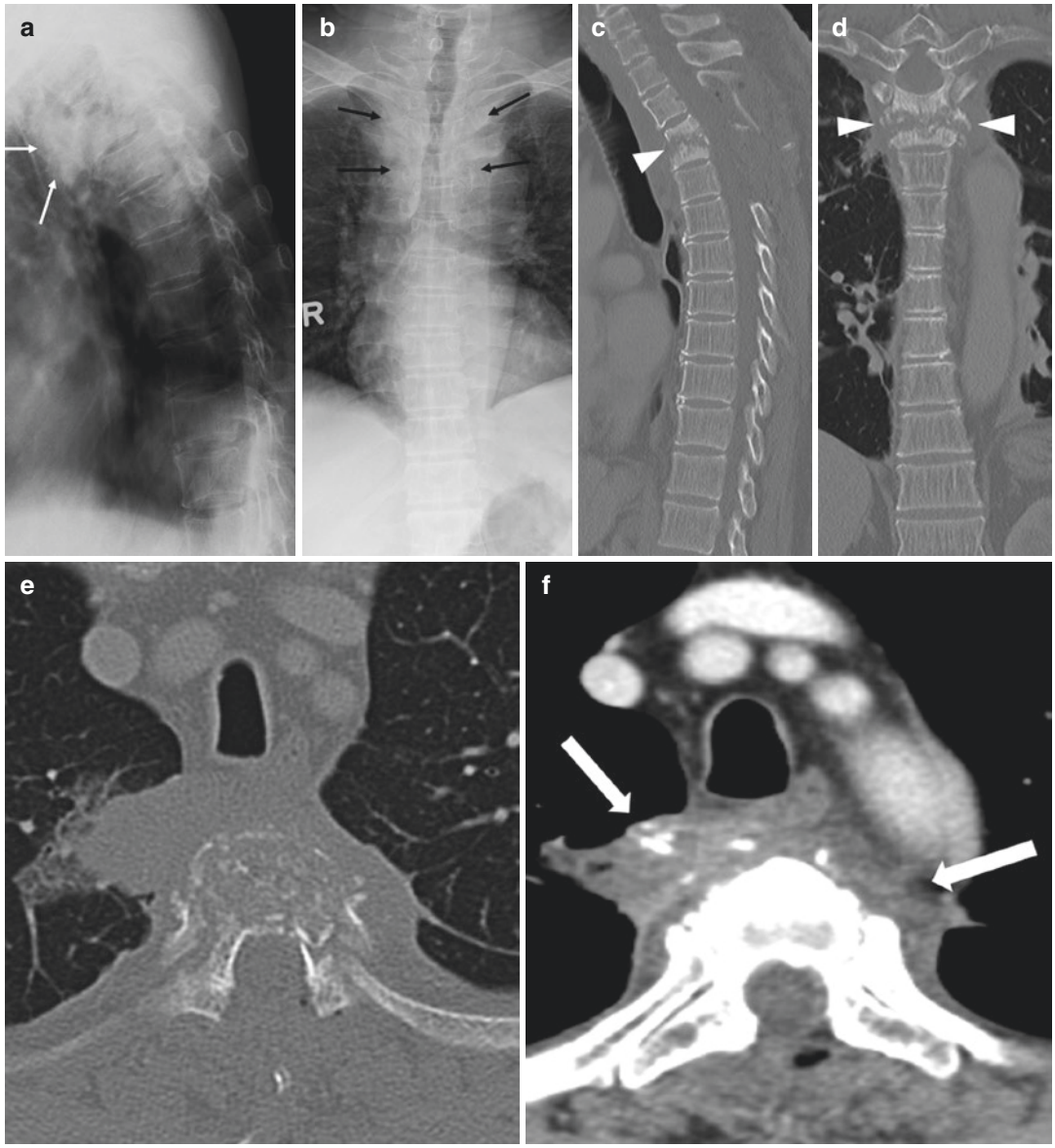

Fig. 6 A 65-year-old man presenting with upper back pain, a month and a half after spinal surgery. Note the missing posterior spinal elements from T2 to T5 vertebral levels. (**a**) Lateral radiograph of the upper thoracic spine is suboptimal due to the multiple overlapping bony and soft tissue structures. Abnormal soft tissue swelling (white arrows) is present adjacent to the anterior thoracic vertebral bodies. (**b**) AP radiograph shows abnormal upper mediastinal/paraspinal soft tissue swelling (black arrows) causing adjacent tracheal narrowing. (**c**) Sagittal and (**d**) coronal bone window CT images clearly show destruction of the T3/4 vertebral body end plates and intervening disk (arrowheads). Axial (**e**) bone window and (**f**) soft tissue window CT images taken at the same level better show prevertebral spread of infection with posterior mediastinitis (white arrows). The displaced tiny bone fragments within the area of infection are well depicted on all the CT images in various planes. CT is extremely useful to evaluate structures in the lower cervical/upper thoracic region and gives an added advantage of showing the spread of infection into the adjacent structures such as the mediastinum and lungs. This patient was treated for pyogenic spondylodiscitis

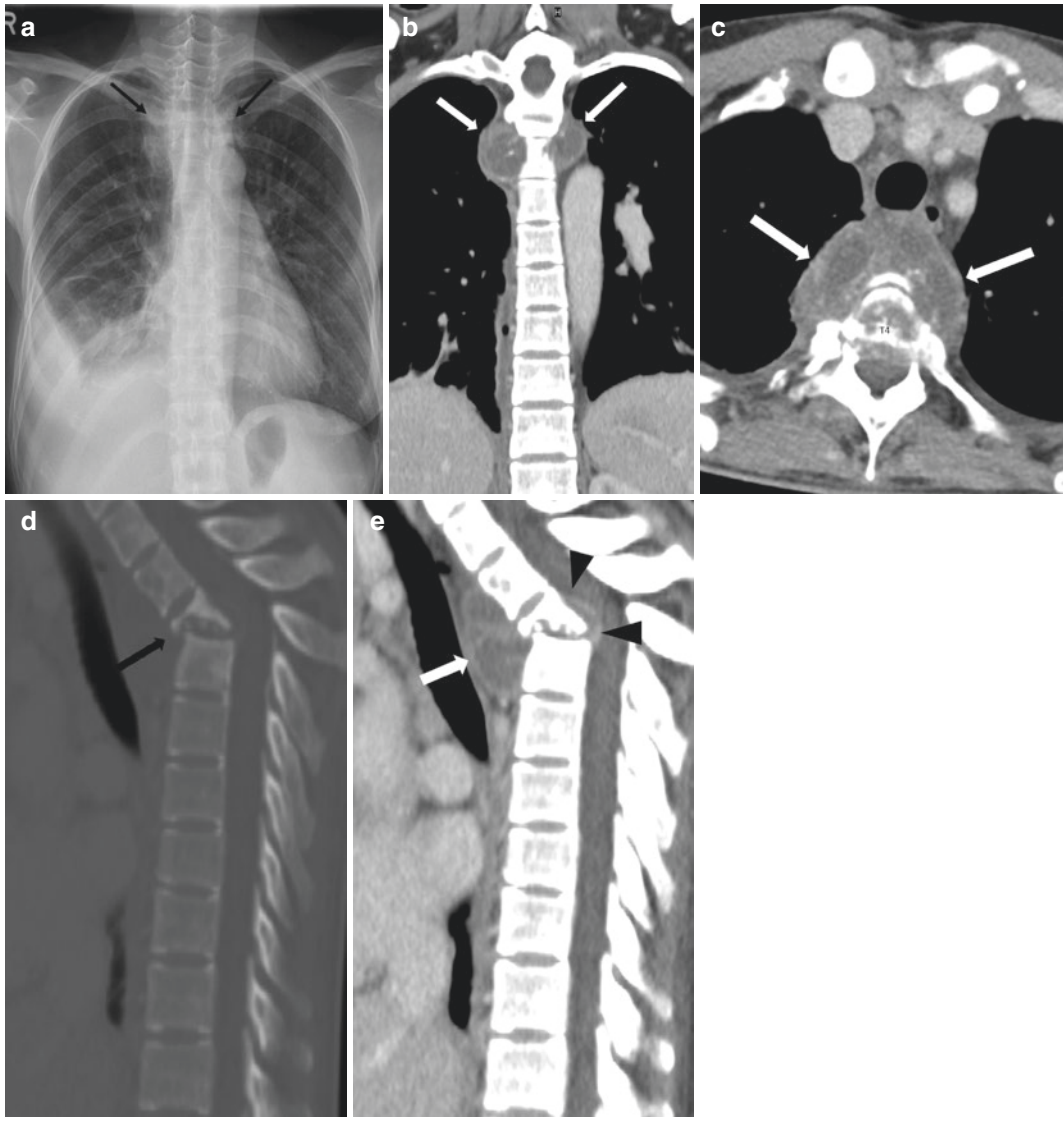

Fig. 7 (**a**) Frontal chest radiograph of a 30-year-old woman presenting with cough and upper limb weakness shows right-sided pleural effusion with underlying right lower lobe collapse consolidation. There are subtle bony changes in the region of T4 vertebra with adjacent abnormal paraspinal soft tissue swelling (black arrows). (**b**) Coronal and (**c**) axial contrast-enhanced soft tissue window CT images show multi-loculated rim-enhancing paravertebral abscesses (white arrows) along with destruction of the T4 vertebral body. (**d**) Sagittal bone window CT image confirms the destruction, partial collapse, and posterior angulation of T4 vertebral body into the spinal canal (black arrow). (**e**) Corresponding sagittal contrast-enhanced soft tissue window CT image better shows the rim-enhancing prevertebral abscess (white arrow) and epidural abscess (arrowheads). Note the intrinsic limitation of radiographs in revealing changes in the upper thoracic spine and the superiority of CT in displaying the bony and soft tissue changes. This was proven to be tuberculous spondylodiscitis with atypical involvement of a single vertebral body. The preferential destruction of the vertebral body over the disk is characteristic of tuberculous infection of the spine

summarized in Table 1. Given that radiographs are insensitive for early disease changes, it is useful to follow a systematic approach to avoid errors when reading a spine radiograph. Radiologists should always correlate with the clinical history of suspected infection and advise consideration of further advanced imaging such as CT and MRI.

Table 1 Outline of normal radiological findings in the thoracolumbar and cervical spine with emphasis on specific findings in the clinical context of spinal infection

	Key points	Thoracolumbar spine	Cervical spine
1.	Views	• AP and lateral • Oblique, coned (L5/S1), and flexion/extension views when indicated	• AP, lateral, and open-mouth (C1/C2) views • Swimmer, oblique views when indicated
2.	Adequate coverage	Whole thoracic and/or lumbar spine	• AP view must show the entire cervical and upper thoracic spine • Lateral view cover C1-C7 vertebrae from skull base till lower margin of the T1 vertebra • Swimmer view if T1 and C7 vertebrae not adequately visualized • Open mouth view for C1/C2 articulation must show lateral C1/C2 joints bilaterally
3.	Alignment	• Check for congruent alignment of vertebral bodies and spinous processes on AP view • Examine anterior and posterior corners of vertebral bodies with the adjacent vertebra on a lateral view	• Check for congruent alignment of lateral margins of the spine on AP view • Congruence of anterior and posterior cervical lines and spinolaminar lines on a lateral view • Odontoid peg must be equidistant from lateral processes of C1 on both sides on open-mouth view
4.	Vertebral body	• Sequentially examine individual vertebral bodies for sharp and intact cortical outline and height reduction on a lateral view (early erosions and blurring at end plates) • Bear in mind a normal sequential mild increase in vertebral body height from top to bottom owing to projectional reasons	• Sequentially examine individual vertebral bodies for sharp and intact cortical outlines and height reduction on a lateral view
5.	Intervertebral disks	• Carefully examine the height of disk spaces for the asymmetrical reduction in height on lateral and left/right asymmetry on AP view (early changes of discitis) • Bear in mind a normal sequential mild increase in disk space height from top to bottom owing to projectional reasons • L5/S1 disk height is normally smaller than the other spaces	• Carefully examine the height of intervening disk spaces for an asymmetrical reduction in height on a lateral view • All spinous processes must be equidistant from each other on AP view. AP view not ideal for examining vertebral body or disk heights
6.	Posterior bony elements	• Integrity and symmetry of pedicles and transverse processes on AP and posterior elements (facet joints and spinous processes) on lateral or oblique views • Destructive changes particularly seen in infection	• Integrity of posterior elements (facet joints and spinous processes) better seen on lateral or oblique views and transverse processes best examined on AP view
7.	Other bones (costo-transverse articulations, ribs and pelvis)	• Integrity of costo-transverse joints and visualized posterior ribs on AP view. Comparison with contralateral side assists in detecting destruction • Examine the visualized pelvic bones (osteomyelitis) and sacroiliac joints (erosive sacroiliitis) on AP view	

(continued)

Table 1 (continued)

	Key points	Thoracolumbar spine	Cervical spine
8.	Soft tissues	• Check for preserved fat planes along the lateral margin of bilateral psoas shadows • Psoas symmetry on AP view • Examine thoracic paraspinal soft tissue thickness (normal right-sided stripe is not visible and left-sided stripe has a normal thickness up to 1 cm) on AP view (specially look for psoas fat plane obliteration, calcifications, and fusiform posterior mediastinal paraspinal bulge in infections)	• Assessment of prevertebral soft tissue thickness (normal prevertebral soft tissue above C4 level ≤1/3rd vertebral body width and below C4 ≤100% vertebral body width) • Prevertebral space abscess manifests with increased prevertebral soft tissue thickness
9.	Deformities	• Kyphoscoliosis, gibbus, and anterior gauge defects	
10.	Edge of the radiograph	• Visible lung abnormalities give major clues towards infection (pneumonia, pleural effusions)	• Visible upper ribs and apices of the lungs (erosions and pneumonia)

4 Role of CT

4.1 CT Acquisition Techniques

CT is the modality of choice for accurate assessment of the bony structures of the spine, especially given the complex anatomy and the multitude of soft tissue structures superimposed on the spine, particularly on AP radiographs of the thoracolumbar regions. CT assessment of the spinal soft tissues, although superior to radiographs, has limitations; thus augmentation with intravenous contrast administration is useful, when indicated. CT is fast and well-tolerated by almost every patient. The image quality depends on the choice of imaging parameters, multiplanar reconstructions, and post-processing techniques, which include reconstruction algorithms and the reformatting parameters. Bone and soft tissue windows may be used to separately assess these tissues (Tins 2010) (Figs. 8 and 9).

The patient is placed in a supine position, which ensures minimal movement of the spine. The long axis of the spine is usually orientated along the z-axis of the scanner, although dynamic flexion/extension and oblique imaging may sometimes be required. External metallic objects are removed to avoid beam hardening artifacts. For the spine, optimal images are acquired with a high kV and mAs and thin collimation (ideally <1.5 mm). Typical parameters for a patient weighing 70–80 kg are 120 kVp and 330 mAs for the cervical spine and 120 kVp and 380 mAs for the thoracolumbar spine, with a pitch of 0.9 and a slice thickness of 1–1.5 mm. Slimmer and younger patients can be imaged with lower kV and mA and larger/obese patients with higher values. Multiplanar coronal and sagittal reconstructions are obtained from the axial source acquisition. Three-dimensional (3D) volume reconstructions may also be useful in improving the diagnostic accuracy (Tins 2010).

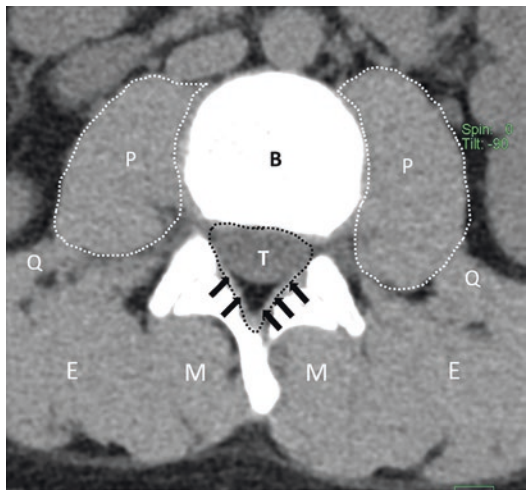

Fig. 8 Axial soft tissue window CT image of the normal lumbar spine shows the vertebral body (B), spinal canal (dotted black line), paired ligamentum flava (small black arrows) posterolaterally, and the thecal sac (T). The axial view is also the best for evaluation of the surrounding muscles anterolaterally, the psoas (P) muscles outlined by dotted white lines, laterally the quadratus lumborum (Q), posteromedially the multifidus (M), and posterolaterally the erector spinae (E) muscles

4.2 CT Findings in Spinal Infection

CT has traditionally played a minor role in the diagnosis of spinal infection and is not the primary modality of investigation. However, owing to its superior anatomical resolution and intrinsic ability in depicting bony detail, it is much more sensitive than radiography and excels in delineating fine bony details when there is a diagnostic conundrum and for preoperative assessment (Tali and Gültekin 2005; Diehn 2012) (Figs. 6 and 7).

The imaging findings and their sequence of appearance follow the same principles as radiographs. However, the earliest changes of end-plate destruction and osteoporosis of the involved vertebral bodies are better delineated on CT than radiographically and may be seen as early as 2 weeks from infection in at least half of the affected patients. They are sometimes even appreciable in the setting of negative radiographs. Careful assessment of the intervening disk may reveal a reduction in height and reduced density (3–4 weeks after infection), when compared to the other non-affected disks (Larde et al. 1982; Golimbu et al. 1984) (Fig. 10).

The sequential medullary osteolysis in the vertebral bodies, end-plate collapse, and forma-

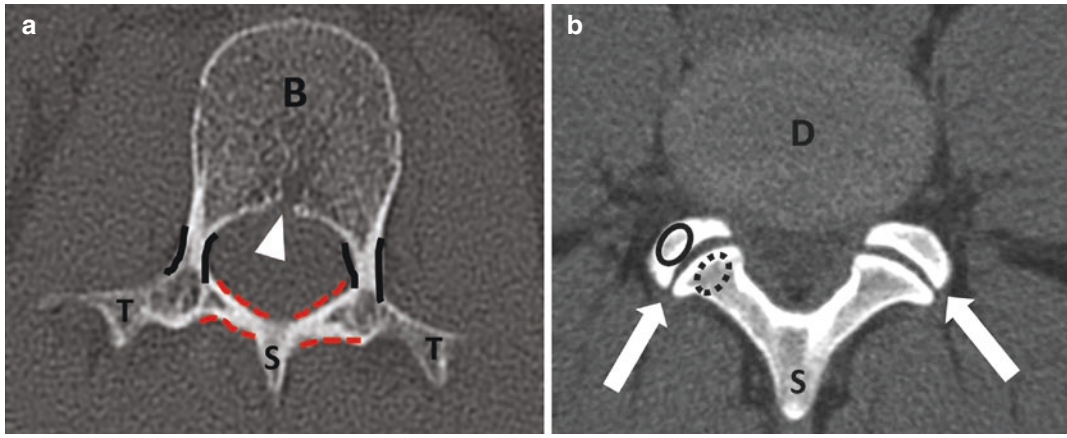

Fig. 9 Axial bone window CT images of the normal lumbar spine taken at (**a**) vertebral body and (**d**) intervertebral disk levels. Fine bony details of the vertebral body (B), basivertebral vein foramen (arrowhead), and components of the posterior elements such as the pedicles (outlined in black lines), transverse processes (T), laminae (outlined in dotted red lines), and spinous process (S) are well shown. The intervertebral disk (D) and the facet joints (white arrows) formed by the superior articular process of the upper vertebra (solid black oval ring) and the inferior articular process of the lower vertebra (dotted black oval ring) are also well shown

tion of vertebral end-plate geodes can be easily identified (Golimbu et al. 1984; McGahan and Dublin 1985; Sans et al. 2012) (Figs. 6, 7, and 10). Involvement of the posterior elements in atypical forms of tuberculosis, immunosuppressed states, intravenous drug abuse, and recent regional procedures can be easily seen, with the precise extent of bony destruction of the facet joint, pedicle, and transverse and spinous processes (Sans et al. 2012; Diehn 2012). This may manifest as partial destruction or complete osteolysis, sclerotic lesions, and expansile tumorlike lesions (Moore and Rafii 2001; Varma et al. 2001; Acharya and Gibbs 2016) (Fig. 11).

The paraspinal soft tissue spread of infection comprising circumferential pre- and paravertebral soft tissue thickening, phlegmonous changes and abscess formation in the iliopsoas muscle (lumbar and pelvic regions), fusiform posterior mediastinal abscess (thoracic region), and prevertebral cervical involvement are also appreciated directly and much earlier on soft tissue windows on CT. Whenever indicated, intravenous contrast administration may be used to facilitate direct visualization of rim-enhancing abscesses and heterogeneously enhancing phlegmonous change in these regions (Figs. 6, 7, and 11). CT with contrast administration also delineates other associated findings such as pyelonephritis and renal abscess; retroperitoneal, pelvic, and mediastinal lymphadenopathy; mediastinitis; and involvement of the tracheobronchial tree and esophagus with secondary fistulous formation (Acharya and Gibbs 2016) (Figs. 6, 7, and 12).

Although it is not the ideal modality and not considered a replacement for MRI, CT can still be useful, to some extent, in the assessment of the structures of the spinal canal. The epidural spread of infection manifesting as an epidural abscess can be directly delineated on contrast-enhanced CT as a heterogeneously enhancing phlegmon or a rim-enhancing abscess (Fig. 7). Additionally, the extent of spinal canal stenosis by the epidural spread can be indirectly assessed. Changes in the cord, nerve roots, leptomeningitis, and epiduritis are best seen directly on MRI, rather than using CT. CT is probably the best technique for direct visualization of bony sequestra formed by destruction and fragmentation of the vertebrae, which may migrate into the

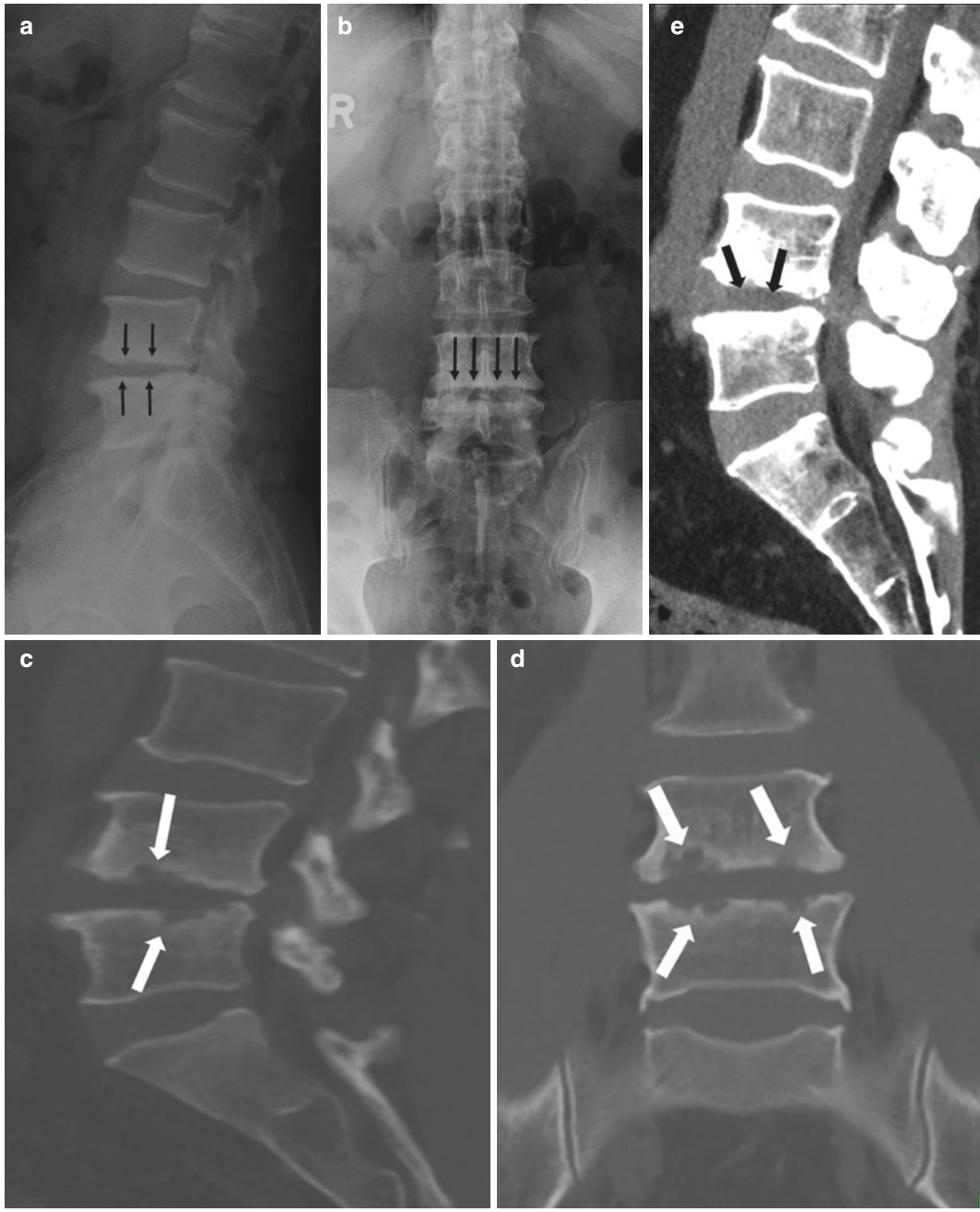

Fig. 10 A 48-year-old woman presenting with 1-month history of low back pain, who was subsequently treated for *E. coli* infection. (**a**) Lateral and (**b**) AP lumbar spine radiographs show L4/L5 disk space reduction with blurring of the adjacent vertebral end plates (thin black arrows). These changes are subtle and may be seen in early infection. (**c**) Sagittal and (**d**) coronal bone window CT images better show the destructive changes at the L4/L5 end plates (white arrows). (**e**) Sagittal soft tissue window CT image shows a reduction in height and reduced density of the L4/5 disk (thick black arrows), when compared to the other non-affected disks. Reduced disk density is usually evident 3–4 weeks after infection

spinal canal and perispinal soft tissues (Fig. 6). CT also is best for showing residual calcifications in the paraspinal soft tissues and presence of gas within the affected disk, spinal canal, and paraspinal abscesses. Overall, the pathognomonic findings of infective spondylodiscitis comprising cortical end-plate erosions of two contiguous vertebral bodies with reduction of the intervening disk space and associated paraspinal soft tissue prominence are earlier and better depicted on CT than radiographs (Sans et al. 2012).

Although CT is not the modality of choice for follow-up of healed infections, there is still limited use in the assessment of the stability of vertebral body height, especially in the thoracic and lower cervical regions which are difficult to view on radiographs due to soft tissue overlap. It is

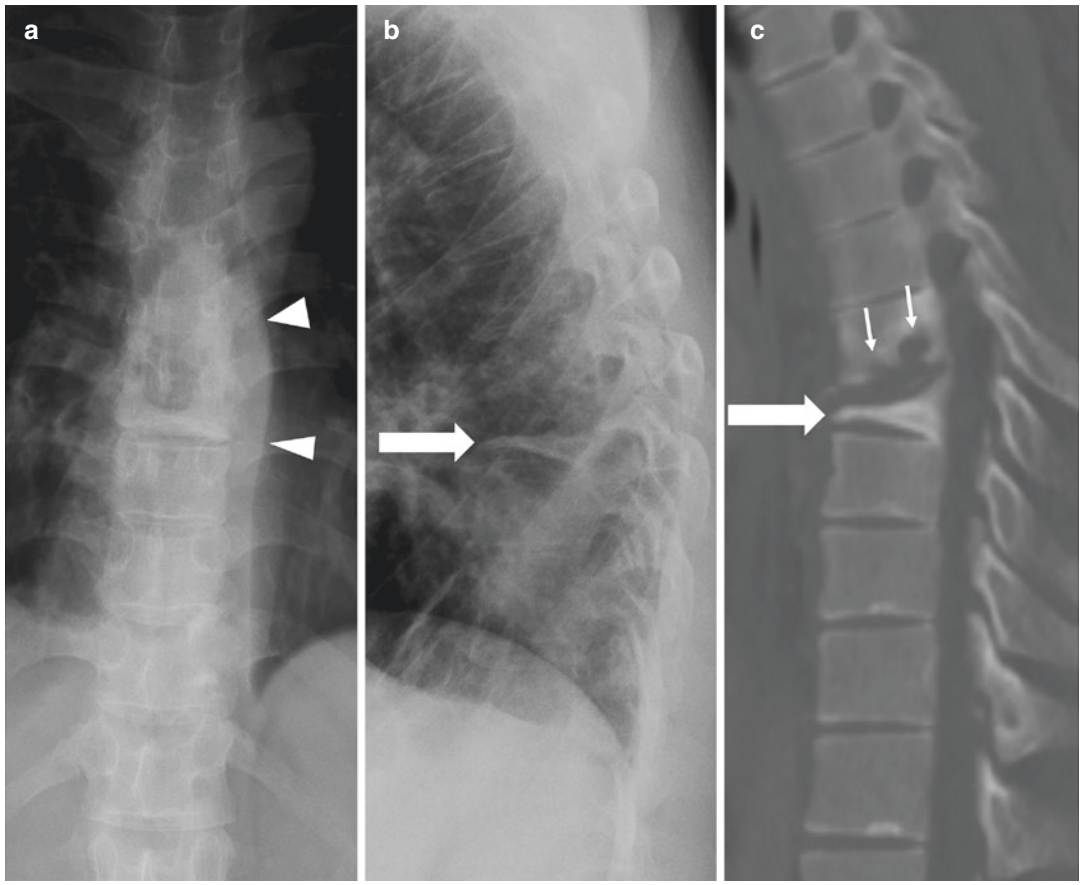

Fig. 11 A 46-year-old woman presenting with back pain and UTI. (**a**) AP and (**b**) lateral radiographs of the thoracic spine show a severe collapse of the T8 vertebral body (large white arrow) with associated abnormal paraspinal mediastinal soft tissue swelling (arrowheads). It is difficult to see other changes on the radiographs alone due to overlapping structures. (**c**) Sagittal bone window CT image confirmed a severe collapse of T8 vertebral body (large white arrow) and also shows inferior end-plate destruction of T7 vertebral body (small white arrows). (**d**) Left parasagittal and (**e**) axial bone window CT images show a lytic lesion involving the left pedicle, and superior articular and transverse processes of T11 vertebra (black arrows). Given that the complex anatomy of the posterior arch makes visualization difficult, CT was useful to show the lesion extent. Contrast-enhanced (**f**) coronal and (**g**) axial soft tissue CT images confirm the paravertebral abscess (arrowheads) at T7/8 vertebral levels. Note also a right-sided pleural effusion with underlying lung collapse. The patient was treated for pulmonary and multilevel spine tuberculosis infection

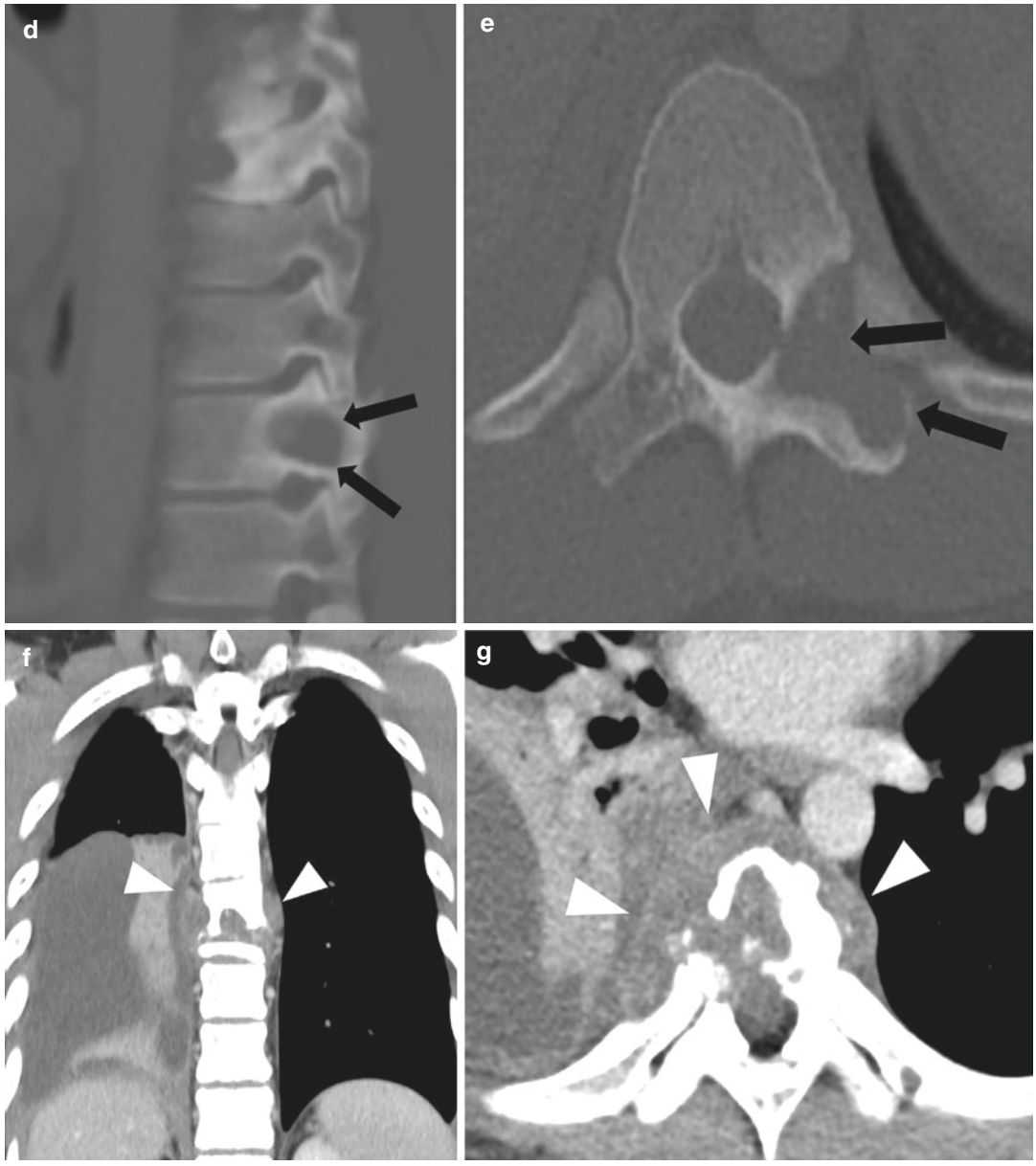

Fig. 11 (continued)

also useful for preoperative delineation of bony anatomy and postoperative assessment of spinal fixation devices (to assess for displacement and spinal canal impingement). Sagittal and axial reconstructions and 3D volume rendering are particularly useful for pre- and postoperative evaluation. CT is also used to assess questionable discitis or osteomyelitis seen on MRI (e.g., when there is confusion regarding Modic type I changes, acute Schmorl nodes, and tumors versus atypical infections), especially when the MRI findings are not strongly suggestive and a biopsy has been requested (Tali and Gültekin 2005; Diehn 2012; Sans et al. 2012).

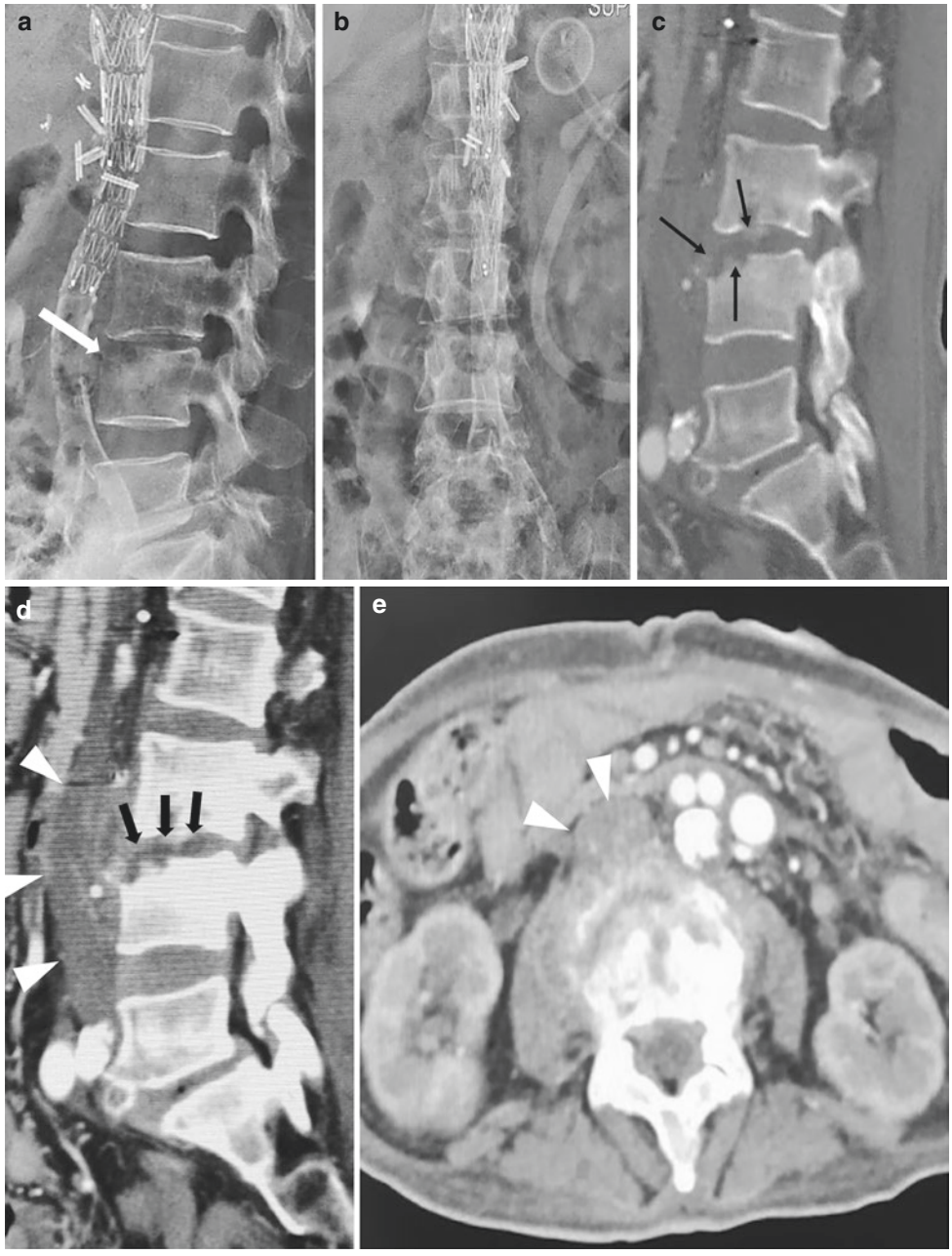

Fig. 12 A 70-year-old man presenting with low back pain, a month after aortic stent grafting. (**a**) Lateral radiograph of the lumbar spine shows the aortic stent as well as partial anterosuperior end-plate destruction of L4 vertebral body (white arrow) with reduction of the L3/L4 disk height. (**b**) AP radiograph is not very helpful due to the overlapping bowel. (**c**) Sagittal bone window CT image confirms partial end-plate destruction of L3 and L4 vertebrae (thin black arrows). (**d**) Sagittal contrast-enhanced soft tissue window CT image shows disk height reduction, an abnormal linear hypodensity affecting L3/L4 disk (short black arrows), and enhancing prevertebral soft tissue swelling (arrowheads). The intradiscal hypodensity is likely to represent phlegmonous change/small discal abscess and, when visible on CT, directly helps confirm discal involvement. (**e**) Axial contrast-enhanced CT image shows that the prevertebral soft tissue swelling is close to the aortic stent. This was confirmed to be a pyogenic infection secondary to the stent

4.3 Dual-Energy CT (DECT)

DECT has made significant recent advances in musculoskeletal imaging and has emerged as an evolving tool in the detection of bone marrow edema. This has been made possible by special post-processing tools which allow detection of marrow edema using the so-called virtual non-calcium technique. However, MRI remains the gold standard for detecting marrow edema. The virtual non-calcium technique decomposes the cancellous bone into red marrow (similar to soft tissue attenuation), yellow marrow (fat attenuation), and calcium. It then subtracts calcium from the cancellous bone, thus allowing assessment of the marrow. The underlying principle in the detection of bone marrow edema is the higher attenuation of the edematous marrow as compared to fatty marrow. Color-coded virtual non-calcium subtracted images have been suggested for better visual detection of attenuation changes in the bone marrow (Pache et al. 2010; Nicolaou et al. 2012).

Conventional CT has intrinsic limitations in the assessment of soft tissue structures, such as the ligaments and intervertebral disks. These structures are composed of type 1 collagen, elastin, proteoglycans, glycosaminoglycans, and glycoproteins. DECT can exploit collagen's specific dual-energy index and decompose it from the surrounding tissue. A three-material collagen decomposition algorithm consisting of collagen, fat, and soft tissue is performed, and collagen can be allotted a color. In this way, DECT allows visualization of collagenous structures such as ligaments and tendons. Recent studies have applied this technique to the intervertebral disk and shown that DECT is suitable for detecting disk edema by demonstrating reduced collagen content in the edematous disk (Nicolaou et al. 2012; Pumberger et al. 2019).

DECT has the future potential for the detection of bone and disk edema via the virtual non-calcium subtraction technique. Most of the research in the field of DECT has been centered mainly on the identification of marrow and disk edema in the setting of acute trauma. However, the same principle can be applied to spondylodiscitis where marrow and disk edema are the early findings. This may be particularly beneficial to patients with contraindications to MRI (Nicolaou et al. 2012; Pumberger et al. 2019).

4.4 Role of CT-Guided Biopsy

Image-guided targeted tissue sampling may be necessary in some cases of spinal infections for identification of the causative organism in order to determine the treatment regimen. Radiologists play an important role in the diagnostic algorithm by performing image-guided percutaneous biopsy. Either fluoroscopy or CT can be used for needle guidance, with the latter being the current modality of choice for spine biopsy (Fig. 13). Ultrasound imaging can sometimes be used to guide the aspiration of superficially located paraspinal abscesses. CT is safer with less likelihood of neurovascular and vital organ injury and much more precisely shows the needle position, when compared to fluoroscopy. The technique of CT fluoroscopy enables real-time imaging and smaller radiation dosage (Figs. 13 and 14).

Following preliminary axial scanning, the radiologist selects the most appropriate slice and plans the most ideal route for biopsy. Factors to consider are the lesion depth, entry point, and the angle of the chosen needle (coaxial technique is preferable to avoid re-puncturing), while avoiding adjacent vital structures such as blood vessels and nerves. At least three or more samples of the disk space, both vertebral end plates, and the adjacent soft tissue should be obtained. The approach routes vary, but the most reliable ones are posterolateral and transpedicular approach for the lumbar spine and inter-costotransverse approach for the thoracic spine (Fig. 13). At the end of the procedure, a later sample can be taken after lavage of the disk space using normal saline solution, with the fluid then aspirated for microbiological analysis. CT-guided needle aspiration has been found to be accurate for identifying active bacterial disk infection but is less reliable for fungal infection (Chew and Kline 2001; Peh 2006; Gogna et al. 2008; Sehn and Gilula 2012; Diehn 2012).

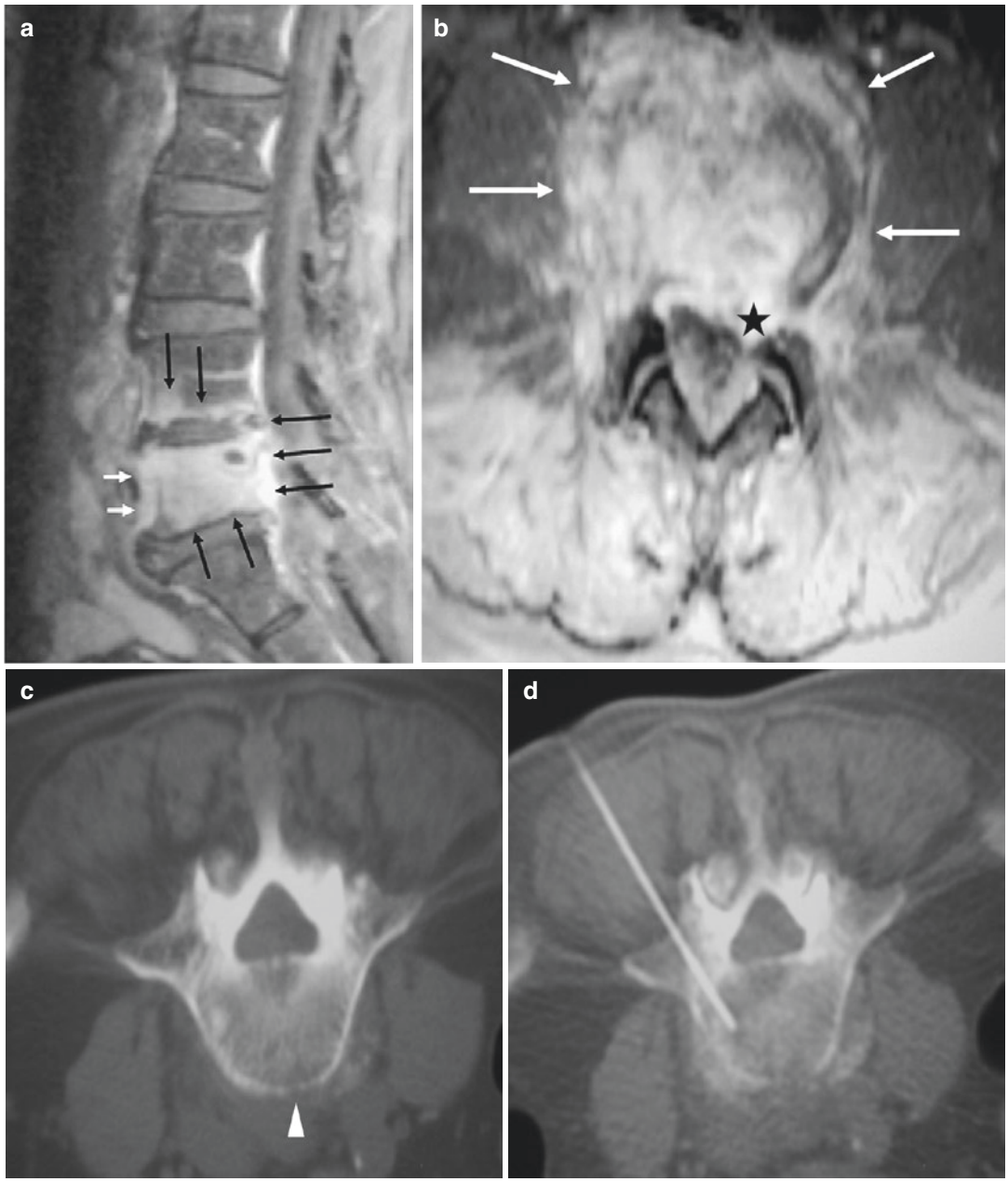

Fig. 13 CT-guided biopsy of a 64-year-old man with L5 vertebral osteomyelitis and L4/5 discitis. (**a**) Sagittal and (**b**) axial contrast-enhanced T1-W MR images show an intensely enhancing lesion involving the whole L5 vertebral body with similar changes in the posterior part of the L4/5 disk and the inferior L4 vertebral body (black arrows). There is soft tissue anterior subligamentous (short white arrows), paravertebral (long white arrows) and posterior extradural extension (asterisk), as well as medial psoas muscle involvement, worse on the right side. (**c**) Pre-biopsy axial CT image of the upper L5 vertebral body, taken with the patient in a prone position, shows mild cortical destruction of the vertebral body, particularly anteriorly (arrowhead). The prominent vertebral body medullary involvement seen on MRI is barely visible on CT. Correlation of the planned biopsy site with corresponding MR images is needed. (**d**) Prone axial CT fluoroscopic image (taken at nearly the same level as Fig. 13c) shows the insertion of a 14.5G Ostycut trephine needle (Angiomed/Bard, Karlsruhe, Germany) into the L5 vertebral body using the transpedicular approach

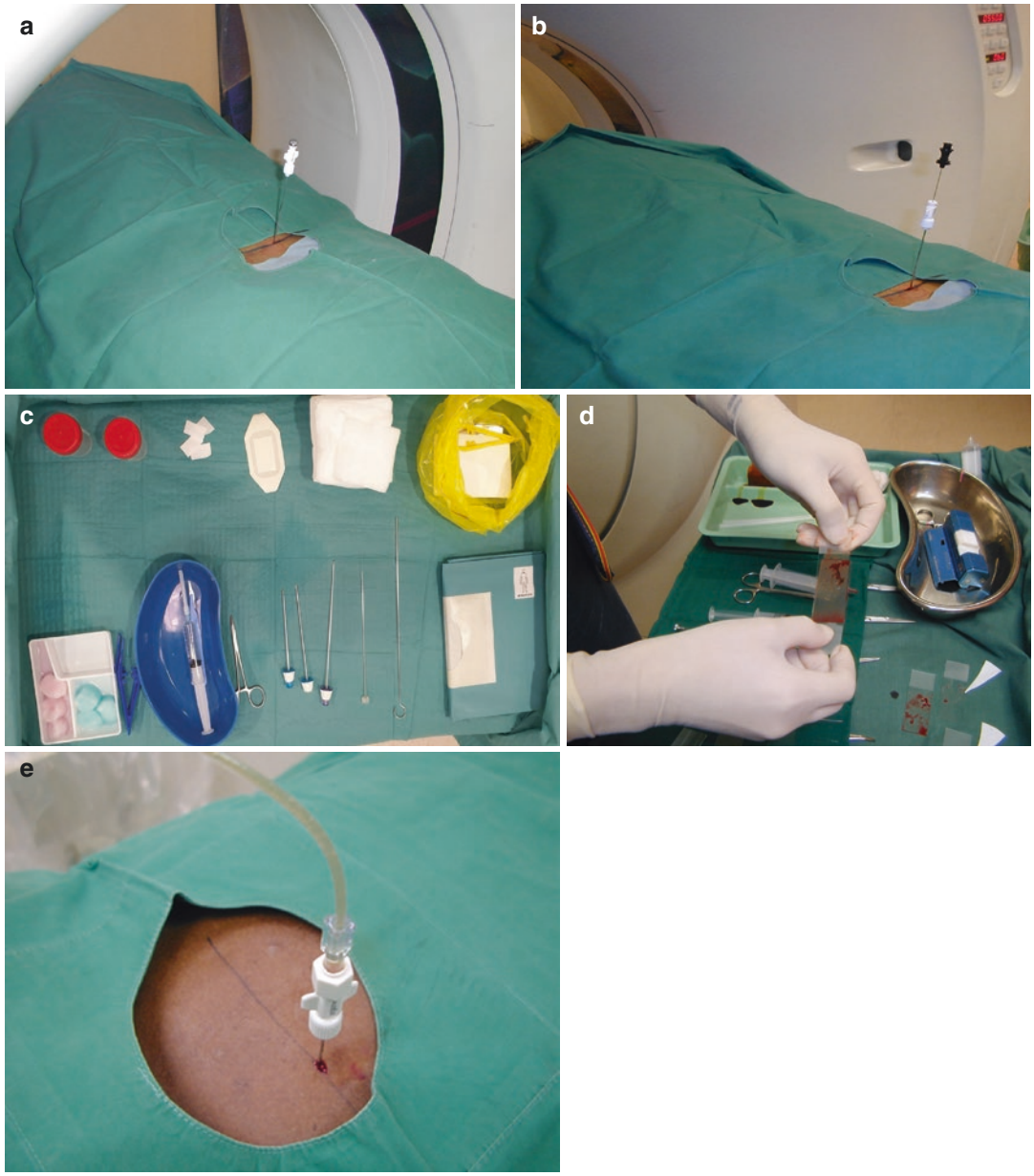

Fig. 14 Photographs taken during CT-guided percutaneous biopsy of the spine. (**a**) Photograph of a CT fluoroscopy unit with the cleaned and draped patient lying in a prone position on the CT table. The Ostycut trephine needle (Angiomed/Bard, Karlsruhe, Germany), used to obtain core specimens of bone, has been inserted through the skin which has been surfaced marked at the selected CT slice. (**b**) The photograph shows a 22G Chiba needle (Cook, Bloomington, Indiana, USA) (black hub) which has been placed coaxially into the shorter 14.5G Ostycut needle (white hub). The fine Chiba needle is ideal for the aspiration of fluid and obtaining cytology specimens. The coaxial method allows multiple passes through a single bone window created by the Ostycut trephine needle. (**c**) The photograph shows the typical trolley setting for a bone biopsy, including the different components of the 13G Bonopty coaxial bone biopsy system (AprioMed AB, Uppsala, Sweden). (**d**) The photograph shows the biopsy specimen being smeared onto a glass slide for cytological examination. Radiologists should be familiar with the various techniques for the preparation of specimens for histology, cytopathology, and microbiology. (**e**) The photograph shows aspiration of pus from a paraspinal abscess. The importance of sorting out and labeling the various specimens for delivery to the various laboratories for processing cannot be overemphasized

Aspiration and core specimens have complementary roles. Ideally, all samples should be sent for histology, cytopathology, and microbiology (Fig. 14). This is highlighted by the potential of histology to distinguish pyogenic from granulomatous infections, diagnose culture-negative chronic osteomyelitis, and detect unsuspected neoplasm. The result is usually negative if the specimens are not of adequate quality or quantity and if biopsy results are compromised by antibiotics prescribed before the intervention (Peh 2006; Diehn 2012; Sans et al. 2012). Three specific contexts must be highlighted, namely, taking a specimen from a large tuberculous paraspinal abscess is often easier and sufficient for diagnosis through microbiology; blood cultures are often negative in postoperative spondylodiscitis which makes this a routine scenario for image-guided aspiration or biopsy; and the clinical history and serology often suffices in the diagnosis of brucellar spondylodiscitis, without the need for intervention (Sans et al. 2012). Details of percutaneous biopsy techniques and diagnostic results can be found in the chapter entitled "Percutaneous Biopsy of Spinal Infection".

4.5 Advantages of CT

Although CT is not the primary modality of choice in spinal infection, it has several advantages over the other imaging modalities (Tins 2010; Sans et al. 2012):

1. Faster to perform, better tolerated, and usually more readily available, compared to MRI.
2. The best modality for evaluating bony changes such as early cortical lesions, areas of osteolysis, vertebral end-plate geodes, and precise extent of posterior element involvement.
3. Offers the options of multiplanar reconstructions, volume rendering/3D reconstruction, and windowing options for bone and soft tissues.
4. Useful for studying areas that are not optimally seen on radiographs, such as the thoracolumbar spine or cervicothoracic junction.
5. Currently the best technique for visualizing bone sequestra within the spinal canal, residual calcifications, and presence of gas within an abscess or disk.
6. Better depiction of paraspinal soft tissue changes compared to radiographs, especially in contrast-enhanced images.
7. Important role in imaging of patients with contraindications to MRI, e.g., ferromagnetic metal implants.
8. The preferred image-guided technique for percutaneous biopsies.

4.6 Disadvantages and Pitfalls of CT

CT has its own share of pitfalls in imaging of spinal infection. It may be well-tolerated and sensitive but lacks specificity (Tins 2010; Diehn 2012; Sans et al. 2012):

1. Artifacts can occur in CT imaging. In particular, movement, noise, and streak artifacts due to very high attenuation materials can cause a problem for image interpretation.
2. CT of the spine can be associated with high radiation doses, and radiation protection should be considered. It is advisable to tailor the imaging parameters in order to adhere to the ALARA (as low as reasonably achievable) principle. For example, using a high pitch, low kVp and mAs, and limiting the region-of-interest should be considered in pediatric patients.
3. CT does not allow full assessment of the changes in the soft tissues, disk, spinal cord, and bone marrow. MRI remains the gold standard in imaging these structures. The presence or absence of dural and leptomeningeal spread, epiduritis, and cord involvement cannot be reliably detected on CT.

5 Conclusion

Radiographs and CT may not be the gold standard imaging techniques in imaging of spinal infection. This chapter aims to emphasize the preliminary and basic role played by radiographs by illustrating the radiographic features, advantages, and pitfalls. It must not be forgotten that evaluating the spine radiograph prior to MRI is often beneficial. CT is a sensitive but not specific investigation, and is not the primary investigation of choice in spinal infection. However, its importance is underlined by the ability to depict fine bony details and the significant role in guiding percutaneous biopsy.

References

Acharya J, Gibbs WN (2016) Imaging spinal infection. Radiol Infect Dis 3:84–91

Alsop C (2005) The vertebral column. In: Clark's positioning in radiography, 12th edn. CRC Press, London, pp 164–192

Cheung WY, Luk KDK (2012) Pyogenic spondylitis. Int Orthop 36:397–404

Chew FS, Kline MJ (2001) Diagnostic yield of CT-guided percutaneous aspiration procedures in suspected spontaneous infectious diskitis. Radiology 218:211–214

Diehn FE (2012) Imaging of spine infection. Radiol Clin North Am 50:777–798

Gogna A, Peh WCG, Munk PL (2008) Image-guided musculoskeletal biopsy. Radiol Clin North Am 46:455–473

Golimbu C, Firooznia H, Rafii M (1984) CT of osteomyelitis of the spine. AJR Am J Roentgenol 142:159–163

Hong SH, Choi JY, Lee JW et al (2009) MR imaging assessment of the spine: infection or an imitation? Radiographics 29:599–612

Larde D, Mathieu D, Frija J et al (1982) Vertebral osteomyelitis: disk hypodensity on CT. AJR Am J Roentgenol 139:963–967

Lee KY (2014) Comparison of pyogenic spondylitis and tuberculous spondylitis. Asian Spine J 8:216–223

Low KTA, Peh WCG (2017) Radiography limitations and pitfalls. In: Peh WCG (ed) Pitfalls in musculoskeletal radiology. Springer, Berlin, pp 3–32

McGahan JP, Dublin AB (1985) Evaluation of spinal infections by plain radiographs, computed tomography, intrathecal metrizamide, and CT-guided biopsy. Diagn Imaging Clin Med 54:11–20

Moore SL, Rafii M (2001) Imaging of musculoskeletal and spinal tuberculosis. Radiol Clin North Am 39:329–342

Nicolaou S, Liang T, Murphy DT et al (2012) Dual-energy CT: a promising new technique for assessment of the musculoskeletal system. AJR Am J Roentgenol 199:78–86

Pache G, Krauss B, Strohm P et al (2010) Dual-energy CT virtual noncalcium technique: detecting posttraumatic bone marrow lesions—feasibility study. Radiology 256:617–624

Peh WCG (2002) Modern imaging of the musculoskeletal system: is there still a role for radiography? Singapore Med J 43:385–386

Peh WCG (2006) CT-guided percutaneous biopsy of spinal lesions. Biomed Imaging Interv J 2(3):e25

Pumberger M, Fuchs M, Engelhard N et al (2019) Disk injury in patients with vertebral fractures—a prospective diagnostic accuracy study using dual-energy computed tomography. Eur Radiol 29:4495–4502

Sans N, Faruch M, Lapègue F et al (2012) Infections of the spinal column-spondylodiscitis. Diagn Interv Imaging 93:520–529

Sehn JK, Gilula LA (2012) Percutaneous needle biopsy in diagnosis and identification of causative organisms in cases of suspected vertebral osteomyelitis. Eur J Radiol 81:940–946

Stäbler A, Reiser MF (2001) Imaging of spinal infection. Radiol Clin North Am 39:115–135

Tali ET, Gültekin S (2005) Spinal infections. Eur Radiol 15:599–607

Tins B (2010) Technical aspects of CT imaging of the spine. Insights Imaging 1:349–359

Tyrrell PNM, Cassar-Pullicino VN, McCall IW (1999) Spinal infection. Eur Radiol 9:1066–1077

Varma R, Lander P, Assaf A (2001) Imaging of pyogenic infectious spondylodiskitis. Radiol Clin North Am 39:203–213

Magnetic Resonance Imaging of Spinal Infection

Kheng Song Leow, Keynes T. A. Low, and Wilfred C. G. Peh

Contents

Abstract

Infection can involve different structures in and around the spine, such as the vertebral bodies, intervertebral disks, spinal canal, spinal cord, nerve roots, and paraspinal soft tissues. A delay in diagnosis and treatment of spinal infection can result in dire consequences for the patient. Magnetic resonance imaging (MRI) is currently the imaging modality of choice for investigating spinal infection. It provides excellent soft tissue resolution, superior sensitivity, and comprehensive assessment of the spine without the risk of ionizing radiation. Applying the correct

K. S. Leow (✉) · K. T. A. Low
Department of Diagnostic Radiology, Woodlands Health Campus, Singapore, Republic of Singapore
e-mail: leow_kheng_song@whc.sg; Low.keynes.ta@gmail.com.sg

W. C. G. Peh
Department of Diagnostic Radiology, Khoo Teck Puat Hospital, Singapore, Republic of Singapore
e-mail: Wilfred.peh@gmail.com.sg

© The Author(s), under exclusive license to Springer Nature Switzerland AG 2021, corrected publication 2021

M. F. Ladeb, W. C. G. Peh (eds.), *Imaging of Spinal Infection*,
Medical Radiology Diagnostic Imaging, https://doi.org/10.1007/978-3-030-70459-9_4

MRI technique and knowing the protocols and pitfalls of MRI are important to optimize imaging of spinal infection.

Abbreviations

CSF	Cerebrospinal fluid
CT	Computed tomography
FS	Fat-suppressed
IV	Intravenous
MRI	Magnetic resonance imaging
STIR	Short tau inversion recovery
T1-W	T1-weighted
T2-W	T2-weighted
TE	Echo time
TR	Repetition time

1 Introduction

Infection of the spine accounts for approximately 2–7% of musculoskeletal infections (Tyrrell et al. 1999; Hong et al. 2009; Cheung and Luk 2012). The incidence has been rising, and it is believed to be contributed by increasing numbers of those "at risk," such as elderly and immunocompromised individuals. Infection can involve different structures in and around the spine, such as the vertebral bodies, intervertebral disks, spinal canal, spinal cord, nerve roots, and paraspinal soft tissues (Ruiz et al. 2000). The consequences can be devastating and deadly, if the diagnosis and treatment are delayed. Some of the morbidities are severe, including paralysis from cord compression, meningoencephalitis from ascending spread of microorganisms, and death resulting from widespread septicemia (Ruiz et al. 2000).

2 Role of MRI in Spinal Infection

Conventional radiography, the first-line imaging modality for back pain, is useful to exclude compression fracture and structural bony changes. It is not sensitive in detecting early infection. Approximately 30–50% bone loss is required before the pathological process is visible on radiographs (Pineda et al. 2011). Computed tomography (CT) provides better delineation of cortical bone destruction and early periosteal reaction, compared to radiographs, and accurately guides percutaneous biopsy. However, CT involves ionizing radiation and has inferior soft tissue resolution compared to magnetic resonance imaging (MRI) (Peh 2006; Chihara and Segreti 2010). Details of the roles of radiographs and CT, and their advantages and limitations, have been covered in the preceding chapter.

MRI is currently regarded as the imaging modality of choice for investigating spinal infection (Leone et al. 2012). It provides excellent soft tissue resolution, superior sensitivity, and more detailed assessment of the spine, without risk of ionizing radiation. The reported sensitivity and specificity of spine MRI are as high as 94–96% (Modic et al. 1985; Cheung and Luk 2012). Its multiplanar ability also allows a better and more detailed evaluation of the various components of the spine.

2.1 MRI of Spine Anatomy

The vertebral bone marrow is composed of a mixture of different proportions of red and yellow marrow. Red marrow is more cellular, containing hematopoietic stem cells and blood cell progenitors, whereas yellow marrow has more fat and is less cellular. Red marrow comprises approximately 40% fat, compared to yellow marrow which comprises 80% fat. This explains the normal T1-W and T2-W MRI appearances of the red and yellow marrow. Red marrow is hypointense relative to subcutaneous fat and slightly hyperintense relative to muscle on T1-W MR images and is hypointense compared to fat on T2-W, STIR, or fat-suppressed T2-W MR images. In comparison, yellow marrow, consisting predominantly of fat, is hyperintense on T1-W images and hypointense on T2-W MR images (Hanrahan and Shah 2011).

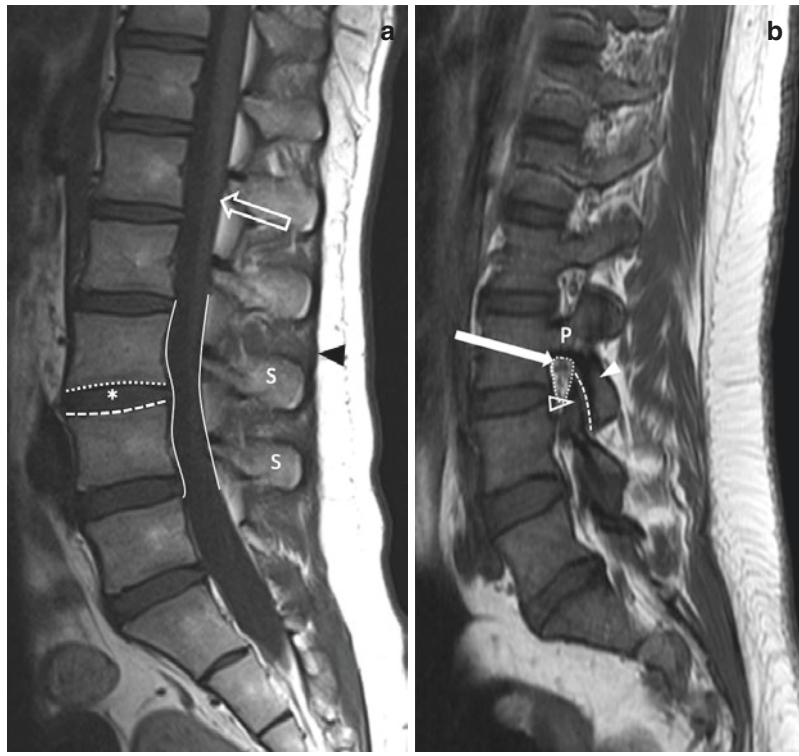

Fig. 1 (**a**) Sagittal T1-W MR image shows the normal anatomy of the lumbar spine in the midsagittal plane. The L3/4 intervertebral disk (asterisk) is bounded by the inferior end plate of the L3 vertebral body (dotted line) and the superior end plate of the L4 vertebral body (dashed line). The anterior and posterior dural margins of the thecal sac are indicated by solid lines. The tip of the spinal cord (conus medullaris) lies at the lower L1 level (open arrow). The epidural space lies outside of the thecal sac but still within the confines of the spinal canal—it is normally occupied by the internal vertebral venous plexus and T1-hyperintense fat, which is better appreciated in the posterior epidural space on this midsagittal image. The vertebral arch forms the posterior bony boundary of the spinal canal and comprises the spinous processes of L3 and L4 vertebrae (labeled "S") on this image. The supraspinous ligament (black arrowheads) connects the posterior spinous processes. (**b**) Sagittal T1-W MR image of the same patient shows the normal anatomy of the lumbar spine in a parasagittal plane. The exiting L3 nerve root is seen en face (arrow), traversing the cranial aspect of the neural foramen (dotted line). The nerve root is clearly seen as it is surrounded by hyperintense fat. Posteriorly, the neural foramen is bounded by the facet joint comprising the inferior articular process of L3 (solid white arrowhead) and superior articular process of L4 (open white arrowhead). The articular margins and joint space of the facet joint are indicated by the dashed line. The pedicle (P) forms the superior border of the neural foramen, and the posterior parts of the L3 vertebral body and L3/4 disc forms its anterior border

The cortex that rims each vertebra is hypointense on both T1-W and T2-W MR images, as is the vertebral end plate which is the transition region where the vertebral body and intervertebral disk interface with each other (Fig. 1).

The intervertebral disk consists of a central gelatinous nucleus pulposus and is surrounded by the collagen fibers of the annulus fibrosus. The relatively high fluid content of the nucleus pulposus explains its T2-hyperintense and T1-iso- to hypointense signal intensity. The annulus fibrosus, comprising mainly of dense fibrous tissue, remains hypointense on both T1-W and T2-W MR images (Fig. 2). The anterior and posterior longitudinal ligament attaches to the ventral and dorsal aspects of the vertebral bodies and intervertebral disks, respectively, and, being composed of fibrous tissue, appears as a hypointense structure on both T1-W and T2-W MR images (Fig. 3).

The spinal cord is located in the spinal canal, contained within the thecal sac, and surrounded

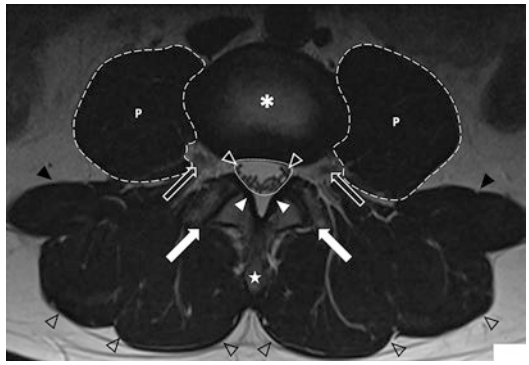

Fig. 2 Axial T2-W MR image shows the normal anatomy of the lumbar spine at the L3/4 intervertebral level. The L3/4 intervertebral disk (asterisk) shows T2-hyperintense central nucleus pulposus and T2-hypointense peripheral annulus fibrosus. The psoas muscles (dashed lines labeled "P") are seen in cross section, occupying paraspinal locations. Given their close relation to the vertebra, it is easy to understand how they can be involved in the setting of spinal infection. Within the spinal canal, the dural margins of the thecal sac are indicated by dotted lines. Note that the dura also extends around exiting the nerve roots and spinal ganglia as dural sheaths. Cauda equina nerve roots are seen within the thecal sac, surrounded by T2-hyperintense CSF. Bilateral descending L4 nerve roots (open white arrowheads) are seen traversing within the lateral recesses. The bilateral exited L3 nerve roots are indicated by open arrows. The facet joints (solid arrows), ligamentum flava (solid white arrowheads), and spinous process of the L3 vertebra (star) are structures enclosing the spinal canal posteriorly at this level. The quadratus lumborum muscles (solid black arrowheads), and paravertebral muscles (open black arrowheads) which include erector spinae and multifidus muscles, are postural muscles that provide support to the vertebral column

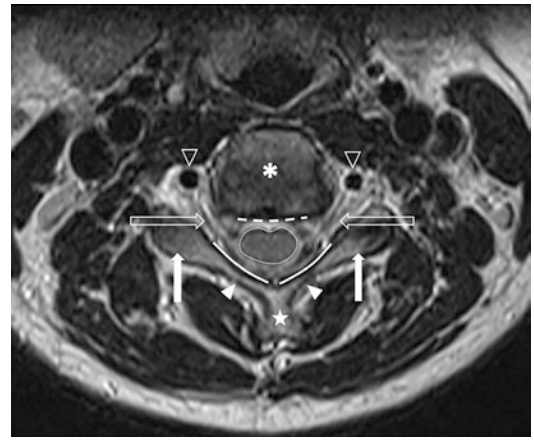

Fig. 3 Axial T2*-W MR image shows the normal anatomy of a cervical spine at the C3/4 intervertebral level. The spinal cord (demarcated by dotted lines) traverses the spinal canal in a central position, surrounded by CSF within the thecal sac. The thecal sac is bounded anteriorly by the C3/4 intervertebral disk (asterisk) and the posterior longitudinal ligament (dashed line) and posteriorly by the ligamentum flava (solid lines) and the vertebral arch comprising the laminae (solid arrowheads), spinous process (star), and inferior articular processes (solid arrows) of the C3 vertebra. The epidural space is a potential space found between the dural margins of the thecal sac and these structures and may be involved by the spread of infection (e.g., epidural abscess) in the setting of spinal infection. The exiting C4 nerve roots are seen traversing the neural foramina bilaterally (open arrows), with the paired vertebral arteries seen in close proximity (open arrowheads)

by CSF (Fig. 3). It extends caudally from the corticomedullary junction (at the level of the foramen magna) to the tip of conus medullaris which usually terminates around L1/L2 vertebral level. The nerve roots exit the spinal canal via the intervertebral (or neural) foramina (Figs. 1, 2, and 3). The collective nerve roots within the thecal sac that extend distally from the conus medullaris are the cauda equina (Fig. 2). The cord and nerve roots are T1- and T2-isointense, while the CSF has typical fluid signal characteristics, i.e., T1-hypointense and T2-hyperintense (Figs. 1 and 2).

The facet joint is a synovial joint formed by the inferior articular process of the superior vertebra cranial to the joint and the superior articular process of the inferior vertebra caudal to the joint (Figs. 1 and 2). The joint articulating surfaces are covered with hyaline cartilage and enveloped by the synovial capsule. The ligamentum flava are paired structures that connect the adjacent laminae of the vertebral bodies (Figs. 2 and 3). The interspinous ligament, along the stronger supraspinous ligament, joins the spinous processes of the adjacent vertebrae (Fig. 1). All these ligaments are hypointense on both T1-W and T2-W MR images.

The psoas muscle originates from the first to fourth lumbar vertebrae, lies in the gutter between the bodies and transverse processes of the lumbar vertebrae, fuses with the iliacus muscle to form the iliopsoas muscle, and inserts into the lesser trochanter of the femur. The quadratus lumborum muscles and paravertebral muscles, including the erector spinae and multifidus muscles, are the postural muscles that provide support to the

vertebral column (Fig. 2). These muscles are isointense on both T1-W and T2-W MR images. Given their close location to the vertebrae, it is not surprising that they are prone to involvement by the spread of spinal infection.

2.2 MRI of Spinal Infection

Spondylodiscitis refers to infection of the intervertebral disk and adjacent vertebrae. The hematogeneous route of infection is the far more common one and usually commences at the anterior subchondral region of the vertebral body. With disease progression, the infective process results in bone infarction, followed by vertebral body and end-plate destruction, and then a direct spread of infection to the adjacent disk space (Shikhare and Peh 2019). Bone marrow involvement manifests as patchy areas of T1-hypointensity, T2-hyperintensity, and corresponding contrast enhancement. End-plate destruction can be appreciated as marked thinning or absence of the normal T1- and T2-hypointense margins of the cortical bone. Abnormal T2-hyperintense signal, sometimes with enhancement, is seen in the intervertebral disc (Fig. 4). Associated soft tissue extension

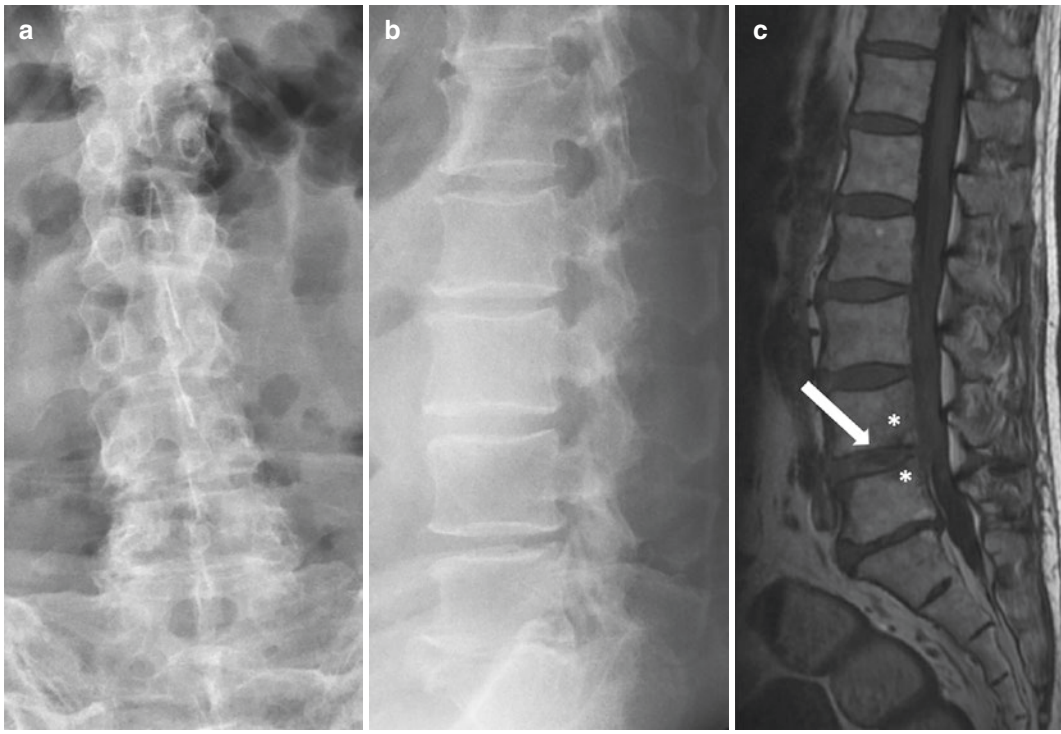

Fig. 4 A 76-year-old man who presented with fever, back pain, and weakness of the lower limbs. (**a**) Frontal and (**b**) lateral radiographs of the lumbar spine show no feature to suggest spinal infection. Background degenerative spondylosis is noted. Sagittal (**c**) T1-W, (**d**) T2-W FS, and (**e**) contrast-enhanced FS T1-W MR images of the lumbar spine, obtained on the same day, show abnormal T1-hypointense T2-hyperintense marrow signal with corresponding enhancement (asterisks) involving the posterior aspects of the L4 and L5 vertebral bodies. Associated destruction of the adjacent inferior L4 and superior L5 end plates are present. There is abnormal fluid signal within the intervening L4–L5 disks (arrows). These features are consistent with spondylodiscitis. There is spread of infection to the anterior epidural space with formation of an epidural abscess (open arrows), extending cranially from the L4–L5 level to the L2–L3 level. The epidural abscess causes significant narrowing of the spinal canal with impingement of the cauda equina nerve roots. Background degenerative changes are noted, with a disk extrusion seen at the L2–L3 level (arrowheads). Small enhancing nodules (open arrowheads) are incidentally noted and closely related to the cauda equina and may represent neurogenic tumors

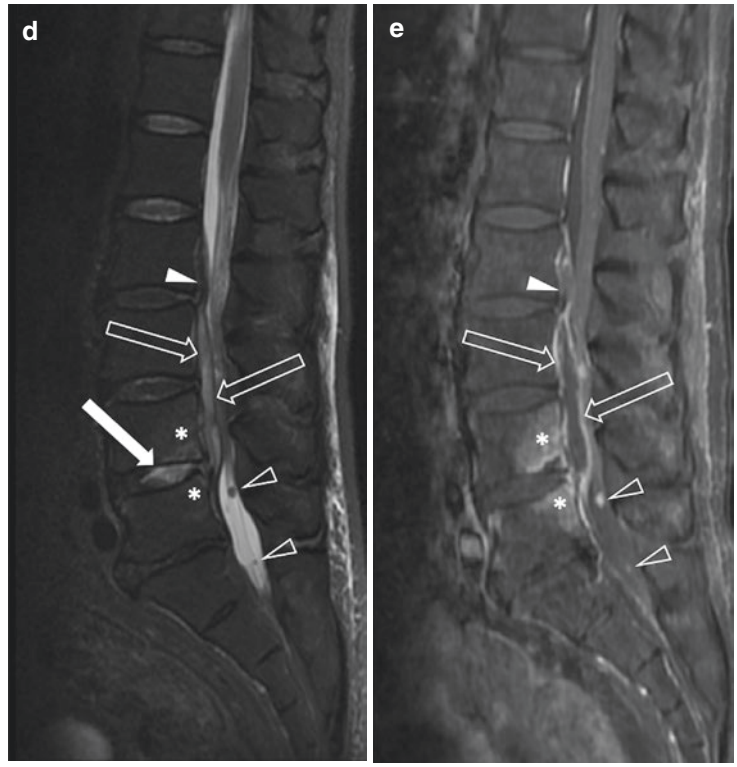

Fig. 4 (continued)

includes epidural and paraspinal soft tissue abscesses, which are seen as fluid collections with rim enhancement, and surrounding soft tissue edema and inflammation (Diehn 2012) (Figs. 4 and 5).

Besides the diagnosis of spinal infection, MRI is also useful for evaluating the full disease extent and to exclude secondary complications and other causes of back pain, e.g., disk prolapse. It also plays an important role in preoperative planning before spinal surgery (Pineda et al. 2011). In selected cases of spinal infection whereby there was no clear clinical or laboratory improvement after 4–8 weeks of antibiotic therapy, MRI can be used to assess the treatment response (Lener et al. 2018). The imaging features of various types of spinal infection, including MRI findings, are discussed in detail in subsequent chapters. The role of MRI in spinal infection is summarized in Table 1.

Table 1 Role of MRI in spinal infection

1.	To diagnose or confirm the clinical suspicion of spinal infection
2.	To exclude differential diagnoses and other causes of back pain
3.	To exclude complications and assess the extent of spinal infection
4.	To guide preoperative planning
5.	To follow up patients with no clear clinical or laboratory improvement post-antibiotics

3 MRI Technique

3.1 Patient Positioning

The "head-in" position is routinely adopted for MRI of the cervical and thoracic spine, while the "feet-in" position has been recommended for MRI of the lumbosacral spine to ensure that the region

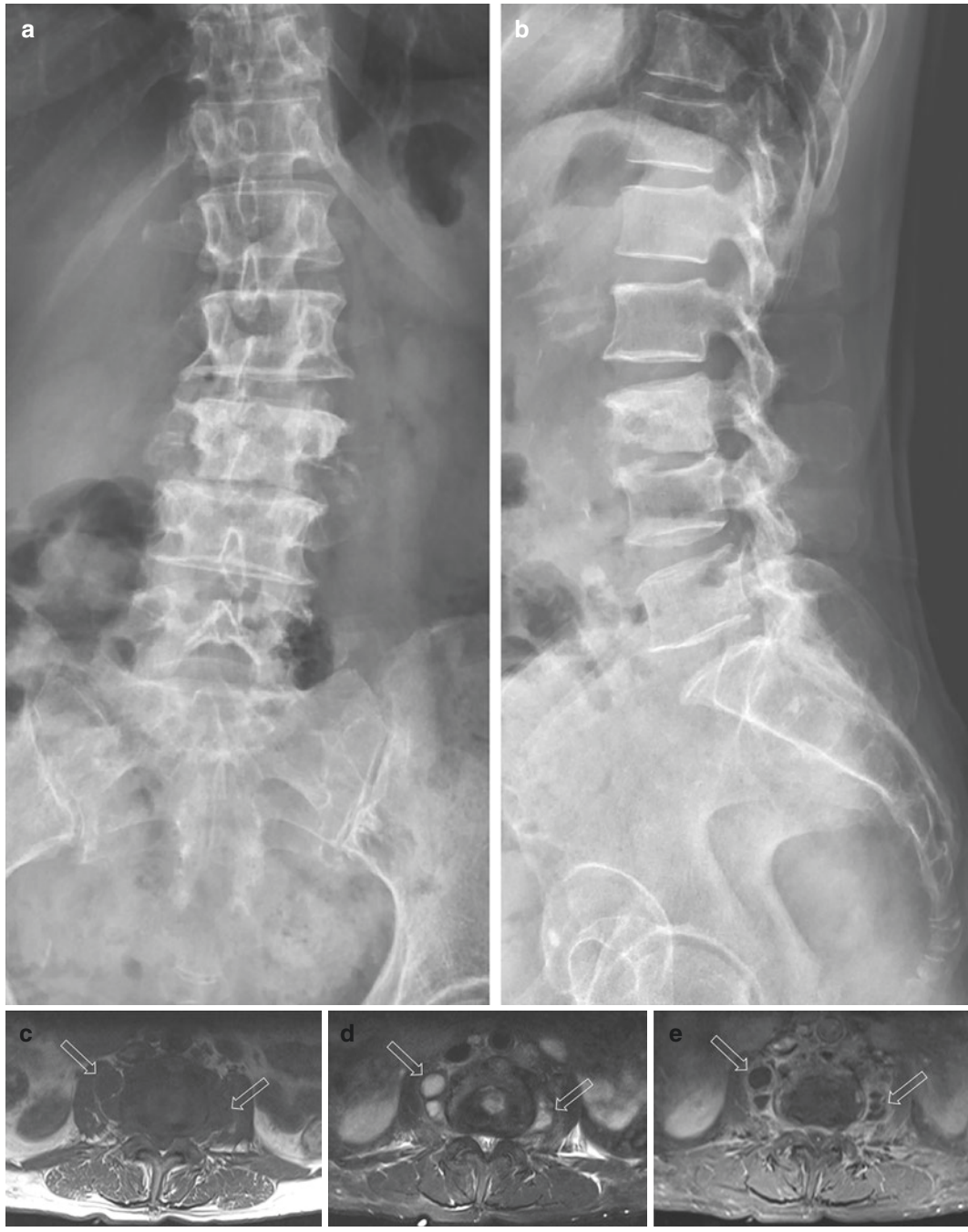

Fig. 5 A 70-year-old woman who presented with constitutional symptoms and back pain of insidious onset. (**a**) Frontal and (**b**) lateral radiographs of the lumbar spine show a reduction of the L3/L4 disk space with lateral vertebral subluxation. There is osteolysis with bone loss involving the anterior inferior aspect of the L3 vertebral body, with associated sclerotic change indicating a degree of chronicity. These features are consistent with spondylodiscitis and vertebral osteomyelitis and in keeping with the eventual diagnosis of tuberculous spondylitis. Axial (**c**) T1-W, (**d**) T2-W FS, and (**e**) contrast-enhanced FS T1-W MR images taken at the L3/4 level show bilateral psoas abscesses (open arrows). The abscesses have internal fluid signal intensity and well-defined enhancing margins. Tuberculous spondylitis has the propensity for large paraspinal abscess formation

of interest is kept in the center of the magnetic field (Van Geothem 2010). In our institution, we routinely perform all our MRI spine in the "head-in" position. This allows sagittal localizer images to be acquired (Fig. 6). Localizer images are important for proper counting of the vertebral bodies, detection of the transitional vertebra, and avoiding the mistake of the surgeon operating at the wrong vertebral level (Peh et al. 1999). Rarely, we may perform MRI of the spine employing the "feet-in" position for patients with claustrophobia who prefer their heads to be outside the MRI machine. Patient comfort is extremely important to reduce movement artifacts and achieve good image quality, with knee supports being useful. Surface marker placement is also useful to indicate the region of interest (Van Geothem 2010).

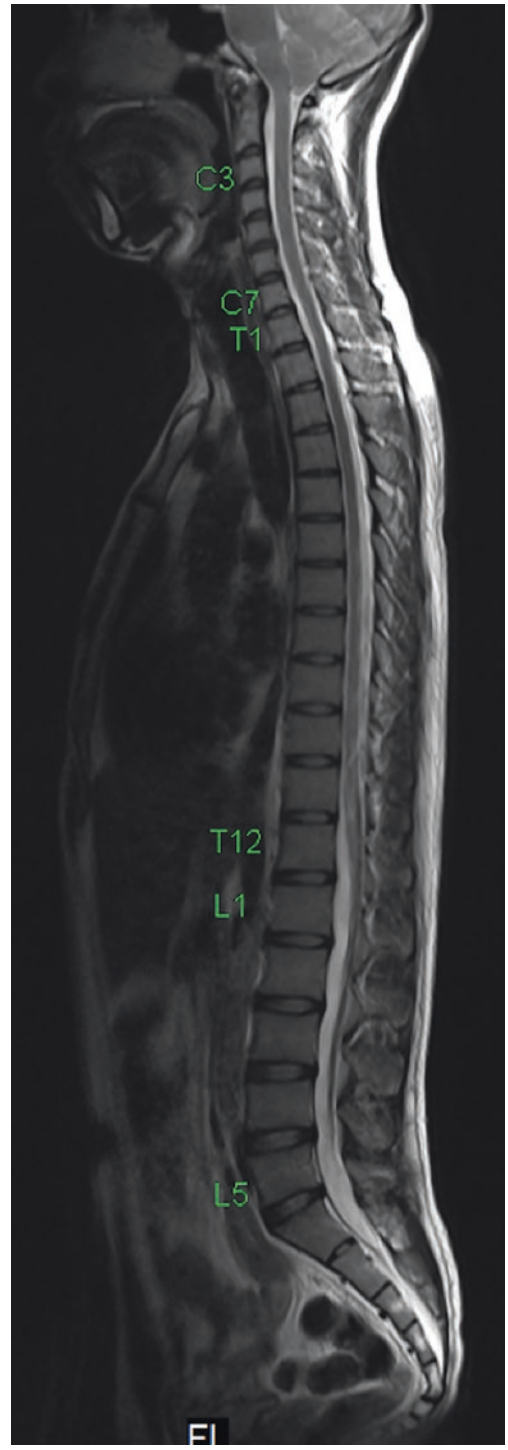

Fig. 6 Localizer sagittal FSE T2-W MR image covers the whole spine from the C1 vertebra down to the coccyx. The vertebral levels are labeled by counting from cranially to caudally. No transitional lumbosacral vertebral segment is identified in this patient

3.2 Coils

Coils play an important role in achieving the best possible image quality. For good image quality, radiofrequency (RF) coils must be able to convert the electromagnetic signals with minimal electrical resistive loss. To achieve this objective, surface coils are placed directly over to the anatomical region of interest to produce a high signal-to-noise ratio (SNR) and resolution. The trade-off is a small field of view (FOV). This limitation has been overcome by the advent of multi-coil technology. Phased array coils are designed carefully to combine many individual coils to allow large FOV image acquisition and still maintain good SNR (Asher et al. 2010). The coil system currently used in spine imaging is built into the table of the MRI machine, allowing imaging of multiple segments of the spine. For the cervical spine, there is an option to add an additional coil, with multi-segment attachment (Broderick 2012) (Fig. 7).

3.3 Pulse Sequences

3.3.1 T1-Weighted Sequence

The spin-echo (SE) T1-weighted (T1-W) sequence has a short repetition time (TR) and a

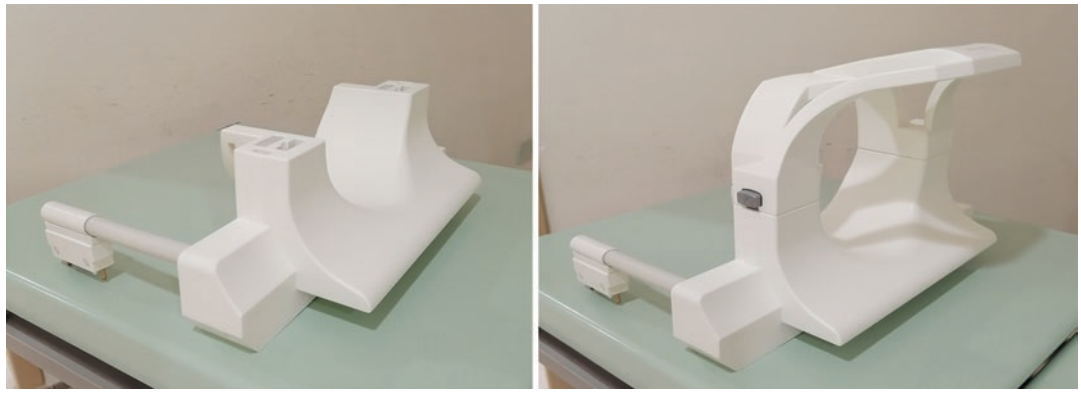

Fig. 7 Photographs of a neck matrix coil with two different segments that are routinely used in MRI of the cervical spine. It has a four-element design with four integrated preamplifiers. The anterior part is removable, while the posterior part usually stays on the table of MRI machine. It operates in an integrated fashion with the spine matrix coil for coverage of the anterior and posterior regions of the neck, with the aim of obtaining better image quality

short echo time (TE), typically with TR < 800 ms and TE < 30 ms (Helms 2009). It is useful for providing information about the anatomy of various spinal structures and to evaluate the bone marrow. The T1 signal hyperintensity of the fat in the bone marrow is contributed by the short T1 relaxation time and efficient spin-lattice relaxation from the hydrophobic carbon-hydrogen groups in the fat (Pooley 2005). As a result, by virtue of its high fat content, yellow bone marrow shows hyperintense signal relative to muscle and intervertebral disk, although not as high as that of the subcutaneous fat. Abnormal bone marrow in osteomyelitis is characterized by hypointense signal relative to the muscle and disk. It has been reported that at 1.5 T, finding of hypointense T1 signal of bone marrow has a high accuracy rate of approximately 94% (when more hypointense than muscle) and 98% (when more hypointense than intervertebral disk) (Carroll et al. 1997).

3.3.2 T2-Weighted Sequence

The T2-weighted (T2-W) sequence has a long TR and long TE, with TR > 2000 ms and TE > 60 ms (Helms 2009). It is a very useful sequence for evaluating normal fluid-containing structures (e.g., disk nucleus pulposus and CSF) and internal neural structures and to demonstrate the edema and hyperintense T2 signal in areas of pathology, e.g., hyperintense vertebral body marrow in osteomyelitis, abnormal fluid accumulated in the facet joints in septic arthritis, and areas of soft tissue hyperintensity in myositis and abscesses. These findings make T2-W sequences ideal for disease detection (Yeom et al. 2016). It is worthwhile to mention that while fat is expectedly hypointense on the conventional spin-echo (SE) T2-W sequence, it is hyperintense on the fast spin-echo (FSE) T2-W sequence. By virtue of being time-saving, FSE sequences are often currently used in routine MRI. Hence, fat suppression is usually applied to FSE T2-W MRI to differentiate between the abnormal signal from the background fat, particularly in patients with suspected spinal infection (Fig. 8).

3.3.3 Short Tau Inversion Recovery Sequence

The short TI inversion recovery (STIR) sequence has a TR > 2000 ms, TE > 30 ms, and TI of 120–150 ms (Helms 2009). It is a technique that suppresses the signal intensity of the fat, with the aim to increase the signal intensity difference between abnormal fluid and adjacent fat. Hence, the STIR sequence is extremely sensitive for the detection of abnormalities in the bone marrow or soft tissues (Helms 2009). The benefits and disadvantages of using STIR sequence as a fat suppression technique will be discussed in the subsequent subsection.

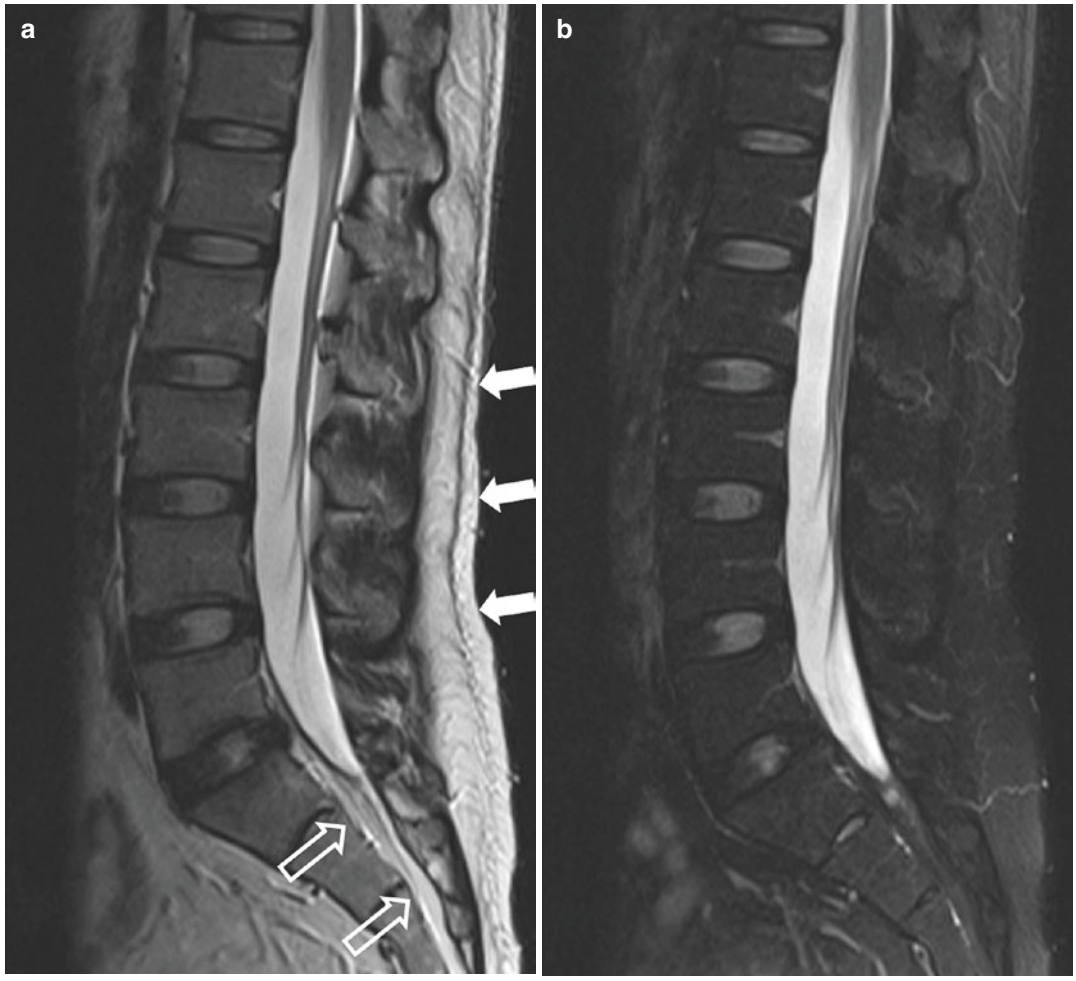

Fig. 8 Usefulness of fat suppression in fast spin-echo MR sequences. (**a**) Sagittal FSE T2-W MR image of the lumbar spine shows hyperintense signal of the subcutaneous fat (solid arrows) and epidural fat (open arrows). Fat is normally hyperintense on fast SE sequences. (**b**) Repeat sagittal FSE T2-W MR image, this time with fat suppression, shows complete signal suppression of fat-containing structures in these areas. The CSF within the thecal sac is distinctly seen, as would any abnormal signal due to a pathologic process within the subcutaneous fat plane or epidural space

3.3.4 Fat Suppression Technique

Two commonly used techniques to achieve fat suppression in MRI of the spine are frequency-selective (chemical) fat suppression and STIR sequences (Helms 2009). Fat suppression is useful to increase the *relative* signal intensity of pathological lesions compared to normal tissue. For example, on T1-W images, fat suppression can accentuate the relatively higher signal intensity of the proteinaceous fluids within an epidural abscess from the epidural fat and also allows better appreciation of abnormal epidural enhancement. On T2-W images, fat suppression nulls the normal bone marrow signal to accentuate the abnormal signal of the edematous bone marrow.

The frequency-selective (chemical) technique makes use of the frequency differences between the fat and water, which is about 210 Hz at 1.5 T, by applying a selective "spoiler" radiofrequency pulse to null the signal from the fat, with no significant effect on the nonlipid tissues (Gerdes et al. 2007). This technique is often applied in

FSE T2-W sequences. Nevertheless, this frequency-selective (chemical) technique has the inherent problem of inhomogeneous fat suppression. Failure of fat suppression is greatest when the fat-air interface is perpendicular to the static magnetic field, with a common site of this artifact being the posterior aspect of the neck (Peh and Chan 2001). It is also highly sensitive to the inhomogeneity of magnetic fields, especially due to the presence of metallic implants (Gerdes et al. 2007).

STIR sequences exploit the differences in the longitudinal relaxation between protons of the fat and water molecules. An inversion time (TI) is identified to null the signal generated by fat. A nonselective 180° RF pulse is applied, followed by a second 90° pulse applied at the TI, which represents the time the previously inverted longitudinal magnetization of fat crosses the null point (Helms 2009). This results in suppression of the fat signal, while preserving the signal of the water in the selected slices. Compared to the frequency-selective (chemical) technique, STIR is less susceptible to magnetic field inhomogeneity and can achieve more a homogeneous fat suppression. Thus, the STIR sequence is favored in the spine imaging protocol of patients with spinal implants at our institution to reduce susceptibility artifact as much as possible, though there is currently no way to completely eliminate it (Fig. 9). The STIR sequence is not used in contrast-enhanced MRI, as gadolinium, which has the similar relaxation properties to the fat protons, would be suppressed along with fat (Helms 2009).

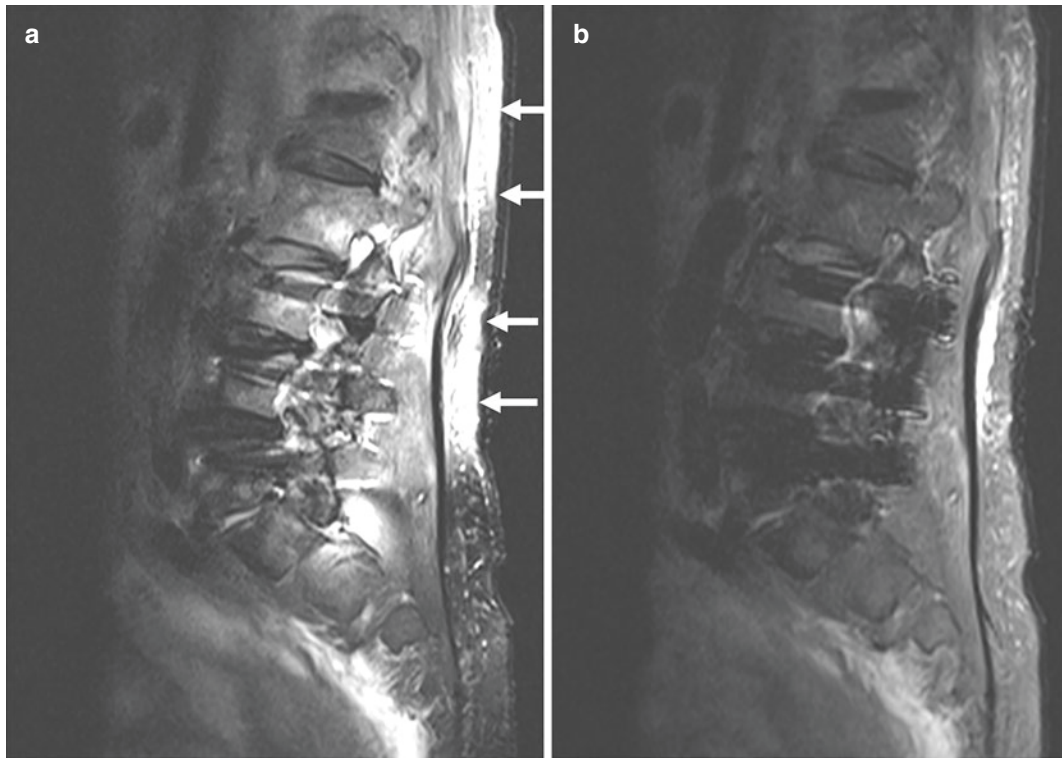

Fig. 9 Failure of fat suppression due to magnetic field inhomogeneity secondary to metallic susceptibility. (**a**) Sagittal FSE FS T2-W MR image of the lumbar spine shows the failure of fat suppression (arrows) due to metallic spinal implants at L3–L5 vertebral levels. (**b**) Repeat sagittal STIR MR image shows the marked improvement of fat suppression. Compared to the frequency-selective (chemical) technique, STIR is less susceptible to an inhomogeneous magnetic field. The STIR sequence is therefore preferred for patients with known metallic implants in the spine

3.4 Intravenous Gadolinium-Based Contrast Agent

Administering an intravenous (IV) gadolinium-based contrast agent is extremely useful in MRI of spinal infection, as it not only increases the sensitivity of the study but is also useful in establishing the extent of infection. It is easier to appreciate abnormal signal in the bone marrow (in osteomyelitis), intervertebral disk (in spondylodiscitis), facet joints (in septic arthritis), spinal cord (in myelitis), and paravertebral soft tissues (abscesses) when IV gadolinium-based contrast agent is administered (Diehn 2012). Contrast-enhanced MRI is also useful to differentiate a drainable abscess from non-drainable phlegmon, abscess from hematoma, abscess from necrotic tumor, and abscess from postoperative epidural scar (Shikhare et al. 2014).

3.5 Diffusion-Weighted Imaging

MRI findings in spinal infection may sometimes be nonspecific, especially in pyogenic and atypical infections, as well as in the postoperative spine (Kowalski et al. 2006). The use of diffusion-weighted imaging (DWI) has been very useful in MRI of the brain to distinguish a brain abscess from necrotic tumor (Lai et al. 2002). DWI is based on the random Brownian movement of water molecules within tissues. Apparent diffusion coefficient (ADC) is a measure of the magnitude of diffusion of water molecules within tissue and is commonly clinically calculated using MRI with DWI (Sener 2001). A higher ADC value indicates more mobile water molecules, while a low ADC value suggests a restricted movement of water molecules in the tissues (Mukherjee et al. 2008).

In challenging cases, DWI and ADC sequences are extremely useful to differentiate between vertebral osteomyelitis from Modic type 1 degenerative bone marrow changes, spondylodiscitis from degenerative disc disease, and epidural and paraspinal abscesses from CSF leak or postoperative seroma. For example, the ADC value of an infected bone marrow has been shown to be significantly higher than degenerated bone marrow attributed to bone edema and necrosis. In spondylodiscitis, the intervertebral disk typically shows high DWI signal, as opposed to desiccated disks in degenerative disk disease. In epidural and paraspinal abscesses, viscous pus collection with restricted water molecule movement often results in high DWI signals with corresponding low ADC values, allowing differentiation from the simple CSF leak and postoperative seroma. High DWI signal with high ADC value is also known as T2-shine through (Eastwood et al. 2002; Eguchi et al. 2011; Moritani et al. 2014).

A cut-off ADC value of less than $1250 \times 10–6$ mm^2/s has been found to be statistically significant to differentiate patients with positive microbiological sampling in suspected spinal infection. It has a sensitivity of 66%, specificity of 88%, positive predictive value of 95%, and negative predictive value of 41% and an accuracy of 70% (Dumont et al. 2019). DWI can also potentially complement the other sequences in MRI of spinal infection and may be a useful marker to assess for response post-antibiotics (Dumont et al. 2019).

3.6 MRI Protocols and Parameters

The MRI protocols and parameters of MRI of the cervical, thoracic, and lumbosacral spine used in our institution are summarized in Tables 2, 3, and 4. Images in sagittal and axial planes are acquired. The basic sequences are FSE T1-W and either FSE T2-W or STIR sequences, with the addition of axial gradient-echo T2*-W sequences in the cervical spine.

4 Disadvantages and Pitfalls of MRI

MRI has poorer sensitivity for detection of soft tissue gas (e.g., in gas-forming or necrotizing infection) and is inferior to CT in detecting early changes of cortical bone destruction. The magnetic field can pose various problems in patients with metallic implants and devices, such as tissue

Table 2 MRI of the cervical spine protocol

Sequence	Plane	TR (ms)	TE (ms)	Flip angle (°)	ETL	Slice thickness (mm)	Interslice gap (mm)	Matrix	FOV (mm)	BW (Hz/Px)	No. of Acq.
FSE T1-W	Sag	531	9.7	150	3	3	0.3	269 × 384	240 × 240	181	3
FRFSE T2-W	Sag	1600	98	150	19	3	0.3	269 × 384	240 × 240	191	2
STIR	Sag	4120	80	150	14	3	0.3	224 × 320	240 × 240	150	2
FSE T1-W	Ax	418	11	150	3	3	0.3	205 × 256	180 × 180	150	3
FSE T2-W FS	Ax	3160	78	150	13	3	0.3	179 × 256	180 × 180	150	2
GRE T2*-W	Ax	470	17	28	NA	3	0.3	70 × 320	180 × 180	150	2
FSE T1-W +c FS	Sag	416	9.6	150	3	3	0.3	205 × 256	240 × 240	181	2
FSE T1-W +c FS	Ax	628	12	150	3	3	0.3	205 × 256	180 × 180	150	2
FSE T1-W +c FS	Cor	416	9.6	150	3	3	0.3	205 × 256	240 × 240	181	2

FSE fast spin-echo, *FRFSE* fast recovery fast spin-echo, *FS* fat suppression, *T1-W* T1-weighted, *T2-W* T2-weighted, *STIR* short tau inversion recovery, *+c* post-contrast, *Sag* sagittal, *Ax* axial, *Cor* coronal, *TR* repetition time, *TE* echo time, *ETL* echo time length, *Matrix* (phase × frequency matrix), *FOV* field of view, *BW* bandwidth, *Hz/Px* Hertz per pixel, *Acq* acquisition

Table 3 MRI of the thoracic spine protocol

Sequence	Plane	TR (ms)	TE (ms)	Flip angle (°)	ETL	Slice thickness (mm)	Interslice gap (mm)	Matrix	FOV (mm)	BW (Hz/Px)	No. of Acq.
FSE T1-W	Sag	684	11	150	3	4	0.4	314 × 448	350 × 350	169	1
STIR	Sag	4730	76	150	16	4	0.4	269 × 384	350 × 350	161	2
FSE T1-W	Ax	462	8.7	150	3	5	0.5	224 × 320	200 × 200	180	2
FRFSE T2-W FS	Ax	2320	76	160	13	5	0.5	224 × 320	200 × 200	161	2
FSE T1-W +c FS	Sag	471	9.6	150	3	4	0.4	224 × 320	350 × 350	180	1
FSE T1-W +c FS	Ax	687	8.7	150	3	5	0.5	179 × 256	200 × 200	179	1
FSE T1-W +c FS	Cor	515	8.7	150	3	4	0.4	179 × 256	350 × 350	179	1

FSE fast spin-echo, *FRFSE* fast recovery fast spin-echo, *FS* fat suppression, *T1-W* T1-weighted, *T2-W* T2-weighted, *STIR* short tau inversion recovery, *+c* post-contrast, *Sag* sagittal, *Ax* axial, *Cor* coronal, *TR* repetition time, *TE* echo time, *ETL* echo time length, *Matrix* (phase × frequency matrix), *FOV* field of view, *BW* bandwidth, *Hz/Px* Hertz per pixel, *Acq* acquisition

Table 4 MRI of the lumbosacral spine protocol

Sequence type	Plane	TR (ms)	TE (ms)	Flip angle (°)	ETL	Slice thickness (mm)	Interslice gap (mm)	Matrix	FOV (mm)	BW (Hz/Px)	No. of Acq.
FSE T1-W	Sag	624	9.9	150	3	4	0.4	314 × 448	330 × 330	180	2
FSE T2-W FS	Sag	4320	96	150	14	4	0.4	314 × 448	330 × 330	90	1
FSE T1-W	Ax	462	8.7	150	3	4	0.4	224 × 320	200 × 200	180	2
FRFSE T2-W FS	Ax	2329	76	160	13	4	0.4	224 × 320	200 × 200	161	2
FSE T1-W +c FS	Sag	480	9.9	150	3	4	0.4	314 × 448	330 × 330	180	2
FSE T1-W +c FS	Ax	573	8.7	150	3	4	0.4	224 × 320	200 × 200	180	2
FSE T1-W +c FS	Cor	480	9.9	150	3	4	0.4	314 × 448	330 × 330	180	2

FSE fast spin-echo, *FRFSE* fast recovery fast spin-echo, *FS* fat suppression, *T1-W* T1-weighted, *T2-W* T2-weighted, *STIR* short tau inversion recovery, *+c* post-contrast, *Sag* sagittal, *Ax* axial, *Cor* coronal, *TR* repetition time, *TE* echo time, *ETL* echo time length, *Matrix* (phase × frequency matrix), *FOV* field of view, *BW* bandwidth, *Hz/Px* Hertz per pixel, *Acq* acquisition

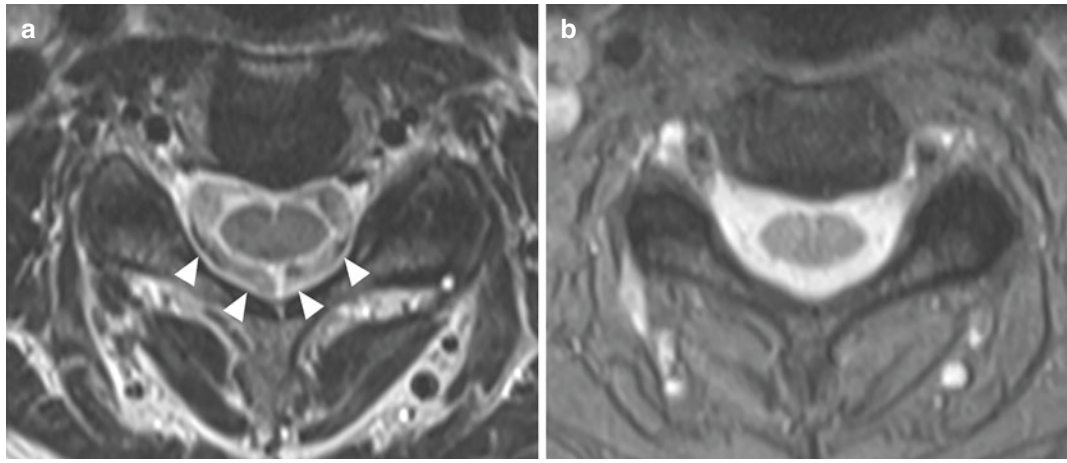

Fig. 10 CSF flow artifact. (**a**) Axial FSE T2-W MR image of the cervical spine shows areas of signal void in the subarachnoid space (arrowheads) around the cervical cord, mimicking an intradural lesion. (**b**) Repeat axial GRE T2*-W MR image shows that this area is normal and the previously seen pseudo-lesion was a CSF flow artifact

heating in spinal fixation, pacemaker malfunction, and migration of aneurysm clips and hearing aids (Tsai et al. 2015). Interpreting MRI of the postoperative spine can be challenging, as the postoperative spine may normally produce disk and end-plate signal changes and enhancement within the first 6 months after surgery. MRI may therefore not reliably differentiate expected postoperative changes from infection. However, there are a few useful tips that can be used to overcome this problem. For example, post-discectomy typically shows two parallel thin bands of enhancement, compared to the more amorphous pattern of enhancement seen in infection. The absence of enhancement or marrow edema adjacent to the vertebral end plate or disk makes infection very unlikely. If paravertebral collections are present, they are highly specific for spinal infection (Yeom et al. 2016).

Postoperative fluid pockets and hematomas may be encountered in the early postoperative phase, while pseudo-meningocele may be seen later on during follow-up MRI. These simple postoperative fluid pockets and hematomas usually resolve spontaneously. Pseudo-meningocele is usually managed conservatively. It is important to distinguish these normal postoperative changes from abscesses. Though hematomas may have variable signal intensities on T1-W and T2-W images, they commonly show magnetic susceptibility on gradient-echo images. Pseudo-meningocele occurs secondary to a tear in the dura, thus it has a signal intensity similar to CSF, enabling the correct diagnosis to be made. In contrast to simple postoperative collections which usually has a similar signal to fluid with an associated thin peripheral enhancing rim, abscesses are often seen as heterogeneous collections due to their proteinaceous contents with a thick irregular rim of enhancement (Shikhare et al. 2014).

Magnetic susceptibility artifacts can compromise the image quality and diagnostic capability of MRI, especially in the assessment of the spinal canal. This can be overcome by utilizing fast spin-echo rather than gradient-echo sequences, scanning the patient in a 1.5 T instead of a 3.0 T MRI machine, switching the frequency-encoding gradient parallel to the long axis of the implants, and exploring the use of newer techniques such as iterative decomposition of water and fat with echo asymmetry and least-squares estimation (IDEAL) (Peh and Chan 2001; Shikhare et al. 2014). Motion artifacts are not uncommon in children and elderly patients who may be in pain or are anxious. This problem can be overcome with efforts at patient reassurance and immobilization, adequate analgesia, and sometimes, the use of sedation or even general anesthesia. Patients with claustrophobia may benefit from earplugs and MRI-compatible headphones playing music, in order to achieve

the best user experience (Peh and Chan 2001; Tsai et al. 2015).

CSF flow artifact is another common artifact in the spine. It is also known as "ghost" artifact. The CSF flow rate is higher in the cervical and thoracic spines than in the lumbosacral spine. Thus, the turbulent flow in the CSF may cause significant dorsal dephasing artifacts, with phase incoherence contributing to signal loss. This artifact is seen as serpentine areas of the signal void, sometimes mimicking intradural lesions (Fig. 10). This problem can overcome by cross-referencing with another imaging plane, comparison with other sequences with short TE, or can be eliminated using a gradient-echo sequence (Peh and Chan 2001; Shikhare et al. 2014) (Fig. 10).

Truncation (Gibb) artifact can appear as alternate parallel bright and dark striations in the spine, more apparent at tissue interfaces whereby there is a marked abrupt change in the signal intensities (Fig. 11). This artifact can simulate a

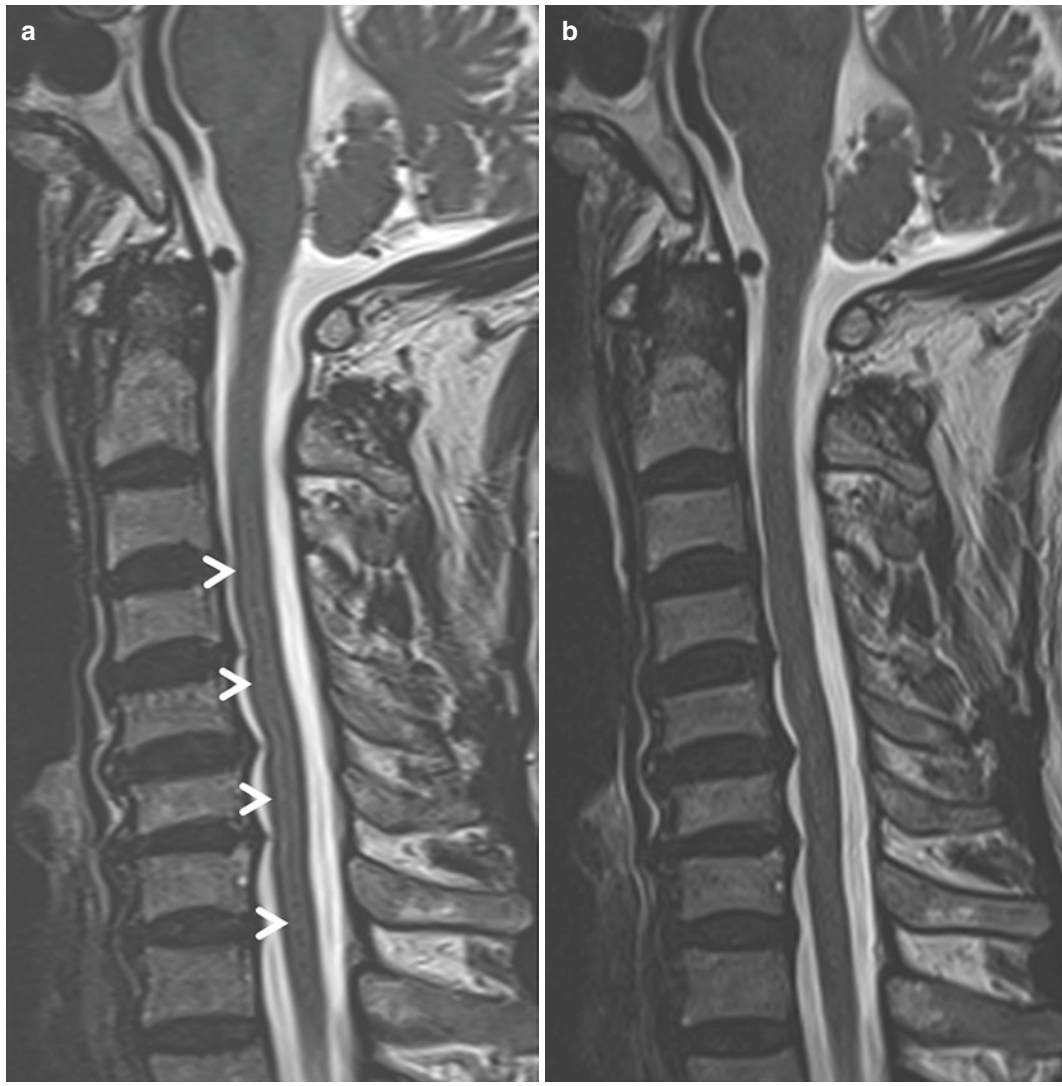

Fig. 11 Truncation (Gibb) artifact. (**a**) Sagittal FSE T2-W MR image of the cervical spine shows vertically oriented hyperintense linear lines in the cervical cord (arrowheads) from C3 to C7 vertebral levels. (**b**) Repeat sagittal FSE T2-W MR image, this time increasing the matrix size along the phase-encoding direction, has eliminated with previously seen truncation artifact. The spinal cord is normal

syrinx in the spinal cord, intramedullary lesion, cord edema, or cord atrophy; hence, failure to recognize this artifact may significantly change the patient's management. It occurs as a result of under-sampling in the phase-encoding direction. This problem can be reduced by increasing the matrix size along the phase-encoding direction, decreasing the field of view (FOV), or switching between the phase- and frequency-encoding directions (Peh and Chan 2001) (Fig. 11).

Nephrogenic systemic fibrosis (NSF) is a rare systemic fibrotic condition, which was first described in 2000 (Cowper et al. 2000). It occurs in patients with existing renal impairment or patients on dialysis who received IV gadolinium-based contrast agent. In patients with normal renal function, virtually all gadolinium-based contrast agents are excreted from the body within 3 days. However, in renal-impaired patients, the prolonged excretory half-life of the contrast agent increases the chance of deposition of the freely dissociated gadolinium ions in the body. Patients who suffer from NSF can present with skin hardening and contracture, and the disease can also involve muscles such as the diaphragm, esophagus, and skeletal muscles (Kaewlai and Abujudeh 2012).

5 Conclusion

Spinal infection can result in devastating morbidity and mortality, if the diagnosis and treatment are delayed. MRI is currently the imaging modality of choice in the investigation of spinal infection. Understanding the technique, protocol, pitfalls, and limitations, as well as practical considerations of MRI, is extremely helpful in the diagnosis and management of spinal infection.

Acknowledgments We would like to thank Mr. Tan Tee Meng, senior principal radiographer, for his input to Subsection 3.2 on MRI coils and MRI radiographers Ms. Tay Ming Wei, Mr. Lin Chih-Ying, Mr. Huang Tsung-Hsiang, Mr. Archel Javier, and Ms. Joyce Tan Mui Sin for their assistance in acquiring some of the images.

References

Asher KA, Bangerter NK, Watkins RD et al (2010) Radiofrequency coils for musculoskeletal magnetic resonance imaging. Top Magn Reson Imaging 21:315–323

Broderick DH (2012) Spine. In: Berquist TH (ed) MRI of the musculoskeletal system, 6th edn. Lippincott Williams & Wilkins, Philadelphia, pp 124–203

Carroll KW, Feller JF, Tirman PF (1997) Useful internal standards for distinguishing infiltrative marrow pathology from hematopoietic marrow at MRI. J Magn Reson Imaging 7:394–398

Cheung WY, Luk KDK (2012) Pyogenic spondylitis. Int Orthop 36:397–404

Chihara S, Segreti J (2010) Osteomyelitis. Dis Mon 56:5–31

Cowper SE, Robin HS, Steinberg SM et al (2000) Scleromyxoedema-like cutaneous diseases in renal-dialysis patients. Lancet 356:1000–1001

Diehn FE (2012) Imaging of spine infection. Radiol Clin North Am 50:777–798

Dumont RA, Keen NN, Bloomer CW et al (2019) Clinical utility of diffusion-weighted imaging in spinal infections. Clin Neuroradiol 29:515–522

Eastwood JD, Vollmer RT, Provenzale JM (2002) Diffusion-weighted imaging in a patient with vertebral and epidural abscesses. AJNR Am J Neuroradiol 23:496–498

Eguchi Y, Ohtori S, Yamashita M et al (2011) Diffusion magnetic resonance imaging to differentiate degenerative from infectious endplate abnormalities in the lumbar spine. Spine 36:E198–E202

Gerdes CM, Kijowski R, Reeder SB (2007) IDEAL imaging of the musculoskeletal system: robust water fat separation for uniform fat suppression, marrow evaluation, and cartilage imaging. AJR Am J Roentgenol 189:W284–W291

Hanrahan CJ, Shah LM (2011) MRI of spinal bone marrow: part 2, T1-weighted imaging-based differential diagnosis. AJR Am J Roentgenol 197:1309–1321

Helms C (2009) Basic principles of musculoskeletal MRI. In: Helms C, Major NM, Anderson MW et al (eds) Musculoskeletal MRI, 2nd edn. Saunders Elsevier, Philadelphia, pp 1–18

Hong SH, Choi JY, Lee JW et al (2009) MR imaging assessment of the spine: infection or an imitation? Radiographics 29:599–612

Kaewlai R, Abujudeh H (2012) Nephrogenic systemic fibrosis. AJR Am J Roentgenol 199:W17–W23

Kowalski TJ, Berbari EF, Huddleston PM et al (2006) Do follow-up imaging examinations provide useful prognostic information in patients with spine infection? Clin Infect Dis 43:172–179

Lai PH, Ho JT, Chen WL et al (2002) Brain abscess and necrotic brain tumor: discrimination with proton MR

spectroscopy and diffusion-weighted imaging. AJNR Am J Neuroradiol 23:1369–1377

Lener S, Hartmann S, Barbagallo GMV et al (2018) Management of spinal infection: a review of the literature. Acta Neurochir 160:487–496

Leone A, Dell'Atti C, Magarelli N et al (2012) Imaging of spondylodiscitis. Eur Rev Med Pharmacol Sci 2:8–19

Modic MT, Feiglin DH, Piraino DW et al (1985) Vertebral osteomyelitis: assessment using MR. Radiology 157:157–166

Moritani T, Kim J, Capizzano AA et al (2014) Pyogenic and non-pyogenic spinal infections: emphasis on diffusion-weighted imaging for the detection of abscesses and pus collections. Br J Radiol 87:20140011

Mukherjee P, Berman JI, Chung SW et al (2008) Diffusion tensor MR imaging and fiber tractography: theoretic underpinnings. AJNR Am J Neuroradiol 29:632–641

Peh WCG (2006) CT-guided percutaneous biopsy of spinal lesions. Biomed Imaging Interv J 2:1–12

Peh WCG, Chan JHM (2001) MR artifacts in musculoskeletal imaging—identification and correction. Skeletal Radiol 30:179–191

Peh WCG, Siu TH, Chan JHM (1999) Determining the lumbar vertebral segments on magnetic resonance imaging. Spine 24:1852–1855

Pineda C, Pena A, Espinosa R et al (2011) Imaging of osteomyelitis: the key is in the combination. Int J Clin Rheumatol 6:25–33

Pooley RA (2005) Fundamental physics of MR imaging. Radiographics 25:1087–1099

Ruiz A, Post MJ, Sklar EM et al (2000) MR imaging of infections of the cervical spine. Magn Reson Imaging Clin N Am 9:561–580

Sener RN (2001) Diffusion MRI: apparent diffusion coefficient (ADC) values in the normal brain and a classification of brain disorders based on ADC values. Comput Med Imaging Graph 25:299–326

Shikhare SN, Peh WCG (2019) Pyogenic spondylodiscitis. In: Taljanovic MS, Omar IM, Hoover KB, Chadaz TS (eds) Musculoskeletal imaging, vol 2. Oxford University Press, Oxford, pp 87–90

Shikhare SN, Singh DS, Peh WCG (2014) Variants and pitfalls in MR imaging of the spine. Semin Musculoskelet Radiol 18:23–35

Tsai LL, Grant AK, Mortele KJ et al (2015) A practical guide to MR imaging safety: what radiologists need to know. Radiographics 35:1722–1737

Tyrrell PNM, Cassar-Pullicino VN, McCall IW (1999) Spinal infection. Eur Radiol 9:1066–1077

Van Geothem JWM (2010) Magnetic resonance imaging of the spine. In: Reimer P, Parizel PM, Meaney JFM et al (eds) Clinical MR imaging, 2nd edn. Springer, Berlin, Heidelberg, New York, pp 147–172

Yeom JA, Lee IS, Suh HB et al (2016) Magnetic resonance imaging findings of early spondylodiscitis: interpretive challenges and atypical findings. Korean J Radiol 17:565–680

Nuclear Medicine Imaging of Spinal Infection

Anbalagan Kannivelu, Aaron K. T. Tong, Kelvin S. H. Loke, and David C. E. Ng

Contents

Abstract

Spinal infection can be challenging to diagnose accurately, as symptoms can be insidious and nonspecific. Advanced radiological imaging procedures can be very useful to aid diagnosis. Nuclear medicine imaging can provide significant information, in addition to more conventional imaging techniques such as radiography and MRI. Nuclear medicine imaging (SPECT and PET) have shown high sensitivity and accuracy with regard to spinal

A. Kannivelu (✉)
Department of Diagnostic Radiology, Khoo Teck Puat Hospital, Singapore, Republic of Singapore
e-mail: kannivelu.anbalagan@ktph.com.sg

A. K. T. Tong · K. S. H. Loke · D. C. E. Ng
Department of Nuclear Medicine and Molecular Imaging, Singapore General Hospital, Singapore, Republic of Singapore
e-mail: aaron.tong.k.t@singhealth.com.sg; kelvin.loke.s.h@singhealth.com.sg; david.ng.c.e@singhealth.com.sg

© The Author(s), under exclusive license to Springer Nature Switzerland AG 2021, corrected publication 2021

M. F. Ladeb, W. C. G. Peh (eds.), *Imaging of Spinal Infection*,
Medical Radiology Diagnostic Imaging, https://doi.org/10.1007/978-3-030-70459-9_5

infection diagnosis, especially when used in combination with conventional radiological investigations such as CT and MRI. By providing additional functional information, nuclear medicine imaging helps to identify possible sites for biopsy, monitor treatment responses, and guide the duration of antimicrobial treatment. Expert consensus guidelines have been published, addressing the use and implementation of nuclear medicine imaging techniques in spinal infection.

Abbreviations

[^{18}F] FDG	Fluorine-18 2′-deoxy-2-fluoro-D-glucose
^{67}Ga	Gallium-67
^{99m}Tc	Technetium-99m
CT	Computed tomography
MRI	Magnetic resonance imaging
PET	Positron emission tomography
SPECT	Single photon emission computed tomography

1 Introduction

Spinal infection includes vertebral osteomyelitis, discitis, and spondylodiscitis and may also involve the posterior elements, epidural space, and paraspinal soft tissues. The usual routes of infections are hematogeneous spread, direct inoculation from interventional procedures or penetrating trauma, and extension from contiguous infection (Raghavan et al. 2018). The majority of spinal infection are pyogenic in origin, most commonly caused by *Staphylococcus aureus* (60%), followed by *Enterobacter* species (30%), and less commonly by non-pyogenic agents such *Mycobacterium tuberculosis*, *Brucella*, fungi, and parasites. Disease involvement is mostly single spinal segment (65%), followed by multilevel contiguous (20%), and noncontiguous infection (10%) (Prodi et al. 2016; Raghavan et al. 2018). Clinical features such as back pain and variable presence of fever are generally nonspecific, and manifestations of neurological deficits are present in only a minority of patients. Therefore, spinal infection can be confused with degenerative process, leading to delayed diagnosis and significant morbidity and mortality (Mylona et al. 2009).

Laboratory findings also vary, depending on the grade, causative agent, the type of spinal infection, and associated pathology. Elevation of erythrocyte sedimentation rate (ESR) is mostly consistent, and white blood cell count and C-reactive protein (CRP) plasma levels are variable. The most definitive diagnosis is identification of the pathogen from biopsy of the bone lesion or the wound, by histopathological analysis or indirectly from blood cultures. As the biopsy specimens and blood cultures can remain negative, noninvasive imaging becomes paramount in diagnosis and assessing response to treatment of spinal infection (Gemmel et al. 2006).

Among the morphological imaging techniques, radiographs are usually the first imaging modality performed, despite their low sensitivity and specificity. Signs are not usually seen radiographically till the bone destruction exceeds 30% and until 2–8 weeks after the initial symptoms (Khoo et al. 2003). Computed tomography (CT) is the best modality for detection of bony abnormalities and detects small areas of destruction earlier than radiographs. Currently, CT is mostly used for percutaneous needle biopsy and percutaneous drainage of abscesses (Lazzeri et al. 2019). Magnetic resonance imaging (MRI) is the reference standard for imaging of spinal infection because of its high sensitivity, specificity, and accuracy. Other advantages are its high-contrast resolution, multiplanar imaging capability, high sensitivity for soft tissue and bone marrow abnormalities, and absence of ionizing radiation. Some of the disadvantages of MRI are overestimation of infected tissue, its inherent limitations in the postoperative setting, and difficulty in differentiating reparative process and therapy failure. Consequently, radionuclide or functional imaging studies are often performed to increase diagnostic accuracy, particularly in postsurgical infections or to complement equivocal MRI findings (Hong et al. 2009; Ohtori et al. 2010; Seifen et al. 2012; Saha et al. 2013).

2 Conventional Nuclear Medicine

Single-photon emitting radiopharmaceuticals used for musculoskeletal infections are labeled diphosphonates (such as Technetium-99m methylene diphosphonate/hydroxymethylene diphosphonate [^{99m}Tc MDP/HDP]), ^{67}Ga citrate, labeled autologous leukocytes and novel radiotracers. Individual centers use different radiotracers, depending upon their availability, technical capability, and their own experience and expertise. Mechanisms of accumulation of these tracers at the site of infection are different (Thang et al. 2014).

2.1 Bone Scintigraphy

^{99m}Tc-labeled diphosphonate bone scintigraphy is widely available worldwide and easily performed. These radiopharmaceuticals bind to the inorganic mineral hydroxyapatite crystalline matrix of the bone. The uptake depends on multiple factors including blood supply, capillary permeability, quantity of mineralized bone, and rate of bone turnover. For clinical suspicion of osteomyelitis, triphasic bone scan is routinely performed in angiographic, blood pool, and delayed bone phases. Soft tissue infection manifests as increased radionuclide accumulation in the angiographic and blood pool phases, with no increased bony tracer activity in the delayed phase. Osteomyelitis shows increased tracer activity in all the three phases due to focal hyperperfusion, hyperemia, and increased bony uptake (Thang et al. 2014; Raghavan et al. 2018).

Bone scintigraphy is sensitive in diagnosing osteomyelitis, but the specificity decreases in the settings of pre-existing conditions such as degenerative changes, fractures, and prosthesis. A meta-analysis of 30 original articles published between 1984 and 2004 regarding the use of different types of radionuclide imaging of spinal infection showed that bone scans had a sensitivity of 81.4% and specificity of 40.7% (Prandini et al. 2006) (Fig. 1). In a prospective study conducted in 30 patients who had vertebral osteomyelitis, the sensitivity of the bone scintigraphy was reported to be 86%, but the target-to-background ratio did not correlate with histological grade and severity of the osteomyelitis. The triphasic bone scan was positive with severe infection but not in individuals with mild or moderate infection (Gratz et al. 2000).

In a retrospective study conducted in 22 patients, planar imaging was found to be 73% sensitive, 31% specific, and 50% accurate for diagnosing infection, and triphasic bone scan improved the specificity to 92% and diagnostic accuracy to 67% (Love et al. 2000). Due to its specific bone affinity, bone scintigraphy is of limited use in the evaluation of associated paraspinal infection in spondylodiscitis. Lisbona et al. (1993) retrospectively reviewed bone scintigraphy in 21 patients with infectious spondylitis (14 nontuberculous and 6 tuberculous). The scan was abnormal in 16 of 17 sites of nontuberculous infection and 6 of 9 sites of tuberculous infection of vertebrae, but none of the 8 paraspinal infections (6 nontuberculous and 2 tuberculous) was detected (Lisbona et al. 1993; Gemmel et al. 2006).

2.2 Gallium-67 (^{67}Ga) Citrate Scintigraphy

^{67}Ga citrate was one of the preferred radiotracers for musculoskeletal infections from the early 1970s till the mid-1980s. Several mechanisms have been proposed for the increased uptake of ^{67}Ga citrate at the sites of infection, namely, (1) about 90% of circulating tracer is bound to transferrin and because of increased blood flow and vascular permeability; it is delivered and accumulated more in the sites of infection; (2) it dissociates from transferrin and binds to lactoferrin which is present in high concentrations at the infection sites; and (3) direct bacterial uptake through siderophores and leukocyte transport. Imaging is usually delayed, performed from 18 to 72 h after injection. The main disadvantages are poor image quality compared to ^{99m}Tc MDP, excretion through the gastrointestinal tract obscuring the infection sites in the abdominopelvic region (requiring the use of laxatives prior to imaging), higher radiation burden,

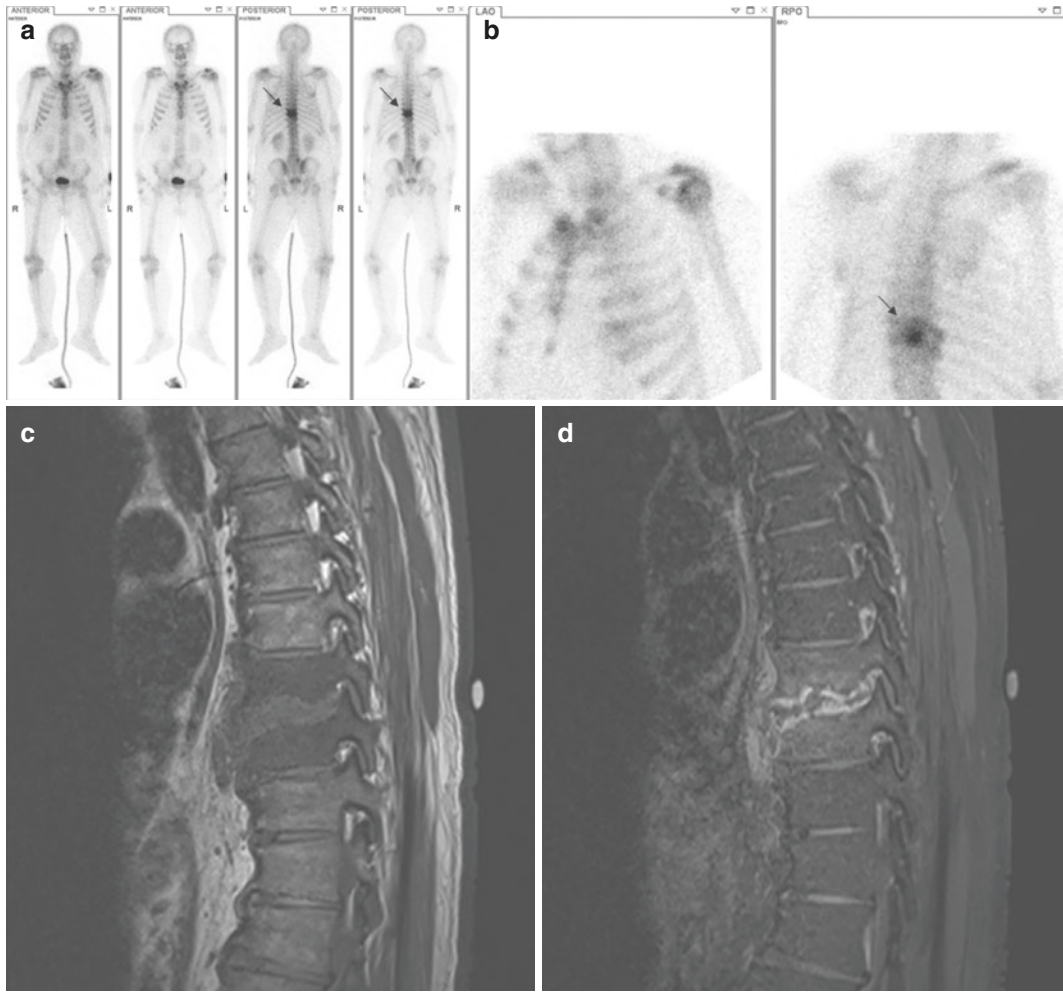

Fig. 1 Whole-body ^{99m}Tc MDP bone scan shows (**a**) intense tracer uptake at T8/T9 vertebrae (black arrows) which is better seen in the (**b**) local views. These findings correlated with spondylodiscitis seen on MRI. Sagittal (**c**) T1-W MR image shows hypointense vertebral marrow signal, and (**d**) contrast-enhanced FS T1-W MR image shows corresponding enhancement pattern typical of T8/T9 infective spondylodiscitis

and nonspecificity for infection versus inflammation (Gemmel et al. 2006; Thang et al. 2014; Raghavan et al. 2018; Lazzeri et al. 2019).

Despite its shortcomings, ^{67}Ga citrate scintigraphy is more useful than bone scintigraphy in the diagnosis of spinal infection due to its high specificity, even though their sensitivity is comparable (Fig. 2). In a retrospective study of 21 patients with infectious spondylitis involving 26 sites of infection, Lisbona et al. (1993) reported that ^{67}Ga citrate scintigraphy identified all 17 sites of nontuberculous infection and 9 sites of tuberculous infection and disclosed 6 sites of paraspinal infection, with the detection rate better than that of bone scintigraphy. Gratz et al. (2000) reported sensitivity, specificity, and diagnostic accuracy of 73%, 61%, and 80%, respectively, for ^{67}Ga planar and SPECT/CT imaging, in a prospective study of 30 patients with suspected diagnosis of spondylodiscitis. Love et al. (2000) retrospectively reviewed the results of ^{67}Ga imaging performed on 22 patients with suspected spondylodiscitis and showed that planar ^{67}Ga imaging had sensitivity, specificity, and accuracy of 82%, 77%, and 79%, respectively, which is better than bone scintigraphy.

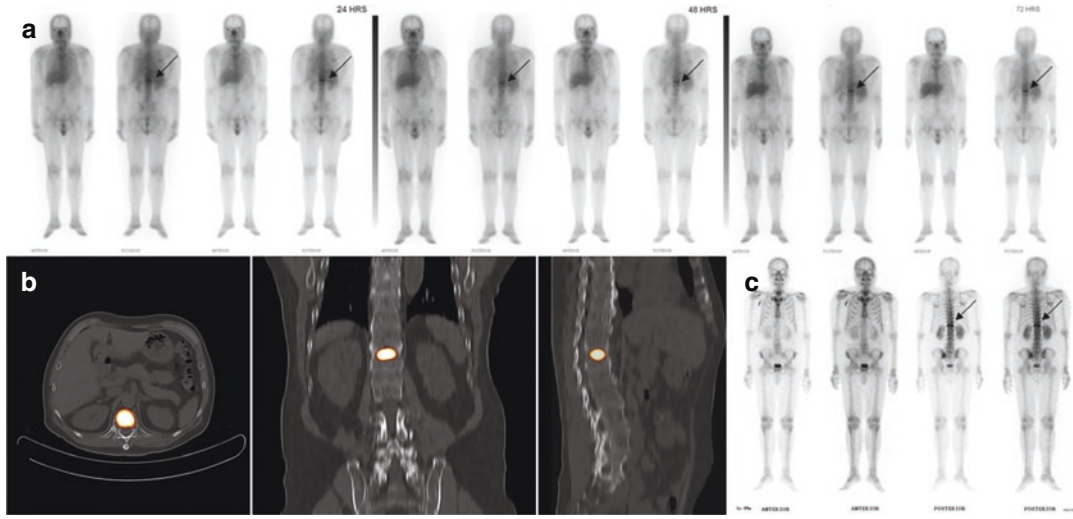

Fig. 2 (**a**) Gallium-67 citrate whole-body images show persistent tracer uptake at the T12 vertebra (black arrows). (**b**) SPECT/CT images localize the intense tracer activity to T12 vertebral body nearer to the upper end plate, suspicious for spondylodiscitis. (**c**) Correlative whole-body ^{99m}Tc MDP bone scan also shows congruent increased tracer uptake at the T11/T12 vertebral junction (black arrows) which is compatible with spondylodiscitis

A combination of bone scintigraphy and ^{67}Ga imaging can be done to increase the diagnostic accuracy, especially in the patients having post-surgical infections and to complement doubtful MRI findings. When performed together with bone scintigraphy, ^{67}Ga imaging improves the specificity, may detect the infection site earlier, and identifies the soft tissue infections which are otherwise undetected (Love and Palestro 2016; Lazzeri et al. 2019). In a prospective study conducted in 34 patients, combined bone scintigraphy and ^{67}Ga imaging were correctly interpreted as positive (true-positive) for spondylitis in 14 of 18 patients and correctly interpreted as negative (true-negative) in 13 of 16 patients. The sensitivity and specificity of the combined imaging were 78% and 81%, respectively, with an overall accuracy of 79%. If the equivocal pattern was considered positive, the sensitivity raised to 100%, but the specificity dropped to 50% (Fuster et al. 2012). Conversely, a retrospective study conducted by Love et al. (2000) concluded that ^{67}Ga SPECT was sufficient to diagnose spondylodiscitis, and bone scintigraphy was not necessary, as the results of combined bone scintigraphy, ^{67}Ga SPECT, and ^{67}Ga SPECT were identical with 91% sensitivity, 92% specificity, and 92% accuracy.

2.3 Radiolabeled Leukocyte Imaging

Labeling of autologous white blood cells (WBC) can be performed with Indium-111 (^{111}In) and Technetium-99m hexamethylpropylene amine oxime (^{99m}Tc HMPAO), with the half-life of Indium-111 being longer than that of Technetium-99m. Labeled leukocytes accumulate at the site of infection as part of the inflammatory process. The uptake depends upon intact chemotaxis, number and types of cells labeled, cellular response, and initiation of antimicrobial therapy, with the scan being most sensitive for detecting acute neutrophil-mediated infections. A combination with ^{99m}Tc sulfur colloid marrow imaging is useful to improve the diagnostic accuracy, since the physiological uptake of leukocytes by the bone marrow may complicate the interpretation of the study (Thang et al. 2014; Raghavan et al. 2018) (Fig. 3).

Unfortunately, radiolabeled leukocyte imaging is not very useful in diagnosing spondylodiscitis. In about 50% of the patients, leukocyte scintigraphy fails to detect vertebral osteomyelitis, and the site of infection appears often "cold" due to decreased or absent activity (Palestro et al.

1991). The explanations for this photopenia are not clearly known, and suggested probable causes are occlusion of the microcirculation of the involved bone, infection-induced death of reticulo-endothelial cells and normal marrow uptake by the viable bone. Patients who are symptomatic for less than 1 month usually show increased tracer uptake, while patients who are symptomatic for more than a month demonstrate decreased tracer uptake. Besides, several noninfectious conditions, such as treated spondylodiscitis, tumor, infection, compression fracture, hemangioma, and Paget disease, may also present with photopenia. This limitation of radiolabeled leukocyte imaging for spinal infection has also been reported with anti-granulocyte antibody imaging (Palestro et al. 1991; Gemmel et al. 2006; Palestro and Love 2007; Raghavan et al. 2018).

2.4 Other Types of Radiotracers

2.4.1 ^{99m}Tc Ciprofloxacin (Infection)

Ciprofloxacin is a fluoroquinolone, and its activity is mediated by inactivation of bacterial DNA gyrase and topoisomerase IV. ^{99m}Tc ciprofloxacin is the radiolabeled antibiotic developed for the diagnosis of infection, based on the fact that it would be incorporated and metabolized by bacteria at the site of infection. In a study conducted in 48 patients with suspected spondylodiscitis, planar and SPECT imaging was performed after injection of ^{99m}Tc ciprofloxacin. A relatively high number of false-positive results were reported in that study, with an explanation being that the patients had undergone surgery recently and had spinal implants at the time of scanning. Subsequent investigations revealed poor specificity and the enthusiasm for radiolabeled antibiotics subsequently faded (Yapar et al. 2001; De Winter et al. 2004; Palestro 2016).

2.4.2 Streptavidin/^{111}In-Biotin

Biotin or vitamin B7 plays a key role in glucose metabolism, and it is also a bacterial growth factor. Streptavidin, a 65-kDa protein, accumulates at the site of infection due to increased capillary permeability. ^{111}In-biotin, given subsequently, binds to streptavidin at the site of infection due to the abovementioned factors (Lazzeri et al. 1999). Lazzeri et al. (2004) evaluated this tracer complex in 55 consecutive patients with suspected spondylodiscitis in a multicenter study and

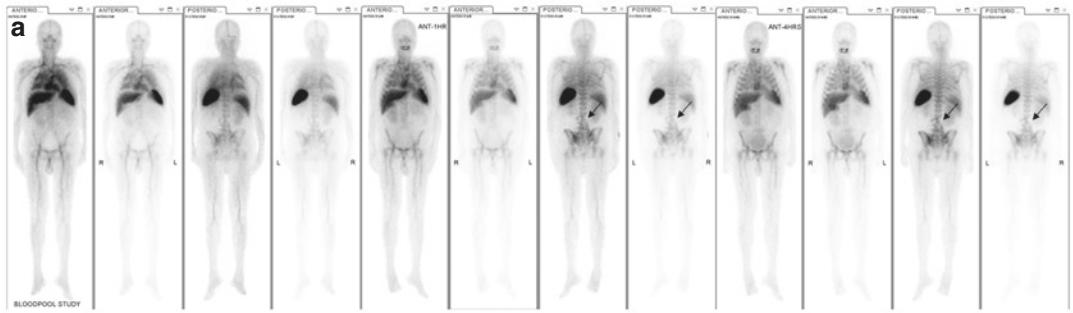

Fig. 3 (**a**) Radiolabeled WBC whole-body planar images show tracer accumulation of degree similar to that of the background marrow noted around the left L3 vertebra pedicle screw, around the L3 posterior elements and right L5 pedicle screw (black arrows). (**b**) Local views of the WBC scan show a close-up of the WBC accumulation in the pedicle screws (black arrows). (**c**) SPECT/CT images clearly demarcate the tracer activity in the L3 pedicle screw (white arrows, left facing) and the L5 pedicle screw (white arrows, right facing). (**d**) Sulfur colloid bone marrow planar images and (**e**) SPECT/CT image show no definite Tc-99m sulfur colloid uptake seen corresponding to the foci of radiolabeled WBC accumulation at the pedicle screws. Tracer accumulation in the posterior elements of L3 vertebra seen on the planar images (black arrows) appear to correspond to the findings seen in the radiolabeled WBC scan and hence unlikely to represent infection. Overall findings are suggestive of the pedicle screws as a source of infection

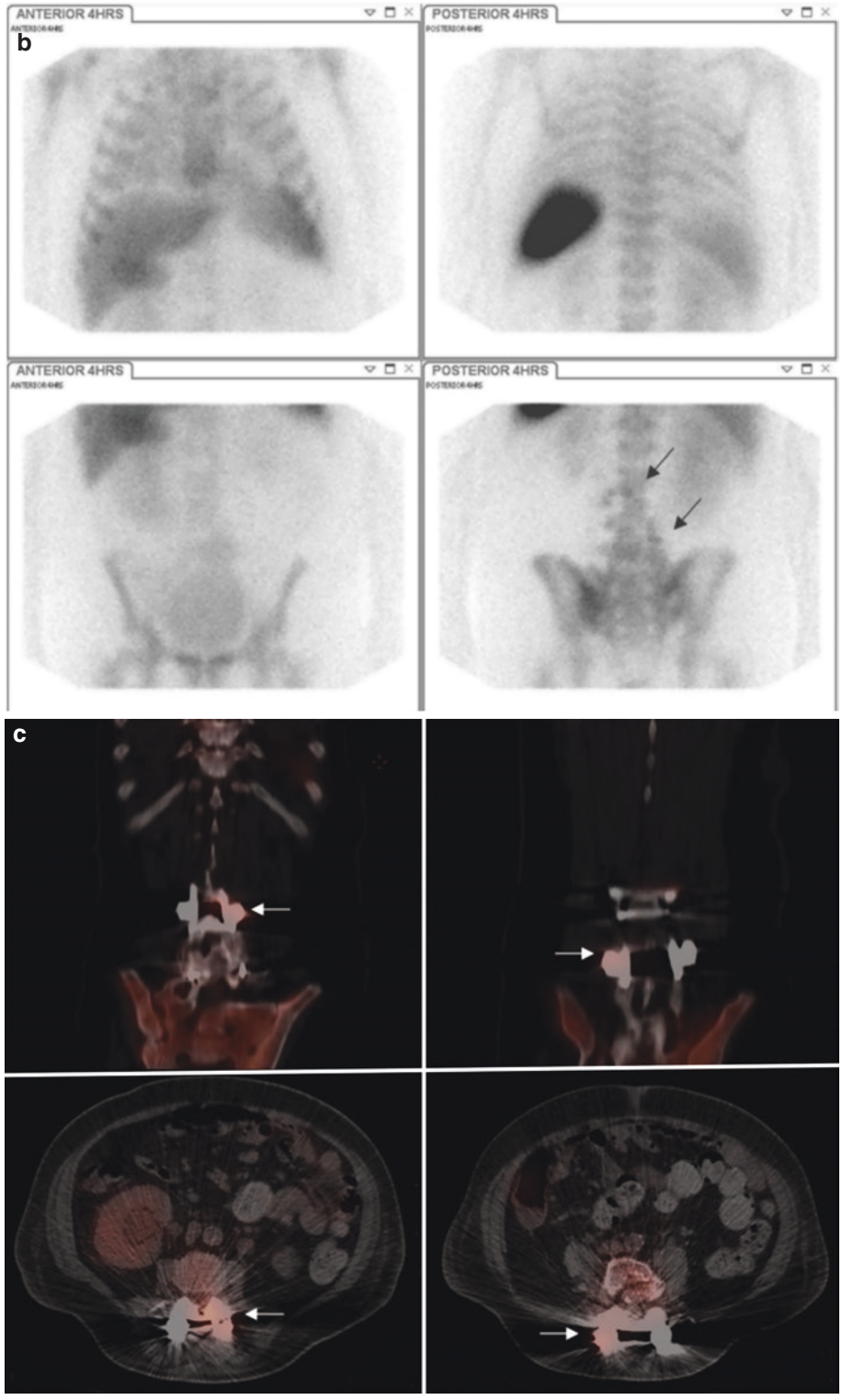

Fig. 3 (continued)

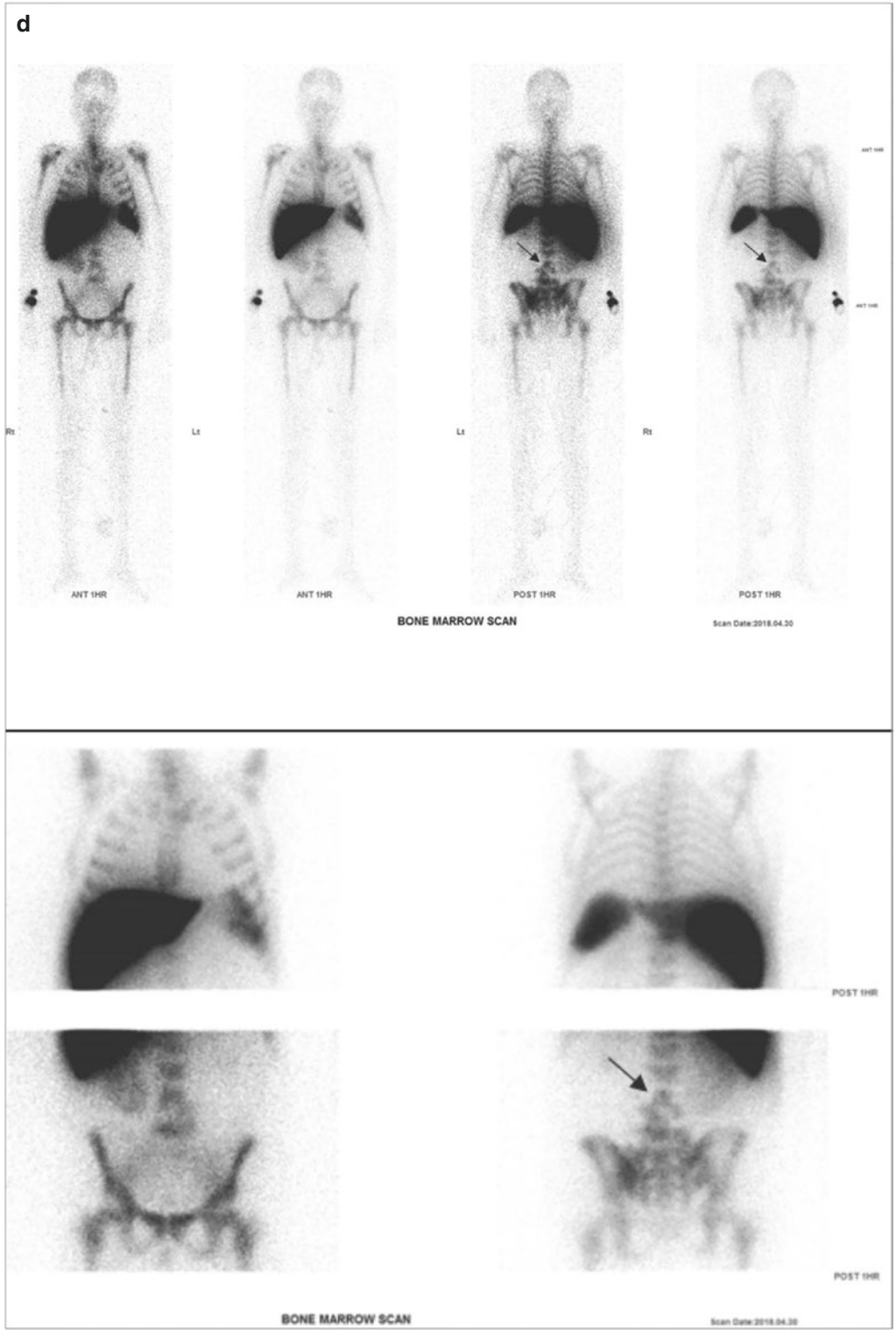

Fig. 3 (continued)

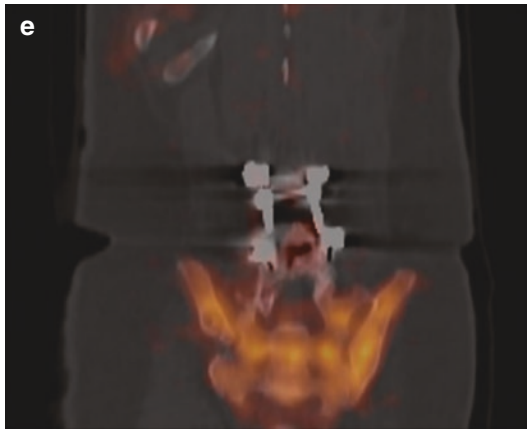

Fig. 3 (continued)

reported that the sensitivity, specificity, and accuracy were 94%, 95%, and 94%, respectively. The advantages of this tracer are same-day imaging (within 6 h), faint bone marrow uptake, relatively low radiation burden, and whole-body imaging capability. The antibiotic treatment did not affect the sensitivity. However, the important disadvantage is the potential for immunogenic reactions to the subsequent administration of the drug which can lead to altered tracer distribution (Lazzeri et al. 2004).

2.4.3 Radiolabeled Antimicrobial Peptides

Antimicrobial peptides are small, cationic and amphipathic, and part of the natural defense mechanism and interact with pathogens by multiple mechanisms. Their therapeutic and diagnostic potentials against a broad spectrum of pathogens are being investigated. One example is ^{99m}Tc-labelled ethambutol or isoniazid for tuberculous infection. Radiolabeled synthetic fragments of ubiquicidine, which is present in murine macrophages, have been investigated for infection-specific imaging. Both ^{99m}Tc- and ^{68}Ga-labeled ubiquicidine successfully detects spinal infection (Palestro et al. 2013; Palestro 2016). Dillmann-Arroyo et al. (2011) evaluated the role of ^{99m}Tc ubiquicidine in 27 patients suspected to have spinal infection and reported that the test was 100% sensitive and 87.5% specific for spondylodiscitis.

3 Single-Photon Emission Computed Tomography/Computed Tomography (SPECT/CT)

The development of hybrid imaging techniques, especially SPECT/CT, has revolutionized nuclear medicine imaging by improving the diagnostic accuracy. The CT data is used for both anatomical correlation and attenuation correction. The differentiation between bone and soft tissue is often very difficult with planar imaging alone and may lead to false-positive results in spinal infection. The introduction of SPECT/CT has improved the localization of spinal infection compared to planar scintigraphy in bone scintigraphy, ^{67}Ga scintigraphy, and radiolabeled leukocyte imaging (Erba and Israel 2014; Thang et al. 2014). Bone scintigraphy has high sensitivity and moderate specificity for diagnosing osteomyelitis in non-violated bones. But the specificity decreases significantly from over 50% to 35% in the presence of previous trauma and surgical intervention. In these clinical situations, SPECT/CT improves the specificity of bone scintigraphy by reducing the number of false-positives and equivocal findings (Erba and Israel 2014).

In a prospective study conducted in 82 patients, Bar-Shalom et al. (2006) evaluated the role of additional SPECT/CT to planar imaging of ^{67}Ga scintigraphy and ^{111}In-labeled WBC scintigraphy. They found that SPECT/CT provided additional contribution to diagnosis in 48% of patients who underwent ^{67}Ga scintigraphy and 55% of patients who underwent ^{111}In-labeled WBC scintigraphy. The study revealed that SPECT/CT enables more precise anatomical localization and accurate delineation of the extent of infection (Fig. 4). However, SPECT/CT did not significantly contribute, if planar imaging was negative (Bar-shalom et al. 2006). Similarly, Lazzeri et al. (2010) also concluded that SPECT/CT imaging provides accurate evaluation of spinal infection by differentiating vertebral and adjacent soft tissue involvement in a study which investigated ^{111}In-biotin SPECT/CT in patients with suspected spinal infection. The authors demonstrated that the diagnostic accuracy of

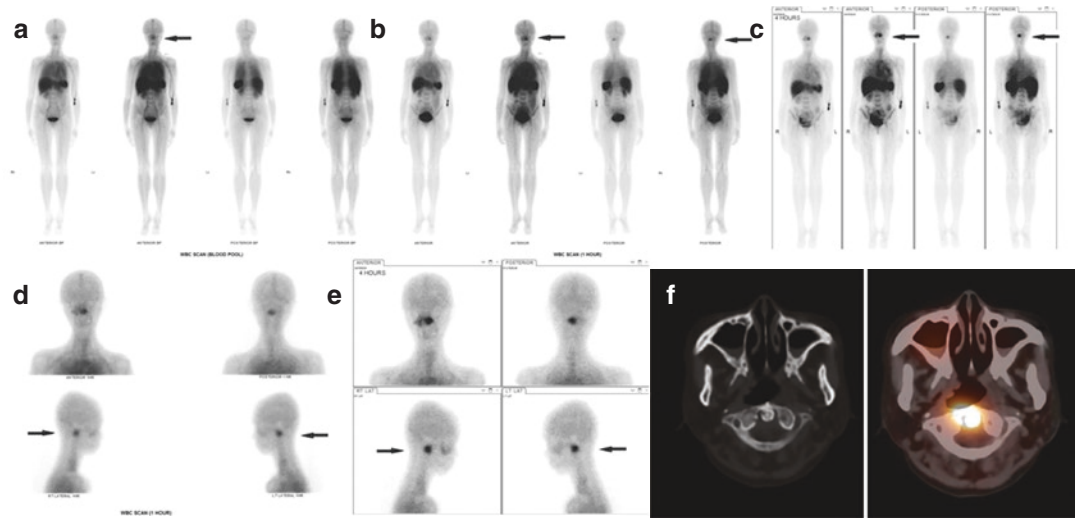

Fig. 4 Radiolabeled WBC whole-body planar images obtained at (**a**) blood pool phase, (**b**) 1 h, and (**c**) 4 h show increasing tracer activity (black arrows) in the midline of the head which appears to be at the upper cervical spine and best appreciated in the local views obtained at (**d**) 1 h and (**e**) 4 h. (**f**) SPECT/CT images localize the tagged WBC accumulation to be centered at the right anterior arch of the C1 vertebra and the medial atlantoaxial joint, suspicious for osteomyelitis with contiguous involvement of the atlantoaxial joint

SPECT/CT (93%) was higher than planar scintigraphy (76.3%) and stand-alone SPECT (90.3%) (Lazzeri et al. 2010).

4 Positron Emission Tomography/Computed Tomography (PET/CT)

Proton-rich unstable nuclei such as fluorine-18 (^{18}F) and gallium-68 (^{68}Ga) decay by electron capture or positron emission. The emitted positron travels a short distance from its origin site, loses energy, annihilates with a resident electron, and emits two 511 keV gamma photons in opposite directions. Hybrid PET/CT scanners identify the annihilation event and localizes it in the cross-sectional images with aid of coincidental detection and computer image reconstruction algorithms. Positron-emitting radiopharmaceuticals have intrinsic high spatial resolution and facilitate the precise localization of uptake in PET/CT, compared to single-photon-emitting isotopes. They have the added advantage of providing widely acceptable semiquantitative analysis, which is helpful in differentiating infectious and noninfectious conditions, monitoring treatment response, and diagnosing relapsed infections during follow-up (Kannivelu et al. 2014; Raghavan et al. 2018).

4.1 Fluorine-18-2′-Deoxy-2-Fluoro-D-Glucose ([^{18}F] FDG)

[^{18}F] FDG is the most commonly used tracer in PET/CT imaging for spinal infection. [^{18}F] FDG is a fluorinated structural analog of glucose and is transported into the cell by glut-1 transporters and initially phosphorylated by the same mechanism, namely, hexokinase. But the phosphorylated [^{18}F] FDG cannot be further metabolized as phosphorylated glucose and gets trapped within the cell in proportion to the rate of glucose uptake. Several factors influence the increased [^{18}F] FDG uptake at the infection sites. Because of hyperemia, more [^{18}F] FDG is distributed to the region of infection. The activated inflammatory cells such as neutrophils, lymphocytes, monocytes, and macrophages are present in increased numbers at the infection zones. They express more glucose transporters in their cell

membranes, resulting in increased affinity and uptake of [^{18}F] FDG. Furthermore, the normal bone marrow physiological uptake of [^{18}F] FDG is low. All these factors, together with its widespread availability, make [^{18}F] FDG an effective tracer and excellent alternative to conventional radionuclide imaging for diagnosis of spinal infection (Gemmel et al. 2006; Palestro 2013).

[^{18}F] FDG PET shows increased tracer uptake in both acute and chronic osteomyelitis, corresponding to the areas of inflammatory cell filtration, neutrophils in the acute phase and macrophages in the chronic phase. In a study conducted in acute and chronic osteomyelitis in 21 patients, [^{18}F] FDG PET yielded true-positive results in all seven patients who had spondylitis (Kälicke et al. 2000). Guhlmann et al. (1998) studied the usefulness of [^{18}F] FDG PET in 15 patients with suspected chronic osteomyelitis, compared it with radiolabeled anti-granulocyte antibody imaging, and concluded that [^{18}F] FDG PET had a higher diagnostic accuracy. Similarly, in evaluation of [^{18}F] FDG PET in 16 consecutive patients with suspected spondylodiscitis, the investigators showed that [^{18}F] FDG PET was true positive in all 12 patients of infection and true negative in 3 of 4 patients without infection. They also demonstrated the advantage of PET in delineation of the involvement of paravertebral soft tissue (Schmitz et al. 2001). In general, [^{18}F] FDG PET/CT performs better than bone scintigraphy and ^{67}Ga scintigraphy in identification of paraspinal soft tissue infection, and differentiation of degenerative arthritis from infection, providing higher diagnostic accuracy (Gratz et al. 2002; Gemmel et al. 2010; Fuster et al. 2012) (Fig. 5). A recent systematic review and bivariate meta-analysis, based on 12 selected studies among 26 articles, for the effectiveness of [^{18}F] FDG PET/CT in patients with suspected spondylitis showed sensitivity of 94.8% and specificity of 91.4% overall (Treglia et al. 2020).

In the presence of severe degenerative changes of the vertebral end plates and intervertebral disks, [^{18}F] FDG PET appears to be superior in differentiation of infection from degeneration, compared to ^{67}Ga scintigraphy and MRI (Gratz et al. 2000; Schmitz et al. 2001; Gemmel et al. 2010) (Fig. 6). In a prospective study of 30 patients with substantial vertebral end-plate

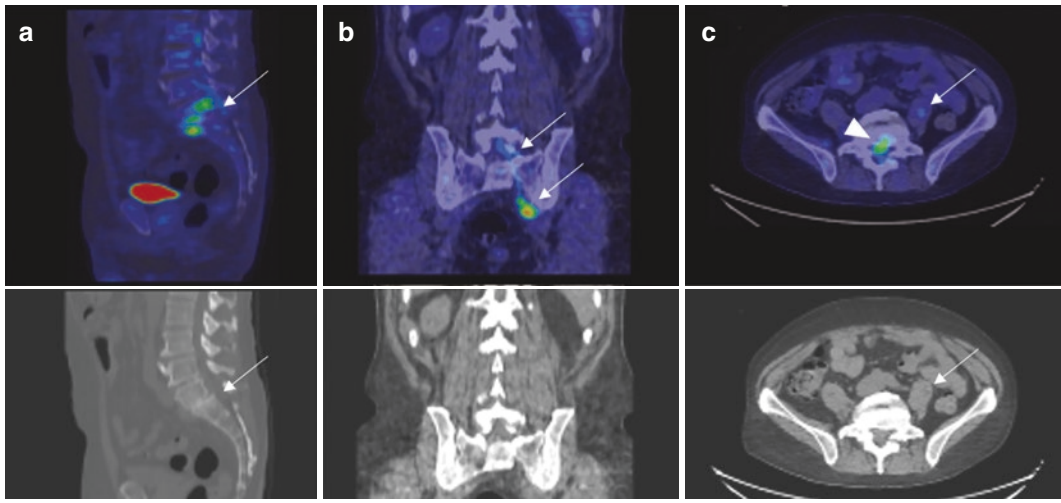

Fig. 5 [18F] FDG PET/CT. (**a**) Sagittal images show a Grade 1 anterolisthesis of L5 on S1 vertebral segments with moderately diffuse FDG uptake at the L5 and S1 vertebrae with epidural extension (white arrows). (**b**) Coronal images show increased FDG avidity along the left S1 nerve (white arrows). (**c**) Axial images also show a hypermetabolic soft tissue lesion in the left psoas muscle (white arrow). The hypermetabolic epidural extension can also be appreciated (white arrowhead). Overall findings are suggestive of L5/S1 spondylodiscitis with epidural extension and a left psoas abscess

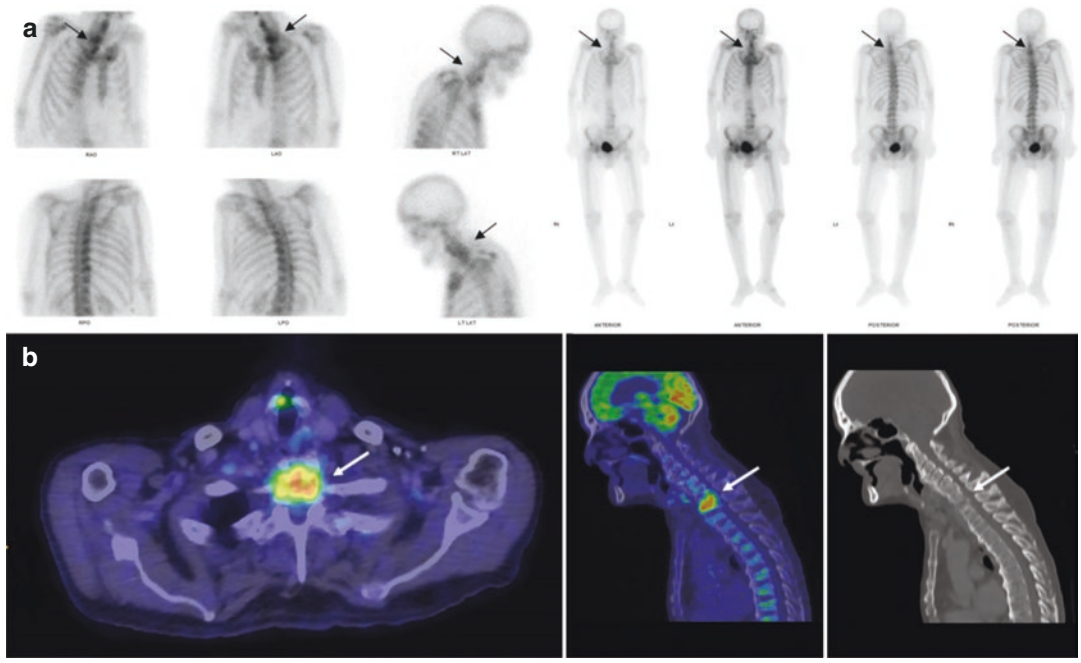

Fig. 6 (**a**) Whole-body ^{99m}Tc MDP bone scan with local views show moderately increased radiotracer uptake in the C7/T1 region (black arrows) suspicious for spondylodiscitis in the background of degenerative changes of the cervical spine. (**b**) Correlative FDG PET/CT images show increased metabolic activity at the C7/T1 level centered on the intervertebral disk with destructive changes at the adjacent vertebral end plates (white arrows), compatible with spondylodiscitis

abnormalities, [^{18}F] FDG PET was true-positive in all 5 foci of infection and true-negative in all 33 uninfected sites with 100% sensitivity and 100% specificity, compared to 50% sensitivity and 96% specificity for MRI (Stumpe et al. 2002). However, Rosen et al. (2006) concluded differently that significant focal [^{18}F] FDG uptake of varying degrees was seen in more than half of patients with degenerative spinal disease, primarily in the lumbosacral spine. Similarly, a few studies conducted to evaluate the potential of [^{18}F] FDG PET to differentiate tuberculous from pyogenic spinal infections contributed variable results. Kim et al. (2008) performed dual time point [^{18}F] FDG PET imaging in 22 consecutive patients with high suspicion of spondylitis at 1 h and 2 h after injection of [18F] FDG. They observed that the SUVmax at 1 h was significantly higher for tuberculous infection than nontuberculous infection. However, at 2 h, the differences were not significant and not useful for differentiating tuberculous and nontuberculous infections. Gunes et al. (2016) investigated the usefulness of [^{18}F] FDG PET/CT in 32 patients with spondylodiscitis. Images were acquired at 90 min and 2 h after injection of [^{18}F] FDG, and they observed no significant differences between pyogenic and tuberculous spondylitis in early and delayed imaging. It would be safe to conclude that neither visual nor semiquantitative analysis, using dual point imaging, could reliably differentiate pyogenic and tuberculous spinal infections (Kim et al. 2008; Gunes et al. 2016).

The diagnosis of spinal infection in the presence of previous trauma and hardware is a great challenge in all available imaging modalities, including [^{18}F] FDG PET/CT. Even in the absence of infection, there can be increased [^{18}F] FDG uptake at the location of instrumentation due to foreign body immune response, aseptic loosening, bone remodeling, and peri-prosthetic fracture. Hungenbach et al. (2013) performed [^{18}F] FDG PET for 42 patients with spondylodiscitis, including 13 who underwent prior surgery. They

evaluated for the intensity and patterns of [^{18}F] FDG uptake and found that the test was 86% sensitive and 95% specific. Hartmann et al. (2007) investigated the diagnostic value of [^{18}F] FDG PET/CT in patients with trauma and suspected chronic osteomyelitis in the axial and appendicular skeleton, including patients with metallic implants. For the subgroup of nine spinal region infections, [^{18}F] FDG PET/CT was true positive in all seven patients with spondylodiscitis and true negative in the two patients without infection (100% diagnostic accuracy). The added value of anatomical localization provided by the CT component in PET/CT imaging to identify the extent of infection and soft tissue involvement for better clinical management was emphasized by these investigators (Hartmann et al. 2007) (Fig. 7).

In the largest prospective series to date, De Winter et al. (2003) evaluated the role of [^{18}F] FDG PET in patients with postoperative spine, including 16 patients in the control group (hematogeneous spondylitis) and 57 patients in the investigation group (30 patients without spinal implants and 27 patients with spinal implants). Using optimal cut-off values, the overall sensitivity, specificity, diagnostic accuracy, positive predictive value, and negative predictive value were 100%, 81%, 86%, 65%, and 100%, respectively. Among the 30 patients without spinal implants, there were two false-positive studies;

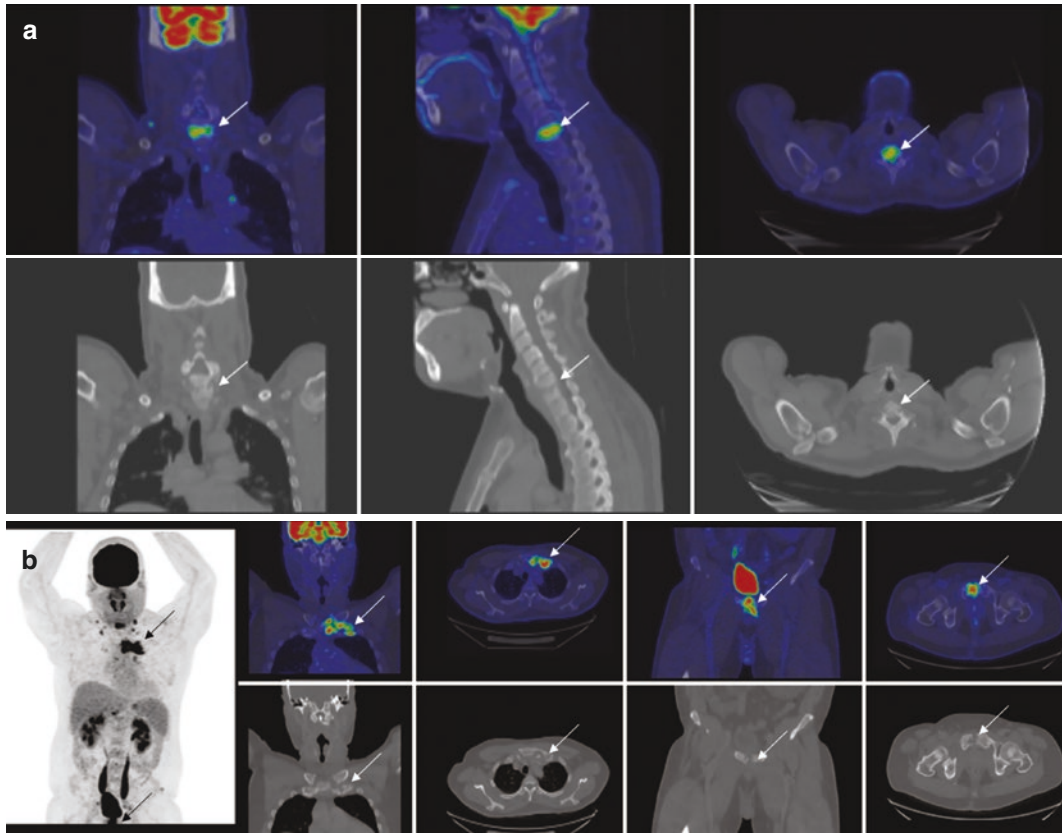

Fig. 7 FDG PET/CT (**a**) coronal, sagittal, and axial images show intense FDG avidity in the C6/C7 vertebrae with bony destruction (white arrows), suspicious for spondylodiscitis. (**b**) MIP image (far left) shows hypermetabolic lesions in the left sternoclavicular junction and the pubic symphysis (black arrows) which correspond to the areas of intense FDG uptake and bony destruction on the coronal and axial FDG PET/CT images (white arrows). The CT component provides accurate anatomical localization. These raise the suspicion for multiple sites of septic arthritis

and among the 27 patients with spinal implants, there were 6 false-positive studies. The specificity was 65% in the group with spinal implants, compared to 92% in the group without spinal implants. The authors concluded that chronic postoperative spinal infection can be excluded in negative [^{18}F] FDG PET studies; however, positive studies must be interpreted cautiously (De Winter et al. 2003).

MRI and [^{18}F] FDG PET/CT are complementary to each other in the diagnosis of spinal infection, especially in the patients in which they are not individually conclusive. There are many comparative studies between MRI and [^{18}F] FDG PET/CT to assess their effectiveness and limitations. Even with their limited resolution, [18F] FDG PET was found to be superior to MRI in detecting low-grade spondylitis and discitis (Gratz et al. 2002). In the presence of degenerative vertebral end-plate changes, [^{18}F] FDG appears to better at diagnosing or ruling out spondylodiscitis (Stumpe et al. 2002; Ohtori et al. 2010). In a prospective study, Fuster et al. (2012) compared [^{18}F] FDG PET/CT and MRI in 26 patients with clinical symptoms of spondylodiscitis. The diagnostic accuracies of MRI and [^{18}F] FDG PET/CT were fairly similar, being 84% and 81%, respectively. They concluded that [^{18}F] FDG PET/CT had a higher specificity than MRI. However, MRI was superior for detecting soft tissue involvement. The combination of [^{18}F] FDG PET/CT and MRI detected spondylodiscitis in all the patients who had infection (Fuster et al. 2012). Comparison studies conducted by various investigators provided comparable but conflicting sensitivity and specificity values for [^{18}F] FDG PET/CT and MRI in diagnosing spinal infection, but all agree that [^{18}F] FDG PET/CT is a useful adjunct to MRI and can be used when MRI is inconclusive and cannot be performed (Seifen et al. 2012; Skanjeti et al. 2012; Palestro 2013; Raghavan et al. 2018).

[^{18}F] FDG PET/CT is very useful during follow-up for monitoring treatment response and detecting relapse. Nanni et al. (2012) evaluated the potential of [^{18}F] FDG PET/CT in the early assessment of treatment response to antibiotics in 34 patients with hematogeneous spondylodiscitis. The SUVmax of the baseline study (SUV1) and SUVmax of the second study (SUV2) which was performed 2–4 weeks after the start of treatment were compared. They found that in responders, SUV2 was significantly less than SUV 1. By using delta-SUVmax {(SUVmax baseline − SUVmax response)/SUVmax baseline}, higher sensitivity and specificity were achieved (Nanni et al. 2012). In addition to the quantification, the tracer uptake pattern in the follow-up scans is also helpful for differentiating active infection and patients without active infection. In active infection, the [^{18}F] FDG uptake is usually seen in the bone and soft tissue, whereas the uptake confined to the margins of destroyed disks after treatment is not indicative of infection (Riccio et al. 2015). In a study conducted in 21 patients with 24 sites of disease, Skanjeti et al. (2012) found that [^{18}F] FDG PET/CT was more accurate than MRI in assessing treatment response. Dauchy et al. (2016) prospectively investigated for relapsed infection in 30 patients, including 19 with spinal hardware who had previously confirmed spondylodiscitis. In a comparison between [^{18}F] FDG PET/CT and MRI using a combination of visual and semiquantitative analysis, the results of [^{18}F] FDG PET/CT were better than those of MRI, though the differences were not significant (Dauchy et al. 2016).

[^{18}F] FDG PET/CT is a promising alternative to conventional nuclear imaging and is becoming a frontline investigation together with MRI for investigation of spinal infection. The disadvantage of limited anatomical information of PET has now been overcome by co-registration with in-line CT in hybrid PET/CT scanners. Still, we should be mindful that the uptake of [^{18}F] FDG is nonspecific and can be seen in infection, inflammation, and tumor. Even though [^{18}F] FDG PET/CT is more effective than other imaging choices in diagnosing spinal infection in the presence of degenerative changes and previous trauma, it is important to note that the specificity is moderately reduced in patients with spinal instrumentation. Other disadvantages of [^{18}F] FDG PET/CT are scarce availability, radiation burden, and relatively higher costs (Gemmel et al. 2010; Lazzeri et al. 2019).

4.2 Gallium-68 (^{68}Ga) and Other Radiotracers

^{68}Ga is a positron-emitting isotope with physical half-life of 68 min, which is shorter than 78-h half-life of ^{67}Ga. The uptake of ^{68}Ga citrate at the sites of inflammation and infection are nonspecific and similar to ^{67}Ga. ^{68}Ga offers superior quality imaging as it is a positron emitter, and imaging should be performed within a few hours after injection because of its short half-life. Little data are available on the role of ^{68}Ga citrate imaging in spinal infection. Nanni et al. (2010) performed ^{68}Ga PET/CT scans on 31 patients with suspected spondylodiscitis, and of these, 23 cases were positive. They reported sensitivity, specificity, and accuracy of 100%, 76%, and 90%, respectively (Nanni et al. 2010). Similar to ^{111}In-biotin, efforts were made to develop a specific infection imaging agent, by complexing biocytin with ^{68}Ga. ^{68}Ga-DOTA-biocytin was stable over 3 h and may prove useful for diagnosing infection (Asti et al. 2012; Raghavan et al. 2018).

^{18}F sodium-fluoride (NaF) is a bone-specific positron-emitting isotope, and NaF PET/CT has been used for the diagnosis of various bone and joint diseases. Recently, this isotope was evaluated for diagnosing bone infection, including spinal infection and postsurgical interventions. A dual-phase NaF PET/CT imaging protocol was introduced to detect infection and inflammation, with early-phase PET imaging performed within 10 min after tracer injection and standard bone phase PET/CT imaging performed 30–90 min after tracer injection (Freesmeyer et al. 2014). In a recent study, Lee et al. (2019) evaluated the role of NaF PET/CT in diagnosing surgical site infection of the 23 patients, and they reported that the sensitivity, specificity, and accuracy of dual-phase NaF bone PET/CT were 92.9%, 100%, and 95.7%, respectively. Based on these results, the authors suggested that NaF PET/CT can be an alternative nuclear medicine imaging modality for detecting orthopedic infections, especially spinal infection (Lee et al. 2019).

5 Positron Emission Tomography/Magnetic Resonance Imaging (PET/MRI)

Hybrid PET/MRI scanners have become increasingly common, after integration was made possible by newer technical advances such as avalanche photodiodes and new MR Dixon sequence (Kannivelu et al. 2012). The combination of the strengths of [^{18}F] FDG PET and MRI offers highly sensitive metabolic and high-resolution anatomical imaging with excellent soft tissue contrast, hence overcoming their individual limitations. The scientific literature and available data are still limited for the role of PET/MRI in the diagnosis of spinal infection. Fahnert et al. (2016) conducted a prospective study in patients with suspected spondylodiscitis with previous inconclusive MRI results. Image datasets of 28 patients (a total of 29 regions) were evaluated. When the PET component was added, the sensitivity, specificity, positive predictive value (PPV), and negative predictive value (NPV) of PET/MRI improved to 100%, 88%, 86%, and 100%, respectively, compared to the sensitivity, specificity, PPV, and NPV of MRI alone which were 50%, 71%, 54%, and 67% respectively. Among the 8 of 29 inconclusive regions of MRI alone, the added PET information changed the diagnosis to spondylodiscitis in 5 regions and to absence of spondylodiscitis in 3 regions. There were no false-negative results using combined PET/MRI. The investigators concluded that the use of [^{18}F] FDG PET/MRI significantly increases the diagnostic certainty of the detection of spinal infection, especially in patients with inconclusive clinical or MRI findings. They concluded that [^{18}F] FDG PET/MRI can become the one-stop-shop approach for earlier initiation of proper treatment to patients with spinal infection (Fahnert et al. 2016).

6 Consensus Guidelines

An expert specialist team, comprising nuclear medicine physicians appointed by the European Association of Nuclear Medicine (EANM),

neuroradiologists appointed by the European Society of Neuroradiology (ESNR), and infectious diseases specialists appointed by the European Society of Clinical Microbiology and Infectious Diseases (ESCMID), reviewed the literature from January 2006 to December 2015 and published guidelines for the diagnosis of spinal infection (spondylodiscitis) in adults. They issued 20 consensus statements which were graded by level of evidence based on the 2011 Oxford Centre of Evidence Based Medicine criteria (Lazzeri et al. 2019). Among them, the issued guidelines (statements) regarding nuclear medicine imaging are summarized below:

- In primary and postsurgical spondylodiscitis, if MRI is contraindicated, the imaging modality of choice is [^{18}F] FDG-PET/CT (Level 2).
- In postsurgical spondylodiscitis, with or without spinal hardware, [^{18}F] FDG-PET/CT can detect both spinal infection and soft tissue infection (Level 2).
- In patients with suspected spinal infection and elevated ESR and/or CRP and doubtful MRI, [^{18}F] FDG-PET/CT should be performed (Level 1).
- In patients with suspected spinal infection, elevated ESR and/or CRP, doubtful or unperformable MRI, and doubtful or unperformable [^{18}F] FDG-PET/CT, a CT scan should be performed with an image-guided biopsy (Level 2).
- The role of hybrid PET/MRI, although promising, needs to be evaluated (Level 5).
- In case of negative MRI or negative [^{18}F] FDG-PET/CT, the diagnosis of spondylodiscitis should be excluded (Level 5).

7 Conclusion

There has been much advance in diagnostic imaging of spinal infection since the advent of CT and MRI which provide exquisite spatial resolution but limited functional data. As clearly illustrated in this chapter, nuclear medicine functional techniques for spinal infection imaging have also come to the forefront, especially with the use of hybrid SPECT/CT, PET/CT, and PET/MRI, which provide traditionally high sensitivity and superior functional information afforded by nuclear imaging and the superior spatial resolution and anatomical detail from CT and MRI. A myriad of radiotracers is available to nuclear medicine physicians in this respect, ranging from SPECT tracers based on SPECT isotopes such as ^{99m}Tc and ^{67}Ga radionuclides, to PET tracers based on PET isotopes such as ^{18}F-fluorine- and ^{68}Ga-labelled positron emitters.

Advantages of hybrid nuclear imaging in spinal infection include their usefulness in patients who had prior spinal instrumentation where conventional anatomical imaging is difficult or cannot detect the source of infection, providing more information to directing targeted biopsy for tissue cultures, and helping to determine treatment response and the efficacy of antimicrobial therapy. Improved specificity with high negative predictive values of FDG PET/CT in this setting has led to it being the preferred noninvasive nuclear medicine diagnostic imaging modality of choice in the diagnosis, management, and clinical decision-making process in spinal infection.

References

Asti M, Iori M, Erba PA et al (2012) Radiosynthesis of 68Ga-labelled DOTA–biocytin (68Ga-r-BHD) and assessment of its pharmaceutical quality for clinical use. Nucl Med Commun 33:1179–1187

Bar-shalom R, Yefremov N, Guralnik L et al (2006) Leukocyte scintigraphy for diagnosis of infection. J Nucl Med 47:587–594

Dauchy FA, Dutertre A, Lawson-Ayayi S et al (2016) Interest of [18 F]fluorodeoxyglucose positron emission tomography/computed tomography for the diagnosis of relapse in patients with spinal infection: a prospective study. Clin Microbiol Infect 22:438–443

De Winter F, Gemmel F, Van De Wiele C et al (2003) 18-Fluorine fluorodeoxyglucose positron emission tomography for the diagnosis of infection in the postoperative spine. Spine (Phila Pa) 28:1314–1319

De Winter F, Gemmel F, Van Laere K et al (2004) 99mTc-Ciprofloxacin planar and tomographic imaging for the diagnosis of infection in the postoperative spine: experience in 48 patients. Eur J Nucl Med Mol Imaging 31:233–239

Dillmann-Arroyo C, Cantú-Leal R, Campa-Núñez H et al (2011) [Application of the ubiquicidin 29-41 scan in

the diagnosis of pyogenic vertebral osteomyelitis]. Acta Ortop Mex 25:27–31
Erba PA, Israel O (2014) SPECT/CT in infection and inflammation. Clin Transl Imaging 2:519–535
Fahnert J, Purz S, Jarvers JS et al (2016) Use of simultaneous 18F-FDG PET/MRI for the detection of spondylodiskitis. J Nucl Med 57:1396–1401
Freesmeyer M, Stecker FF, Schierz J-H et al (2014) First experience with early dynamic 18F-NaF-PET/CT in patients with chronic osteomyelitis. Ann Nucl Med 28:314–321
Fuster D, Solà O, Soriano A et al (2012) A prospective study comparing whole-body FDG PET/CT to combined planar bone scan with 67Ga SPECT/CT in the diagnosis of spondylodiskitis. Clin Nucl Med 37:827–832
Gemmel F, Dumarey N, Palestro CJ (2006) Radionuclide imaging of spinal infections. Eur J Nucl Med Mol Imaging 33:1226–1237
Gemmel F, Rijk PC, Collins JMP et al (2010) Expanding role of 18F-fluoro-d-deoxyglucose PET and PET/CT in spinal infections. Eur Spine J 19:540–551
Gratz S, Dörner J, Oestmann JW et al (2000) 67Ga-Citrate and 99Tcm-MDP for estimating the severity of vertebral osteomyelitis. Nucl Med Commun 21:111–120
Gratz S, Dörner J, Fischer U et al (2002) 18F-FDG hybrid PET in patients with suspected spondylitis. Eur J Nucl Med 29:516–524
Guhlmann A, Brecht-Krauss D, Suger G et al (1998) Fluorine-18-FDG PET and technetium-99m antigranulocyte antibody scintigraphy in chronic osteomyelitis. J Nucl Med 39:2145–2152
Gunes BY, Onsel C, Sonmezoglu K et al (2016) Diagnostic value of F-18 FDG PET/CT in patients with spondylodiscitis: is dual time point imaging time worthy? Diagn Microbiol Infect Dis 85:381–385
Hartmann A, Eid K, Dora C et al (2007) Diagnostic value of 18F-FDG PET/CT in trauma patients with suspected chronic osteomyelitis. Eur J Nucl Med Mol Imaging 34:704–714
Hong SH, Choi JY, Lee JW et al (2009) MR imaging assessment of the spine: infection or an imitation? Radiographics 29:599–612
Hungenbach S, Delank K-S, Dietlein M et al (2013) 18F-fluorodeoxyglucose uptake pattern in patients with suspected spondylodiscitis. Nucl Med Commun 34:1068–1074
Kälicke T, Schmitz A, Risse JH et al (2000) Fluorine-18 fluorodeoxyglucose positron emission tomography in infectious bone diseases: results of histologically confirmed cases. Eur J Nucl Med Mol Imaging 27:524–528
Kannivelu A, Kok TY, Padhy AK (2012) The conundrum of PET/MR. World J Nucl Med 11:1–2
Kannivelu A, Loke KSH, Kok TY et al (2014) The role of PET/CT in the evaluation of skeletal metastases. Semin Musculoskelet Radiol 18:149–165
Khoo LA, Heron C, Patel U et al (2003) The diagnostic contribution of the frontal lumbar spine radiograph in community referred low back pain—a prospective study of 1030 patients. Clin Radiol 58:606–609
Kim SJ, Lee JS, Suh KT et al (2008) Differentiation of tuberculous and pyogenic spondylitis using double phase F-18 FDG PET. Open Med Imaging J 2:1–6
Lazzeri E, Manca M, Molea N et al (1999) Clinical validation of the avidin/indium-111 biotin approach for imaging infection/inflammation in orthopaedic patients. Eur J Nucl Med 26:606–614
Lazzeri E, Pauwels EKJ, Erba PA et al (2004) Clinical feasibility of two-step streptavidin/111In-biotin scintigraphy in patients with suspected vertebral osteomyelitis. Eur J Nucl Med Mol Imaging 31:1505–1511
Lazzeri E, Erba P, Perri M et al (2010) Clinical impact of SPECT/CT with In-111 biotin on the management of patients with suspected spine infection. Clin Nucl Med 35:12–17
Lazzeri E, Bozzao A, Cataldo MA et al (2019) Joint EANM/ESNR and ESCMID-endorsed consensus document for the diagnosis of spine infection (spondylodiscitis) in adults. Eur J Nucl Med Mol Imaging 46:2464–2487
Lee JW, Yu SN, Yoo ID et al (2019) Clinical application of dual-phase F-18 sodium-fluoride bone PET/CT for diagnosing surgical site infection following orthopedic surgery. Medicine (Baltimore) 98:e14770
Lisbona R, Derbekyan V, Novales-Diaz J, Veksler A (1993) Gallium-67 scintigraphy in tuberculous and nontuberculous infectious spondylitis. J Nucl Med 34:853–859
Love C, Palestro CJ (2016) Nuclear medicine imaging of bone infections. Clin Radiol 71:632–646
Love C, Patel M, Lonner BS et al (2000) Diagnosing spinal osteomyelitis: a comparison of bone and Ga-67 scintigraphy and magnetic resonance imaging. Clin Nucl Med 25:963–977
Mylona E, Samarkos M, Kakalou E et al (2009) Pyogenic vertebral osteomyelitis: a systematic review of clinical characteristics. Semin Arthritis Rheum 39:10–17
Nanni C, Errani C, Boriani L et al (2010) 68Ga-Citrate PET/CT for evaluating patients with infections of the bone: preliminary results. J Nucl Med 51:1932–1936
Nanni C, Boriani L, Salvadori C et al (2012) FDG PET/CT is useful for the interim evaluation of response to therapy in patients affected by haematogenous spondylodiscitis. Eur J Nucl Med Mol Imaging 39:1538–1544
Ohtori S, Suzuki M, Koshi T et al (2010) 18F-Fluorodeoxyglucose-PET for patients with suspected spondylitis showing Modic change. Spine (Phila Pa) 35:E1599–E1603
Palestro CJ (2013) FDG-PET in musculoskeletal infections. Semin Nucl Med 43:367–376
Palestro CJ (2016) Radionuclide imaging of musculoskeletal infection: a review. J Nucl Med 57:1406–1412
Palestro CJ, Love C (2007) Radionuclide imaging of musculoskeletal infection: conventional agents. Semin Musculoskelet Radiol 11:335–352
Palestro CJ, Kim CK, Swyer AJ et al (1991) Radionuclide diagnosis of vertebral osteomyelitis: indium-111-

leukocyte and technetium-99m-methylene diphosphonate bone scintigraphy. J Nucl Med 32:1861–1865

Palestro CJ, Glaudemans AWJM, Dierckx RAJO (2013) Multiagent imaging of inflammation and infection with radionuclides. Clin Transl Imaging 1:385–396

Prandini N, Lazzeri E, Rossi B et al (2006) Nuclear medicine imaging of bone infections. Nucl Med Commun 27:633–644

Prodi E, Grassi R, Iacobellis F, Cianfoni A (2016) Imaging in spondylodiskitis. Magn Reson Imaging Clin N Am 24:581–600

Raghavan M, Lazzeri E, Palestro CJ (2018) Imaging of spondylodiscitis. Semin Nucl Med 48:131–147

Riccio SA, Chu AKM, Rabin HR, Kloiber R (2015) Fluorodeoxyglucose positron emission tomography/computed tomography interpretation criteria for assessment of antibiotic treatment response in pyogenic spine infection. Can Assoc Radiol J 66:145–152

Rosen RS, Fayad L, Wahl RL (2006) Increased 18F-FDG uptake in degenerative disease of the spine: characterization with 18F-FDG PET/CT. J Nucl Med 47:1274–1280

Saha S, Burke C, Desai A et al (2013) SPECT-CT: applications in musculoskeletal radiology. Br J Radiol 86:1–15

Schmitz A, Risse J, Grünwald F et al (2001) Fluorine-18 fluorodeoxyglucose positron emission tomography findings in spondylodiscitis: preliminary results. Eur Spine J 10:534–539

Seifen T, Rettenbacher L, Thaler C et al (2012) Prolonged back pain attributed to suspected spondylodiscitis. Nuklearmedizin 51:194–200

Skanjeti A, Penna D, Douroukas A et al (2012) PET in the clinical work-up of patients with spondylodiscitis: a new tool for the clinician? Q J Nucl Med Mol Imaging 56:569–576

Stumpe KDM, Zanetti M, Weishaupt D et al (2002) FDG positron emission tomography for differentiation of degenerative and infectious endplate abnormalities in the lumbar spine detected on MR imaging. AJR Am J Roentgenol 179:1151–1157

Thang S, Tong A, Lam W, Ng D (2014) SPECT/CT in musculoskeletal infections. Semin Musculoskelet Radiol 18:194–202

Treglia G, Pascale M, Lazzeri E et al (2020) Diagnostic performance of 18F-FDG PET/CT in patients with spinal infection: a systematic review and a bivariate meta-analysis. Eur J Nucl Med Mol Imaging 47:1287–1301

Yapar Z, Kibar M, Yapar AF et al (2001) The efficacy of technetium-99m ciprofloxacin (Infecton) imaging in suspected orthopaedic infection: a comparison with sequential bone/gallium imaging. Eur J Nucl Med 28:822–830

Percutaneous Biopsy of Spinal Infection

Mouna Chelli Bouaziz, Mohamed Fethi Ladeb, Soumaya Rammeh, Wafa Achour, and Hend Riahi

Contents

M. Chelli Bouaziz (✉) · M. F. Ladeb · H. Riahi
Department of Radiology, MT Kassab Institute of Orthopaedics, Tunis, Tunisia

Faculty of Medicine of Tunis, Tunis-El Manar University, Tunis, Tunisia
e-mail: bouaziz_mouna@yahoo.fr; fethiladeb@hotmail.fr; hend.riahi@gmail.com

S. Rammeh
Department of Pathology, Charles Nicolle Hospital, Tunis, Tunisia

Faculty of Medicine of Tunis, Tunis-El Manar University, Tunis, Tunisia
e-mail: rammehs@yahoo.fr

W. Achour
Laboratory Department, National Bone Marrow Transplant Center, Tunis, Tunisia

Faculty of Medicine of Tunis, Tunis-El Manar University, Tunis, Tunisia
e-mail: wafaachour@gmail.com

© The Author(s), under exclusive license to Springer Nature Switzerland AG 2021
M. F. Ladeb, W. C. G. Peh (eds.), *Imaging of Spinal Infection*, Medical Radiology Diagnostic Imaging, https://doi.org/10.1007/978-3-030-70459-9_6

Abstract

Percutaneous spine biopsy is an effective modality for the diagnosis and management of spinal infection when a microbiological diagnosis for a known associated organism has not been established by blood cultures or serological tests. It allows obtaining of specimens for microbiological and histopathological diagnosis. This safe and cost- and time-saving procedure is less painful and less invasive than open surgical biopsy. Several imaging-guidance methods are available, including fluoroscopy, computed tomography (CT), ultrasonography, and magnetic resonance imaging, but CT and fluoroscopy remain the most frequently used ones. A good knowledge of spinal anatomy, meticulous biopsy technique, and close collaboration among the interventional radiologist, pathologist, microbiologist, and clinician is essential to obtaining good results and avoiding complications.

Abbreviations

CT Computed tomography

1 Introduction

An accurate diagnosis of spinal infection is essential for its successful management, but it remains a challenging exercise. Percutaneous spine biopsy is an effective modality for the prompt diagnosis and proper management of spinal infection when the other biological tests are negative. It allows obtaining of specimens for microbiological and histopathological diagnosis. One or more spinal biopsies are sometimes needed before the causative agent can be isolated from the specimen. Percutaneous imaging-guided biopsy has several advantages over surgical open biopsy. It is a safe and cost- and time-saving procedure and is less painful and less invasive than surgical biopsy. It usually does not require hospitalization or general anesthesia and results in fewer complications (Peh 2006; Colmenero et al. 2013).

Apart from investigating spinal infection, percutaneous spinal biopsy may be indicated to determine the nature of a solitary spine lesion or exclude malignancy by differentiating infections (most commonly tuberculosis) from malignant lesions (Aithala 2016). Several image-guidance technologies are available including fluoroscopy, computed tomography (CT), ultrasonography, and magnetic resonance imaging (MRI) (Wu et al. 2012; Liu et al. 2015) but CT and fluoroscopy remain the most frequently used ones. A good knowledge of spinal anatomy and a meticulous technique is important to obtain good results and to avoid complications.

2 General Principles, Indications, and Pre-biopsy Work-Up

First described by Coley and Martin in the early 1930s, percutaneous bone biopsy was used for spine lesions in 1935 by Robertson and Ball. The use of trephine and radiographs during the procedure was reported by Siffert et al. in 1949, and the use of CT for biopsy guidance was first reported by Adapon in 1981 (Nourbakhsh 2015). Percutaneous spinal biopsy is expected to serve as an effective modality for the prompt diagnosis and proper management of spinal infection (Colmenero et al. 2013). It is indicated in patients with suspected spinal infection, aiming to obtain samples of organism when a microbiological diagnosis for a known associated organism has not been established by blood cultures or serological tests (Peh 2006; Berbari et al. 2015). There are two other clinical scenarios of spinal infection that need biopsy, namely, to differentiate malignant lesion from infection (most commonly tuberculosis) and, secondly, treatment failure in a patient with clinical and imaging evidence of spinal infection (Berbari et al. 2015; Aithala 2016).

A well-planned and executed biopsy is however essential for accurate diagnosis and therefore appropriate treatment (Peh 2006). It should be performed in referral centers as it has been proven that the complication rates are lower (Nourbakhsh 2015). The only absolute contraindication of percutaneous spinal biopsy is bleeding diathesis with

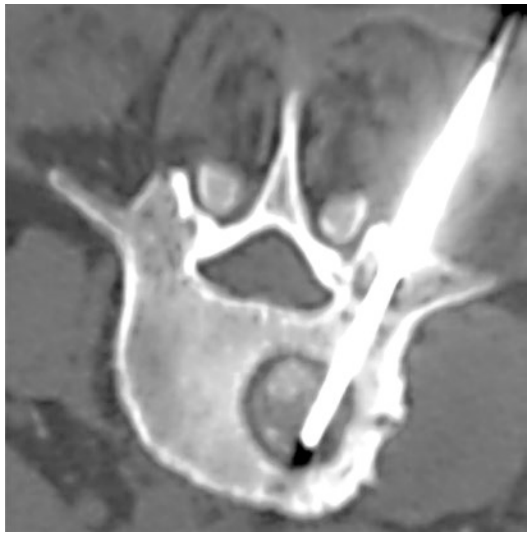

Fig. 1 Percutaneous spinal biopsy. Axial CT image shows the transpedicular approach in the lumbar vertebral body of a patient with vertebral infection

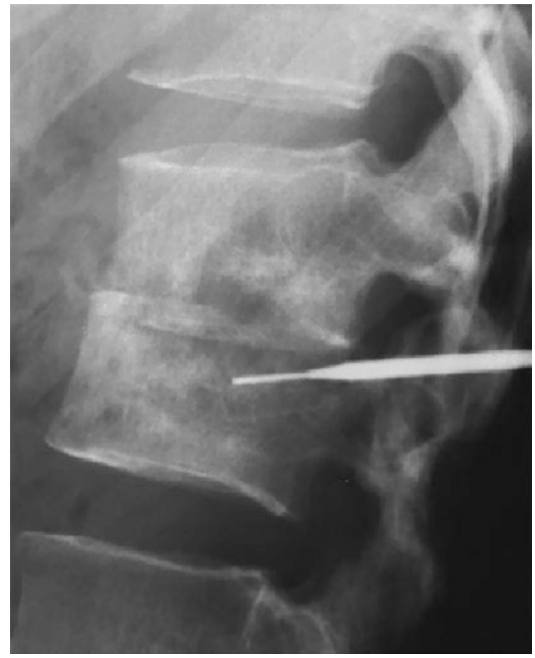

Fig. 2 Percutaneous spinal biopsy. Lateral radiograph shows the costovertebral approach in the lower thoracic vertebral body of a patient with vertebral infection

decreased platelet count <50,000/mm^3 (Peh 2006; Nourbakhsh 2015). The pre-biopsy work-up should include routine spine radiographs, CT, and/or MRI of the spine, complete blood count, activated partial thromboplastin time (APTT), and prothrombin time (PT). The radiologist should carefully study the radiographs, CT, and/or MRI before the biopsy: firstly, to rule out some conditions that do not need biopsy such as spinal echinococcosis and degenerative disk disease and, secondly, to choose the most appropriate approach and therefore to avoid vital structures (Peh 2006; Ladeb et al. 2019). The diagnostic algorithm for patients with clinical suspicion of spinal infection (Fig. 1) is found in the chapter entitled "Diagnostic Algorithm of Spinal Infection".

Percutaneous spinal biopsy is usually performed under local anesthesia. The need for sedation or antianxiety premedication should be evaluated and written informed consent obtained (Peh 2006; Nourbakhsh 2015). Anticoagulants, aspirin, and nonsteroidal anti-inflammatory drugs should be discontinued 7 days before the biopsy (Nourbakhsh 2015). Spinal biopsy should be performed before starting antibiotics, with samples sent for both pathological and bacteriological examinations (Rankine et al. 2004). Otherwise, antibiotics should be stopped at least 48 h before the procedure. However, apart from the lower success rate, antibiotic therapy should not be considered as a reason for not performing percutaneous biopsy in cases of suspected infection (Rehm et al. 2016). The diagnostic algorithm for management and etiological diagnosis of spinal infection (Fig. 2), including the role of imaging-guided percutaneous biopsy, is found in the chapter entitled "Diagnostic Algorithm of Spinal Infection".

3 Biopsy Technique

3.1 Guidance Methods

A variety of imaging modalities, such as fluoroscopy, CT, CT fluoroscopy, ultrasonography, and MRI, may be used for biopsy guidance. The choice of imaging guidance modality to be employed is determined by individual operator preference and the availability of equipment and facilities (Peh 2006; Shrestha et al. 2015). CT is currently the modality of choice for guiding percutaneous biopsy of spinal lesions. It has been shown to be slightly superior to fluoroscopy for percutaneous biopsy, with regard to adequacy

(92.6% in CT versus 90.1% in fluoroscopy), accuracy (90.2% in CT versus 88.1% in fluoroscopy), and complications (3.3% in CT versus 5.3% in fluoroscopy); although the differences were not statistically significant (Nourbakhsh 2015; Chaudhary et al. 2019).

Compared with fluoroscopy, CT more precisely shows the needle position and is potentially safer. Some lesions may be inaccessible under fluoroscopy guidance due to their small size or anatomical site. Additionally, visualization of the neural arch and paravertebral lesions is difficult by fluoroscopy, while CT ensures accurate biopsy of these lesions (Nourbakhsh 2015). However, a meta-analysis did not show any difference between percutaneous spinal biopsy performed under fluoroscopy compared to CT guidance (Pupaibool et al. 2015; Sahoo et al. 2019). With CT fluoroscopy, near real-time imaging is possible using a relatively small radiation dosage compared with conventional diagnostic CT (Peh 2006).

Ultrasonography has been advocated for guiding biopsy of lesions in the cervical spine and posterior elements of the thoracic and lumbar spine. The reasons for considering ultrasonography are cost-effectiveness, real-time monitoring, and avoidance of ionizing radiation. This modality cannot be used for deeply located bone lesions without invasion to the cortex. However, it can successfully be used for vertebral posterior elements or paraspinal lesions.

Independently of the chosen method of guidance, percutaneous spinal biopsy must be performed in aseptic conditions, identical to those achieved in the operating room. The decision also depends on the availability of imaging guidance and the expertise of the physician. There might be a steep learning curve to gain expertise in the wide variety of approaches used to obtain adequate specimens. The duration of biopsy depends on the radiologist's expertise and lesion site. Rehm et al. (2016) observed a strong correlation between the anatomical level and the biopsy duration; following the rule that the closer to the sacrum, the faster the biopsy was carried out. An overview of CT-guided percutaneous biopsy is provided in the chapter entitled "Radiography and Computed Tomography of Spinal Infection".

3.2 Patient Positioning and Biopsy Approach

The approach to be adopted by the interventional radiologist should be appropriately tailored for each patient. It depends on the involved spine level, the exact site of the lesion, and patient positioning (Peh 2006; Gallucci and D'Orazio 2015). A lateral extrapedicular approach may be used for the lumbar spine and the transpedicular approach (Fig. 1) or transcostovertebral approach (Figs. 2 and 3) for the thoracic and lumbar spine or posteriorly located cervical lesions (Peh 2006; Wiesner et al. 2018).

In biopsy of anteriorly located lesions in the mid- and lower cervical spine, an anterolateral approach is usually adopted (Fig. 4). The radiologist's fingers are used to guard the carotid artery, the internal jugular vein, and adjacent nerves, while the needle is inserted and directed towards the vertebral lesion. The patient's right side is preferably used, to avoid puncturing the esophagus and trachea (Peh 2006; Wiesner et al. 2018). The trans-oral approach is recommended for anteriorly located lesions of the first three cervical vertebrae, with this procedure preferably referred to the otolaryngological surgeon (Peh 2006; Nourbakhsh 2015).

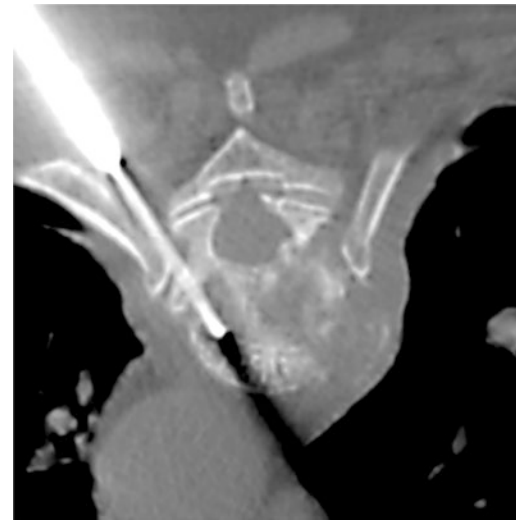

Fig. 3 Percutaneous spinal biopsy. Axial CT image shows the costovertebral approach in the thoracic vertebral body of a patient with vertebral infection

For sacral lesions, either a posterior or posterolateral approach may be used (Nourbakhsh 2015).

The patient's position depends on the guidance method and biopsy site and aims to facilitate needle access to the lesion and ensure as much comfort as possible to the patient while limiting movement. The prone position is usually used for CT-guided spinal biopsy of the thoracic and lumbosacral spine, as well as posterior elements of the cervical spine, whereas the supine position is used for anteriorly located cervical spinal lesions. Lateral decubitus and semi-prone or semi-supine position are rarely used. Care should still be taken to minimize irradiation to both the patient and the operator (Peh 2006). The patient's vital signs should be continuously monitored during the procedure.

Following preliminary scanning, the most appropriate image is selected to plan the most optimal needle route (entry point, lesion depth, and angle), taking care to avoid vital anatomical structures, major blood vessels, nerves, peritoneal cavity, as well as the spinal canal and its contents. The skin is then cleaned and draped. After administration of local anesthesia (1% lignocaine), a small skin incision is made, and the biopsy needle is inserted and directed into the lesion under imaging guidance (Peh 2006; Ladeb et al. 2019). The determinants of the approach, instruments, and imaging method used for spinal biopsy include the lesion type, location of the lesion in the vertebrae, and the involved spinal level (Nourbakhsh 2015).

3.3 Biopsy Methods and Needles

Three main methods of percutaneous spine biopsy are currently used, namely, discovertebral core biopsy in which the operator performs a biopsy on the disk and adjacent vertebral end plates; fine needle aspiration or biopsy of the intervertebral disk; and biopsy of the paravertebral abscess wall (Fig. 5). International scien-

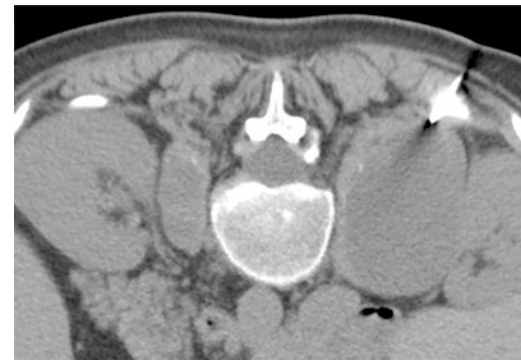

Fig. 5 Axial CT image shows percutaneous biopsy of the psoas abscess wall in a patient with infectious spondylodiscitis

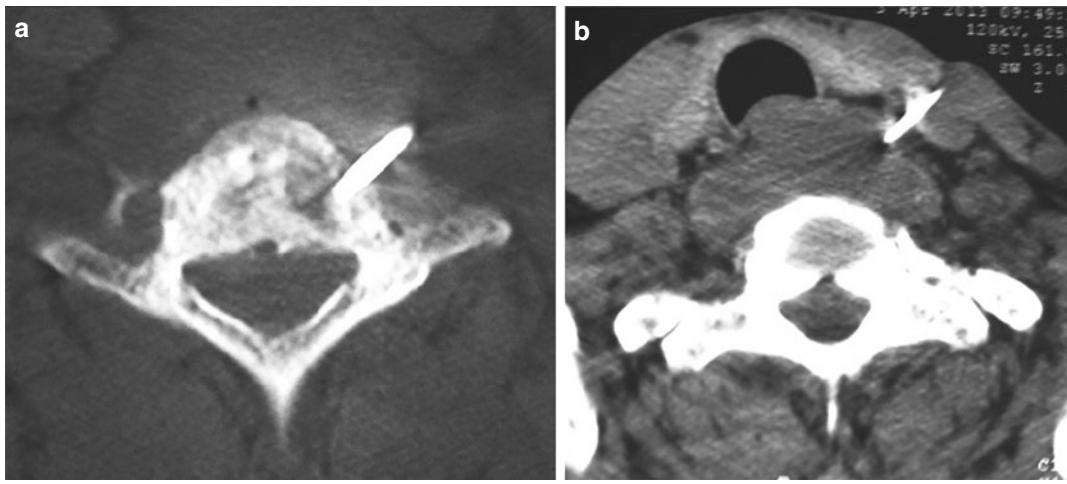

Fig. 4 Percutaneous biopsy of the cervical spine in a patient with infectious spondylodiscitis. (**a**) Axial CT image obtained in bone window setting shows the anterolateral approach. (**b**) Aspiration of the prevertebral abscess was performed at the end of the procedure

tific societies recommend discovertebral biopsy, advising radiologists to obtain at least three specimens during biopsy (Spilf 2007; Berbari et al. 2015; Ladeb et al. 2019). The combination of aspiration and biopsy is preferred (Nourbakhsh 2015).

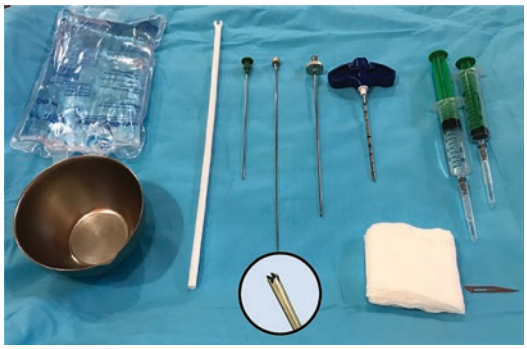

Fig. 6 Photograph shows tray setting for percutaneous spine biopsy, including trephine 11G coaxial needle (inset—the cutting tip of needle), syringes for lidocaine and saline solution

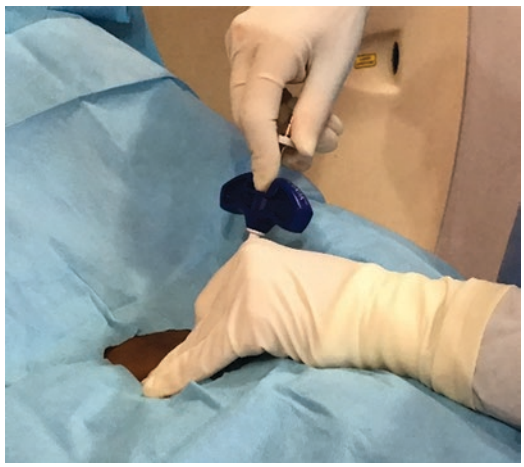

Fig. 7 Photograph shows percutaneous spinal biopsy performed under CT fluoroscopic guidance using a coaxial needle biopsy system

The type of needle used depends on the biopsy method, the nature of the lesion, and the operator's personal preference. A large variety of needles are available: aspiration needles (e.g., spinal or Chiba) are mainly used for fine needle aspiration of the disk and cutting, or Tru-cut needles are mostly used in paravertebral soft tissue biopsy, and trephine needles are used for discovertebral biopsy (Fig. 6). They range in size from 11G to 22G. The needle should be long enough to reach the lesion and have the appropriate bore size to obtain an adequate amount of specimen (Peh 2006; Sahoo et al. 2019).

Whichever needle type and imaging method are employed, imaging should be continuously or at least intermittently done: firstly, to ensure that the needle tip is in a safe position during its insertion and, secondly, to confirm its placement within the lesion. Ideally, the needle should be placed into different parts of the lesion to ensure representative sampling (Peh 2006). Coaxial biopsy needle systems facilitate the procedure and allow easy and rapid obtention of multiple samples (Fig. 7).

3.4 Specimen Handling

All material, tissue or fluid obtained, including blood clots, should be sent for cytology, culture, and histopathological examination (Fig. 8). As there are different methods of specimen handling and fixation, pre-procedure consultation among the radiologist, microbiologist, and pathologist is

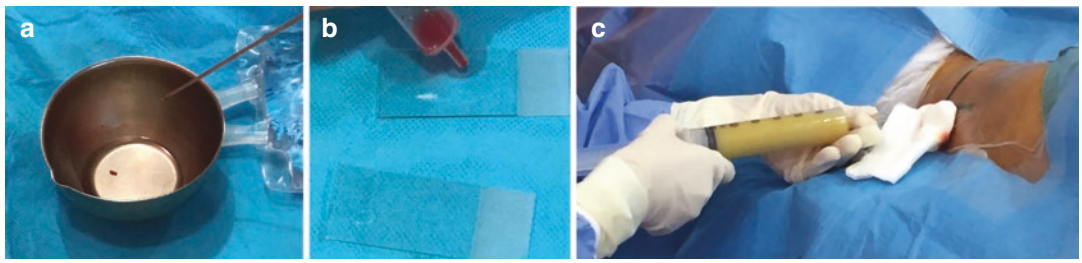

Fig. 8 Photographs show different types of specimens obtained during spinal biopsy for (**a**) histological, (**b**) cytological, and (**c**) pus for microbiological studies

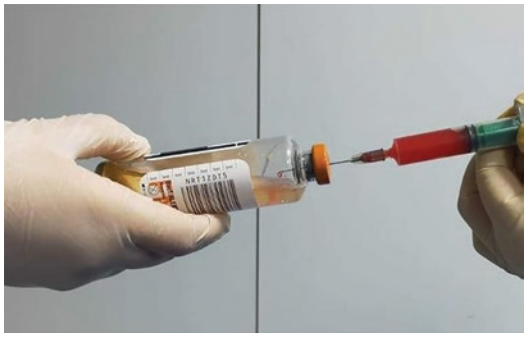

Fig. 9 Photograph shows immediate culturing of liquid samples in blood culture bottles in the procedure room

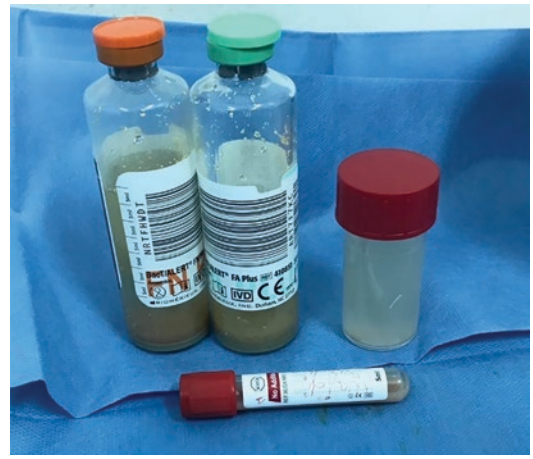

Fig. 10 Photograph shows the various types of containers used for culture and histopathological specimens

required to ensure that the adequate number of specimens are obtained, and proper tests are ordered. The latter includes cultures, gram staining, gene amplification techniques, and histology tests (Nourbakhsh 2015). As many specimens as possible should be submitted to the laboratory and may include aspirates and/or tissue biopsies. However, there is no available data demonstrating which and how many tests should be utilized to be the ideal "combined reference standard" (Pupaibool et al. 2015).

Solid samples are usually sent for histopathological examination, but at least one of them should be collected in a sterile container and then submitted for culture. Liquid samples should ideally be immediately cultured in blood culture bottles in the procedure room (Fig. 9). If anaerobics are the expected causative organisms, rapid handling to the microbiologist is necessary. When an infection is suspected and no fluid could be obtained, several sterile saline injections and aspirations should be tried. Specimens should be transported immediately to the laboratory at room temperature.

All the specimens should be carefully labeled and dispatched promptly by a responsible person. The radiologist should also be familiar with smear preparation on glass slides and the various types of containers to be used for culture and histopathological specimens (Peh 2006) (Fig. 10). Clinical and epidemiologic information should be provided on the request form because additional testing may be required (Ladeb et al. 2019). The histological examination of the blood clots increases the accuracy of the biopsy and hence should be treated like a tissue specimen (Nourbakhsh 2015).

3.5 Follow-Up

Post-biopsy care monitoring of the patient may vary in duration from 1 h to overnight observation. Some authors recommend a chest radiograph after thoracic spine biopsy. In cases of wide-bore trephine use or high-risk patients, cardiopulmonary monitoring is recommended (Nourbakhsh 2015). Post-procedure blood cultures are recommended by some authors, but this practice is still controversial (Ladeb et al. 2019).

Negative results in the presence of high clinical suspicion necessitate a repeat biopsy before institution of prolonged antibiotic therapy (Ozsarlak et al. 2003; Kasalak et al. 2018). In cases of a negative initial biopsy, repeat CT-guided biopsy improves the overall yield (Terreaux et al. 2016; Husseini et al. 2020). Open biopsy should be considered when percutaneous needle biopsy yields a negative result, to enable administration of organism-specific antibiotics for a successful outcome. Furthermore, empirical antibiotics should be delayed until the results of cultures are available, unless the patient is severely septic, critically ill, neutropenic, or neurologically compromised (Nourbakhsh 2015).

4 Results

4.1 Microbiological Diagnosis of Spinal Infection

The epidemiology of the causative agents for spinal infection depends on the geographical area. Typical bacterial agents such as *Staphylococcus aureus*, *Streptococcus* spp., enterobacteria, and other gram-negative rods are the most common pathogens isolated in most regions of the world. However, *Mycobacterium tuberculosis* and *Brucella* spp. are among the common pathogens in certain endemic regions. Fungi are rare and are essentially reported in immunocompromised patients (Berbari et al. 2015).

Current Infectious Disease Society of America guidelines suggest the addition of fungal, mycobacterial, or brucellar cultures on image-guided biopsy and aspiration specimens in patients with suspected spinal infection, if epidemiological host risk factors or characteristic imaging clues are present. They also suggest the addition of fungal and mycobacterial cultures and bacterial nucleic acid amplification testing to appropriately stored specimens if aerobic and anaerobic bacterial cultures reveal no growth in patients with suspected spinal infection. Molecular diagnostic tools had been especially useful in the diagnosis of brucellar, mycobacterial, and fungal spinal infections (Berbari et al. 2015). When brucellar native vertebral osteomyelitis is suspected, the physician is advised to alert the microbiology laboratory personnel to mitigate the risk of laboratory-acquired brucellar infection and to use appropriate techniques (Berbari et al. 2015).

The reported overall accuracy of CT-guided spinal bone biopsy varies from 67 to 97% (Peh 2006; Nourbakhsh 2015). However, in cases of spinal infection, the reported accuracy is more variable, with positive microbiological results obtained in 29–70% of cases (Rankine et al. 2004; Sehn and Gilula 2012; Pupaibool et al. 2015; Joo et al. 2016; Ladeb et al. 2019; Özmen et al. 2019; Sertic et al. 2019). This is lower than the diagnostic yield of blood cultures which is approximately 59% and open biopsies estimated at 91%. This could be explained by the fact that more severe cases requiring surgical management could correlate to higher pathogen load (Sertic et al. 2019).

The location and type of the lesion, needle bore size, and imaging guidance modality have been mentioned as determinants of the accuracy of spinal biopsy (Nourbakhsh 2015; Aithala 2016). The wide range of success rates depends on the organism and multiple other factors, including inadequate amount of specimen, sampling error, and empirical antibiotics at the time of the biopsy, as well as experience and skill of radiologist and sometimes difficulty of the paraspinal approach (Nam et al. 2011; Pupaibool et al. 2015; Rehm et al. 2016). The puncture site and biopsy method do not seem to influence the results: no statistical difference was found among yields of end-plate disk, disk-only, and paravertebral soft-tissue biopsies, either for microbiological or histological study (Chang et al. 2015; Özmen et al. 2019).

However, improvements can be made in biopsy technique and specimen transfer to optimize culture yield and increase the clinical value of the procedure. Taking several cores seem to improve the diagnostic yield. However, obtaining more than three biopsies of the lesion does not increase the likelihood of positive results (Nourbakhsh 2015). Previous antibiotic therapy administration has been recognized as a major cause for negative results of microbiological examination of the specimen obtained. Some authors advise repeating the biopsy after at least 1 week without antibiotic therapy (Gallucci and D'Orazio 2015). Despite this, spinal biopsy is still worthwhile performing, even if the patient has been started on antibiotics (Rankine et al. 2004). In a recent meta-analysis, McNamara et al. (2017) did not find a significantly different biopsy yield between patients with and without prior antibiotic exposure.

4.2 Histopathological Diagnosis of Spinal Infection

In routine practice, fixation and decalcification are required for processing tissues obtained from

the spine. The control of these key steps is crucial to preserve tissue morphology for histopathological examination and deoxyribonucleic acid (DNA) for molecular analysis. Fixation of core bone specimens in buffered formalin for at least 6 h is recommended. Ethylene diamine tetracetic acid (EDTA) is recommended for the decalcification of core bone specimens. However, for surgical specimens, decalcification with EDTA is slow and time-consuming. The histological examination of the blood clots increases the accuracy of the biopsy and should be treated as a tissue specimen (Nourbakhsh 2015). Although the diagnosis of infectious spondylodiscitis is mainly confirmed by microbiological investigations, histopathological examination of bone specimens is a key tool for the etiological diagnosis of the disease. Positive culture is not always obtained due to the low load of microorganisms and the difficulty of cultivating them. The etiological agent is never identified in approximately one-third of infectious spondylodiscitis (Sheikh et al. 2017).

Histopathology provides valuable information on cell morphology and tissue changes that allow the determination of the etiological diagnosis of infectious spondylodiscitis. Histopathological features show a large spectrum, which vary from neutrophil-rich infiltrate to granulomatous infection (Duarte and Vaccaro 2013). Positive histopathological results in patients with suspected infectious spondylodiscitis vary in the literature from 55 to 74% (Romdhane et al. 2020; Özmen et al. 2019), reaching more than 96% for spinal tuberculosis (Ladeb et al. 2019; Rammeh et al. 2021). The main goal of the histological study is to distinguish granulomatous from non-granulomatous spinal infections, and in the case of spinal tuberculosis, it may be sufficient to confirm the diagnosis, even in the absence of microbiological positivity (Romdhane et al. 2020). Pyogenic spinal infection is histologically characterized by edematous fibrosis and neutrophil-rich infiltrate (Li et al. 2016). The composition of the infiltrate depends on the stage of the disease. Neutrophils are numerous in the early stage (Fig. 11). But these features are not pathognomonic, as neutrophil-rich infiltrate is also observed in rare forms of tuberculous spondylodiscitis, in fungal spondylodiscitis, and even in brucellar spondylodiscitis (Rammeh et al. 2020).

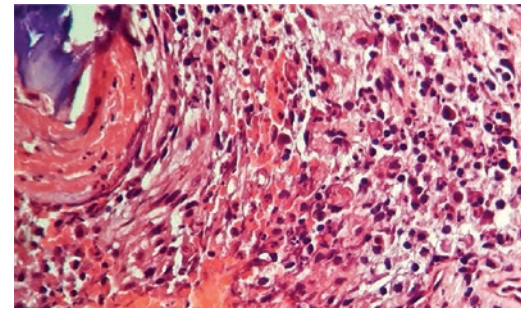

Fig. 11 Pyogenic spondylodiscitis. Photomicrograph shows neutrophil-rich inflammatory infiltrate in a medullary space. [Hematoxylin and eosin ×400]

Tuberculous spondylodiscitis is characterized by necrotizing epithelioid granulomas (Romdhane et al. 2020), which is observed in 59–76% of spinal tuberculosis (Cottle and Riordan 2008). Epithelioid granulomas are nodular-like focal collections of macrophage-derived cells called epithelioid cells, with elongated nuclei, abundant and eosinophilic cytoplasm, and poorly defined margins. Epithelioid granulomas include also lymphocytes and giant cells called Langhans cells, which are multinucleated cells characterized by numerous nuclei arranged peripherally in the shape of a horseshoe. As Langhans giant cells are seen in other granulomatous inflammations, they are not pathognomonic of tuberculosis. Caseous necrosis is highly suggestive of tuberculosis but is also not pathognomonic, as it may be also seen in other granulomatous diseases, e.g., fungal infection (Romdhane et al. 2020; Rammeh et al. 2021). Caseous necrosis is a distinctive form of coagulative necrosis. Macroscopically, it has a soft and white proteinaceous cheese-like appearance. Histologically, it appears as an eosinophilic, amorphous granular area, and often surrounded by a rim of epithelioid cells (Figs. 12, 13, and 14).

Granulomatous inflammation, in an appropriate clinical setting, is highly suggestive of tuberculous spondylodiscitis. Other granulomatous inflammations such as brucellosis, fungal spondylodiscitis, and sarcoidosis must be excluded (Duarte and Vaccaro 2013; Rammeh et al. 2021). In our series, tuberculosis represented 89.5% of

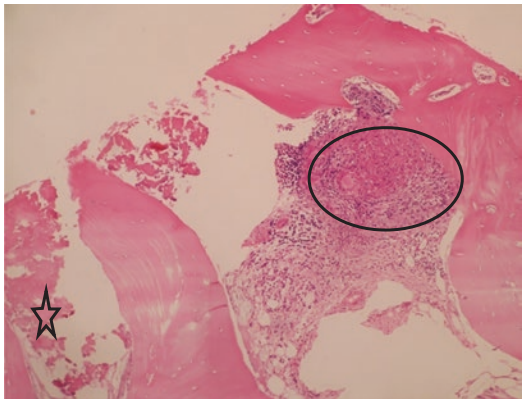

Fig. 12 Tuberculous spondylodiscitis. Photomicrograph shows caseous necrotic material (star) and epithelioid granuloma (circled) with giant cells in a medullary space. [Hematoxylin and eosin ×400]

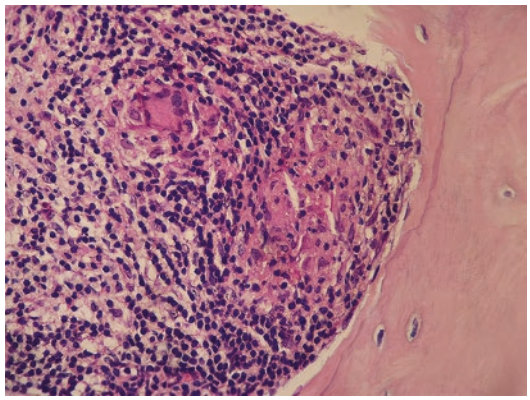

Fig. 13 Tuberculous spondylodiscitis. Photomicrograph shows a well-formed epithelioid granuloma with a giant cell. [Hematoxylin and eosin ×400]

granulomatous spondylodiscitis, while brucellosis represented 5.3%, fungi 3.5%, and sarcoidosis 1.7% (Rammeh et al. 2021). Suppurative forms of tuberculous spondylodiscitis mimicking pyogenic and fungal spondylodiscitis exist (Rammeh et al. 2021). The detection of acid-fast bacilli by Ziehl-Neelsen staining on formalin-fixed, paraffin-embedded tissues (FFPET) confirms the diagnosis of tuberculous spondylodiscitis. But due to the paucibacillary character of the disease in the spinal location, Ziehl-Neelsen staining often fails to visualize acid-fast bacilli. Immunohistochemistry using specific anti-*Mycobacterium tuberculosis* antibodies can be an

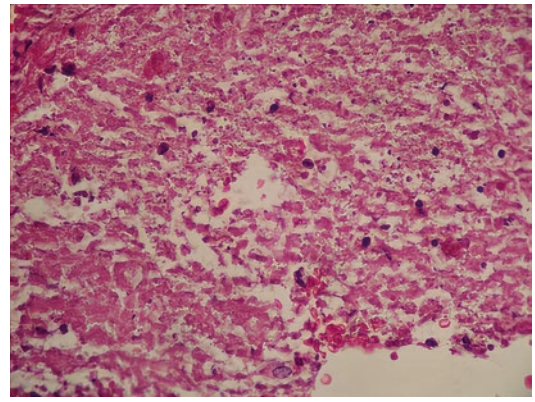

Fig. 14 Tuberculous spondylodiscitis. Photomicrograph shows typical caseous necrosis with eosinophilic, amorphous, and granular appearance. [Hematoxylin and eosin ×400]

alternative to Ziehl-Neelsen staining (Kohli et al. 2014).

Fungal spondylodiscitis is rare. Histologically, it displays suppurative and granulomatous forms, mimicking pyogenic and tuberculous spondylodiscitis. Many fungal microorganisms, such as *Candida albicans*, *Aspergillus* spp., and *Cryptococcus neoformans*, can be visualized by hematoxylin and eosin staining. Periodic acid Schiff and Gomori methenamine silver staining demonstrates spores and mycelial filaments in yeast infections and hyphae in fungal infections (Guarner and Brandt 2011). These stains must be systematically performed in the context of infectious spondylodiscitis to rule out fungal spondylodiscitis. Histopathological examination may suggest the nature of the fungal agent; for example, *Candida albicans* is a yeast-like fungus with budding and non-septated hyphae filamentous (pseudohyphal and hyphal) forms. *Aspergillus* spp. have septate hyphae with dichotomous branching. *Cryptococcus neoformans* is a yeast-like fungus. The yeast forms of cryptococcosis are usually widely separated by a thick mucoid capsule decorated by Periodic acid-Schiff and by mucicarmine stains (Figs. 15, 16, 17, and 18).

The diagnosis of brucellar spondylodiscitis is commonly based on clinical data and confirmed by the detection of specific antibodies (Wright, Rose Bengal, immunofluorescence) and/or the isolation of the causative agent from blood or

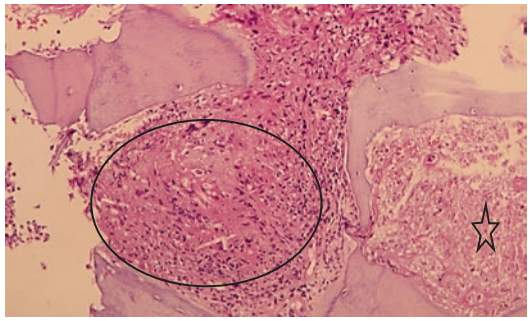

Fig. 15 Aspergillus spondylodiscitis. Photomicrograph shows medullary dense inflammatory infiltrate with ill-defined histiocytic granuloma and caseous-like necrotic material (star). [Hematoxylin and eosin ×400]

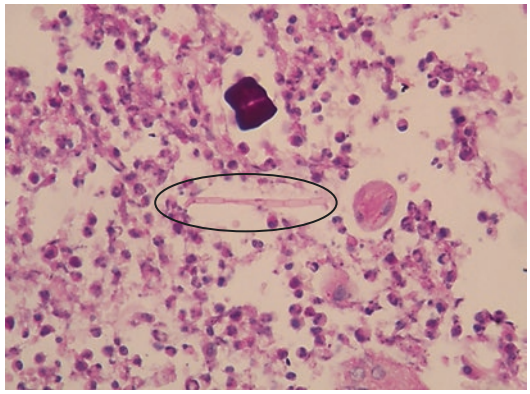

Fig. 16 Aspergillus spondylodiscitis. Photomicrograph shows septate hyphae in a dense neutrophil infiltrate. [Hematoxylin and eosin ×400]

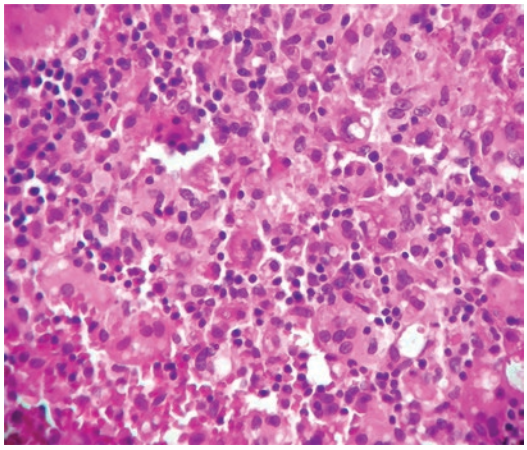

Fig. 17 Cryptococcal spondylodiscitis. Photomicrograph shows histiocytic-rich infiltrate containing weakly stained spores. [Hematoxylin and eosin ×400]

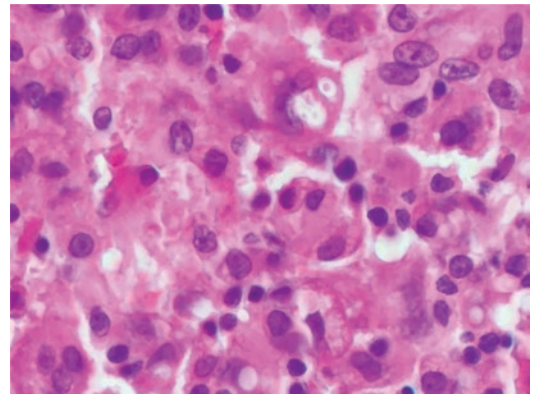

Fig. 18 Cryptococcal spondylodiscitis. Photomicrograph shows intracellular round/oval yeast, with a size of 4–10 microns with a thick capsule. [Hematoxylin and eosin ×600]

tissues (Al Dahouk and Nöckler 2011; Bozbaş et al. 2016). The histopathological examination is carried out in two circumstances, namely, in cases with negative microbiological tests and high clinical suspicion of brucellosis and to exclude a tuberculous coinfection. In these circumstances, biopsy is advisable to obtain tissue samples for microbiological and histopathological investigations to confirm brucellar spondylodiscitis (Rammeh et al. 2020). The histopathological diagnosis of brucellar spondylodiscitis is challenging because it shows a large spectrum of histopathological lesions with nonspecific and granulomatous forms—each observed in about half of the cases (Fuentes Ferrer et al. 2012; Li et al. 2016; Rammeh et al. 2020).

The brucellar granuloma, highly suggestive of brucellar spondylodiscitis, is surrounded by a chronic inflammatory reaction composed of lymphocytes, plasmocytes, and neutrophils (Mondal and Misra 1994). It is typically small, not well-formed, noncaseating, and composed of aggregates of histiocytes with round nuclei without epithelioid appearance (Fig. 19). Granulomas with an epithelioid appearance and even caseous-like necrosis, although rare, are possible in brucellar spondylodiscitis (Rammeh et al. 2020). Epithelioid granulomas formed by eosinophilic cells with elongated nuclei are rarely observed in brucellar spondylodiscitis. They are typically associated with histiocytic-type granulomas and are not well-

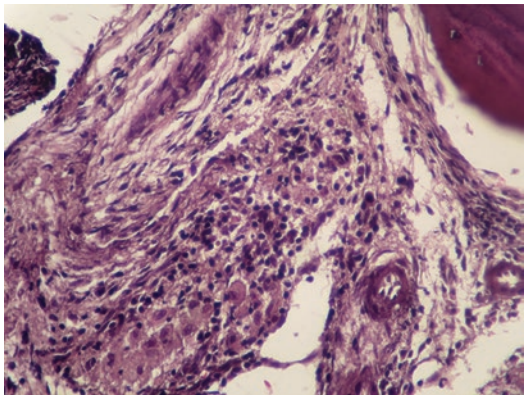

Fig. 19 Brucellar granuloma. Photomicrograph shows small aggregates of histiocytes with round nuclei, surrounded by a chronic inflammatory reaction. [Hematoxylin and eosin ×400]

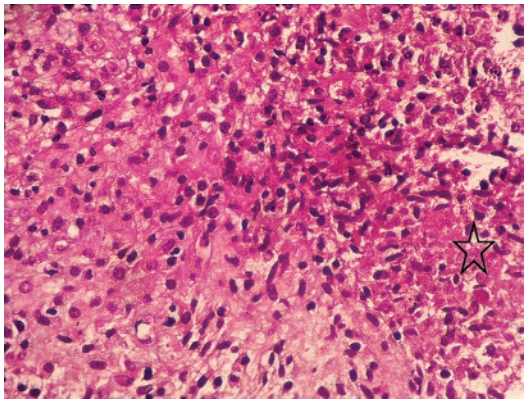

Fig. 20 Brucellar spondylodiscitis. Photomicrograph shows epithelioid granuloma with caseous-like necrosis. [Hematoxylin and eosin ×400]

formed like those classically observed in tuberculous spondylodiscitis (Fig. 20). The association of histiocytic and epithelioid granulomas has also been reported in fungal and tuberculous spondylodiscitis (Cottle and Riordan 2008). Nonspecific forms of brucellar spondylodiscitis characterized by non-granulomatous infiltrate show typically a polymorphous infiltrate with the predominance of lymphocytes and plasmocytes (Figs. 21 and 22). As these forms mimic pyogenic spondylodiscitis, their distinction is histologically challenging. Pyogenic spondylodiscitis is characterized by predominant neutrophil infiltration (Landi et al. 2017). The predominance of the mononuclear

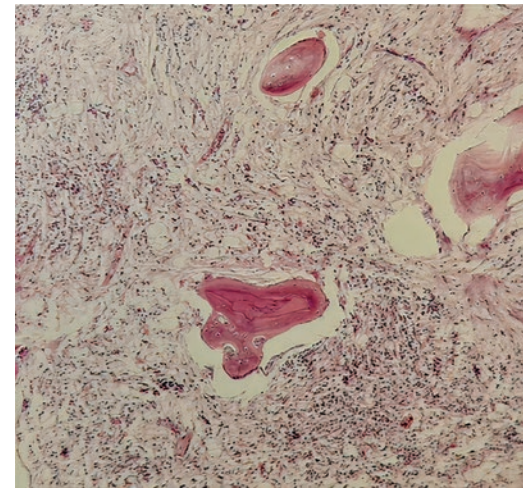

Fig. 21 Brucellar spondylodiscitis. Photomicrograph shows polymorphous inflammatory infiltrate without epithelioid granuloma. [Hematoxylin and eosin ×100]

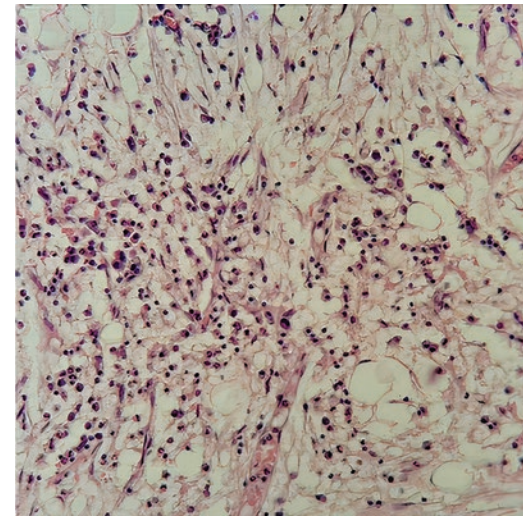

Fig. 22 Brucellar spondylodiscitis. Nonspecific form. Photomicrograph shows inflammatory infiltrate with plasmocytes and neutrophils. [Hematoxylin and eosin ×400]

cells should alert the pathologist to suggest the diagnosis of brucellar spondylodiscitis.

4.3 Cytological Diagnosis of Spinal Infection

CT-guided fine needle aspiration cytology (FNAC) is a simple and economical tool in the

diagnosis of spinal infection, compared with core-needle biopsy or excision biopsy. It can provide an accurate diagnosis of spinal infection when it is used with a proper combination of experience and diligence (Mondal and Misra 1994). FNAC is cytologist- and operator-dependent procedure which requires experienced cytologists and radiologists, sufficient material, good sampling method, and coordination among the cytologist, radiologist, and physician (Jorda et al. 2000). It is recommended for paravertebral abscesses and for osteolytic lesions with cortical disruption (De Lucas et al. 2009). In countries with high tuberculosis endemicity, FNAC may be an alternative to histopathology and is also suitable for obtaining material for microbiology. *Mycobacterium tuberculosis* is easily isolated from these sites. The cytological diagnosis of spinal tuberculosis depends upon the demonstration of epithelioid granuloma with necrotic material which is observed in 50–68% of cases (Handa et al. 2010). The rate of noncontributory FNAC is one of the major limitations of this technique, which ranges from 10 to 31% (Phadke et al. 2001).

4.4 Molecular Diagnosis of Spinal Infection

With the advent of molecular techniques, the diagnosis of spinal infection has become prompt and accurate, allowing the initiation of adequate treatment and preventing neurological complications (Lecouvet et al. 2004; Gouliouris et al. 2010; Jacquier et al. 2019). These techniques are validated on fresh samples and can be helpful on FFPET but only a few studies have assessed the value of molecular diagnosis on FFPET. Molecular diagnosis provides a considerable gain in terms of sensitivity and rapidity. It is performed on biopsies frozen at −20 °C when cultures remain negative. It is particularly useful in case of decapitated infections or in case of infections due to microorganisms rarely isolated or with fastidious culture. It is based on specific or universal PCR techniques, which are currently accepted but whose indications are not well-established due to their lack of standardization (Ladeb et al. 2019).

Specific real-time PCR has shown good performance in the diagnosis of *Staphylococcus aureus*, brucellosis, and mycobacterial and fungal spinal infections (Berbari et al. 2015; Chebbi et al. 2019). PCR methods are widely used for the detection and the identification of *Brucella* spp. from peripheral blood or from fresh tissues (Kaden et al. 2017). They can be combined with clinical findings to differentiate between the different stages of brucellosis (Wang et al. 2014; Kaden et al. 2017). The efficacy of molecular methods depends mainly on the specificity of primers. Various targets used for the diagnosis of brucellosis include gene encoding BCSP 31, a sequence 16S rRNA of *B. abortus*, and a gene encoding omp2 (Wang et al. 2014). Colmenero et al. (2013) reported a sensitivity of 100% using the gene BCSP 31.

The utility of molecular diagnostic tools is also proved for diagnosing pyogenic spondylodiscitis. Several studies have demonstrated the advantage of targeting 16S rDNA for rapid identification of *Staphylococcus aureus* (Sheikh et al. 2017) and the gene mecA for the detection of methicillin-resistant *Staphylococcus aureus* (Kobayashi et al. 2009). The detection of galactomannan antigen by PCR is known to be a rapid tool for the diagnosis of invasive fungal infections. Given the rarity of this disease, the performance of PCR for the diagnosis of fungal infection has not been widely reported (Jorge et al. 2012). Molecular methods allow a rapid diagnosis of tuberculous spondylodiscitis. Most of the studies have used the insertion sequence IS6110 because *Mycobacterium tuberculosis* contains between 6 and 25 copies of this repetitive element. The majority of the studies reported the performances of uniplex, multiplex, and real-time PCRs. The sensitivity and specificity of PCR in fresh tissue for the diagnosis of spinal tuberculosis vary from 61 to 91% and from 63.7 to 93.7%, respectively (Rammeh et al. 2021).

The major limitation of molecular analyses on FFPET is the degradation of DNA due to fixation which are required for the histological processing of tissues. During the process of fixation, the for-

malin causes the formation of cross-linking between proteins and DNA which might interfere with the amplification process. Besides cross-linking, the oxidation of formalin to formic acid leads to the depurination, and strand DNA breaks (Dietrich et al. 2013). The control of these key steps is crucial to preserve tissue morphology for histopathological examination and nucleic acids for molecular analyses. Molecular techniques on FFPET with validated pre-analytic steps are useful tools for the diagnosis of tuberculous spondylodiscitis, especially for cases where microbiological investigations are negative or not carried out, mainly because clinical features were in favor of noninfectious pathology, e.g., metastasis and noninfectious disease (Choe et al. 2014; Jacquier et al. 2019).

5 Complications

The overall complication rate of spine biopsy varies from 0 to 10%, with serious complication rates being less than 1% (Peh 2006; Nourbakhsh 2015). The complication rate of CT-guided spinal biopsies (3.3%) is low, compared with 5.3% for fluoroscopy and compared to the open biopsy complication rate of 16% (Nourbakhsh 2015; Rehm et al. 2016). The types and incidence of complications depend on the anatomical level, the chosen approach, and the type of needle used (Peh 2006; Rehm et al. 2016). Potential complications include pneumothorax, hematoma, nerve root injury, transient paresis, transient spinal anesthesia, meningitis, radiculopathy, and paraplegia (Nourbakhsh 2015). Ultrasonography-guided biopsy has been used in the cervical and lumbar spine without any reported complications (Nourbakhsh 2015).

6 Conclusion

Percutaneous spine biopsy is an effective modality for assessment and management of spinal infection when a microbiological diagnosis for a known associated organism has not been established by blood cultures or serologic tests. It allows obtaining a specimen for microbiological and histopathological diagnosis in order to choose the appropriate treatment.

Adherence to biopsy guidelines, good planning, and execution of the procedure with accurate sample handling and close collaboration among the interventional radiologist, pathologist, microbiologist, and clinician are determinants of a successful percutaneous spinal biopsy. Compared to surgical open biopsy, percutaneous imaging-guided biopsy is a safe and cost- and time-saving procedure, which is less painful and less invasive, with good accuracy. CT and fluoroscopy remain the most frequently used imaging modalities to guide spinal biopsies. A good knowledge of the spine anatomy and of biopsy technique is essential to obtain good results.

References

Aithala JP (2016) Role of percutaneous image guided biopsy in spinal lesions: adequacy and correlation with MRI findings. J Clin Diagn Res 10(8):RC11–RC15

Al Dahouk S, Nöckler K (2011) Implications of laboratory diagnosis on brucellosis therapy. Expert Rev Anti-Infect Ther 9:833–845

Berbari EF, Kanj SS, Kowalski TJ et al (2015) Infectious Diseases Society of America (IDSA) clinical practice guidelines for the diagnosis and treatment of native vertebral osteomyelitis in adults. Clin Infect Dis 61:e26–e46

Bozbaş GT, Ünübol Aİ, Gürer G (2016) Seronegative brucellosis of the spine: a case of psoas abscess secondary to brucellar spondylitis. Eur J Rheumatol 3:185–187

Chang CY, Simeone FJ, Nelson SB, Taneja AK, Huang AJ (2015) Is biopsying the paravertebral soft tissue as effective as biopsying the disk or vertebral endplate? 10-year retrospective review of CT-guided biopsy of diskitis-osteomyelitis. AJR Am J Roentgenol 205:123–129

Chaudhary RK, Acharya S, Chahal RS, Kalra KL (2019) Fluoroscopy guided percutaneous transpedicular biopsy of vertebral body lesion. J Nepal Health Res Counc 17:163–167

Chebbi Y, Riahi H, Bouaziz MC, Romdhane E, Mhiri E, Rammeh S, Saidi LS, Achour W, Ladeb MF (2019) Mycobacterium bovis Spondylodiscitis: Report of 4 Cases. J Clin Rheumatol. https://doi.org/10.1097/RHU.0000000000001040. Online ahead of print

Choe H, Aota Y, Kobayashi N, Nakamura Y et al (2014) Rapid sensitive molecular diagnosis of pyogenic spinal infections using methicillin-resistant Staphylococcus-

specific polymerase chain reaction and 16S ribosomal RNA gene-based universal polymerase chain reaction. Spine J 14:255–262

Colmenero JD, Ruiz-Mesa JD, Sanjuan-Jimenez R, Sobrino B, Morata P (2013) Establishing the diagnosis of tuberculous vertebral osteomyelitis. Eur Spine J 22(Suppl 4):579–586

Cottle L, Riordan T (2008) Infectious spondylodiscitis. J Infect 56:401–412

De Lucas EM, González Mandly A, Gutiérrez A et al (2009) CT-guided fine-needle aspiration in vertebral osteomyelitis: true usefulness of a common practice. Clin Rheumatol 28:315–320

Dietrich D, Uhl B, Sailer V et al (2013) Improved PCR performance using template DNA from formalin-fixed and paraffin-embedded tissues by overcoming PCR inhibition. PLoS One 8(10):e77771

Duarte RM, Vaccaro AR (2013) Spinal infection: state of the art and management algorithm. Eur Spine J 22:2787–2799

Fuentes Ferrer M, Gutiérrez Torres L, Ayala Ramírez O, Rumayor Zarzuelo M, del Prado González N (2012) Tuberculosis of the spine. A systematic review of case series. Int Orthop 36:221–231

Gallucci PM, D'Orazio F (2015) Image guided interventions in spinal infections. Neuroimaging Clin N Am 25:281–294

Gouliouris T, Aliyu SH, Brown NM (2010) Spondylodiscitis: update on diagnosis and management. J Antimicrob Chemother 65(Suppl 3):iii11–iii24

Guarner J, Brandt ME (2011) Histopathologic diagnosis of fungal infections in the 21st century. Clin Microbiol Rev 24:247–280

Handa U, Garg S, Mohan H, Garg SK (2010) Role of fine-needle aspiration cytology in tuberculosis of bone. Diagn Cytopathol 38:1–4

Husseini JS, Simeone FJ, Nelson SB, Chang CY (2020) CT-guided discitis-osteomyelitis biopsies: needle gauge and microbiology results. Skeletal Radiol 49:1431–1439

Jacquier H, Fihman V, Amarsy R et al (2019) Benefits of polymerase chain reaction combined with culture for the diagnosis of bone and joint infections: a prospective test performance study. Open Forum Infect Dis 6(12):ofz511

Joo EJ, Yeom JS, Ha YE et al (2016) Diagnostic yield of computed tomography-guided bone biopsy and clinical outcomes of tuberculous and pyogenic spondylitis. Korean J Intern Med 31:762–771

Jorda M, Rey L, Hanly A, Ganjei-Azar P (2000) Fine-needle aspiration cytology of bone: accuracy and pitfalls of cytodiagnosis. Cancer 90:47–54

Jorge VC, Cardoso C, Noronha C et al (2012) Fungal spondylodiscitis in a non-immunocompromised patient. BMJ Case Rep 2012:bcr1220115337

Kaden R, Ferrari S, Alm E, Wahab T (2017) A novel real-time PCR assay for specific detection of Brucella melitensis. BMC Infect Dis 17(1):230

Kasalak Ö, Adams HJA, Jutte PC et al (2018) Culture yield of repeat percutaneous image-guided biopsy after a negative initial biopsy in suspected spondylodiscitis: a systematic review. Skeletal Radiol 47:1327–1335

Kobayashi N, Inaba Y, Choe H et al (2009) Rapid and sensitive detection of methicillin-resistant Staphylococcus periprosthetic infections using real-time polymerase chain reaction. Diagn Microbiol Infect Dis 64:172–176

Kohli R, Punia RS, Kaushik R, Kundu R, Mohan H (2014) Relative value of immunohistochemistry in detection of mycobacterial antigen in suspected cases of tuberculosis in tissue sections. Indian J Pathol Microbiol 57:574–578

Ladeb F, Ben Aissa H, Tiouiri H et al (2019) Clinical practice guidelines for the diagnosis and treatment of native vertebral osteomyelitis. Tunis Med 97: 14–92

Landi A, Grasso G, Iaiani G et al (2017) Spontaneous spinal discitis and spondylodiscitis: clinico-therapeutic remarks. J Neurosci Rural Pract 8:642–646

Lecouvet F, Irenge L, Vandercam B et al (2004) The etiologic diagnosis of infectious discitis is improved by amplification-based DNA analysis. Arthritis Rheum 50:2985–2994

Li T, Liu T, Jiang Z, Cui X, Sun J (2016) Diagnosing pyogenic, brucella and tuberculous spondylitis using histopathology and MRI: a retrospective study. Exp Ther Med 12:2069–2077

Liu M, Sequeiros RB, Xu Y et al (2015) MRI-guided percutaneous transpedicular biopsy of thoracic and lumbar spine using a 0.23t scanner with optical instrument tracking. J Magn Reson Imaging 42:1740–1746

McNamara AL, Dickerson EC, Gomez-Hassan DM, Cinti SK, Srinivasan A (2017) Yield of image-guided needle biopsy for infectious discitis: a systematic review and meta-analysis. AJNR Am J Neuroradiol 38:2021–2027

Mondal A, Misra DK (1994) CT-guided needle aspiration cytology (FNAC) of 112 vertebral lesions. Indian J Pathol Microbiol 37:255–261

Nam KH, Song GS, Han IH, Choi BK, Cha SH (2011) Diagnostic value of biopsy techniques in lumbar spondylodiscitis: percutaneous needle biopsy and open biopsy. Korean J Spine 8:267–271

Nourbakhsh A (2015) Percutaneous spine biopsy: a literature review. Int J Radiol Radiat Oncol 1:23–28

Özmen D, Özkan N, Guberina N et al (2019) Computed-tomography-guided biopsy in suspected spondylodiscitis: single-center experience including 201 biopsy procedures. Orthop Rev (Pavia) 11(1):7793

Ozsarlak O, De Schepper AM, Wang X, De Raeve H (2003) CT-guided percutaneous needle biopsy in spine lesions. JBR-BTR 86:294–296

Peh WCG (2006) CT-guided percutaneous biopsy of spinal lesions. Biomed Imaging Interv J 2(3):e25

Phadke DM, Lucas DR, Madan S (2001) Fine-needle aspiration biopsy of vertebral and intervertebral disc lesions: specimen adequacy, diagnostic utility, and pitfalls. Arch Pathol Lab Med 125:1463–1468

Pupaibool J, Vasoo S, Erwin PJ, Murad MH, Berbari EF (2015) The utility of image-guided percutaneous needle aspiration biopsy for the diagnosis of spontaneous vertebral osteomyelitis: a systematic review and meta-analysis. Spine J 15:122–131

Rammeh S, Romdhane E, Riahi H et al (2021) Granulomatous spondylodiscitis: a case series with focus on histopathological features. J Spinal Cord Med 44:282–287

Rammeh S, Romdhane E, Riahi H et al (2020) Brucellar spondylodiscitis: a case series with focus on histopathological features. J Clin Neurosci 78:360–364

Rankine JJ, Barron DA, Robinson P, Millner PA, Dickson RA (2004) Therapeutic impact of percutaneous spinal biopsy in spinal infection. Postgrad Med J 80:607–609

Rehm J, Veith S, Akbar M, Kauczor HU, Weber MA (2016) CT-guided percutaneous spine biopsy in suspected infection or malignancy: a study of 214 patients. Rofo 188:1156–1162

Romdhane E, Rammeh S, Riahi H et al (2020) The value of histology in the diagnosis of tuberculous spondylodiscitis. J Clin Rheumatol 26:63–66

Sahoo MM, Mahapatra SK, Sethi GC, Sahoo A, Kar BK (2019) Role of percutaneous transpedicular biopsy in diagnosis of spinal tuberculosis and its correlation with the clinico-radiological features. Indian J Tuberc 66:388–393

Sehn JK, Gilula LA (2012) Percutaneous needle biopsy in diagnosis and identification of causative organisms in cases of suspected vertebral osteomyelitis. Eur J Radiol 81:940–946

Sertic M, Parkes L, Mattiassi S et al (2019) The efficacy of computed tomography-guided percutaneous spine biopsies in determining a causative organism in cases of suspected infection: a systematic review. Can Assoc Radiol J 70:96–103

Sheikh AF, Khosravi AD, Goodarzi H et al (2017) Pathogen identification in suspected cases of pyogenic spondylodiscitis. Front Cell Infect Microbiol 7:60

Shrestha D, Shrestha R, Dhoju D (2015) Fluoroscopy guided percutaneous transpedicular biopsy for thoracic and lumbar vertebral body lesion: technique and safety in 23 consecutive cases. Skeletal Radiol 47:1327–1335

SPILF (2007) Primary infectious spondylitis, and following intradiscal procedure, without prothesis. Recommendations. Med Mal Infect 37: 573–538

Terreaux W, Geoffroy M, Ohl X et al (2016) Diagnostic contribution of a second percutaneous needle biopsy in patients with spontaneous diskitis and negative blood cultures and first biopsy. Joint Bone Spine 83:715–719

Wang Y, Wang Z, Zhang Y et al (2014) Polymerase chain reaction-based assays for the diagnosis of human brucellosis. Ann Clin Microbiol Antimicrob 13:31

Wiesner EL, Hillen TJ, Long J, Jennings JW (2018) Percutaneous CT-guided biopsies of the cervical spine: technique, histopathologic and microbiologic yield, and safety at a single academic institution. AJNR Am J Neuroradiol 39:981–985

Wu HT, Chang CY, Chang H et al (2012) Magnetic resonance imaging guided biopsy of musculoskeletal lesions. J Chin Med Assoc 75:160–166

Imaging of Hematogeneous Pyogenic Spondylodiscitis

Sumer N. Shikhare and Wilfred C. G. Peh

Contents

Abstract

Pyogenic spondylodiscitis (PSD) is an infection of the intervertebral disk and adjacent vertebrae, which may also involve the paravertebral soft tissues. The incidence of PSD is increasing because of the growing number of elderly people and immunocompromised patients. Hematogeneous spread is by far the commonest route of spinal infection, due to the rich arterial supply of the vertebral body. PSD warrants early diagnosis and prompt treatment to prevent morbidity and mortality. Diagnosis is often challenging and requires a high index of clinical suspicion, blood and tissue cultures, appropriate imaging, and/or imaging-guided biopsy to enable an early diagnosis. This chapter aims to provide an overview of PSD, particularly its pathophysiology and imaging features. The roles of different imaging modalities such as radiography, computed tomography,

S. N. Shikhare (✉) · W. C. G. Peh
Department of Diagnostic Radiology, Khoo Teck Puat Hospital, Singapore, Republic of Singapore
e-mail: sumershikhare@yahoo.co.in; Wilfred.peh@gmail.com.sg

© The Author(s), under exclusive license to Springer Nature Switzerland AG 2021, corrected publication 2021

M. F. Ladeb, W. C. G. Peh (eds.), *Imaging of Spinal Infection*,
Medical Radiology Diagnostic Imaging, https://doi.org/10.1007/978-3-030-70459-9_7

magnetic resonance imaging (MRI), and nuclear scintigraphy are discussed, with a focus on MRI as the imaging modality of choice.

Abbreviations

CT	Computed tomography
FS	Fat-suppressed
MRI	Magnetic resonance imaging
STIR	Short-tau inversion recovery
T1-W	T1-weighted
T2-W	T2-weighted

1 Introduction

Pyogenic spondylodiscitis (PSD) is an infection of the spine which affects primarily the intervertebral disk and the adjacent vertebra. The incidence of PSD has been on the rise over the recent few years, due to the increasing life expectancy of older patients and several other factors. The indolent nature of the disease usually contributes to a delay in timely diagnosis and treatment, thus affecting clinical outcome. The diagnosis cannot be established solely on the basis of clinical assessment and almost always requires imaging. Characteristic imaging findings, together with image-guided microbiological isolation of the causative agent, are the main tools for appropriate diagnosis. This chapter discusses various aspects of PSD such as its epidemiology, pathogenesis, and clinical features, with emphasis on the role of various imaging modalities in confirming its diagnosis.

2 Epidemiology

PSD is relatively rare and comprises only 2–7% of all cases of musculoskeletal infections (Tyrrell et al. 1999; Stäbler and Reiser 2001; Cheung and Luk 2012). The reported incidence in developed countries ranges from 4 to 24 per million per year (Lazzeri et al. 2019). The incidence of PSD has been rising in the recent few years, due to improved life expectancy of older patients with chronic debilitating diseases and increased prevalence of chronic liver or renal disease, diabetes mellitus, long-term steroid use, intravenous drug abuse, and human immunodeficiency virus infection. The increase in number of spinal surgeries and improved diagnostic sensitivity, particularly related to the more widespread use of magnetic resonance imaging (MRI), has also contributed to these rising numbers (Kehrer et al. 2014; Nickerson and Sinha 2016; Lazzeri et al. 2019).

PSD can affect any age group but is most frequently seen between the fifth to seventh decades, with a male preponderance (Cheung and Luk 2012; Lazzeri et al. 2019). The most frequent site of vertebral infection is the lumbar spine (50%), followed by the thoracic (35%) and cervical spine (15%) (Cheung and Luk 2012). In approximately 95% of cases, PSD involves the vertebral body, with or without the intervening disk. Involvement of the posterior elements is seen in only 5% of cases (Cheung and Luk 2012). The common organisms causing PSD are *Staphylococcus aureus* including methicillin-resistant *Staphylococcus aureus* (MRSA) and streptococci, accounting for more than 50% of the cases (Cheung and Luk 2012; Boody et al. 2018). Other organisms causing PSD are *Escherichia coli*, *Klebsiella* spp., *Proteus* spp., *Enterobacter* spp., *Salmonella*, and *Pseudomonas aeruginosa* (Fantoni et al. 2012). Moreover, 1 in 10 cases of PSD is polymicrobial, highlighting the importance of blood cultures (Boody et al. 2018).

3 Pathogenesis

PSD commonly results from hematogeneous spread of bacteria from the skin, respiratory tract, gastrointestinal tract, genitourinary tract, or oral cavity (Govender 2005; Skaf et al. 2010). The arterial mode of spread is more common than the venous route (Figs. 1 and 2). This is explained by a rich arterial supply of the vertebral bodies derived from the vertebral arteries, the aorta, or the iliac arteries, depending on vertebral location. In septicemia, microemboli are carried in the arterial system and get impacted in the vertebral end arterioles (Ratcliffe 1985; Leone et al. 2012). PSD typically involves two adjacent vertebral bodies and the intervening disk and is explained by the

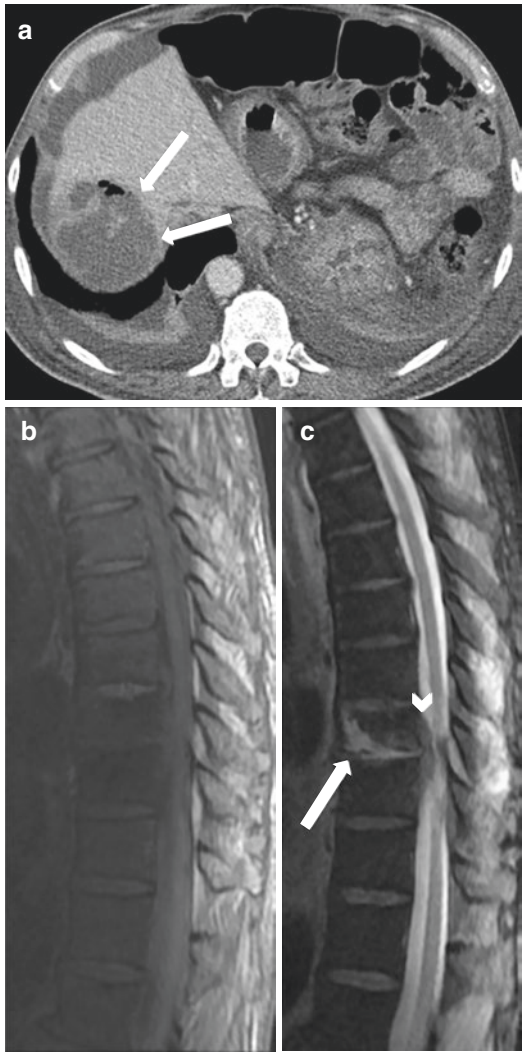

Fig. 1 A 69-year-old man with pyogenic spondylodiscitis due to hematogeneous spread of infection from liver abscess secondary to *Klebsiella pneumoniae*. (**a**) Axial contrast-enhanced CT image of the abdomen shows a large necrotic liver abscess with air locules within (arrows). Two months later, the patient presented with fever and back pain. Sagittal (**b**) T1-W and (**c**) STIR MR images show changes of pyogenic spondylodiscitis involving T8 and T9 vertebral bodies as well as the T8/T9 disk in the form of T8 and T9 vertebral body end-plate irregularity (arrow) and diffuse T1-hypointense signal in the T8 and T9 vertebral bodies with corresponding subtle T2-hyperintense signal. The T8/T9 disk also demonstrates marked T2-hyperintense signal intensity similar to that of fluid. There is an epidural component with resultant T8/T9 anterior epidural space indentation (arrowhead)

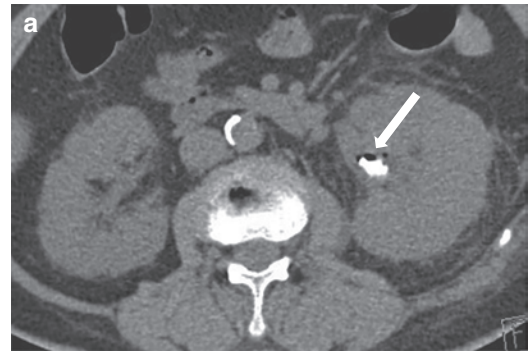

Fig. 2 A 73-year-old woman with pyogenic spondylodiscitis due to hematogeneous spread of infection from left emphysematous pyelonephritis due to *Escherichia coli*. (**a**) Axial unenhanced CT image of the abdomen shows air foci within the left renal pelvis (arrow) with a renal calculus. The left kidney is swollen with perinephric fat stranding. One month later, the patient developed fever and low back pain. Sagittal (**b**) T1-W, (**c**) FS T2-W, and (**d**) contrast-enhanced FS T1-W MR images show typical changes of pyogenic spondylodiscitis involving the L4-L5 vertebral bodies. The intervening disk demonstrates increased signal intensity on STIR images (arrow). There is T1-hypointensity, T2-hyperintensity, and marrow enhancement involving L4-L5 vertebral bodies (star). There is an enhancing epidural component with resultant L4/L5 anterior thecal sac indentation (curved arrow)

arterial supply of the axial skeleton. The same segmental spinal artery bifurcates and supplies the lower portion of the upper vertebra, the upper portion of the adjacent lower vertebra, and the intervening disk (Cheung and Luk 2012). The arterioles enter the vertebral body through central nutrient foramina, undergo ramification, and are most abundant at the vertebral body end plates, particularly in the anterior subchondral region where the infective process usually commences (Wiley and Trueta 1959; Ratcliffe 1985; Leone et al. 2012).

The intervertebral disk is avascular in adults; hence it is usually not directly infected by hematogeneous spread of infection. In elderly patients however, disk degeneration may be followed by ingrowth of vascularized granulation tissue. This secondary vascularization of the disk material may be the reason why primary discitis is possible in older patients (Yeom et al. 2016). As infection worsens, it causes bone infarction, followed by vertebral body and end-plate destruction, and direct extension of infection through the end plates into the intervertebral disk (Fantoni et al.

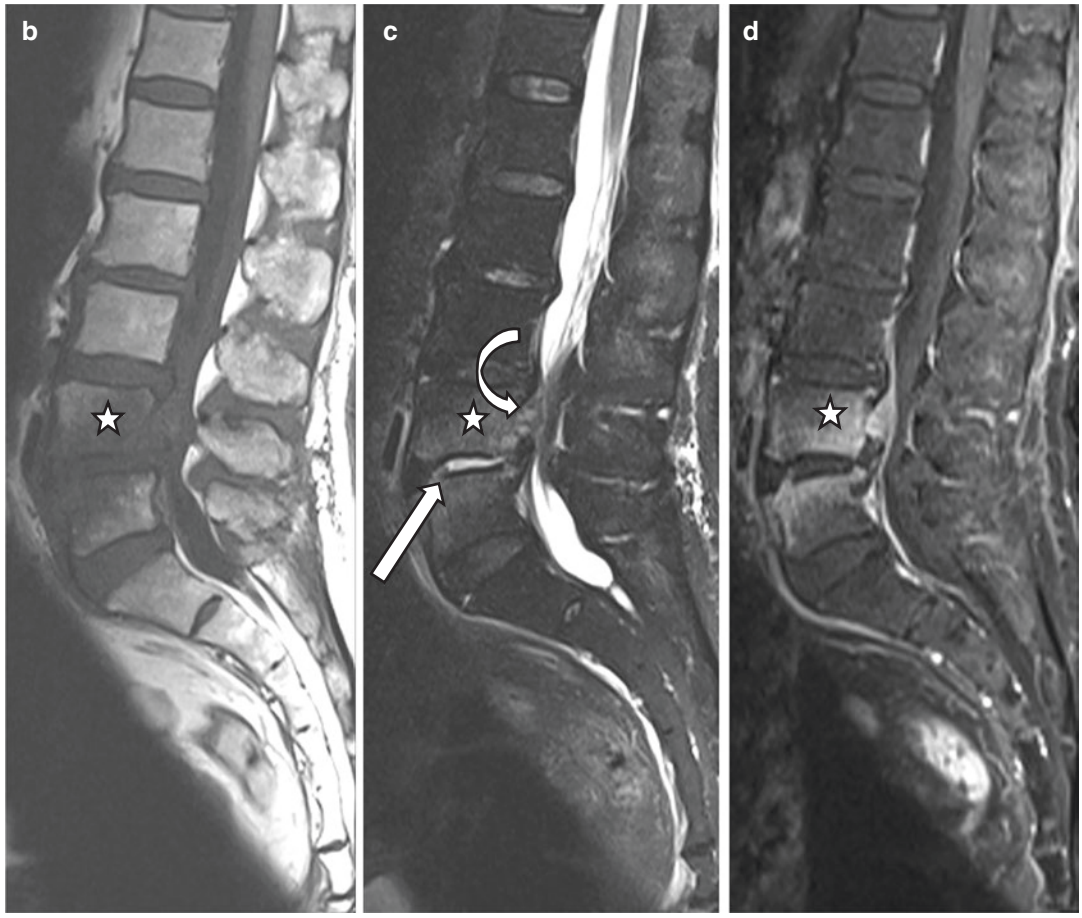

Fig. 2 (continued)

2012). If untreated, the infection may progress and spread into the paravertebral soft tissue and the spinal canal.

Due to their poor blood supply, the posterior elements of the vertebrae such as facet joints are rarely involved by the hematogeneous spread of infection (Babinchak et al. 1997; Yeom et al. 2016). Facet joint infection is an uncommon condition which may result from hematogeneous spread of infection from the skin and respiratory and urinary systems (Narváez et al. 2006; Diehn 2012; Yeom et al. 2016). It may also result from direct inoculation during an interventional procedure, such as therapeutic facet joint injection. When present, facet joint infection is most commonly found in the lumbar spine and usually affects the facet joint unilaterally. Occasionally, when bilateral facet joints are involved, the suggested route of transmission is through the retro-ligamentous space of Okada (Narváez et al. 2006; Diehn 2012; Yeom et al. 2016).

The venous spread of infection, such as via epidural venous plexus within the central canal and Batson paravertebral plexus, is less common. These are a series of valveless veins along the length of the spinal canal. The venous route of spread is of particular importance in instances of sepsis originating in the urinary bladder, bowel, and female pelvic organs. As the Batson plexus is a valveless system, increasing intra-abdominal pressure allows retrograde hematogeneous spread from the pelvis and abdominal organs to the vertebral column, particularly the lumbar spine (Tyrrell et al. 1999; Govender 2005; Cheung and Luk 2012; Tali et al. 2015). In the cervical spine, the infection may spread via the prevertebral pharyngeal venous plexus

in patients with infections in the head and neck region (Wiley and Trueta 1959; Cheung and Luk 2012).

4 Clinical Features

PSD is often an indolent disease with nonspecific symptoms and signs. Hence, the time from onset of symptoms to diagnosis is often long, ranging from 2 to 12 weeks, and on occasion, even 3 months or more (Cheung and Luk 2012). The commonest presenting symptom is unremitting back or neck pain which is present in more than 90% of patients (An and Seldomridge 2006; Cottle and Riordan 2008; Skaf et al. 2010). Fever is less common and occurs in 60–70% of patients (Gasbarrini et al. 2005; An and Seldomridge 2006; Skaf et al. 2010). A nonspecific back pain with no significant fever may be due to a wide list of differential diagnoses, the most common being degenerative spine disease. This symptom does not necessarily prompt spinal imaging, with possible resultant delayed diagnosis, unless there is a high index of suspicion.

Other constitutional symptoms include nausea, vomiting, malaise, anorexia, and weight loss (Cottle and Riordan 2008). Patients with PSD of the cervical spine may present with difficulty in swallowing, secondary to a retropharyngeal abscess (Cheung and Luk 2012). In later stages of PSD, patients may present with limb weakness, numbness, sphincter loss, and paralysis, which may be related to neurological compromise caused by spinal cord or cauda equina compression (An and Seldomridge 2006; Leone et al. 2012). Physical examination may reveal localized paravertebral muscle tenderness and spasm, with a limited range of motion (Cottle and Riordan 2008).

5 Laboratory Investigations

The white blood cell count (WBC) can be normal and may be elevated in less than 50% of cases (Hadjipavlou et al. 2000; Cottle and Riordan 2008). C-reactive protein (CRP) and erythrocyte sedimentation rate (ESR) levels are elevated in more than 90% of patients with spinal infection (Lam and Webb 2004; An and Seldomridge 2006; Cottle and Riordan 2008). Although not pathognomonic, elevated CRP and ESR levels serve as good screening and surveillance tests in the diagnosis and treatment of spinal infections. In suspected cases of PSD, blood cultures, urinalysis, and urine for culture should be obtained. These may be helpful in guiding the choice of antimicrobial therapy (Cheung and Luk 2012). If blood cultures are negative, an attempt should be made to obtain direct cultures using computed tomography (CT)-guided needle biopsy or a surgical biopsy (Skaf et al. 2010). Unless the patient is critically ill, antibiotic therapy should not be started until the appropriate cultures have been performed.

6 Imaging

6.1 Radiography

Radiographs are usually the first imaging study employed in patients with suspected spinal infection. However, radiographs have a very low sensitivity and specificity. Infection usually results in loss of normal bone matrix, causing reduced bone density and osteolysis. In general, osteolysis must compromise 30–40% of bone mineral content to produce noticeable changes on radiographs. These radiographic changes may take at least 2 weeks after acute onset of infection (Gillams et al. 1996; Tali et al. 2015). Thus, a negative study does not rule out an underlying infection. The earliest radiographic sign is ill-defined and irregular borders of the anterior corner of the vertebral body end plate occurring at 2–8 weeks after infection onset. Vertebral body end-plate destruction is considered the most reliable radiographic sign (Tali et al. 2015). This is followed by reduced disk space, vertebral osteolysis, and loss of height of the affected vertebral bodies (Fig. 3a).

As infection progresses, further osteolysis results in vertebral body collapse and wedging, causing a gibbus deformity (Leone et al. 2012). The posterior elements of the vertebral body are uncommonly involved. Paraspinal extension may

be seen radiographically as an abnormal psoas shadow or widening of the mediastinum or retropharyngeal space (An and Seldomridge 2006; Cottle and Riordan 2008). In the later stages of spinal infection, increased bone density due to sclerosis, obliteration of the disk space, ankylosis of the vertebral bodies, and kyphotic or scoliotic deformities may be seen (Leone et al. 2012) (Fig. 3b).

6.2 Computed Tomography

CT is not the modality of choice for diagnosing PSD. However, due to its superior anatomical resolution, CT is more sensitive than spine radiographs in the early detection of loss of disk height, vertebral body end-plate destruction, vertebral osteolysis, and paravertebral soft tissue involvement (Fig. 4). CT can also be useful in identifying other causes of back pain such as degenerative spine disease, fracture, or metastatic disease. Intravenous contrast agent is usually not administered, unless MRI is contraindicated. Compared to radiographs, CT enables better evaluation of paraspinal abscess, seen as a rim-enhancing fluid collection (Raghavan et al. 2018). CT may also be used in the evaluation of facet joint infection and may demonstrate bony destruction at or soft tissue changes around the infected facet joint (Diehn 2012) (Fig. 5a).

Another major application of CT is in guiding percutaneous needle biopsy and abscess drainage. Currently, the modality of choice for

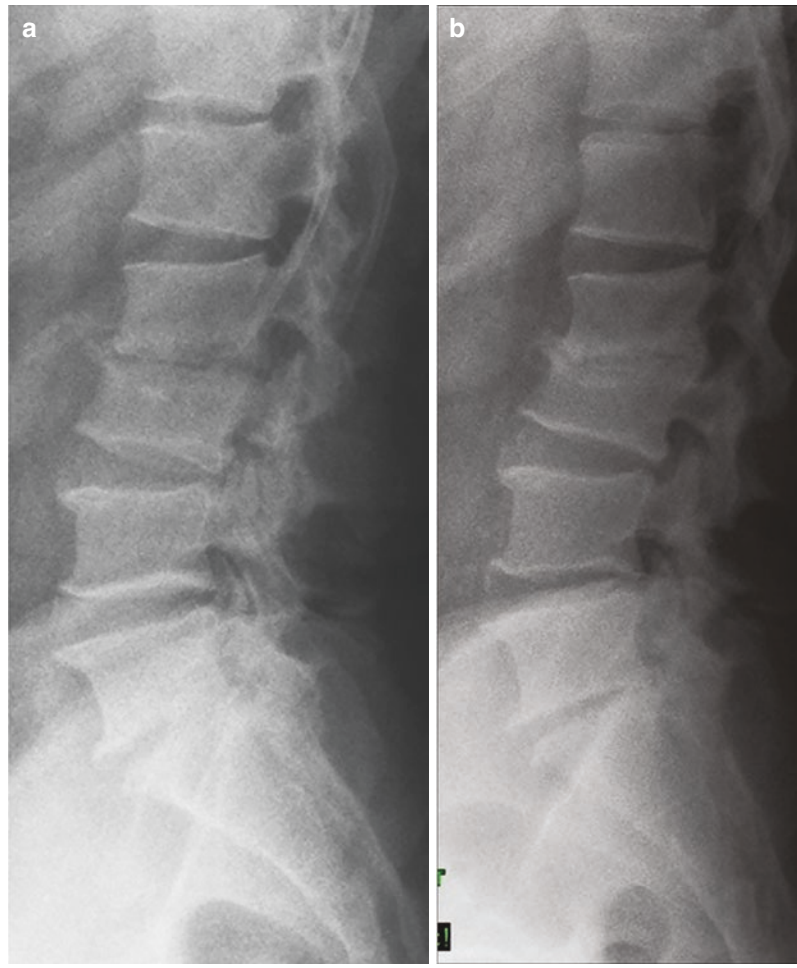

Fig. 3 A 73-year-old man presenting with fever and lower back pain. (**a**) Lateral radiograph of the lumbar spine shows a reduction of the L2/3 disk space with ill-defined irregularities of the adjacent vertebral body end plates and mild loss in height of both L2 and L3 vertebral bodies, indicating early spondylodiscitis. (**b**) Lateral radiograph of the lumbar spine taken 9 months later, following completion of antibiotic treatment, shows chronic changes in the form of obliteration of the L2/L3 disk space with L2 and L3 vertebral body end-plate sclerosis, vertebral body collapse, and mild kyphotic wedging. Causative organism on blood cultures was *Staphylococcus aureus*

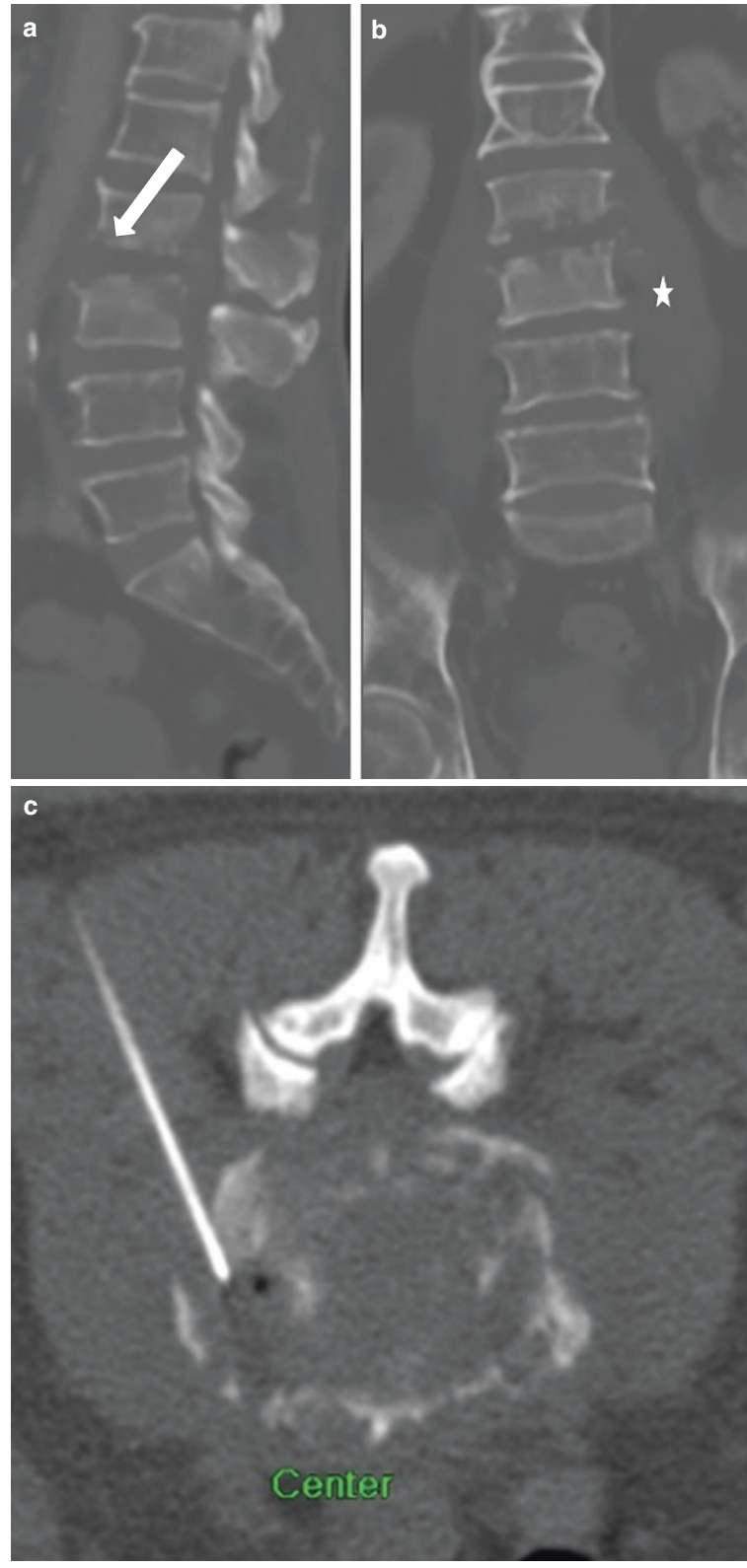

Fig. 4 An 80-year-old woman presenting with constitutional symptoms and back pain of insidious onset. (**a**) Sagittal and (**b**) coronal CT images of the lumbar spine show vertebral body end-plate destruction (arrow) and reduced disk space at L2 and L3 vertebral levels with associated paravertebral soft tissue swelling (star). (**c**) CT-guided percutaneous biopsy was performed and *Escherichia coli* was isolated

performing percutaneous biopsies of the spine is CT fluoroscopy, due to its higher accuracy and repeatability in the event of an inconclusive result (Fig. 4c). Other advantages are patient comfort, ability to be performed as a day procedure, and significantly lower post-procedure complications and patient morbidity compared to open biopsy (Gogna et al. 2008; Srinivasan and Peh 2011). CT-guided percutaneous needle biopsy has better a diagnostic yield than blood cultures, ranging from 70 to 100%; while open biopsies are diagnostic in more than 80% of patients (An et al. 2006; Skaf et al. 2010).

6.3 Magnetic Resonance Imaging

MRI is the modality of choice for the diagnosis and assessment of PSD due to its high sensitivity (96%), specificity (94%), and accuracy (94%). Other advantages are high-contrast resolution, high sensitivity to detect soft tissue and bone marrow abnormalities, multiplanar imaging capability, and lack of ionizing radiation (Varma et al. 2001; Lazzeri et al. 2019; Shikhare and Peh 2019). The major advantage of MRI is its capability to diagnose PSD at an early stage, when other imaging modalities are usually normal (Cheung and Luk 2012; Tali et al. 2015). The protocol should include fat-suppressed (FS) T2-weighted (T2-W) or short-tau inversion recovery (STIR) sequences which are fluid-sensitive sequences that are highly sensitive in demonstrating marrow edema before destructive changes appear; T1-weighted (T1-W) imaging for morphological assessment; and contrast-enhanced FS T1-W sequences to complete a full diagnostic assessment and to differentiate between vascularized and necrotic inflammatory components (Yeom et al. 2016; Lazzeri et al. 2019).

Hematogeneous PSD in adults usually begins near the anterior subchondral region of the vertebral body and subsequently spreads to involve the intervertebral disk and adjacent vertebral body. The infection causes marrow edema which is seen as an area of hypointense signal on T1-W images and hyperintense signal on FS T2-W or STIR images, with corresponding contrast enhancement (Tins and Cassar-Pullicino 2004; Tali et al. 2015; Kawakyu-O'Connor et al. 2016; Lazzeri et al. 2019) (Figs. 2, 6, and 7). When destruction of the vertebral body end plates occurs, there is loss of definition or absence of the normal hypointense rim of cortical bone on T1-W images (Go et al. 2012; Yeom et al. 2016) (Figs. 2 and 7). The infected intervertebral disk may have abnormal hyperintense fluid signal on T2-W images (Figs. 1, 2, 7, and 8). Another reliable finding of spondylodiscitis is the loss of the disk intranuclear cleft on T2-W images (Tali

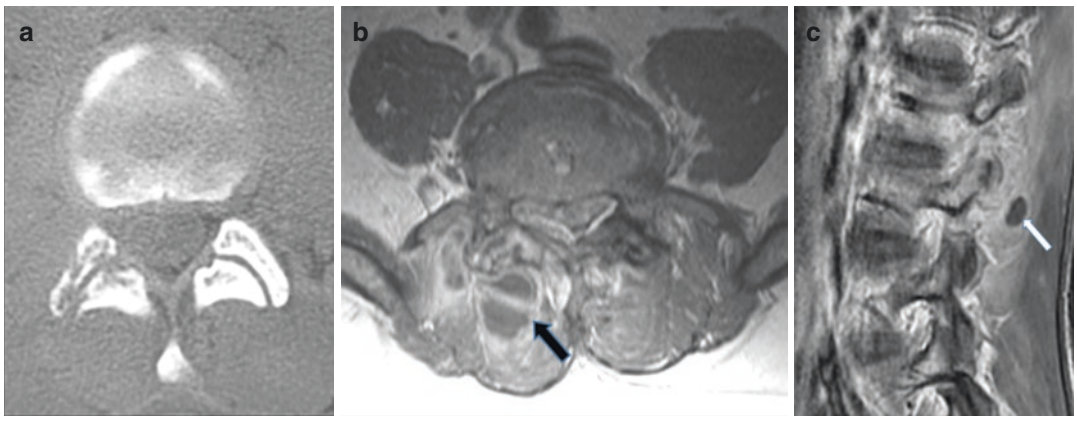

Fig. 5 A 42-year-old man with fever and back pain. (**a**) Axial CT image of the lumbar spine shows destructive subchondral osteolysis of the right facet joint. (**b**) Axial and (**c**) sagittal contrast-enhanced T1-W images confirm subchondral osteolysis involving the right facet joint with intra- and periarticular abscesses (arrows) and extension to the right posterior epidural space. [Case courtesy of Professor Fethi Ladeb, Tunis, Tunisia]

2004) (Figs. 2 and 8). On contrast-enhanced images, the disk may demonstrate homogeneous enhancement, patchy non-confluent areas of enhancement, or thick or thin areas of peripheral enhancement (Hong et al. 2009) (Figs. 2, 6, and 7). The involvement of disk helps differentiate infection from neoplasm, as the disk is usually not affected in neoplasm (Shikhare and Peh 2019). The early changes of PSD may involve only one vertebral body, one vertebral body and one disk, or two vertebral bodies without intervening disk involvement (Varma et al. 2001).

Dagirmanjian et al. (1999) showed that T1-hypointense signal in the vertebral body and disk with associated end-plate changes is a more reliable and consistent finding of PSD than

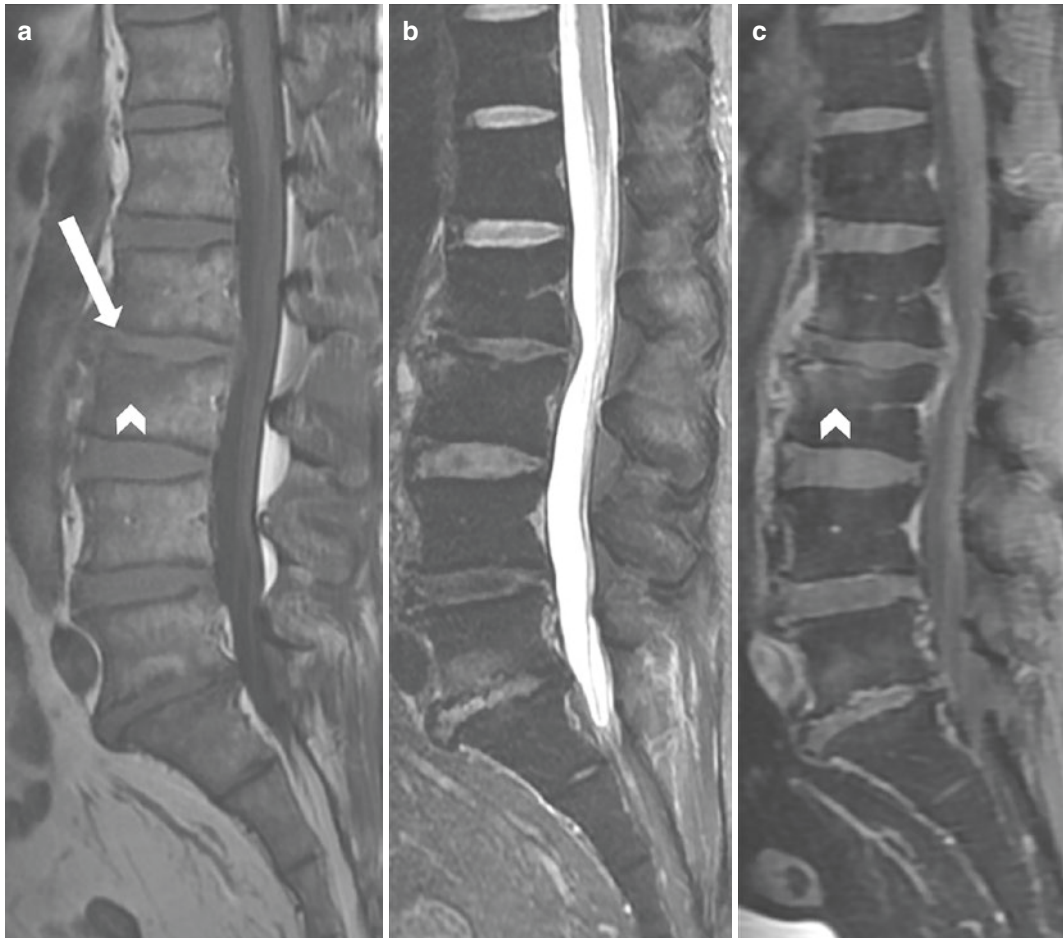

Fig. 6 A 73-year-old woman presenting with constitutional symptoms and back pain of insidious onset. (**a**) Sagittal T1-W, (**b**) FS T2-W, and (**c**) contrast-enhanced FS T1-W images show early changes of pyogenic spondylodiscitis (PSD). There is L2 and L3 vertebral body end-plate irregularity (arrow) and T1-hypointense signal in anterior subchondral regions of L2-L3 vertebral bodies, with corresponding subtle T2-hyperintense signal and contrast enhancement (arrowhead). This case demonstrates a hypointense signal on T1-W images as a more reliable and consistent finding of PS than T2-hyperintense signal. There are Modic-type II vertebral body end-plate changes at L5-S1 level. One month later, (**d**) sagittal T1-W, (**e**) FS T2-W, and (**f**) contrast-enhanced FS T1-W MR images show the progression of PSD involving L2-L3 vertebral bodies, with extensive T1-hypointensity (star), T2-hyperintensity, and marrow enhancement (star). The L2/L3 disk also demonstrates marked T2-hyperintense signal intensity similar to that of fluid (arrow), with patchy enhancement. There is an enhancing epidural component with resultant L2/L3 anterior thecal sac indentation (curved arrow). Causative organism on blood cultures was methicillin-resistant *Staphylococcus aureus*

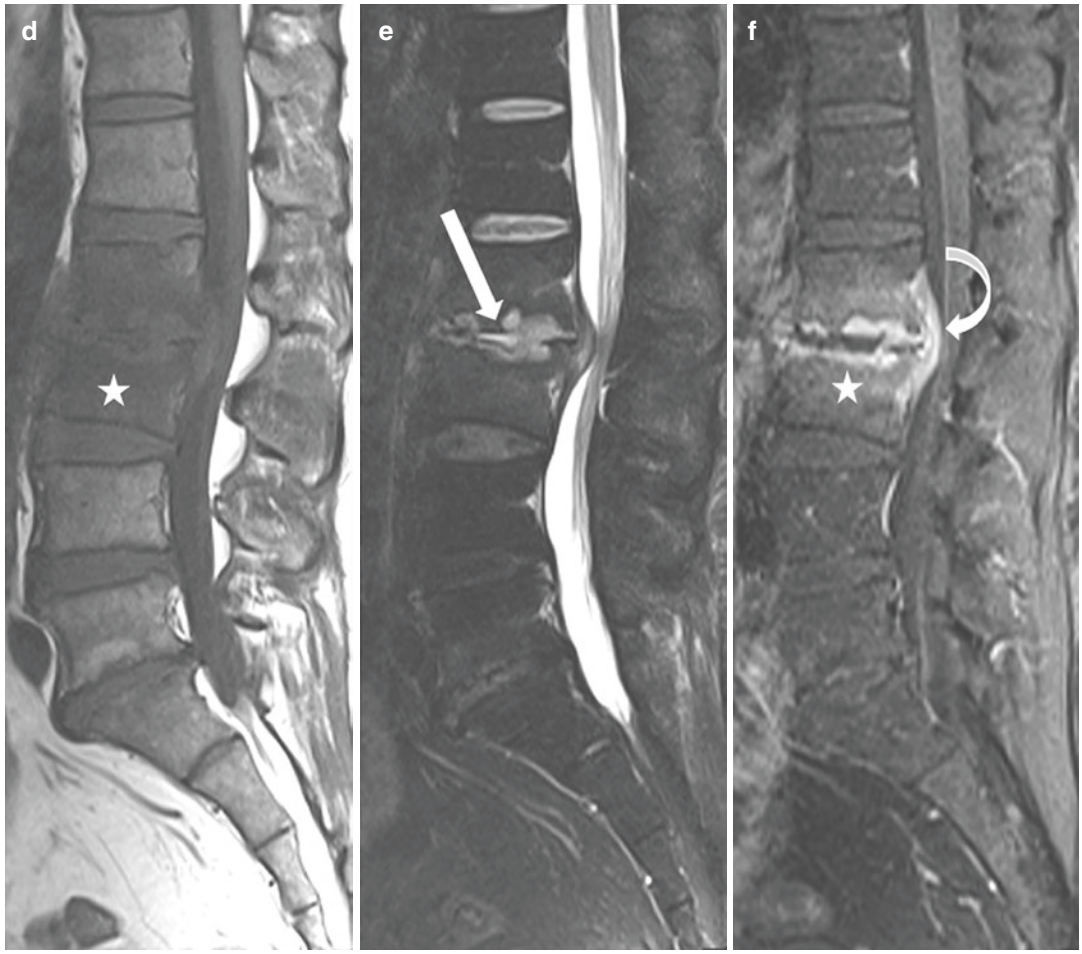

Fig. 6 (continued)

hyperintense signal seen on T2-W images (Fig. 6a, b). Abnormal T2-hyperintense signal may not be that consistent, due to the presence of sclerosis in the vertebral bodies which may cause T2-hypointense signal (Dagirmanjian et al. 1999; Varma et al. 2001). Contrast enhancement of the vertebral body marrow and adjacent intervertebral disk, however, remains a consistent diagnostic finding (Dagirmanjian et al. 1999) (Figs. 2, 6, and 7). Age-related changes in the MRI signal intensity caused by the marrow composition should be considered. Younger patients have predominant red marrow which is relatively hypointense on T1-W images. This may mask marrow edema-related hypointense signal, which is more apparent in elderly patients due to hyperintense signal from predominant fatty marrow (Dagirmanjian et al. 1996). Radiologists should be aware of these diagnostic pitfalls.

Contrast-enhanced FS T1-W sequences are also useful in assessing paravertebral space involvement (Leone et al. 2012; Shikhare and Peh 2019). In early spondylodiscitis, enhancement of paravertebral soft tissue may be the only MRI finding in the absence of vertebral body end-plate changes (DeSanto and Ross 2011; Yeom et al. 2016). Paravertebral soft tissue may be involved in the form of either a phlegmon or an abscess. Phlegmons are seen as poorly defined areas of signal hyperintensity on T2-W images with diffuse contrast enhancement, in contrast to abscesses which demonstrate hyperintense signal intensity on T2-W images with thick irregular rim-like enhancement on FS T1-W images (An

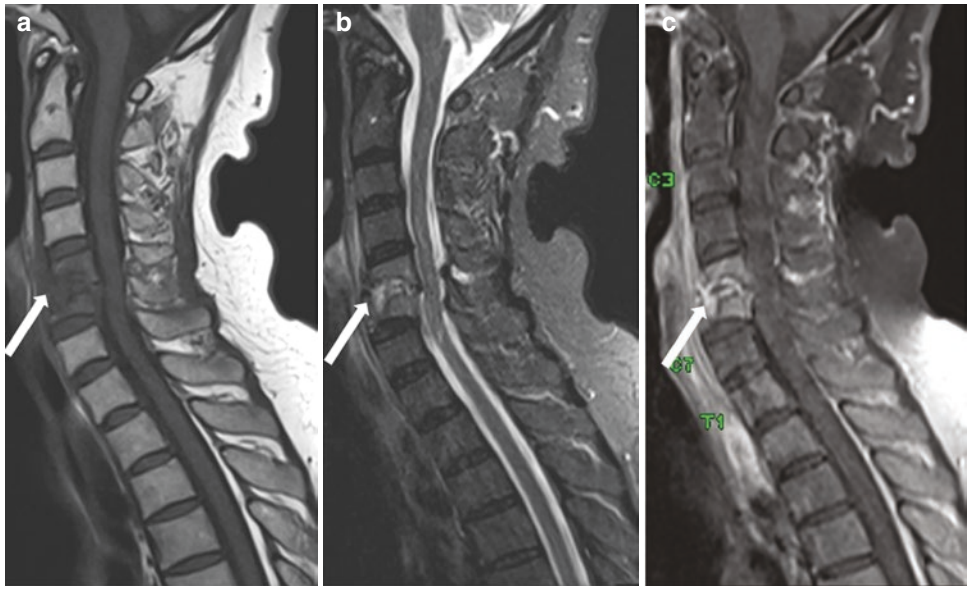

Fig. 7 A 52-year-old man presenting with fever and neck pain. Sagittal (**a**) T1-W, (**b**) STIR, and (**c**) contrast-enhanced FS T1-W MR images show vertebral body endplate destruction with T1-hypointensity, T2-hyperintensity, and marked enhancement involving C5 and C6 vertebral bodies. The intervening C5/C6 disk also shows marked T2-hyperintensity similar to that of fluid, with heterogeneous contrast enhancement (arrow). Causative organism on blood cultures was *Staphylococcus aureus*

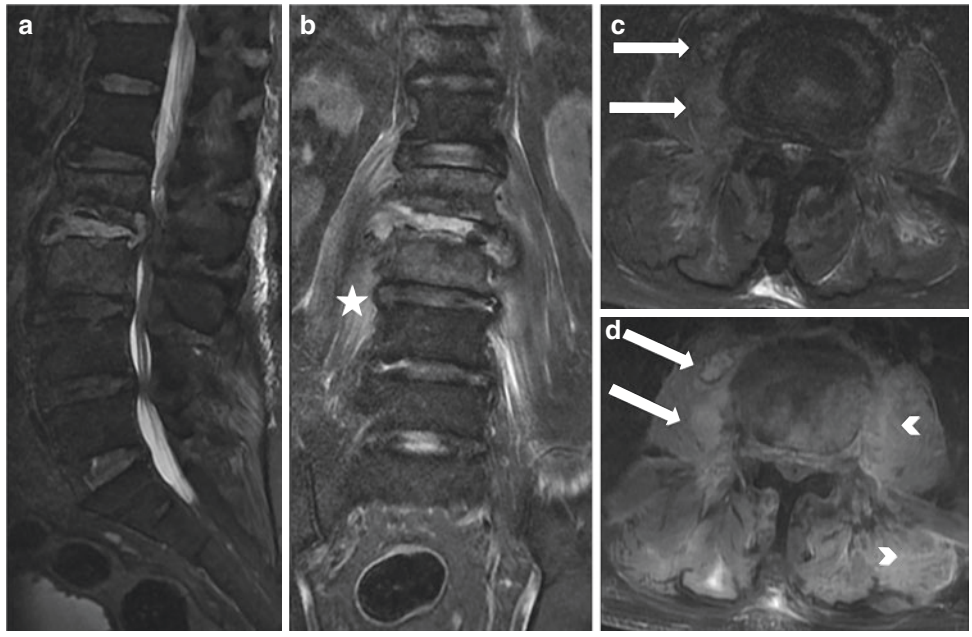

Fig. 8 An 80-year-old woman presenting with fever and severe low back pain. (**a**) Sagittal, (**b**) coronal, and (**c**) axial FS T2-W MR images show changes of pyogenic spondylodiscitis involving the L2 and L3 vertebral bodies with T2 hyperintense signal within both the psoas muscles (star). The L2/L3 disk also shows marked T2-hyperintensity similar to that of fluid. (**d**) Axial contrast-enhanced FS T1-W image shows corresponding pre- and paravertebral soft tissue enhancement with phlegmons (arrowheads) and rim-enhancing abscesses (arrows) in the psoas muscles, as well as the erector spinae and multifidus muscles. CT-guided percutaneous biopsy was performed, and *Escherichia coli* was isolated

et al. 2006) (Fig. 8). In facet joint infection, MRI may demonstrate destruction of the subchondral bone surface of the facet joint, fluid-filled facet joint with surrounding edema, and facet capsular enhancement (Diehn 2012). Associated periarticular abscesses and epidural extension are also well shown (Fig. 5b, c).

Imaging features of PSD may mimic tuberculous (TB) spondylodiscitis in approximately 75% of cases (Shikhare et al. 2011). MRI features which favor TB spondylodiscitis and help differentiate it from PSD include relative preservation of the intervertebral disk, multiple vertebral or entire vertebral body involvement, skip lesions with subligamentous spread of infection involving three or more vertebral levels (Fig. 9), well-defined abnormal signal in the paraspinal region, thin and smooth-walled abscess, presence of paraspinal or intraspinal abscess, and thoracic spine involvement (Smith et al. 1989; Jung et al. 2004; Harada et al. 2008).

MRI may also be used as a tool in assessing the therapeutic response and to help guide clinical decision-making (Hong et al. 2009). However, this can sometimes be challenging as MRI findings can lag behind the clinical picture by 4–8 weeks, or even months, after the initiation of antibiotic therapy. Hence, MRI is not a

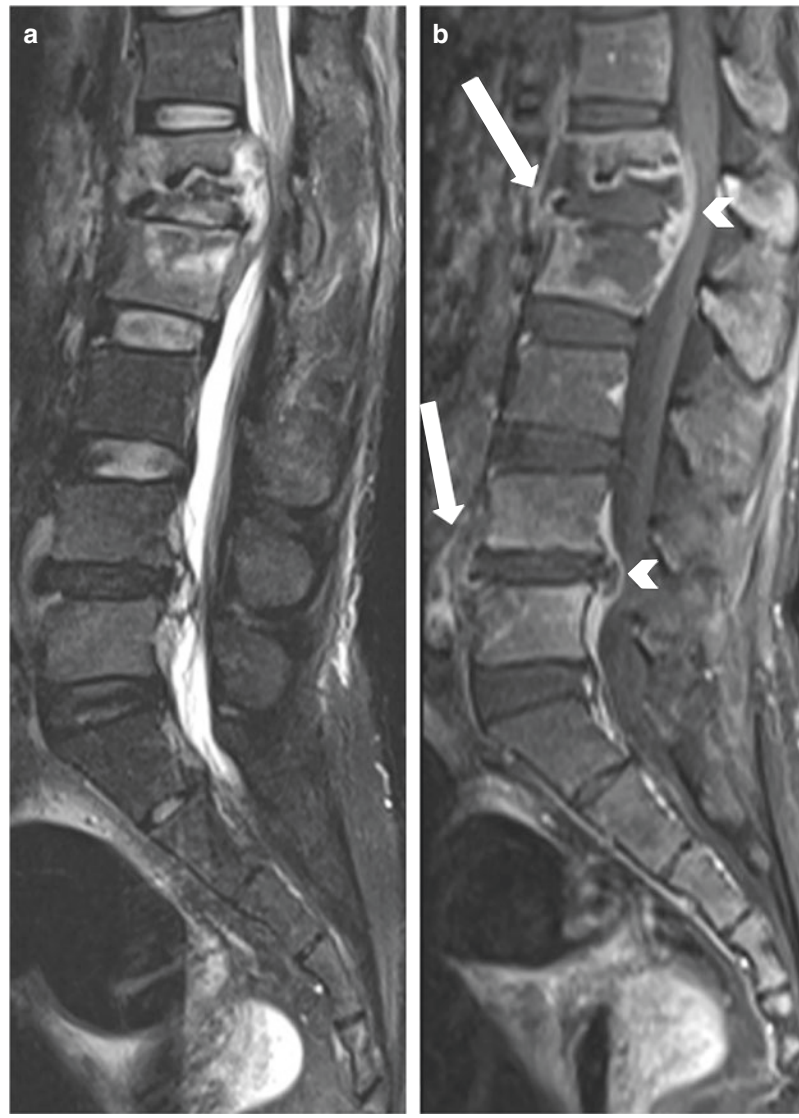

Fig. 9 Tuberculous spondylodiscitis in a 68-year-old man presenting with evening fever, chills, weight loss, and severe back pain. Sagittal (**a**) T2-W and (**b**) contrast-enhanced FS T1-W MR images show involvement of multiple vertebral bodies (L1-L2 and L4-L5). There are skip lesions with a subligamentous spread of infection (arrow) and epidural extension at both levels (arrowhead). Both L1/L2 and L4/L5 disks are relatively preserved

fully reliable technique in evaluating treatment response. The early marker of healing at follow-up MRI is the reduction in contrast enhancement, which may be seen few weeks to months after the initiation of treatment. Other signs of healing include fatty marrow restoration, seen as reinstitution of hyperintense signal in the bone marrow on T1-W images and corresponding decrease of hyperintense marrow signal on STIR or T2-W images (Fig. 10), as well as resolution of paravertebral soft tissue changes. The disk space, however, may appear persistently narrowed on follow-up imaging (Tins and Cassar-Pullicino 2004; Leone et al. 2012; Tali et al. 2015) (Fig. 10).

6.4 Nuclear Medicine Imaging

Radionuclide studies are more sensitive than radiographs in detecting early infection. Radiopharmaceuticals commonly used in the assessment of spinal infection include technetium-99m-labeled methylene diphosphonate (99mTc-MDP), gallium-67 citrate, and fluorine-18 [18F] fluoro-deoxyglucose positron

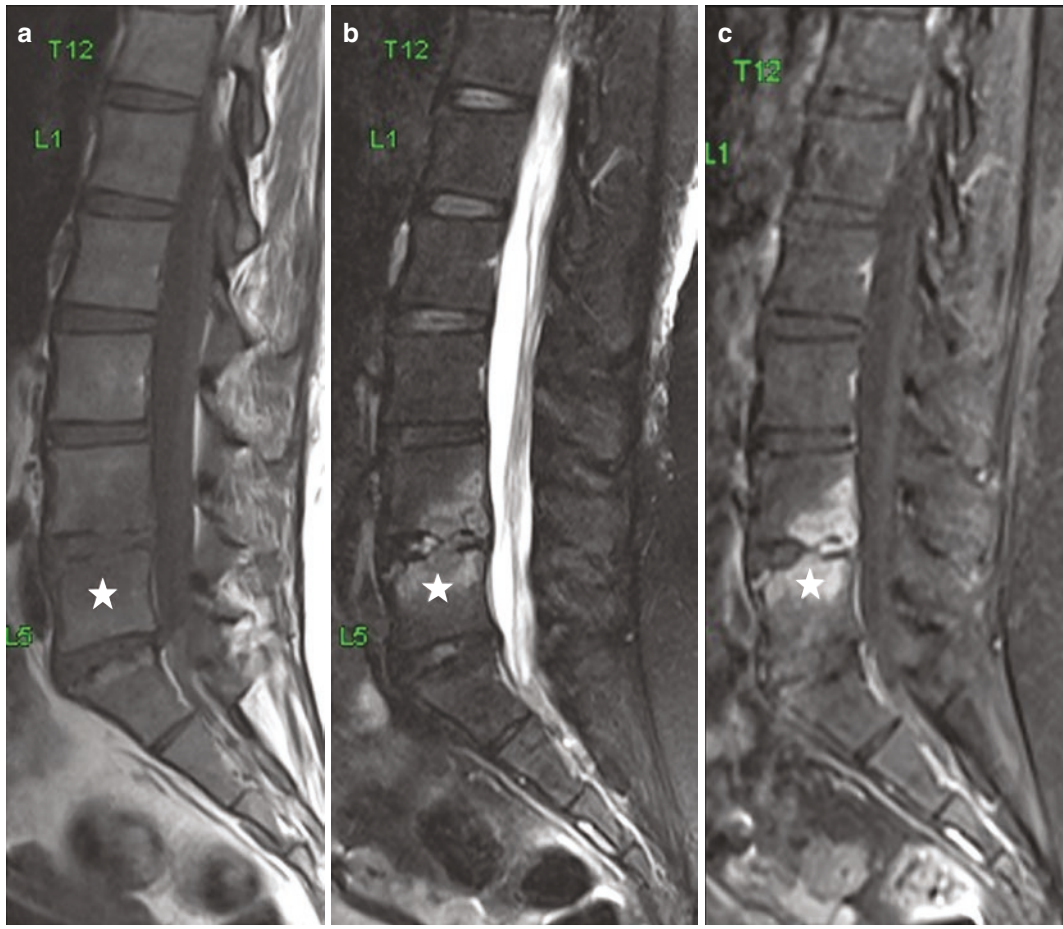

Fig. 10 A 72-year-old woman presenting with fever and back pain. Sagittal (**a**) T1-W, (**b**) FS T2-W, and (**c**) contrast-enhanced FS T1-W MR images show typical appearances of pyogenic spondylodiscitis at L4-L5 level (star) secondary to *Staphylococcus aureus*. The patient was treated with antibiotics. Ten months later, corresponding sagittal (**d**) T1-W, (**e**) FS T2-W, and (**f**) contrast-enhanced FS T1-W MR images show features of healing in the L4 and L5 vertebral bodies with fatty marrow restoration, seen as reinstitution of normal fatty signal in the bone marrow on T1-W (star) and T2-W images. There is no significant enhancement. The previously seen abnormal T2-hyperintense L4/L5 disk signal has resolved but the disk remains slightly narrowed (arrowhead)

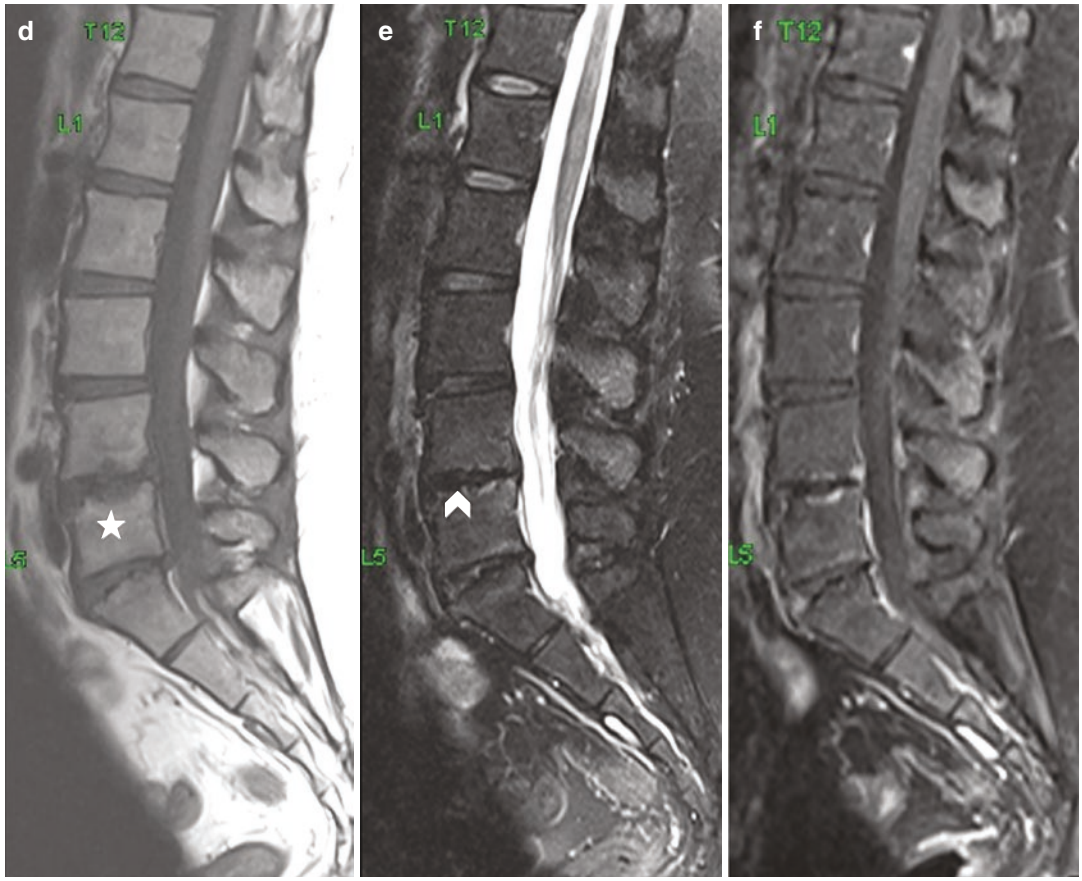

Fig. 10 (continued)

emission tomography (FDG-PET) (Lazzeri et al. 2019). Three-phase 99mTc-MDP scan has a sensitivity of 87–98% and a specificity of 91–100%, whereas the sensitivity and specificity of gallium-67 citrate bone scans is 89% and 85%, respectively, for diagnosing spinal infection (Govender 2005; Cheung and Luk 2012). Radionuclide studies lack specificity, as they may show increased activity in other conditions such as degenerative disk disease, osteoporotic fractures, and neoplasms. Additionally, bone scintiscans provide poor anatomical detail and may show persistent increased activity, even after the vertebral infection has healed (Tali et al. 2015; Shikhare and Peh 2019).

The diagnostic accuracy can be increased by using combination of technetium and gallium radionuclides, with sensitivity rates of up to 94% (Tali et al. 2015). Gallium scan is a better tool for follow-up treatment response compared to technetium, as they provide a more accurate degree of the infectious activity (Go et al. 2012; Tali et al. 2015). FDG-PET has a reported sensitivity of 97% and specificity of 88% for the diagnosis of PSD (Prodromou et al. 2014). FDG-PET combined with CT provides better anatomical details (Lazzeri et al. 2019). The advantages of FDG-PET/CT include its high negative predictive value, short acquisition time, and superior image quality. Drawbacks are its low specificity (ranging from 35 to 88%) and failure to consistently differentiate infection from marked degenerative spine disease and neoplastic lesions (Rosen et al. 2006).

7 Treatment

PSD is usually treated conservatively using antimicrobial therapy and nonpharmacological treatments such as bed rest and physiotherapy

(Gouliouris et al. 2010) (Fig. 10). Patients are often started on empirical antibiotic therapy, covering *S. aureus*, gram-negative organisms, and anaerobes, while microbiological results are still pending (Gouliouris et al. 2010). Afterwards, specific antibiotic treatment is continued intravenously, once an organism has been isolated. The recommended duration of intravenous antibiotics is 6–8 weeks, aiming to reduce failure and recurrence rates (Cheung and Luk 2012). Surgical intervention is usually indicated in cases of failed response to conservative management, intractable pain, neurological complications, and chronic infection causing extensive bone destruction leading to spinal instability or severe kyphotic deformity (Gouliouris et al. 2010). Surgical management usually includes aggressive radical debridement and decompression, along with anterior fusion for spinal stabilization (Pola et al. 2012) (Fig. 11).

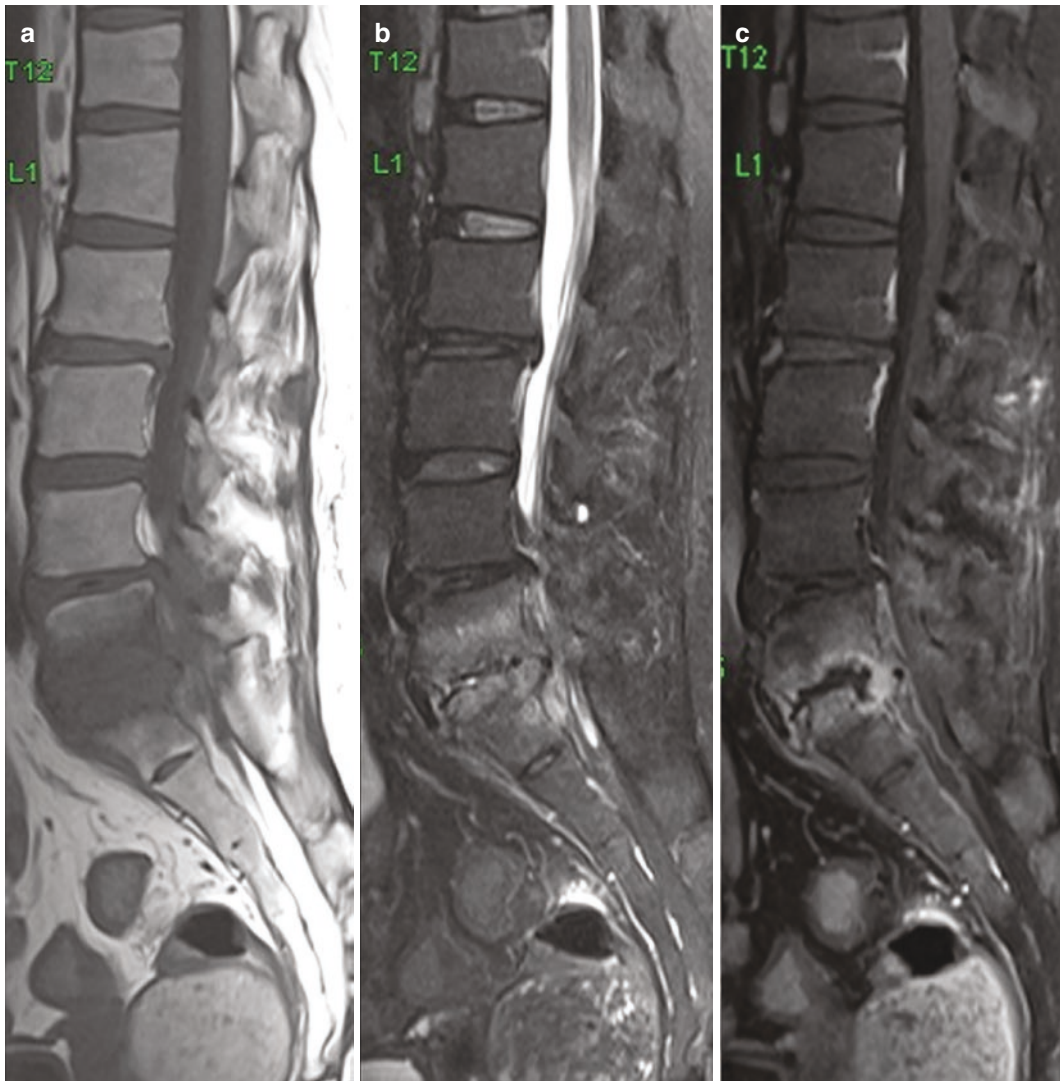

Fig. 11 A 71-year-old woman presenting with fever and back pain. Sagittal (**a**) T1-W, (**b**) FS T2-W, and (**c**) contrast-enhanced FS T1-W MR images show typical appearances of pyogenic spondylodiscitis at L5-S1 level secondary to methicillin-resistant *Staphylococcus aureus*. Patient failed conservative management and developed neurological complications, hence underwent surgery (laminectomy at L4-L5 level). Three years later, sagittal (**d**) T1-W and (**e**) STIR MR images show features of healing and bony ankylosis at L5-S1 level

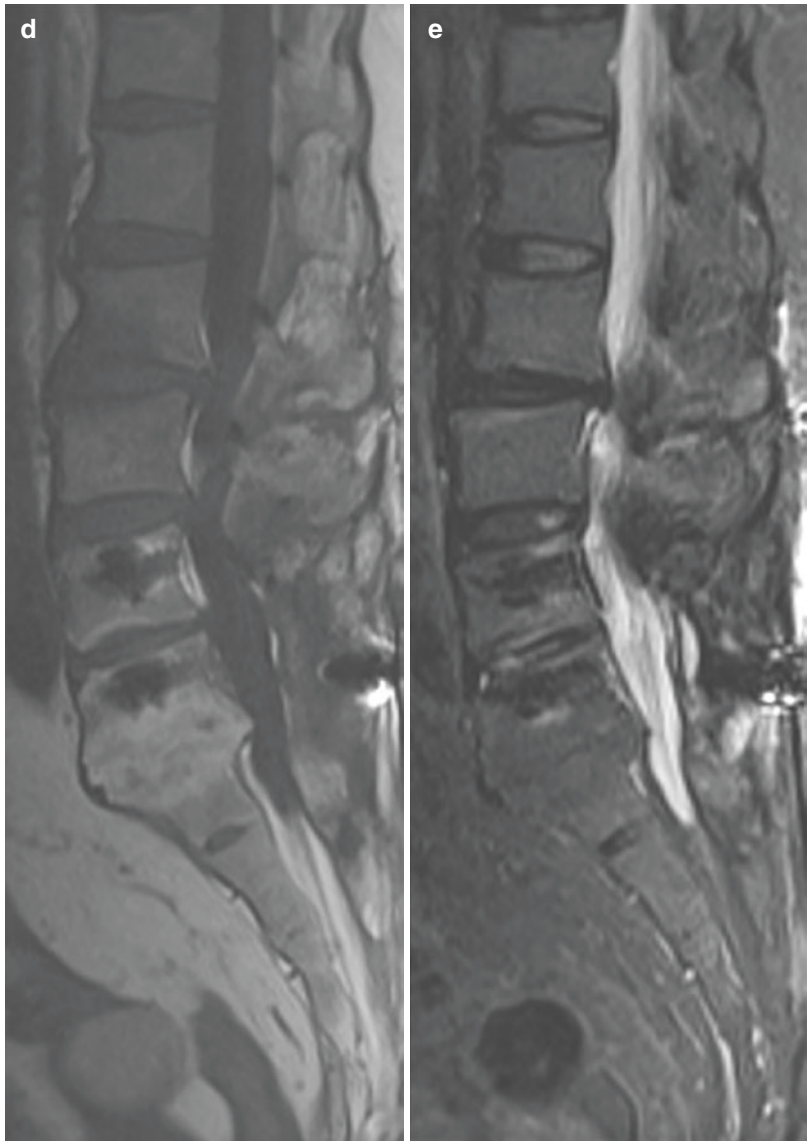

Fig. 11 (continued)

8 Conclusion

The incidence of PSD has been on the rise over the recent few years. Early diagnosis requires a high degree of clinical suspicion and knowledge of early imaging features, with the aim of preventing morbidity and mortality. The use of multiple imaging modalities has led to a greater sensitivity and specificity in the diagnosis of PSD. Radiologists thus play a crucial role and should be aware of varied imaging manifestations of PSD, particularly the MRI features. Currently, MRI is the modality of choice for diagnosing PSD at an early stage and to differentiate PSD from other conditions such as neoplasms. MRI is also useful for defining the extent of disease process and complications.

References

An HS, Seldomridge JA (2006) Spinal infections: diagnostic tests and imaging studies. Clin Orthop Relat Res 444:27–33

An HS, Masuda K, Inoue N (2006) Intervertebral disc degeneration: biological and biomechanical factors. J Orthop Sci 11:541–552

Babinchak TJ, Riley DK, Rotheram EB Jr (1997) Pyogenic vertebral osteomyelitis of the posterior elements. Clin Infect Dis 25:221–224

Boody BS, Tarazona DA, Vaccaro AR (2018) Evaluation and management of pyogenic and tubercular spine infections. Curr Rev Musculoskelet Med 11:643–652

Cheung WY, Luk KDK (2012) Pyogenic spondylitis. Int Orthop 36:397–404

Cottle L, Riordan T (2008) Infectious spondylodiscitis. J Infect 56:401–412

Dagirmanjian A, Schils J, McHenry MC et al (1996) MR imaging of vertebral osteomyelitis revisited. AJR Am J Roentgenol 167:1539–1543

Dagirmanjian A, Schils J, McHenry MC (1999) MR imaging of spinal infections. Magn Reson Imaging Clin North Am 7:525–538

DeSanto J, Ross JS (2011) Spine infection/inflammation. Radiol Clin North Am 49:105–127

Diehn FE (2012) Imaging of spine infection. Radiol Clin North Am 50:777–798

Fantoni M, Trecarichi EM, Rossi B et al (2012) Epidemiological and clinical features of pyogenic spondylodiscitis. Eur Rev Med Pharmacol Sci 16:2–7

Gasbarrini AL, Bertoldi E, Mazzetti M et al (2005) Clinical features, diagnostic and therapeutic approaches to haematogenous vertebral osteomyelitis. Eur Rev Med Pharmacol Sci 9:53–66

Gillams AR, Chaddha B, Carter AP (1996) MR appearances of the temporal evolution and resolution of infectious spondylitis. AJR Am J Roentgenol 166:903–907

Go JL, Rothman S, Prosper A et al (2012) Spine infections. Neuroimaging Clin North Am 22:755–772

Gogna A, Peh WCG, Munk PL (2008) Image-guided musculoskeletal biopsy. Radiol Clin North Am 46:455–473

Gouliouris T, Aliyu SH, Brown NM (2010) Spondylodiscitis: update on diagnosis and management. J Antimicrob Chemother 65:11–24

Govender S (2005) Spinal infections. J Bone Joint Surg Br 87:1454–1458

Hadjipavlou AG, Mader JT, Necessary JT et al (2000) Hematogenous pyogenic spinal infections and their surgical management. Spine 25:1668–1679

Harada Y, Tokuda O, Matsunaga N (2008) Magnetic resonance imaging characteristics of tuberculous spondylitis vs. pyogenic spondylitis. Clin Imaging 32:303–309

Hong SH, Choi JY, Lee JW et al (2009) MR imaging assessment of the spine: infection or an imitation? Radiographics 29:599–612

Jung NY, Jee WH, Ha KY et al (2004) Discrimination of tuberculous spondylitis from pyogenic spondylitis on MRI. AJR Am J Roentgenol 182:1405–1410

Kawakyu-O'Connor D, Bordia R, Nicola R (2016) Magnetic resonance imaging of spinal emergencies. Magn Reson Imaging Clin North Am 24:325–344

Kehrer M, Pedersen C, Jensen TG et al (2014) Increasing incidence of pyogenic spondylodiscitis: a 14-year population-based study. J Infect 68:313–320

Lam KS, Webb JK (2004) Discitis. Hosp Med 65: 280–286

Lazzeri E, Bozzao A, Cataldo MA et al (2019) Joint EANM/ESNR and ESCMID-endorsed consensus document for the diagnosis of spine infection (spondylodiscitis) in adults. Eur J Nucl Med Mol Imaging 46:2464–2487

Leone A, Dell'Atti C, Magarelli N et al (2012) Imaging of spondylodiscitis. Eur Rev Med Pharmacol Sci 16:8–19

Narváez J, Nolla JM, Narváez JA et al (2006) Spontaneous pyogenic facet joint infection. Semin Arthritis Rheum 35:272–283

Nickerson EK, Sinha R (2016) Vertebral osteomyelitis in adults: an update. Br Med Bull 117:121–138

Pola E, Logroscino CA, Gentiempo M et al (2012) Medical and surgical treatment of pyogenic spondylodiscitis. Eur Rev Med Pharmacol Sci 16:35–49

Prodromou ML, Ziakas PD, Poulou LS et al (2014) FDG PET is a robust tool for the diagnosis of spondylodiscitis: a meta-analysis of diagnostic data. Clin Nucl Med 39:330–335

Raghavan M, Lazzeri E, Palestro CJ (2018) Imaging of spondylodiscitis. Semin Nucl Med 48:131–147

Ratcliffe JF (1985) Anatomic basis for the pathogenesis and radiologic features of vertebral osteomyelitis and its differentiation from childhood discitis: a microarteriographic investigation. Acta Radiol Diagn 26:137–143

Rosen RS, Fayad L, Wahl RL (2006) Increased 18F-FDG uptake in degenerative disease of the spine: characterization with 18F-FDG PET/CT. J Nucl Med 47:1274–1280

Shikhare SN, Peh WCG (2019) Pyogenic spondylodiscitis. In: Taljanovic MS, Omar IM, Hoover KB, Chadaz TS (eds) Musculoskeletal imaging, vol 2. Oxford University Press, Oxford, pp 87–90

Shikhare SN, Singh DR, Shimpi TR, Peh WCG (2011) Tuberculous osteomyelitis and spondylodiscitis. Semin Musculoskelet Radiol 15:446–458

Skaf GS, Domloj NT, Fehlings MG et al (2010) Pyogenic spondylodiscitis: an overview. J Infect Public Health 3:5–16

Smith AS, Weinstein MA, Mizushima A et al (1989) MR imaging characteristics of tuberculous spondylitis vs vertebral osteomyelitis. AJR Am J Roentgenol 153:399–405

Srinivasan S, Peh WCG (2011) Imaging-guided biopsy in musculoskeletal infections. Semin Musculoskelet Radiol 15:561–568

Stäbler A, Reiser MF (2001) Imaging of spinal infection. Radiol Clin North Am 39:115–135

Tali ET (2004) Spinal infections. Eur J Radiol 50:120–133

Tali ET, Oner AY, Koc AM (2015) Pyogenic spinal infections. Neuroimaging Clin North Am 25:193–208

Tins BJ, Cassar-Pullicino VN (2004) MR imaging of spinal infection. Semin Musculoskelet Radiol 8: 215–229

Tyrrell PNM, Cassar-Pullicino VN, McCall IW (1999) Spinal infection. Eur Radiol 9:1066–1077

Varma R, Lander P, Assaf A (2001) Imaging of pyogenic infectious spondylodiskitis. Radiol Clin North Am 39:203–213

Wiley AM, Trueta J (1959) The vascular anatomy of the spine and its relationship to pyogenic vertebral osteomyelitis. J Bone Joint Surg Br 41:796–809

Yeom JA, Lee IS, Suh HB et al (2016) Magnetic resonance imaging findings of early spondylodiscitis: interpretive challenges and atypical findings. Korean J Radiol 17:565–680

Imaging of Iatrogenic Spinal Infection

Jesper Dierickx, Johan Van Goethem, Bart Poffyn, Koenraad Luc Verstraete, and Filip Vanhoenacker

Contents

J. Dierickx
Faculty of Medicine and Health Sciences, Ghent University, Ghent, Belgium

General Hospital Sint-Maarten Mechelen, Mechelen, Belgium

J. Van Goethem
Department of Radiology, Antwerp University Hospital, Edegem, Belgium

Faculty of Medicine and Health Sciences, Antwerp University, Edegem, Belgium

B. Poffyn
Department of Orthopedics and Traumatology, Faculty of Medicine and Health Sciences, Ghent University, Ghent, Belgium

K. L. Verstraete
Faculty of Medicine and Health Sciences, Department of Radiology, Ghent University, Ghent, Belgium

F. Vanhoenacker (✉)
Faculty of Medicine and Health Sciences, Ghent University, Ghent, Belgium

General Hospital Sint-Maarten Mechelen, Mechelen, Belgium

Department of Radiology, Antwerp University Hospital, Edegem, Belgium

Faculty of Medicine and Health Sciences, Antwerp University, Edegem, Belgium
e-mail: filip.vanhoenacker@telenet.be

© The Author(s), under exclusive license to Springer Nature Switzerland AG 2021, corrected publication 2021

M. F. Ladeb, W. C. G. Peh (eds.), *Imaging of Spinal Infection*,
Medical Radiology Diagnostic Imaging, https://doi.org/10.1007/978-3-030-70459-9_8

Abstract

Spinal infection may occur due to iatrogenic causes. Its pathogenesis, clinical presentation, management, various imaging techniques, and its application in instrumented and noninstrumented spines are discussed. We provide an overview of the typical infection locations and its imaging correlates, such as spondylodiscitis, epidural and paravertebral abscesses, facet joint infection, and myelomeningitis. Iatrogenic spinal infection should be differentiated from postoperative fluid collections, such as hematoma, seroma, and pseudomeningocele.

Abbreviations

CT Computed tomography
MRI Magnetic resonance imaging

1 Introduction

Over the years, spinal infection has steadily increased in incidence, partly due to the aging population, increasing the number of immunocompromised patients, and the more frequent application of spinal procedures and the improved imaging techniques (Jiménez-Mejías et al. 1999; Babic and Simpfendorfer 2017). Iatrogenic spinal infection is defined as spinal infection due to medical intervention and can be either post-procedural or non-post-procedural. Post-procedural infection can be classified as infection following minimally invasive procedures or postoperative infection. Minimally invasive procedures are defined as procedures using a percutaneous approach, such as facet joint injection, epidural injection, discography, or myelography. Postoperative infection consists of infections complicating standard, open surgery, either with or without instrumentation. Non-post-procedural, iatrogenic spine infection are mainly infections that occur in immunocompromised patients.

2 Epidemiology

Among post-procedural spinal infections, infection is less frequent after minimally invasive procedures than after surgery. Di Martino et al. (2019) reported an incidence ranging from 0.26 to 2.75% for minimally invasive procedures, while an incidence of 2.1 to 8.5% was reported after instrumented surgery. After open surgery without instrumentation, an incidence of less than 1% has been reported. It has a higher incidence among older patients and pediatric patients and a slight male predominance (Jiménez-Mejías et al. 1999; Chahoud et al. 2014). The reported incidence of postoperative spinal infection in the current literature, however, has a wide range, from 0.5 to 18.8% (Chahoud et al. 2014). The incidence of non-post-procedural iatrogenic spondylodiscitis is increasing as well, mainly due to renal dialysis and immunosuppressants in the treatment of malignancy or autoimmune disease (Cervan et al. 2012; Venugopal Menon and Sorour 2016). It is estimated that 1.3% of hemodialysis patients with bacteremia develop spondylodiscitis (Ethier et al. 2008; García-García et al. 2010).

3 Pathogenesis

3.1 Spread

Direct inoculation is the most frequent route of post-procedural infection, in both minimally invasive procedures and surgery. Hematogeneous spread and early postoperative contamination are less frequent (Jiménez-Mejías et al. 1999; Taşdemiroglu et al. 2004; Gerometta et al. 2012a; Chahoud et al. 2014). Several cases of spinal infection after minimally invasive procedures have been reported, e.g., following epidural catheterization (Arun et al. 2007), facet joint (corticosteroid) injection (Cook et al. 1999; Falagas et al. 2006; Weingarten et al. 2006), lumbar epidural corticosteroid injection (Hooten et al. 2006), or intradiscal therapy

(Subach et al. 2012). Bosnak et al. (2017) reported ten cases of spondylodiscitis after intradiscal electrothermal therapy, a therapy applied in low back pain patients in tertiary hospitals. Clifton and Selby (2018) reported a man with an epidural abscess after prolotherapy, an alternative medical treatment for chronic musculoskeletal pain.

In non-post-procedural spondylodiscitis, the main pathogenic mechanism is hematogeneous spread (Jiménez-Mejías et al. 1999). It occurs in the context of bacteremia, with microorganisms spreading to the anterior aspect of the vertebral body end plates through the end arterioles (see chapter on "Pathophysiology of Spinal Infection"). The pathogens spread from the vertebral body into the disk space and the adjacent end plate (Go et al. 2012). Several authors have reported spinal infection secondary to catheter-induced septicemia (Corso et al. 1995; Gezici and Ergün 2010). Corso et al. (1995) described a patient with spinal osteomyelitis occurring after total parental nutrition (TPN) catheter-induced septicemia, while Gezici and Ergün (2010) reported two male hemodialysis patients with cervical epidural abscesses.

Another possible mechanism for non-post-procedural spinal infection is direct spread through a transvenous route. The Batson plexus, an epidural venous plexus, may enable the spread of microorganisms from other infectious sites (Go et al. 2012). The most common coexisting infection in spondylodiscitis is genitourinary infection, potentially spreading through this transvenous mechanism (Taşdemiroglu et al. 2004). Two case reports have described patients with spondylodiscitis developing after a transrectal ultrasonography-guided needle biopsy of the prostate (Taşdemiroglu et al. 2004; Kalenderov et al. 2018).

Opportunistic spinal infections can occur as a complication of immunosuppressive therapy in rheumatoid arthritis (Giri et al. 2014) or transplant patients, either through hematogeneous spread, transvenous spread, or direct inoculation. The occurrence of spinal tuberculosis (TB) after liver transplantation, most likely due to hematogeneous origin, has been reported (Lou et al. 2010). Bacteremia in renal dialysis patients is another frequent cause of non-post-procedural spondylodiscitis (Cervan et al. 2012).

3.2 Microorganisms

The most common causative organism in the post-procedural setting is *Staphylococcus aureus*. Weinstein et al. (2000) showed that this was the most commonly cultured pathogen in 74% of 46 cases of postoperative spinal wound infection. The second most common organisms are coagulase-negative staphylococci, such as *S. epidermis*, often associated with implanted spinal prosthesis. This is followed by gram-negative organisms, such as *Escherichia coli*, *Pseudomonas aeruginosa*, and *Proteus* species. They have been associated with urinary and fecal incontinence, posterior lumbar approach, intravenous drug use, and long hospital admission (Weinstein et al. 2000; McDermott et al. 2012; Di Martino et al. 2019). In infection occurring several months after initial procedures, *Propionibacterium acnes* is another common microorganism. Due to its low virulence and slow growth rate, it is rather difficult to isolate this organism (Haidar et al. 2010; McDermott et al. 2012; Di Martino et al. 2019). Fungal microorganisms or *Mycobacterium tuberculosis* causing postoperative spondylodiscitis are quite rare and are most probably due to direct intraoperative inoculation. It has been suggested that *Aspergillus* and *Candida* are the most common fungal pathogens. Fungal and mycobacterial infection should be suspected when cultures are negative for bacteria and there is deterioration of the clinical findings after antibiotic treatment (Lotfinia and Vahedi 2010; Gerometta et al. 2012a).

4 Etiology

The incidence of postoperative spinal infection is determined by several risk factors. Both preoperative and intraoperative risk factors play a role (Tables 1 and 2).

4.1 Preoperative Risk Factors

Diabetes mellitus is an independent risk factor for postoperative spinal infection (Jiménez-Mejías et al. 1999; Pull ter Gunne and Cohen 2009; Veeravagu et al. 2009; Chahoud et al. 2014). Patients with diabetes mellitus have microangiopathic changes, leading to local tissue ischemia and lower tissue concentrations of antibiotics. The relative immune suppression in diabetes mellitus impairs wound healing and further increases the risk for infection. Cigarette smoking has a similar mechanism. It is associated with microangiopathy and tissue ischemia. It has been shown that obesity increases the overall risk of surgical spinal infection (SSI), as well as superficial SSI and deep SSI (Pull ter Gunne and Cohen 2009; Veeravagu et al. 2009). The thick subcutaneous adipose layer is poorly perfused, and its large space predisposes it to infection. Since the use of corticosteroids is associated with impaired wound healing and immune suppression, it increases the risk for SSI. Blood loss and the perioperative need for transfusion of blood products are correlated with a higher risk for postoperative spinal infection (Pull ter Gunne and Cohen 2009; Chahoud et al. 2014), as well as alcohol abuse. Young children and elderly people have an increased risk for postoperative spinal infection (Pull ter Gunne and Cohen 2009; Chahoud et al. 2014). The incidence of iatrogenic spinal infection varies among the different types of surgery. Trauma patients are reported to have the highest infection rates. Patients with bone metastases or pre-existing discitis have high SSI rates as well, while patients with surgery for degenerative disease have lower infection rates (Blam et al. 2003; Veeravagu et al. 2009; Smith et al. 2011; Chahoud et al. 2014).

Table 1 List of preoperative risk factors for surgical site infection

Diabetes mellitus
Smoking
Obesity
Corticosteroids
Perioperative need for blood transfusion
Alcohol abuse
Young children or elderly
Type of surgery: trauma > metastasis = infection > degeneration

Table 2 List of intraoperative risk factors

Location: thoracic > lumbar > cervical
Approach: combined anterior and posterior approach > isolated posterior > isolated anterior
Open approach > minimally invasive approach
Presence of implants
Revision surgery
Long operation duration
Intraoperative fraction of inspired oxygen of less than 50%

4.2 Intraoperative Risk Factors

Surgery in the thoracic spine has the highest rate of postoperative infection, followed by lumbar and cervical surgery (Blam et al. 2003; Maragakis et al. 2009; Chahoud et al. 2014). Other risk factors include the presence of implants and spinal fusion, with isolated anterior fusion having a significantly lower infection rate compared to a posterior, or a combined anterior and posterior approach (Maragakis et al. 2009; Veeravagu et al. 2009; Smith et al. 2011; Chahoud et al. 2014). A minimally invasive approach has a lower infection rate, compared to an open approach (Smith et al. 2011). Revision cases tend to have a higher chance of SSI (Smith et al. 2011). An intraoperative fraction of inspired oxygen of less than 50% and a long operation duration are risk factors for SSI as well (Blam et al. 2003; Maragakis et al. 2009; Veeravagu et al. 2009).

5 Clinical Presentation

The clinical presentation of iatrogenic spondylodiscitis is not specific and does not differ from non-iatrogenic spondylodiscitis (Jiménez-Mejías

et al. 1999). It is characterized by back pain, worsening after any motion. Muscle spasms and limited range of motion are very common. Localized swelling or pus in the superficial surgical wound may be present. However, the clinical presentation is usually unremarkable. Neurological deficits are rare as well (Skaf et al. 2010). Several studies show that fever is present in only 33–52% of affected patients (Jiménez-Mejías et al. 1999). In atypical pathogens, such as fungal and mycobacterial microorganisms, and in delayed infections caused by *P. acnes*, fever is even less frequent (Haidar et al. 2010; Babic and Simpfendorfer 2017). Epidural abscesses may compress the dural sac, causing neurological symptoms. Facet joint infection typically has a unilateral and more acute and severe presentation, compared to spondylodiscitis (Tali et al. 2015). Patients with spinal meningitis and/or myelitis present with fever, headache, spinal pain, and neurological deficits, such as loss of consciousness, motor or sensory deficit, or bladder dysfunction (Tali et al. 2015).

Inflammatory markers, such as white blood cell count (WBC), C-reactive protein (CRP), and erythrocyte sedimentation rate (ESR), can be used as an indicator of infection. Raised CRP levels are more sensitive for spondylodiscitis than raised ESR levels or WBC, especially in a postoperative context (Gerometta et al. 2012b), and are the most useful inflammatory marker. However, it has a low specificity and low positive predictive value (McDermott et al. 2012).

6 Imaging

6.1 Imaging Techniques

6.1.1 Noninstrumented Spine

Radiography has a low sensitivity and specificity for spinal infection. Osteolytic changes are not visible at an early stage, causing a diagnostic delay of at least 2 weeks (Torres and Zakhari 2017). While computed tomography (CT) is superior in the detection of bony destructive changes compared to radiography, magnetic resonance imaging (MRI) is a better modality to assess soft tissue, the intervertebral disk, and early changes in the vertebral end plates. T1- and T2-weighted images in the sagittal and axial planes should be obtained. The MRI protocol should include fat-suppression sequences, such as fat-suppressed T2-weighted images, short-tau inversion recovery (STIR), Dixon method, or IDEAL sequences. IDEAL is an acronym for iterative decomposition of water and fat with echo asymmetry and least squares estimation. These sequences, along with hypointense signal on T1-weighted images, aid detection of bone marrow edema. If an abnormality is seen on these fat-suppressed images, additional axial T1-weighted images after intravenous gadolinium contrast administration should be acquired in order to assess enhancement of the intervertebral disk, vertebral end plates, and surrounding soft tissues (Torres and Zakhari 2017).

6.1.2 Instrumented Spine

6.1.2.1 Radiographs

Radiographs are used as first-line modality for follow-up of the postoperative spine, in order to assess any callus formation or hardware complications (Allouni et al. 2013). However, in the instrumented spine, the value of radiography for early detection of spinal infection is limited.

6.1.2.2 CT

Although less sensitive than MRI, CT is a useful imaging tool in the assessment of the postoperative spine in patients with a contraindication for MRI. However, artifacts related to metallic hardware can compromise the visualization of the surrounding bone and soft tissue, possibly influencing the diagnosis of infectious disease. Metallic hardware attenuates large numbers of X-ray photons, preferentially low energy photons. As a consequence, the beam of photons is "hardened" and leads to a decrease of voxel density in the area surrounding the metallic implants. Additionally, the lower number of photons leads to a noisier image and to an aliasing effect, representing areas with lower spatial frequency (Rassner 2019). These artifacts depend on both fixed and modified variables (McLellan et al.

2014). The former includes factors related to the composition and the geometry of the material. For example, implants based on titanium, polyethylenes, or fibrocarbons have less artifacts than steel or vitallium hardware, due to their lower attenuation coefficients (Nouh 2012; Rassner 2019). The extent of hardware-related artifact is associated with the thickness of the implant.

Modifiable variables are related to CT acquisition parameters (Table 3), including X-ray kilovolt peak (kVp), X-ray tube current, pitch, and image reconstruction parameters (Stradiotti et al. 2009; McLellan et al. 2014). Increasing the kVp reduces the attenuation by metal, resulting in fewer artifacts (Fig. 1) (McLellan et al. 2014). The X-ray beam can penetrate the metallic hardware more efficiently with higher tube current settings (Stradiotti et al. 2009). However, an increase in both kVp and tube current significantly increases the patients' radiation dose. For example, an increase in kVp from 120 to 140 increases the radiation dose by 40% (McLellan et al. 2014).

Table 3 Recommendations on CT acquisition parameter adjustments for reduction of metal-related artifacts

Increasing kVp
Increasing X-ray tube current
Minimal section thickness (1 or 2 mm)
Minimal pitch (0.2)
Iterative reconstruction techniques
Dual-energy CT technique

The slice thickness has an important impact on the beam hardening artifact. The smallest possible slice thickness is indicated, and a minimal pitch and minimal section thickness should be used (Fig. 2). More voxel data can be collected with a lower pitch setting, thus reducing the artifacts (Stradiotti et al. 2009; McLellan et al. 2014). Douglas-Akinwande et al. (2006) suggest

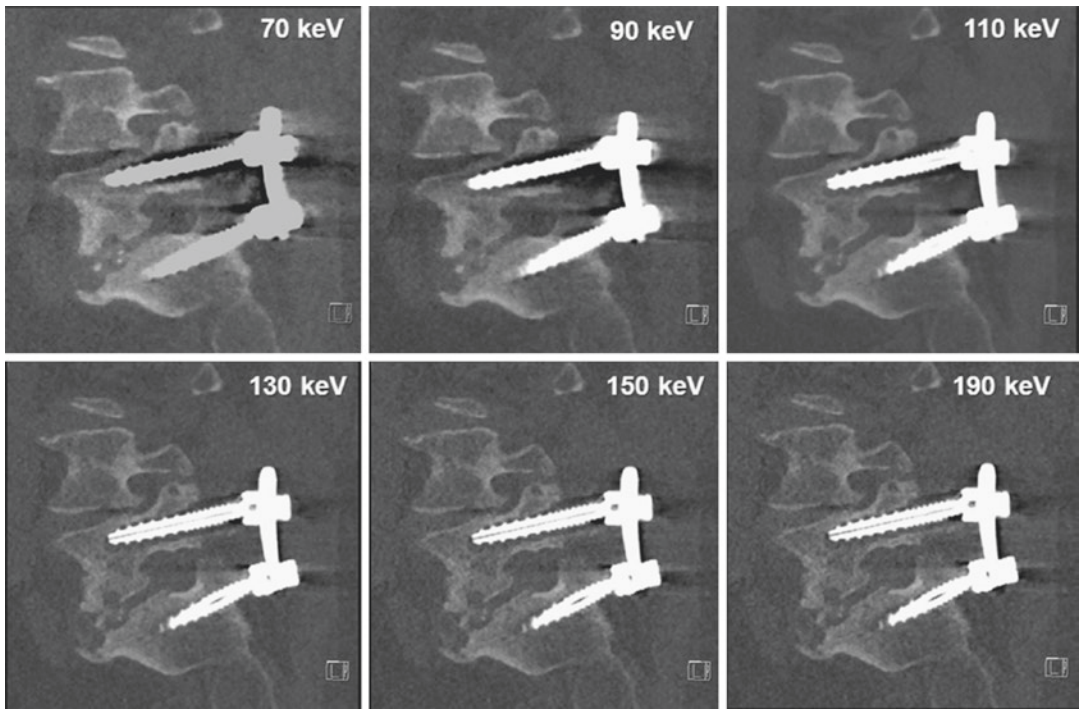

Fig. 1 Metal artifact reduction on CT by modification of energy level. When the energy level increases, the metal-related artifacts become less apparent, and the structure of the metallic implants can be evaluated better. However, the contrast resolution decreases as the energy level rises. [Reprinted with permission from Elsevier: McLellan A M, Daniel S, Corcuera-Solano I, Joshi V, Tanenbaum L N (2014) Optimized imaging of the postoperative spine. Neuroimag Clin North Am 24:349–364]

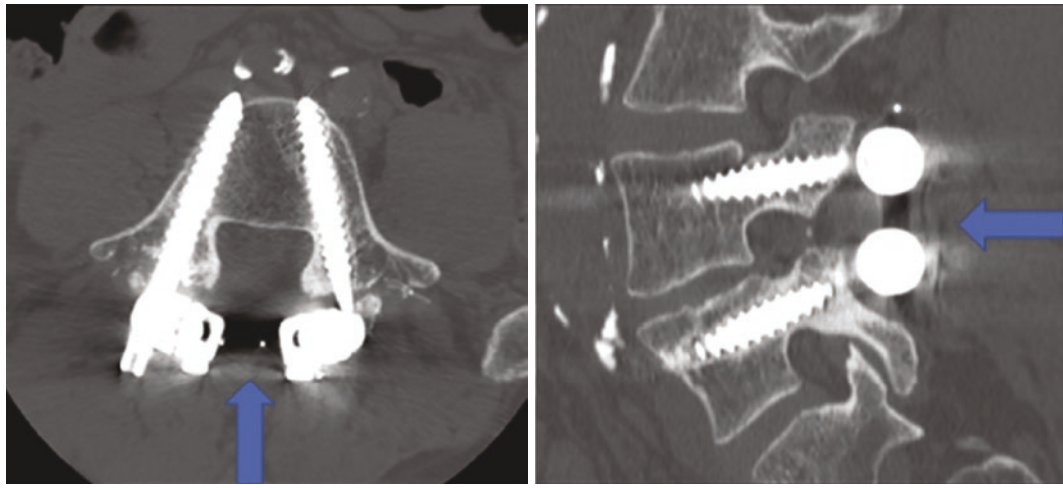

Fig. 2 Metal artifact reduction on CT by using thin slices. CT images with thin slices show minimal metal-related artifact. Only the posterior part of the metallic implants produces artifacts (blue arrows). [Reprinted with permission from Elsevier: McLellan A M, Daniel S, Corcuera-Solano I, Joshi V, Tanenbaum L N (2014) Optimized imaging of the postoperative spine. Neuroimag Clin North Am 24:349–364]

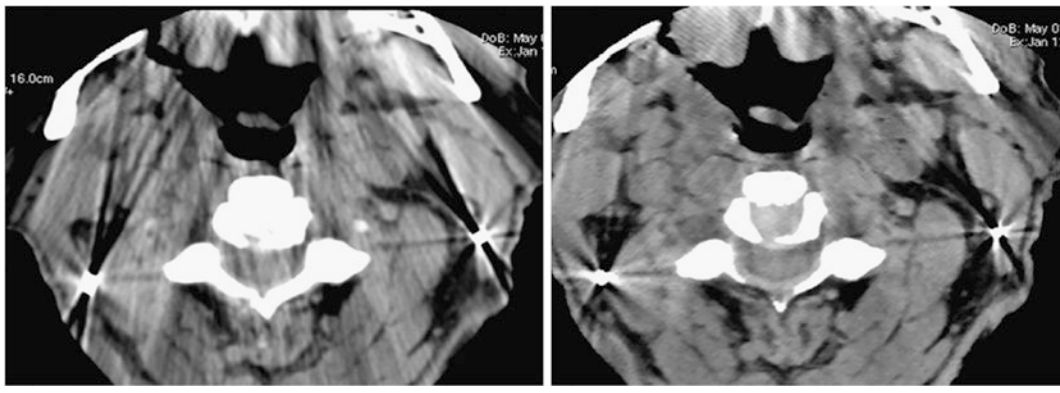

Fig. 3 Metal artifact according to reconstruction algorithm. Metal-related artifacts are more extensive on CT image acquired through filtered back reconstruction (left) than through iterative reconstruction (right). [Reprinted with permission from Elsevier: McLellan A M, Daniel S, Corcuera-Solano I, Joshi V, Tanenbaum L N (2014) Optimized imaging of the postoperative spine. Neuroimag Clin North Am 24:349–364]

a pitch of 0.2 and a section thickness of 1 or 2 mm in multichannel CT protocols. Iterative reconstruction techniques have a role in removing metallic hardware artifacts (Fig. 3). Dual-energy CT obtains an image in two different kVp levels, typically 80 and 140 kVP. This technique obtains information about the atomic number of the different tissue components through information about tissue attenuation at different energy levels. It plays a role in the reduction of metallic hardware artifacts (McLellan et al. 2014).

6.1.2.3 MRI

In the assessment of postoperative spinal infection, MRI is preferred to CT, due to its higher contrast resolution. The absence of ionizing radiation is an additional advantage. However, metallic hardware disrupts the local magnetic field, with anatomical distortion, pixel pile up, and signal loss of the surrounding tissue. This is affected by both the type of metal and the field strength, with 3 Tesla (T) images generating more artifacts compared to 1.5 T images (McLellan et al. 2014).

Non-ferromagnetic materials, such as titanium and polycarbon-enforced implants, produce less pronounced artifacts compared to ferromagnetic implants, such as stainless steel (Nouh 2012). The implant size correlates with the severity of the artifacts (Stradiotti et al. 2009).

Artifacts can be minimized through frequency encoding in the direction of the long axis of screws. In spinal imaging, this means the anterior-to-posterior direction in both axial and sagittal MR images (McLellan et al. 2014). In MR images, smaller voxel sizes result in smaller signal voids related to metal artifacts, due to the increased spatial definition. This can be achieved by a smaller field of view and by thin slices. The trade-off of smaller voxel sizes is a lower signal-to-noise ratio (SNR). This can possibly be compensated with an increased number of excitations (Stradiotti et al. 2009). A slice thickness of 4 mm and a field of view of 32 × 32 cm for sagittal fast spin-echo (FSE) T2-weighted images and 20 × 20 cm for axial FSE-T2-weighted images are recommended as optimal parameters (Zou et al. 2015).

Another parameter that may influence metal artifacts is the receiver bandwidth (BW). Increasing the BW results in less artifacts, with reduced SNR as a disadvantage (Van Goethem et al. 2002). Zou et al. (2015) demonstrated that 142.86 kHz is the optimized bandwidth for imaging orthopedic metal implants. Field inhomogeneity can be partially corrected by the refocusing pulse of 180° in SE and FSE sequences. This 180° pulse is absent in gradient echo (GRE) sequences, resulting in significantly larger areas of distortion and signal loss in GRE compared to SE or FSE sequences (Rassner 2019). Additionally, FSE, with reduced echo spacing (ES), is less susceptible to metal artifacts compared to SE sequences.

Among fat suppression techniques, the use of the radiofrequency (RF)-based fat suppression technique is limited. The inhomogeneous magnetic field, caused by the presence of metallic hardware, results in areas of reduced fat suppression. Short-tau inversion recovery (STIR) imaging technique is less dependent on field homogeneity and offers more homogeneous fat suppression (Fig. 4), with a reduced SNR as a trade-off (Stradiotti et al. 2009; McLellan et al. 2014). Chemical shift imaging techniques, such as IDEAL (GE Healthcare, New York, USA) and DIXON (Siemens Healthineers, Munich, Germany), are other alternatives for RF-based fat suppression. Selective water and fat images can be obtained by adding and subtracting images from in-phase and opposed-phase imaging. They offer more homogeneous fat suppression, due to its insensitivity to the inhomogeneous magnetic field (McLellan et al. 2014). However, the robustness of DIXON techniques is lower than that of STIR techniques in the presence of metallic implants. The advantage of DIXON sequences is the higher SNR and the production of both in-phase and fat-suppressed sequences within one acquisition (Jungmann et al. 2017). Dedicated MRI sequences have been developed to reduce metal artifacts.

In view angle tilting (VAT), the angle from which the excited slice is viewed is tilted and causes a "shearing" of voxels (Fig. 5). All off-resonance-induced shifts along the readout direction within the excited slice are eliminated (Ariyanayagam et al. 2015). It corrects in-plane distortions. This technique has a few limitations. Firstly, it does not correct through-plane distortions. Secondly, the sheared slices have a more blurred appearance. This limitation can partially be corrected by using thin slices (Jungmann et al. 2017). Multi-sequence imaging (MSI) is another new imaging technique and includes multiacquisition variable-resonance image combination (MAVRIC; GE Healthcare, New York, USA) and slice-encoding for metal artifact correction (SEMAC; Siemens Healthineers, Munich, Germany) (McLellan et al. 2014; Jungmann et al.

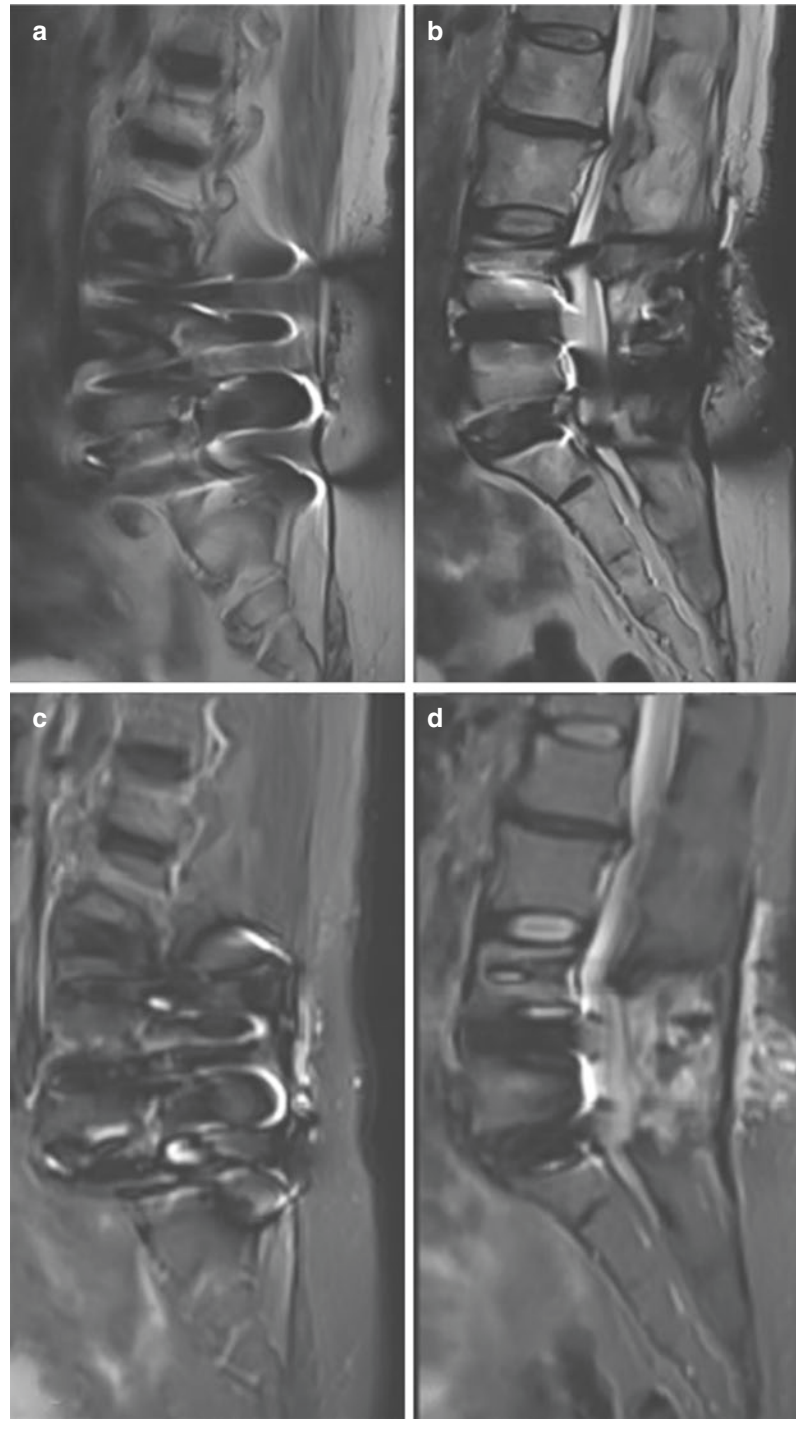

Fig. 4 Metal artifact reduction on MRI. A 74-year-old woman with a history of laminectomy and posterior lumbar fixation with transpedicular screws and disk prosthesis. (**a**, **b**) Sagittal T2-W images with spectral fat suppression show extensive areas of inhomogeneous fat suppression. (**c**, **d**) Sagittal STIR images show more homogeneous fat suppression. The anatomical distortion and signal loss at the level of the metallic implants are less pronounced in the STIR image than in the T2-W image

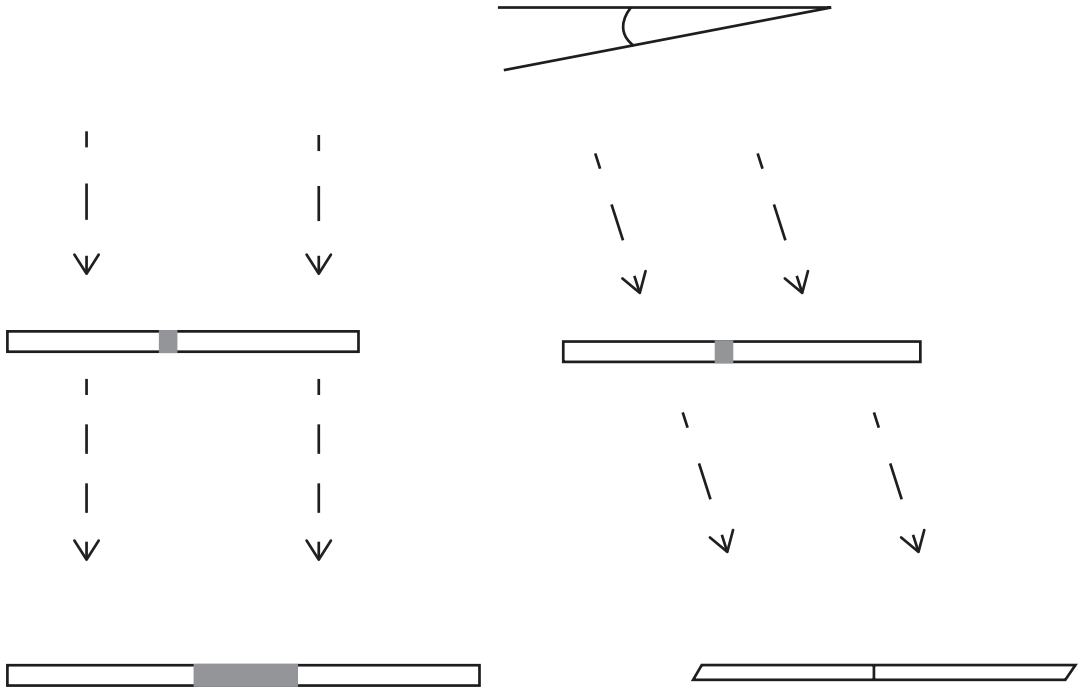

Fig. 5 Schematic representation of view angle tilting. The angle from which the excited slice is viewed is tilted and causes a "shearing" of voxels. All off-resonance-induced shifts along the readout direction within the excited slice are eliminated

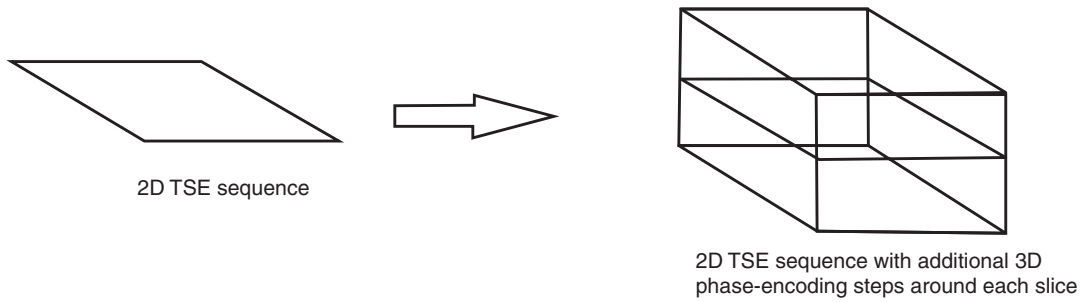

Fig. 6 SEMAC is based on a 2D TSE sequence. It applies additional phase-encoding steps in a 3D slab around each slice, in order to register through-plane distortions

2017). SEMAC is often used in combination with VAT and reduces both in-plane and through-plane distortions. This technique is based on a two-dimensional (2D) TSE sequence and applies additional phase-encoding steps in a three-dimensional (3D) slab around each slice, in order to register through-plane distortions (Fig. 6). A disadvantage is the duration of the scan time, which depends on the extent of the field inhomogeneity (Jungmann et al. 2017). MAVRIC is a 3D technique that acquires several 3D slaps multiple times with discretely varying resonance frequency offsets. An analysis of these 3D slaps builds an image with reduced artifacts (Ariyanayagam et al. 2015; Jungmann et al. 2017). Aliasing in the through-plane direction can be a trade-off. Several different metal artifact-reducing sequences, such as single-point imaging

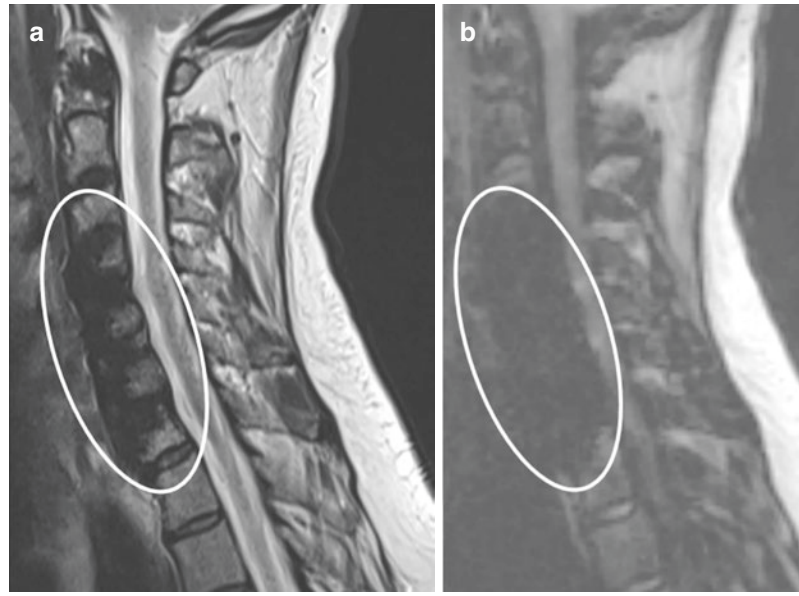

Fig. 7 Sagittal (**a**) T2-W and (**b**) DWI MR images of metallic implants causing artifacts. Sagittal DWI shows more extensive artifacts due to the presence of metallic implants at the C4-C7 level, compared to the sagittal T2-W image (white circle). An assessment of the vertebral bone marrow and the surrounding soft tissue at these levels is not possible on the DWI MR images

or pre-polarized MRI, have been developed. Due to long acquisition times or low spatial resolution, however, they are clinically not feasible (Jungmann et al. 2017).

Diffusion-weighted imaging (DWI) usually uses single-shot echo planar pulse sequences (SS-EPI). This allows rapid imaging with minimal motion artifacts. However, the presence of metal implants produces extreme distortions due to off-resonance effects (Koch et al. 2018) (Fig. 7). Koch et al. (2018) demonstrated that multispectral DWI (PROPELLER DWI; GE Healthcare, New York, USA) can produce images with reduced metal artifacts, compared to SS-EPI DWI. Currently, its clinical application is still limited because of the long scan times. It should also be noted that the measured apparent diffusion coefficient (ADC) values differ between EPI DWI and PROPELLER DWI, which might affect the appearance of pathology (Rassner 2019). Table 4 summarizes the recommendations for reduction of metal artifacts on MRI (Table 4).

Table 4 Recommendations on MRI acquisition parameter adjustments for metal-related artifact reduction

Lower field strength (1.5 T)
Using non-ferromagnetic metallic implants (i.e. titanium)
Frequency encoding in the anterior-to-posterior direction
Small field-of-view
Thin slices (4 mm)
Increasing the receiver BW (142.86 kHz)
FSE sequences (instead of SE or GRE sequences)
Chemical shift imaging techniques or STIR techniques (instead of RF-based fat suppression)
VAT techniques
MSI techniques
Multispectral DWI techniques

6.1.2.4 Nuclear Medicine Imaging

Bone scintigraphy has several limitations in the diagnosis of postoperative spinal infection. It may produce false-negative results in the elderly and in spondylodiscitis. Increased uptake may persist after resolution of the infection. Additionally, bone scintigraphy is not reliable for the detection of adjacent soft tissue infection, such as abscesses. Gallium-67 (^{67}Ga) citrate imaging can be used as a complementary examination to improve specificity and detection of soft tissue infection. However, this technique has a few disadvantages, such as the use of two different

radioisotopes, and the injection and imaging being on different days. The injection of ^{67}Ga should be performed 24–72 h before imaging (Gemmel et al. 2010).

Positron emission tomography (PET)/CT imaging is based on the detection of two gamma rays emitted at the same time by a positron and electron, while single-photon emission computed tomography (SPECT)/CT is based on the detection of a single gamma ray emitted by a radioisotope. Fluorine-18 2′-deoxy-2-fluoro-D-glucose ([^{18}F] FDG) PET/CT imaging provides higher resolution than that of SPECT/CT. Additionally, an imaging session is completed within 1–2 h. Compared to ^{67}Ga SPECT/CT and bone scintigraphy, it has a lower radiation dose. [^{18}F] FDG PET/CT imaging has a high sensitivity for spinal infection, and negative [^{18}F] FDG PET/CT can exclude spinal infection (Gemmel et al. 2010). However, foreign body reaction and aseptic loosening of metallic implants may demonstrate increased FDG uptake as well. [^{18}F] FDG PET/CT imaging is more useful than SPECT/CT imaging in evaluating postoperative infection in the axial skeleton. Artifacts on PET images are generally less pronounced compared to MRI. Due to attenuation correction, metal artifacts can show higher FDG avidity in the areas with metallic implants on PET/CT fused images (Goerres et al. 2003). Therefore, to avoid false-positive results, non-attenuation corrected images should be assessed as well.

The role of radiolabelled leukocyte imaging is limited in the diagnosis of iatrogenic spinal infections. In more than 50% of all cases, radiolabeled leukocyte imaging does not demonstrate increased activity in the infected area (Gemmel et al. 2010). This is due to a poor migration of radiolabelled white blood cells into an infected and edematous vertebra. On the contrary, radiolabelled leukocytes may correctly identify extravertebral soft tissue infection.

6.2 Location

6.2.1 Spondylodiscitis

6.2.1.1 Post-Procedural Spondylodiscitis

In a post-procedural spine, the identification of spondylodiscitis on MRI is hampered by many factors. Aside from potential metal artifacts in an instrumented spine, discal and vertebral changes in spondylodiscitis should be differentiated from normal post-procedural changes. After surgery, the intervertebral disk usually has a decreased height (Grand et al. 1993). In a normal post-procedural setting, the intervertebral disks and adjacent vertebral body end-plate bone marrow can demonstrate signal intensity changes (Fig. 8). In the vertebral body end-plates, the signal intensity decreases on T1-weighted and increases on T2-weighted images, correlating with postoperative edema and are described as Modic type I end-plate changes (Boden et al. 1992; Dufour et al. 2005). Contrast-enhanced T1-weighted MR images can show enhancement of these edematous areas at the vertebral body end plate (Boden et al. 1992; Dufour et al. 2005).

In a study by Van de Kelft et al. (1996), 6 weeks after operation, all asymptomatic patients showed enhancement of the soft tissues along the surgical tract, in the subcutaneous layers, the peridural space, and/or the intervertebral disk. Even after 6 months, a significant number of asymptomatic patients demonstrated persisting epidural, paraspinal, or intervertebral enhancement. This most likely correlates to postoperative granulation or scar tissue (Van De Kelft et al. 1996). Normal postoperative intervertebral disk enhancement patterns have been described in the literature. Ross et al. (1996) reported linear bands of enhancement in the superior and inferior aspects of the intervertebral disk that parallels the vertebral body end plates as a normal postoperative finding. Boden et al. (1992)

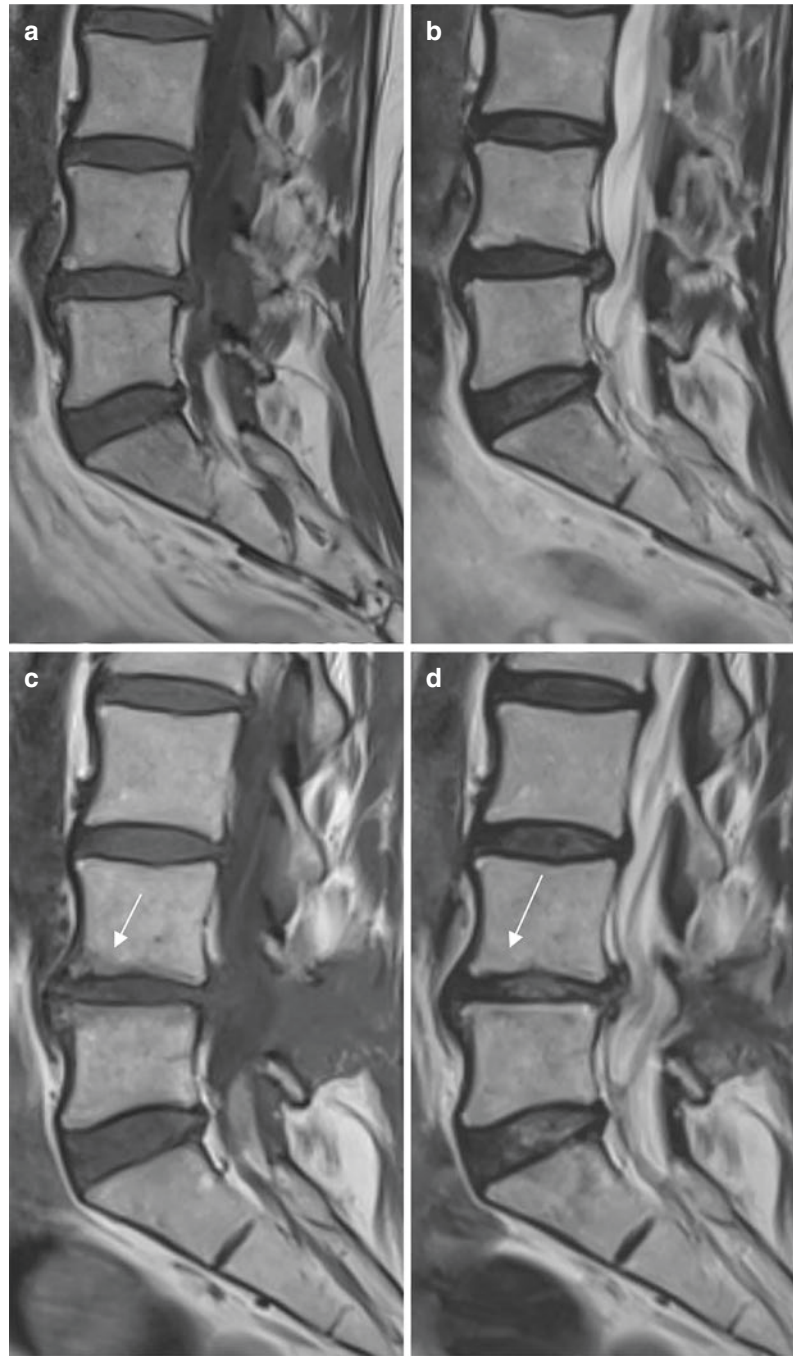

Fig. 8 MRI of normal postoperative changes in a 58-year-old woman with a history of discectomy at the L4/L5 level a few months prior. Preoperative sagittal (**a**) T1-W and (**b**) T2-W images show a disk protrusion at the L4/L5 level. Postoperative sagittal (**c**) T1-W and (**d**) T2-W images show T2-hyperintense signal in the L4/L5 intervertebral disk and Modic type I vertebral body end-plate changes (white arrows), with subtle T1-hypointense and T2-hyperintense signal

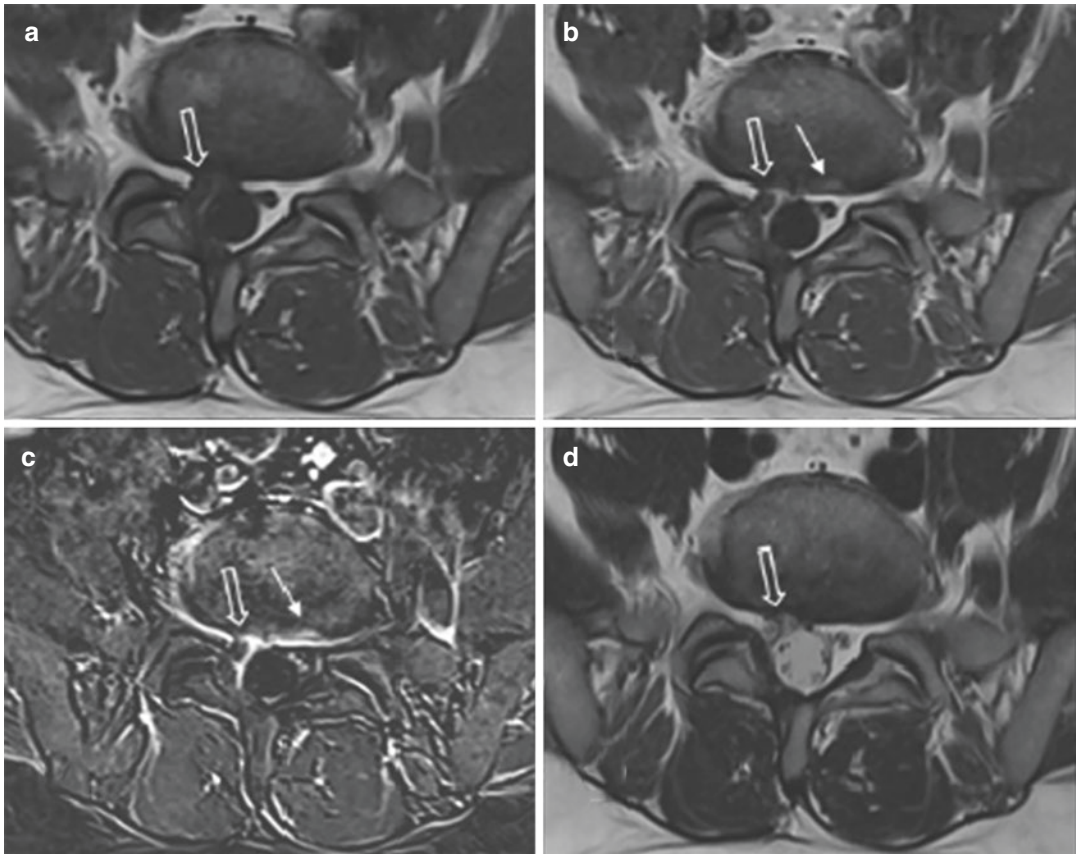

Fig. 9 MRI of normal postoperative changes in a 38-year-old man with a history of discectomy at the L5/S1 level 3 years prior. Axial (**a**) unenhanced, (**b**) contrast-enhanced, and (**c**) subtracted contrast-enhanced T1-W and (**d**) T2-W images show the right anterolateral epidural space is of hypointense signal on both T1-W and T2-W sequences and demonstrates subtle contrast enhancement (white open arrow). The posterior part of the annulus fibrosis shows contrast enhancement (white arrow)

reported another type of normal postoperative enhancement that is localized in the posterior part of the annulus fibrosus (Fig. 9).

In postoperative spondylodiscitis, vertebral bone marrow edema (BME) is a sensitive and early MRI parameter and is more frequently present than in non-iatrogenic spondylodiscitis. Vertebral BME may be either global or posteriorly located (Fig. 10). Isolated anterior spondylodiscitis rarely presents in a postoperative spine (Dufour et al. 2005; Kim et al. 2017), since direct inoculation is the main route of spread in a post-procedural setting. Vertebral BME in postoperative spondylodiscitis presents as horizontal, band-like T1-hypointense, and T2-hyperintense area, which enhances after contrast administration. This is not a specific finding, since these features can be seen in some normal postoperative cases (Ross et al. 1996; Grane et al. 1998). Compared to normal postoperative enhancement, the enhancement pattern in disk space infection is typically more pronounced and nonlinear (Ross et al. 1996).

In patients with spondylodiscitis, a T2-hyperintense disk can be expected (Grand et al. 1993), compared to a typical lower signal intensity in normal postoperative changes. However, Boden et al. (1992) showed that not all patients with spondylodiscitis have signal intensity changes or enhancement of the intervertebral

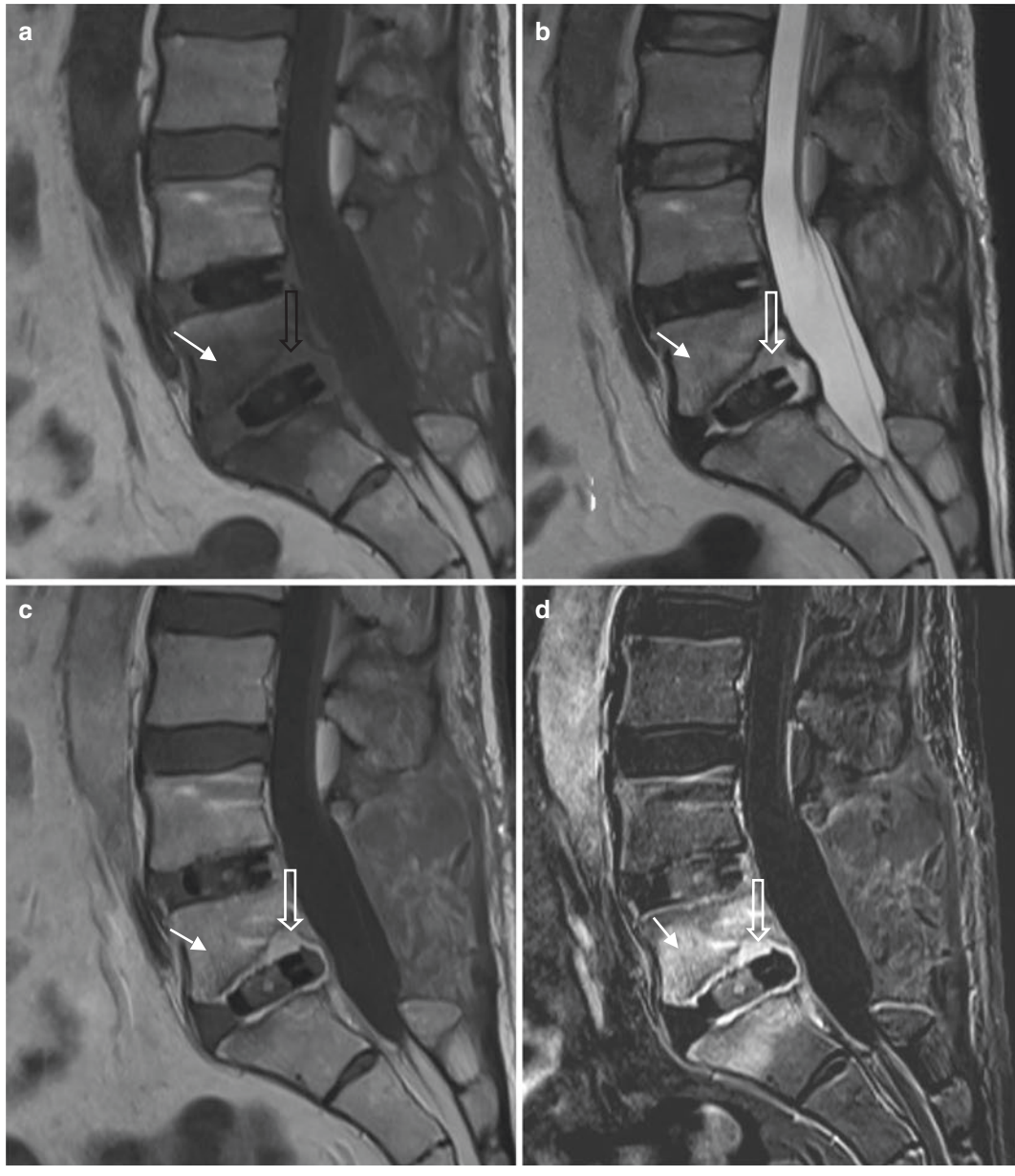

Fig. 10 MRI of a postoperative spondylodiscitis in a 47-year-old man with a history of discectomy at the L4-L5-S1 levels, with a disk prosthesis insertion. Sagittal (**a**) T1-W, (**b**) T2-W, (**c**) contrast-enhanced T1-W, and (**d**) subtracted contrast-enhanced T1-W images show vertebral body end-plate edema with contrast enhancement, anteriorly and posteriorly at the L5/S1 level (white arrow). The intervertebral disk space shows T2-hyperintense signal and peripheral contrast enhancement (white open arrow)

disk. The differentiation between normal postoperative changes and spondylodiscitis on MRI is often difficult, especially in the first weeks and months after surgery. In the presence of nonlinear disk enhancement or vertebral body end-plate edema, postoperative spondylodiscitis and normal postoperative changes often cannot reliably be differentiated in the first 6 months (Diehn

Table 5 Imaging features differentiating normal postoperative changes from postoperative spondylodiscitis

	Normal postoperative changes	Spondylodiscitis
Vertebral body end-plate edema	– No specific location	– Globally located or isolated posterior location
Vertebral body end-plate destruction	– No vertebral end-plate destruction	– Vertebral end-plate destruction and vertebral collapse in advanced cases
Contrast enhancement pattern	– Superior and inferior thin linear enhancement, paralleling the vertebral body end plates – Enhancement of the posterior part of the annulus fibrosus	– Marked, nonlinear enhancement
Soft tissue mass	– No enhancing soft tissue mass	– Paravertebral or epidural enhancing soft tissue mass
^{18}F-FDG-PET/CT features	– No ^{18}F-FDG avidity	– ^{18}F-FDG avidity

2012). A paravertebral or epidural enhancing soft tissue mass at the affected spinal level is a feature highly suggestive of spondylodiscitis (Van Goethem et al. 2000; Salgado et al. 2006). Table 5 summarizes the differential diagnosis of normal postoperative changes and postoperative spondylodiscitis.

In more advanced cases, imaging findings of spondylodiscitis include loss of disk space height, vertebral body end-plate destruction, vertebral body collapse, and displacement of any grafts or implants (Ortiz et al. 2018) (Figs. 11 and 12). In cases of healing, the bone marrow will progressively demonstrate fatty reconversion, resulting in a T1-hyperintense signal and T2-hypointense signal. Other possible sequelae of healing are vertebral fusion due to ossification of the annular ligaments or intervertebral fusion (Visuri et al. 2005) (Fig. 13). Spondylitis should also be differentiated from Modic type I changes in degenerative disk disease (Fig. 14). In patients after spinal fusion, degenerative disk disease can develop in intervertebral levels, adjacent to the postoperative level. The imaging features should be compared with features on preoperative MRI (Boden et al. 1992). Features of degenerative disk disease include vertebral osteophyte formation, vacuum phenomenon, disk space narrowing, and vertebral end-plate changes (Modic type 1, 2 and/or 3) (Miller 2004; Farshad-Amacker et al. 2015).

DWI, with a *b*-value of 1000 and ADC, is useful in the diagnosis of infectious processes. Mean ADC values in infectious bone marrow are significantly higher compared to both normal and degenerative vertebral end plates. Eguchi et al. (2011) reported mean ADC values of

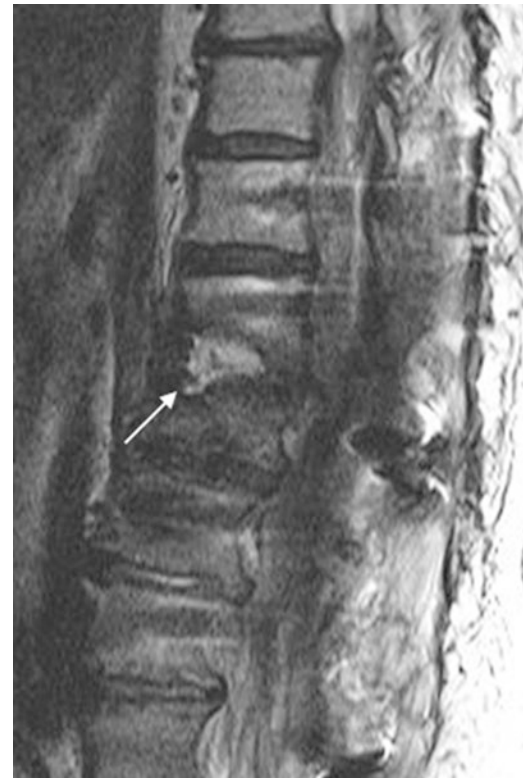

Fig. 11 MRI of advanced postoperative spondylodiscitis in a 59-year-old patient with a history of posterior lumbar fusion with transpedicular screws from T12 to S1 levels. Sagittal T2-W image shows vertebral body end-plate destruction at the L1/2 level with T2-hyperintense signal of the intervertebral disk (white arrow)

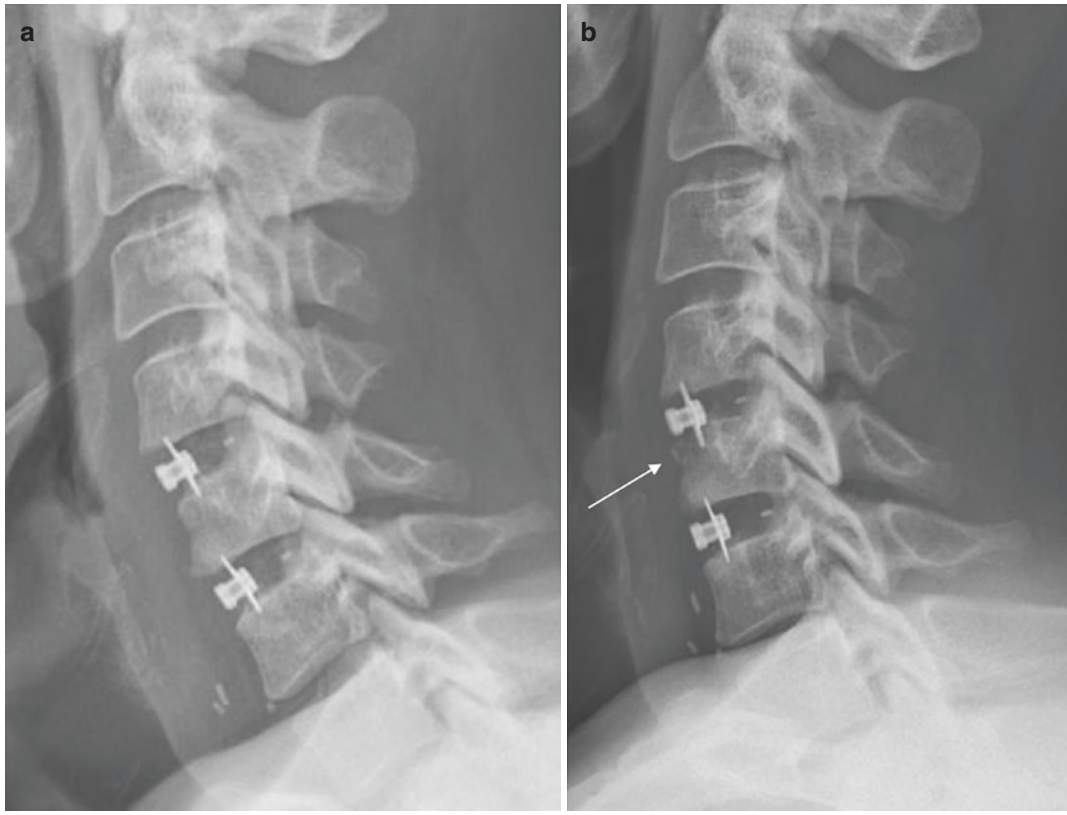

Fig. 12 Lateral radiographs of advanced postoperative spondylodiscitis in a 51-year-old patient with disk prostheses at the C4/C5 and C5/C6 levels. (**a**) Early postoperative radiograph shows no osseous lesion. (**b**) Radiograph taken 2 months later shows an osteolytic area in the anterior part of the superior C5 vertebral end plate (white arrow)

1.067×10^{-3} mm^2/s in infectious marrow and 0.624×10^{-3} mm^2/s in degenerative disk disease with Modic type changes. Other studies, however, demonstrated that DWI has limited use in evaluating infectious processes in the vertebral bone marrow and intervertebral disk (Moritani et al. 2014). Due to the prominent paramagnetic susceptibility artifacts near metallic implants on DWI-EPI sequences, this technique has little clinical use in patients with instrumented spines (Eguchi et al. 2011; Moritani et al. 2014). As mentioned previously, a recent study shows that DWI images with less paramagnetic susceptibility artifacts can be obtained through multispectral techniques, at the cost of acquisition time (Koch et al. 2018).

^{18}F-FDG-PET/CT is more reliable than MRI to differentiate between normal postoperative changes and spondylodiscitis. MRI features cannot reliably differentiate early postoperative spondylodiscitis and normal postoperative changes in the first 6 months after surgery. ^{18}F-FDG-PET/CT demonstrates a significantly higher standard uptake value (SUV) ratio for infection than for degeneration or noninfected bone marrow (Smids et al. 2017; Follenfant et al. 2019; Rutenberg et al. 2019). Another advantage of ^{18}F-FDG-PET/CT is the capability to identify multifocal infectious foci (Smids et al. 2017; Rutenberg et al. 2019). In addition to its use in the initial diagnosis, ^{18}F-FDG-PET/CT is also more reliable in the follow-up of infection, com-

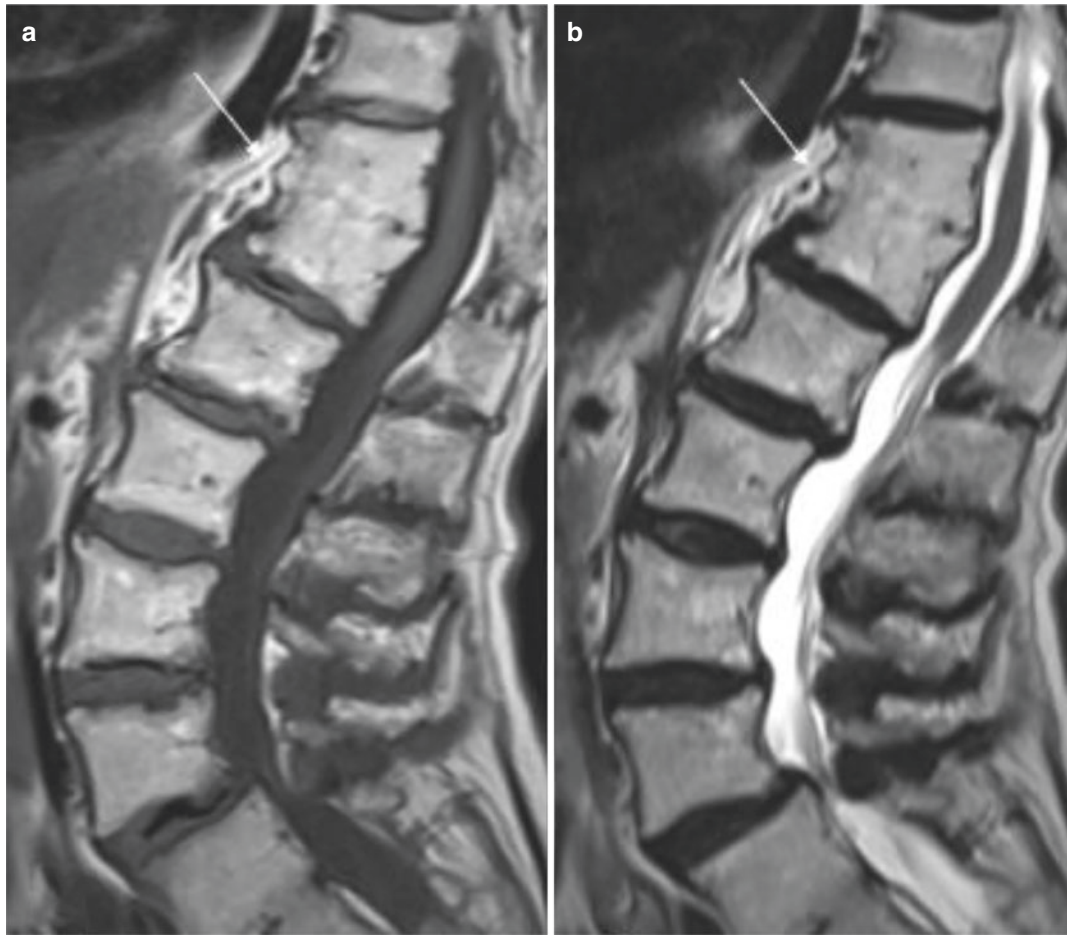

Fig. 13 MRI of healed spondylodiscitis in an 81-year-old woman with a history of spondylodiscitis at the T11/T12 level 18 years ago. Sagittal (**a**) T1-W and (**b**) T2-W images show a fusion of the T11 and T12 vertebral bodies (white arrows). The bone marrow of the fused vertebral bodies has the typical signal of normal fatty marrow on both T1- and T2-W sequences

pared to MRI (Russo et al. 2019) (Fig. 15). Follow-up MRI is not useful to monitor treatment response (Fig. 16), as there is no correlation between clinical features and follow-up MRI (Kowalski et al. 2007).

6.2.1.2 Non-Post-Procedural Spondylodiscitis

In a non-post-procedural setting, iatrogenic spondylodiscitis should be differentiated from degenerative disk disease, more specifically Modic type 1 changes. This corresponds to vertebral body end-plate edema that is T1-hypointense and T2-hyperintense. After gadolinium contrast administration, these areas may enhance (Diehn 2012). Several features may be assessed to distinguish infection from degeneration. In degenerative disk disease, the intervertebral disk often shows T2-hypointense signal, while in spondylodiscitis the disk is often T2-hyperintense (Diehn 2012). The lack of paraspinal or epidural abscesses and the lack of disk or vertebral body end-plate enhancement suggest degeneration. On CT, vacuum phenomenon, vertebral osteophytes,

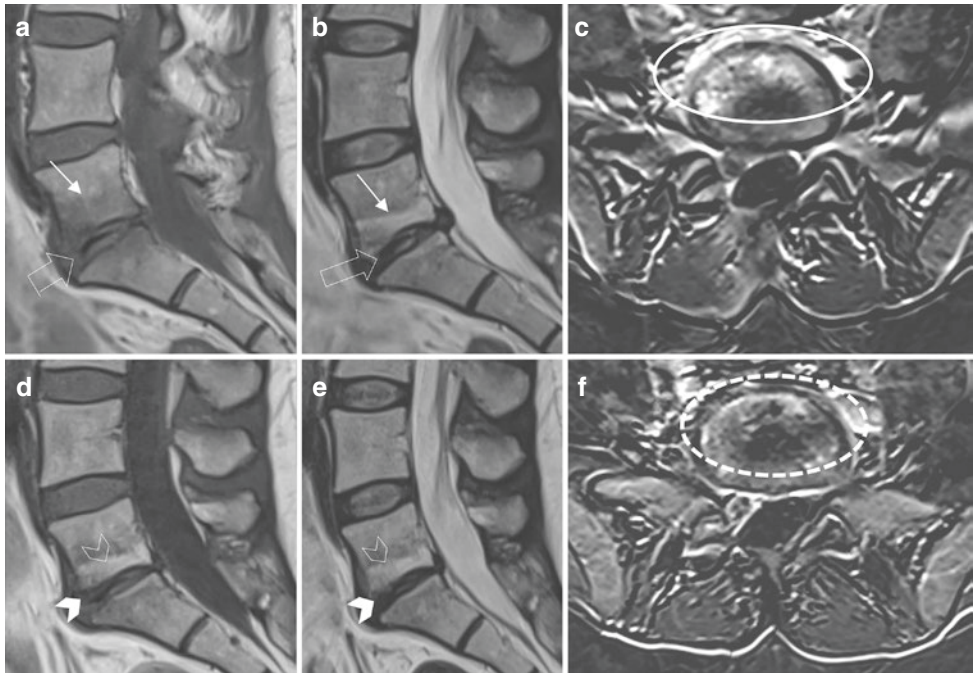

Fig. 14 MRI of degenerative disk disease in a 34-year-old woman presenting with lower back pain 2 years after discectomy. Sagittal (**a**) T1- and (**b**) T2-W and (**c**) axial subtracted contrast-enhanced T1-W images taken at the L5/S1 level show Modic type I changes, with areas of T1-hypointense and T2-hyperintense signal (white arrows) and contrast enhancement in the vertebral end plates (white circle). Vacuum phenomenon (open white arrows) is visible in the intervertebral disk. Repeat sagittal (**d**) T1- and (**e**) T2-W and (**f**) axial subtracted contrast-enhanced T1-W images taken of the same patient 3 years later show vertebral end-plate Modic type 2 changes (open white arrowheads), with less pronounced contrast enhancement (dashed white circle). The vacuum phenomenon is still visible in the intervertebral disk (white arrowheads)

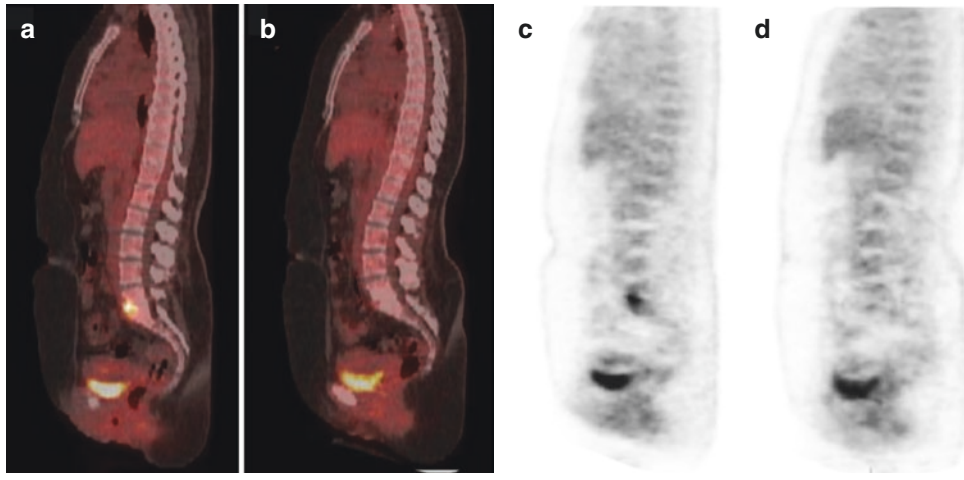

Fig. 15 ^{18}F-FDG-PET/CT of L5/S1 spondylodiscitis in a 35-year-old patient with spondylodiscitis, obtained before and after 5 months of antibiotic therapy. (**a**, **c**) Initial PET/CT images show increased ^{18}F-FDG avidity at the L5-S1 level. (**b**, **d**) Repeat images taken 5 months later show only minimal ^{18}F-FDG uptake. [Figure provided is licensed under CC BY 4.0: Smids C, Kouijzer IJE, Vos FJ, Sprong T, Hosman AJF, de Rooy JWJ, Aarntzen EHJG, de Geus-Oei L, Oyen WJG, Bleeker-Rovers CP. A comparison of the diagnostic value of MRI and ^{18}F-FDG-PET/CT in suspected spondylodiscitis]

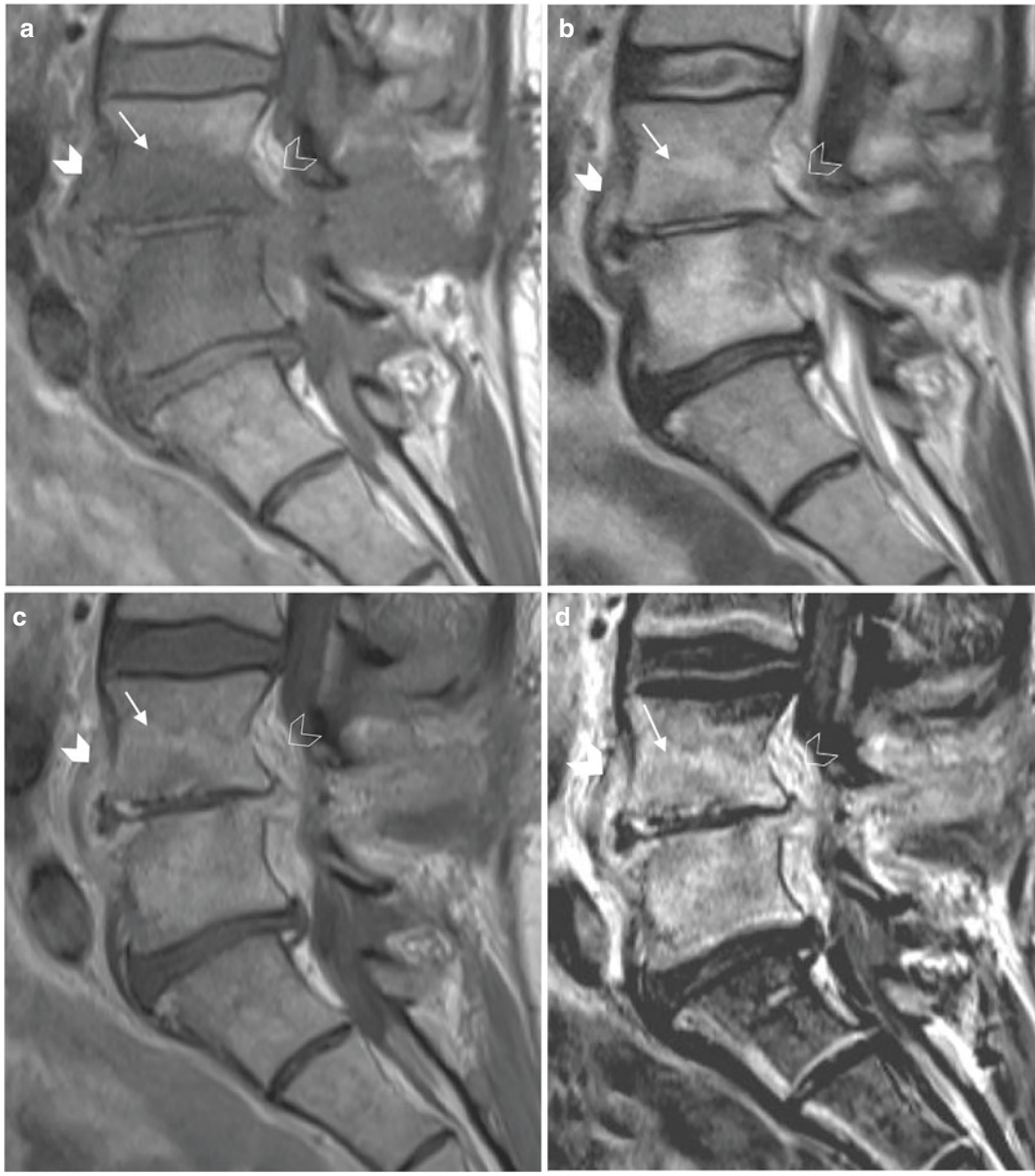

Fig. 16 MRI of postoperative spondylodiscitis, with paravertebral and anterior epidural phlegmon, in a 41-year-old patient with a history of discectomy. Sagittal (**a**) T1- and (**b**) T2-W images show L4/L5 intervertebral disk narrowing with vertebral body end-plate edema (white arrows). The vertebral body end plates and a fluid collection in the anterior epidural space (open white arrowheads) and the anterior paravertebral space (white arrowheads) demonstrate enhancement on sagittal (**c**) contrast-enhanced and (**d**) subtracted contrast-enhanced T1-W images. Bone erosion can be seen in the anterior corner of the superior L5 vertebral body end plate. Follow-up MRI was done 10 months after the initial diagnosis of postoperative spondylodiscitis. Sagittal (**e**) T1-W, (**f**) T2-W, (**g**) contrast-enhanced T1-W, and (**h**) subtracted contrast-enhanced T1-W images show persisting vertebral body end-plate edema with contrast enhancement (white arrows). There are increased signs of vertebral sclerosis, seen as hypointense areas on T1- and T2-W images. The paravertebral (white arrowhead) and anterior epidural (open white arrowhead) phlegmon persists, although the patient had clinical improvement

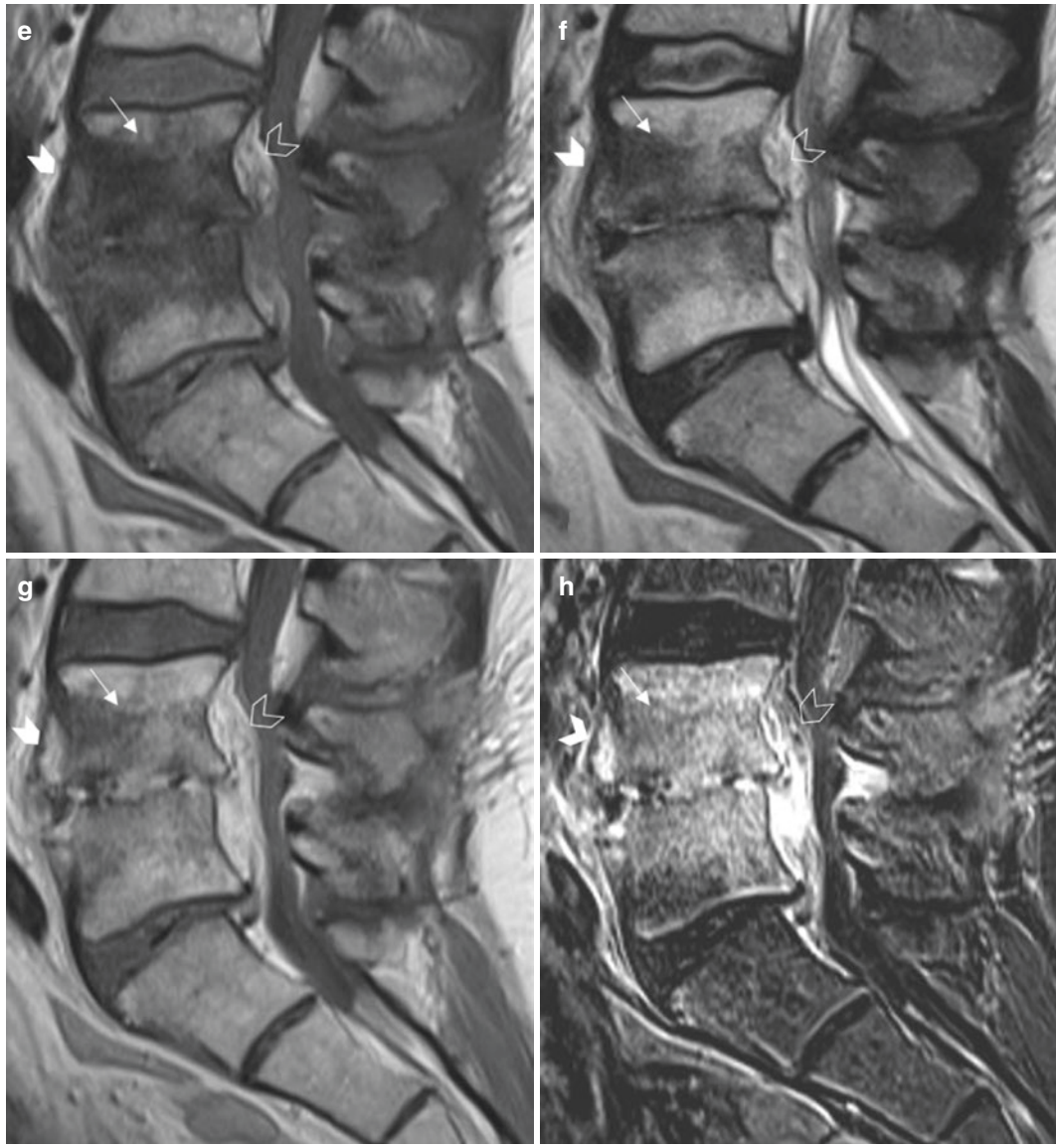

Fig. 16 (continued)

and the lack of vertebral body end-plate destruction indicate degenerative disk disease (Miller 2004; Diehn 2012). Unlike post-procedural spondylodiscitis, non-post-procedural spondylodiscitis tends to start in the anterior part of the vertebral body end plate due to its hematogeneous spread (Dufour et al. 2005). However, other early and advanced MRI features of non-post-procedural spondylodiscitis are similar to those of post-procedural cases. Complete fusion of two adjacent vertebrae may occur as late sequelae (Fig. 17).

DWI, with a *b*-value of 1000 and ADC maps, has a controversial role in the evaluation of spondylodiscitis. Eguchi et al. (2011) concluded that DWI can be used to differentiate between infected vertebral end plate and normal or degenerative end plate. However, other studies found that DWI has limited use in the evaluation of spondylodiscitis (Moritani et al. 2014). Since metallic

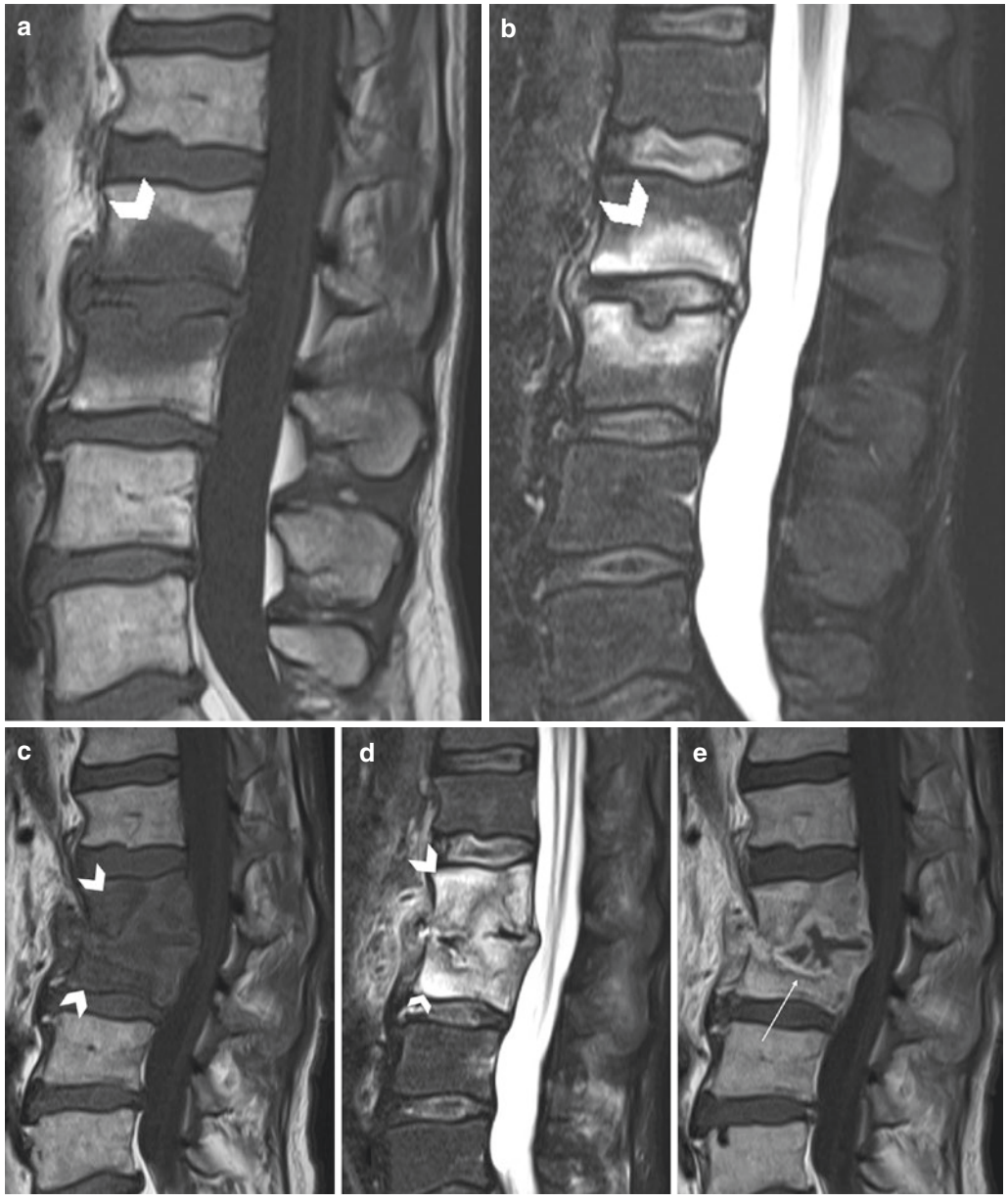

Fig. 17 Iatrogenic spondylodiscitis in a 62-year-old patient treated with immunosuppressants. Sagittal (**a**) T1-W and (**b**) fat-suppressed T2-W MR images show horizontal bands of marked T1-hypointense signal and marked T2-hyperintense signal at the L2/L3 vertebral body end plates, corresponding to vertebral end-plate edema (white arrowheads). A small erosion is visible in the center of the superior L3 vertebral body end plate (white arrows). These changes are consistent with early iatrogenic spondylodiscitis. This patient subsequently developed advanced changes of iatrogenic spondylodiscitis, seen on sagittal (**c**) T1-W, (**d**) fat-suppressed T2-W and (**e**) contrast-enhanced T1-W MR images, (**f**) CT and (**g**) ^{18}F-FDG-PET images, and (**h**) lateral radiograph. Extensive bone marrow edema at the L2/L3 level (white arrowheads) are seen on the (**c**) T1-W and (**d**) T2-W MR images. There are extensive erosions in the central and posterior part of the L2 and L3 vertebral body end plates, resulting in early signs of vertebral body collapse. Marked contrast enhancement and increased ^{18}F-FDG uptake of the L2/3 intervertebral disk space (white arrows) are present. Follow-up sagittal (**i**) T1-W and (**j**) T2-W MR images taken 7 years later show a complete fusion of the collapsed L2 and L3 vertebral bodies (white arrows), indicative of healing

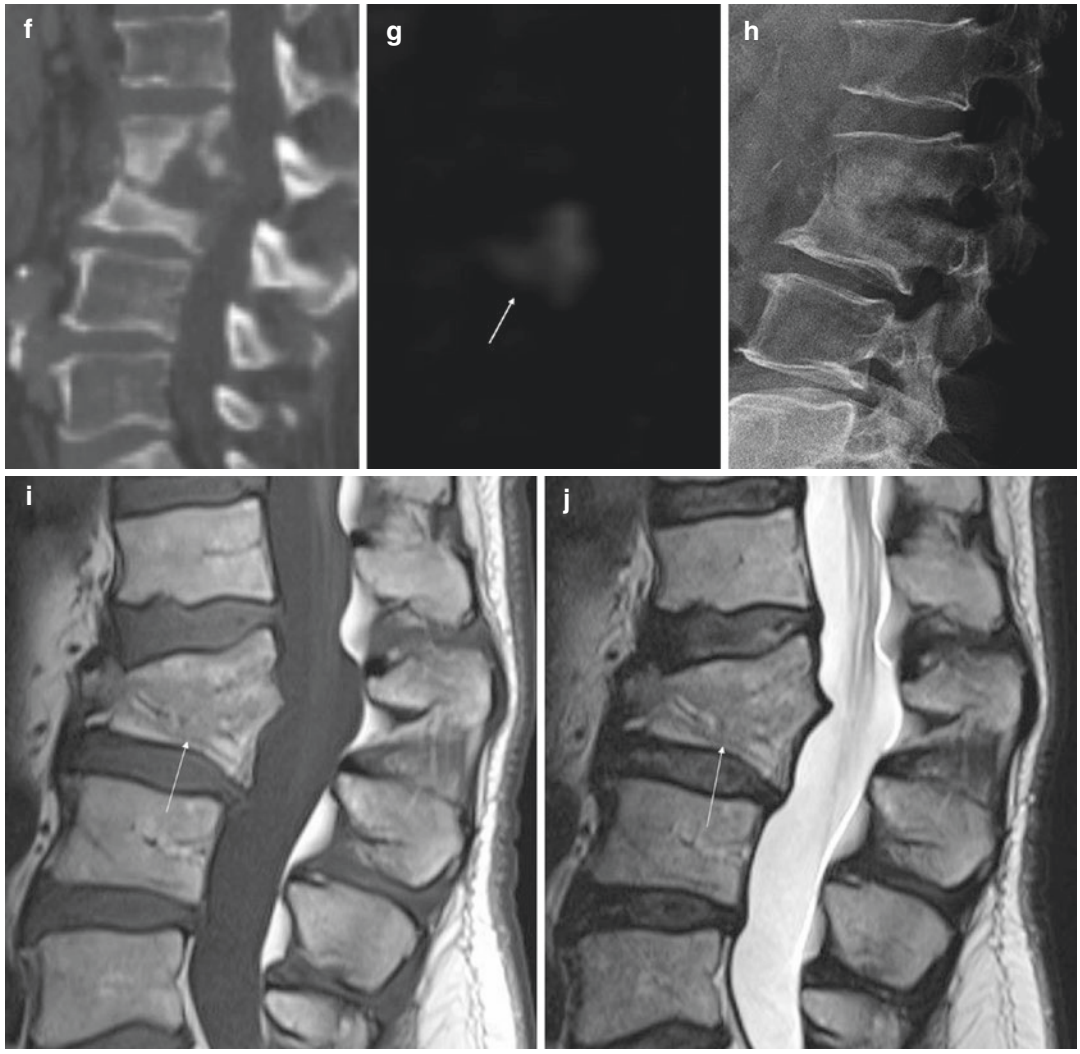

Fig. 17 (continued)

implants are absent in a non-postoperative spine, SS-EPI DWI sequences can potentially be used in the MRI protocol. Similar to the post-procedural spine, ^{18}F-FDG-PET/CT has diagnostic value in non-post-procedural spondylodiscitis, especially for early detection (Smids et al. 2017). High sensitivity and specificity have been reported for differentiating spondylodiscitis and degeneration. However, specificity is controversial when distinguishing between infection and malignancy (Smids et al. 2017).

6.2.2 Epidural and Paravertebral Abscess

Similar to non-iatrogenic cases, an abscess can either occur secondarily to facet joint infection or spondylodiscitis or as an isolated lesion. In facet joint infection, abscesses tend to spread to the posterior part of the epidural space or the paraspinal musculature (Moritani et al. 2014). In spondylodiscitis, abscesses either spread to the anterior epidural space or the anterior paravertebral space (Fig. 18). At the cervical and thoracic

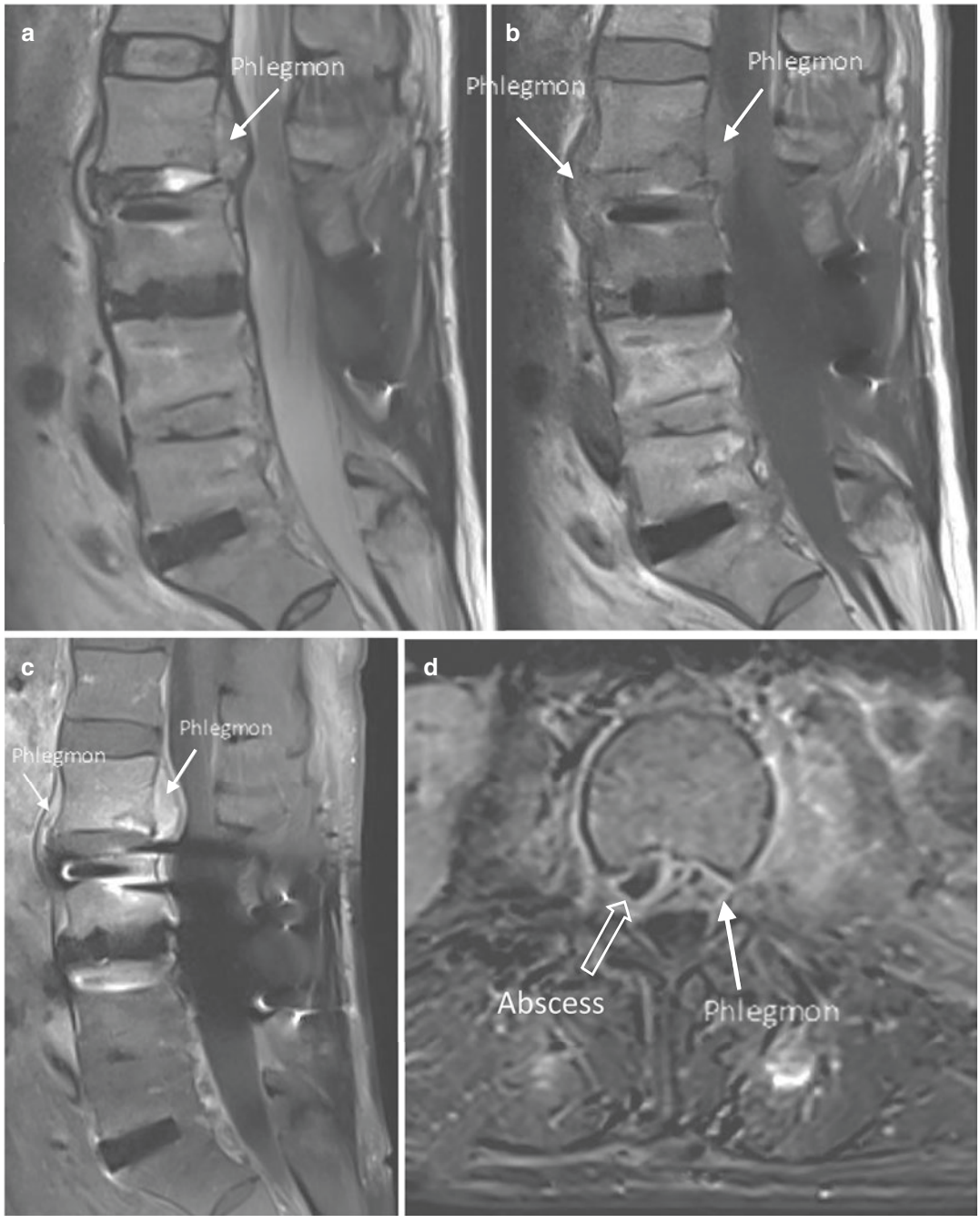

Fig. 18 MRI of epidural abscess and paravertebral and epidural phlegmon in a 60-year-old woman with a history of posterior lumbar fusion. Sagittal (**a**) T2-W, (**b**) T1-W, and (**c**) contrast-enhanced T1-W images show a T2-hyperintense intervertebral disk with contrast enhancement of the vertebral body end plates. Note the paravertebral and epidural phlegmon with contrast enhancement on (**c**) sagittal T1-W image and (**d**) axial subtracted contrast-enhanced T1-W images obtained at the L3 level (white arrow). A peripheral contrast-enhancing collection at the right side of the epidural space (open white arrow) represents the epidural abscess

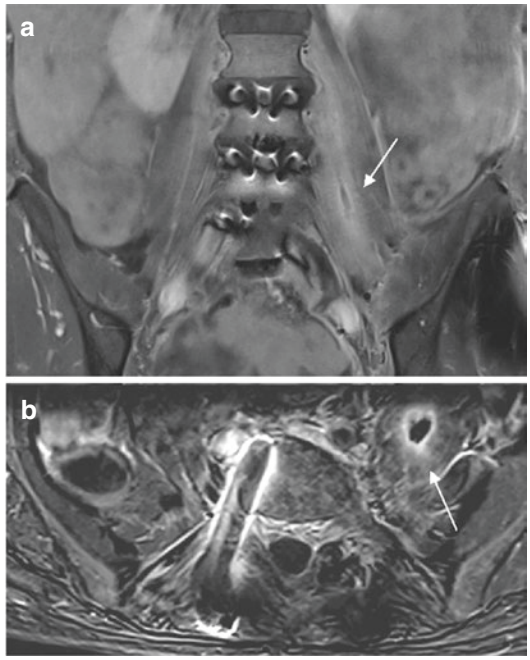

Fig. 19 MRI of a patient with post-operative psoas muscle abscess. (**a**) Coronal fat-suppressed contrast-enhanced T1-W and (**b**) axial subtracted contrast-enhanced T1-W images show a peripheral contrast-enhancing collection in the left psoas muscle (white arrows)

spine, abscesses can cause mediastinitis, empyema, and pericarditis, while at the lumbar spine, psoas abscesses and peritoneal and pelvic infection can occur (Moritani et al. 2014) (Fig. 19). An anterior epidural abscess tends to extend anteriorly and laterally to the dural sac, causing compression on the dural sac and congestion of the epidural venous plexus, eventually leading to ischemia of the spinal cord (Go et al. 2012). In anterior paravertebral abscesses, the involvement of the vessels can lead to vasculitis or mycotic aneurysms, frequently affecting the aorta (Go et al. 2012). An anterior epidural abscess should be differentiated from subligamentous spondylodiscitis displacing the posterior longitudinal ligament (PLL) posteriorly. In contrast to epidural abscesses, subligamentous spondylodiscitis does not spread to the lateral side of the dural sac or the paravertebral tissues and is posteriorly delineated by the posterior longitudinal ligament.

Imaging features of iatrogenic abscesses are similar to those of non-iatrogenic cases. An abscess appears as a hypodense to isodense fluid collection on CT. Unlike other postoperative fluid collections, gas may be present in some abscesses (Torres and Zakhari 2017). On MRI, most abscesses are T1-hypointense and T2-hyperintense (Jain et al. 2014). A phlegmon, an early stage lesion, enhances homogeneously or heterogeneously, while an abscess demonstrates peripheral enhancement with central pus formation (Diehn 2012; Yeom et al. 2016). In patients without metallic implants, DWI is very useful in both the early detection and follow-up of small abscesses, evaluating its location, size, and the grade of dural sac compression (Numaguchi et al. 1993; Diehn 2012; Moritani et al. 2014; Yeom et al. 2016). It is helpful in differentiating abscesses and other postoperative fluid collections (Moritani et al. 2014; Torres and Zakhari 2017). Abscesses typically display diffusion restriction on DWI sequences (Moritani et al. 2014). Smids et al. (2017) showed that MRI is superior to ^{18}F-FDG-PET/CT in the detection of epidural abscesses, while the sensitivity of paravertebral and psoas abscesses is higher in ^{18}F-FDG-PET/CT than MRI. However, since very few studies are available in the current literature on the value of MRI and ^{18}F-FDG-PET/CT in the diagnosis of postoperative abscesses, these conclusions should be confirmed by future studies. Abscesses should be differentiated from other postoperative fluid collections (see Sect. 6.2.5).

6.2.3 Facet Joint Infection

Imaging features of iatrogenic facet joint infection are similar to non-iatrogenic cases. Findings of infection on conventional radiography have a delay of several weeks, demonstrating erosions of the articular surface and widened joint space. On CT, these features are visible in an earlier stage than on radiographs, and CT allows evaluation of soft tissue, epidural, and paraspinal extension (Babic and Simpfendorfer 2017). However, MRI is the most sensitive modality and

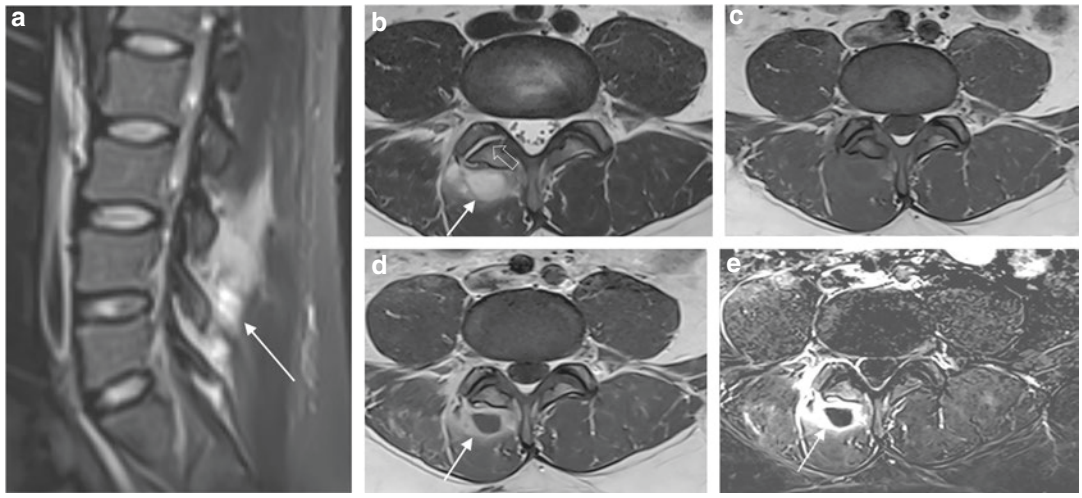

Fig. 20 MRI of facet joint infection with extensive paravertebral abscesses in a 33-year-old man on methylprednisolone treatment. (**a**) Sagittal STIR image and (**b**) axial T2-W image at the L4/L5 level show joint space widening of the right facet joint (open white arrow), with extensive edema and abscesses in the paravertebral musculature extending from the L3 to S1 levels (white arrows). Axial (**c**, **d**) T1-W and (**e**) subtracted contrast-enhanced T1-W images show enhancement of the joint capsule and adjacent abscess

shows early signs of facet joint infection. Bone marrow edema and enhancement can be seen, along with joint capsule enhancement and a fluid-filled widened joint space (Fig. 20). Articular and subchondral erosions, surrounding soft tissue edema and enhancement, appear at a later stage (Torres and Zakhari 2017; Talbott et al. 2018). Similar to non-iatrogenic facet joint infection, these findings are usually unilateral (Babic and Simpfendorfer 2017). Abscess formation may occur in the posterior epidural space or paraspinal musculature (Moritani et al. 2014; Yeom et al. 2016). DWI is useful to detect secondary paraspinal or epidural abscesses (Moritani et al. 2014). ^{18}F-FDG-PET/CT has a high sensitivity and negative predictive value (NPV) for facet joint infection (Gemmel et al. 2010). In an early post-procedural setting, it has a higher value than MRI to differentiate normal postoperative changes and infection. Due to its high NPV, a negative ^{18}F-FDG-PET/CT scan excludes facet joint infection (Follenfant et al. 2019; Rutenberg et al. 2019).

MRI features of spinal infection should be differentiated from normal postoperative changes. Van De Kelft et al. (1996) demonstrated that facet joint enhancement is a normal postoperative finding in 53% of patients 6 months after lumbar discectomy. However, facet joint erosions and paravertebral and epidural abscesses are absent in a normal postoperative spine (Van Goethem et al. 2000; Ortiz et al. 2018). MRI can differentiate facet joint degeneration from infection. In mild cases, patients with facet joint degeneration present with joint space narrowing and/or osteophytes, while moderate to severe cases also demonstrate erosion (Berg et al. 2019). Joint space narrowing and osteophytes are typically not seen in facet joint infection.

6.2.4 Myelomeningitis

The imaging features of iatrogenic myelitis and meningitis are comparable to non-iatrogenic cases. In an early acute stage, linear, focal-nodular, or patchy contrast enhancement of the meninges can be seen, without any features on unenhanced sequences (Tali et al. 2015). In advanced cases, meningeal thickening, thickening of neural roots, and cerebrospinal fluid (CSF) space obliteration can be seen, with possible spread to the spinal cord (Tali et al. 2015).

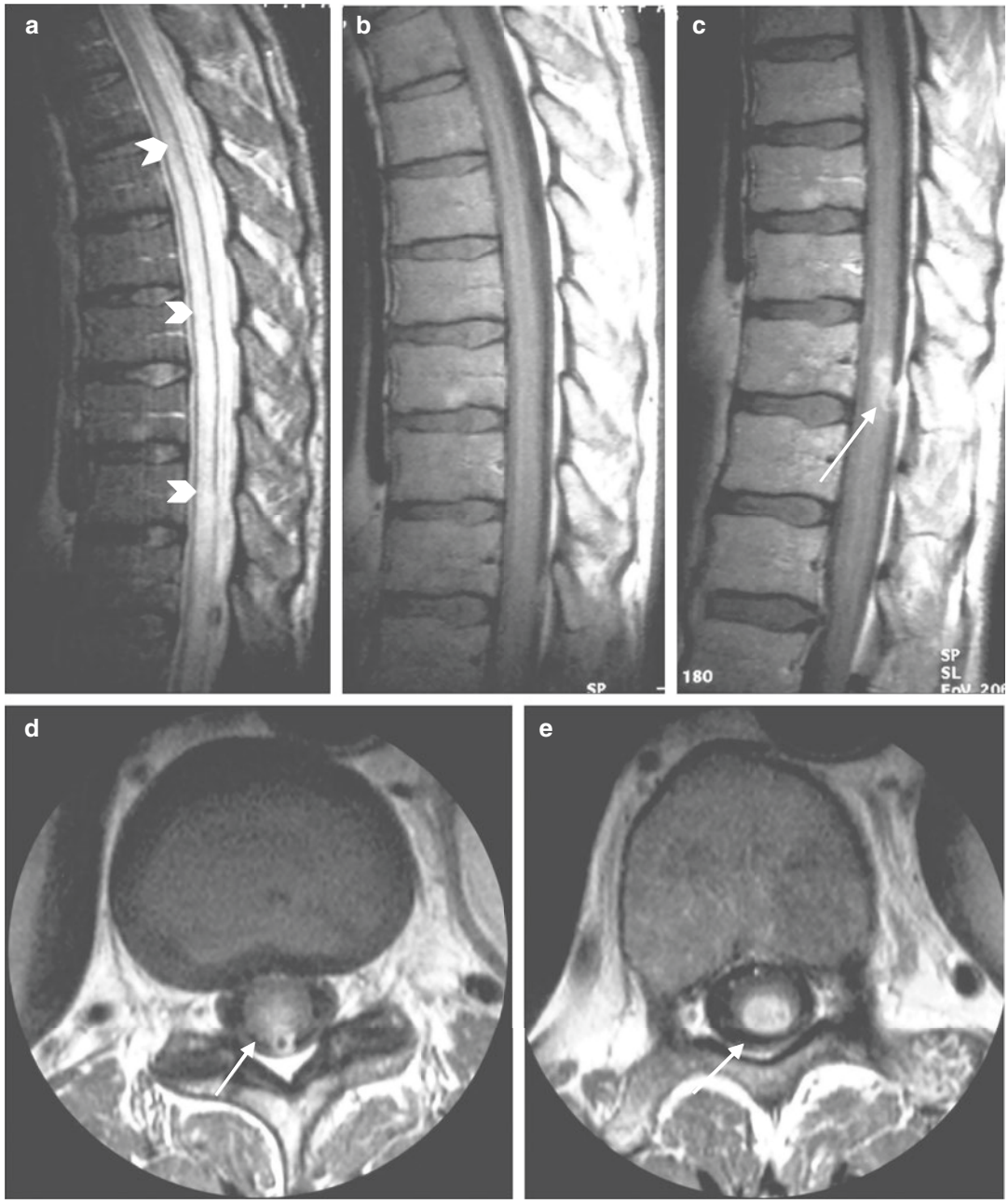

Fig. 21 MRI of myelomeningitis in a patient with a morphine catheter. (**a**) Sagittal T2-W image shows extensive multilevel hyperintense signal in the spinal cord, compatible with edema (white arrowheads). Sagittal (**b**) T1-W and (**c**) contrast-enhanced T1-W and (**d**, **e**) axial contrast-enhanced T1-W images show focal meningeal enhancement spreading to the spinal cord at one vertebral level (white arrow)

Myelitis manifests as T1-hypointense and T2-hyperintense signal, with diffuse enlargement of the spinal cord, signs compatible with an area of edema (Fig. 21). A central area of slightly less hyperintense signal on T2-weighted images may correspond to the infected area. The lesion may show either homogeneous or heterogeneous contrast enhancement (Tali et al. 2015).

6.2.5 Differential Diagnosis

6.2.5.1 Hematoma

A variety of postoperative paraspinal fluid collections may mimic abscesses (Table 6). In typical cases, postoperative hematomas present several hours to days after the surgical intervention (Salgado et al. 2006). Its imaging features are dependent on the age of the blood collection (Table 7). An acute hematoma is hyperdense to isodense to muscle on CT and has heterogeneous signal intensities on T1- and T2-weighted MR images, with foci of hypointense signal on GRE sequences (Jain et al. 2014). In the subacute phase, the collection has T1- and T2-hyperintense signal (Fig. 22). In the chronic phase, the hematoma progressively demonstrates fluid signal intensity, being T1-hypointense and T2-hyperintense, and has a hypodense appearance on CT (Hancock and Quencer 2008; Moritani et al. 2014). The hematoma collection may show mild peripheral enhancement (Jain et al. 2014). A hematoma may show diffusion restriction on DWI in the chronic phase, hindering the differentiation from abscesses (Moritani et al. 2014).

6.2.5.2 Seroma

A seroma contains lymphatic fluid and may be encapsulated by fibrous tissue. It appears as a fluid collection on all imaging modalities, being anechoic or hypoechoic on ultrasonography and hypodense on CT. On MRI, a seroma is T1-hypointense and T2-hyperintense, without diffusion restriction on DWI (Hancock and Quencer 2008; Jain et al. 2014) (Figs. 23 and 24). Small foci of hemorrhage may be present, with increased echogenicity on ultrasonography, hyperdensity on CT, and a small fluid-fluid level on axial T2-weighted MR images (Jain et al. 2014).

6.2.5.3 Pseudomeningocele

A pseudomeningocele represents a CSF collection, extending from the dural sac to the paraspinal soft tissue, and is delineated by reactive fibrous tissue. It develops after meningeal laceration during surgery (Salgado et al. 2006). It typically appears as an irregular or lobulated collection with fluid imaging characteristics, adjacent to the dural sac and surgical bone defect (Jain et al. 2014). Mild peripheral enhancement may be visible, in contrast to a thick rim of contrast enhancement in abscesses (Hancock and Quencer 2008; Jain et al. 2014). The dural leak is sometimes visible on MRI as an area of T2-hypointense signal, indicating CSF flow (Hancock and Quencer 2008). In other cases, immediate and delayed post-myelogram CT images may show the dural leakage (Jain et al. 2014).

Table 6 Imaging features differentiating abscesses from other postoperative fluid collections

	Abscess	Hematoma	Seroma	Pseudomeningocele
Diffusion restriction	Yes	May be present in chronic phase	No	No
Contrast enhancement	Thick peripheral enhancement	Mild peripheral enhancement	Mild peripheral enhancement	Mild peripheral enhancement
T1-WI features	Hypointense	Depending on the age of the hematoma	Hypointense	Hypointense
T2-WI features	Hyperintense	Depending on the age of the hematoma	Hyperintense	Hyperintense

Table 7 Imaging features differentiating the age of the hematoma

	Acute	Subacute	Chronic
T1-WI	Heterogeneous	Hyperintense	Hypointense
T2-WI	Heterogeneous	Hyperintense	Hyperintense
Diffusion restriction	No	No	Possible
CT	Hyper- to isodense	Iso- to hypodense	Hypodense

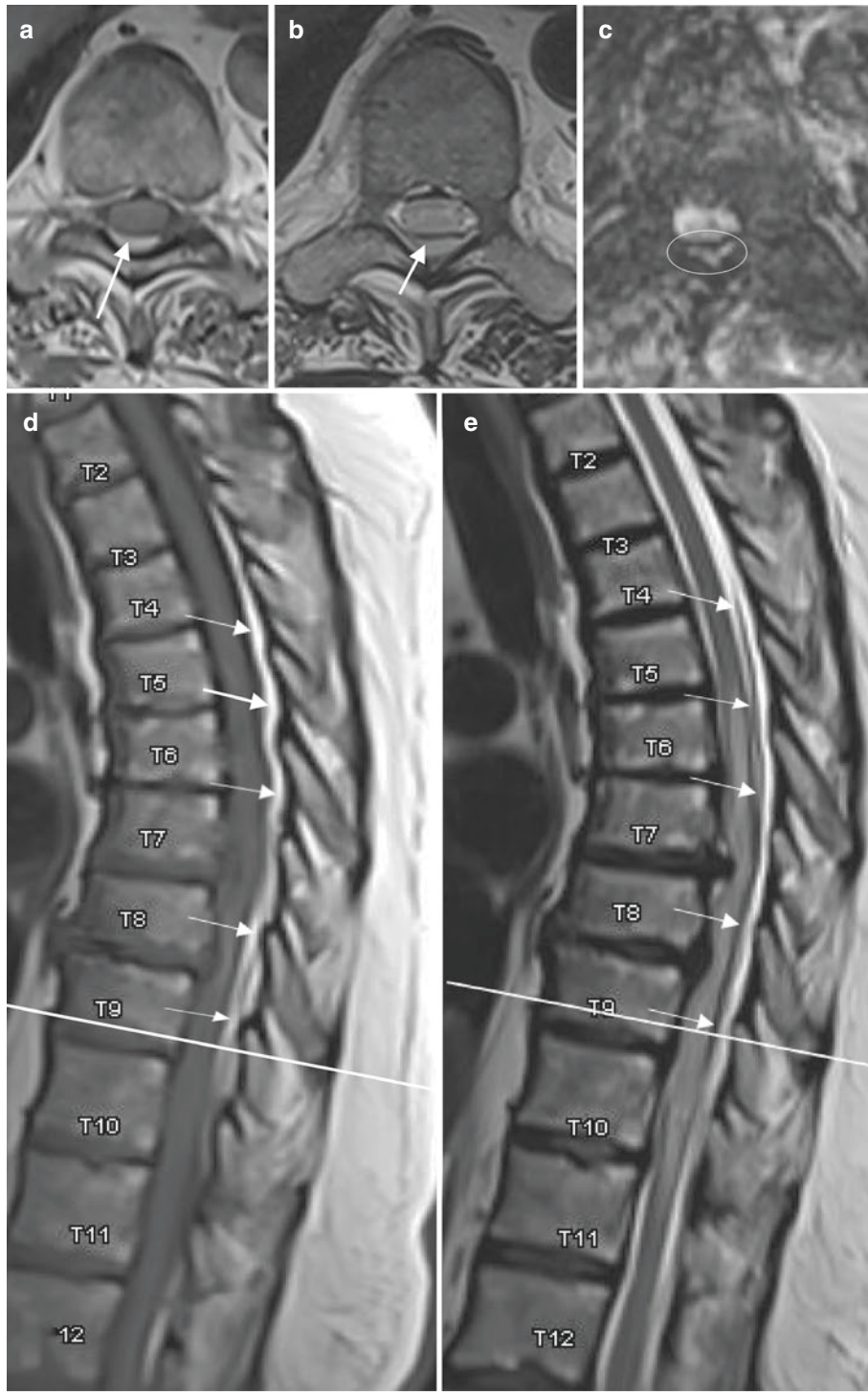

Fig. 22 MRI of subacute hematoma and disk herniation with signs of myelomalacia in a 69-year-old woman presenting with paraplegia in the lower limbs. Axial (**a**) T1-W, (**b**) T2-W and (**c**) SWI at the T9 level (white line on sagittal images), and sagittal (**d**) T1-W and (**e**) T2-W images show a T1- and T2-hyperintense posterior epidural collection extending from T3 to T9 levels (white arrows), with peripheral hypointense signal on axial SWI (white circle). The spinal cord is T2-hyperintense, compatible with medullary edema. Disk herniations are visible at the T7/T8 and T8/T9 levels, compressing the spinal cord

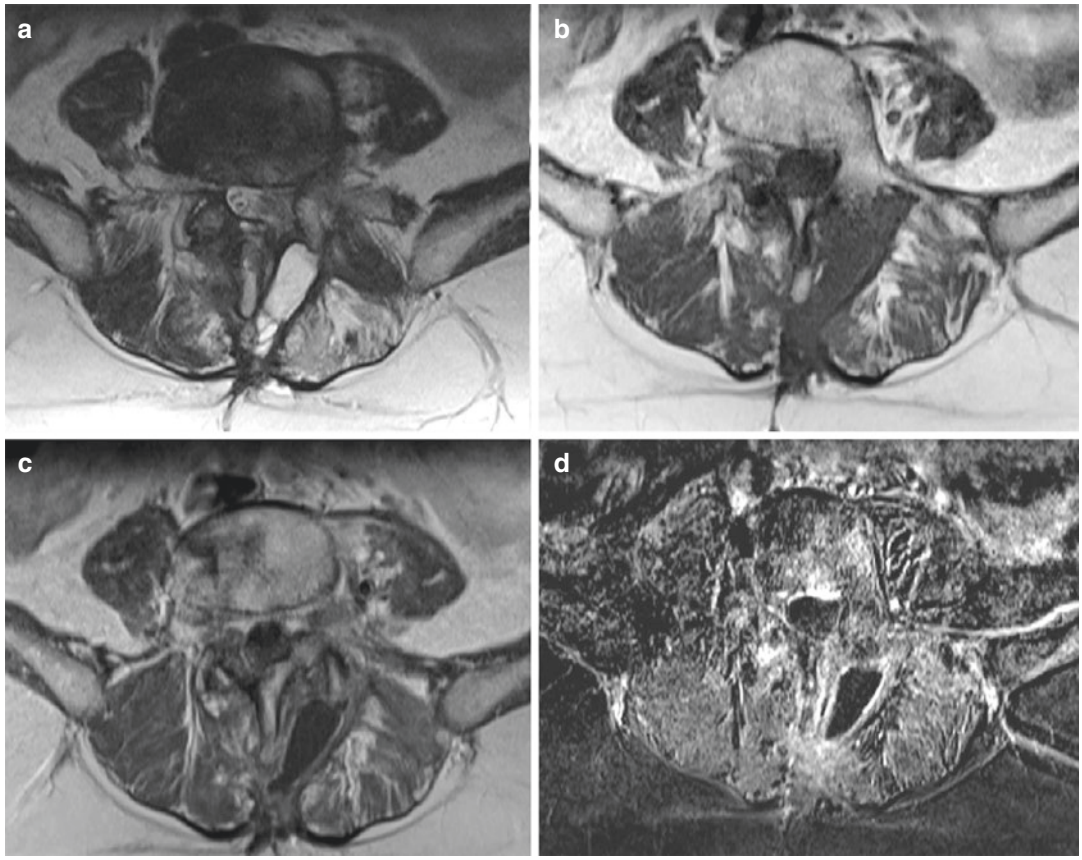

Fig. 23 MRI of seroma in a 65-year-old patient with a history of microlaminectomy at L4/L5 level. Axial (**a**) T2-W, (**b**) T1-W, (**c**) contrast-enhanced T1-W, and (**d**) subtracted contrast-enhanced T1-W images show a lobulated collection near the dural sac at the microlaminectomy site, extending to the paraspinal soft tissue. The collection is T2-hyperintense and T1-hypointense, comparable to CSF. The fluid collection has a mild peripheral contrast enhancement

7 Management

CT-guided spine biopsy is mandatory in both spondylodiscitis and facet joint infection, in order to isolate the pathogen and administer appropriate antibiotic treatment. Specimens for microbiological analysis, culture, and histopathological examination should be acquired. In addition, multiple biopsy specimens of the paraspinal soft tissue, intervertebral disk, and subchondral bone are necessary to optimize diagnostic yield. However, spine biopsy has a rather low diagnostic yield of about 48% (Mazzie et al. 2014; Talbott et al. 2018). Biopsy should preferably be done before starting antibiotic treatment.

Initially, spinal infection requires conservative management with antibiotics and immobilization (Babic and Simpfendorfer 2017; Di Martino et al. 2019). Antibiotic treatment should be adapted to the results of the culture, if available. Alternatively, empiric treatment could be started. A surgical approach through debridement of necrotic tissue, decompression, and abscess drainage is indicated in case of failure of conservative treatment, in the case of vertebral deformity and in patients with neurological symptoms caused by epidural abscesses (Mazzie et al. 2014). In patients with spinal fusion, treatment differs between early- and late-onset infection. In early infection, spinal implants should not be removed, whenever possible, in which spinal

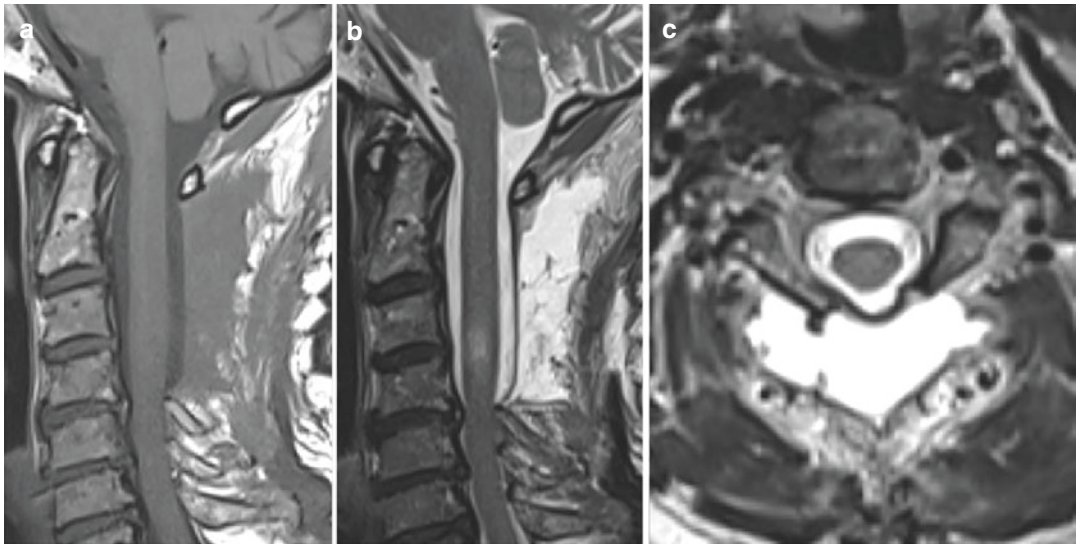

Fig. 24 MRI of seroma in a 70-year-old woman with a history of laminectomy at the C2-C4 levels. Sagittal (**a**) T1-W and (**b**) T2-W images and (**c**) axial T2-W image taken at the C2/C3 level show a collection in the posterior epidural space, with T2-hyperintense and T1-hypointense signal, comparable to CSF. The fluid collection demonstrates no connection with the dural sac. The spinal cord has an area of T2-hyperintense signal at C3/C4 level, compatible with myelomalacia. Disk protrusions at the C4/C5 and C5/C6 levels are present

fusion is not yet completed. In late infection, spinal fusion is established, and instrumentation should be removed (Di Martino et al. 2019). The treatment of epidural abscesses differs from psoas muscle abscesses. While emergent surgical decompression is indicated in epidural abscesses due to dural compression, psoas muscle abscesses are often treated conservatively with antibiotics (Babic and Simpfendorfer 2017). However, larger psoas muscle abscesses usually require percutaneous drainage (Mazzie et al. 2014).

Several preventive measures can be taken to avoid iatrogenic spinal infection. Prophylactic administration of antibiotics is an important measure in spinal procedures and should be given preoperatively until 24–48 h postoperatively (Che et al. 2011). Irrigation of the spinal wound with detergent solution or with diluted povidone-iodine solution has been described as useful preventive methods (Gerometta et al. 2012a, b). In catheter-related spinal infection, such as in patients on hemodialysis, minimizing the use of chronic catheters and treating other catheter-related infections are mandatory in the prevention (García-García et al. 2010). In immunocompromised patients, preventive measures, such as prophylactic administration of antibiotics, can be taken. Following bone marrow transplantation, antifungal prophylaxis significantly reduces fungal infection (Morrison et al. 1993).

8 Conclusion

In patients with a clinical suspicion of iatrogenic spinal infection, MRI is indicated as the initial imaging modality. The imaging protocol should be adjusted if metallic spinal implants are present. Conventional radiography and CT have a limited role in detecting early iatrogenic spinal infection. In an early post-procedural setting, spinal infection can be difficult to differentiate from normal postoperative changes on MRI, for both spondylodiscitis and facet joint infection. Abscesses can be differentiated from other postoperative spinal infections and detected by DWI with ADC mapping, in the absence of metallic implants. When MRI is indeterminate for diagnosis of iatrogenic spinal infection, ^{18}F-FDG-PET/CT is indicated.

References

Allouni AK, Davis W, Mankad K et al (2013) Modern spinal instrumentation. Part 2: multimodality imaging approach for assessment of complications. Clin Radiol 68:75–81

Ariyanayagam T, Malcolm PN, Toms AP (2015) Advances in metal artifact reduction techniques for periprosthetic soft tissue imaging. Semin Musculoskelet Radiol 19:328–334

Arun R, Al-Nammari SS, Mehdian SMH (2007) Multilevel vertebral osteomyelitis and facet joint infection following epidural catheterisation. Acta Orthop Belg 73:665–669

Babic M, Simpfendorfer CS (2017) Infections of the spine. Infect Dis Clin North Am 31:279–297

Berg L, Thoresen H, Neckelmann G et al (2019) Facet arthropathy evaluation: CT or MRI? Eur Radiol 29:4990–4998

Blam OG, Vaccaro AR, Vanichkachorn JS et al (2003) Risk factors for surgical site infection in the patient with spinal injury. Spine (Phila Pa 1976) 28:1475–1480

Boden SD, Davis DO, Dina TS et al (1992) Postoperative diskitis: distinguishing early MR imaging findings from normal postoperative disk space changes. Radiology 184:765–771

Bosnak VK, Karaoglan I, Erkutlu I, Namiduru M (2017) Nosocomial spondylodiscitis after intradiscal electrothermal therapy: case series. J Pak Med Assoc 67:1290–1292

Cervan AM, Colmenero JDD, Del Arco A et al (2012) Spondylodiscitis in patients under hemodialysis. Int Orthop 36:421–426

Chahoud J, Kanafani Z, Kanj SS (2014) Surgical site infections following spine surgery: eliminating the controversies in the diagnosis. Front Med 1:1–10

Che W, Li RY, Dong J (2011) Progress in diagnosis and treatment of cervical postoperative infection. Orthop Surg 3:152–157

Clifton T, Selby M (2018) Epidural abscess from prolotherapy: a cautionary tale. ANZ J Surg 88:E216–E217

Cook NJ, Hanrahan P, Song S (1999) Paraspinal abscess following facet joint injection. Clin Rheumatol 18:52–53

Corso FA, Wolfe BM, Shaul DB (1995) Spinal osteomyelitis after TPN catheter-induced septicemia. J Parenter Enter Nutr 19:291–295

Di Martino A, Papalia R, Albo E et al (2019) Infection after spinal surgery and procedures. Eur Rev Med Pharmacol Sci 23:173–178

Diehn FE (2012) Imaging of spine infection. Radiol Clin North Am 50:777–798

Douglas-Akinwande AC, Buckwalter KA, Rydberg J et al (2006) Multichannel CT: evaluating the spine in postoperative patients with orthopedic hardware. Radiographics 26:S97–S111

Dufour V, Feydy A, Rillardon L et al (2005) Comparative study of postoperative and spontaneous pyogenic spondylodiscitis. Semin Arthritis Rheum 34:766–771

Eguchi Y, Ohtori S, Yamashita M et al (2011) Diffusion magnetic resonance imaging to differentiate degenerative from infectious endplate abnormalities in the lumbar spine. Spine (Phila Pa 1976) 36:198–202

Ethier J, Mendelssohn DC, Elder SJ et al (2008) Vascular access use and outcomes: an international perspective from the dialysis outcomes and practice patterns study. Nephrol Dial Transplant 23:3219–3226

Falagas ME, Bliziotis IA, Mavrogenis AF, Papagelopoulos PJ (2006) Spondylodiscitis after facet joint steroid injection: a case report and review of the literature. Scand J Infect Dis 38:295–299

Farshad-Amacker NA, Farshad M, Winklehner A, Andreisek G (2015) MR imaging of degenerative disc disease. Eur J Radiol 84:1768–1776

Follenfant E, Balamoutoff N, Lawson-Ayayi S et al (2019) Added value of [18F]fluorodeoxyglucose positron emission tomography/computed tomography for the diagnosis of post-operative instrumented spine infection. Joint Bone Spine 86:503–508

García-García P, Rivero A, Del Castillo N et al (2010) Infectious spondylodiscitis in hemodialysis. Semin Dial 23:619–626

Gemmel F, Rijk PC, Collins JMP et al (2010) Expanding role of 18F-fluoro-d-deoxyglucose PET and PET/CT in spinal infections. Eur Spine J 19:540–551

Gerometta A, Bittan F, Rodriguez Olaverri JC (2012a) Postoperative spondilodiscitis. Int Orthop 36:433–438

Gerometta A, Olaverri JCR, Bitan F (2012b) Infections in spinal instrumentation. Int Orthop 36:457–464

Gezici AR, Ergün R (2010) Cervical epidural abscess in haemodialysis patients by catheter related infection: report of two cases. J Korean Med Sci 25:176–179

Giri U, Thavalathil BC, Varghese R, Regional A (2014) Vertebral osteomyelitis in an immunosuppressed patient with rheumatoid arthritis. BMJ Case Rep 2014:9–11

Go JL, Rothman S, Prosper A et al (2012) Spine infections. Neuroimaging Clin North Am 22:755–772

Goerres GW, Ziegler SI, Burger C et al (2003) Artifacts at PET and PET/CT caused by metallic hip prosthetic material. Radiology 226:577–584

Grand CM, Bank WO, Balériaux D et al (1993) Gadolinium enhancement of vertebral endplates following lumbar disc surgery. Neuroradiology 35:503–505

Grane P, Josephsson A, Seferlis A, Tullberg T (1998) Septic and aseptic post-operative discitis in the lumbar spine—evaluation by MR imaging. Acta Radiol 39:108–115

Haidar R, Najjar M, Der Boghossian A, Tabbarah Z (2010) Propionibacterium acnes causing delayed postoperative spine infection: review. Scand J Infect Dis 42:405–411

Hancock C, Quencer R (2008) Challenges and pitfalls in postoperative spine imaging. Appl Radiol 37:23–34

Hooten WM, Mizerak A, Carns PE, Huntoon MA (2006) Discitis after lumbar epidural corticosteroid injection: a case report and analysis of the case report literature. Pain Med 7:46–51

Jain NK, Dao K, Ortiz AO (2014) Radiologic evaluation and management of postoperative spine paraspinal fluid collections. Neuroimaging Clin N Am 24:375–389

Jiménez-Mejías ME, de Dios Colmenero J, Sánchez-Lora FJ et al (1999) Postoperative spondylodiskitis: etiology, clinical findings, prognosis, and comparison with nonoperative pyogenic spondylodiskitis. Clin Infect Dis 29:339–345

Jungmann PM, Agten CA, Pfirrmann CW, Sutter R (2017) Advances in MRI around metal. J Magn Reson Imaging 46:972–991

Kalenderov R, Soukratos N, Kirat Rai P, Warsi A (2018) Early presentation of vertebral osteomyelitis following a transrectal ultrasound-guided prostate biopsy with delayed radiological findings. BMJ Case Rep 11:10–12

Kim SJ, Lee SH, Chung HW et al (2017) Magnetic resonance imaging patterns of post-operative spinal infection: relationship between the clinical onset of infection and the infection site. J Korean Neurosurg Soc 60:448–455

Koch KM, Bhave S, Gaddipati A et al (2018) Multispectral diffusion-weighted imaging near metal implants. Magn Reson Med 79:987–993

Kowalski TJ, Layton KF, Berbari E et al (2007) Follow-up MR imaging in patients with pyogenic spine infections: lack of correlation with clinical features. AJNR Am J Neuroradiol 28:693–699

Lotfinia I, Vahedi P (2010) Late-onset post-diskectomy tuberculosis at the same operated lumbar level: case report and review of literature. Eur Spine J 19:226–232

Lou XF, Wu RH, Xu SZ, Lin XJ (2010) Spinal tuberculosis in post-liver transplantation patients: case reports. Transpl Infect Dis 12:132–137

Maragakis LL, Cosgrove SE, Martinez EA et al (2009) Intraoperative fraction of inspired oxygen is a modifiable risk factor for surgical site infection after spinal surgery. Anesthesiology 110:556–562

Mazzie JP, Brooks MK, Gnerre J (2014) Imaging and management of postoperative spine infection. Neuroimaging Clin N Am 24:365–374

McDermott H, Bolger C, Humphreys H (2012) Postprocedural discitis of the vertebral spine: challenges in diagnosis, treatment and prevention. J Hosp Infect 82:152–157

McLellan AM, Daniel S, Corcuera-Solano I et al (2014) Optimized imaging of the postoperative spine. Neuroimaging Clin N Am 24:349–364

Miller TT (2004) Imaging of disk disease and degenerative spondylosis of the lumbar spine. Semin Ultrasound CT MRI 25:506–522

Moritani T, Kim J, Capizzano AA et al (2014) Pyogenic and non-pyogenic spinal infections: emphasis on diffusion-weighted imaging for the detection of abscesses and pus collections. Br J Radiol 87:20140011

Morrison W, Schweitzer M, Bock G et al (1993) Diagnosis of osteomyelitis: utility of fat-suppressed contrast-enhanced MR imaging. Radiology 189:251–257

Nouh MR (2012) Spinal fusion-hardware construct: basic concepts and imaging review. World J Radiol 4:193–207

Numaguchi Y, Rigamonti D, Rothman MI et al (1993) Spinal epidural abscess: evaluation with gadolinium-enhanced MR imaging. Radiographics 13:545–559

Ortiz AO, de Moura A, Johnson BA (2018) Postsurgical spine: techniques, expected imaging findings, and complications. Semin Ultrasound CT MRI 39:630–650

Pull ter Gunne A, Cohen D (2009) Incidence of surgical site infection following adult spinal surgery and analysis and prevalence of risk factors. Spine J 34:1422–1428

Rassner U (2019) Pearls and pitfalls of spine imaging. Radiol Clin North Am 57:233–255

Ross JS, Zepp R, Modic MT (1996) The postoperative lumbar spine: enhanced MR evaluation of the intervertebral disk. AJNR Am J Neuroradiol 17:323–331

Russo A, Graziano E, Carnelutti A et al (2019) Management of vertebral osteomyelitis in an 8-year period: the UDIPROVE (UDIne PROtocol on VErtebral osteomyelitis). Int J Infect Dis 89:116–121

Rutenberg TF, Baruch Y, Ohana N et al (2019) The role of F-Fluorodeoxyglucose positron-emission tomography/computed tomography in the diagnosis of postoperative hardware-related spinal infections. Isr Med Assoc J 21:532–537

Salgado R, Van Goethem JWM, van den Hauwe L, Parizel PM (2006) Imaging of the postoperative spine. Semin Roentgenol 41:312–326

Skaf GS, Domloj NT, Fehlings MG et al (2010) Pyogenic spondylodiscitis: an overview. J Infect Public Health 3:5–16

Smids C, Kouijzer IJE, Vos FJ et al (2017) A comparison of the diagnostic value of MRI and 18F-FDG-PET/CT in suspected spondylodiscitis. Infection 45:41–49

Smith JS, Shaffrey CI, Sansur CA et al (2011) Rates of infection after spine surgery based on 108,419 procedures: a report from the Scoliosis Research Society morbidity and mortality committee. Spine (Phila Pa 1976) 36:556–563

Stradiotti P, Curti A, Castellazzi G, Zerbi A (2009) Metal-related artifacts in instrumented spine. Techniques for reducing artifacts in CT and MRI: state of the art. Eur Spine J 18:102–108

Subach BR, Copay AG, Martin MM et al (2012) Epidural abscess and cauda equina syndrome after percutaneous intradiscal therapy in degenerative lumbar disc disease. Spine J 12:e1–e4

Talbott JF, Shah VN, Uzelac A et al (2018) Imaging-based approach to extradural infections of the spine. Semin Ultrasound CT MRI 39:570–586

Tali ET, Oner AY, Koc AM (2015) Pyogenic spinal infections. Neuroimaging Clin N Am 25:193–208

Taşdemiroglu E, Sengöz A, Bagatur E (2004) Iatrogenic spondylodiscitis. Case report and review of literature. Neurosurg Focus 16:1–5

Torres C, Zakhari N (2017) Imaging of spine infection. Semin Roentgenol 52:17–26

Van De Kelft EJZ, Van Goethem JWM, De La Porte C, Verlooy JSA (1996) Early postoperative gadolinium-DTPA-enhanced MR imaging after successful lumbar discectomy. Br J Neurosurg 10:41–49

Van Goethem JWM, Parizel PM, Verlooy J, De Schepper AMA (2000) The value of MRI in the diagnosis of postoperative spondylodiscitis. Neuroradiology 42:580–585

Van Goethem JWM, Parizel PM, Jinkins JR (2002) Review article: MRI of the postoperative lumbar spine. Neuroradiology 44:723–739

Veeravagu A, Patil CG, Lad SP, Boakye M (2009) Risk factors for postoperative spinal wound infections after spinal decompression and fusion surgeries. Spine (Phila Pa 1976) 34:1869–1872

Venugopal Menon K, Sorour TMM (2016) Epidemiologic and demographic attributes of primary spondylodiscitis in a Middle Eastern population sample. World Neurosurg 95:31–39

Visuri T, Pihlajamäki H, Eskelin M (2005) Long-term vertebral changes attributable to postoperative lumbar discitis: a retrospective study of six cases. Clin Orthop Relat Res 97–105

Weingarten TN, Hooten WM, Huntoon MA (2006) Septic facet joint arthritis after a corticosteroid facet injection. Pain Med 7:52–56

Weinstein MA, McCabe JP, Cammisa J (2000) Postoperative spinal wound infection: a review of 2,391 consecutive index procedures. J Spinal Disord 13:422–426

Yeom JA, Lee IS, Suh HB et al (2016) Magnetic resonance imaging findings of early spondylodiscitis: interpretive challenges and atypical findings. Korean J Radiol 17:565–580

Zou YF, Chu B, Wang CB, Hu ZY (2015) Evaluation of MR issues for the latest standard brands of orthopedic metal implants: plates and screws. Eur J Radiol 84:450–457

Imaging of Pyogenic Epidural Abscess

Hong Chou, Teck Yew Chin, and Wilfred C. G. Peh

Contents

Abstract

Spinal epidural abscess is an uncommon but severe infection affecting the spinal canal with the potential for causing serious complications such as spinal cord compression and infarct with resultant paralysis, if treatment is delayed. Despite advances in medical knowledge and imaging techniques, it is often misdiagnosed at initial presentation due to its insidious onset and nonspecific clinical signs. The classical triad of spinal pain, fever, and neurological deficit is often not present at initial presentation, making the diagnosis based on clinical findings alone challenging. Imaging thus plays a crucial role in the evaluation and early detection of this condition, allowing for prompt treatment to improve prognosis and clinical outcome. This chapter serves to describe the use of various techniques available for imaging pyogenic abscesses in spinal infections, particularly magnetic resonance imaging which is the modality of choice for diagnosis.

H. Chou (✉) · T. Y. Chin · W. C. G. Peh
Department of Diagnostic Radiology, Khoo Teck Puat Hospital, Singapore, Republic of Singapore
e-mail: Chou.hong@ktph.com.sg; Chin.teck.yew@ktph.com.sg; wilfred.peh@ktph.com.sg

© The Author(s), under exclusive license to Springer Nature Switzerland AG 2021, corrected publication 2021

M. F. Ladeb, W. C. G. Peh (eds.), *Imaging of Spinal Infection*,
Medical Radiology Diagnostic Imaging, https://doi.org/10.1007/978-3-030-70459-9_9

Abbreviations

CRP	C-reactive protein
CSF	Cerebrospinal fluid
CT	Computed tomography
ESR	Erythrocyte sedimentation rate
MRI	Magnetic resonance imaging
SEA	Spinal epidural abscess
STIR	Short tau inversion recovery
T1-W	T1-weighted
T2-W	T2-weighted
WBC	White blood cell count

1 Introduction

Spinal epidural abscess (SEA) is defined as an infection of the spinal extradural space with abscess formation and is also called spinal epidural empyema. It is commonly caused by hematogeneous spread and direct extension from adjacent spondylodiscitic infections. If left untreated, it can cause serious neurological sequelae due to a combination of cord compression and ischemic injury and may also progress to cause life-threatening sepsis. Diagnosis of SEA is often delayed due to its insidious onset and nonspecific clinical findings. They are considered infectious emergencies, requiring urgent intervention, including surgery in cases where there is cord compression, progressive neurological deficit, or persistent severe pain. Expedient diagnosis and prompt treatment are crucial to prevent adverse outcomes and to improve prognosis.

The relative incidence of SEA has been reported at 0.2–1.2 cases per 10,000 hospital admissions in the 1970s (Baker et al. 1975). This has increased over the last several decades to 2.5–3 cases per 10,000 hospital admissions. This rise can be attributed to the increase in predisposing factors such as an aging population, diabetes mellitus, chronic renal failure, immunodeficiency, local steroid injections, the increasing use of spinal instrumentation and vascular access, and intravenous drug abuse (Darouiche 2006; Sendi et al. 2008; Go et al. 2012). It may also be partly explained by the widespread availability and use of advanced imaging techniques, increasing the detection rates of SEA which may have previously been undiagnosed (Sendi et al. 2008). Although SEA may occur in all age groups, the greatest prevalence of the disease has been reported between the fifth to seventh decades of life, with a male preponderance (Hlavin et al. 1990; Rigamonti et al. 1999).

2 Anatomy and Pathogenesis

Knowledge of the vascular anatomy of the vertebral column is important for understanding the pathogenesis of spinal infection. The basic arrangement of the arterial supply consists of a metameric grid of transversely oriented paired segmental vessels at each vertebral level, connected by various longitudinal channels. The origin of the segmental arteries varies at different levels. In the cervical and upper thoracic spine, they arise from the vertebral arteries and subclavian artery branches, respectively. Large parts of the thoracic and lumbar spine are supplied by segmental arteries arising from the dorsal aspect of the descending aorta and the iliac arteries. The segmental arteries course along the equatorial plane around each vertebral body, giving off metaphyseal and nutrient branches into the vertebral end plates and central vertebral body (Ratcliffe 1980).

It is in the most richly vascularized vertebral end plates that infective spondylodiscitis often begins and subsequently spread to the adjacent disk, vertebral body, and epidural space. Several other extraosseous anastomotic branches from the segmental arteries form an arcade of vascular channels, often spanning multiple and sometimes noncontiguous vertebral segments (Wiley and Trueta 1959; Ratcliffe 1980). It is through these channels that longitudinal spread of bacteria occurs to other levels of the spine. The venous drainage of the vertebral body consists of valveless veins that exit through the dorsal nutrient foramen into the extradural venous plexus with drains into the paravertebral plexus of Batson (Batson 1957). It has been postulated that the spread of infection from the abdominal and pelvic organs, such as the bowel and urinary system,

may occur via the venous route (Sundaram and Doshi 2016). However, the arterial route is still widely recognized as the main route of hematogeneous transmission.

The spinal epidural space is a continuous sleevelike space that extends craniocaudally within the spinal canal. It separates the thecal (or dural) sac from the bony structures of the spinal canal. The thecal sac is the membranous sheath that represents a continuation of the intracranial dura mater, contains cerebrospinal fluid (CSF), and encloses the spinal cord and cauda equina. From the skull, the dura mater of the thecal sac adheres to bone at the foramen magnum and extends caudally to the second sacral vertebra where it tapers to cover over the filum terminale. The thecal sac has projections that follow the spinal nerves along their paths exiting the vertebral canal through the neural foramina, where they become the dural root sheaths.

Being located immediately external to the thecal sac, the extent of the spinal epidural space mirrors that of the thecal sac, except caudally where it is bound inferiorly by the sacrococcygeal membrane. Laterally, it extends around the dural sheaths of the exiting nerve roots (Richardson and Groen 2005). In the lumbar region, the dura mater apposes the vertebral periosteum, giving a segmented appearance. The posterior epidural space is larger than the anterior space as the dura mater, posterior longitudinal ligament, and the periosteum of the vertebral body are in close contact with each other anteriorly. The posterior epidural space is most capacious in the mid-thoracic (T4–T8) and lumbosacral (L3–S2) regions, which are the most common sites of SEA (Browder and Meyers 1941; Sendi et al. 2008). The spinal epidural space contains mainly fat, arteries, and venous complexes (Fig. 1).

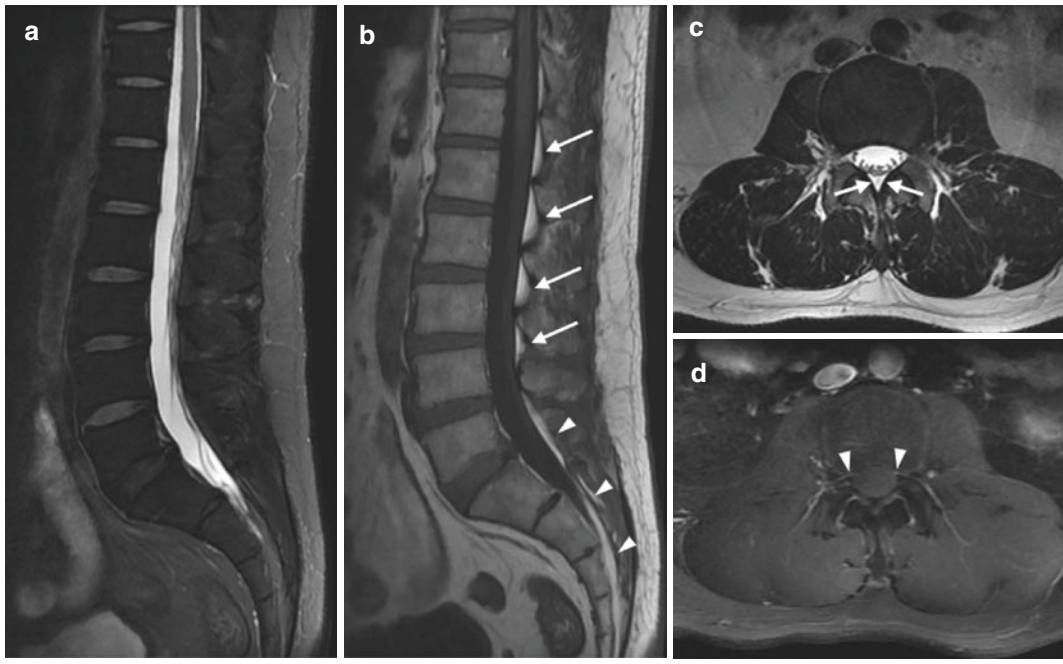

Fig. 1 Sagittal (**a**) T1-W and (**b**) FS T2-W MR images show the segmented appearance of the posterior epidural space in the lumbar spine (arrows) and more capacious, non-segmented, epidural fat in the sacral region (arrowheads). The anterior epidural space is not seen as the dura closely apposes the posterior periosteum of the vertebral bodies and the posterior longitudinal ligament. Axial (**c**) T2-W and (**d**) contrast-enhanced FS T1-W MR images show the triangular appearance of posterior epidural fat (arrows) and enhancing vessels within the neural foramina (arrowheads)

Bacteria may gain access to the epidural space via hematogeneous spread, extension from adjacent infection, and iatrogenic or silent inoculation. Hematogeneous spread from other sites of infection in the body account for approximately half the cases. The most common sources of septic emboli are from skin and soft tissue infections, followed by urinary infections. Other relatively common primary sites of infection include respiratory tract and abdominal infections. Up to 11% of cases are associated with previous sepsis of unknown origin. Less common sources include endocarditis, infected vascular access, dental abscesses, and ear, nose, and throat infections (Sendi et al. 2008). Direct extension from vertebral osteomyelitis, spondylodiscitis, septic arthritis of the facet joints, or paravertebral abscesses accounts for about a third of the cases. An estimated 15% of cases can be attributed to iatrogenic causes such as spinal interventions or surgery. In some cases, no cause can be ascertained, possibly due to silent direct inoculation of bacteria into the epidural space (Darouiche 2006; Sendi et al. 2008).

Several predisposing factors to SEA have been described; most of these cause some form of immunosuppression and are common to all forms of severe infections. Diabetes mellitus is one of the most important risk factors, seen in up to 54% of cases. Intravenous drug abuse is another factor that has been reported in up to 40% of cases. The presence of remote infection has been described in up to 44% (Grewal et al. 2006). Other risk factors include alcoholism, chronic renal failure, pre-existing cancer, immunosuppressive therapy, underlying spinal abnormalities, and antecedent trauma. A history of preceding spinal anesthetic procedures such as epidural injection or catheterization can also predispose to iatrogenic causes of SEA (Sendi et al. 2008).

The vast majority of SEA are caused by pyogenic organisms. *Staphylococcus aureus*, including methicillin-resistant *Staphylococcus aureus* (MRSA), is the organism implicated in about two-thirds of SEAs. Other less common organisms include coagulase-negative staphylococci such as *Staphylococcus epidermidis*, *Escherichia coli* (usually from urinary tract infections), and *Pseudomonas aeruginosa* (especially in intravenous drug abusers). Mycobacterial, fungal, and parasitic infections are rare causes of epidural abscess (Kaufman et al. 1980; Darouiche 2006). Polymicrobial infections in the spine are rare (<2.5%), except in postoperative scenarios (~50%) (Sapico 1996).

SEA can form either anterior or posterior to the spinal cord. Anteriorly sited abscesses often but not exclusively extend contiguously from adjacent vertebral osteomyelitis or spondylodiscitis. The expanding abscess dissects the epidural space and usually spans across three to four adjoining vertebral segments. Posteriorly located abscesses are frequently found in the thoracolumbar regions where the posterior epidural space is most capacious. These are usually secondary to hematogeneous spread and tend to be more extensive and multifocal, forming the so-called skip lesions (Darouiche 2006; Arbelaez et al. 2014). A less common source of posterior or posterolateral abscesses is from direct extension from septic arthritis of the facet joints (Muffoletto et al. 2001; Tins and Cassar-Pullicino 2004).

Neurological deficits seen in patients with epidural abscesses are attributed to direct mechanical compression due to the mass effect of the abscess upon the spinal cord. Indirect injury to the cord may also occur secondary to vascular occlusion and ischemic damage postulated to be due to thrombophlebitis of the spinal vessels (Darouiche 2006). Animal studies have shown both a primary role for mechanical compression of the cord and additive effect of cord ischemia on neurological function (Feldenzer et al. 1988). The rapid improvement of neurological function seen in patients following decompressive laminectomy is further evidence of a mechanical pathophysiology (Khanna et al. 1996). Postmortem examinations have also detected thrombosed vessels, pointing to an ischemic

cause (Browder and Meyers 1941). Mechanical compression and vascular occlusion may both contribute to neurological compromise in different phases of the disease.

3 Clinical Features

The clinical signs of SEA are often variable and nonspecific, especially in the early course of the disease. The three most common symptoms described are the classical triad of back pain, fever, and neurological deficit. However, this combination of findings is only seen in 10–15% of cases at initial presentation (Davis et al. 2004; Curry Jr et al. 2005). Back pain is the most consistent symptom, being reported in 75% of cases. It is often severe and may be described as a "stabbing pain." Fever is seen in up to half the patients and neurological deficit of varying severity in up to a third of patients (Darouiche 2006; Sendi et al. 2008).

Four stages of clinical progression have been described. In stage one, clinical signs of back pain at the affected level, spinal tenderness, and fever predominate. Early neurological signs in stage 2 manifest as radicular pain in the affected nerve distribution, neck stiffness, and changes in reflexes. As the disease progresses to stage 3, more severe neurological signs become apparent in the form of sensory disturbances, motor weakness, and bladder and bowel dysfunction. The final stage represents paralysis, the most feared complication of epidural abscess, which rapidly becomes irreversible without urgent treatment (Heusner 1948; Peterson et al. 1987). There is a large variability in the duration of symptoms prior to clinical presentation, ranging from a few days to more than a month. The time course of neurological deterioration is also unpredictable, with some patients progressing rapidly to paralysis within hours of diagnosis and others who follow a more indolent course over several days (Darouiche 2006; Sendi et al. 2008).

As a result of nonspecific and variable clinical signs in the early stages of the disease, SEA is often misdiagnosed in more than half the cases at initial presentation (Tang et al. 2002; Davis et al. 2004). Infectious conditions such as osteomyelitis, discitis, meningitis, urinary tract infection, sepsis, and endocarditis are common mimickers in patients with fever and back pain without neurological signs. More common noninfectious conditions such as intervertebral disk prolapse, degenerative joint disease, spinal tumor, demyelinating illness, transverse myelitis, and spinal hematoma are some conditions frequently diagnosed at the time of initial evaluation (Hlavin et al. 1990; Darouiche et al. 1992; Reihsaus et al. 2000). A high index of suspicion based on risk factors and careful neurological examination are required to direct subsequent laboratory and imaging studies.

4 Laboratory Investigations

Routine laboratory investigations for suspected SEA include white blood cell count (WBC) as part of a full blood count panel and inflammatory markers such as erythrocyte sedimentation rate (ESR) and C-reactive protein (CRP). These parameters are elevated in most cases but remain nonspecific for diagnosis of SEA. Leukocytosis is seen in 60–80% of cases, and ESR is elevated to >20 mm/h in 95% of patients (Tang et al. 2002; Sendi et al. 2008). The mean CRP levels in a study of 25 patients with epidural abscesses have been found to be 150 mg/L, which is significantly increased from the normal value of <5 mg/L (Soehle and Wallenfang 2002).

Microbiological investigations are important to isolate the causative microorganism and to direct antibiotic therapy. Bacteremia is detected in about 60% of patients; however, in the remaining 40%, blood cultures will return a negative finding (Davis et al. 2004; Curry Jr et al. 2005). In these instances, specimens may be obtained directly from the abscess, either from surgical

decompression or from needle aspiration under computed tomography (CT) guidance. Additional samples should also be taken from potential sources of primary infection, such as the urinary tract or respiratory system.

CSF analysis has been shown to be of limited value in the evaluation of SEA. Positive cultures are obtained in less than 25% of cases. Findings of pleocytosis, elevated protein, and lactate levels are typical but again nonspecific for epidural infection (Maslen et al. 1993; Darouiche 2006; Sendi et al. 2008). As such, lumbar punctures are not routinely performed for suspected SEA. If a lumbar puncture is to be performed in these patients, magnetic resonance imaging (MRI) is highly recommended to evaluate the location and extent of any SEA to avoid traversing the infected tissues and hence spreading the infection into the subarachnoid space, potentially causing meningitis (Darouiche 2006; Sendi et al. 2008; Arbelaez et al. 2014).

5 Imaging

The possibility of SEA is first suspected based on clinical and laboratory findings. Ultimately, the definitive diagnosis is established by imaging studies. Several imaging modalities are available, with MRI representing the gold standard. Ultrasonography and nuclear medicine studies are of limited value in the diagnosis and evaluation of SEA, and will not be discussed in this chapter.

5.1 Radiography

Radiographs are of limited utility in the evaluation of spinal infections and are often normal in the early stages of the disease. They are found to be useful in less than 20% of cases. Epidural abscesses are not visible on radiographs in the absence of myelography (Grewal et al. 2006). In cases with concomitant spondylodiscitis, features such as vertebral osteolysis, end-plate destruction, and loss of intervertebral disk space may be evident. However, these are late signs and are only apparent when there is 30–40% loss of bone matrix (Stäbler and Reiser 2001; Grewal et al. 2006; Arbelaez et al. 2014).

5.2 Computed Tomography

Contrast-enhanced CT may initially be performed as a screening tool to determine the source of infection as part of the workup of a patient with sepsis. SEA may be detected occasionally if actively sought after and with the appropriate window level settings on CT (Fig. 2a, b). Associated findings of spondylodiscitis, facet joint septic arthritis, paravertebral soft tissue swelling, and psoas collection may be apparent. However, findings on CT are neither sensitive nor specific for SEA and, ideally, should not replace MRI (Angtuaco et al. 1987; Wong and Raymond 1998). CT myelography involves the intrathecal administration of contrast agent followed by CT. This technique can detect SEA with similar sensitivity as MRI. However, it may not completely delineate the entire extent of the abscess in cases where there is an obstruction to the flow of contrast agent within the thecal sac. It is also an invasive procedure and carries the risk of puncturing the abscess and spreading the infection along the subarachnoid space, potentially causing subsequent meningitis (Hlavin et al. 1990; Rigamonti et al. 1999; Butler et al. 2006; Grewal et al. 2006). Due to these reasons, CT myelography is only reserved for a selected group of patients for which MRI is not possible or contraindicated (Gerstein 2007).

5.3 Magnetic Resonance Imaging

Contrast-enhanced MRI has specificity, sensitivity, and accuracy of more than 90% and is the diagnostic method of choice for diagnosis of SEA (Angtuaco et al. 1987; Wong and Raymond 1998; Rigamonti et al. 1999). It enables rapid and

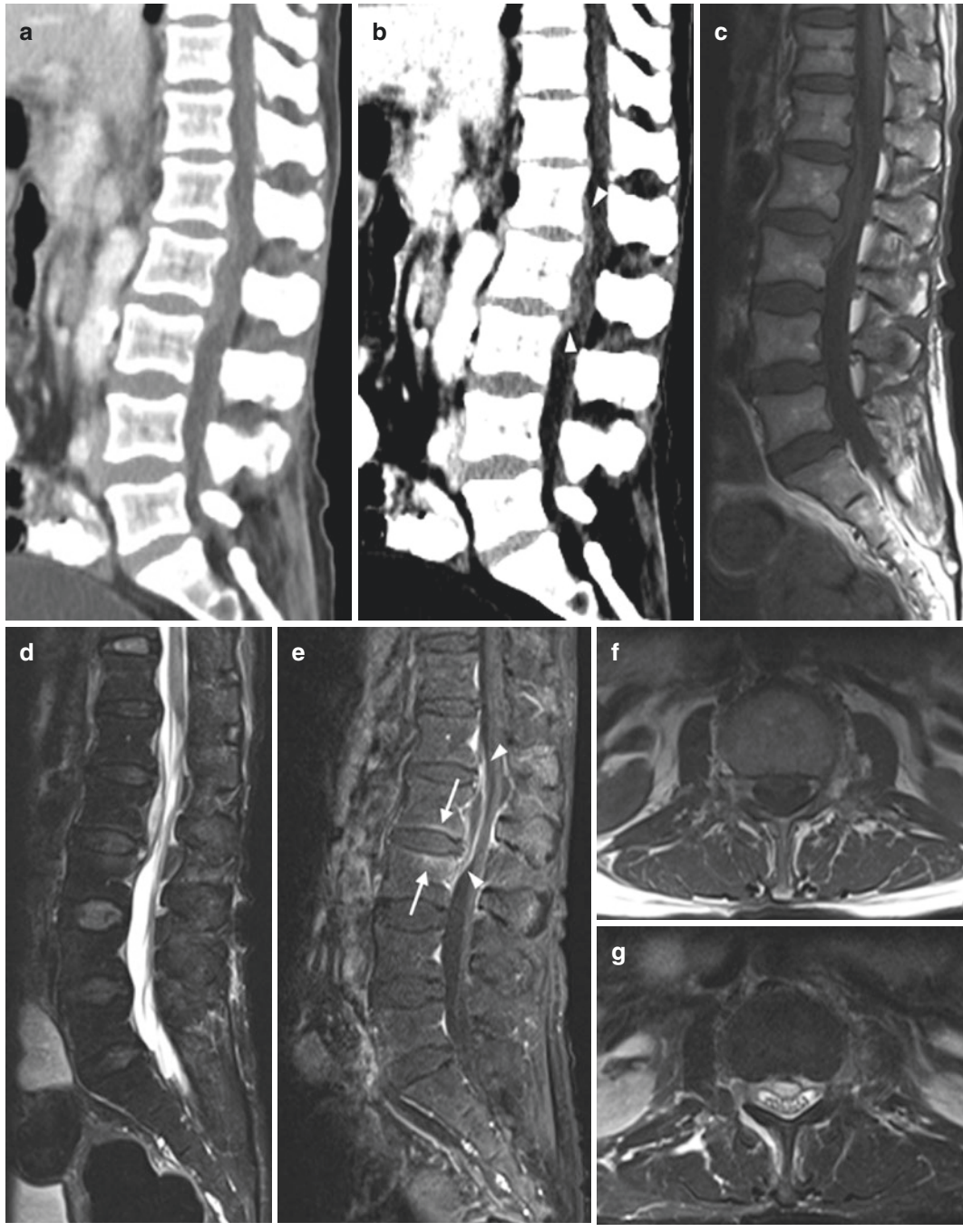

Fig. 2 A 62-year-old woman presenting with severe back pain, lower limb weakness, and fever. She had WBC of 14.5×10^9/L and CRP of 165 mg/L. (**a**) Initial sagittal contrast-enhanced CT image shows curvilinear epidural soft tissue swelling posterior to L2 vertebral body, which is accentuated by (**b**) further soft tissue windowing (arrowheads). Sagittal (**c**) T1-W, (**d**) FS T2-W, and (**e**) contrast-enhanced FS T1-W and axial (**f**) T1-W (**g**) FS T2-W and (**h**) contrast-enhanced FS T1-W MR images show a corresponding rim-enhancing epidural abscess (arrowheads) causing moderate compression of the thecal sac and its contents. Patchy area of T1-hypointensity, T2-hyperintensity, and enhancement in the posterior inferior L2 and posterior superior L3 vertebral end plate represents early spondylitis (arrows). Blood cultures revealed methicillin-sensitive *Staphylococcus aureus* (MSSA) infection

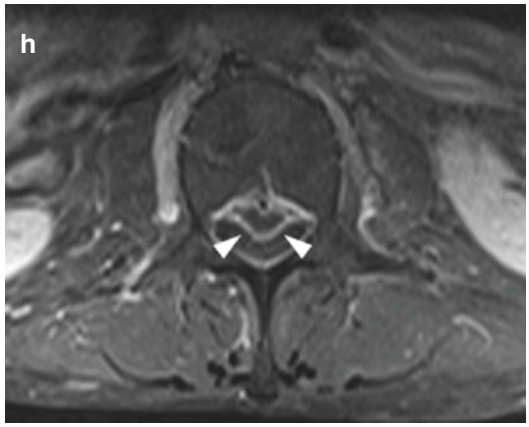

Fig. 2 (continued)

accurate detection of abscesses, defines their anatomical extent, and assists in preoperative planning. SEA is characteristically identified as a collection within the epidural space that is hypointense on T1-weighted (T1-W) and hyperintense on short tau inversion recovery (STIR) and T2-W MR sequences. They may show mixed T1-W and T2-W signal intensities, depending on the contents of the collection, but are generally hyperintense to CSF on T1-W sequences and hypointense to CSF on T2-W sequences (Tins and Cassar-Pullicino 2004) (Fig. 2c–h).

There are typically two main patterns of contrast enhancement in SEA. The first is diffuse homogeneous or heterogeneous enhancement, representing inflammatory phlegmon or granulation tissue (Fig. 3a–c). The second pattern is thick or thin rim enhancement around a fluid collection with a non-enhancing central component that represents pus (Tins and Cassar-Pullicino 2004; Arbelaez et al. 2014) (Figs. 2, 4, 5, and 6) Internal septations may be seen within the abscess, like abscesses in other anatomical locations. The cranio-caudal extent of involvement is best assessed on the sagittal images (Figs. 4a–f and 5c, d). Axial images are useful in demonstrating the degree of cord compression and to assess for the lateral extension to the neural foramina as well as paravertebral soft tissue involvement (Numaguchi et al. 1993; Rothman 1996; Küker et al. 1997; Dagirmanjian et al. 1999; Sundaram and Doshi 2016) (Figs. 4g, h, 5f, g, and 6c–e). Both sagittal and axial images should be interpreted in tandem, as some collections have a spiral appearance that can only be fully appreciated in both planes as a single collection rather than separate abscesses (Sundaram and Doshi 2016).

MRI also enables evaluation of secondary effects of SEA. These include assessing the cord for signal changes of cord ischemia or compression, typically depicted as abnormal enhancement and T2-signal hyperintensity due to cord edema (Sundaram and Doshi 2016). Engorgement of the epidural and basivertebral veins has also been described. These are seen as dilated venous structures above and below the SEA (Numaguchi et al. 1993). Features of other concomitant spinal infections such as spondylodiscitis, facet joint septic arthritis, vertebral osteomyelitis, and paravertebral abscesses can also be seen (Figs. 3, 5, 6, and 7). There should a low threshold for imaging the entire spine to avoid missing skip lesions or other sites of spinal infection. Involvement of noncontiguous vertebral segments has been shown to be more common in patients with symptoms of more than 7 days, presence of extraspinal infection, or elevated ESR level of more than 95 mm/h at presentation (Ju et al. 2015).

More recently, diffusion-weighted imaging (DWI) MR sequences, with b-value of 1000 along with a corresponding apparent diffusion coefficient (ADC) map, have been used to image the spine and spinal cord. Abscesses and pus collections contain cellular debris and necrotic material which restrict the movement of water molecules. These result in the appearance of hyperintense signal on DWI. It can be a useful tool in cases when there are equivocal findings with conventional sequences and in selected cases where there is contraindication to the administration of gadolinium chelate. It can also serve to differentiate SEA from mimickers such as epidural hemorrhage, CSF leak, disk herniation, synovial cyst, granulation tissue, spinal tumors, and postsurgical fluid collections (Tsuchiya et al. 2003; Moritani et al. 2014).

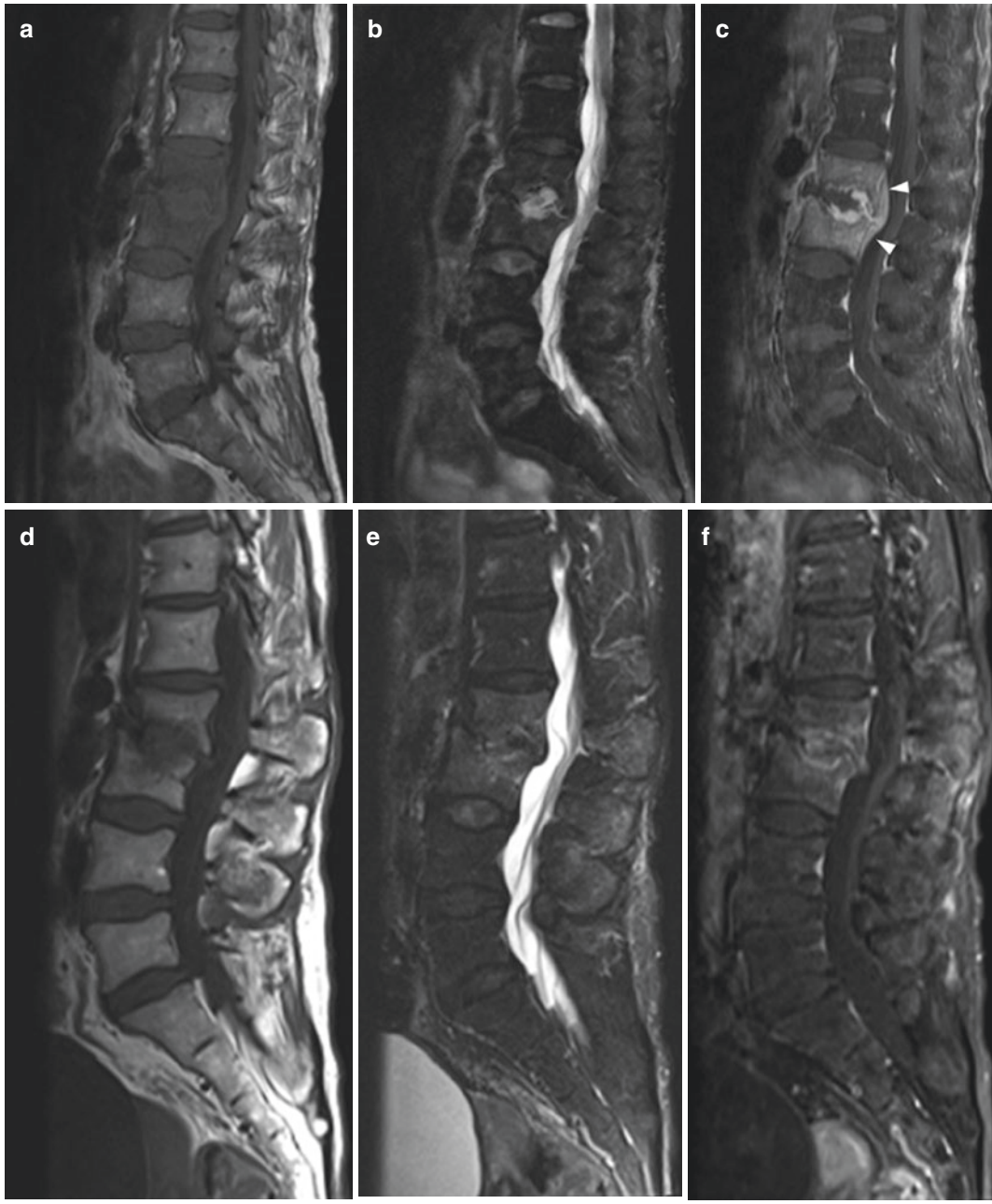

Fig. 3 MSSA spinal infection. The same patient as in Fig. 2. Follow-up MRI after 6 weeks of intravenous antibiotic therapy. Sagittal (**a**) T1-W, (**b**) FS T2-W, and (**c**) contrast-enhanced FS T1-W MR images show marrow infiltration and enhancement of L2 and L3 vertebral bodies with fluid signal within the intervening disk and adjacent end-plate destruction. The previously seen epidural abscess now shows solid enhancement representing granulation tissue (arrowheads). Although imaging findings of spondylodiscitis are now more apparent, the patient showed clinical improvement without further deterioration of neurological signs and was discharged. (**d–f**) Follow-up MRI 3 months after discharge. Sagittal (**d**) T1-W, (**e**) FS T2-W, and (**f**) contrast-enhanced FS T1-W MR images show marked improvement of spondylodiscitic changes and resolution of epidural abscess. The patient remained clinically well

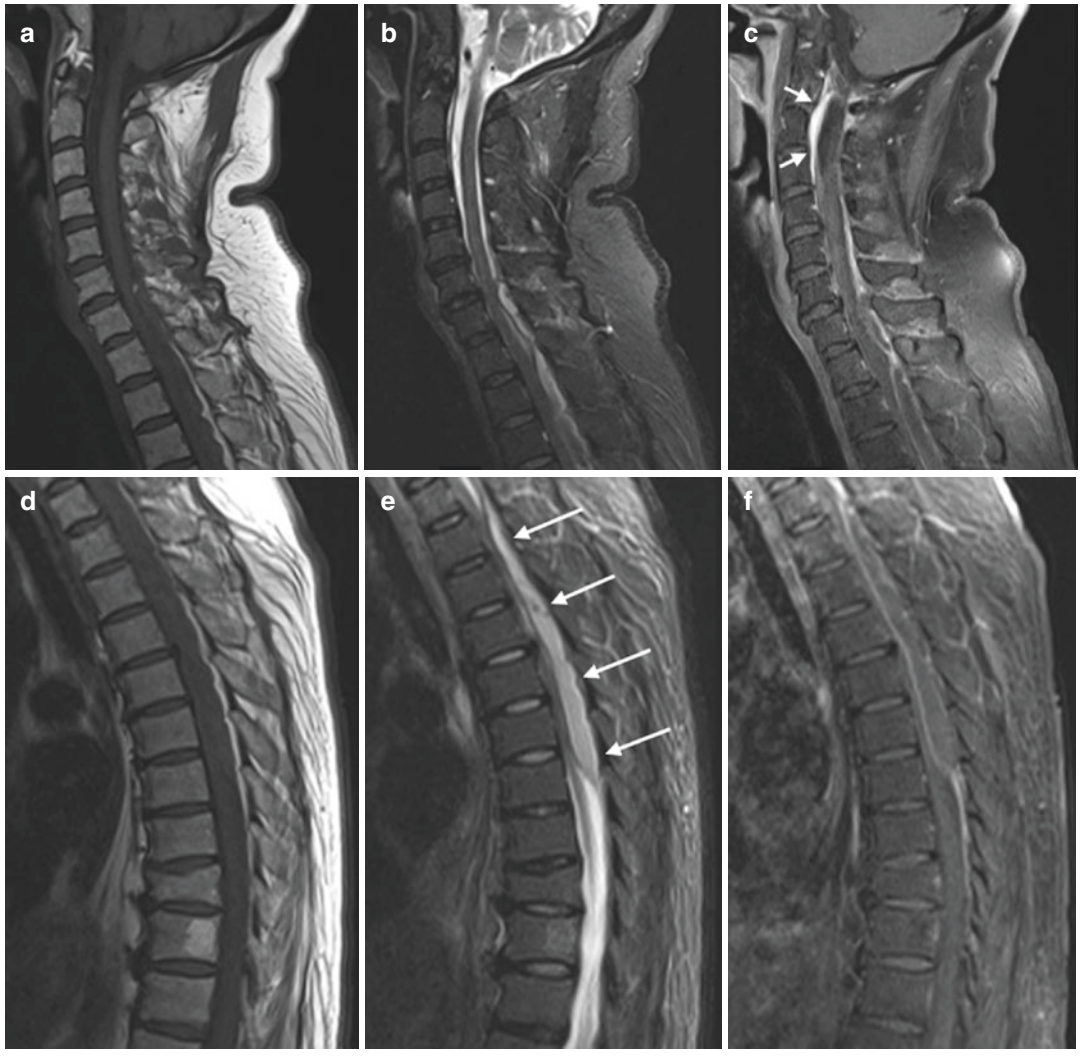

Fig. 4 A 62-year-old woman, with a background history of diabetes mellitus and previous breast carcinoma, presenting with left lower limb swelling and erythema as well as neckache. She also had previous severe left lower limb cellulitis with infected collections for which she received surgical incision and drainage. Sagittal (**a**) T1-W, (**b**) FS T2-W, and (**c**) contrast-enhanced FS T1-W MR images of the cervical spine and sagittal (**d**) T1-W, (**e**) FS T2-W, and (**f**) contrast-enhanced FS T1-W MR images of the thoracic spine show extensive rim-enhancing posterior epidural abscess (long arrows) extending from C7 to T7, with a smaller loculated cranial component at C2 level (short arrows). Axial (**g**) FS T2-W and (**h**) contrast-enhanced FS T1-W MR images taken at T5 vertebral level show epidural abscess (arrows) compressing the spinal cord (arrowheads). Due to the absence of neurological deficits and posterior location of the abscess, CT-guided needle aspiration was preferred as the treatment of choice. (**i**, **j**) Axial CT images with patient in prone position show left posterior interlaminar approach for CT-guided drainage of the posterior epidural abscess. Approximately 5 mL of pus was obtained which yielded group B streptococcus. The patient made an uneventful recovery after completing a course of antibiotics

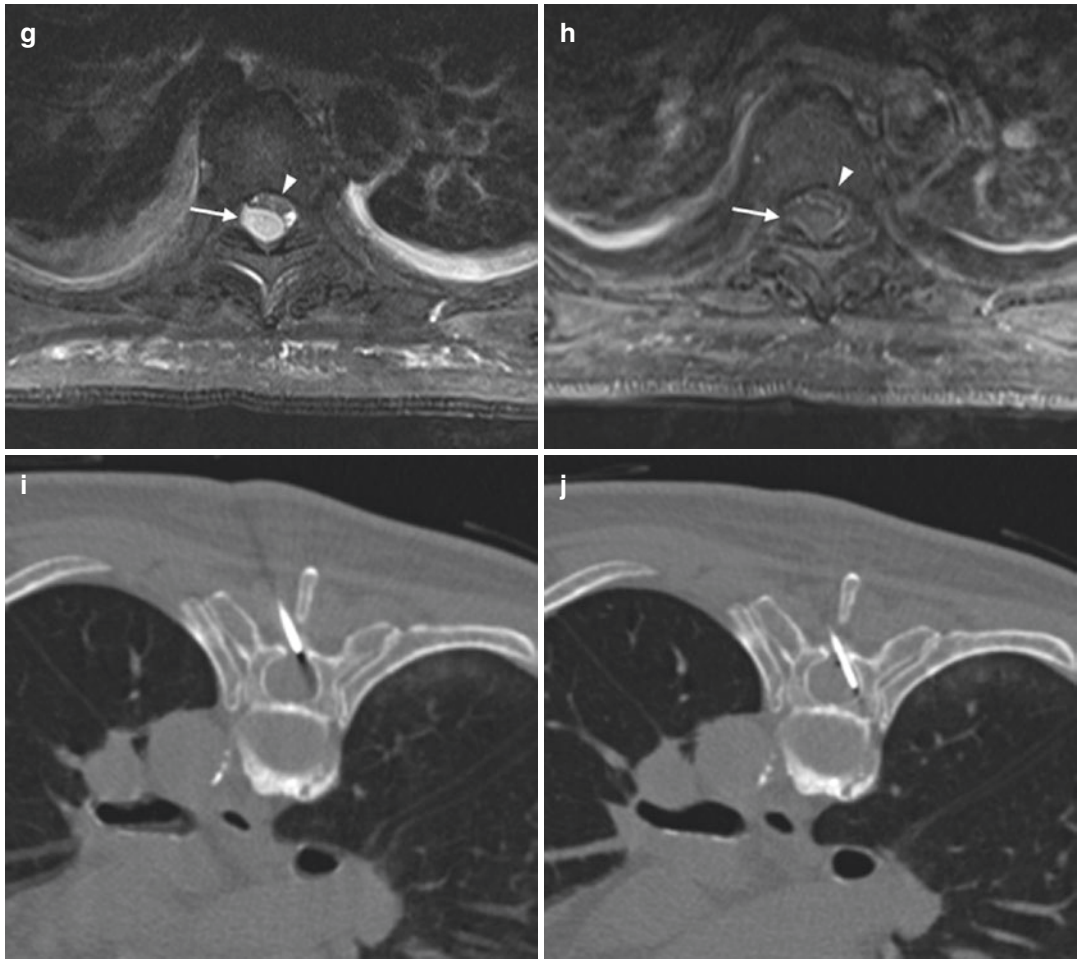

Fig. 4 (continued)

Differential diagnoses for epidural abscesses on MRI include epidural hematoma, extruded or sequestered disk, epidural tumor, vertebral metastasis with extradural extension, CSF leak, and postoperative spinal seroma. Spinal epidural hematoma is the top differential diagnosis for SEA. Appearances of blood on MRI varies with its stage of evolution and can appear similar to SEA in the hyperacute stage, where they show T1-iso- to hypointensity and T2-hyperintensity. At this acute stage, epidural hematomas tend to show more heterogeneous T1-hypointensity and less marked T2-hyperintensity when compared to SEA. In the late subacute stage, hematomas will exhibit T1-hyperintensity which often distinguishes it from SEA. Varying patterns of contrast enhancement can be seen in epidural hematomas, including rim and solid enhancement, similar to SEAs. Secondary imaging features of infection such as paraspinal collections and disk and bony involvement are absent in epidural hematomas. Clinical findings of fever and elevated inflammatory markers are useful for distinguishing the two conditions (Pierce et al. 2018) (Fig. 8).

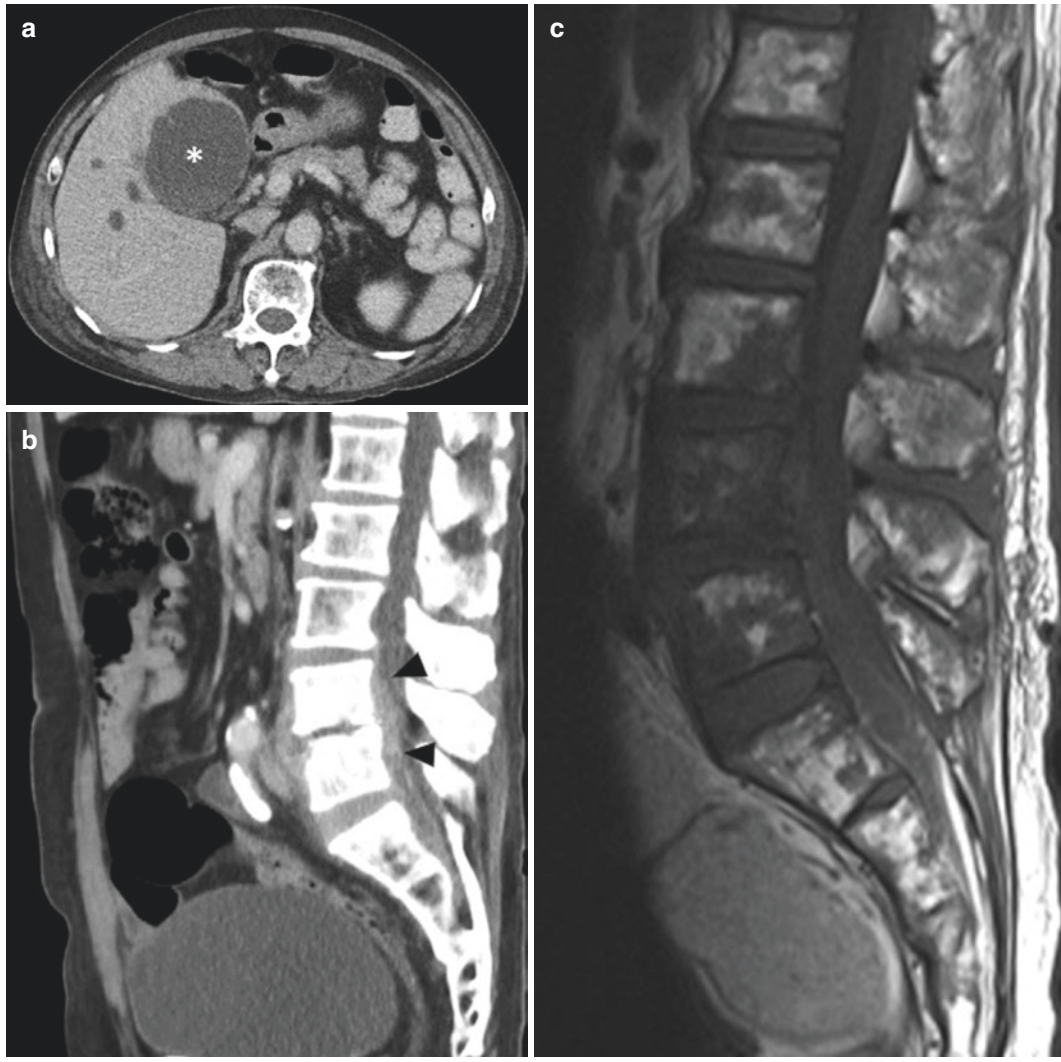

Fig. 5 A 64-year-old man presenting with fever, back pain, and abdominal discomfort. Found to have *Klebsiella* bacteremia and abnormal liver function tests. CRP was 347 mg/L. (**a**) Axial contrast-enhanced CT image shows a thin-walled, rim-enhancing right hepatic lobe abscess (asterisk). (**b**) Sagittal CT image shows disk space narrowing at L4–L5 level with adjacent anterior epidural abscess extending caudally into the sacral region (black arrowheads). Sagittal (**c**) T1-W and (**d**) FS T2-W MR images confirm L4–L5 spondylodiscitis, L4 vertebral osteomyelitis, and anterior epidural abscess from L3 to S2 levels. (**e**) Sagittal contrast-enhanced FS T1-W MR image shows solid enhancement of the cranial portion of the epidural abscess from L3 to L5 levels (arrows), in contrast to the rim-enhancing portion in the caudal portion from L5 to S2 levels (arrowheads). Axial (**f**) T1-W, (**g**) FS T2-W, and (**h**) contrast-enhanced FS T1-W MR images taken at L5 vertebral level show the mass effect of the abscess on the thecal sac with enclosed cauda equina (arrowheads). The epidural abscess was managed medically due to the absence of neurological symptoms. The patient recovered well following percutaneous liver abscess drainage and a prolonged course of intravenous antibiotics

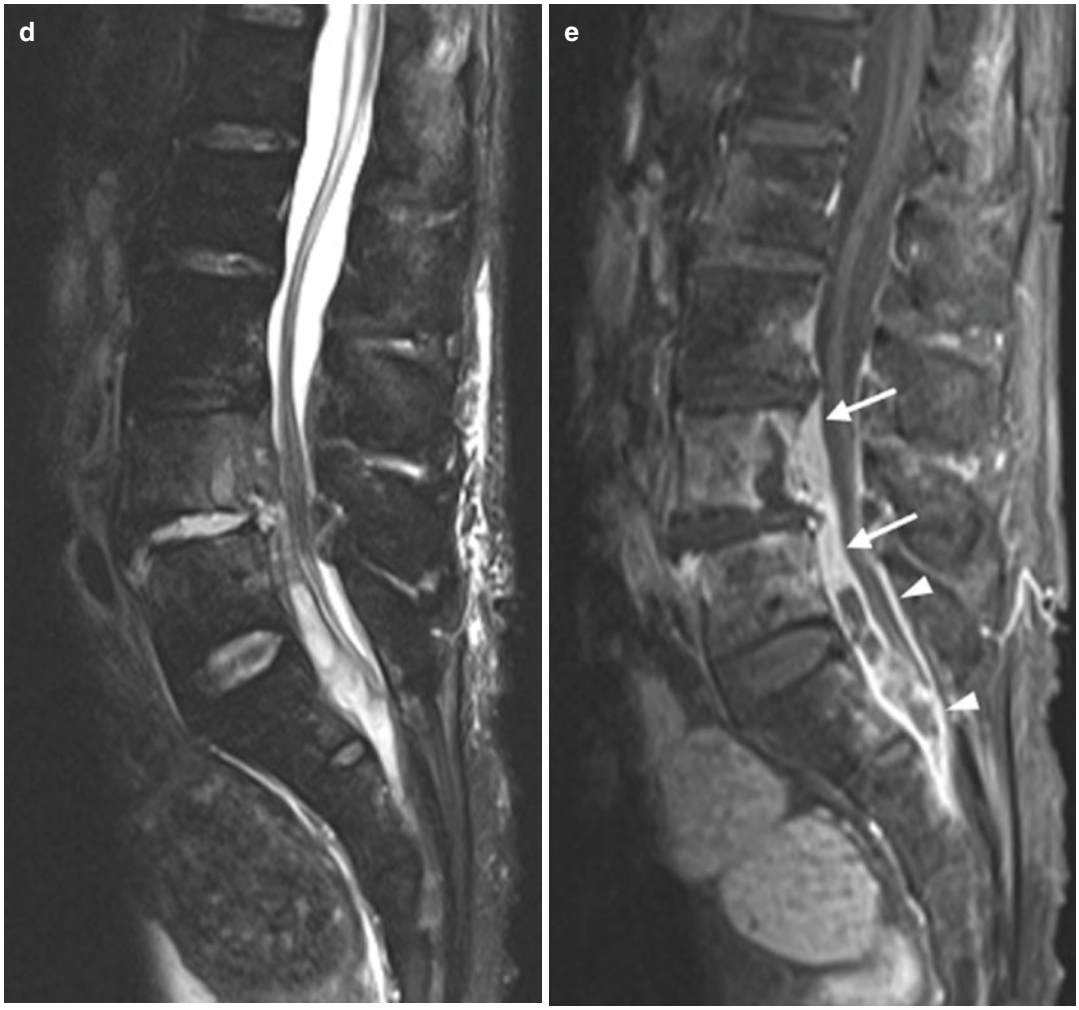

Fig. 5 (continued)

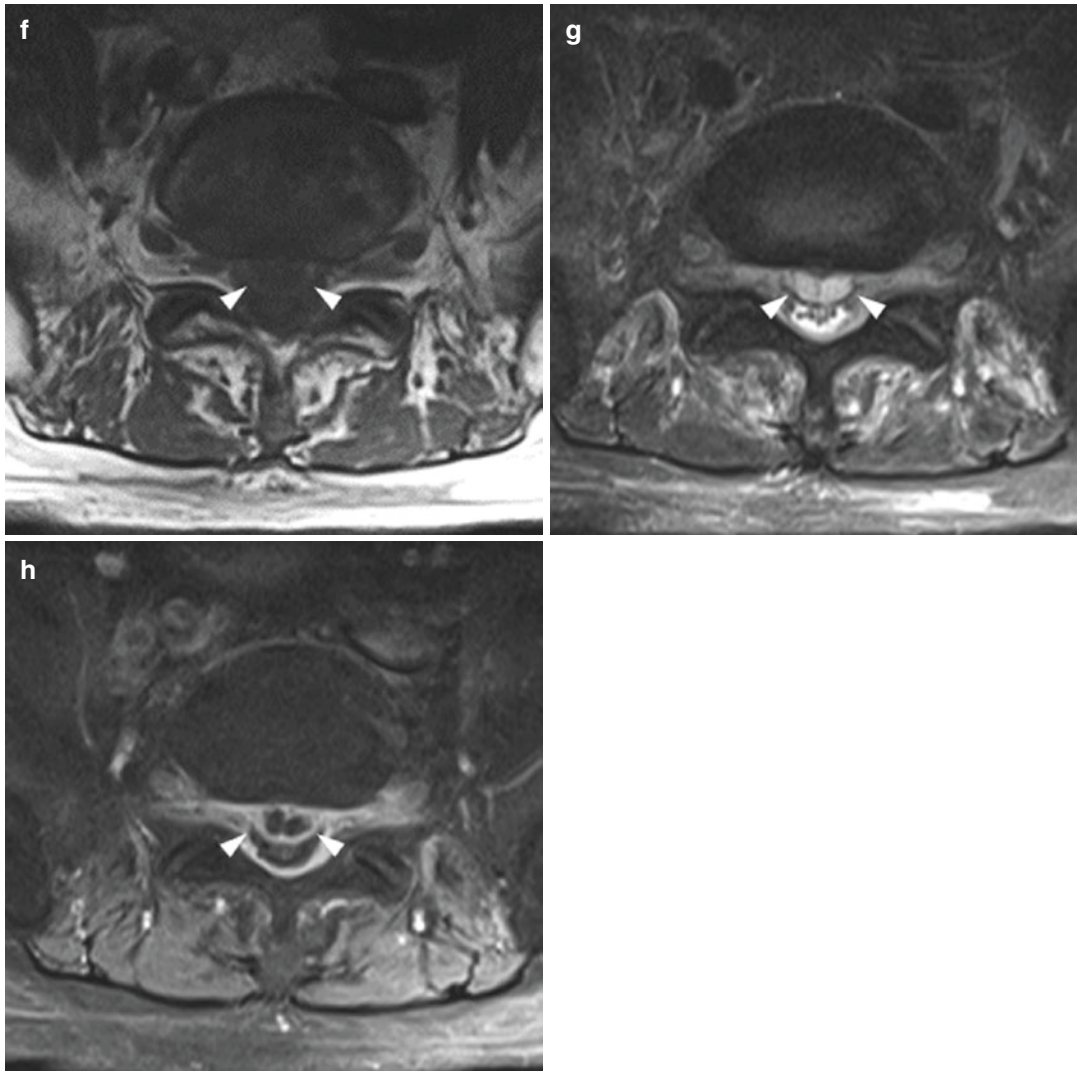

Fig. 5 (continued)

A sequestered disk may also mimic SEA, especially when it has migrated from the parent disk. These can show fluid signal intensities and peripheral enhancement pattern, similar to the features of an abscess. It can be distinguished by identifying degenerative changes in the parent disk, involvement of a shorter length of the epidural space, and absence of other imaging and clinical signs of infection (Chee and Peh 2009) (Fig. 9). CSF leaks and postoperative spinal seromas can dissect along the epidural space and can appear similar to SEA. DWI will show restricted diffusion in SEA but not in a sequestered disk, CSF leak, or seroma (Moritani et al. 2014). Epidural tumors will appear more focal and show solid and homogeneous contrast enhancement. Metastatic vertebral lesions with extradural extension are frequently multiple and may show associated bone marrow changes (Fig. 10).

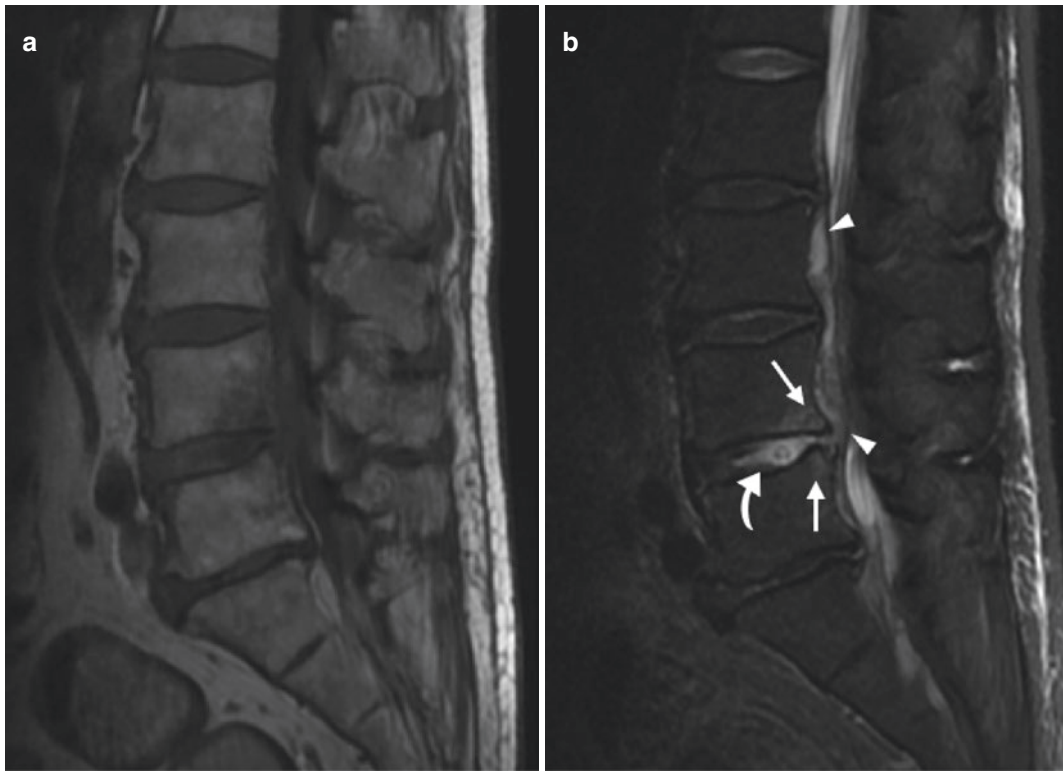

Fig. 6 A 76-year-old man with a background of diabetes mellitus and previous colon carcinoma presenting with fever, cough, and back pain. Laboratory investigations showed WBC of 13.3 × 10^9/L and CRP of 277 mg/L. Imaging revealed septic arthritis of the right sternoclavicular joint (not shown). Sagittal (**a**) T1-W and (**b**) FS T2-W and axial (**c**) T1-W, (**d**) FS T2-W, and (**e**) contrast-enhanced FS T1-W MR images show T2-hyperintensity in the L4–L5 disk (curved arrow) and marrow edema in the adjacent endplates (straight arrows), representing early features of spondylodiscitis. There is an anterior epidural abscess posterior to L3 and L4 vertebral bodies which demonstrates rim enhancement and severe thecal sac compression at L4 vertebral level (arrowheads). The patient subsequently underwent decompressive spinal surgery with debridement of epidural abscess in view of severe cauda equina compression with corresponding neurological signs. Follow-up MRI 6-weeks postsurgery consisting of sagittal (**f**) T1-W, (**g**) FS T2-W, and (**h**) contrast-enhanced FS T1-W, and axial (**i**) T1-W, (**j**) FS T2-W, and (**k**) contrast-enhanced FS T1-W MR images show improvement of an epidural abscess with residual granulation tissue posterior to L4 vertebral body (arrows). There is, however, development of a deep abscess at the laminectomy site spanning from L3 to L4 vertebral levels (arrowheads) necessitating further debridement and wound closure

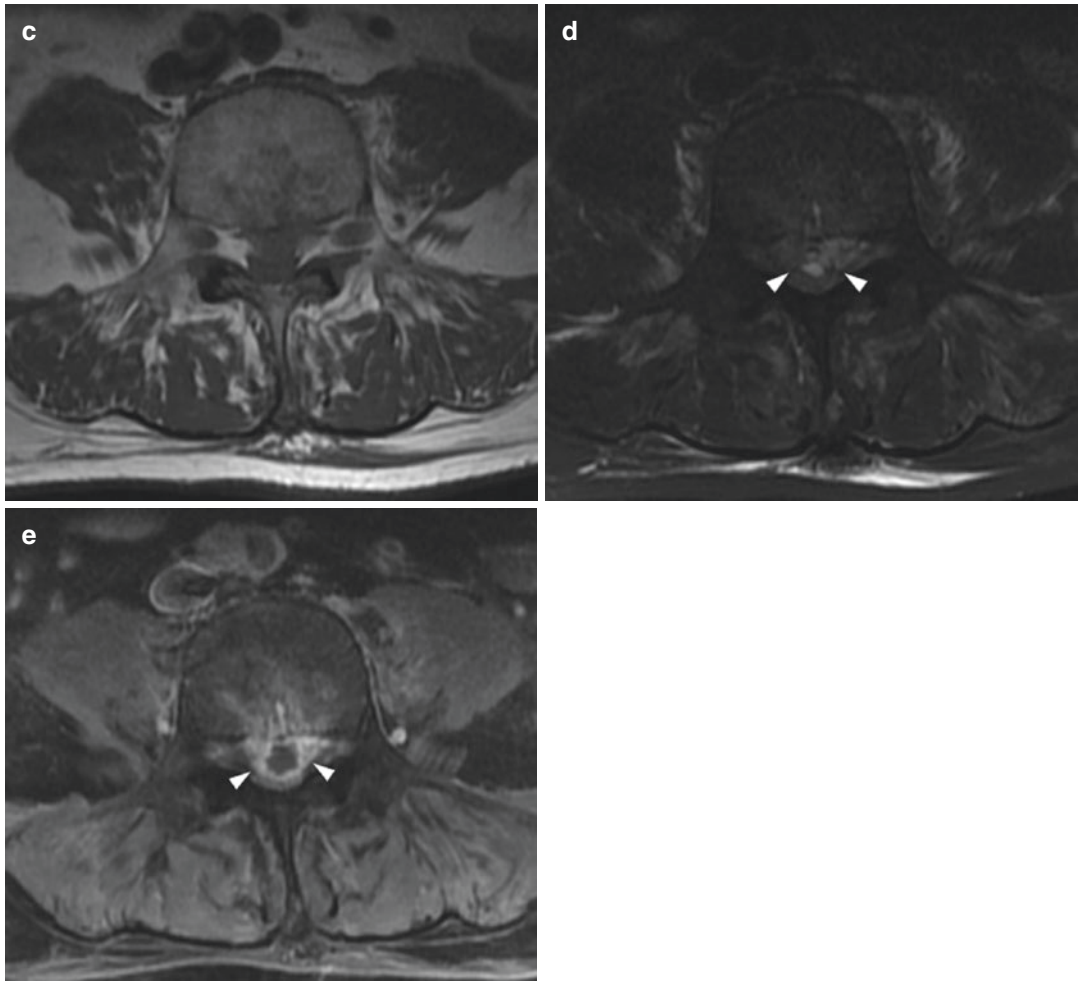

Fig. 6 (continued)

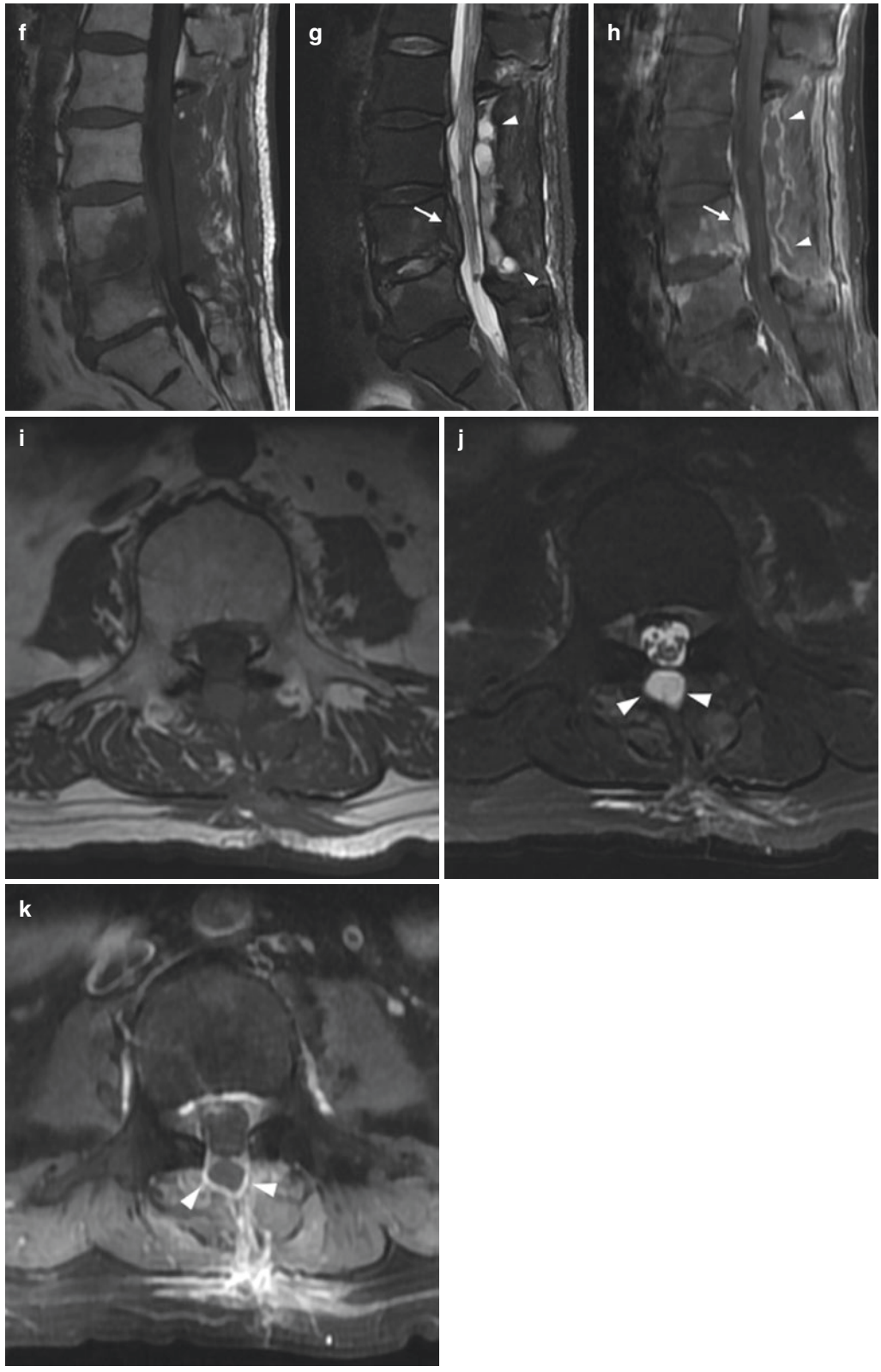

Fig. 6 (continued)

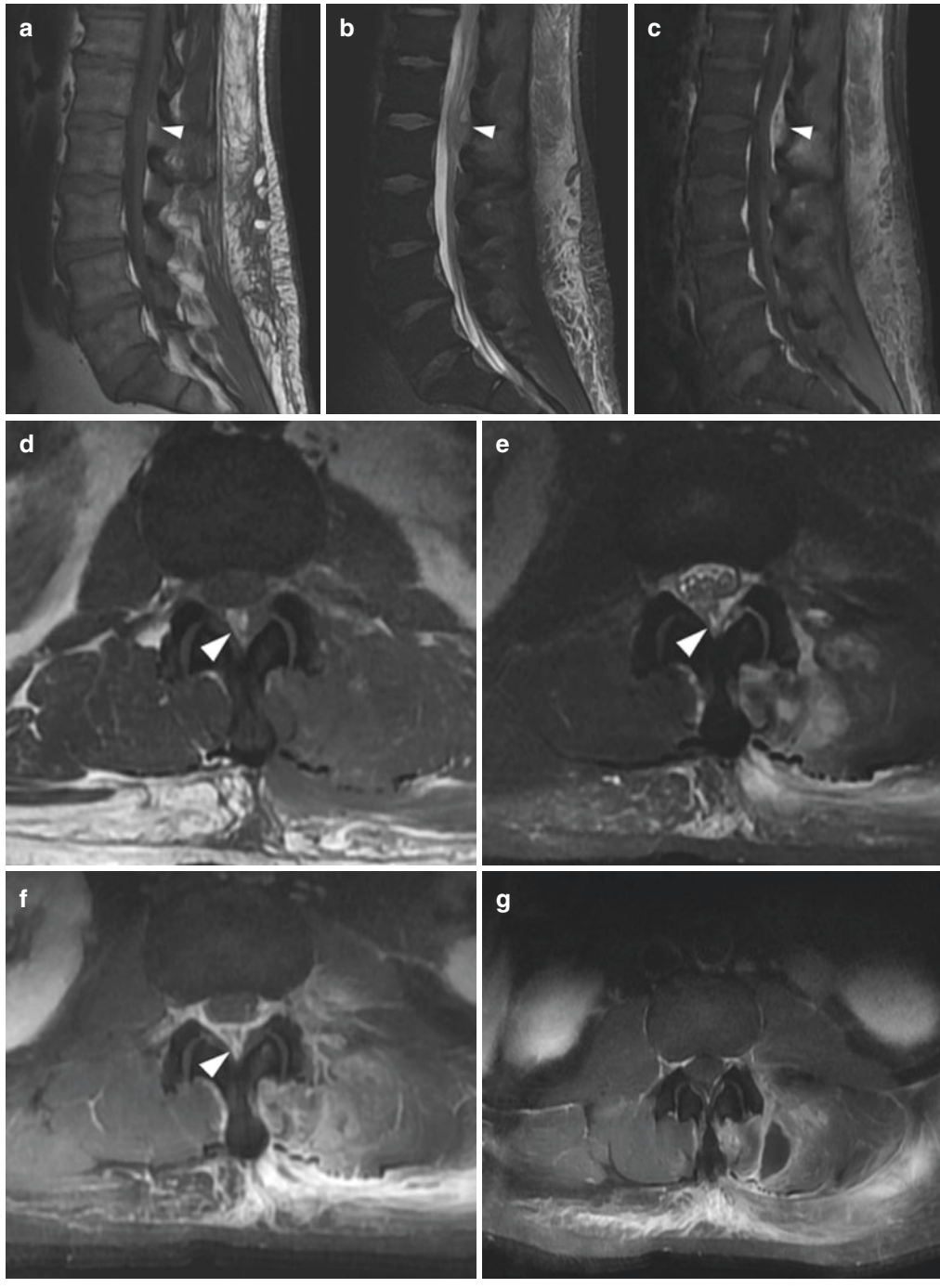

Fig. 7 A 49-year-old man with newly diagnosed diabetes mellitus presenting with left flank pain, WBC of 22.9×10^9/L and CRP of 340 mg/L. Sagittal (**a**) T1-W, (**b**) FS T2-W, and (**c**) contrast-enhanced FS T1-W MR images show enhancing posterior epidural abscess at L1–L2 level (arrowheads) with extensive associated subcutaneous edema in the lower back. Axial (**d**) T1-W, (**e**) FS T2-W, and (**f**) contrast-enhanced FS T1-W MR images at L1–L2 level show the epidural abscess (arrowheads) located adjacent to the left L1–L2 facet joint with surrounding inflammatory changes in the left paravertebral muscles. Additional (**g**) axial, (**h**) sagittal, and (**i**) coronal contrast-enhanced FS T1-W MR images show several rim-enhancing abscesses in the left paravertebral (mainly the erector spinae and multifidus) muscles at L2 and L3 levels. Blood cultures revealed methicillin-sensitive *Staphylococcus aureus* (MSSA) infection

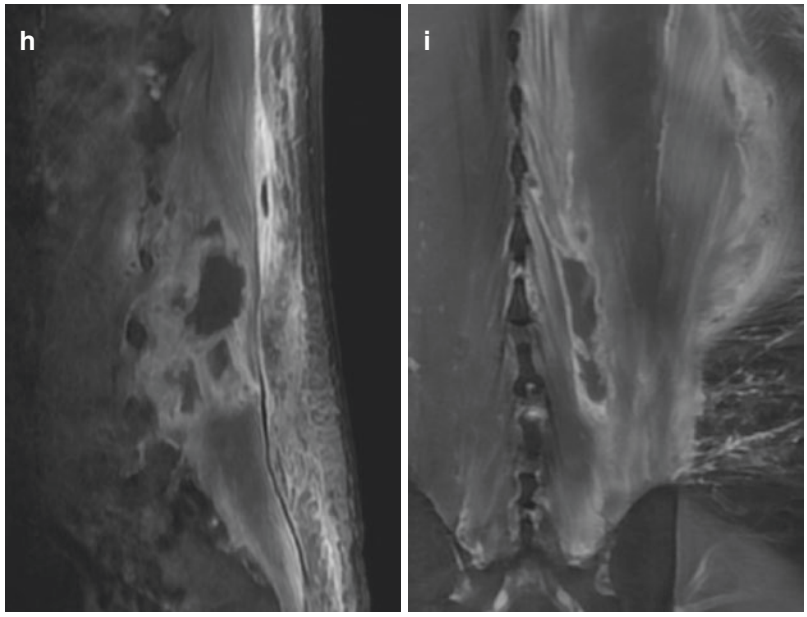

Fig. 7 (continued)

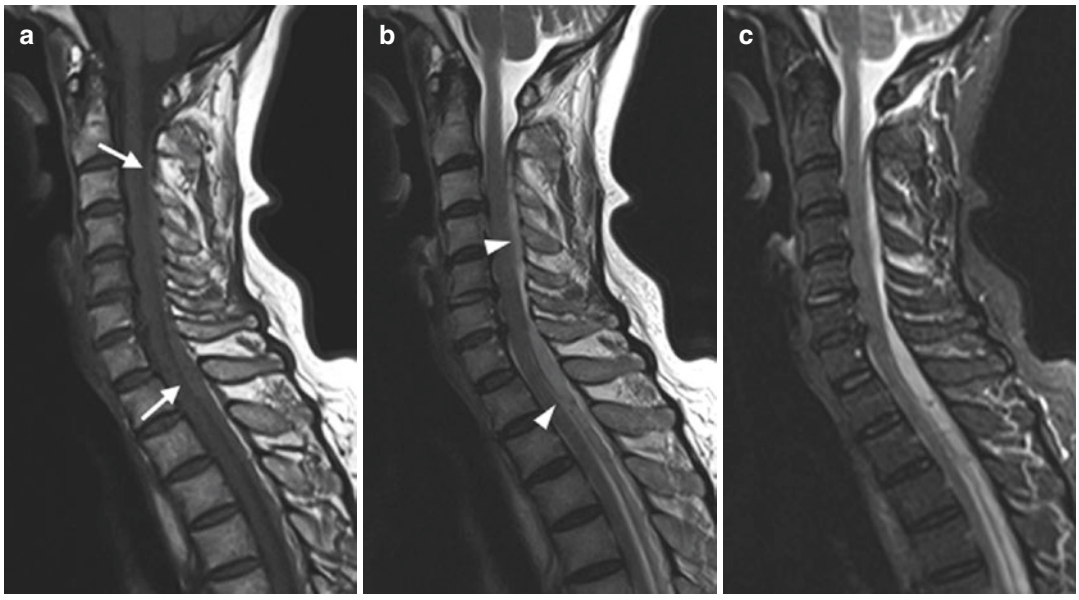

Fig. 8 Spontaneous epidural hematoma in a 47-year-old man presenting with sudden onset of neck pain. Sagittal (**a**) T1-W, (**b**) T2-W, (**c**) FS T2-W, and (**d**) contrast-enhanced FS T1-W MR images show an acute spontaneous posterior epidural hematoma extending from C2 to the upper thoracic spine. It appears slightly hyperintense to the cord on T1-W sequences (arrows). T2-signal is hyperintense relative to the cord but hypointense compared to CSF (arrowheads). Thin peripheral enhancement is seen posteriorly from T1 to T3 levels (curved arrows). Axial (**e**) T1-W, (**f**) FS T2-W, and (**g**) GRE T2*-W MR images taken at the C6 vertebral level show the right posterolateral location of the hematoma with slight compression of the adjacent cord (arrowheads). There is no significant susceptibility artifact on GRE image at this stage

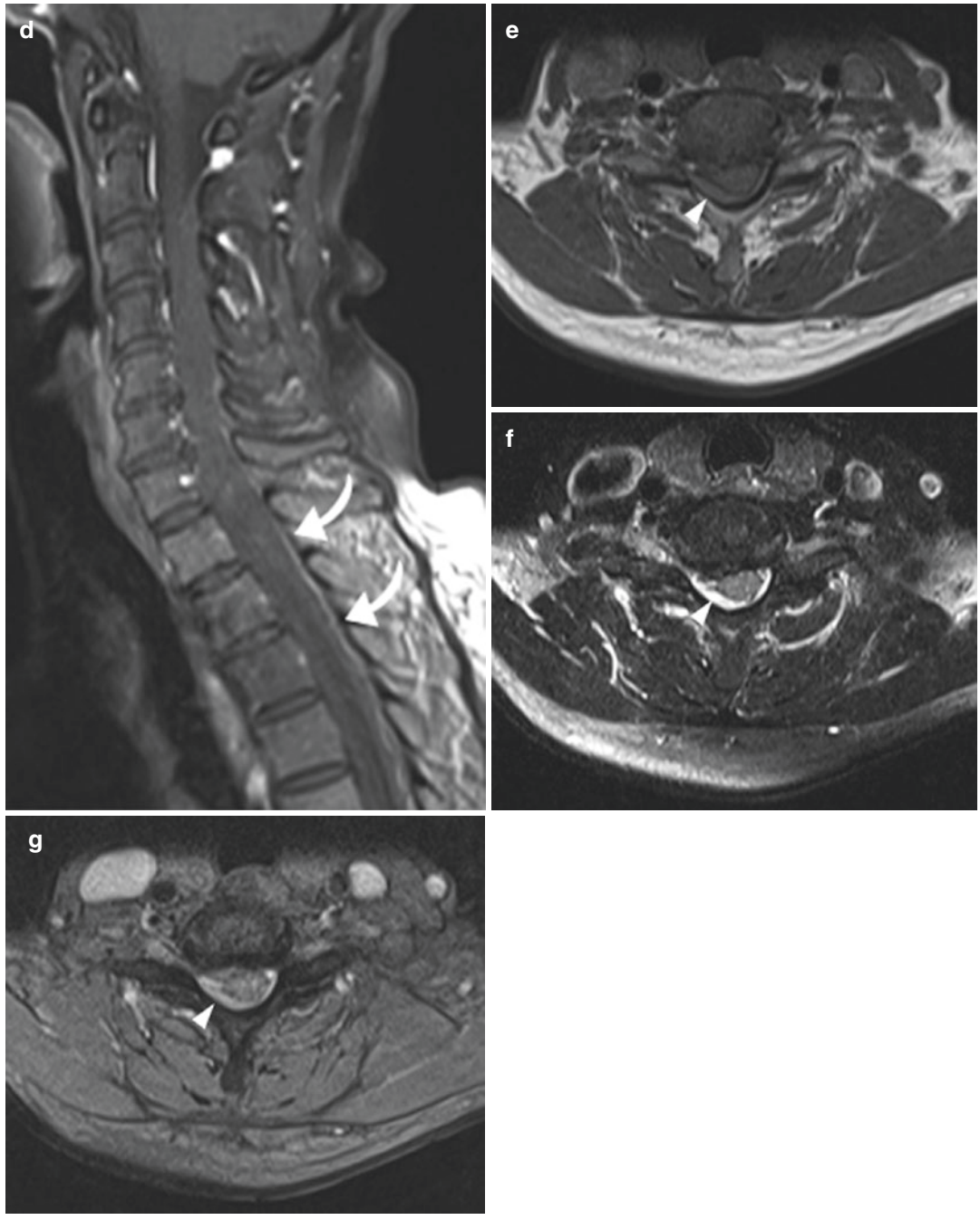

Fig. 8 (continued)

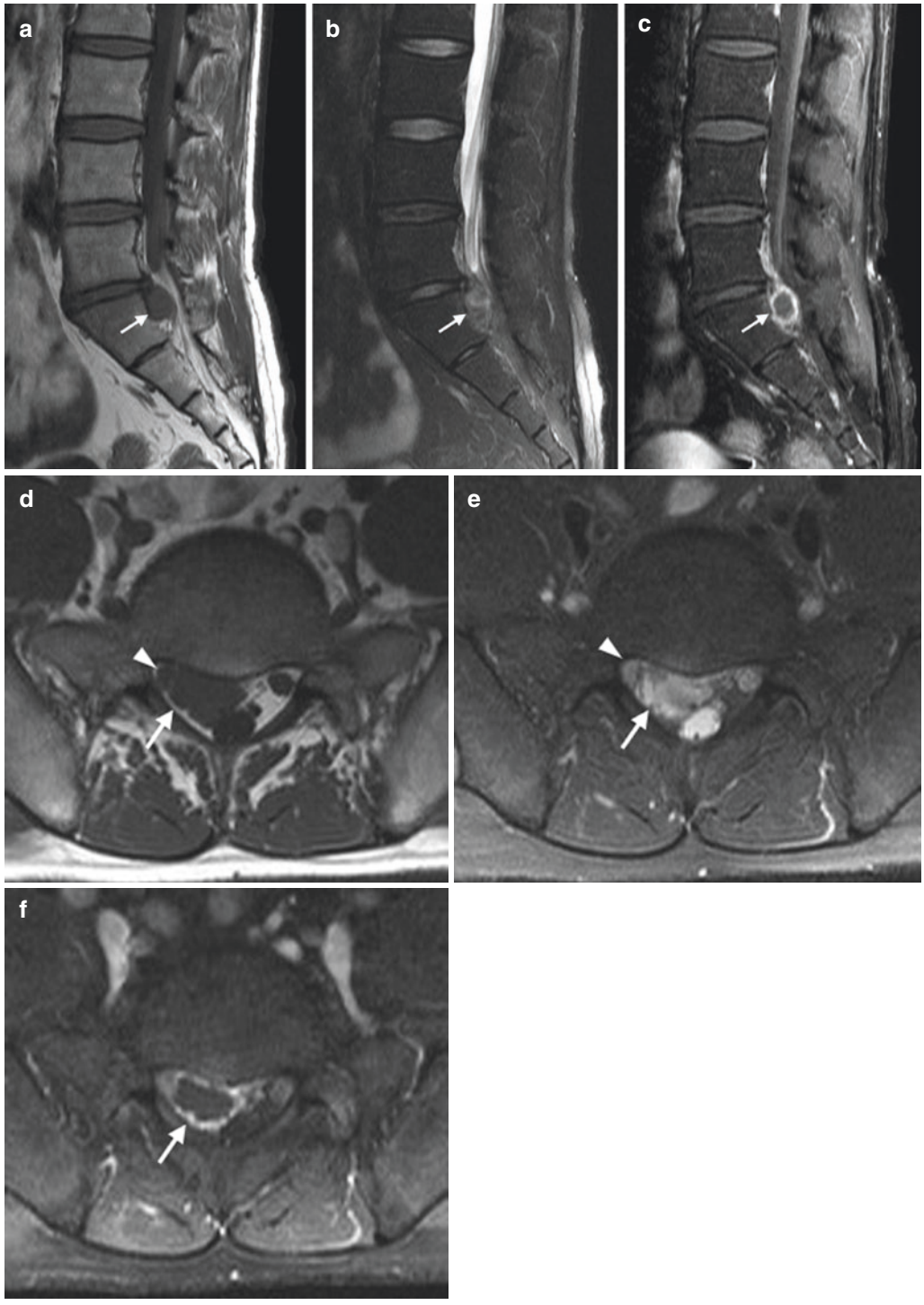

Fig. 9 Sequestered disk in a 31-year-old man presenting with low back pain and right sciatica. Sagittal (**a**) T1-W, (**b**) FS T2-W, and (**c**) contrast-enhanced FS T1-W and axial (**d**) T1-W, (**e**) FS T2-W, and (**f**) contrast-enhanced FS T1-W MR images show a T1-isointense, heterogeneous T2-hyperintense, and peripherally enhancing sequestered disk at S1 level (arrows) which had migrated from the L5/S1 disk. The right S1 nerve root is involved (arrowhead). There are no other clinical or imaging features to suggest spinal infection

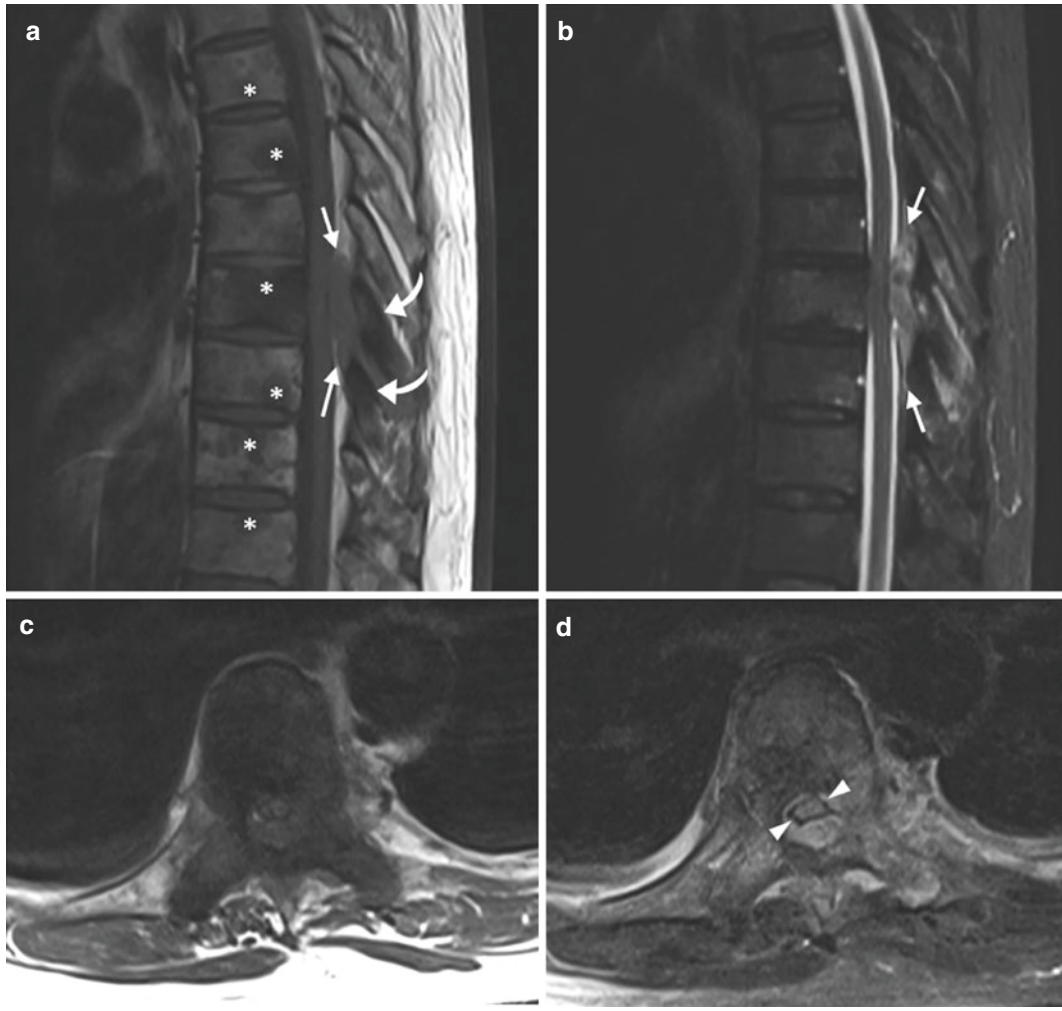

Fig. 10 Epidural tumor extension from vertebral metastases in a 71-year-old man with known metastatic prostate carcinoma presenting with bilateral lower limb weakness and recurrent falls. Sagittal (**a**) T1-W and (**b**) FS T2-W MR images show posterior epidural metastatic lesion at T8 level (arrows). There are multiple vertebral body lesions (asterisks) as well as the involvement of the adjacent posterior elements (curved arrows). Axial (**c**) T1-W and (**d**) FS T2-W MR images show a mass effect upon the compressed cord which is T2-hyperintense (arrowheads). Extensive tumor bony involvement is present

6 Treatment

The principles of treatment for SEA revolve around the relief of spinal cord compression and eradication of the offending microorganism. A multidisciplinary approach involving emergency physicians, spinal surgeons, radiologists, and infectious disease specialists is required (Sendi et al. 2008). Early surgical drainage within 24 h along with administration of systemic antibiotics is the treatment of choice in patients with neurological deficits. This serves the dual purpose of reducing neurological deficits from cord compression, as well as controlling sepsis. This is achieved by laminectomy and decompression of the affected spinal levels along with debridement of the abscess (Sendi et al. 2008) (Fig. 6). Proposed indications for surgical intervention

include worsening neurological deficits, persistent severe back pain, increasing body temperature, and elevated WBC (Baker et al. 1992).

Depending on local practice, empirical antibiotics may be commenced with coverage of the most common pathogens while awaiting the results of cultures and sensitivities. Subsequent therapy should be ideally tailored to specific organisms obtained from either blood cultures or specimens from the drainage of the abscess (Darouiche 2006; Sendi et al. 2008). Most patients receiving appropriate antibiotics show clinical improvement within 48 h of commencement of therapy (Hlavin et al. 1990). The duration of antibiotic treatment is variable and largely dependent on the presence of concomitant infection and response to treatment. They typically last from 4 to 8 weeks and up to 12 weeks in cases with associated vertebral osteomyelitis (Darouiche 2006; Sendi et al. 2008).

There has been a shift from conventional surgical treatment as the first line of intervention of SEA to medical therapy for patients without acute neurological deficit (Rigamonti et al. 1999; Siddiq et al. 2004; Curry Jr et al. 2005). Patients should be stratified according to clinical presentation, degree of neurological deficit, laboratory markers, and imaging findings to determine the most appropriate treatment strategy. Patients with elevated CRP greater than 115 mg/L, leukocytosis more than 12.5×10^9/L, bacteremia, and diabetes mellitus have been shown to have a 76.9% chance of medical failure. In these patients, close follow-up and frequent neurological evaluation are required for detection of neurological deterioration and to assess response to treatment (Patel et al. 2014). There should be a low threshold for consideration of surgical treatment. CT-guided needle aspiration may be considered for patients with posterior collections who have minimal neurological deficit or with high surgical risk, and who do not respond satisfactorily to antimicrobial treatment alone. It is a minimally invasive procedure with a low risk of dural puncture, if carefully performed by experienced musculoskeletal interventional radiologists under CT-guidance (Cwikiel 1991; Lyu et al. 2002) (Fig. 4).

Follow-up imaging has been recommended 4–8 weeks after commencement of treatment to evaluate for treatment response (Kowalski et al. 2006, 2007). Earlier follow-up imaging may be indicated in cases where there is poor response to treatment or to evaluate for postoperative complications (Fig. 6). No specific imaging finding has been found to correlate with the clinical status of the patient. Soft tissue findings, including paraspinal and epidural abscesses, tend to show improvement at this time, compared to vertebral infection which is more likely to persist or even worsen, despite successful medical treatment and improvement in clinical signs (Gillams et al. 1996; Visuri et al. 2005; Kowalski et al. 2007) (Figs. 2 and 3). Follow-up of clinical status and inflammatory biomarkers at 4–8 weeks may be helpful in identifying patients who may benefit from additional MRI (Kowalski et al. 2006). Further imaging studies at a later stage show no additional benefit, if clinical and laboratory investigations are unremarkable (Veillard et al. 2000).

7 Outcome and Prognosis

The outcome measures for SEA are mortality and recovery of neurological deficit (Sendi et al. 2008). Despite falling mortality rates since the early twentieth century, the rates reported in various studies have remained in the range of 2–20%, averaging 15% in the late 1990s (Khanna et al. 1996; Reihsaus et al. 2000). The causes of death are mainly due to severe sepsis in patients with multiple comorbidities. Other causes of death indirectly related to SEA are pulmonary embolism, meningitis, and pneumonia (Maslen et al. 1993; Rigamonti et al. 1999; Soehle and Wallenfang 2002; Butler et al. 2006). The eventual outcome for afflicted patients correlates closely with the duration and severity of neurological deficit before surgery or definitive treatment. Patients with stage 3 (sensory disturbances, motor weakness, bladder and bowel dysfunction) and stage 4 (paralysis or paresis) symptoms and a duration of symptoms of more than 24–36 h show the worst outcomes (Baker et al. 1975;

Rigamonti et al. 1999; Davis et al. 2004; Curry Jr et al. 2005). Rapid surgical intervention within 24 h has been shown to correlate with improved neurological recovery (Rigamonti et al. 1999; Curry Jr et al. 2005). MRI findings may also correlate with the outcome. Tung et al. (1999) reported that spinal stenosis of more than 50%, presence of peripheral enhancement, and an abscess length exceeding 3 cm were significantly associated with a worse clinical outcome. Unfortunately, up to one-third of patients diagnosed with SEA have been reported to have a poor outcome (Rigamonti et al. 1999; Soehle and Wallenfang 2002; Tang et al. 2002; Davis et al. 2004). Delay in diagnosis, identified in 85% of patients in the study of Davis et al. (2004), plays a significant role in unsatisfactory outcomes.

8 Conclusion

The diagnosis of SEA remains challenging in current medical practice. Nonspecific clinical signs and laboratory markers contribute to diagnostic delay and suboptimal management which may result in neurological deficit, irreversible paralysis, and life-threatening sepsis. Increased awareness of this condition, recognition of at-risk population, and thorough neurological assessment and evaluation of laboratory findings should raise the clinical suspicion for SEA and direct subsequent imaging studies. The ready availability of imaging modalities, especially MRI, and alternative treatment options such as CT-guided needle aspiration help pave the way for early diagnosis, prompt treatment, and improved outcomes in the management of SEA.

References

Angtuaco EJ, McConnell JR, Chadduck WM et al (1987) MR imaging of spinal epidural sepsis. AJR Am J Roentgenol 149:1249–1253

Arbelaez A, Restrepo F, Castillo M (2014) Spinal infections: clinical and imaging features. Top Magn Reson Imaging 23:303–314

Baker AS, Ojemann RG, Swartz MN et al (1975) Spinal epidural abscess. N Engl J Med 293:463–468

Baker AS, OJemann RG, Baker RA (1992) To decompress or not to decompress—spinal epidural abscess. Clin Infect Dis 15:28–29

Batson O (1957) The vertebral vein system. Caldwell lecture 1956. Am J Roentgenol Radium Ther Nucl Med 78:195–212

Browder J, Meyers R (1941) Pyogenic infections of the spinal epidural space: a consideration of the anatomic and physiologic pathology. Surgery 10:296–308

Butler JS, Shelly MJ, Timlin M et al (2006) Nontuberculous pyogenic spinal infection in adults: a 12-year experience from a tertiary referral center. Spine 31:2695–2700

Chee DWY, Peh WCG (2009) Clinics in diagnostic imaging (127). Singapore Med J 50:834–839

Curry WT Jr, Hoh BL, Amin-Hanjani S et al (2005) Spinal epidural abscess: clinical presentation, management, and outcome. Surg Neurol 63:364–371

Cwikiel W (1991) Percutaneous drainage of abscess in psoas compartment and epidural space. Case report and review of the literature. Acta Radiol 32:159–161

Dagirmanjian A, Schils J, McHenry MC (1999) MR imaging of spinal infections. Magn Reson Imaging Clin N Am 7:525–538

Darouiche RO (2006) Spinal epidural abscess. N Engl J Med 355:2012–2020

Darouiche RO, Hamill RJ, Greenberg SB et al (1992) Bacterial spinal epidural abscess: review of 43 cases and literature survey. Medicine (Baltimore) 71:369–385

Davis DP, Wold RM, Patel RJ et al (2004) The clinical presentation and impact of diagnostic delays on emergency department patients with spinal epidural abscess. J Emerg Med 26:285–291

Feldenzer JA, McKeever PE, Schaberg DR et al (1988) The pathogenesis of spinal epidural abscess: microangiopathic studies in an experimental model. J Neurosurg 69:110–114

Gerstein N (2007) Spinal epidural abscess. N Engl J Med 356:639

Gillams AR, Chaddha B, Carter AP (1996) MR appearances of the temporal evolution and resolution of infectious spondylitis. AJR Am J Roentgenol 166:903–907

Go JL, Rothman S, Prosper A et al (2012) Spine infections. Neuroimaging Clin N Am 22:755–772

Grewal S, Hocking G, Wildsmith JAW (2006) Epidural abscesses. Br J Anaesth 96:292–302

Heusner AP (1948) Nontuberculous spinal epidural infections. N Engl J Med 239:845–854

Hlavin ML, Kaminski HJ, Ross JS et al (1990) Spinal epidural abscess: a ten-year perspective. Neurosurgery 27:177–184

Ju KL, Kim SD, Melikian R et al (2015) Predicting patients with concurrent noncontiguous spinal epidural abscess lesions. Spine J 15:95–101

Kaufman DM, Kaplan JG, Litman N (1980) Infectious agents in spinal epidural abscesses. Neurology 30:844–850

Khanna RK, Malik GM, Rock JP et al (1996) Spinal epidural abscess: evaluation of factors influencing outcome. Neurosurgery 39:958–964

Kowalski TJ, Berbari EF, Huddleston PM et al (2006) Do follow-up imaging examinations provide useful prognostic information in patients with spine infection? Clin Infect Dis 43:172–179

Kowalski TJ, Layton KF, Berbari EF et al (2007) Follow-up MR imaging in patients with pyogenic spine infections: lack of correlation with clinical features. AJNR Am J Neuroradiol 28:693–699

Küker W, Mull M, Mayfrank L et al (1997) Epidural spinal infection; variability of clinical and magnetic resonance imaging findings. Spine 22:544–551

Lyu RK, Chen CJ, Tang LM et al (2002) Spinal epidural abscess successfully treated with percutaneous, computed tomography-guided, needle aspiration and parenteral antibiotic therapy: case report and review of the literature. Neurosurgery 51:509–512

Maslen DR, Jones SR, Crislip MA et al (1993) Spinal epidural abscess. Optimizing patient care. Arch Intern Med 153:1713–1721

Moritani T, Kim J, Capizzano AA et al (2014) Pyogenic and non-pyogenic spinal infections: emphasis on diffusion-weighted imaging for the detection of abscesses and pus collections. Br J Radiol 87:20140011

Muffoletto AJ, Ketonen LM, Mader JT et al (2001) Hematogenous pyogenic facet joint infection. Spine 26:1570–1576

Numaguchi Y, Rigamonti D, Rothman MI et al (1993) Spinal epidural abscess: evaluation with gadolinium-enhanced MR imaging. Radiographics 13:545–559

Patel AR, Alton T, Bransford R et al (2014) Spinal epidural abscesses: risk factors, medical versus surgical management, a retrospective review of 128 cases. Spine J 14:326–330

Peterson JA, Paris P, Williams AC (1987) Acute epidural abscess. Am J Emerg Med 5:287–290

Pierce JL, Donahue JH, Nacey NC et al (2018) Spinal hematomas: what a radiologist needs to know. Radiographics 38:1516–1535

Ratcliffe JF (1980) The arterial anatomy of the adult human lumbar vertebral body: a microarteriographic study. J Anat 131:57–79

Reihsaus E, Waldbaur H, Seeling W (2000) Spinal epidural abscess: a meta-analysis of 915 patients. Neurosurg Rev 23:175–204

Richardson J, Groen GJ (2005) Applied epidural anatomy. Contin Educ Anaesth Crit Care Pain 5:98–100

Rigamonti D, Liem L, Sampath P et al (1999) Spinal epidural abscess: contemporary trends in etiology, evaluation, and management. Surg Neurol 52:189–196

Rothman SL (1996) The diagnosis of infections of the spine by modern imaging techniques. Orthop Clin North Am 27:15–31

Sapico FL (1996) Microbiology and antimicrobial therapy of spinal infections. Orthop Clin North Am 27:9–13

Sendi P, Bregenzer T, Zimmerli W (2008) Spinal epidural abscess in clinical practice. QJM 101:1–12

Siddiq F, Chowfin A, Tight R et al (2004) Medical vs surgical management of spinal epidural abscess. Arch Intern Med 164:2409–2412

Soehle M, Wallenfang T (2002) Spinal epidural abscesses: clinical manifestations, prognostic factors, and outcomes. Neurosurgery 51:79–85

Stäbler A, Reiser MF (2001) Imaging of spinal infection. Radiol Clin North Am 39:115–135

Sundaram VK, Doshi A (2016) Infections of the spine: a review of clinical and imaging findings. Appl Radiol 45:10–20

Tang HJ, Lin HJ, Liu YC et al (2002) Spinal epidural abscess—experience with 46 patients and evaluation of prognostic factors. J Infect 45:76–81

Tins BJ, Cassar-Pullicino VN (2004) MR imaging of spinal infection. Semin Musculoskelet Radiol 8:215–229

Tsuchiya K, Osawa A, Katase S et al (2003) Diffusion-weighted MRI of subdural and epidural empyemas. Neuroradiology 45:220–223

Tung GA, Yim JW, Mermel LA et al (1999) Spinal epidural abscess: correlation between MRI findings and outcome. Neuroradiology 41:904–909

Veillard E, Guggenbuhl P, Morcet N et al (2000) Prompt regression of paravertebral and epidural abscesses in patients with pyogenic discitis. Sixteen cases evaluated using magnetic resonance imaging. Joint Bone Spine 67:219–227

Visuri T, Pihlajamaki H, Eskelin M (2005) Long-term vertebral changes attributable to postoperative lumbar discitis: a retrospective study of six cases. Clin Orthop Relat Res 433:97–105

Wiley A, Trueta J (1959) The vascular anatomy of the spine and its relationship to pyogenic vertebral osteomyelitis. J Bone Joint Surg Br 41:796–809

Wong D, Raymond NJ (1998) Spinal epidural abscess. N Z Med J 111:345–347

Imaging of Spinal Brucellosis

Mouna Chelli Bouaziz, Mohamed Fethi Ladeb, Hend Riahi, Wafa Achour, Aida Berriche, Lamia Ammari, and Soumaya Rammeh

Contents

M. Chelli Bouaziz (✉) · M. F. Ladeb · H. Riahi
Department of Radiology, MT Kassab Institute of Orthopaedics, Tunis, Tunisia

Faculty of Medicine of Tunis, Tunis-El Manar University, Tunis, Tunisia
e-mail: bouaziz_mouna@yahoo.fr; fethiladeb@hotmail.fr; hend.riahi@gmail.com

W. Achour
Laboratory Department, National Bone Marrow Transplant Center, Tunis, Tunisia

Faculty of Medicine of Tunis, Tunis-El Manar University, Tunis, Tunisia
e-mail: wafaachour@gmail.com

A. Berriche · L. Ammari
Department of Infectious Diseases, Rabta Hospital, Tunis, Tunisia

Faculty of Medicine of Tunis, Tunis-El Manar University, Tunis, Tunisia
e-mail: aida.berricheg@gmail.com; lamia_ammarib@yahoo.fr

S. Rammeh
Department of Pathology, Charles Nicolle Hospital, Tunis, Tunisia

Faculty of Medicine of Tunis, Tunis-El Manar University, Tunis, Tunisia
e-mail: rammehs@yahoo.fr

© The Author(s), under exclusive license to Springer Nature Switzerland AG 2021
M. F. Ladeb, W. C. G. Peh (eds.), *Imaging of Spinal Infection*,
Medical Radiology Diagnostic Imaging, https://doi.org/10.1007/978-3-030-70459-9_10

Abstract

Brucellosis is a systemic infection caused by facultative intra-cellular bacteria of the *Brucella* genus that may involve multiple organs and tissues. The disease is a zoonosis of worldwide distribution, occurring in all continents, but is more frequent in many countries of the Middle East, the Mediterranean region, and Latin America. The spine is the most common site of musculoskeletal involvement, followed by the sacroiliac joints. This chapter aims to assess the clinical, biological, and imaging features of spinal brucellosis.

Abbreviations

CT	Computed tomography
MRI	Magnetic resonance imaging

1 Introduction

Brucellosis is one of the most common zoonoses worldwide (Kursun et al. 2013; Kazak et al. 2016). It remains a major public health problem, mainly in the Mediterranean region, the Middle East, and parts of Central and South America (Harman et al. 2001). The disease affects mainly young and middle-aged adults, with infants and elderly patients being less vulnerable (Sharif et al. 1989). Skeletal brucellosis is a very old disease, with the earliest published case being dated to the Middle Bronze Age. Other studies demonstrated that spinal brucellosis occasionally affected our ancestors 2.3–2.5 million years ago. The disease would also almost certainly have been endemic in Roman society and during the Middle Ages (D'Anastasio et al. 2011).

Brucellosis is transmitted to humans by direct contact with infected animals; through damaged skin, nasal or conjunctival mucosa, or consumption of unpasteurized milk and milk products obtained from infected animals (Kursun et al. 2013; Kazak et al. 2016); or by airborne transmission through contaminated aerosols in laboratories and meat-packing plants (Sharif et al. 1989). It is more frequently transmitted by occupational exposure in endemic countries. The causative agent of brucellosis is a small, gram-negative coccobacillus from the *Brucella* genus. Four of these are known to produce disease in humans, namely, *Brucella abortus*, *B. melitensis*, *B. suis*, and *B. canis* (Güzey et al. 2007).

Brucellosis is a multisystem disease, and patients may present with a broad spectrum of clinical manifestations and develop various complications. Almost every organ can be affected.

Musculoskeletal complications are the leading complications of brucellosis. In brucellosis, any region in the musculoskeletal system may be affected (Hamza et al. 1990; Zorompala et al. 2000; Pourbagher et al. 2006). The most important clinical forms of osteoarticular involvement are arthritis, spondylodiscitis, bursitis, tenosynovitis, and osteomyelitis. Arthritis is usually observed in large joints and especially in the sacroiliac joint (Turan et al. 2011).

2 Pathophysiology

Brucellar infection mainly affects organs rich in mononuclear phagocytes, such as the liver, spleen, lymph nodes, and bone marrow (Resnick 1995). The type of skeletal involvement depends on the patient's age (Turgut Tali 2004). The spine is the targeted site in the elderly, while the sacroiliac joints and knee arthritis predominate in children and young adults. Musculoskeletal complications may have a genetic predisposition, as recent data suggest an association with HLA-B39 (Pappas et al. 2005).

Spinal brucellosis represents 6–58% of musculoskeletal infection sites (Sharif et al. 1990).

It typically occurs in men over 40 years of age. The most affected site is the lumbar spine (60%), particularly at the L4–L5 level, followed by thoracic (19%) and cervical spine (12%). More than one spinal level is affected in 6–14% of the cases. Involvement of the spine may be either focal or diffuse (Hamza et al. 1990; Sharif et al. 1990; Al-Shahed et al. 1994; Resnick 1995; Ben Taarit et al. 2002; Pourbagher et al. 2006; Turan et al. 2011).

The focal form is confined to the anterior part of the vertebral body. This typically occurs in the anterosuperior corner of a lumbar vertebra at the discovertebral junction because of its rich blood supply (Hamza et al. 1990; Sharif et al. 1990). The diffuse form may involve the entire vertebral body and extend to the adjacent disk, paravertebral, and epidural space. Infection diffuses via the ligaments and vascular communications. Facet joint arthritis is uncommon (Hamza et al. 1990; Sharif et al. 1990; Resnick 1995; Ben Taarit et al. 2002; Yin et al. 2015). Soft tissue involvement typically results in the formation of small and well-defined abscess with smooth walls.

3 Clinical Features

Kulowski and Vinke first described involvement of the spine in brucellosis in 1932 (Arkun and Mete 2011). Clinical symptoms of spinal brucellosis may include manifestations of chronic infection, such as fever, night sweats, malaise, anorexia, and spinal pain of variable intensity. Physical examination may reveal hepatomegaly and splenomegaly. There are usually localized signs such as back pain or intercostal pain, with tenderness on palpation, segmental spinal stiffness, and paravertebral muscle contracture. It is uncommon for brucellar spondylodiscitis to present with spinal cord or nerve root compression. However, neurological deficits such as sensory, motor, and reflex changes can be detected (Arkun and Mete 2011). The long latent stage between the onset of symptoms and the appearance of the radiological changes (from 2 to 8 weeks) may prevent early diagnosis (Al-Shahed et al. 1994).

4 Imaging Features

Initial radiographs of the spine and pelvis may be normal. Radiographic manifestations usually appear 3–5 weeks after the onset of clinical symptoms. Focal erosions of the superior or inferior vertebral body corner (brucellar epiphysitis) are characteristic of brucellosis (Fig. 1). Focal anterior or diffuse decrease in disk height is very frequent. A vacuum phenomenon may be

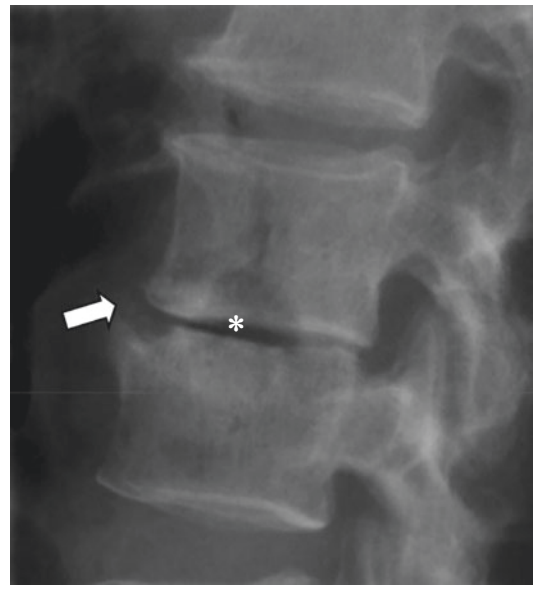

Fig. 1 L2/L3 brucella spondylodiscitis : Lateral radiograph of the lumbar spine show erosion of the antero-superior angle of L3 vertebra with parrot beak appearance (arrow), disc narrowing and vacuum phenomenon (*)

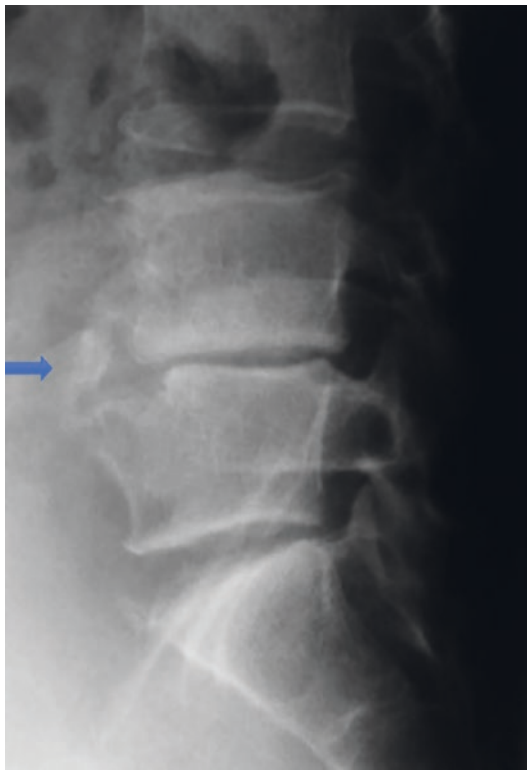

Fig. 2 Brucellar spondylodiscitis. Lateral radiograph of the lumbar spine shows erosion of anterosuperior corner of L5 vertebral body with disk collapse and the parrot beak appearance (arrow)

observed, especially in the anterior part of the disk, possibly secondary to ischemic changes in the disk, with subsequent necrosis (Sharif et al. 1990; Chelli Bouaziz et al. 2008) (Fig. 1).

Bone destruction is less important than in tuberculous spondylodiscitis. Perilesional bone formation with osteophytes at the anterior vertebral corners (parrot beak appearance) is typical (Fig. 2). Productive bone changes occur earlier than in tuberculous spondylodiscitis. Because bony remodelling may progress slowly, radiographical changes might not be easy to distinguish from those of degenerative disease. Evidence of infective spondylodiscitis is best documented by bone scintigraphy, computed tomography (CT), or magnetic resonance imaging (MRI) (Al-Shahed et al. 1994; Turgut et al. 2006).

Bone scintigraphy enables early total body assessment of the extent and distribution of musculoskeletal involvement, with sensitivity ranging from 69 to 91% (El-Desouki 1991; Yin et al. 2015). Several scintigraphic patterns may be observed, with increased uptake limited to the anterior vertebral body corner being highly suggestive of brucellosis (Lifeso et al. 1985; Madkour et al. 1988; Sharif et al. 1990). 2-Deoxy-2-[fluorine-18]fluoro-D-glucose positron emission tomography CT (18F-FDG PET/CT) is not routinely performed. It may be used in atypical forms to evaluate the extent of disease and show high uptake in the same areas (Alduraibi et al. 2019).

CT yields positive findings early in the course of the disease. It shows disk height loss and vertebral destruction, which may not be visible on initial radiographs (Fig. 3). A small amount of disk gas may be observed in 25–30% of the cases (Zorompala et al. 2000) (Fig. 4). The extent of the inflammatory process can be also defined using CT (Figs. 4 and 5). Paravertebral abscess is easily diagnosed after intravenous administration of contrast agent (Fig. 6). The intra-spinal extent of epidural abscesses causing posterior displacement of the dural sac can be shown on contrast-enhanced CT, but these changes are better defined on MRI (Hamza et al. 1990; Sharif et al. 1990; Ben Taarit et al. 2002).

CT and MRI allow early detection of the bony destructive focus, the extent of the inflammatory process, and the location of the epidural abscess. In patients with neural arch brucellosis, the bony destructive focus is usually located in the spinous or transverse process, the inflammatory region mainly involves the local paravertebral muscles, and the epidural abscess is positioned posterior to the dural sac. In patients with brucellar spondylitis, the bony destructive focus and inflammatory area are located in the vertebrae, while in patients with brucellar spondylodiscitis, they are located in the vertebral end plate and intervertebral disk. The epidural abscess is positioned anterior to the dural sac in both brucellar spondylitis and spondylodiscitis (Yin et al. 2015).

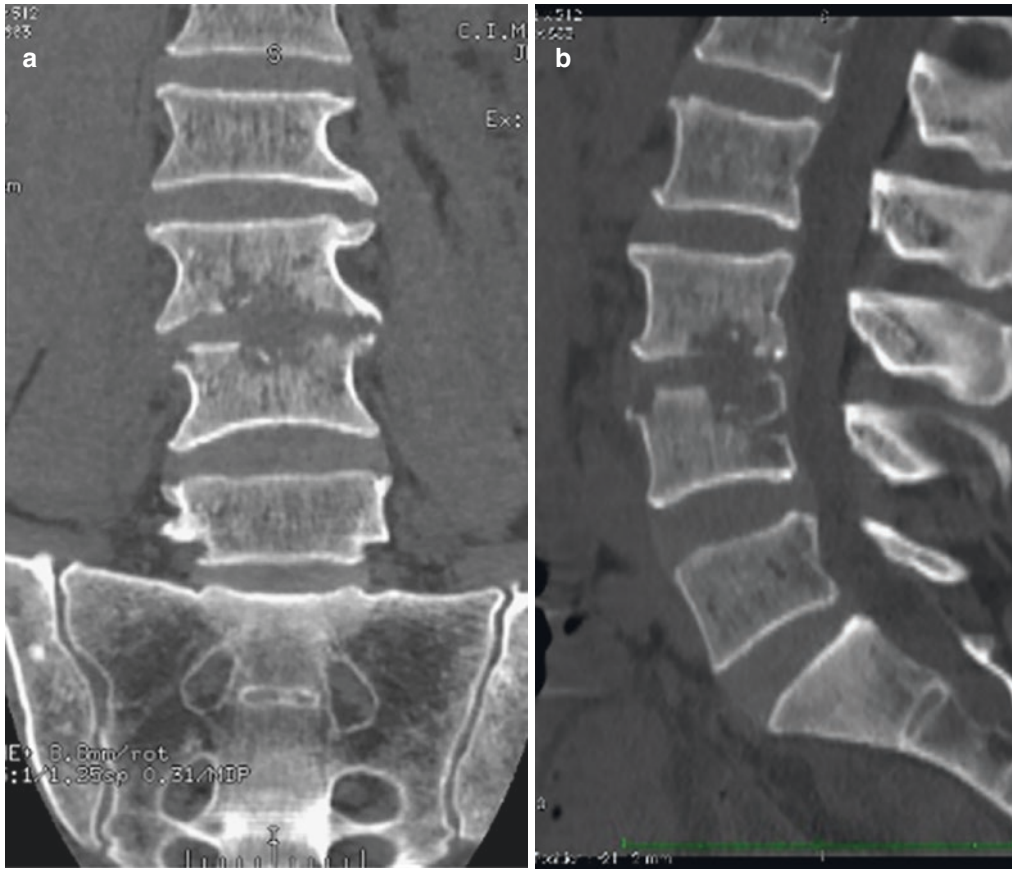

Fig. 3 Brucellar spondylodiscitis in a 63-year-old man. (**a**) Coronal and (**b**) sagittal CT images show L2/L3 disk narrowing with destruction of the adjacent vertebral end plates

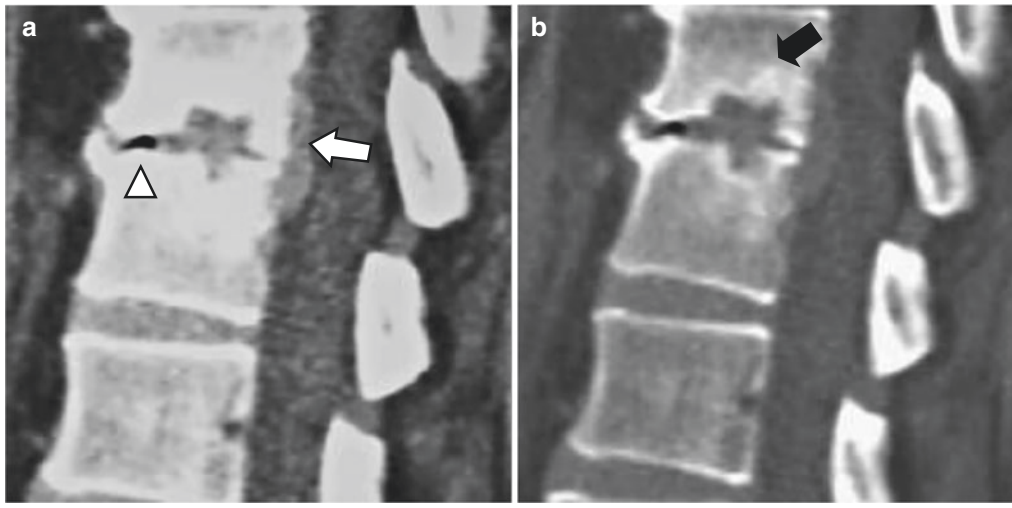

Fig. 4 L1/L2 brucellar spondylodiscitis. Sagittal CT images taken in (**a**) soft tissue and (**b**) bone window settings show vertebral end-plate destruction (black arrow), parrot beak appearance with anterior vacuum phenomenon (arrowhead), and epidural extension (white arrow)

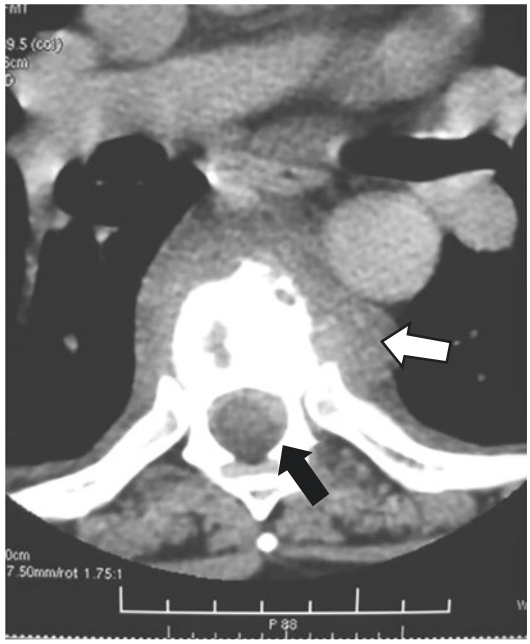

Fig. 5 T5/T6 brucellar spondylodiscitis. Axial CT image shows paravertebral (white arrow) and epidural (black arrow) soft tissue involvement

MRI is the method of choice for the diagnosis and follow-up of spinal brucellosis. MRI has a high sensitivity for detecting the disease in the early stages and provides excellent definition of paravertebral and epidural extension (Sharif et al. 1990; Ben Taarit et al. 2002; Pourbagher et al. 2006) (Fig. 7). It allows the detection of otherwise unsuspected additional non-contiguous spinal foci (Fig. 8) and sacroiliac arthritis (Zorompala et al. 2000). In acute spinal brucellosis, T1-weighted MR images show intermediate signal intensity of the intervertebral disk and signal hypointensity of the adjacent vertebral bodies. The signal in these areas becomes hyperintense on T2-weighted MRI sequences, with either a homogeneous or heterogeneous pattern. Intravenous administration of contrast agent allows better definition of the spinal inflammatory lesions (Hamza et al. 1990; Sharif et al. 1990) and a more complete assessment of soft tissue involvement and epidural extent (Fig. 9). These features are best shown when

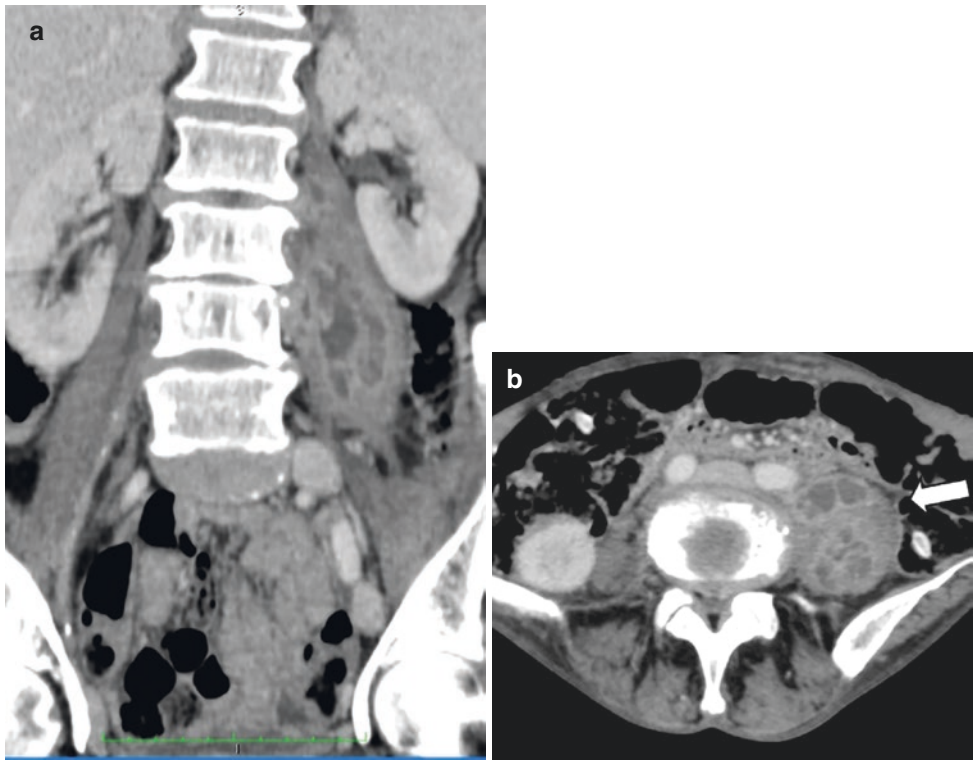

Fig. 6 Lumbar spine brucellar spondylodiscitis. (**a**) Coronal and (**b**) axial contrast-enhanced CT images show a large abscess within the left psoas muscle (arrow)

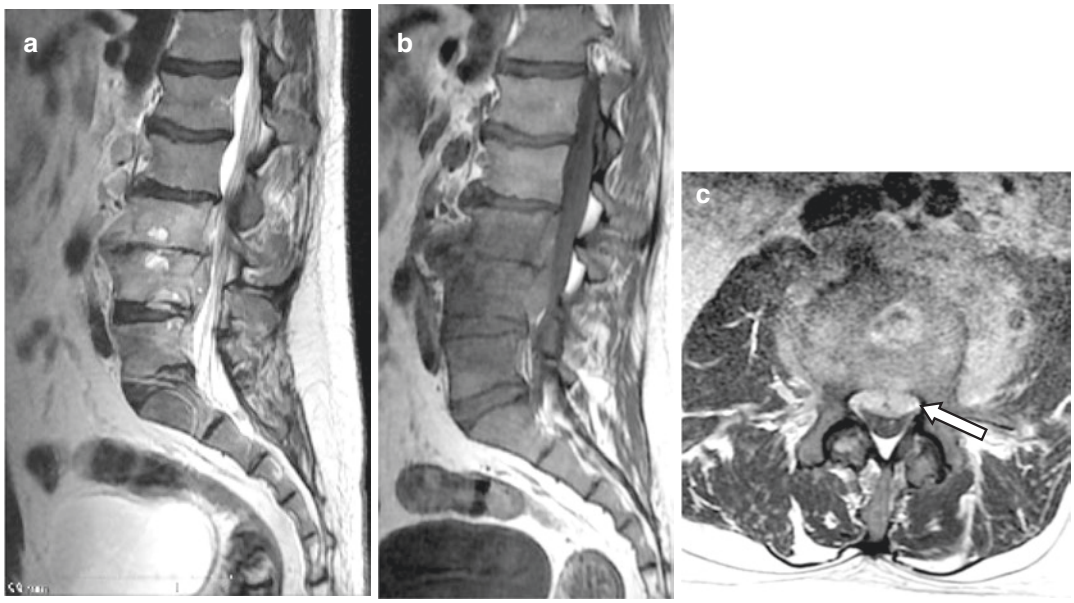

Fig. 7 Brucellar spondylodiscitis in a 40-year-old man. Sagittal (**a**) T2-W and (**b**) T1-W MR images show intermediate signal intensity of a narrowed L3/L4 intervertebral disk and T1-hypointense signal of the adjacent L3 and L4 vertebral bodies, which are T2-hyperintense. (**c**) Axial contrast-enhanced T1-W MR image allows a better assessment of soft tissue involvement and epidural extent (arrow)

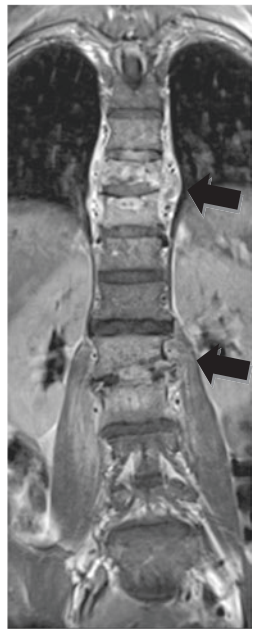

Fig. 8 Multilevel spinal brucellosis. Coronal contrast-enhanced T1-W MR image shows non-contiguous thoracic and lumbar spine involvement

fat-suppression techniques are applied to the contrast-enhanced images. Paravertebral abscesses are observed in approximately 30% of cases and are typically characterized by its small size and well-defined margins (Harman et al. 2001).

Spinal brucellosis may take many unusual and atypical forms because of its location or imaging features. An atypical form is pseudo-Pott brucellar spondylitis which refers to extensive bone destruction and large or calcified paraspinal soft tissue collection (Figs. 10 and 11). Unusual locations are cervical, thoracic, and multifocal spine involvement (Fig. 12) (Hamza et al. 1990; Chelli Bouaziz et al. 2010; Yang et al. 2014). Other atypical imaging features include isolated osteitis of the vertebral body (Fig. 13) and neural arch (Fig. 14) and T2 signal hypointensity of the intervertebral disk (Fig. 15) (Sharif et al. 1990; Al-Shahed et al. 1994; Resnick 1995; Zorompala et al. 2000). Isolated vertebral involvement is a rare presentation of spinal brucellosis which may lead to a vertebral collapse (Ekici et al. 2014).

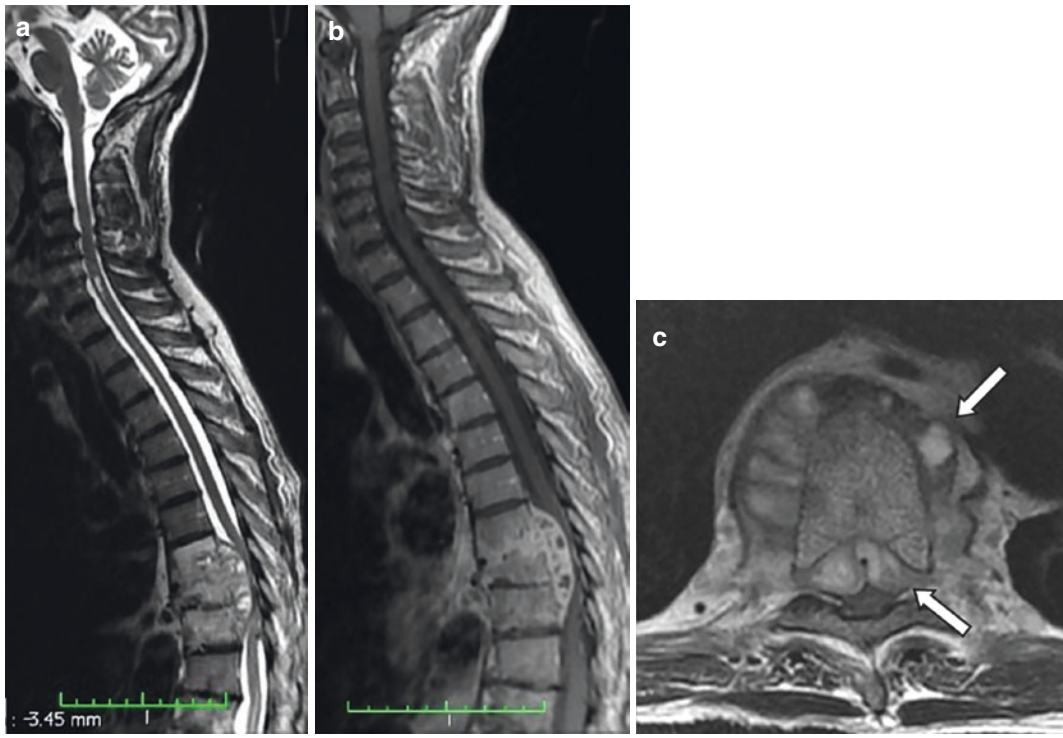

Fig. 9 Brucellar spondylodiscitis of the thoracic spine with spinal cord compression. Sagittal (**a**) T2-W and (**b**) contrast-enhanced T1-W MR images show hyperintense signal of T8, T9, and T10 vertebral bodies and intervertebral disks associated with a large epidural abscess resulting in the compression of the spinal cord. (**c**) Axial T2-W MR image shows the well-defined appearance of paravertebral and epidural abscess (arrows)

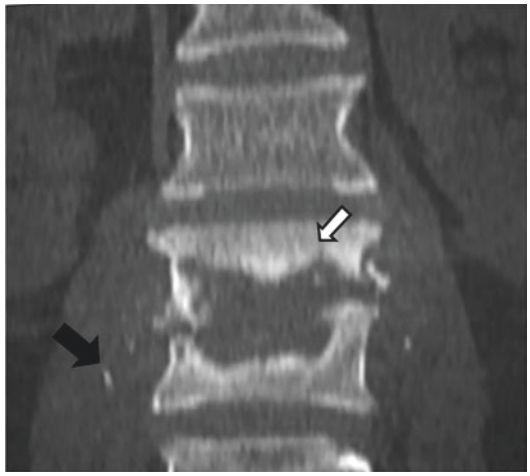

Fig. 10 Pseudo-Pott brucellar spondylodiscitis. Coronal CT image shows extensive destruction of vertebral end plates surrounded by bone sclerosis (white arrow) and the presence of small paravertebral soft tissue calcifications (black arrow)

5 Differential Diagnosis

Degenerative disk disease is the main differential diagnosis of spinal brucellosis, particularly when intradiscal gas is observed together with vertebral bone sclerosis and osteophytosis. Tuberculous spondylodiscitis and pyogenic spondylodiscitis should also be considered in the differential diagnosis (Resnick 1995; Arkun and Mete 2011). Marked destruction, vertebral body collapse, gibbus deformity, large soft tissue abscesses, and paraspinal calcification are the main differentiating findings of the tuberculous spondylodiscitis.

The co-infection of *M. tuberculosis* and *B. melitensis* is rare, and the exact mechanism of this co-infection remains unclear. Macrophage dysfunction in patients with tuberculosis may be associated with this mechanism (Ekici et al. 2014). Other findings that are reported to be

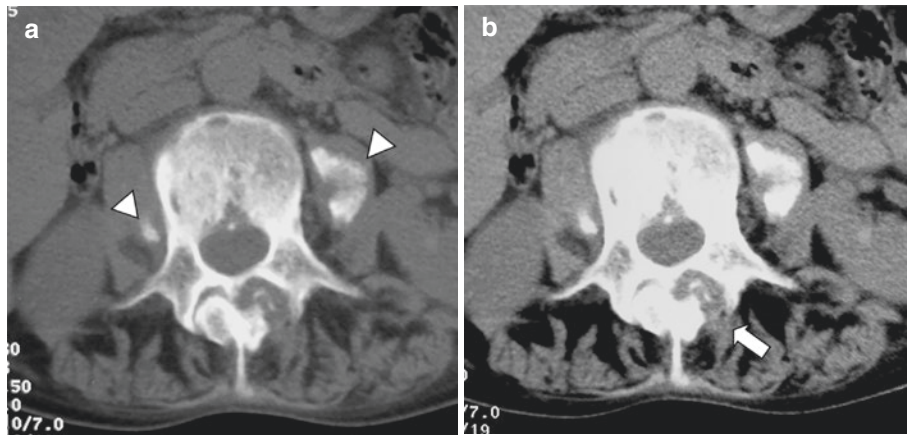

Fig. 11 Pseudo-Pott brucellar spondylodiscitis. Axial CT images taken in (**a**) bone and (**b**) soft tissue window settings show bilateral calcified psoas abscesses (arrowheads) associated with destruction of the left facet joint (white arrow)

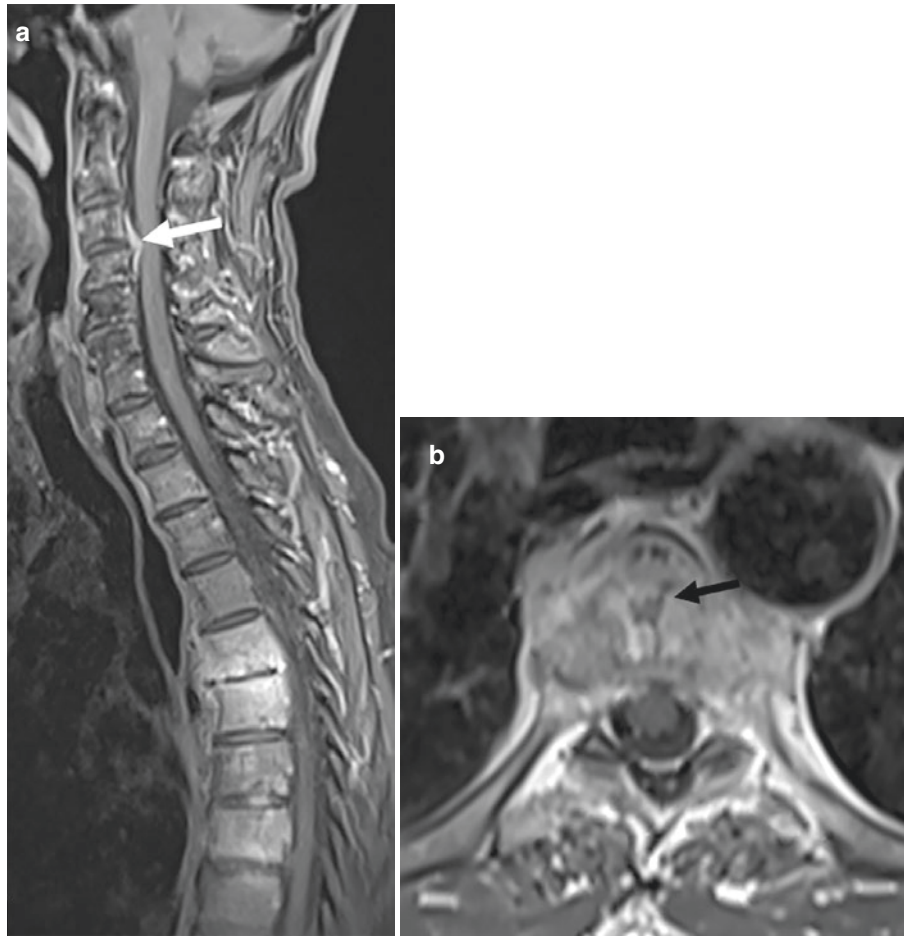

Fig. 12 Atypical brucellar spondylodiscitis. (**a**) Sagittal and (**b**) axial contrast-enhanced T1-W MR images show multifocal involvement of the cervical and thoracic spine with an epidural phlegmon (white arrow) and intraosseous abscess (black arrow)

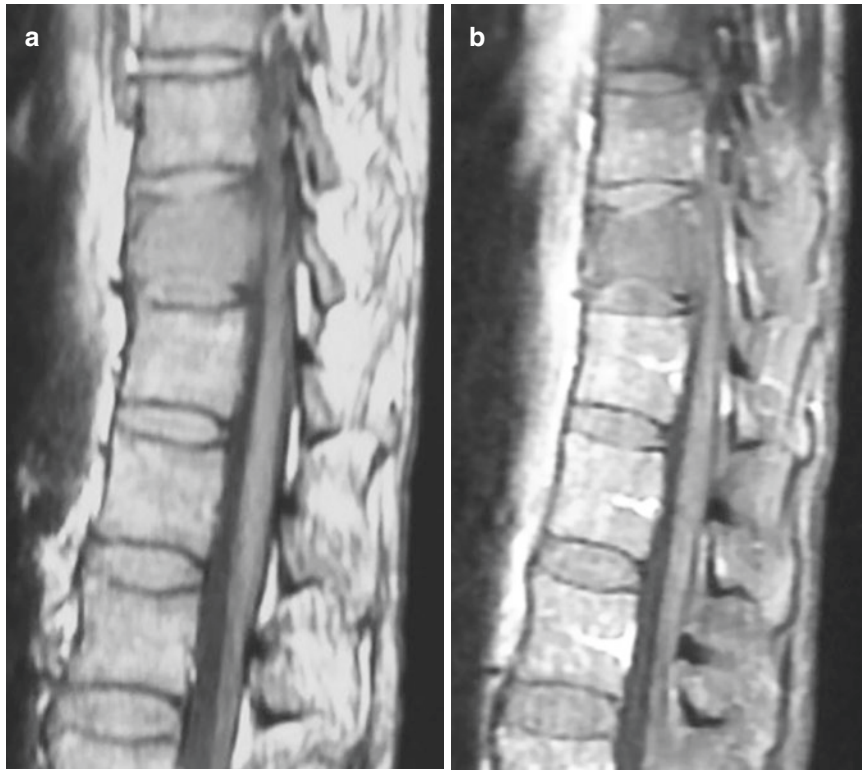

Fig. 13 Brucellar spondylitis with isolated vertebral involvement. Sagittal (**a**) T1-W and (**b**) contrast-enhanced fat-suppressed T1-W MR images show T1-hypointense signal of T10 vertebra without enhancement after IV contrast administration. Differential diagnosis includes tuberculous spondylodiscitis and primitive or metastatic vertebral tumor

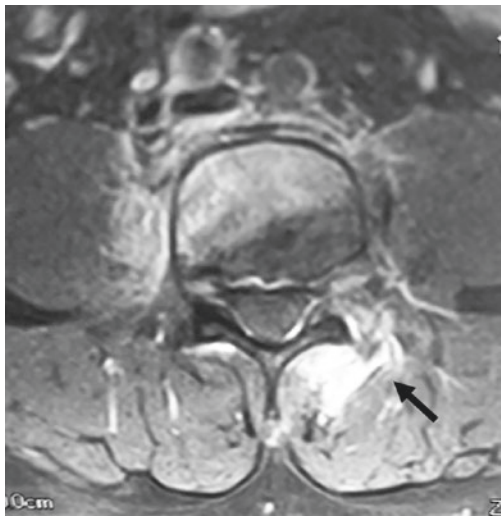

Fig. 14 Brucellar spondylodiscitis with additional neural arch involvement. Axial contrast-enhanced fat-suppressed T1-W MR image shows hyperintense signal at the right anterior corner of the discovertebral junction and of the left facet joint with adjacent soft tissue enhancement (black arrow)

more characteristic of brucellosis than of tuberculosis are less disk space loss and more commonly evident bone fusion between the affected vertebral bodies. Peripherally located intradiscal gas collection also may be characteristic of brucellosis. Pyogenic spondylodiscitis is usually more acute than brucellar spondylodiscitis (Pappas et al. 2005). The main differences between brucellosis, pyogenic spondylodiscitis, and degenerative disc disease are summarized in Table 1.

6 Biological Diagnosis

Hematological and biochemical testing yields no specific findings to suggest the diagnosis of focal brucellosis. Complete blood counts most frequently reveal leukopenia; and pancytopenia may be observed in as many as 20% of patients (Güzey

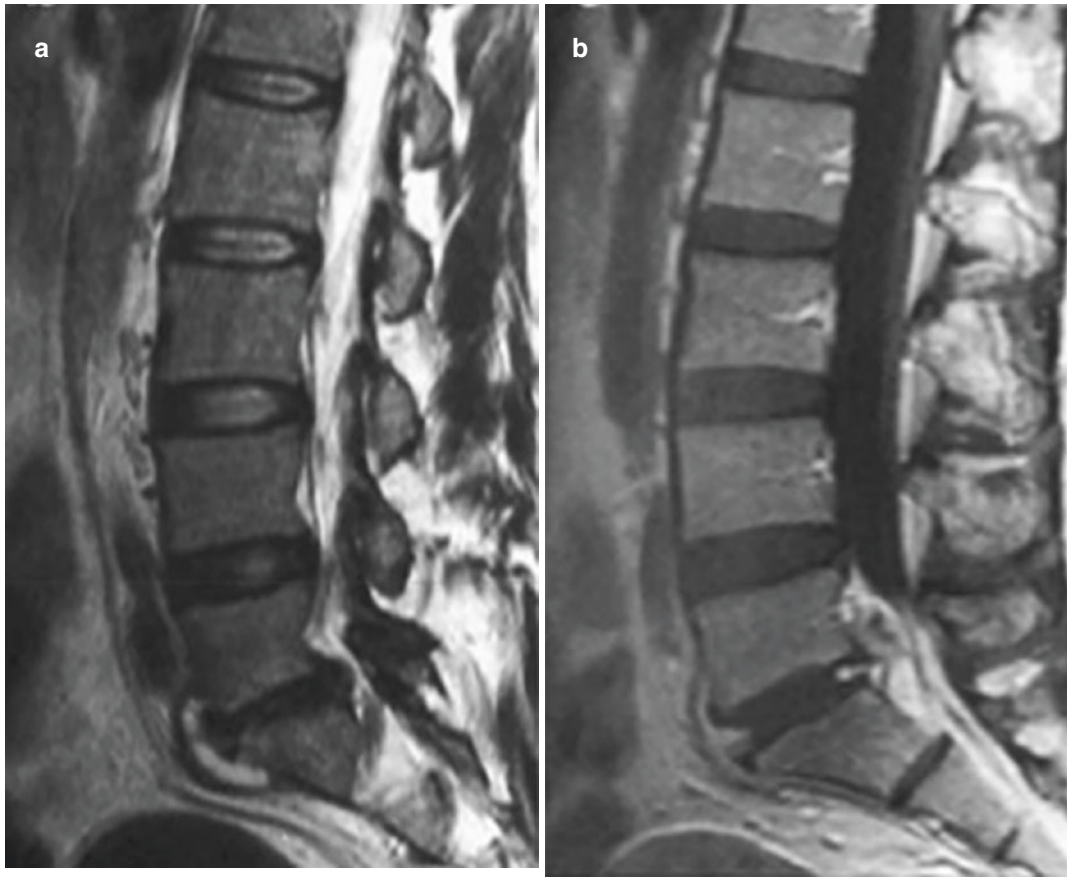

Fig. 15 L5/S1 brucellar spondylodiscitis. Sagittal (**a**) T2-W and (**b**) contrast-enhanced T1-W MR images show T2 hypointensity of the L5–S1 intervertebral disk and subtle peripheral enhancement. Note the small epidural abscess

Table 1 List of features to differentiate among brucellar spondylodiscitis, tuberculous spondylodiscitis, pyogenic spondylodiscitis, and degenerative disc disease

	Brucellar spondylodiscitis	Tuberculous spondylodiscitis	Pyogenic spondylodiscitis	Degenerative disc disease
Disk narrowing	Late and moderate	Late and marked	Early and moderate	Variable
Vertebral body destruction	Mild	Marked	Marked	Absent
Vertebral sclerosis	Early and marked	Late and moderate	Early and marked	Variable
Vacuum phenomenon	Possible: peripheral and small	Absent	Absent	Variable
Soft tissue abscess	Inconstant, small and well-defined	Frequent, large and well-defined	Variable size and ill-defined	Absent
Preferential location	Lower lumbar spine	Thoracic and thoraco-lumbar spine	Lumbar spine	Lumbar spine

et al. 2007). The levels of C-reactive protein (CRP) may be elevated (Resnick 1995).

The definitive diagnosis of brucellosis is based on culture and identification of *Brucella* spp. from clinical specimens or evidence of a fourfold or greater rise in *Brucella* antibody titers between acute and convalescent phase serum specimens obtained greater than or equal to 2 weeks apart. The presumptive diagnosis of brucellosis is based on *Brucella* total antibody titers greater than or equal to 1:160 by standard tube agglutination test (STAT) or *Brucella* microagglutination test (BMAT) in one or more serum specimens obtained after onset of symptoms or the detection of *Brucella* DNA in a clinical specimen by polymerase chain reaction (PCR) assay.

Culture is the gold standard, but it is time-consuming, hazardous, and not sensitive. Indeed, culture from primary specimens may require up to 21 days of incubation. Moreover, the use of automated blood culture systems has shortened the detection time of *Brucella* spp. (Andriopoulos et al. 2007). Patients with chronic infections are also less likely to be culture-positive. If the diagnosis is suspected clinically, one should be careful to notify laboratory personnel of the concern for brucellosis so that proper specimen processing occurs. *Brucella* sp. is most commonly isolated from blood cultures. It can also be isolated from the bone marrow, cerebrospinal fluid, wounds, purulent discharge, joint fluid, or image-guided procedures, such as CT-guided percutaneous biopsy. Surgical intervention is indicated for patients with neurological deficits (Solera et al. 1999). Blood culture results are not always positive for the bacteria (35–92%) because of inadequate microbiological techniques, the possible previous administration of antimicrobial agents, and the intermittent feature of the bacteremia. Also, the sensitivity depends on both the stage of disease, which decreases as the disease duration progresses (Araj 2010). Pus culture gives positive findings in 10–20% of cases (Sarigüzel et al. 2011).

Published information on molecular diagnosis techniques in focal complications of brucellosis is scarce. The most important study investigated, by PCR and by conventional microbiological techniques, 34 non-blood samples (comprising four bone tissue samples) with different focal forms of brucellosis. The sensitivity of PCR and that of the parallel culture in samples other than blood were 97.1% and 29.4%, respectively (Morata et al. 2001). Li et al. (2018) recently reported a sensitivity of 93.5% of real-time PCR assay on 31 formalin-fixed paraffin-embedded samples from patients with brucellar vertebral osteomyelitis.

Numerous serological methods are used in the diagnosis of human brucellosis. Combination of these methods may help to warrant quality performance by reducing false-negative results due to low antigen quality or poor technical standards (Sascha et al. 2011). The most popular can be ranked, according to their overall accuracy in clinical settings, such as ELISA > Rose Bengal test (RBT) > serum agglutination test (SAT) > Coombs' test (Al Dahouk and Nöckler 2011). The standard tube agglutination test (STAT) (Wright test) is the reference method (Sarigüzel et al. 2011). It gives positive findings in almost all patients with the disease.

In rare instances, positive blood culture results and negative serology findings have been reported (Güzey et al. 2007). As the definite cure of a patient correlates well with lower SAT titers, patients should be followed up clinically and serologically (Sascha et al. 2011). In endemic countries, RBT has been traditionally used as a rapid screening test. The diagnostic gain of this test is excellent in patients without previous exposure to *Brucella* or a history of brucellosis (Sascha et al. 2011). ELISA is more sensitive than SAT in chronic and past brucellosis. However, in acute cases, agglutination tests show the same results and are less expensive (Al Dahouk and Nöckler 2011).

Agglutination tests detect antibodies of IgM, IgG, and IgA classes. IgM antibodies are predominant in acute infection but decline within weeks. Relapses are accompanied by transient elevations of IgG and IgA antibodies but not IgM. False-positive *Brucella* test results can be caused by cross-reactivity of antibodies to *Escherichia coli* O157, *Francisella tularensis*, *Moraxella phenylpyruvica*, *Yersinia enterocolit-*

ica, and certain *Salmonella* serotypes and from persons vaccinated against *Vibrio cholerae*. This is due to antigenic similarity between the smooth lipopolysaccharide (S-LPS) of *Brucella* species, the primary immunodeterminant factor, and the lipopolysaccharide of other gram-negative rods (Al Dahouk and Nöckler 2011).

7 Histopathological Diagnosis

Histopathological examination is not routinely practiced for the diagnosis of brucellar spondylodiscitis because clinical and biological examinations are usually sufficient. It is carried out in two circumstances: in cases with negative microbiological tests and high clinical suspicion of brucellosis and in cases of bad response to the treatment. In these circumstances, biopsy is advisable to obtain tissue samples for microbiological and histopathological investigations to confirm brucellar spondylodiscitis (Rammeh et al. 2021). Discovertebral specimens are usually obtained by imaging-guided needle biopsy. The histopathological diagnosis of brucellar spondylodiscitis is challenging, because it shows a large spectrum of histopathological lesions with non-specific and granulomatous forms, each observed in about half of the cases (Turunc et al. 2007; Li et al. 2018; Rammeh et al. 2021).

The brucellar granuloma, highly suggestive of brucellar spondylodiscitis, is surrounded by a chronic inflammatory reaction composed of lymphocytes, plasmocytes, and neutrophils (Rammeh et al. 2021). It is typically small, not well-formed, non-caseating, and composed of aggregates of histiocytes with round nuclei without epithelioid appearance. But granulomas with epithelioid appearance and even caseous-like necrosis, although rare, are possible in brucellar spondylodiscitis (Rammeh et al. 2021). Epithelioid granuloma formed by eosinophilic cells with elongated nuclei is rarely observed in brucellar spondylodiscitis. They are typically associated with histiocytic-type granulomas and are not well-formed like those classically observed in tuberculous spondylodiscitis. The association of histiocytic and epithelioid granulomas has also been reported in fungal and tuberculous spondylodiscitis (Madkour 2001).

Non-specific forms of brucellar spondylodiscitis characterized by non-granulomatous infiltrate show typically a polymorphous infiltrate with predominance of lymphocytes and plasmocytes. These forms mimic pyogenic spondylodiscitis. Their distinction is histologically challenging. Pyogenic spondylodiscitis is characterized by predominant neutrophil infiltration (Li et al. 2016). The predominance of the mononuclear cells should alert the pathologist to suggest the diagnosis of brucellar spondylodiscitis.

8 Treatment

Patients with brucellar spondylodiscitis usually require antibiotherapy and immobilization (Ariza et al. 1992). Treatment of brucellosis must aim at controlling the illness effectively and preventing complications, including relapse. The regimen of choice and duration of antimicrobial therapy should be based on the presence of focal disease and underlying conditions that contraindicate certain specific antibiotics. Currently, the most commonly used antibiotics in the treatment of brucellosis are tetracycline, rifampicin, aminoglycosides, trimethoprim-sulfamethoxazole, and quinolones. Combined drug therapy with a prolonged course is recommended (Pourbagher et al. 2006).

Treatment of spinal brucellosis is based on dual or trial antibiotic therapy. The treatment recommended for brucellosis is the combination of doxycycline (200 mg/day) and rifampicin (15 mg/kg/day). The combination of doxycycline and streptomycin (1 g/day intramuscularly during the first 21 days) is more effective than doxycycline-rifampicin. Streptomycin combined to doxycycline has been reported to have a superior efficacy and lower relapse rates (Ulu-Kilic et al. 2013). However, the side effects of streptomycin limit its use, particularly in elderly patients. Another alternative therapy that can be used for the treatment of spinal brucellosis is a combination of ciprofloxacin (1000 mg/day) and rifampicin (Alp and Doganay 2008). Other

regimens including ciprofloxacin 1 g/day and/or trimethoprim/sulfamethoxazole have also been proposed (Perez-Calvo et al. 1994).

Many studies have shown that the combination of rifampicin and ciprofloxacin can be used in spinal brucellosis due to the ability of these drugs to penetrate and achieve high concentration in bone and soft tissues, particularly in spinal brucellosis with complications. Therefore, a regimen that includes fluoroquinolones may be a better therapeutic option to doxycycline and streptomycin (Alp et al. 2006; Liang et al. 2019). The optimal duration of therapy is unknown, but at least 3–6 months of treatment would be beneficial in osteoarticular brucellosis. Streptomycin or gentamycin is used for 3 weeks. CT-guided percutaneous drainage is necessary only when a large paravertebral abscess is present. Surgery is reserved for those exceptional cases of intraspinal abscesses and progressive signs of spinal cord and nerve root compression.

Brucellar spondylodiscitis usually has a good prognosis. With medical treatment, patients usually recover in 1–3 months. Radiographs show progressive bony sclerosis. Partial or complete vertebral ankylosis may be seen in approximately one-third of patients. MRI is generally not required in the post-therapeutic course of brucellar spondylodiscitis but may be useful to document progressive improvement. According to Harman et al. (2001), changes in the signal intensity of the bone marrow tend to regress sometime between 6 weeks and many months, following effective medical management. Signal changes in the marrow reflect progressive regression of the inflammatory process and formation of fibrous tissue and bone (Harman et al. 2001).

9 Conclusion

Brucellosis occurs in all continents and is a serious hazard in Mediterranean countries, the Middle East, and Latin America. This systemic infection, caused by facultative intra-cellular bacteria of the *Brucella* genus, can involve many organs and tissues. Osteoarticular involvement is a common complication, with the lumbar spine the most frequently affected site. Some imaging characteristics, although not specific, may lead the radiologist to suggest spinal brucellosis. Positive diagnosis is based on serological tests.

References

Al Dahouk S, Nöckler K (2011) Implications of laboratory diagnosis on brucellosis therapy. Expert Rev Anti-Infect Ther 9:833–845

Alduraibi AK, Naddaf S, Alzayed MF (2019) FDG PET/CT of spinal brucellosis. Clin Nucl Med 44:465–466

Alp E, Doganay M (2008) Current therapeutic strategy in spinal brucellosis. Int J Infect Dis 12:573–577

Alp E, Koc RK, Durak A et al (2006) Doxycycline plus streptomycin versus ciprofloxacin plus rifampicin in spinal brucellosis. BMC Infect Dis 6:72

Al-Shahed MS, Sharif HS, Haddad MC et al (1994) Imaging features of musculoskeletal brucellosis. Radiographics 14:333–348

Andriopoulos P, Tsironi M, Deftereos S, Aessopos A, Assimako-poulos G (2007) Acute brucellosis: presentation, diagnosis and treatment of 144 cases. Int J Infect Dis 11:62–67

Araj GF (2010) Update on laboratory diagnosis of human brucellosis. Int J Antimicrob Agents 36(1 Suppl):S12–S17

Ariza J, Gudiol F, Pallares R et al (1992) Treatment of human brucellosis with doxycycline plus rifampicin or doxycycline plus streptomycin. Ann Intern Med 117:25–30

Arkun R, Mete BD (2011) Musculoskeletal brucellosis. Semin Musculoskelet Radiol 15:470–479

Ben Taarit CH, Turki S, Ben Maiz H (2002) Spondylodiscites infectieuses: étude d'une série de 151 cas. Acta Orthop Belg 68:381–387

Chelli Bouaziz M, Ladeb MF, Chakroun M, Chaabane S (2008) Spinal brucellosis: a review. Skeletal Radiol 37:785–790

Chelli Bouaziz M, Bougamra I, Kaffel D et al (2010) Noncontiguous multifocal spondylitis: an exceptional presentation of spinal brucellosis. Tunis Med 88:280–284

D'Anastasio R, Staniscia T, Milia ML, Manzoli L, Capasso L (2011) Origin, evolution and paleoepidemiology of brucellosis. Epidemiol Infect 139:149–156

Ekici MA, Ozbek Z, Kazancı B, Güçlü B (2014) Collapsed L4 vertebral body caused by brucellosis. J Korean Neurosurg Soc 55:48–50

El-Desouki M (1991) Skeletal brucellosis: assessment with bone scintigraphy. Radiology 181:415–418

Güzey FK, Emel E, Sel B et al (2007) Cervical spinal brucellosis causing epidural and prevertebral abscesses

and spinal cord compression: a case report. Spine J 7:240–244
Hamza M, Elleuch M, Amara A et al (1990) Brucellose pelvirachidi-enne a propos de quinze patients tunisiens. Sem Hop Paris 66:1939–1943
Harman M, Unal O, Onbasi KT (2001) Brucellar spondylodiscitis MRI diagnosis. J Clin Imaging 25:421–427
Kazak E, Akalın H, Yılmaz E et al (2016) Brucellosis: a retrospective evaluation of 164 cases. Singapore Med J 57:624–629
Kursun E, Turunc T, Demiroglu Y, Arslan H (2013) Evaluation of four hundred and forty seven brucellosis cases. Intern Med 52:745–750
Li T, Liu T, Jiang Z, Cui X, Sun J (2016) Diagnosing pyogenic, brucella and tuberculous spondylitis using histopathology and MRI: a retrospective study. Exp Ther Med 12:2069–2077
Li M, Zhou X, Li J, Sun L, Chen X, Wang P (2018) Real-time PCR assays for diagnosing brucellar spondylitis using formalin-fixed paraffin-embedded tissues. Medicine (Baltimore) 97:e0062
Liang C, Wei W, Liang X, De E, Zheng B (2019) Spinal brucellosis in Hulunbuir, China, 2011-2016. Infect Drug Resist 12:1565–1571
Lifeso RM, Harder E, Mc Corkell SJ (1985) Spinal brucellosis. J Bone Joint Surg Br 67:345–351
Madkour MM (2001) Madkour's brucellosis, 2nd edn. Springer, Berlin
Madkour MM, Sharif HS, Aabed MY, Al Fayez MA (1988) Osteoarticular brucellosis: results of bone scintigraphy in 140 patients. AJR Am J Roentgenol 150:1101–1105
Morata P, Queipo-Ortuño MI, Reguera JM, Miralles F, Lopez-Gonzalez JJ, Colmenero JD (2001) Diagnostic yield of a PCR assay in focal complications of brucellosis. J Clin Microbiol 39:3743–3746
Pappas G, Akriditis N, Bosilkovski M, Tsianos E (2005) Brucellosis. N Engl J Med 352:2325–2336
Perez-Calvo J, Matamala C, Sanjoaquin I et al (1994) Epidural abscess due to acute Brucella melitensis infection. Arch Intern Med 154:1410–1411
Pourbagher A, Pourbagher MA, Savas L et al (2006) Epidemiologic, clinical and imaging findings in brucellosis patients with osteoarticular involvement. AJR Am J Roentgenol 187:873–880
Rammeh S, Romdhane E, Riahi H et al. (2021) Granulomatous spondylodiscitis: a case series with focus on histopathological features. J Spinal Cord Med 44:282–287
Resnick D (1995) Diagnosis of bone and joint disorders, vol 4, 3rd edn. Saunders, Philadelphia, pp 2448–2558
Sarigüzel FM, Kayman T, Çelik I, Koç N (2011) Comparison of standard tube agglutination, Coombs' and Brucellacapt tests in the diagnosis of Brucellosis. N Engl J Med 28:113–115
Sharif HS, Aiden OA, Clark DC (1989) Brucellar and tuberculous spondylitis: comparative imaging features. Radiology 171:419–425
Sharif HS, Clark DC, Aabed MY (1990) Granulomatous spinal infections: MR imaging. Radiology 177:101–107
Solera J, Lozano E, Martínez-Alfaro E et al (1999) Brucellar spondylitis: review of 35 cases and literature survey. Clin Infect Dis 29:1440–1449
Turan H, Serefhanoglu K, Karadeli E, Togan T, Arslan H (2011) Osteoarticular involvement among 202 brucellosis cases identified in Central Anatolia region of Turkey. Intern Med 50:421–428
Turgut Tali E (2004) Spinal infections. Eur J Radiol 50:120–133
Turgut M, Turgut AT, Koşar U (2006) Spinal brucellosis: Turkish experience based on 452 cases published during the last century. Acta Neurochir (Wien) 148:1033–1044
Turunc T, Demiroglu YZ, Uncu H, Colakoglu S, Arslan H (2007) A comparative analysis of tuberculous, brucellar and pyogenic spontaneous spondylodiscitis patients. J Infect 55:158–163
Ulu-Kilic A, Sayar MS, Tütüncü E, Sezen F, Sencan I (2013) Complicated brucellar spondylodiscitis: experience from an endemic area. Rheumatol Int 33:2909–2912
Yang X, Zhang Q, Guo X (2014) Value of magnetic resonance imaging in brucellar spondylodiscitis. Radiol Med 119:928–933
Yin Z, He E, Ding H, Chen J (2015) Brucella infection of the thoracic vertebral arch presenting with an epidural abscess: a case report. J Med Case Rep 9:237
Zorompala A, Skopelitis E, Thanos L (2000) An unusual case of brucellar spondylitis involving both the cervical and lumbar spine. J Clin Imaging 24:273–275

Imaging of Salmonella Spondylodiscitis

Emna Labbène, Wafa Achour,
Mohamed Fethi Ladeb, and Nadia Hammami

Contents

E. Labbène (✉) · M. F. Ladeb
Department of Radiology, MT Kassab Institute of Orthopaedics, Tunis, Tunisia

Faculty of Medicine of Tunis, Tunis-El Manar University, Tunis, Tunisia
e-mail: emnasensei@gmail.com; fethiladeb@hotmail.fr

W. Achour
Laboratory Department, National Bone Marrow Transplant Center, Tunis, Tunisia

Faculty of Medicine of Tunis, Tunis-El Manar University, Tunis, Tunisia
e-mail: wafaachour@gmail.com

N. Hammami
Department of Neuroradiology, National Institute of Neurology Mongi-Ben Hamida, Tunis, Tunisia

Faculty of Medicine of Tunis, Tunis-El Manar University, Tunis, Tunisia
e-mail: nadiahamaied@hotmail.com

Abstract

Salmonella osteomyelitis is uncommon and generally associated with sickle cell disease. Vertebral location is extremely rare and has mainly been reported in case reports. Magnetic resonance imaging (MRI) is the modality of choice for assessing discovertebral and soft tissue abnormalities. Imaging features are similar to other spondylodiscitis. Bacteria isolation is necessary for definitive diagnosis and antibiotic susceptibility testing, allowing adequate medical treatment.

© The Author(s), under exclusive license to Springer Nature Switzerland AG 2021

M. F. Ladeb, W. C. G. Peh (eds.), *Imaging of Spinal Infection*,
Medical Radiology Diagnostic Imaging, https://doi.org/10.1007/978-3-030-70459-9_11

Abbreviations

CT	Computed tomography
MRI	Magnetic resonance imaging

1 Introduction

Salmonella osteomyelitis is a rare condition that generally occurs in immunocompromised patients and mainly affects those with sickle cell disease (Mavrogenis et al. 2017). Vertebral location is extremely rare and has mainly been reported in case reports (Santos and Sapico 1998). In patients with sickle cell disease, differentiating between vaso-occlusive crisis and early osteomyelitis is a diagnostic challenge. Magnetic resonance imaging (MRI) is the modality of choice for spondylodiscitis assessment showing vertebral and disk signal abnormalities at an early stage (Sans et al. 2012). Definitive diagnosis is based on pathogen isolation (Santos and Sapico 1998).

2 Epidemiology

Salmonella is known to cause a broad spectrum of human illnesses and involves strains belonging essentially to *Salmonella enterica* subsp. *enterica.* These strains can be divided into typhoidal (serovars *typhi* and *paratyphi*) and non-typhoidal strains. Typhoidal strains cause typhoid in areas with unsafe water and poor sanitation. Non-typhoidal strains most commonly cause gastroenteritis transmitted through the consumption of contaminated food of animal origin and are the leading causes of bloodstream infection in low-resource settings (Stephanie and Schmalzle 2019). The incidence of *S. typhi* and *S. paratyphi* varies among countries. It is high (greater than 100 cases per 100,000 per year) in South-Central Asia and Southeast Asia; medium (10–100 cases per 100,000 per year) in Africa, Latin America, the Caribbean, the rest of Asia and Oceania; and low (less than 10 cases per 100,000 per year) in Europe, Australia, New Zealand and North America (Sánchez-Vargas et al. 2011).

Osteomyelitis is a rare extra-intestinal manifestation of Salmonella infection, due essentially to *Salmonella typhimurium* and *Salmonella enteritidis* and rarely to *Salmonella typhi*. It accounts for 1–4% of all bone infections (Kumar et al. 2008) and represents less than 1% of total Salmonella infection cases (Weston and Moran 2015). In a review of 7779 cases of Salmonella infection, only 59 patients (0.76%) had osteomyelitis (Saphra and Winter 1957). It is predominantly seen in patients with hemoglobinopathies such as sickle cell disease or thalassemia, presenting as a significant cause of morbidity and mortality in this population, and it is mainly located in long bones (Chambers et al. 2000; McAnearney 2015). Indeed, Salmonella is the main etiologic agent of osteomyelitis in patients with sickle cell disease (Burnett et al. 1998), with rates differing by region (Stephanie and Schmalzle 2019). However, it is a rare cause of osteomyelitis in patients with no sickle cell disease, accounting for approximately 0.5% of all cases (Khoo et al. 2016). Other risk factors are diabetes mellitus, a history of intravenous drug abuse, pulmonary diseases, hemodialysis, human immunodeficiency virus, chronic immunocompromised states like systemic lupus erythematous, collagen diseases, liver cirrhosis, lymphoma, steroid treatment, atherosclerosis, achlorhydria (Khoo et al. 2016), and biliary and urinary tract abnormalities and co-infections (Stephanie and Schmalzle 2019).

Vertebral location of salmonella infection is extremely rare, representing approximately one quarter of salmonella osteomyelitis cases (Santos and Sapico 1998). Its occurrence seems to be increasing in recent years, attributed probably to the aging population and the increasing number of immunocompromised individuals. The lumbar spine is the most common site of involvement (Cheng et al. 2018). The largest review of salmonella spondylodiscitis reported in the English literature, published by Santos and Sapico (1998), includes 46 reported cases. The majority of the other published articles are case reports. Forty-six of these articles were reviewed which included 104 patients (Miller 1954; Greenspan and Feinberg 1957; Weiss and

Table 1 Patients' characteristics in 104 cases of salmonella spondylodiscitis

Feature	Value or percentage
Age	
Range	1–79 years
Mean	42 years
Gender	
Male	64%
Female	46%
Predisposing factors	
Sickle cell disease	9%
Others	42%
Level of infection	
Lumbar	56%
Thoracic	24%
Cervical	2%

Katz 1970; Bussiere et al. 1979; Carvell and Maclarnon 1981; Gardner 1985; O'Keeffe 1991; Tsui et al. 1997; Santos and Sapico 1998; Skoutelis et al. 2001; Akiba et al. 2001; Chen et al. 2001; Gupta et al. 2004; Rajesh et al. 2004; Barkai et al. 2005; Devrim et al. 2005; Laloum et al. 2005; Altay et al. 2006; Liu et al. 2006; Ozturk et al. 2006; Khan and El-Hiday 2007; Abdullah et al. 2008; Chen et al. 2008; Kumar et al. 2008; Osebold 2008; Zheng et al. 2009; Rostom et al. 2009; Learch et al. 2009; Suwanpimolkul et al. 2010; Amritanand et al. 2010; Choi et al. 2010; Berngard and Miller 2013; Feng et al. 2014; Shrestha et al. 2015; McAnearney 2015; Effendi et al. 2016; Fukuda et al. 2016; Khoo et al. 2016; Oki et al. 2016; Fareed et al. 2017; Banerjee et al. 2018; Cheng et al. 2018; Dahlberg et al. 2018; Myojin et al. 2018; Popa et al. 2019). Their main characteristics are summarized in Table 1. Among those 104 patients, 64% were male and had a mean age of 42 years (range 1–79 years). Sickle cell disease was reported in 9% of cases and other predisposing factors in 42% of cases. By excluding the cases reported by Santos and Sapico (1998) who found 54% had predisposing factors, the percentage drops to 33%. This difference could be explained by the fact that atherosclerosis, the main predisposing factor in the study of Santos and Sapico, was not specified in other reported cases.

3 Pathophysiology

Vertebral osteomyelitis due to Salmonella occurs by the hematogeneous route. Contiguous spread from adjacent infected tissues is rare. Contamination after invasive diagnostic or therapeutic procedures is also possible (Cheng et al. 2018). Since clinical imaging nearly always reveals disease involving two adjacent vertebrae and subsequently the adjacent intervertebral disk, an arterial route is the probable source as the segmental arteries supplying the vertebrae bifurcate to supply both adjacent vertebral segments. In some patients, inflammation of the disk occurs before vertebral infection (Berngard and Miller 2013). In children, since there are persisting vascular channels in the disk, infective discitis may occur after bacteremia (Cheng et al. 2018).

The exact pathogenesis is not well established, although, theoretically, bowel micro-infarcts causing hematogeneous spread of Salmonella are likely to be the cause. Cases due to direct contiguous spread from an adjacent infected aortic aneurysm have also been reported (Effendi et al. 2016). Indeed, Salmonella is one of the major causes of mycotic aneurysm of the aorta (Chen et al. 2008). In sickle cell disease, Salmonella osteomyelitis seems to be due to a combination of factors. Sickling events may lead to infarct of both gut and bone, creating a permissive environment for both bacterial entry from the gut to the bloodstream and seeding of damaged bone by blood-borne bacteria.

4 Sites of Infection

The lumbar spine is the most frequent site of Salmonella spondylitis accounting for approximately 56% of infections, followed by thoracic spine with 24%. The cervical spine, along with cervicothoracic and thoracolumbar levels, is less frequently involved. Some authors have reported multifocal osteomyelitis (Rostom et al. 2009; Zheng et al. 2009). Involvement of multiple sites is usually reported in immunocompromised

patients (Shrestha et al. 2015). Table 1 summarizes the different sites of infection of 104 cases of Salmonella spondylodiscitis (Miller 1954; Greenspan and Feinberg 1957; Weiss and Katz 1970; Bussiere et al. 1979; Carvell and Maclarnon 1981; Gardner 1985; O'Keeffe 1991; Tsui et al. 1997; Santos and Sapico 1998; Akiba et al. 2001; Skoutelis et al. 2001; Chen et al. 2001; Gupta et al. 2004; Rajesh et al. 2004; Devrim et al. 2005; Laloum et al. 2005; Barkai et al. 2005; Liu et al. 2006; Altay et al. 2006; Ozturk et al. 2006; Khan and El-Hiday 2007; Abdullah et al. 2008; Chen et al. 2008; Kumar et al. 2008; Osebold 2008; Learch et al. 2009; Rostom et al. 2009; Zheng et al. 2009; Choi et al. 2010; Amritanand et al. 2010; Suwanpimolkul et al. 2010; Berngard and Miller 2013; Feng et al. 2014; McAnearney 2015; Shrestha et al. 2015; Effendi et al. 2016; Fukuda et al. 2016; Khoo et al. 2016; Oki et al. 2016; Fareed et al. 2017; Cheng et al. 2018; Dahlberg et al. 2018; Myojin et al. 2018; Banerjee et al. 2018; Popa et al. 2019).

5 Clinical Presentation

Clinical presentation can be acute, subacute, or chronic. The duration of symptoms before diagnosis can vary from a few days to several years (Santos and Sapico 1998). Back pain is the most common symptom, reported in more than 90% of cases. It can be a lower back pain, thoracic pain, and/or cervical pain, depending on the site of the infection. This symptom can be isolated (Banerjee et al. 2018). Fever is the second most frequent sign, reported in 65% of cases. It can precede back pain, occur at the same time, or appear during evolution (Feng et al. 2014; Cheng et al. 2018; Myojin et al. 2018). Neurological signs, present in 27% of cases, constitute an emergency and reflect spinal cord or nerve root compression mainly by an epidural spread of infection. They include numbness, weakness or paralysis of the limbs, cauda equina syndrome, and hyperreflexia (Berngard and Miller 2013; Fareed et al. 2017; Popa et al. 2019).

Gastrointestinal symptoms at the moment of presentation are found in 25% of cases, consisting mainly of abdominal pain and diarrhea (Kumar et al. 2008; Fareed et al. 2017). A pre-existing history of typhoid fever with abdominal pain, diarrhea and fever occurring weeks or months before spondylodiscitis is sometimes reported by patients and should raise suspicion of Salmonella spondylodiscitis, particularly if the patients are residing in or have travelled to an endemic area (Rajesh et al. 2004; Altay et al. 2006; Shrestha et al. 2015; Popa et al. 2019). Indeed, chronic carriage of Salmonella (persistence in stool or urine for periods greater than 1 year) has been reported in 1–4% of patients with untreated enteric fever (Stephanie and Schmalzle 2019).

Other signs, such as night sweats, weight loss, or fatigue, have also been reported (Gupta et al. 2004; Abdullah et al. 2008).

Table 2 summarizes the clinical findings in 55 patients with Salmonella spondylodiscitis (Miller 1954; Greenspan and Feinberg 1957; Weiss and Katz 1970; Bussiere et al. 1979; Carvell and Maclarnon 1981; Gardner 1985; O'Keeffe 1991; Tsui et al. 1997; Santos and Sapico 1998; Akiba et al. 2001; Skoutelis et al. 2001; Chen et al. 2001; Gupta et al. 2004; Rajesh et al. 2004; Devrim et al. 2005; Laloum et al. 2005; Barkai et al. 2005; Liu et al. 2006; Altay et al. 2006; Ozturk et al. 2006; Khan and El-Hiday 2007; Abdullah et al. 2008; Chen et al. 2008; Kumar et al. 2008; Osebold 2008; Learch et al. 2009; Rostom et al. 2009; Zheng et al. 2009;

Table 2 Review of clinical features in 55 patients with Salmonella spondylodiscitis

Feature	Value or percentage
Symptoms	
Back/neck pain	94%
Fever	65%
Neurological signs	27%
Gastrointestinal symptoms	25%
Others	31%
Duration of symptoms before diagnosis	
Range	1 day–7 years
Median	4 weeks

Choi et al. 2010; Suwanpimolkul et al. 2010; Berngard and Miller 2013; Feng et al. 2014; McAnearney 2015; Shrestha et al. 2015; Effendi et al. 2016; Fukuda et al. 2016; Khoo et al. 2016; Oki et al. 2016; Fareed et al. 2017; Cheng et al. 2018; Dahlberg et al. 2018; Myojin et al. 2018; Banerjee et al. 2018; Popa et al. 2019).

6 Imaging

The diagnosis of spondylodiscitis is largely based on imaging with MRI being the modality of choice. However, there are no specific signs allowing the precise diagnosis of the causative pathogen. Indeed, findings are common to all spondylodiscitis and include abnormalities of the intervertebral disk, adjacent vertebral bodies, and surrounding soft tissues (Sans et al. 2012). Spinal radiographs and MRI are the two main modalities used for diagnosis (Sans et al. 2012). CT is mainly used to guide percutaneous procedures such as needle tissue biopsy or paravertebral abscess drainage (Tsui et al. 1997; Khan and El-Hiday 2007; Zheng et al. 2009; Effendi et al. 2016). Bone scintigraphy can be useful in multifocal infections, showing an increased uptake at the sites of infection.

Table 3 summarizes the imaging features reported in 50 patients with Salmonella spondylodiscitis (Miller 1954; Greenspan and Feinberg 1957; Weiss and Katz 1970; Bussiere et al. 1979; Carvell and Maclarnon 1981; Gardner 1985; O'Keeffe 1991; Tsui et al. 1997; Santos and Sapico 1998; Akiba et al. 2001; Skoutelis et al. 2001; Gupta et al. 2004; Rajesh et al. 2004; Devrim et al. 2005; Laloum et al. 2005; Barkai et al. 2005; Liu et al. 2006; Altay et al. 2006; Ozturk et al. 2006; Khan and El-Hiday 2007; Abdullah et al. 2008; Chen et al. 2008; Kumar et al. 2008; Osebold 2008; Learch et al. 2009; Rostom et al. 2009; Zheng et al. 2009; Choi et al. 2010; Amritanand et al. 2010; Suwanpimolkul et al. 2010; Berngard and Miller 2013; Feng et al. 2014; McAnearney 2015; Shrestha et al. 2015; Effendi et al. 2016; Fukuda et al. 2016; Khoo et al. 2016; Oki et al. 2016; Fareed et al. 2017; Cheng et al. 2018; Dahlberg et al. 2018; Myojin et al. 2018; Banerjee et al. 2018; Popa et al. 2019).

Disk space abnormalities have been reported in 36 cases. Disk space narrowing is the most consistent sign (Fig. 1), reported in 83% of cases. The other abnormalities are disk abscess (17%), disk enhancement (14%), and T2 signal hyperintensity (28%). In two cases, disk space height was normal (Gardner 1985; Zheng et al. 2009). Bone abnormalities were reported in 38 cases. Vertebral end-plate erosion or blurring were found in 39% of cases (Figs. 1 and 2), and bone destruction was reported in 31% of cases and vertebral body collapse in 31% of cases. Bone marrow signal abnormalities (T2 signal hyperintensity and bone enhancement) were found in 55% of cases (Fig. 1). In two cases, bone sclerosis and construction were associated with destructive lesions (Tsui et al. 1997; Kumar et al. 2008). Involvement of the posterior arch has not been reported.

Table 3 Review of imaging features in 50 patients with Salmonella spondylodiscitis

Feature (no. of patients with findings)	Percentage
Disk abnormalities (n = 36)	
Disk height narrowing	83%
Hyperintense T2 signal (MRI)	28%
Enhancement (MRI)	14%
Disk abscess (MRI)	17%
Vertebral body abnormalities (n = 38)	
End-plate erosion/blurring	39%
Bone destruction	31%
Vertebral body collapse	31%
Bone marrow signal abnormalities (hyperintense T2 signal, enhancement) (MRI)	55%
Bone sclerosis and construction signs	5%
Paravertebral tissue extension of infection (n = 32)	
Paravertebral phlegmon	28%
Paravertebral abscess	72%
Epidural extension of infection (n = 17)	
Epidural abscess (MRI)	82%
Epidural phlegmon (MRI)	18%
Spinal cord/cauda equina compression (MRI)	47%

Paravertebral abscesses were reported in 23 cases. They were well-defined and had a thin smooth wall (Feng et al. 2014; Cheng et al. 2018). Epidural extension of infection has been reported in 17 cases (Fig. 1). Epidural abscess was found in 82% of cases. Spinal cord or cauda equina compression was reported in 47% of cases.

In sickle cell disease, differentiation between bone infection and infarction is difficult without local histological and bacteriological findings. MRI is considered to be an efficient tool for the diagnosis of osteomyelitis in patients with sickle cell disease. However, bone marrow edema, fluid collection in adjacent soft tissues, and abnormal gadolinium enhancement of muscle and fat are seen with infarction as well as with infection. Bone scintigraphy is not helpful in distinguishing bone infarction from osteomyelitis, since normal and increased uptake may be seen in both. A combination of 99mTc-sulfur colloid and 99mTc diphosphonate or 99mTc with gallium seems to improve the test accuracy. Labeled leucocyte scan is not reliable in the spine. Associated abnormalities reported include spleen abscesses or infected abdominal aortic aneurysm (Santos and Sapico 1998). The latter has mainly been reported in elderly patients (Santos and Sapico 1998; Chen et al. 2008; Learch et al. 2009) and is an emergency, generally requiring surgical treatment. CT and MRI show a saccular aortic aneurysm contiguous to the spondylodiscitis site, with soft tissue swelling and possible periaortic gas.

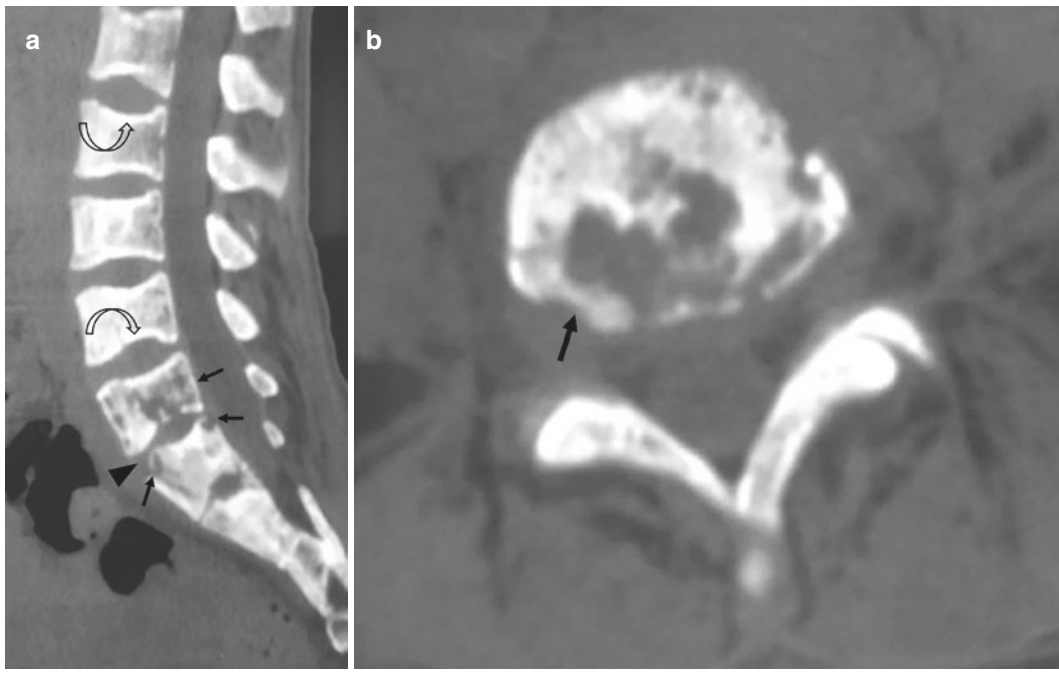

Fig. 1 Salmonella spondylodiscitis in a patient with sickle cell disease. (**a**) Sagittal and (**b**) axial CT images show narrowing of disk space at the L5/S1 level (black arrowhead) with adjacent end-plate erosions and vertebral body destruction (black arrows). Similar findings are present at the S1/S2 level. Notice the H-shape of vertebral bodies consistent with end-plate osteonecrosis characteristic of sickle cell disease (curved arrows). Sagittal (**c**) T2-W, (**d**) T1-W, and (**e**) contrast-enhanced T1-W and (**f**) axial contrast-enhanced T1-W MR images show T2-hyperintense signal of the disk at the L5/S1 and S1/S2 levels (white arrowheads) without enhancement and T2-hyperintense signal of vertebral bodies with enhancement (stars). There is also anterior (small white arrows) and paravertebral (curved arrows) phlegmon at the L5/S1 level along with epidural phlegmon (small black arrow)

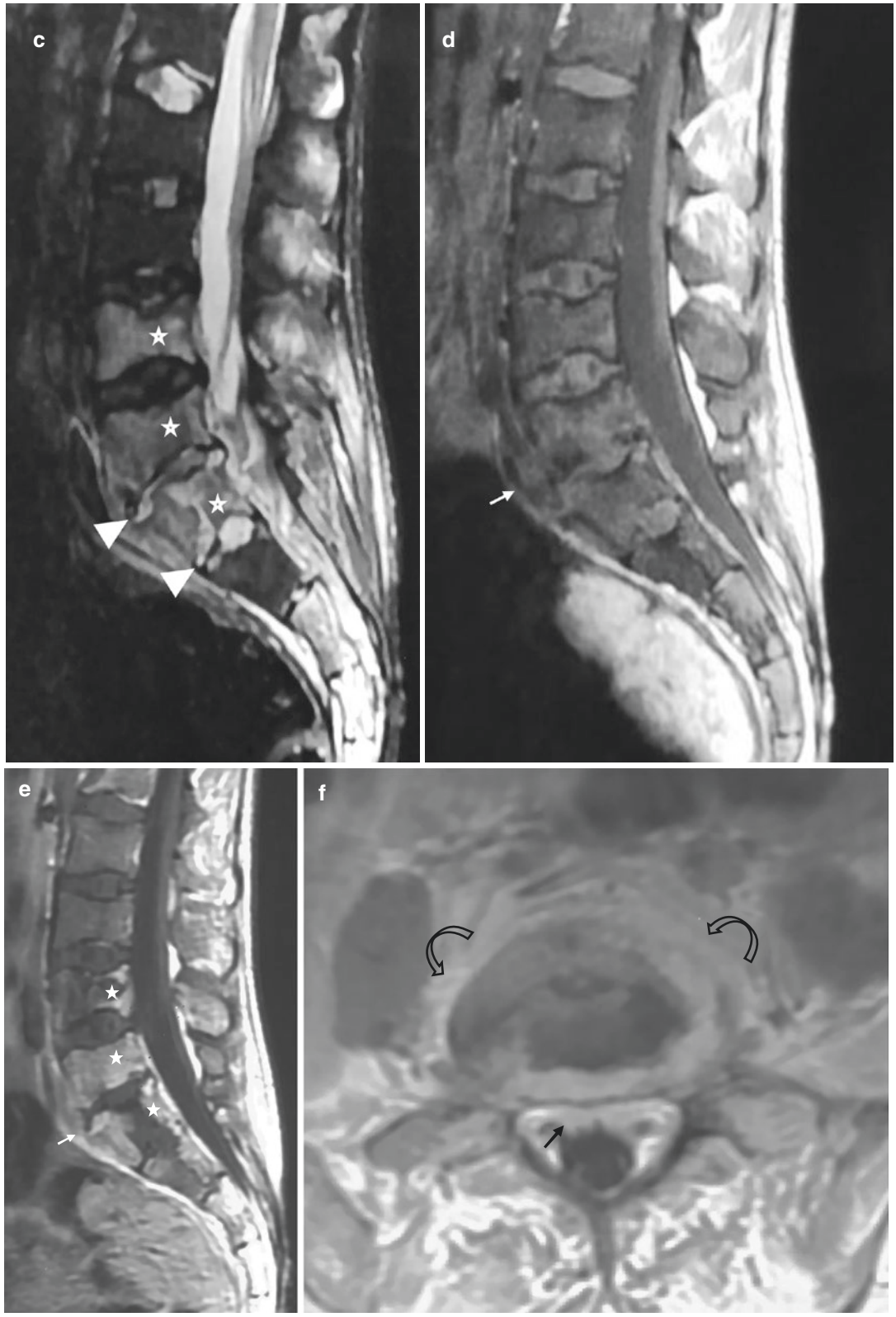

Fig. 1 (continued)

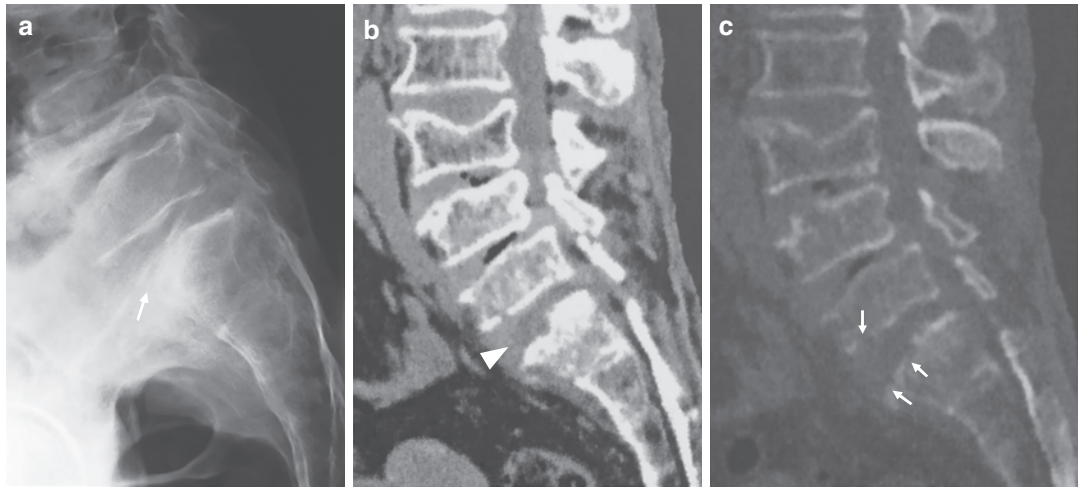

Fig. 2 (**a**) Lateral radiograph of the lumbar spine shows erosion of the anterosuperior corner of S1 segment (white arrow). (**b**, **c**) Sagittal CT images of the same patient show hypodensity of the disk at the L5/S1 level (arrowhead) with erosions of adjacent vertebral end plates (white arrows)

7 Diagnosis

The key to the diagnosis of Salmonella vertebral osteomyelitis is the identification of the organism mainly from a bone specimen obtained by needle or open biopsy (the gold standard), an aspirate of an adjacent fluid collection, or blood (Effendi et al. 2016; Cheng et al. 2018). The diagnosis can also be based on other clinical specimens (stool, urine, cerebrospinal fluid culture, joint fluid culture) (Santos and Sapico 1998; Rostom et al. 2009; Oki et al. 2016). In a review of 46 cases, Santos and Sapico (1998) found that culture of blood (n = 46), percutaneous or surgery specimen, stool (n = 31), and urine (n = 31) were positive in 22 (48%), 24 (52%), 11 (36%), and 7 (23%) cases, respectively. Forty-six articles including 66 patients with salmonella spondylodiscitis were reviewed. Cultures of specimens obtained by percutaneous procedure or surgery, blood culture, stool culture, and urine culture were positive in 93%, in 54%, and in 7/15 and 3/10 of cases, respectively.

Table 4 shows the different methods of diagnosis used by reviewing 46 articles (Miller 1954; Greenspan and Feinberg 1957; Weiss and Katz 1970; Bussiere et al. 1979; Carvell and Maclarnon 1981; Gardner 1985; O'Keeffe 1991; Tsui et al. 1997; Santos and Sapico 1998; Akiba et al. 2001; Skoutelis et al. 2001; Chen et al. 2001; Gupta et al. 2004; Rajesh et al. 2004; Devrim et al. 2005; Laloum et al. 2005; Barkai et al. 2005; Liu et al. 2006; Altay et al. 2006; Ozturk et al. 2006; Khan and El-Hiday 2007; Abdullah et al. 2008; Chen et al. 2008; Kumar et al. 2008; Osebold 2008; Learch et al. 2009; Rostom et al. 2009; Zheng et al. 2009; Choi et al. 2010; Amritanand et al. 2010; Suwanpimolkul et al. 2010; Berngard and Miller 2013; Feng et al. 2014; McAnearney 2015; Shrestha et al. 2015; Effendi et al. 2016; Fukuda et al. 2016; Khoo et al. 2016; Oki et al. 2016; Fareed et al. 2017; Cheng et al. 2018; Dahlberg et al. 2018; Myojin et al. 2018; Banerjee et al. 2018; Popa et al. 2019).

Table 4 Microbiological methods of diagnosis in 66 patients with Salmonella spondylodiscitis

Positive bacterial culture (no. of patients with findings)	Value or percentage
Blood culture (n = 41)	54%
Culture of specimen (percutaneous procedure or open surgery) (n = 44)	93%
Urine culture (n = 10)	3/10
Stool culture (n = 15)	7/15

The rate of positive blood culture associated with Salmonella vertebral osteomyelitis (48%)

is higher than that associated with pyogenic vertebral osteomyelitis due to other causes (25%) (Santos and Sapico 1998). Serum agglutination may be helpful if *S. typhi* infection is suspected. Its sensitivity is higher in osteomyelitis than in gastroenteritis, probably because of sufficient time for antibody response (Santos and Sapico 1998). In a study including 11 cases of Salmonella spondylodiscitis, Widal test was positive in all patients. In two patients, no organism was isolated, and the diagnosis was made based on Widal test along with histological features and a characteristic history (Amritanand et al. 2010). Nevertheless, Widal test can be negative at an early stage of disease, in cases of inadvertent administration of antibiotics, or in waning humoral immune response. Moreover, pathogen identification is necessary for antibiotic susceptibility testing. Laboratory markers, including white blood cell count, erythrocyte sedimentation rate, and C-reactive protein, are, to a certain extent, sensitive indicators of spinal infection. Nevertheless, none of them is specific enough in revealing the pathogens (Cheng et al. 2018).

8 Treatment and Outcome

The success of treatment depends on pathogen identification and antibiotic susceptibility testing (Santos and Sapico 1998). Outcome under antibiotic therapy and eventual surgery is favorable in the majority of cases with good recovery in 86% (57 out of 66 cases). Nevertheless, some patients are left with sequelae (Chen et al. 2008; Berngard and Miller 2013; Popa et al. 2019). Duration of medical treatment varies from 4 weeks to 6 months. Association with infected abdominal aortic aneurysm is characterized by a poorer prognosis with higher mortality. In these cases, surgery is generally needed. In a review of 46 cases of Salmonella spondylodiscitis, 12 patients out of 46 died, and the deaths were all related to infected abdominal aortic aneurysm (Santos and Sapico 1998). The usefulness of follow-up MRI has not been demonstrated. In a study including 33 patients with spinal infection, no correlation was found between imaging findings and clinical features (Kowalski et al. 2007). In another study including 253 patients with spinal infection, the follow-up MRI did not significantly affect outcome (McHenry 2002).

Table 5 Treatment and outcome in 66 patients with Salmonella spondylodiscitis

Features	Percentage
Medical treatment	100%
Surgery	44%
Outcome	
Good recovery	86%
Death	5%
Recovery with sequelae	9%

Table 5 summarizes the treatment and outcome of 66 cases by reviewing 46 articles (Miller 1954; Greenspan and Feinberg 1957; Weiss and Katz 1970; Bussiere et al. 1979; Carvell and Maclarnon 1981; Gardner 1985; O'Keeffe 1991; Tsui et al. 1997; Santos and Sapico 1998; Akiba et al. 2001; Skoutelis et al. 2001; Chen et al. 2001; Gupta et al. 2004; Rajesh et al. 2004; Devrim et al. 2005; Laloum et al. 2005; Barkai et al. 2005; Liu et al. 2006; Altay et al. 2006; Ozturk et al. 2006; Khan and El-Hiday 2007; Abdullah et al. 2008; Chen et al. 2008; Kumar et al. 2008; Osebold 2008; Learch et al. 2009; Rostom et al. 2009; Zheng et al. 2009; Choi et al. 2010; Amritanand et al. 2010; Suwanpimolkul et al. 2010; Berngard and Miller 2013; Feng et al. 2014; McAnearney 2015; Shrestha et al. 2015; Effendi et al. 2016; Fukuda et al. 2016; Khoo et al. 2016; Oki et al. 2016; Fareed et al. 2017; Cheng et al. 2018; Dahlberg et al. 2018; Myojin et al. 2018; Banerjee et al. 2018; Popa et al. 2019).

9 Conclusion

Salmonella is an uncommon cause of osteomyelitis, occurring generally in immunocompromised patients and mainly affects those with sickle cell disease. Vertebral location is very rare. MRI is the modality of choice to enable the diagnosis and assess the extent of infection. However, imaging does not allow differentiation between

Salmonella infection and infection caused by other pathogens. Bacteria isolation is necessary for definitive diagnosis and antibiotic susceptibility testing allows adequate antibiotic treatment. Blood culture and culture of specimens obtained by aspiration or biopsy are the two main ways of isolating the pathogen. CT may be used to guide percutaneous biopsy when other laboratory tests are negative and if surgery is not needed. Outcome is generally favorable under antibiotic therapy.

References

Abdullah SH, Ata OA, El-Adwan N (2008) Thoracic spinal epidural abscess caused by Salmonella typhi—case report. Neurol Med Chir (Tokyo) 48:140–142

Akiba T, Arai T, Ota T et al (2001) Vertebral osteomyelitis and paravertebral abscess due to Salmonella oranienburg in a child. Pediatr Int 43:81–83

Altay M, Kanbay M, Kurultak I et al (2006) A case of bilateral psoas abscesses and lumbar osteomyelitis due to recurrent salmonella infection. J Natl Med Assoc 98:1855–1856

Amritanand R, Venkatesh K, Sundararaj GD (2010) Salmonella spondylodiscitis in the immunocompetent: our experience with eleven patients. Spine (Phila Pa 1976) 35:1317–1321

Banerjee B, Madiyal M, Madhava PK et al (2018) Typhoid spondylodiscitis mimicking tuberculosis in a teenage girl. J Infect Public Health 11:136–137

Barkai G, Leibovitz E, Smolnikov A et al (2005) Salmonella diskitis in a 2-year old immunocompetent child. Scand J Infect Dis 37:232–235

Berngard SC, Miller M (2013) Salmonella spinal infection: a rare case in a patient with advanced AIDS. J Int Assoc Provid AIDS Care 12:241–244

Burnett MW, Bass JW, Cook BA (1998) Etiology of osteomyelitis complicating sickle cell disease. Pediatrics 101:296–297

Bussiere JL, Lopitaux R, Sirot J et al (1979) Spondylodiscites à Salmonella dublin. A propos d'une observation. Med Mal Infect 9:561–567

Carvell JE, Maclarnon JC (1981) Chronic osteomyelitis of the thoracic spine due to salmonella typhi: a case report. Spine (Phila Pa 1976) 6:527–530

Chambers JB, Forsythe DA, Bertrand SL et al (2000) Retrospective review of osteoarticular infections in a pediatric sickle cell age group. J Pediatr Orthop 20:682–685

Chen POQ, Yang SH, Yen CC et al (2001) Salmonella spondylitis in non-sickle cell patients. J Musculoskelet Res 5:253–260

Chen SH, Lin WC, Lee CH, Chou WY (2008) Spontaneous infective spondylitis and mycotic aneurysm: incidence, risk factors, outcome and management experience. Eur Spine J 17:439–444

Cheng W, Lian K, Luo D et al (2018) Salmonella potsdam causing lumbar vertebral osteomyelitis. Medicine (Baltimore) 97(18):e0682

Choi YS, Cho WJ, Yun SH et al (2010) A case of back pain caused by Salmonella spondylitis. Korean J Anesthesiol 59:233–237

Dahlberg RK, Lyvers ME, Dahlberg TK (2018) Diagnostic quandary: Salmonella agbeni vertebral osteomyelitis and epidural abscess. Case Rep Orthop 2018:1–4

Devrim I, Kara A, Kanra G et al (2005) Atypical presentation of spondylitis in a case with sickle cell disease. Turk J Pediatr 47:369–372

Effendi FM, Ibrahim MI, Mohd Miswan MF (2016) Salmonella spondylodiscitis of the thoracic vertebrae mimicking spine tuberculosis. BMJ Case Rep 2016:bcr2016215909. https://doi.org/10.1136/bcr-2016-215909

Fareed S, Nashwan AJ, Jarir SA et al (2017) Spinal abscess caused by salmonella bacteremia in a patient with primary myelofibrosis. Am J Case Rep 18:859–864

Feng ZY, Guo F, Chen Z (2014) Literature review and clinical presentation of cervical spondylitis due to Salmonella enteritidis in immunocompetent. Asian Spine J 8:206–210

Fukuda T, Bouchi R, Minami I et al (2016) Retrograde pyelonephritis and lumbar spondylitis as a result of Salmonella typhi in a type 2 diabetes patient with neurogenic bladder. J Diabetes Investig 7:436–439

Gardner RV (1985) Salmonella vertebral osteomyelitis and epidural abscess in a child with sickle cell anemia. Pediatr Emerg Care 1:87–89

Greenspan RH, Feinberg SB (1957) Salmonella bacteremia: a case with miliary lung lesions and spondylitis. Radiology 68:860–862

Gupta SK, Pandit A, White DG, Evans PD (2004) Salmonella osteomyelitis of the thoracic spine: an unusual presentation. Postgrad Med J 80:110–111

Khan FY, El-Hiday AH (2007) Typhoid osteomyelitis of the spine. Hong Kong Med J 12:391–393

Khoo HW, Chua YY, Chen JLT (2016) Salmonella typhi vertebral osteomyelitis and epidural abscess. Case Rep Orthop 2016:1–3

Kowalski TJ, Layton KF, Berbari EF et al (2007) Follow-up MR imaging in patients with pyogenic spine infections: lack of correlation with clinical features. AJNR Am J Neuroradiol 28:693–699

Kumar P, Mahmoodi SM, Kalaparambil Moosa N et al (2008) Salmonella paratyphi spondylitis: a case report. Eur Spine J 17:754–755

Laloum E, Zeller V, Graff W et al (2005) Salmonella typhi osteitis can mimic tuberculosis. A report of three cases. Joint Bone Spine 72:171–174

Learch TJ, Sakamoto B, Ling AC, Donovan SM (2009) Salmonella spondylodiscitis associated with a mycotic abdominal aortic aneurysm and paravertebral abscess. Emerg Radiol 16:147–150

Liu WH, Hsieh CT, Chan HB et al (2006) Salmonella spondylitis in the thoracic spine. J Med Sci 26:223–225

Mavrogenis AF, Megaloikonomos PD, Igoumenou VG et al (2017) Spondylodiscitis revisited. EFORT Open Rev 2:447–461
McAnearney S (2015) Salmonella osteomyelitis. Ulster Med J 84:171–172
McHenry MC (2002) Vertebral osteomyelitis: long-term outcome for 253 patients from 7 Cleveland-area hospitals. Infect Dis Clin Pract 11:169–170
Miller AA (1954) Salmonella dublin osteomyelitis of the spine. Br Med J 1:194–195
Myojin S, Kamiyoshi N, Kugo M (2018) Pyogenic spondylitis and paravertebral abscess caused by Salmonella Saintpaul in an immunocompetent 13-year-old child: a case report. BMC Pediatr 18:1–6
O'Keeffe M (1991) Brief report. J Nerv Ment Dis 179:108
Oki M, Ueda A, Tsuda A et al (2016) Salmonella enterica serotype enteritidis vertebral osteomyelitis and epidural abscess complicated with meningitis. Tokai J Exp Clin Med 41:169–171
Osebold WR (2008) Systemic leptospirosis followed by salmonella vertebral osteomyelitis without sickling or immunosuppression. Spine (Phila Pa 1976) 33:55–61
Ozturk C, Tezer M, Mirzanli C et al (2006) An uncommon cause of paraplegia: Salmonella spondylodiscitis. J Spinal Cord Med 29:234–236
Popa C, Mbaye M, Thioub M et al (2019) Acute paraplegia due to salmonella brandenburg spondylodiscitis: case report. Open J Mod Neurosurg 9:327–337
Rajesh PK, Mythili S, Subramaniam L (2004) Typhoid spine—a case report. Indian J Med Microbiol 22:128–191
Rostom S, Bahiri R, Srifi N, Hajjaj-Hassouni N (2009) Arthrite septique multifocale et spondylodiscites infectieuses à salmonelle chez un patient drépanocytaire. Press Med 38:1189–1191
Sánchez-Vargas FM, Abu-El-Haija MA, Gómez-Duarte OG (2011) Salmonella infections: an update on epidemiology, management, and prevention. Travel Med Infect Dis 9:263–277
Sans N, Faruch M, Lapègue F et al (2012) Infections of the spinal column-spondylodiscitis. Diagn Interv Imaging 93:520–529
Santos EM, Sapico FL (1998) Vertebral osteomyelitis due to Salmonellae: report of two cases and review. Clin Infect Dis 27:287–295
Saphra I, Winter JW (1957) Clinical manifestations of Salmonellosis in man. N Engl J Med 256:1128–1134
Shrestha P, Mohan S, Roy S (2015) Bug on the back: vertebral osteomyelitis secondary to fluoroquinolone resistant Salmonella typhi in an immunocompetent patient. BMJ Case Rep 2015:10–12
Skoutelis A, Gogos C, Siampi V et al (2001) Salmonella westerstede vertebral osteomyelitis and sepsis in an immunocompetent patient. Int J Infect Dis 5:228–229
Stephanie S, Schmalzle SA (2019) Salmonella enterica serovar Typhi osteomyelitis in a young adult with sickle cell and thalassemia traits: a possible association. IDCases 15:e00478
Suwanpimolkul G, Nilgate S, Suankratay C (2010) Typhoid spondylodiscitis: the first reported case in Southeast Asia and review of the literature. J Med Assoc Thail 93:137–141
Tsui HF, Chiu KH, Leung KS (1997) Osteomyelitis of the spine due to Salmonella infection—conservative treatment with quinolone: a case report. Can J Surg 40:48–50
Weiss H, Katz S (1970) Salmonella paravertebral abscess and cervical osteomyelitis in sickle-thalassemia disease. South Med J 63:339–341
Weston N, Moran E (2015) Salmonella newport causing osteomyelitis in a patient with diabetes. BMJ Case Rep 2015:2–4
Zheng X, Wang J, Wu C, Mehbod AA (2009) Salmonella osteomyelitis of multiple ribs and thoracic vertebra with large psoas muscle abscesses. Spine J 9:e1–e4

Imaging of Spinal Tuberculosis

Mouna Chelli Bouaziz, Mohamed Fethi Ladeb, Emna Labbène, Hend Riahi, Wafa Achour, Aida Berriche, and Soumaya Rammeh

Contents

M. Chelli Bouaziz (✉) · M. F. Ladeb · E. Labbène
H. Riahi
Department of Radiology, MT Kassab Institute of Orthopaedics, Tunis, Tunisia

Faculty of Medicine of Tunis, Tunis-El Manar University, Tunis, Tunisia
e-mail: bouaziz_mouna@yahoo.fr; fethiladeb@hotmail.fr; emnaensei@gmail.com; hend.riahi@gmail.com

W. Achour
Laboratory Department, National Bone Marrow Transplant Center, Tunis, Tunisia

Faculty of Medicine of Tunis, Tunis-El Manar University, Tunis, Tunisia
e-mail: wafaachour@gmail.com

A. Berriche
Department of Infectious Diseases, La Rabta Hospital, Tunis, Tunisia

Faculty of Medicine of Tunis, Tunis-El Manar University, Tunis, Tunisia
e-mail: aida.berricheg@gmail.com

S. Rammeh
Department of Pathology, Charles Nicolle Hospital, Tunis, Tunisia

Faculty of Medicine of Tunis, Tunis-El Manar University, Tunis, Tunisia
e-mail: rammehs@yahoo.fr

© The Author(s), under exclusive license to Springer Nature Switzerland AG 2021
M. F. Ladeb, W. C. G. Peh (eds.), *Imaging of Spinal Infection*,
Medical Radiology Diagnostic Imaging, https://doi.org/10.1007/978-3-030-70459-9_12

Abstract

Spinal tuberculosis represents 25–60% of all musculoskeletal tuberculosis. It remains frequent in low- and middle-income countries, and an increased incidence of infections has been recently observed in developed countries. Three main anatomico-radiological patterns have been described, namely, tuberculous spondylodiscitis (also called Pott disease), isolated tuberculous vertebral osteomyelitis, and primitive neural arch tuberculosis. Magnetic resonance imaging allows an early diagnosis of spinal tuberculosis. In the absence of early and adequate treatment, tuberculosis progresses and may lead to spinal deformities and/or neurological complications. A positive diagnosis is usually straightforward when the patient already has an existing extra-skeletal tuberculosis. Otherwise, spinal tuberculosis is typically confirmed by bacteriological and/or histopathological tests.

Abbreviations

CT	Computed tomography
MRI	Magnetic resonance imaging
TB	Tuberculosis

1 Introduction

Tuberculosis (TB) remains endemic in most developing countries. It is still frequently encountered, with incidences varying between 191 every 100,000 inhabitants in sub-Saharan Africa and 237 every 100,000 inhabitants in Southeast Asia (Durieux 1990; Lacut et al. 1995; Billo 1996; Huchon 1997). However, a resurgence of TB, with a rising incidence of spinal TB, has also been reported in the recent decades. Since 1980, cases in industrialized countries of Europe and the USA have emerged, mainly in immigrants from endemic countries with a high prevalence, in some groups with poor social conditions, and in immunocompromised patients, such as those with acquired immunodeficiency syndrome (AIDS) (Durieux 1990; Aït Khaled et al. 1997; Garg and Somvanshi 2011; Moon 2014).

2 Epidemiology

Musculoskeletal TB accounts for 1–5% of all tuberculous infections and 9–19% of extrapulmonary TB (Eschard et al. 1993; Lacut et al. 1995; Murray 1996; Aït Khaled et al. 1997; Bernard and Perronne 1997; Pertuiset et al. 1997; Moon 2014). Spinal TB represents 25–60% of musculoskeletal TB (Hamza 1993; Resnick 1995; Cotten et al. 1996; Engin et al. 2000; Tuli 2002; Ben Taarit et al. 2003; De Backer et al. 2006). However, the exact incidence and prevalence of spinal TB are unknown in most parts of the world. Currently, most of the patients with spinal TB in developed countries are immigrants from countries where TB is endemic (Garg and Somvanshi 2011). In Europe, the mean age of musculoskeletal TB varies from 45 to 72 years in native patients and from 27 to 39 years in patients originating from developing countries (Aït Khaled et al. 1997). Children are more frequently involved in developing countries (Lacut et al. 1995; Garg and Somvanshi 2011). In most European and American series, there is no gender predilection, with the disease involving males and females equally (Garg and Somvanshi 2011; Aït Khaled et al. 1997).

3 Pathophysiology

Musculoskeletal TB is generally due to *Mycobacterium tuberculosis*. In our experience, *Mycobacterium bovis* is observed in about 20% of cases (Chebbi et al. 2019). Musculoskeletal TB results from reactivation of a pulmonary primary infection focus (Murray 1996; Aït Khaled et al. 1997) after a variable delay, which is usually shorter in children (Eschard et al. 1993; Lacut et al. 1995; Aït Khaled et al. 1997; Pertuiset et al. 1997; Garg and Somvanshi 2011; Moon 2014). Tuberculous bacillus spreads by blood and inoculates the spine, hips, and knees (Moon 2014). Direct inoculation is rare (Lacut et al. 1995; Garg and Somvanshi 2011; Moon 2014). Spinal

involvement usually results from hematogeneous spread of *Mycobacterium tuberculosis* into the dense vasculature of the cancellous vertebral body. The primary infection site is usually either a pulmonary or a genitourinary lesion. Spread occurs either via the arterial or venous route (Garg and Somvanshi 2011). The predilection for spinal disease may be explained by the fact that the vertebrae are extremely well vascularized, even in adulthood (Agrawal et al. 2010).

Local or general predisposing factors are noted in 17–50% of cases, including poverty, overcrowding, illiteracy, malnutrition, alcoholism, drug abuse, diabetes mellitus, chronic hemodialysis, immunosuppressive treatment, and human immunodeficiency virus (HIV) infection (Eschard et al. 1993; Lacut et al. 1995; Aït Khaled et al. 1997; Moon 2014). However, musculoskeletal TB seems to be less frequent compared to infections due to atypical mycobacteria in patients infected by HIV (up to 9%) (Durieux 1990; Lacut et al. 1995; Aït Khaled et al. 1997; Pertuiset et al. 1997; Garg and Somvanshi 2011; Moon 2014).

Genetic susceptibility to spinal TB has recently been demonstrated, with an association found between FokI polymorphism in the vitamin D receptor gene and susceptibility to spinal TB (Garg and Somvanshi 2011).

4 Anatomico-Radiological Patterns

Three main anatomico-radiological patterns of spinal TB have been described, namely, tuberculous spondylodiscitis, also called Pott disease; solitary vertebral involvement, also called tuberculous spondylitis or vertebral osteomyelitis; and primitive neural arch tuberculosis. Spondylodiscitis corresponds to the involvement of the disk and vertebra, accounting for 47–94% of spinal TB (Davies et al. 1984; Eschard et al. 1993; Cotten et al. 1996; Chebbi et al. 2019). Spondylitis or vertebral osteomyelitis is an exclusive involvement of the vertebra sparing the adjacent disks. These "skip lesions" are due to the spread of infection along the Batson paravertebral plexus of veins (Agrawal et al. 2010). They may result in a vertebral collapse or extend into the spinal canal (Stabler and Reiser 2001). Subligamentous extension to contiguous or noncontiguous vertebrae without disk involvement is quite frequent, resulting in a multilevel tuberculous spondylitis. In a series of 206 cases of spinal TB, spondylitis accounted globally for 50%, varying from 30% in autochthonous inhabitants to 61% in immigrants (Aït Khaled et al. 1997). In spinal TB studied by MRI, spondylitis accounted for 28–54% of cases (Pertuiset et al. 1999).

Primitive neural arch tuberculosis represents 1–37% of spinal tuberculosis and is characterized by the frequency of epidural abscesses, spinal instability, and spinal cord compression (Eschard et al. 1993; Cotten et al. 1996; Naim-Ur-Rahaman et al. 1999; Ansari et al. 2001; Stabler and Reiser 2001; Boussel et al. 2002; Chebbi et al. 2019). Other patterns of spinal TB seem to be rare, although limited data are available in the literature. Subligamentous TB is a rare presentation which is initially located under the anterior longitudinal ligament and results in anterior erosion of multiple vertebral bodies with adjacent abscess (Morvan et al. 1998; Ansari et al. 2001; Stabler and Reiser 2001; Narlawar et al. 2002; Nassar et al. 2002). This presentation is more frequently observed in children (Sharif et al. 1995; Mahboubi and Morris 2001; Moorthy and Prabhu 2002; Chebbi et al. 2019). Primitive tuberculous epidural abscesses usually involve males and are located in the thoracic spine (Stabler and Reiser 2001; Ben Taarit et al. 2003). Spinal cord and nerve root involvement may be isolated or associated with spondylodiscitis. It may be observed at any age but usually occur in young adults (Ben Taarit et al. 2003; Gupta et al. 2015; Mishra et al. 2015).

4.1 Tuberculous Spondylodiscitis (Pott Disease)

Tuberculous spondylodiscitis was first described by Sir Percivall Pott in 1779.

4.1.1 Pathogenesis

TB initially locates in the subchondral bone of the anterior corners of the vertebral bodies which are the most vascularized region. Then it usually

extends to the adjacent vertebral body by contiguity beneath the anterior or posterior longitudinal ligament or through vascular anastomoses (Eschard et al. 1993; Lacut et al. 1995), causing progressive destruction of the disk and vertebra (Morvan et al. 1998; Ben Taarit et al. 2003; Chebbi et al. 2019). In spinal TB, more than one vertebra is usually involved because of the possibility of spread via the longitudinal vascular anastomosis. In adults, the involvement of the intervertebral disk is secondary to spread from the adjacent infected vertebra, whereas in children, the disk can be primarily involved by the hematogeneous route due to its vascularized nature (Morvan et al. 1998; Engin et al. 2000; Rasouli et al. 2012).

The disease may extend to the paravertebral soft tissues or to the spinal canal (Lacut et al. 1995). Tissue necrosis results in paravertebral abscess formation (Narlawar et al. 2002). Tuberculous abscesses are typically large, surrounded by a smooth wall, and may result in sinus tract formation (Dorcas and David 1995; Huchon 1997). A lack of proteolytic enzymes in mycobacterial infections, in comparison with pyogenic infections, has been suggested as the possible cause of the subligamentous spread and would also explain the abscess delimitation. The abscess extension is related to the site of vertebral infection, adjacent soft tissue anatomy, and gravity (Resnick 1995). At the cervical spine, abscesses develop anteriorly and laterally, whereas thoracic abscesses develop beneath the longitudinal spinal ligament. Lumbar abscesses develop along the psoas muscle and may reach the iliac fossa and the Scarpa's triangle. The presence of central or peripheral calcifications is characteristic of tuberculous abscesses (Resnick 1995; Naim-Ur-Rahaman et al. 1999; Stabler and Reiser 2001; Moorthy and Prabhu 2002; Chelli Bouaziz et al. 2013).

4.1.2 Topography

The upper lumbar and lower thoracic spine are the most frequently involved sites (80%) (Turgut 2001; Ben Taarit et al. 2003; Teo and Peh 2004). The cervical spine is involved in only 4–15% of cases (Cotten et al. 1996; Pertuiset et al. 1997) and the lumbosacral spine in 2–3% of cases (Pertuiset et al. 1999; Harisinghani et al. 2000; Moore and Rafii 2001). More than one vertebra is involved in 5–23% of cases, usually in children, immigrants, and immunocompromised persons (Pertuiset et al. 1997; Lamer et al. 1998; Papavero et al. 1999; Turgut 2001; Colmenero et al. 2004; Golden and Vikram 2005; Le Roux et al. 2005). The vertebral body is more frequently involved than the posterior arch.

4.1.3 Clinical Presentation

Clinical presentation of spinal TB is typically insidious. The delay between the initial symptoms and the diagnosis has decreased from 6 to 24 months in the past to a mean of 3 months in recent studies (Hamza 1993; Pertuiset et al. 1997). Spinal pain, usually marked, may be mechanical at the early stages, becoming inflammatory later on (Lacut et al. 1995; Murray 1996; Ben Taarit et al. 2003; Colmenero et al. 2004). Night sweats are observed in 20% of cases, with fatigue and weight loss. Fever is present in about 50% of cases. Neurological impairment is frequent (35–60% of cases) with variable patterns and severity. Spinal cord compression and cauda equina syndrome are observed in about 25–30% of cases (Pertuiset et al. 1997). Spinal TB revealed by the presence of a sinus tract is unusual in developed countries (Davies et al. 1984; Resnick 1995; Cotten et al. 1996; Pertuiset et al. 1999; Rasouli et al. 2012). Clinical examination shows segmental spine stiffness with paravertebral contracture or soft tissue abscesses (15–30% of cases). Spinal deformity is exceptional (Ladeb et al. 2019).

4.1.4 Imaging Features

4.1.4.1 Radiographs

Radiographs are usually the initial investigation when spinal TB is suspected. Osteolytic appearance of the vertebral body anterior corners and subchondral bone resorption are the first radiographic manifestations (Fig. 1). At an

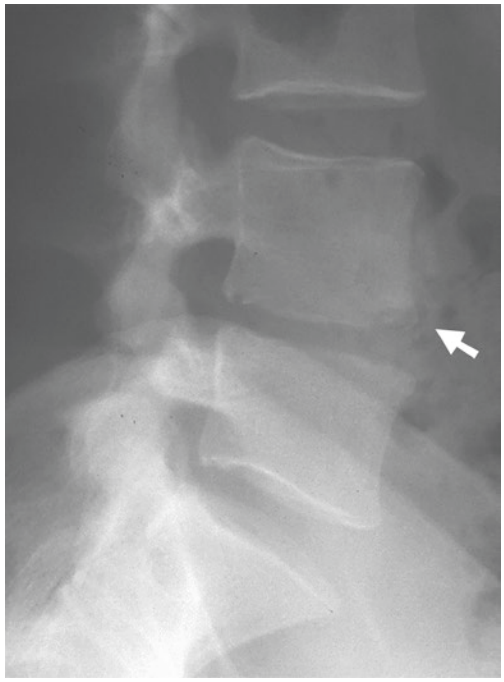

Fig. 1 Tuberculous spondylodiscitis of the lumbar spine. Lateral radiograph shows narrowing of L4/5 intervertebral disk space with subchondral destruction of the adjacent L4 vertebral anterior corner (arrow)

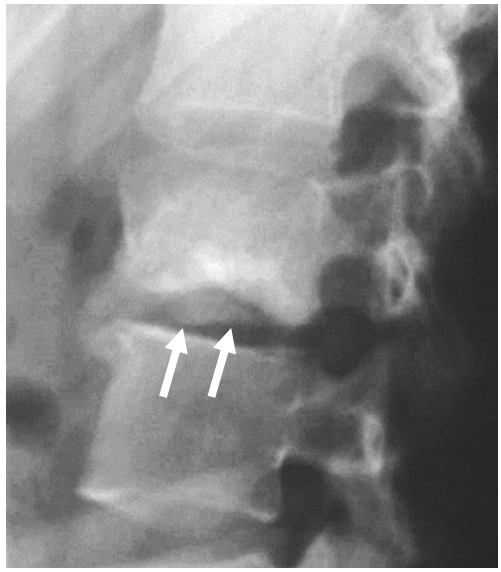

Fig. 2 Tuberculous spondylodiscitis. Lateral radiograph of the lumbar spine shows an osteolytic area of the inferior aspect of L3 vertebral body containing a sequestrum (arrows). There is adjacent sclerosis and narrowing of L3/4 intervertebral disk space

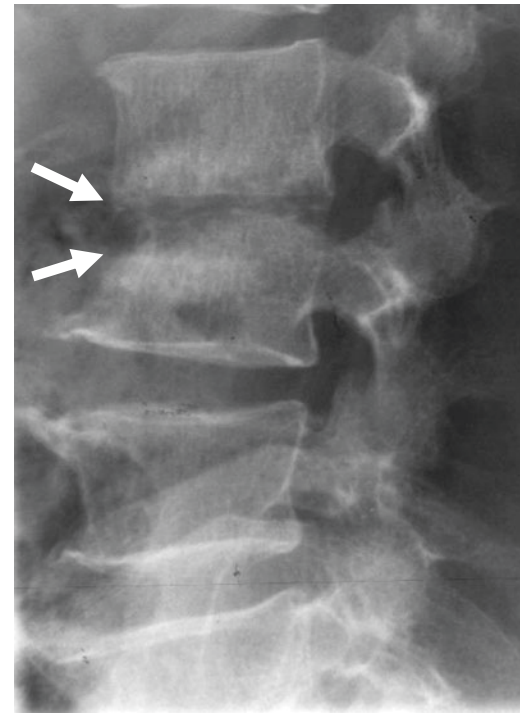

Fig. 3 Tuberculous spondylodiscitis. Lateral radiograph of the lumbar spine shows destruction of the anterior corners of L2 and L3 vertebral bodies and of the L2/3 intervertebral disk with peripheral bone sclerosis (arrows)

advanced stage of the disease, large intravertebral cavities continuous with the disk may be observed, typically limited by thin sclerotic rims and containing sequestra in half of the cases (Fig. 2) (Hamza 1993; Dorcas and David 1995). Bone sclerosis is seen less frequently than in brucellar or pyogenic spondylodiscitis (Moore and Rafii 2001; Stabler and Reiser 2001; Dinc et al. 2002).

The intervertebral disk is initially preserved. Subsequently, there is complete or partial disk narrowing, usually involving the anterior aspect (Fig. 3). The association of a normal disk height with intravertebral cavities is highly suggestive of spinal TB (Davies et al. 1984; Naim-Ur-Rahaman et al. 1999; Mahboubi and Morris 2001). Spontaneous evolution may result in vertebral collapse or anterior vertebral fusion, causing subsequent kyphosis (Fig. 4). Paravertebral abscess of the cervical spine appears on

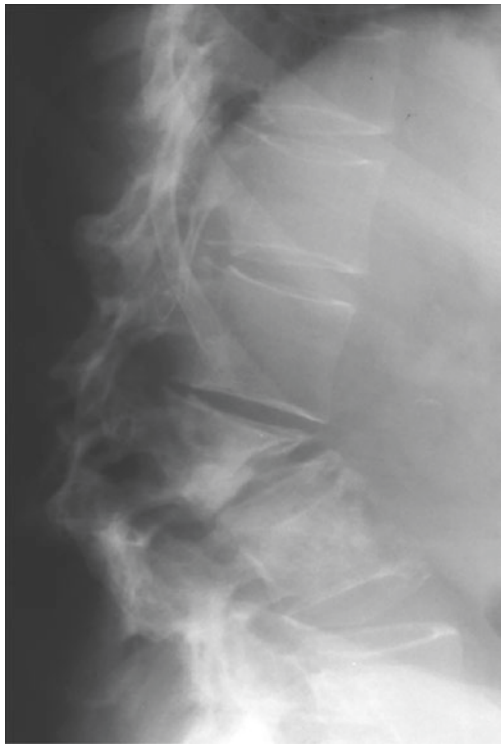

Fig. 4 Tuberculous spondylodiscitis. Lateral radiograph of the lumbar spine shows L2-L3 fusion with angular kyphosis

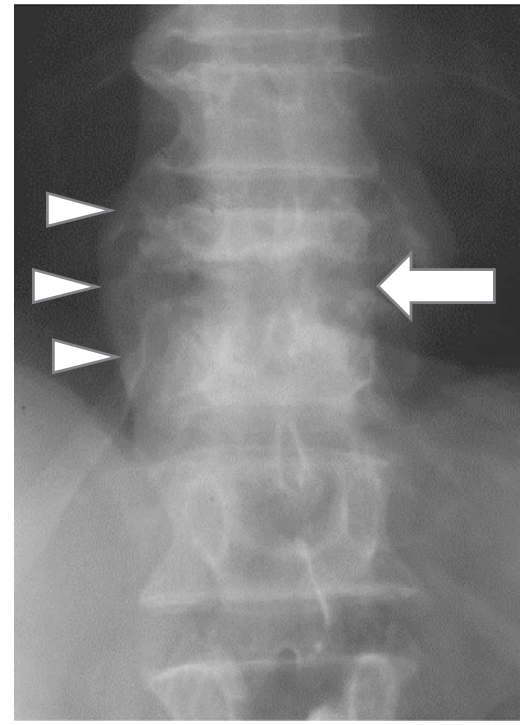

Fig. 6 T11-T12 tuberculous spondylodiscitis. Frontal radiograph of the thoracolumbar junction shows prominent discovertebral destruction (arrow) and paravertebral soft tissue thickening (arrowheads)

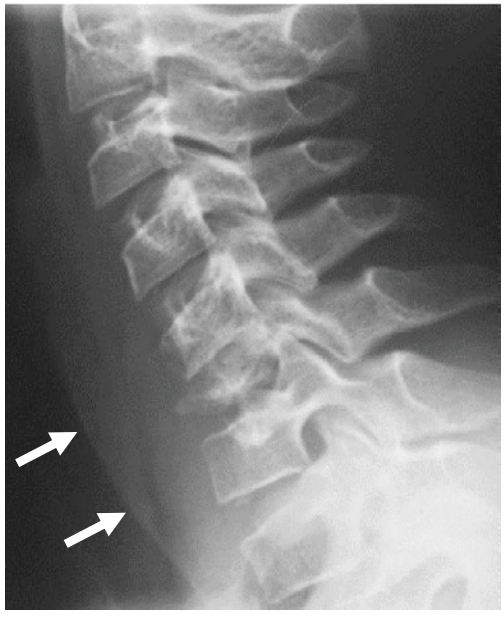

Fig. 5 C6 tuberculous spondylitis. Lateral radiograph of the cervical spine shows collapse of C6 vertebral body and thickening of the prevertebral soft tissues (arrows)

radiographs as a thickening of the prevertebral soft tissues (Fig. 5), whereas in the thoracic spine, it appears as a mediastinal opacity (Fig. 6) that may extend far from the discovertebral lesion. In the lumbar spine, paravertebral abscess may be seen as convexity of the lateral aspect of the psoas muscle (Dorcas and David 1995; Boussel et al. 2002; Dinc et al. 2002).

4.1.4.2 Ultrasonography

Ultrasonography plays a limited role in the diagnosis of spinal TB. It may be used at the cervical or lumbar level in the assessment of paravertebral abscesses and/or to guide needle aspiration or biopsy of these abscesses (Harisinghani et al. 2000) (Fig. 7).

4.1.4.3 Magnetic Resonance Imaging (MRI)

MRI is the method of choice in the diagnosis and follow-up of spinal TB (Sharif et al. 1995; Ridley

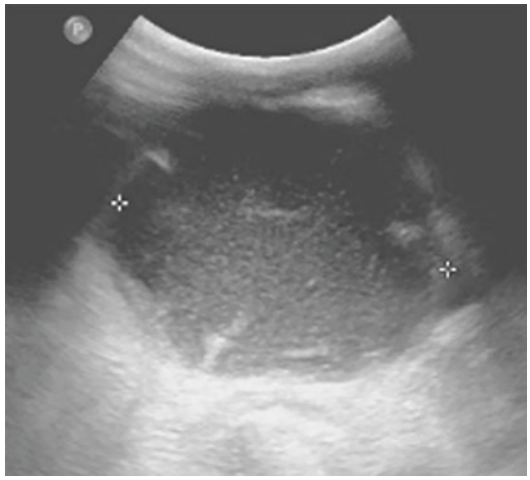

Fig. 7 Tuberculous spondylodiscitis of the cervical spine. Ultrasonographic image shows a large soft tissue abscess surrounded by a thin and smooth wall

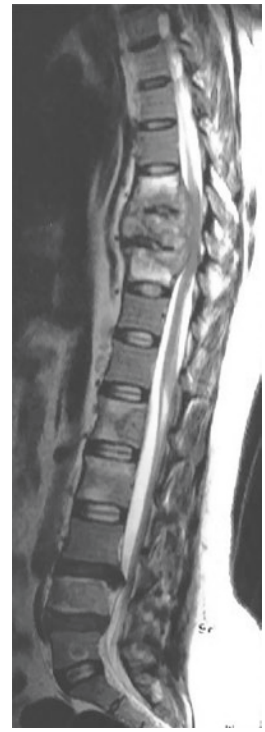

Fig. 8 Multifocal spinal tuberculosis. Sagittal T2-W MR image shows contiguous T8-T10 spondylodiscitis with multiple skip infections involving L1, L2, L4, and L5 vertebral bodies with relative sparing of the disks

et al. 1998; Moore and Rafii 2001; Stabler and Reiser 2001; Boussel et al. 2002; Moorthy and Prabhu 2002; Nassar et al. 2002; Teo and Peh 2004). The sensitivity of MRI allows early detection of bone changes before they appear on radiographs and CT. Moreover, this non-irradiating modality allows an assessment of the whole spine to look for additional asymptomatic spine locations, also called "skip infections," which may be observed in 16–70% of cases (Cotten et al. 1996; Morvan et al. 1998; Engin et al. 2000; Harisinghani et al. 2000; Jain 2010; Rivas-Garcia et al. 2013) (Fig. 8).

MRI is performed using a spine array coil, with spin echo T1-weighted sequences before and after intravenous gadolinium contrast administration in at least two orthogonal planes. The coronal plane is particularly useful to assess the extension of paravertebral abscesses and to rule out additional involvement of sacroiliac and/or coxofemoral joints (Sharif et al. 1995; Boussel et al. 2002). Spin echo or fast spin echo T2-weighted images with fat suppression or contrast-enhanced fat-suppressed T1-weighted MR images are more sensitive to detect early abnormalities of bone, spinal canal, and paravertebral soft tissues (Narlawar et al. 2002).

The involved vertebral body usually appears T1 hypointense and T2 hyperintense, with heterogeneous enhancement on contrast-enhanced T1-weighted images (Morvan et al. 1984; Ridley et al. 1998; Harisinghani et al. 2000; Nassar et al. 2002; Teo and Peh 2004). Intraosseous abscesses appear as areas of T1 hypointensity and T2 hyperintensity, with rim enhancement (Figs. 9 and 10). The penumbra sign described on T1-weighted sequences represents a relatively high T1 intensity of the internal layer of the abscess wall due to the presence of paramagnetic free radicals produced by activated macrophages. It appears to be very specific (99%) for abscess (Fig. 11) (Moser et al. 2012). Atypical MRI patterns have been reported, including intermediate to hypointense T2 signal or hyperintense T1 signal of the vertebral body (Pertuiset et al. 1999). This latter sign, usually observed in young patients, may be explained by the

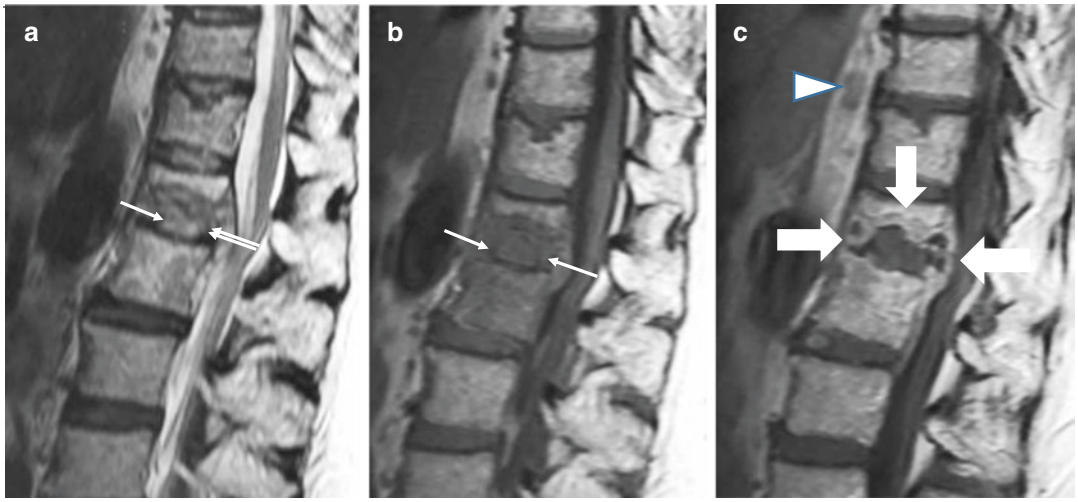

Fig. 9 Tuberculous spondylodiscitis. Sagittal (**a**) T2-W, (**b**) T1-W and (**c**) contrast-enhanced T1-W MR images show T1 hypointensity and T2 hyperintensity of the disk (small arrows) and adjacent vertebrae with peripheral enhancement after contrast administration (large arrows), epidural abscess, and spinal cord compression. Note the prevertebral lymph nodes (arrowhead)

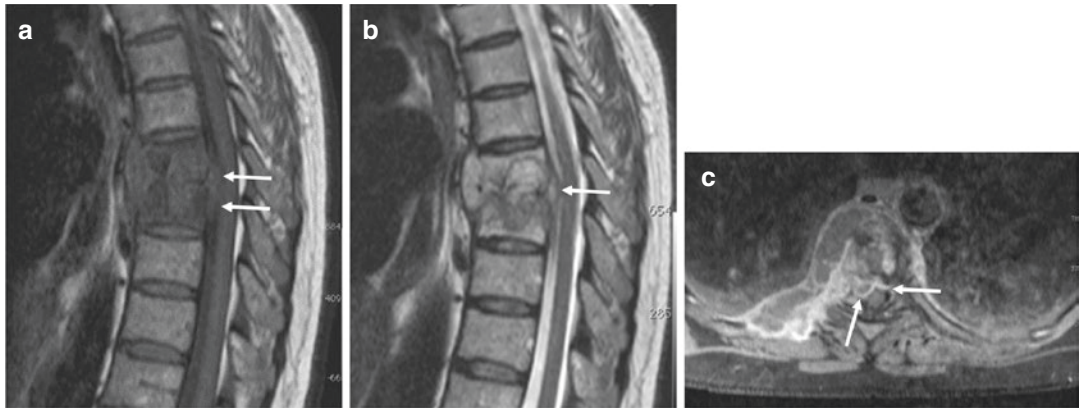

Fig. 10 T8-T9 tuberculous spondylodiscitis. Sagittal (**a**) T1-W, (**b**) T2-W, and (**c**) axial contrast-enhanced fat-suppressed T1-W MR images show T1 hypointensity and T2 hyperintensity of the vertebral body and intervertebral disk with epidural extension (arrows). Note the bilobed appearance of the epidural abscess (arrows) and the extension to the right costovertebral joint

increased level of proteins in the caseum (central necrotic material of tuberculous lesions) (Boussel et al. 2002).

Upon infection, the intervertebral disk T2 signal remains normal for a long time, and then the signal increases with the disappearance of the disk cleft. On T1-weighted images, the intervertebral disk is of intermediate signal intensity (Pertuiset et al. 1999; Boussel et al. 2002). Intravenous contrast administration results either in a diffuse or rim enhancement. A normal or T2-hypointense disk signal may be observed in children, at the early stage of the disease, in granulomatous spondylodiscitis, or in vertebral spondylitis (Teo and Peh 2004; Chelli Bouaziz et al. 2013, 2017). MRI allows a precise assessment of disease extension to the paravertebral soft tissues and the spinal canal.

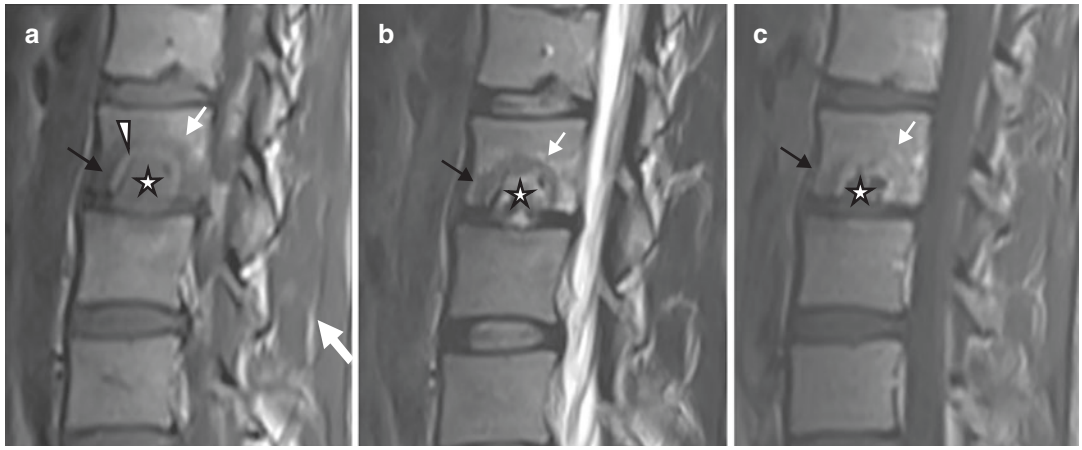

Fig. 11 L2-L3 tuberculous spondylodiscitis with the penumbra sign. Sagittal (**a**) T1-W, (**b**) T2-W, and (**c**) contrast-enhanced T1-W MR images show a target appearance of the L2 subchondral vertebral body abscess with four concentric layers: the abscess center (pus) has T1-hypointense and T2-hyperintense signal (star), the abscess wall with T1-hyperintense signal corresponding to granulation tissue (penumbra sign) (arrowhead), reactive sclerosis with hypointense T1 and T2 signal (black arrow), and the peripheral bone edema with T1-hypointense and T2-hyperintense signal and contrast enhancement (white arrow)

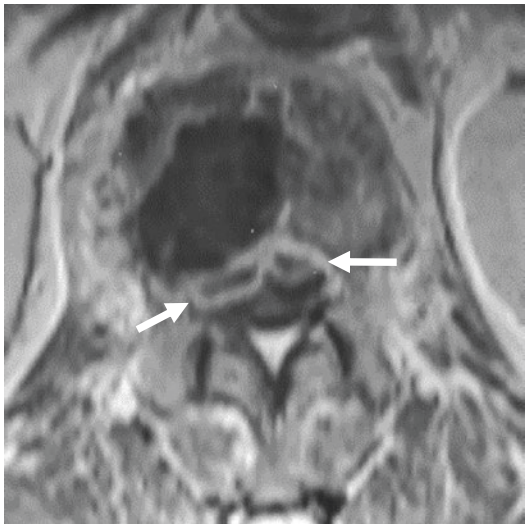

Fig. 12 Tuberculous spondylodiscitis. Axial contrast-enhanced fat-suppressed T1-W MR image shows a bilobed epidural abscess (arrows)

Abscesses show hyperintense T2 signal and hypointense to intermediate T1 signal, surrounded by smooth well-defined and well-vascularized walls (Morvan et al. 1984; Boussel et al. 2002; Teo and Peh 2004). Epidural phlegmon appears as an epidural mass of intermediate T1 and hyperintense T2 signal, with enhancement on contrast-enhanced T1-weighted images (Boussel et al. 2002). Epidural abscess and phlegmon typically show a "bilobed" shape (Madhok and Sachdeva 2016) (Fig. 12). MRI is an excellent tool to assess the longitudinal extent of the epidural abscess or mass and its effects on the spinal cord or the cauda equina (Morvan et al. 1998; Boussel et al. 2002).

Associated lesions, including arachnoiditis, myelitis, or intramedullary tuberculomas, are well depicted by MRI, particularly on contrast-enhanced T1-weighted images. They appear as linear or nodular enhancement of the subarachnoid space, spinal cord, or nerve roots (Davies et al. 1984) (Fig. 13). Intramedullary tuberculomas are characterized by areas of central hypointensity and rim enhancement on contrast-enhanced T1-weighted MR images, with or without central T2 hyperintensity (Mishra et al. 2015). Nerve root involvement may present as meningeal enhancement, clumping of nerve roots or nerve radicles, a soft tissue mass replacing subarachnoid space, or a mixed pattern (Gupta et al. 2015).

Currently, functional MRI sequences are generally not used in routine practice. Diffusion MRI has been proposed to distinguish tuberculous spondylitis from vertebral metasta-

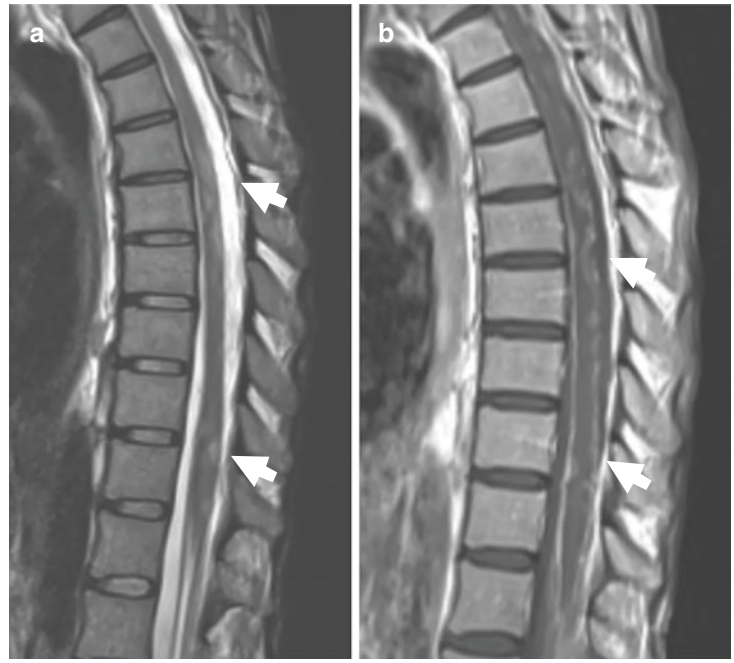

Fig. 13 Tuberculous arachnoiditis. Sagittal (**a**) T2-W and (**b**) contrast-enhanced fat-suppressed T1-W MR images show hyperintense signal intensity and nodular enhancement of the spinal cord and the subarachnoid space (arrows) [Image courtesy of Prof. Cyrine Drissi]

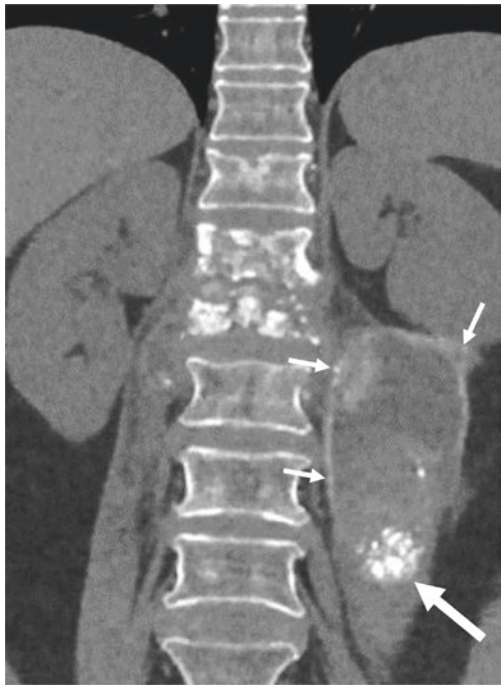

Fig. 14 Tuberculous spondylodiscitis. Coronal CT image of the thoracolumbar spine shows a destructive spondylodiscitis with a left psoas absess. Note the small calcifications in the abscess wall (small arrows) and center (large arrow) of the left psoas abscess, in addition to the thoracolumbar junction spondylodiscitic destructive changes

ses by demonstrating the absence of restriction in cases of infection. However, some doubtful cases have been observed (Ansari et al. 2013; Ladeb et al. 2013). Some authors have evaluated the role of magnetic resonance spectroscopy (MRS) and showed an increased lipid/lactate peaks in the diagnosis of spinal TB (Rauf et al. 2015).

4.1.4.4 Computed Tomography (CT)

CT is more sensitive than radiographs for detecting early bone destruction. It also allows a precise assessment of disease extension to the spinal canal and posterior elements and to look for an associated posterior arthritis (Cotten et al. 1996). The details of vertebral collapse are better assessed by sagittal and coronal CT images (Dorcas and David 1995; Sharif et al. 1995; Pertuiset et al. 1999; Boussel et al. 2002; Dinc et al. 2002; Teo and Peh 2004). Calcifications and bone sequestra are better seen on CT than MRI (Cotten et al. 1996) (Figs. 14 and 15). The involved disk may show intradiscal hypodensity which is better depicted on sagittal and coronal images (Boussel et al. 2002).

Paravertebral tuberculous abscesses are usually large and bilateral (Cotten et al. 1996; Ridley

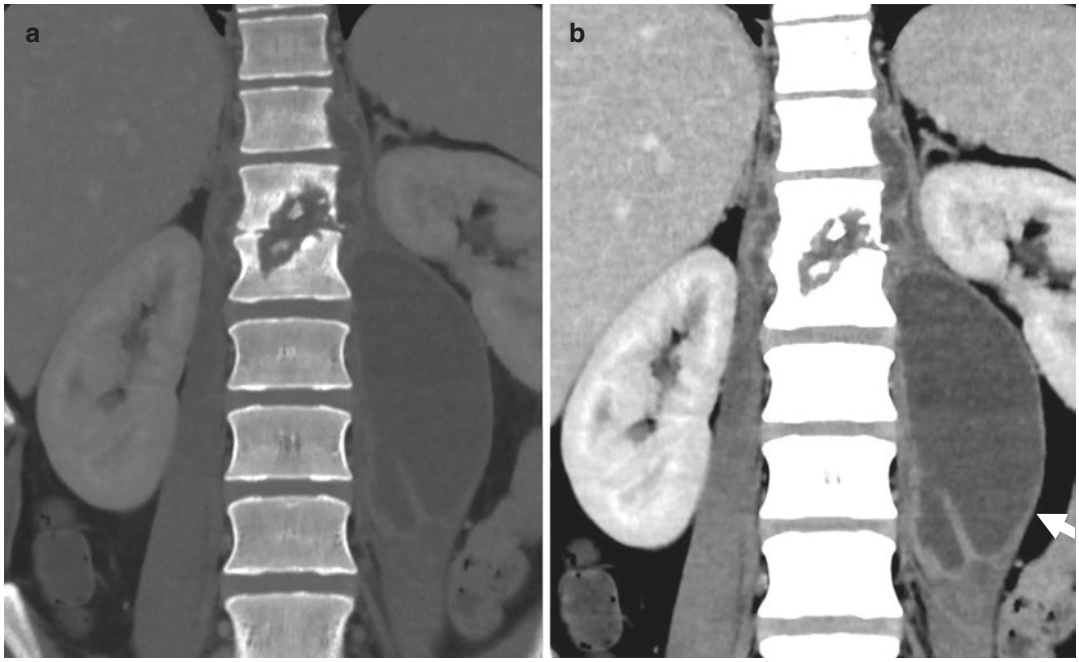

Fig. 15 Tuberculous spondylodiscitis. Coronal CT images of the thoracolumbar spine obtained in (**a**) bone and (**b**) soft tissue window settings show areas of adjacent vertebral bone destruction containing sequestra and a large left psoas abscess with thin and smooth walls (arrow)

et al. 1998; Naim-Ur-Rahaman et al. 1999; Mahboubi and Morris 2001; Stabler and Reiser 2001). They appear on CT as hypodense collections limited by thin, smooth, and well-vascularized walls (Fig. 15). The presence of calcifications at the center or the periphery of the abscess is characteristic of TB (Figs. 16 and 17) (Sharif et al. 1995; Cotten et al. 1996; Pertuiset et al. 1999). Epidural extension is inconstant and visible as an epidural abscess or mass of spontaneously high density that is homogeneously enhanced after contrast administration. Abscess and phlegmon respect the posterior longitudinal ligament and show a bilobed pattern on axial images (Stabler and Reiser 2001; Boussel et al. 2002) (Figs. 10 and 12).

CT is more frequently performed compared to MRI for the assessment of bone destruction. In our practice, CT is reserved for spinal cord compression secondary to vertebral destruction that extends to the neural arch, for suspicion of spinal instability, and when there are MRI contraindications. It is also used for percutaneous biopsy guidance to obtain histological and bacteriological specimens. It is indicated in the preoperative assessment of secondary spine deformities (Sharif et al. 1995; Harisinghani et al. 2000; Stabler and Reiser 2001; Turgut 2001; Teo and Peh 2004).

4.1.4.5 Scintigraphic Imaging

Scintigraphic imaging is particularly recommended in patients with suspected spinal infection, when MRI cannot be obtained (Berbari et al. 2015). Technetium-99m (^{99m}Tc) scintigraphy has a place in the diagnosis of spinal TB, with a sensitivity varying from 65 to 100% but a low specificity. It allows early diagnosis of spinal infection and detection of other asymptomatic locations. The most commonly used tracers are ^{99m}Tc-diphosphonates and Gallium-67 (^{67}Ga)-citrate, with both being sensitive but not specific. The usefulness of ^{67}Ga bone scintiscan remains uncertain, with several authors report many false negatives (Cotten et al. 1996; Pertuiset et al. 1999; Boussel et al. 2002; Shikhare et al. 2011).

Three-phase bone scintigraphy may demonstrate hyperemia and increased blood pool activ-

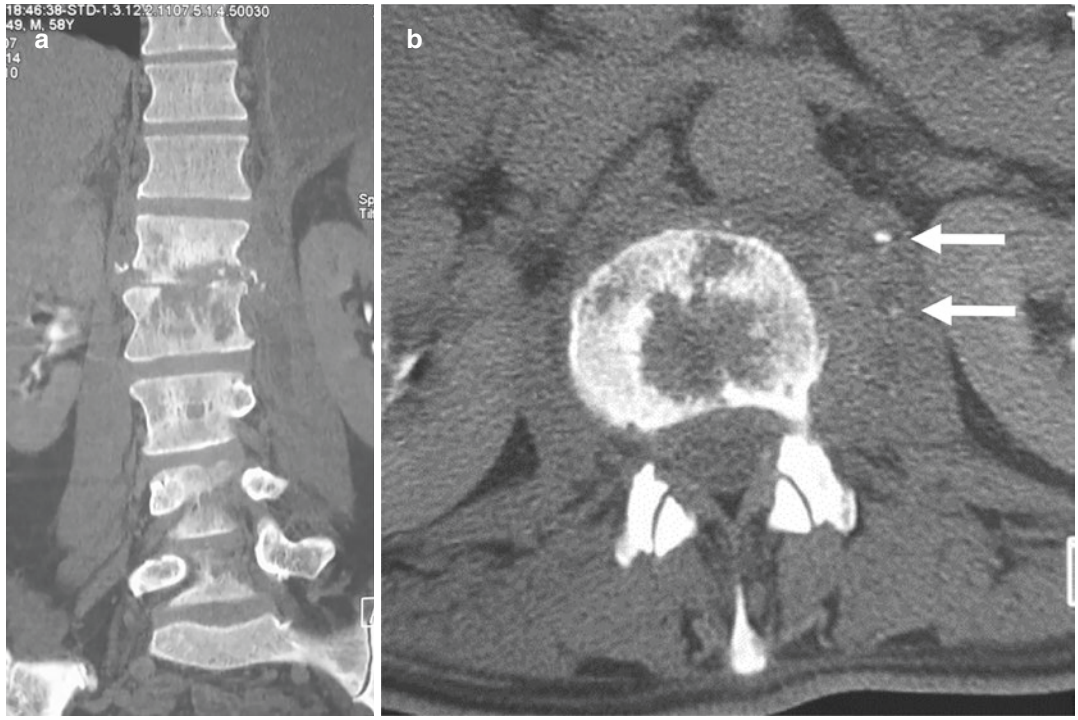

Fig. 16 L1-L2 tuberculous spondylodiscitis. (**a**) Coronal and (**b**) axial CT images obtained in bone window setting show discovertebral destruction and small calcifications of the abscess walls (arrows)

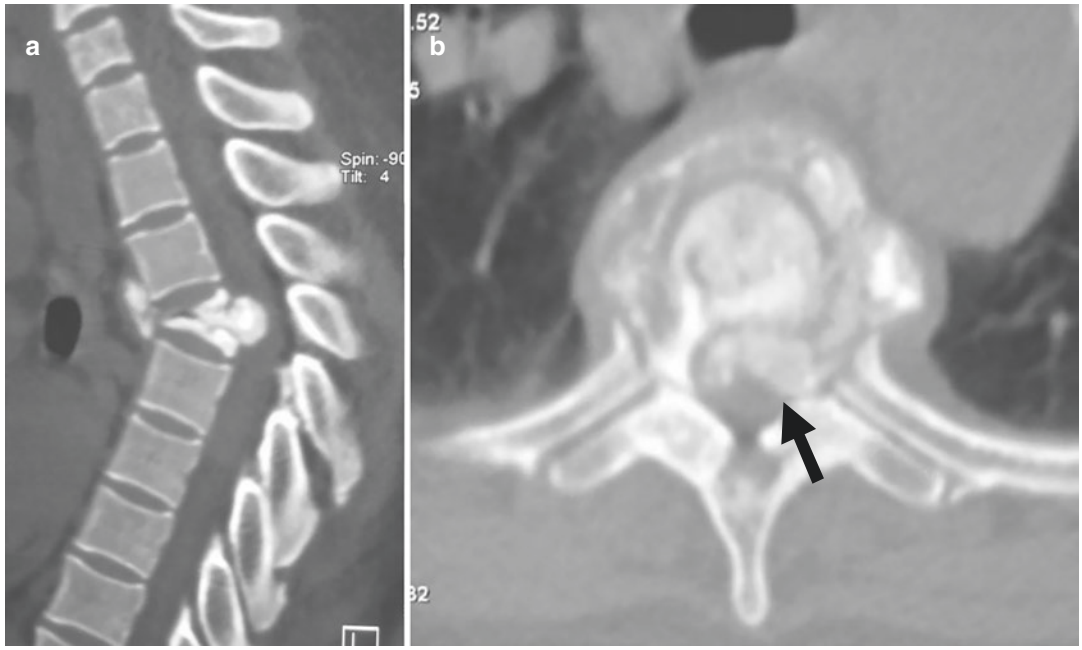

Fig. 17 Long-standing T4-T6 tuberculous spondylodiscitis. (**a**) Sagittal and (**b**) axial CT images taken in bone window setting show prominent discovertebral destruction with bone sclerosis and calcified paravertebral and epidural abscesses (arrow)

ity. Single photon emission tomography (SPET) and single photon emission computed tomography (SPECT) have a better spatial resolution than bone scintigraphy and may thus reveal abnormalities not seen on the planar images (Shikhare et al. 2011). Bone scintigraphy is now being gradually replaced by fluorine-18 2′-deoxy-2-fluoro-D-glucose positron emission tomography ([^{18}F] FDG-PET). PET using [^{18}F] FDG has a sensitivity of 97.5% and a specificity of 86.3% in the diagnosis of musculoskeletal infections. At the moment of diagnosis, it detects additional tuberculous foci in 60–80% of patients, which has, in certain cases, an impact on the treatment (Ladeb et al. 2015). Some authors have noted elevated standardized uptake values (SUV) (>21) compared to pyogenic infections (Yang et al. 2003; Heysell et al. 2013). Recent studies showed that [^{18}F] FDG-PET/CT had a superior diagnostic value for detecting spondylodiscitis within the first 2 weeks (Smids et al. 2017). After this period, for the diagnosis of spondylodiscitis, the diagnostic value of [^{18}F] FDG-PET/CT is comparable to that of MRI for the evaluation of the entire spine (Altini et al. 2020). PET allows follow-up after treatment, as FDG uptake returns to its normal value in 3–4 months, and quantification of SUV has been proposed to detect residual lesions (Rivas-Garcia et al. 2013).

4.1.5 Topographic Pattern: Cranio-cervical Junction Tuberculosis

TB of the cranio-cervical junction (Figs. 18 and 19) is a rare presentation of spinal tuberculosis (2% of spondylodiscitis) involving the first two cervical vertebrae, as well as atlanto-occipital

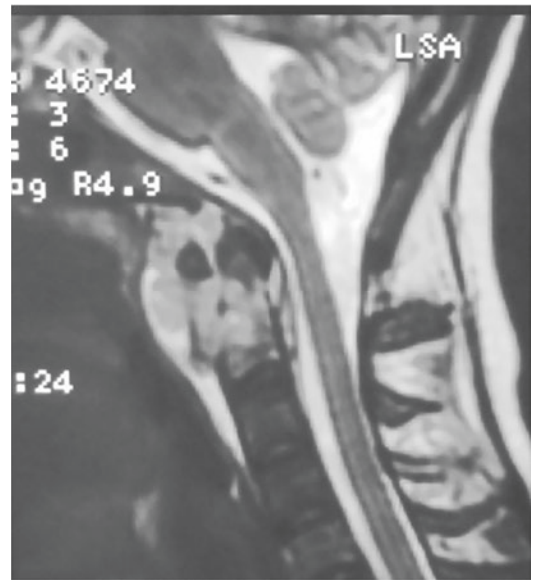

Fig. 19 Cranio-cervical junction tuberculosis. Sagittal T2 MR image shows signal hyperintensity of C1 and C2 vertebral bodies with epidural and paravertebral extension

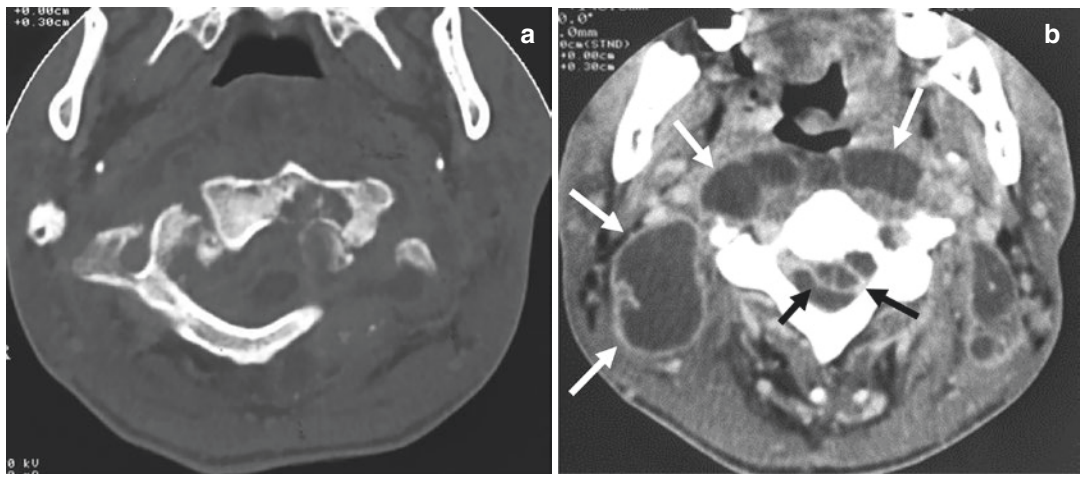

Fig. 18 Cranio-cervical junction tuberculosis. Axial CT images obtained in (**a**) bone and (**b**) soft tissue window settings show destruction of C1 and C2 vertebrae with atlantoaxial dislocation and epidural (black arrows) and paravertebral abscesses (white arrows)

and atlantoaxial joints (Resnick 1995; Boussel et al. 2002). Two hypotheses have been suggested to explain its pathogenesis, namely, (1) initial involvement of lateral C1 masses with destruction of the transverse ligament and extension of the infection to the retropharyngeal space and neighboring joints and (2) initial involvement of the retropharyngeal space followed by extension to C1-C2 vertebrae by lymphatic and venous anastomoses. Cranio-cervical junction TB may cause spinal cord compression by C1-C2 dislocation (disruption of the transverse ligament), by ascending dislocation of the odontoid, or by extension of an anterior epidural abscess (Boussel et al. 2002). Radiographic assessment of this condition may be rather difficult. CT is useful to depict bone destruction, especially of the neural arch, and MRI is the method of choice for the assessment of spinal canal extension.

4.1.6 Differential Diagnosis

Differential diagnosis of Pott disease mainly includes other spondylodiscitis (Table 1) and erosive degenerative disk disease (Table 2) (Resnick 1995; Cotten et al. 1996; Narlawar et al. 2002; Nassar et al. 2002). Clinical findings may help, but the distinction between tuberculous, brucellar, mycotic, and pyogenic spinal infections may be difficult (Morvan et al. 1984; Ridley et al. 1998; Harisinghani et al. 2000; Moore and Rafii 2001; Attia et al. 2004).

In typical cases, the differential diagnosis between tuberculous and brucellar spinal infection is quite straightforward. However, brucellar spondylodiscitis may mimic TB (multifocal spinal involvement, discovertebral extensive destruction, large abscesses with or without calcifications), the so-called pseudo-Pott brucellar spondylitis (Fig. 20). Bacteriological and/or immunological tests are needed to make the positive diagnosis (Madkour et al. 1988; Sharif et al. 1989; Al-Shahed et al. 1994; Chelli Bouaziz et al. 2008, 2010).

Fungal spondylodiscitis is a very uncommon condition, accounting for 0.6–1.6% of infective spondylodiscitis (Fig. 21). However, their incidence has recently been increasing, due to rise in immunosuppressive conditions such as diabetes

Table 1 Main differentiating signs among tuberculous spondylodiscitis (Pott disease), brucellar spondylodiscitis, and pyogenic spondylodiscitis

	Tuberculous spondylodiscitis	Brucellar spondylodiscitis	Pyogenic spondylodiscitis
Disk narrowing	Late and marked	Late and moderate	Early and moderate
Vertebral body destruction	Marked	Mild	Marked
Vertebral sclerosis	Late and moderate	Early and marked	Early and marked
Vacuum phenomenon	Absent	Possible: peripheral and small	Absent
Soft tissue abscess	Frequent, large, and well-defined	Inconstant, small, well-defined	Variable size and ill-defined
Preferential location	Thoracic and thoracolumbar spine	Lower lumbar spine	Lumbar spine

Table 2 Main differentiating MRI features between Pott disease and erosive degenerative disk disease

	Erosive degenerative disk disease	Pott disease
Disk	Vacuum phenomenon T2-hypointense +/− linear T2-hyperintense signal Linear enhancement	Diffuse T2-hyperintense signal Diffuse or rim enhancement
Vertebral body	Marked sclerosis Superficial erosions Homogeneous enhancement	Moderate and late sclerosis Important bone destruction Heterogeneous enhancement
Paravertebral abscess	Absent	50–70% of cases

mellitus, HIV, and patients undergoing chemotherapy (Comacle et al. 2016). The most frequently encountered agents are *Candida* spp. and *Aspergillus* spp. Clinical and radiological findings are not specific, and the diagnosis is often delayed and made on anatomicopathological study of the discovertebral specimen (Williams et al. 1999; Wrobel et al. 2001). Blood cultures are negative in 24–50% of cases (Arias et al. 2004).

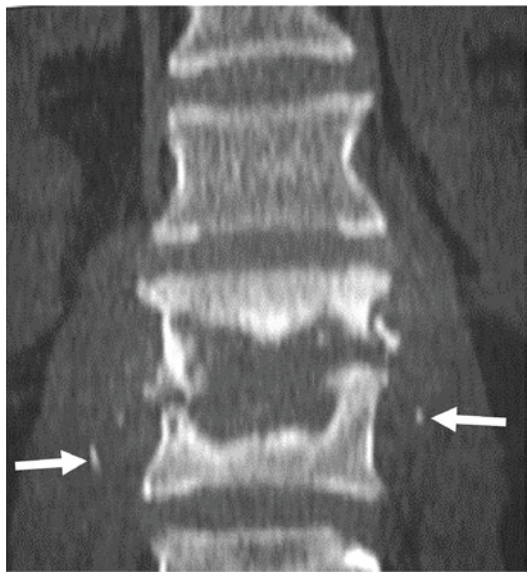

Fig. 20 Pseudo-Pott brucellar spondylitis. Coronal CT image shows extensive destruction of vertebral end plates surrounded by bone sclerosis with multiple adjacent small calcifications (arrows)

Antigen and antibody detection assays based on the detection of circulating cell wall fungal antigens are useful in fungal infections, where they have a high positive predictive value for the diagnosis of *Candida albicans*. Molecular techniques have also been used with fungal infection and have enhanced the sensitivity of conventional methods utilized in diagnostic mycology (Skaf et al. 2010). The imaging appearances of fungal spondylodiscitis often mimic tuberculous spondylodiscitis due to the frequency of subligamentous extension and involvement of multiple contiguous or noncontiguous vertebral bodies (skip lesions). The hypointense T2 signal of the disk and subchondral bone may be observed in both conditions. However, the abscess wall is typically thin and smooth in spinal TB and thick and irregular in fungal spondylodiscitis.

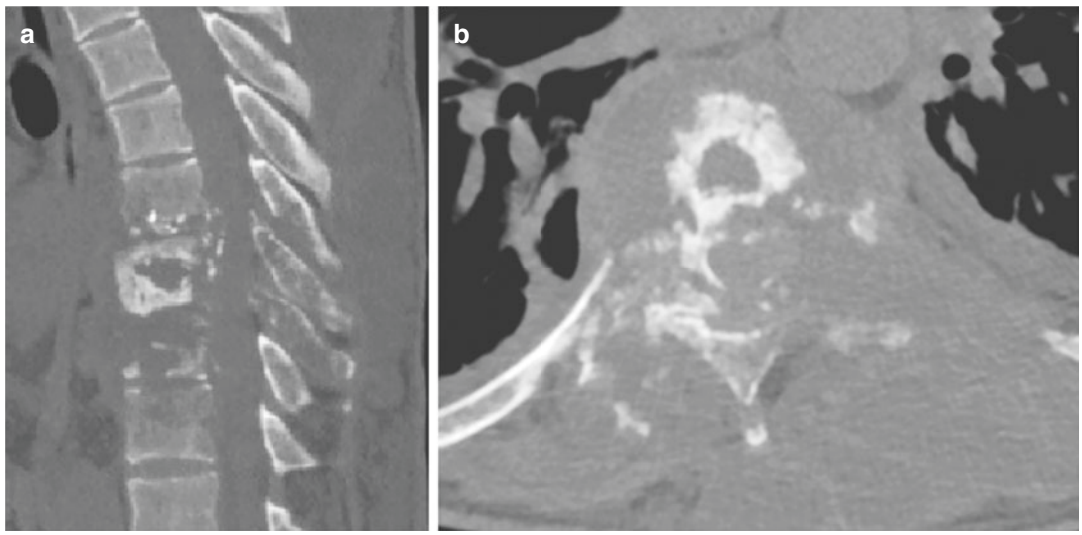

Fig. 21 Fungal spondylodiscitis. (**a**) Sagittal and (**b**) axial CT images obtained in bone window settings show extensive destruction of T8, T9, T10, and T11 vertebral bodies and posterior elements with costovertebral and costotransverse septic arthritis and soft tissue extension

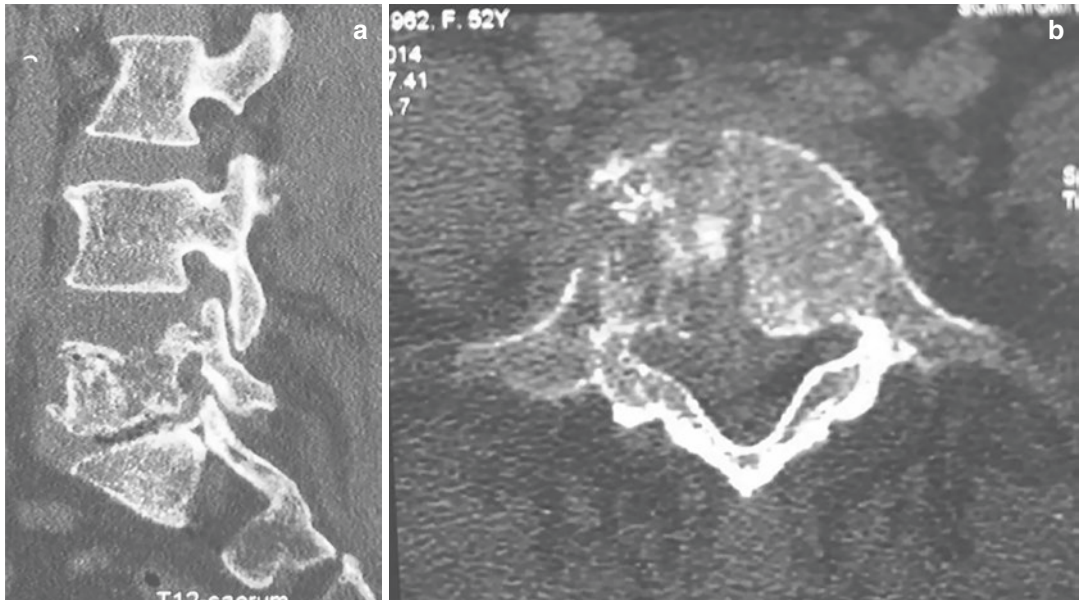

Fig. 22 Spinal sarcoidosis. (**a**) Sagittal and (**b**) axial CT images show destructive areas in the L5 vertebral body without disk or soft tissue involvement

Bone sarcoidosis usually involves the small tubular bones of the hands and feet but may also involve the axial or appendicular skeleton, with an incidence varying from 1 to 14% (Rua-Figueroa et al. 2002). Bone lesions may be single or multiple or osteolytic, sclerotic, or mixed (Fig. 22). On MRI, the vertebral body shows T1-hypointense and T2-hyperintense signal, with variable enhancement after IV gadolinium contrast administration. The posterior elements and intervertebral disks are rarely involved (Lefere et al. 2014). Chest CT is indicated to show mediastinal and pulmonary abnormalities that are suggestive of sarcoidosis. Bone scintigraphy and PET/CT are sensitive but not specific (Valencia et al. 2009).

Spinal hydatidosis (caused by the parasite *Echinococcus granulosus*) may mimic TB at an advanced stage of the disease, following disk involvement. The conservation of vertebral body height and shape is suggestive of echinococcosis, as well as the presence of multiple intra- and extra-osseous vesicles on ultrasonography, CT, and MRI. Other features are the lack of bone marrow edema and the frequent extension to the neighboring bones (e.g., ribs, iliac bone) (Ladeb et al. 2013).

4.1.7 Imaging Follow-Up

Radiological follow-up of tuberculous spondylodiscitis evolves in three steps. First, a progression of the lesions may be observed (progression of disk narrowing, bone destruction, and vertebral collapse), indicating a diagnostic error or a resistance to antibiotics. After 1 or 2 months of treatment, stabilization of the disease is observed, with subsequent signs of bone healing (peripheral sclerosis and osteophytes). The late phase depends on the importance of discovertebral lesions at the time of treatment instauration. Complete vertebral fusion (Fig. 23) results from bone destruction which exposes the vertebral cancellous bone. In cases of moderate bone destruction, vertebral fusion may be incomplete. Restoration to original condition can be obtained only in cases of early treatment. On MRI, the disk and the vertebral body signal decreases on T2-weighted and contrast-enhanced T1-weighted images. Fatty reconversion of the vertebral body marrow correlates to a favorable clinical outcome (Fig. 24). The

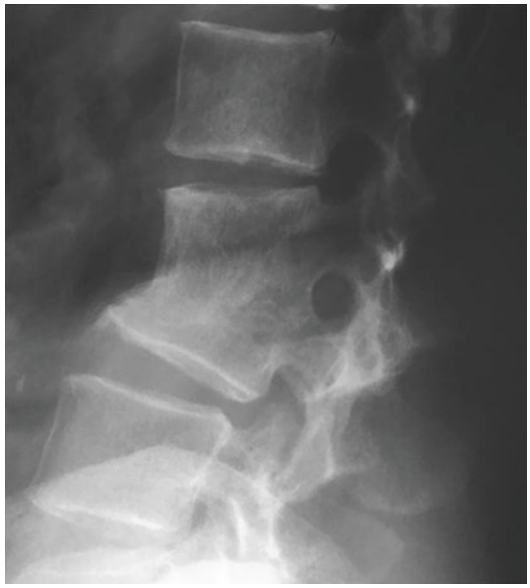

Fig. 23 Patient treated for tuberculous spondylodiscitis. Two-year follow-up lateral radiograph shows complete vertebral fusion

abscesses should disappear in 1–12 months. Signal abnormalities may remain but do not indicate failure of treatment. PET/CT allows follow-up of spondylodiscitis after treatment.

4.1.8 Complications

The main complications of tuberculous spondylodiscitis are kyphosis and spinal cord compression. Spinal cord compression following tuberculous spondylodiscitis is observed in 30–40% of cases (Hamza 1993; Pertuiset et al. 1997; Lolge et al. 2003). Early compression following an evolutive TB must be distinguished from late compression appearing several years after recovery. Early compression may result from epidural abscesses, bone sequestra, subluxation, arachnoiditis, spinal cord ischemia, or a combination of these, whereas late compression mainly results from kyphosis (Martini 1988). Neurological impairment in tuberculous spondylodiscitis is usually symmetrical and progressive

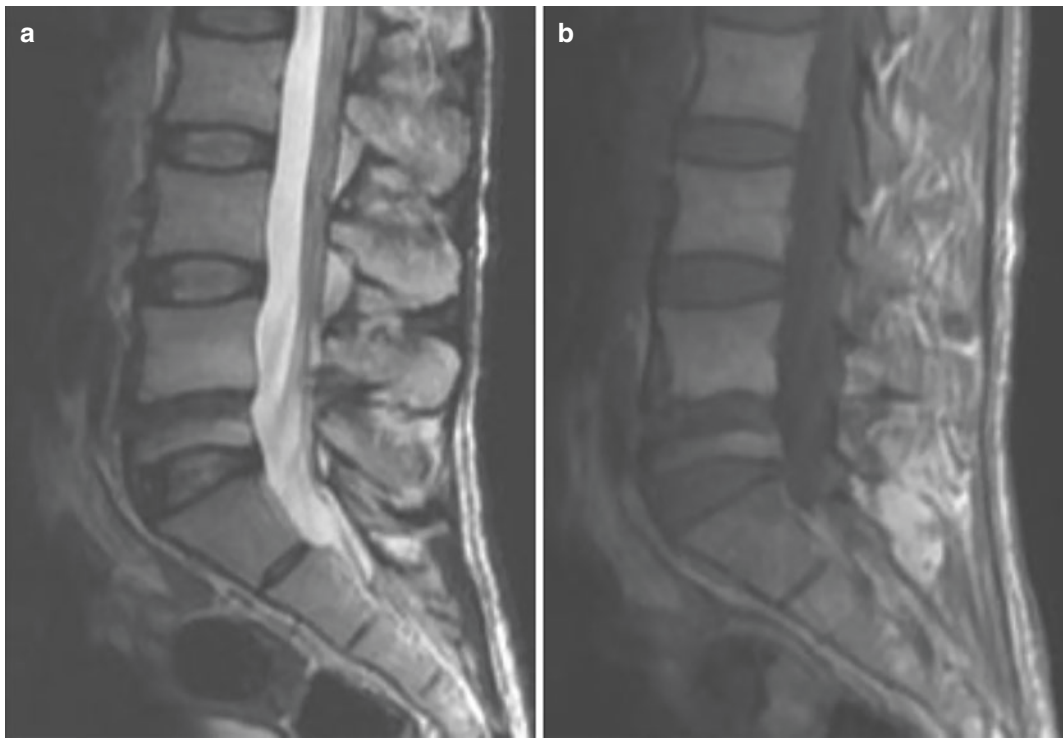

Fig. 24 Patient treated for tuberculous spondylitis. Two-year follow-up sagittal (**a**) T2-W and (**b**) T1-W MR images show fatty marrow reconversion of the vertebral bodies, indicative of healing

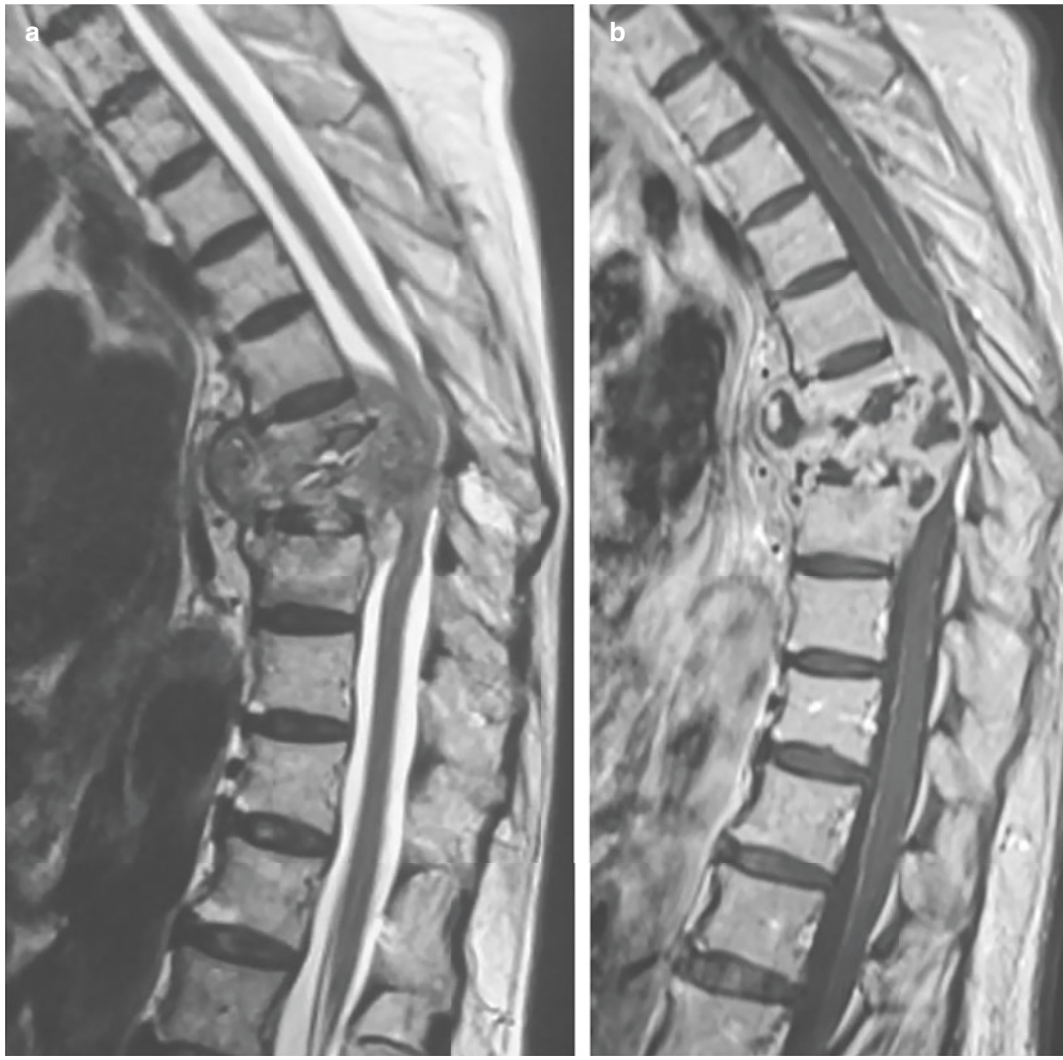

Fig. 25 Pott's paraplegia. Sagittal (**a**) T2-W and (**b**) contrast-enhanced T1-W MR images show discovertebral destruction with a large epidural abscess and spinal cord compression

(Ridley et al. 1998). Pott's paraplegia usually regresses after medical treatment.

CT (Fig. 17) and MRI (Fig. 25) are useful to identify the cause of compression, with osseous causes being better depicted by CT than MRI (Sharif et al. 1995; Cotten et al. 1996; Morvan et al. 1998; Pertuiset et al. 1999; Dinc et al. 2002; Moorthy and Prabhu 2002; Narlawar et al. 2002; Teo and Peh 2004). Kyphosis is the consequence of spondylodiscitis with destruction of several vertebral bodies. It is radiologically assessed by Cobb method. Kyphosis progression may be caused by incomplete bone repair, more frequent in children than in adults. Kyphosis may cause chronic pain, spinal cord compression, or cardiorespiratory issues.

4.2 Vertebral Osteomyelitis (Solitary Vertebral Involvement)

In solitary spinal involvement, the infection exclusively involves the vertebra, sparing the

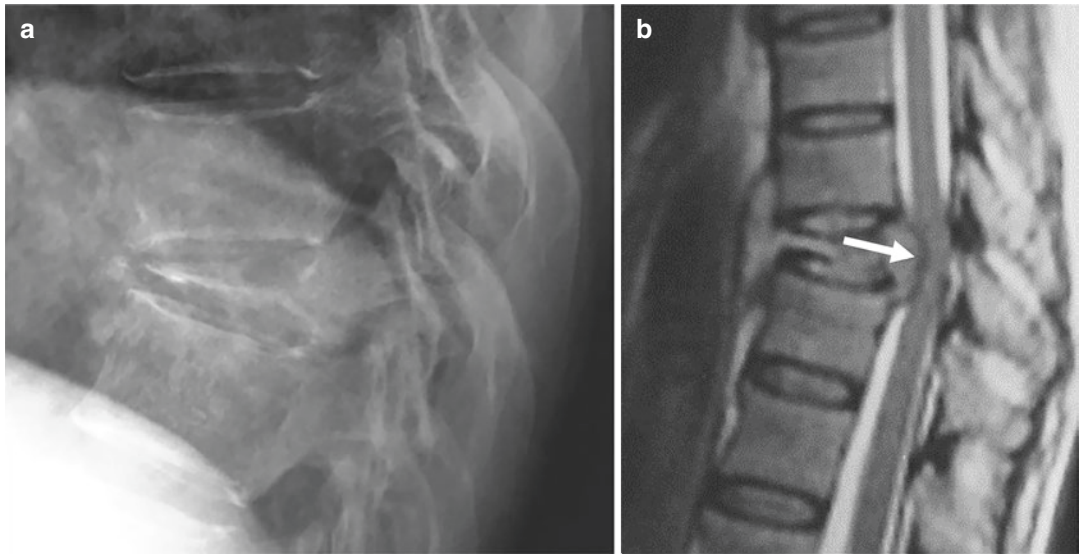

Fig. 26 Tuberculous spondylitis (solitary vertebral involvement). (**a**) Lateral radiograph shows a single severe vertebral collapse sparing the adjacent disks. (**b**) Sagittal T2-W MR image shows spinal cord compression (arrow)

intervertebral disk. However, one or more vertebrae, contiguous or not, may be involved. Radiographs are normal in about 45% of cases (Lolge et al. 2003). Otherwise, they may show a round or oval osteolytic lesion, usually at the center of the vertebral body with a peripheral sclerotic rim (Cotten et al. 1996; Pertuiset et al. 1999; Boussel et al. 2002). Moth-eaten osteolysis may also be observed, sometimes resulting in vertebral collapse, with homogeneous or heterogeneous bone sclerosis that may hide the underlying osteolysis (Fig. 26).

Differential diagnoses includes lymphoma, myeloma, metastasis, and eosinophilic granuloma. Clinical and biological findings as well as the presence of paravertebral and/or epidural abscesses are helpful to make the diagnosis. Vertebral destruction is better depicted by CT. MRI usually shows intermediate T1 and hyperintense T2 signal of one or several vertebral bodies, with sparing of the intervertebral disks. Intravenous gadolinium administration shows diffuse or heterogeneous vertebral enhancement and allows assessment of intraspinal and paravertebral extension of the disease. The presence of discovertebral and/or perivertebral abscesses is essential to distinguish tuberculous solitary vertebral involvement from the other differential diagnoses of a solitary vertebral lesion. When abscesses are not present and when there is no clinical and biological evidence of infection, percutaneous biopsy may be required to obtain diagnostic confirmation.

4.3 Primitive Neural Arch Tuberculosis

Neural arch tuberculosis may involve one or more spinal levels and is usually observed in the cervicothoracic spine (Fig. 27) (Resnick 1995; Sharif et al. 1995; Cotten et al. 1996; Pertuiset et al. 1999; Boussel et al. 2002; Ben Taarit et al. 2003). The neural arch involvement may occasionally be the initial site of tuberculosis (Resnick 1995). Involvement of a single vertebral arch is far more common (Wallace and Cohen 1976; Kumar 2017). Imaging plays an important role in the diagnosis (Morvan et al. 1998; Nassar et al. 2002). The analysis of radiographs is not always easy, and the detection of neural arch abnormalities is possible in less than 10% of the cases

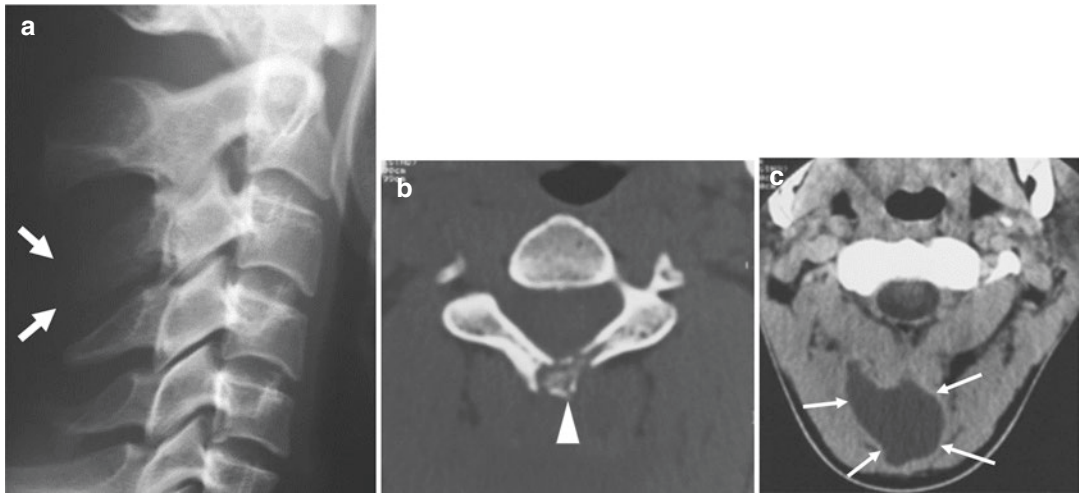

Fig. 27 Neural arch tuberculosis. (**a**) Lateral radiograph of the cervical spine shows an osteolytic lesion of C3 spinous process (arrows). Axial CT images obtained in (**b**) bone and (**c**) soft tissue window settings after contrast administration show osteolysis, sequestrum (arrowhead), and adjacent soft tissue abscess (small arrows)

(Morvan et al. 1998; Narlawar et al. 2002). Radiographs may show an osteolysis of a spinous process, a lamina or a pedicle. Bone destruction may extend to the posterior cortex of the vertebral body or the adjacent ribs with relative sparing of the intervertebral disks (Resnick 1995; Morvan et al. 1998). Well-defined or ill-defined bone sclerosis may also be observed (Cotten et al. 1996).

CT allows a more precise assessment of bone and adjacent soft tissues. It shows intraspinal and extra-spinal extension of the infection, which is particularly frequent in this presentation (Cotten et al. 1996; Narlawar et al. 2002; Nassar et al. 2002). The presence of an associated zygapophyseal, costovertebral, or costo-transversal arthritis is of great diagnostic value (Cotten et al. 1996). On MRI, the lesions show hypointense T1 and hyperintense T2 signal intensity with contrast enhancement (Morvan et al. 1998). Neural arch involvement may cause spinal instability, in which imaging diagnosis is important for surgical planning (Narlawar et al. 2002). Differential diagnoses include metastases, primitive spinal tumors, and hydatidosis (Garg and Somvanshi 2011; Momjian and George 2014).

5 Spinal Tuberculosis Diagnosis

5.1 Presumptive Diagnostic Signs

TB is suspected when there is a history of recent primary infection (30%), another active TB focus (19–30%), satellite lymphadenopathy (10%), and positive tuberculin intradermal reaction (IDR) (75–100%). During tuberculous spondylodiscitis, the increase in erythrocyte sedimentation rate and C-reactive protein is observed in 55% and 75% of cases, respectively. The radiological presumptive signs are listed in Table 3.

5.2 Diagnosis Confirmation

Etiological confirmation is usually established by either the demonstration of acid-fast bacilli on microscopy/culture or by histological examination of material obtained following biopsy of the lesion (Garg and Somvanshi 2011). Ziehl-Neelsen microscopy of the collection is positive in 17–30% of cases. Its low sensitivity is explained by the paucibacillary nature of

Table 3 Radiological signs suggesting spinal TB

Location	Thoracolumbar junction or lower thoracic spine
Extension	Multifocal Subligamentous extension at three vertebra or more
Vertebra	Bone osteolysis adjacent to the disk Sequestra Involvement of vertebral bodies sparing the disk Intravertebral abscess Neural arch involvement: frequent (68% in children, 52% in adults). May be isolated Heterogeneous enhancement of the vertebral body
Disk	Late involvement
Epidural extension	Bilobed appearance of the epidural abscess or phlegmon
Soft tissue abscesses	Frequent, large, well-defined, and smooth walls Calcifications at the center or the periphery of the abscess
Extra-osseous locations	Pulmonary, genitourinary, lymph nodes

osteoarticular TB. Culture is necessary to identify *M. tuberculosis* complex and test its sensitivity to anti-TB drugs. *M. tuberculosis* is isolated by culture of pus from paravertebral abscesses in 42% of cases (Wallace and Cohen 1976). *M. tuberculosis* grows on solid media (Lowenstein's medium) in 4 weeks (2–6 weeks). The use of liquid media reduces the culture time to 2 weeks (8–14 days). Gene amplification techniques identify the mycobacteria of *M. tuberculosis* complex, with a sensitivity of 98% in the case of a positive smear and of 75% in the case of a negative smear. They also offer early and rapid diagnosis of tuberculosis (Garg and Somvanshi 2011).

Improvements in percutaneous biopsy techniques have reduced the number of surgical biopsies. Discovertebral biopsy allows rapid histopathological examination by showing epithelioid and giant cell granulomas, with or without necrosis, in approximately 90% of cases (Trecarichi et al. 2012). False negatives are seen at an advanced stage of the disease when fibrosis sets in (Francis et al. 1999). Cytological puncture is a cheap, rapid, and fairly nonaggressive technique and with a very low risk of complications (Masood 2013). In countries with a high endemicity of TB, cytopathological examination can constitute an alternative to histopathology, provided that the proceduralist and the cytopathologist are well trained (Masood 2013). It is particularly recommended for paravertebral abscesses and osteolytic lesions with cortical interruption; these are frequently observed in tuberculous spondylodiscitis (Gupta et al. 1999).

In cytology, epithelioid granulomas, giant cells, and caseous necrosis are observed with frequencies varying from 50 to 68% (Ben Taarit et al. 2003). If there is a discrepancy between clinico-radiological and cytological results, a vertebral or discovertebral biopsy is necessary for diagnosis (Kang et al. 1999; Jorda et al. 2000; Handa et al. 2009; Gasbarrini et al. 2012). The histopathological differential diagnosis of spinal TB arises with other granulomatous infections, such as brucellosis, mycoses, and sarcoidosis. Suppurative forms are rare and can be considered in the absence of an epithelioid granuloma for an infection with pyogenic bacteria. It is the positivity of Ziehl-Neelsen staining on the histological sections, and especially the bacteriological examination, which allows the correct diagnosis to be made.

Conventionally, the inflammatory infiltrate of brucellosis is polymorphic, rich in lymphocytes, and associated with plasma cells and neutrophils, and the small histiocytic granuloma is made up of small groups of histiocytes (Li et al. 2016), but cases of associated granulomatous brucellosis with necrosis have been reported (Halimi et al. 1999). Mycotic spondylodiscitis can also be granulomatous and necrotizing. Demonstration by special stains of spores and mycelial filaments in yeast infection and hyphae in filamentous fungal infection confirms the mycotic origin. In the

absence of caseous necrosis, the histological distinction between spinal sarcoidosis and TB is not easy.

6 Treatment

Anti-TB drug treatment is the gold standard for the treatment of tuberculous spondylodiscitis, whereas surgical treatment plays an important role as adjunctive therapy.

6.1 Anti-tuberculosis Treatment

The treatment of spinal TB is essentially medical. It consists of four antibiotics (isoniazid [INH], rifampicin, ethambutol, and pyrazinamide) for 2 months, followed by two antibiotics (INH and rifampicin) for the 7–10 months, for a total treatment duration of 9–12 months (Eschard et al. 1993; Ramachandran et al. 2005). Adherence to treatment is an essential condition for healing and must be adhered to. The frequency of side effects to anti-TB drugs requires regular clinical and biological monitoring.

6.2 Associated Treatment

Vertebral immobilization is necessary in cervical spine TB and in TB complicated by spinal compression or instability (Hamza 1993). Rehabilitation must be considered after the acute phase of rest and stabilization of the bone lesions. It is necessary to prevent muscular atrophy (Eschard et al. 1993). The aim of surgery is to completely remove a lesion, achieve spinal decompression and stability, and restore a normal spinal balance (De Backer et al. 2006). The indications for surgery are as follows: (1) acute spinal compression, compression of bone origin, and flaccid paraplegia (Hamza 1993); (2) large paravertebral abscesses resistant to medical treatment and percutaneous drainage; and (3) progressive kyphosis with spinal instability (Golden and Vikram 2005; Ramachandran et al. 2005).

7 Conclusion

Spinal TB accounts for 25–60% of musculoskeletal TB. Three main anatomico-radiological patterns are tuberculous spondylodiscitis (Pott disease), tuberculous spondylitis, and primary neural arch TB. Time to diagnosis has improved from 6–24 months in the past to 3 months on average in the more recent series, thanks to advances in imaging. Imaging also helps to clarify the extent of the infection and its impact on the spinal cord and nerve roots, but it only provides presumptive diagnosis of spinal TB. In the absence of active extra-spinal TB, confirmation of diagnosis of TB is provided by histology and/or bacteriology.

References

Agrawal V, Patgaonkar PR, Nagariya SP (2010) Tuberculosis of spine. J Craniovertebr Junction Spine 1:74–85

Aït Khaled N, Enarson D, Billo N (1997) Epidémiologie de la tuberculose et de la résistance aux antituberculeux. Rev Mal Resp 14:5S8–5S18

Al-Shahed MS, Sharif HS, Haddad MC et al (1994) Imaging features of musculoskeletal brucellosis. Radiographics 14:333–348

Altini C, Lavelli V, Niccoli-Asabella A et al (2020) Comparison of the diagnostic value of MRI and whole body ^{18}F-FDG PET/CT in diagnosis of spondylodiscitis. J Clin Med 9:1581. https://doi.org/10.3390/jcm9051581

Ansari S, Ashraf AN, Al-Moutaery K (2001) Spinal infection: a review. Neurosurg Q 11:112–123

Ansari S, Amanullah MF, Ahmad K, Rauniyar RK (2013) Pott's spine: diagnostic imaging modalities and technology advancements. N Am J Med Sci 5:404–411

Arias F, Mata-Essayag S, Landaeta ME et al (2004) Candida albicans osteomyelitis: case report and literature review. Int J Infect Dis 8:307–314

Attia M, Harnof S, Knoller N et al (2004) Cervical Pott's disease presenting as a retropharyngeal abscess. Isr Med Assoc J 6:438–439

Ben Taarit C, Turki S, Ben Maïz H (2003) La tuberculose ostéoarticulaire en Tunisie: étude rétrospective de 180 cas. Med Mal Infect 33:210–214

Berbari EF, Kanj SS, Kowalski TJ et al (2015) Infectious Diseases Society of America (IDSA) clinical practice guidelines for the diagnosis and treatment of native vertebral osteomyelitis in adults. Clin Infect Dis 61:e26–e46

Bernard L, Perronne C (1997) La tuberculose ostéoarticulaire aujourd'hui. Presse Med 26:308–310

Billo NE (1996) Tendances épidémiologiques de la tuberculose. Rev Prat 46:1332–1335

Boussel L, Marchand B, Blineau N et al (2002) Imagerie de la tuberculose ostéo-articulaire. J Radiol 83:1025–1034

Chebbi Y, Riahi H, Bouaziz MC et al (2019) Mycobacterium bovis spondylodiscitis: report of 4 cases. J Clin Rheumatol 10:1097

Chelli Bouaziz M, Ladeb MF, Chakroun M, Chaabane S (2008) Spinal brucellosis: a review. Skeletal Radiol 37:785–790

Chelli Bouaziz M, Bougamra I, Kaffel D, Hamdi W, Ghannouchi M, Kchir MM (2010) Non-contiguous multilevel spondylitis: an exceptional presentation of spinal brucellosis. Tunis Med 88:280–284

Chelli Bouaziz M, Ladeb MF, Chakroun M (2013) Tuberculose rachidienne. In: Laredo JD, Wybier M, Petrover D (eds) Imagerie rhumatologique et orthopédique. Ed Sauramps Medical, pp 523–538

Chelli Bouaziz M, Riahi H, Ladeb MF, Chakroun M, Rammeh S (2017) Imagerie de la tuberculose rachidienne. Encycl Med Chir Radiologie et imagerie médicale-musculosquelettique-neurologique-maxillofaciale 31-670-C-10

Colmenero JD, Jimenez-Mejias ME, Reguera JM et al (2004) Tuberculous vertebral osteomyelitis in the new millennium: still a diagnostic and therapeutic challenge. Eur J Clin Microbiol Infect Dis 23: 477–483

Comacle P, Le Govic Y, Hoche-Delchet C et al (2016) Spondylodiscitis due to Aspergillus terreus in an immunocompetent host: case report and literature review. Mycopathologia 181:575–581

Cotten A, Flipo RM, Drouot MH et al (1996) La tuberculose vertébrale. Etude des aspects cliniques et radiologiques à partir d'une série de 82 cas. J Radiol 77:419–426

Davies PD, Humphries MJ, Byfield SP et al (1984) Bone and joint tuberculosis. A survey of notifications in England and Wales. J Bone Joint Surg Br 66: 326–330

De Backer AI, Mortelé KJ, Vanhoenacker FM, Parizel PM (2006) Imaging of extraspinal musculoskeletal tuberculosis. Eur J Radiol 57:119–130

Dinc H, Ahmetoglu A, Baykal S et al (2002) Image-guided percutaneous drainage of tuberculous iliopsoas and spondylodiskitic abscesses: midterm results. Radiology 225:353–358

Dorcas CY, David JS (1995) Musculoskeletal tuberculosis. Radiol Clin North Am 33:679–689

Durieux P (1990) Epidémiologie de la tuberculose. Rev Prat 40:703–705

Engin G, Acunas B, Acunas G, Tunaci M (2000) Imaging of extrapulmonary tuberculosis. Radiographics 20:471–488

Eschard JP, Leone J, Etienne JC (1993) Tuberculose osseuse et articulaire des membres. Encycl Méd Chir, Appareil locomoteur, 14-185-A-10, 15 p

Francis IM, Das DK, Luthra UK et al (1999) Value of radiologically guided fine needle aspiration cytology (FNAC) in the diagnosis of spinal tuberculosis: a study of 29 cases. Cytopathology 10:390–401

Garg RK, Somvanshi DS (2011) Spinal tuberculosis: a review. J Spinal Cord Med 34:440–454

Gasbarrini A, Boriani L, Salvadori C et al (2012) Biopsy for suspected spondylodiscitis. Eur Rev Med Pharmacol Sci 16:26–34

Golden MP, Vikram HR (2005) Extrapulmonary tuberculosis: an overview. Am Fam Physician 72:1761–1768

Gupta S, Takhtani D, Gulati M et al (1999) Sonographically guided fine-needle aspiration biopsy of lytic lesions of the spine: technique and indications. J Clin Ultrasound 27:123–129

Gupta R, Garg RK, Jain A et al (2015) Spinal cord and spinal nerve root involvement (myeloradiculopathy) in tuberculous meningitis. Medicine (Baltimore) 94(3):e404

Halimi C, Bringard N, Boyer N et al (1999) Brucellome hépatique: deux nouveaux cas et revue de la littérature. Gastroenterol Clin Biol 23:513–517

Hamza M (1993) Tuberculose articulaire et vertébrale. Rev Rhum (Ed Fr) 60:115–118

Handa U, Garg S, Mohan H, Garg SK (2009) Role of fine-needle aspiration cytology in tuberculosis of bone. Diagn Cytopathol 38:1–4

Harisinghani MG, Mcloud TC, Shepard JA et al (2000) Tuberculosis from head to toe. Radiographics 20:449–470

Heysell SK, Thomas TA, Sifri CD, Rehm PK, Houpt ER (2013) 18-fluorodeoxyglucose positron emission tomography for tuberculosis diagnosis and management: a case series. BMC Pulm Med 13:14

Huchon G (1997) Tuberculose et mycobactérioses non tuberculeuses Encycl Med Chir, Maladies Infectieuses, 8-038-C-10, 20 p

Jain AK (2010) Tuberculosis of the spine: a fresh look at an old disease. J Bone Joint Surg Br 92:905–913

Jorda M, Rey L, Hanly A, Ganjei-Azar P (2000) Fine-needle aspiration cytology of bone: accuracy and pitfalls of cytodiagnosis. Cancer 90:47–54

Kang M, Gupta S, Khandelwal N et al (1999) CT-guided fine-needle aspiration biopsy of spinal lesions. Acta Radiol 40:474–478

Kumar K (2017) Posterior spinal tuberculosis: a review. Mycobact Dis 7:243

Lacut JY, Dupon M, Paty MC (1995) Tuberculoses extrapulmonaires. Revue et possibilités de diminution des délais d'intervention thérapeutiques. Méd Mal Infect 25:304–320

Ladeb MF, Chelli Bouaziz M, Chakroun M, Loussaief C (2013) Atteintes parasitaires de l'appareil locomoteur. Encycl Med Chir Radiologie et imageriemédicale - musculosquelettique - neurologique – maxillofaciale 31-225-A-10

Ladeb MF, Chelli Bouaziz M, Riahi H, Chakroun M (2015) Imagerie de la tuberculose articulaire extra-rachidienne. Encycl Med Chir Radiologie et imagerie médicale-musculosquelettique-neurologique-maxillofaciale 31-220-A-10

Ladeb MF, Riahi H, Chelli Bouaziz M, Mechri M (2019) Clinical evolution of tuberculous spondylodiscitis in Tunisia. Bull Acad Natl Med 203:328–333

Lamer S, Garel C, Holvoet-Vernaut L, Hassan M (1998) Lésion lytique épiphyso-métaphysaire. Presse Med 27:1197–1198

Le Roux P, Quinque K, Bonnel AS, Le Luyer B (2005) Les atteintes extrapulmonaires de la tuberculose de l'enfant. Arch Pédiatr 12:S122–S126

Lefere M, Larbi A, Malghem J, Vande Berg B, Dallaudière B (2014) Vertebral sarcoidosis: long-term follow-up with MRI. Skeletal Radiol 43:1185–1190

Li T, Liu T, Jiang Z, Cui X, Sun J (2016) Diagnosing pyogenic, brucella and tuberculous spondylitis using histopathology and MRI: a retrospective study. Exp Ther Med 12:2069–2077

Lolge S, Maheshwari M, Shah J, Patkar D, Chawla A (2003) Isolated solitary vertebral body tuberculosis-study of seven cases. Clin Radiol 58:545–550

Madhok R, Sachdeva P (2016) Evaluation of apparent diffusion coefficient values in spinal tuberculosis by MRI. J Clin Diagn Res 10:TC19–TC23

Madkour MM, Sharif HS, Abed MY, Al-Fayez MA (1988) Osteoarticular brucellosis. AJR Am J Roentgenol 150:1101–1105

Mahboubi S, Morris MC (2001) Imaging of spinal infections in children. Radiol Clin North Am 39:215–222

Martini M (1988) Tuberculosis of bone and joints. Springer, Berlin, Heidelberg

Masood S (2013) Ultrasound guided fine needle aspiration biopsy: the new challenges and opportunities for cytopathologists. Diagn Cytopathol 41:1017–1018

Mishra SS, Das D, Das S, Mohanta I, Tripathy SR (2015) Spinal cord compression due to primary intramedullary tuberculoma of the spinal cord presenting as paraplegia: a case report and literature review. Surg Neurol Int 6:42

Momjian R, George M (2014) Atypical imaging features of tuberculous spondylitis: case report with literature review. J Radiol Case Rep 8:1–14

Moon MS (2014) Tuberculosis of spine: current views in diagnosis and management. Asian Spine J 8:97–111

Moore SL, Rafii M (2001) Imaging of musculoskeletal and spinal tuberculosis. Radiol Clin North Am 39:329–342

Moorthy S, Prabhu NK (2002) Spectrum of MR imaging findings in spinal tuberculosis. AJR Am J Roentgenol 179:979–983

Morvan G, Martin N, Massare C, Nahum H (1984) La tuberculose du rachis cervical: étude radiologique à propos d'une série multicentrique de 53 cas. Rev Chir Orthop Reparatrice Appar Mot 70:76–80

Morvan G, Laredo JD, Wibier M (1998) Imagerie ostéo-articulaire, vol 2. Médecine-Sciences-Flammarion, Paris, pp 756–763

Moser T, Ehlinger M, Chelli Bouaziz M, Ladeb MF, Durckel J, Dosch JC (2012) Pitfalls in osteoarticular imaging: how to distinguish bone infection from tumour? Diagn Interv Imaging 93:351–359

Murray JF (1996) Expressions cliniques actuelles de la tuberculose. Rev Prat 46:1344–1349

Naim-Ur-Rahaman, El Bakry A, Jamjoom ZA, Kolawole TM (1999) Atypical forms of spinal tuberculosis: case report and review of the literature. Surg Neurol 51:602–607

Narlawar RS, Shah JR, Pimple MK et al (2002) Isolated tuberculosis of posterior elements of spine: magnetic resonance imaging findings in 33 patients. Spine 27:275–281

Nassar I, Mahi M, Semlali S et al (2002) Tuberculose de l'arc vertebral postérieur. J Neuroradiol 29: 204–207

Papavero R, Bissuel F, Gruel S et al (1999) Tuberculose vertébrale de l'enfant. Place de l'imagerie dans la démarche diagnostique et thérapeutique. Presse Med 28:1980–1982

Pertuiset E, Beaudreuil J, Horusitzky F et al (1997) Aspects épidémiologiques de la tuberculose ostéo-articulaire de l'adulte. Etude rétrospective de 206 cas diagnostiqués en région parisienne de 1980 à 1994. Presse Med 26:311–315

Pertuiset E, Beaudreuil J, Liote F et al (1999) Spinal tuberculosis in adults. A study of 103 cases in a developed country, 1980-1994. Medicine 78:309–320

Ramachandran S, Clifton IJ, Collyns TA, Watson JP, Pearson SB (2005) The treatment of spinal tuberculosis: a retrospective study. Int J Tuberc Lung Dis 9:541–544

Rasouli MR, Mirkoohi M, Vaccaro AR, Yarandi KK, Rahimi-Movaghar V (2012) Spinal tuberculosis: diagnosis and management. Asian Spine J 6:294–308

Rauf F, Chaudhry UR, Atif M, ur Rahaman M (2015) Spinal tuberculosis: our experience and a review of imaging methods. Neuroradiol J 28:498–450

Resnick D (1995) Osteomyelitis, septic arthritis and soft tissue infection: organisms. In: Resnick D (ed) Diagnosis of bone and joint disorders, vol 4, 3rd edn. Saunders, Philadelphia, pp 2448–2558

Ridley N, Shaikh MI, Remedios D, Mitchell R (1998) Radiology of skeletal tuberculosis. Orthopaedics 21:1213–1220

Rivas-Garcia A, Sarria-Estrada S, Torrents-Odin C, Casas-Gomila L, Franquet E (2013) Imaging findings of Pott's disease. Eur Spine J 22(Suppl 4): 567–578

Rua-Figueroa I, Gantes MA et al (2002) Vertebral sarcoidosis: clinical and imaging findings. Semin Arthritis Rheum 31:346–352

Sharif HS, Aideyan OA, Clark DC et al (1989) Brucellar and tuberculous spondylitis: comparative imaging features. Radiology 171:419–425

Sharif HS, Morgan JL, Al Shahed MS, Al Thagafi MY (1995) Role of CT and MR imaging in the management of tuberculous spondylitis. Radiol Clin North Am 33:787–804

Shikhare SN, Singh DR, Shimpi TR, Peh WCG (2011) Tuberculous osteomyelitis and spondylodiscitis. Semin Musculoskelet Radiol 15:446–458

Skaf GS, Kanafani ZA, Araj GF, Kanj SS (2010) Non-pyogenic infections of the spine. Int J Antimicrob Agents 36:99–105

Smids C, Kouijzer IJ, Vos FJ et al (2017) A comparison of the diagnostic value of MRI and ^{18}F-FDG-PET/CT in suspected spondylodiscitis. Infection 45:41–49

Stäbler A, Reiser MF (2001) Imaging of spinal infection. Radiol Clin North Am 39:115–135

Teo HEL, Peh WCG (2004) Skeletal tuberculosis in children. Pediatr Radiol 34:853–860

Trecarichi EM, Di Meco E, Mazzotta V, Fantoni M (2012) Tuberculous spondylodiscitis: epidemiology, clinical features, treatment, and outcome. Eur Rev Med Pharmacol Sci 16:58–72

Tuli SM (2002) General principles of osteoarticular tuberculosis. Clin Orthop 398:11–19

Turgut M (2001) Multifocal extensive spinal tuberculosis (Pott's disease) involving cervical, thoracic and lumbar vertebrae. Br J Neurosurg 15:142–146

Valencia MP, Deaver PM, Mammarappallil MC (2009) Sarcoidosis of the thoracic and lumbar vertebrae, mimicking metastasis or multifocal osteomyelitis by MRI: case report. Clin Imaging 33:476–481

Wallace R, Cohen AS (1976) Tuberculous arthritis: a report of two cases with review of biopsy and synovial fluid findings. Am J Med 61:277–282

Williams RL, Fukui MB, Meltzer CC et al (1999) Fungal spinal osteomyelitis in the immunocompromised patient: MR findings in three cases. AJNR Am J Neuroradiol 20:381–385

Wrobel CJ, Chappell ET, Taylor W (2001) Clinical presentation, radiological findings, and treatment results of coccidioidomycosis involving the spine: report on 23 cases. J Neurosurg 95(1 Suppl):33–39

Yang CM, Hsu CH, Lee CM, Wang FC (2003) Intense uptake of [F-18]-fluoro-2 deoxy-D-glucose in active pulmonary tuberculosis. Ann Nucl Med 17:407–410

Imaging of Spinal Hydatidosis

Mohamed Fethi Ladeb, Hend Riahi, Meriem Mechri, Mouna Chelli Bouaziz, Sonia Trabelsi, and Soumaya Rammeh

Contents

M. F. Ladeb (✉) · H. Riahi · M. Mechri · M. Chelli Bouaziz
Department of Radiology, MT Kassab Institute of Orthopaedics, Tunis, Tunisia

Faculty of Medicine of Tunis, Tunis-El Manar University, Tunis, Tunisia
e-mail: fethiladeb@hotmail.fr; hend.riahi@gmail.com; meriem_mechri@yahoo.fr; bouaziz_mouna@yahoo.fr

S. Trabelsi
Department of Parasitology, Charles Nicolle Hospital, Tunis, Tunisia

Faculty of Medicine of Tunis, Tunis-El Manar University, Tunis, Tunisia
e-mail: trabelsi.sonia@gmail.com

S. Rammeh
Department of Pathology, Charles Nicolle Hospital, Tunis, Tunisia

Faculty of Medicine of Tunis, Tunis-El Manar University, Tunis, Tunisia
e-mail: rammehs@yahoo.fr

Abstract

Cystic echinococcosis, also known as hydatid disease, is a worldwide zoonosis caused by the larval stage of *Echinococcus granulosus.* This disease usually affects adults. The frequency of osseous involvement in hydatid disease is 0.5–4%. The clinical and radiographic features of spinal hydatidosis may be nonspecific, although there are some suggestive imaging patterns of spinal involvement. Computed tomography (CT) and magnetic resonance imaging (MRI) are the best imaging tools for diagnostic confirmation, assessment of local extension, and postoperative follow-up. Results of surgical treatment of

© The Author(s), under exclusive license to Springer Nature Switzerland AG 2021

M. F. Ladeb, W. C. G. Peh (eds.), *Imaging of Spinal Infection*,
Medical Radiology Diagnostic Imaging, https://doi.org/10.1007/978-3-030-70459-9_13

bone hydatidosis are not gratifying. Apparent radical removal is not a guarantee that recurrence can be avoided. Medical treatment may help to reduce the risk of recurrence.

Abbreviations

CT Computed tomography
MRI Magnetic resonance imaging

1 Introduction

Cystic echinococcosis (hydatidosis) is a parasitic infection caused by the larval stage of *Echinococcus granulosus*, a small tapeworm. Definitive hosts are from the canid family (e.g., dogs, wolves, and foxes). Intermediate hosts include ungulates or other herbivores (e.g., sheep and goats). Humans are incidental intermediate hosts.

2 *Echinococcus granulosus* Life Cycle (Fig. 1)

The adult *E. granulosus* resides in the small bowel of the definitive hosts, such as dogs or other canids. It measures from 3 to 6 mm in length. It is attached to the mucosa by a specialized attachment organ, the scolex ("head"). The scolex has four muscular suckers and two rows of hooks, one large and one small, on the rostellum (Moro and Schantz 2009; Steinmetz et al. 2014). The body (or strobili) is segmented into three proglottids ("segments"), namely, an immature proglottid, a mature proglottid, and a gravid proglottid (segments containing eggs). The gravid

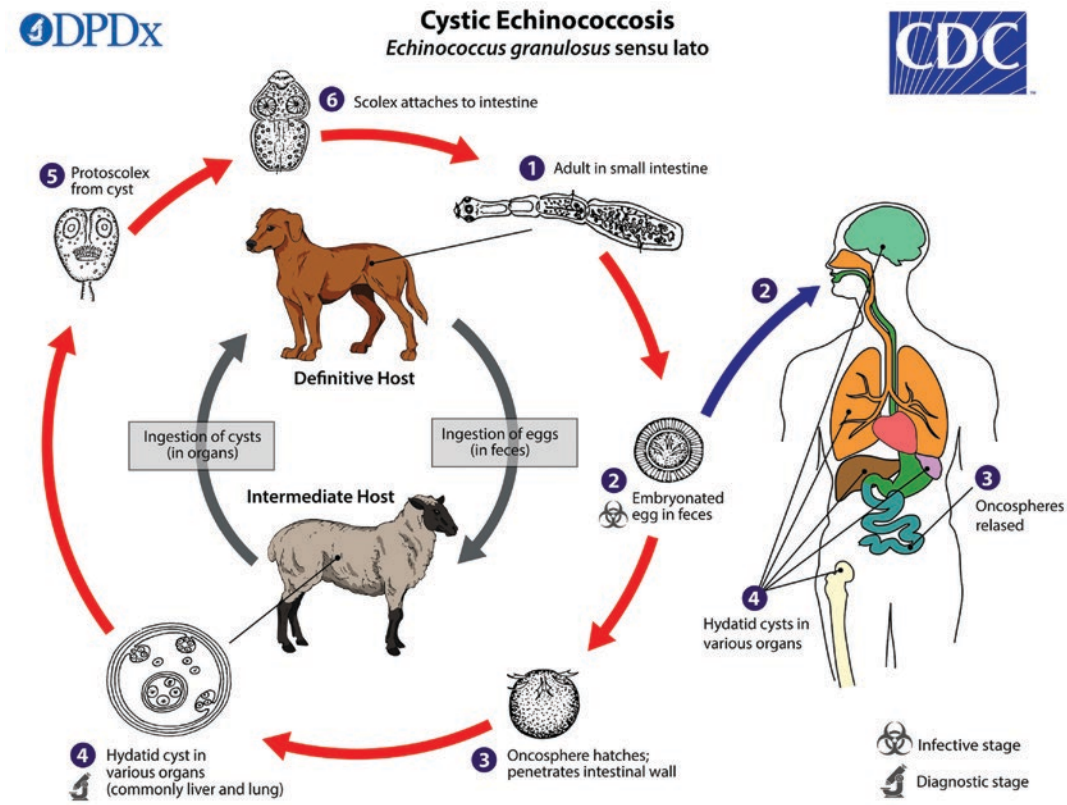

Fig. 1 Life cycle of *Echinococcus granulosus* (Reproduced from the Centers for Disease Control and Prevention at http://www.dpd.cdc.gov/dpdx/html/Echinococcosis.htm)

proglottid passes in the feces (Moro and Schantz 2009; Steinmetz et al. 2014).

This waste is excreted in the environment. After ingestion by a suitable intermediate host such as sheep, the egg hatches in the stomach and releases an oncosphere containing a hexacanth embryo that passes through the intestinal wall and migrates through the circulatory system into various organs, especially the liver and the lungs. In these organs, the embryo develops into a cyst that enlarges gradually. The wall of the cyst differentiates into an outer laminated nonnucleated layer and an inner nucleated germinal layer that produces protoscoleces and daughter vesicles filling the cyst interior (Moro and Schantz 2009; Steinmetz et al. 2014).

The cycle becomes complete when the definitive host ingests the cyst-containing organs of the infected intermediate host. After ingestion, the protoscoleces evaginate, attach to the intestinal mucosa, and develop into adult stages in 1–3 months. Humans may become intermediate hosts after ingesting eggs through contact with a contaminated dog or through consumption of contaminated water or vegetables (Brunetti et al. 2010).

3 Geographic Distribution and Prevalence

The global prevalence of hydatidosis is estimated at 2–3 million human cases. It is ubiquitously distributed, with more frequent occurrence in the Mediterranean Basin, Middle East, South America, Australia, Central Asia, and China (Liu et al. 2004; Chelli Bouaziz et al. 2008). By 2002, two countries, Iceland and New Zealand, and one island-state, Tasmania, had already declared that hydatid disease had been eliminated from their territories. In the endemic regions, the rate of incidence of human hydatidosis has been recorded as being more than 50 per 100,000 person-years, with the prevalence rate reaching 5–10% in some parts of East Africa, Central Asia, China, Peru, and Argentina (WHO 2011).

The most commonly affected organs, where 90% of human hydatidosis develop, are the liver (65–70%) and lungs (20–25%). All the other organs are considered to be uncommon sites of disease. The frequency of osseous involvement in hydatid disease is 0.5–4%. In a literature review of 721 cases, the median age was 37 years. Among the 721 patients, 78% were males. Bone hydatidosis is most commonly seen in the spine and pelvis (50–60%), followed by the femur, tibia, humerus, skull, and ribs (Neumayr et al. 2013a, b). Spinal hydatidosis most commonly affects the thoracic spine, although any part of the spine can be affected (Song et al. 2007; Scarlata et al. 2011).

4 Pathophysiology of Osseous Hydatidosis

Bone hydatidosis may occur via two main mechanisms, namely, hematogeneous spread (the most common mechanism) and direct invasion from extra-osseous structures (Neumayr et al. 2013a, b). Hydatidosis manifests differently in the bone, compared to the liver or the lungs, because of the mechanical resistance that bone offers to the growth of hydatid cysts (Vicidomini et al. 2007; Papakonstantinou et al. 2011). Hydatid cysts proliferate by vesiculation, penetrate the bone trabeculae in the direction of least resistance, and incite a slow destruction and expansion of the bone with trabecular resorption (Dorn et al. 1984). The parasite grows multilocularly with enlargement of the spongiosa spaces without adventitia formation. In the bone, the disease usually starts in the metaphysis.

Grossly, the viable cysts are filled with colorless fluid which contains daughter cysts. The shape of the involved bone remains unchanged initially (Papakonstantinou et al. 2011). With time, the parasite reaches and destroys the cortex, with subsequent spread of the disease to surrounding soft tissues, forming extraosseous collections (ossifluent abscess) (Papakonstantinou et al. 2011), which may calcify (Torricelli et al. 1990). Bone sclerosis is rare or absent, except when there is bone infection or after bone surgery. Joint involvement is usually due to exten-

sion from the adjacent bone and is frequently observed in the hip and shoulder (Engin et al. 2000).

Spinal involvement is due to the rich vascular spongiosa in the vertebral body and paradoxal "emboli" phenomena caused by the atypical passage of embryos to the inferior vena cava through portocaval anastomoses and subsequently toward the retroperitoneum via the epidural Batson venous plexus (Dorn et al. 1984). The disease begins primarily in the vertebral body and subsequently extends into the posterior vertebral elements and extradural and paravertebral spaces (Karray et al. 1990).

5 Spinal Hydatidosis

Spinal hydatidosis occurs in more than 50% of the 0.5–4% of cases affecting bones and is most commonly located in thoracic spine (50%), followed by lumbar (20%), sacral (20%), and cervical spine (Song et al. 2007; Scarlata et al. 2011) (Fig. 2). Associated extra-spinal hydatidosis is

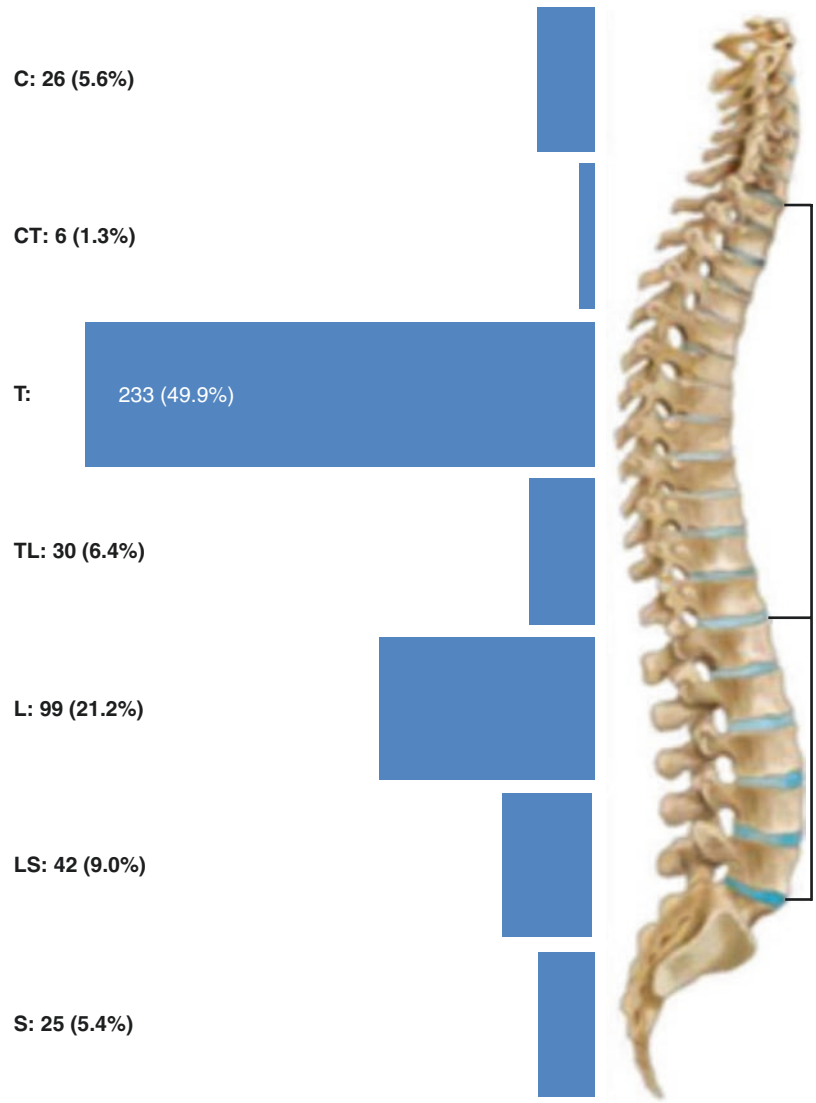

Fig. 2 Anatomical location of spinal hydatidosis. Left, frequency of involved spine levels in 467 cases [*C* cervical, *CT* cervicothoracic, *T* thoracic, *TL* thoracolumbar, *L* lumbar, *LS* lumbosacral, *S* sacral] (Adapted from Neumayr et al. 2013a, b)

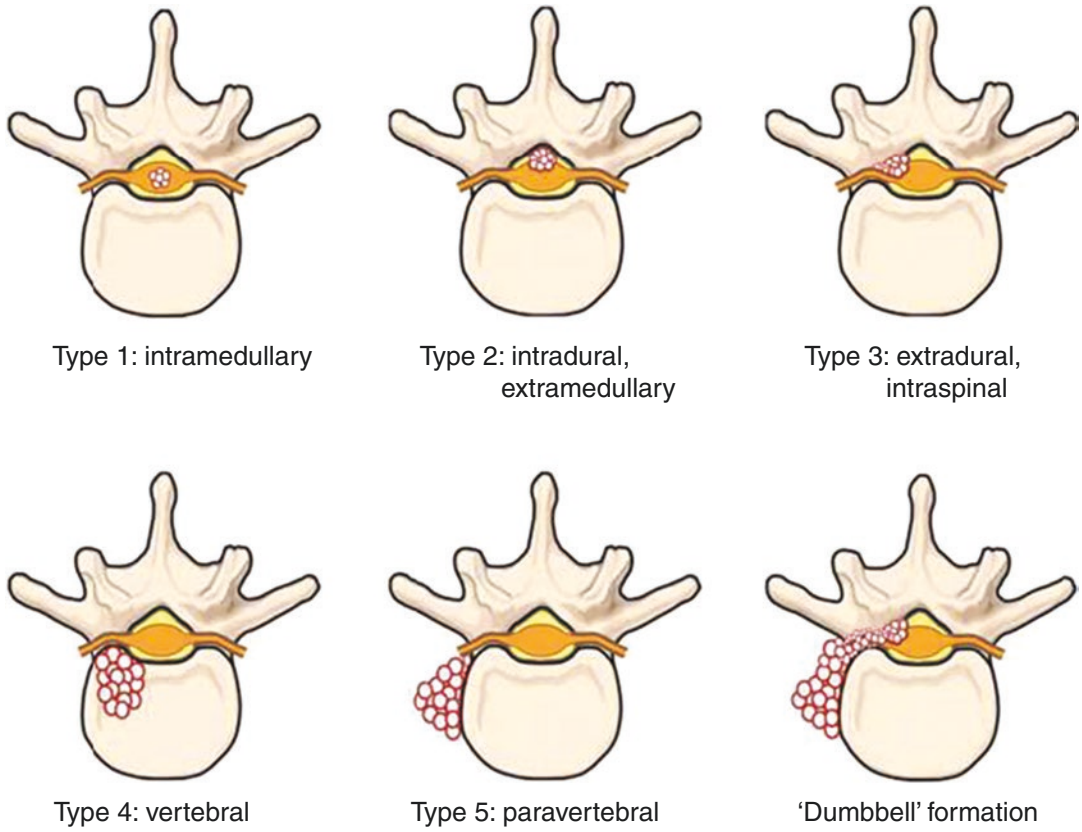

Fig. 3 Classification of spinal hydatidosis according to the Dew/Braithwaite and Lees classification (type 1–5) and "dumbbell" formation Neumayr et al. 2013a, b

seen only in 17.9% of cases. According to Dew/Braithwaite and Lees (Neumayr et al. 2013a, b) (Fig. 3), spinal hydatidosis may be classified into type 1, intramedullary; type 2, intradural, extramedullary; type 3, extradural intraspinal; type 4, vertebral; and type 5, paravertebral (or "dumbbell" formation). Types 1 and 2 are very rare. Ninety percent are confined to the bone and extradural space (Neumayr et al. 2013a, b).

5.1 Clinical Features

Bone hydatidosis usually affects adults and, rarely, children. The clinical symptoms are variable, depending on the localization. Spinal hydatidosis is a slowly progressive disease with a latent period of many years. Clinical symptoms are not specific, and patients may complain of pain but often delay consulting a physician until neural compromise or development of pathological fracture. Neurological symptoms are generally related to spinal cord compression, which tends to cause radicular symptoms of pain and segmental neurological deficits such as sphincter disturbances, paresthesia, paraparesis, and paraplegia. Patients with long bone hydatidosis usually present with pain, swelling, or pathological fracture.

5.2 Imaging

Radiographs show non-specific, pure osteolysis of the vertebral body, sometimes extending to posterior vertebral elements (Fig. 4). Some imaging characteristics have been described as being typical of spinal hydatidosis, such as lack

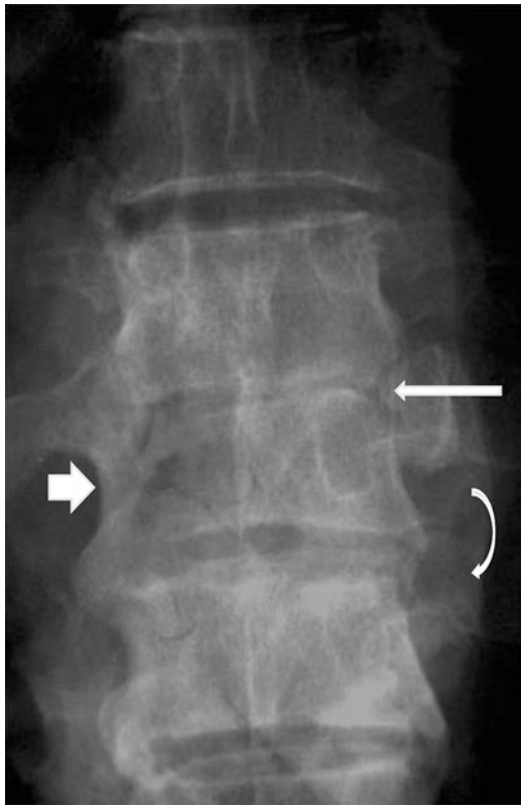

Fig. 4 Thoracic spine hydatidosis. Frontal thoracic spine radiograph shows a destructive lesion involving T9 vertebral body with partial vertebral collapse (short thick arrow), obliteration of T8/T9 disk space (long arrow), and paraspinal mass (curved arrow)

of surrounding bone sclerosis, preservation of vertebral body height, intervertebral extension via a subperiosteal and subligamentous pathway, paraspinal extension, and, particularly, involvement of a contiguous rib or the ilium (Engin et al. 2000; Karantanas et al. 2003) (Fig. 5).

Scalloping of the vertebral body posterior cortex and enlargement of the interpedicular space or intervertebral foramina are indirect signs of extension into the spinal canal. In cases of paravertebral extension, radiographs may show paravertebral masses, which may calcify (Engin et al. 2000). At the thoracic level, extension to the paravertebral soft tissues is frequent, forming ossifluent abscess which present as paraspinal opacities with well-defined rounded or polycyclical and sometimes calcified contours (Fig. 6).

Ultrasonography is effective for assessing soft tissue collections, which may show a multicystic (Fig. 5) or hypoechoic appearance. In cases of musculoskeletal hydatidosis, abdominal ultrasonography should also be done to search for concomitant abdominal involvement, especially of the liver.

CT is the best imaging tool for the assessment of bone destruction. It shows hypodense multivesicular cystic masses, infiltrating bone with endosteal scalloping, and cortical interruption (Zlitni et al. 2001) (Fig. 7). In spinal hydatidosis, CT

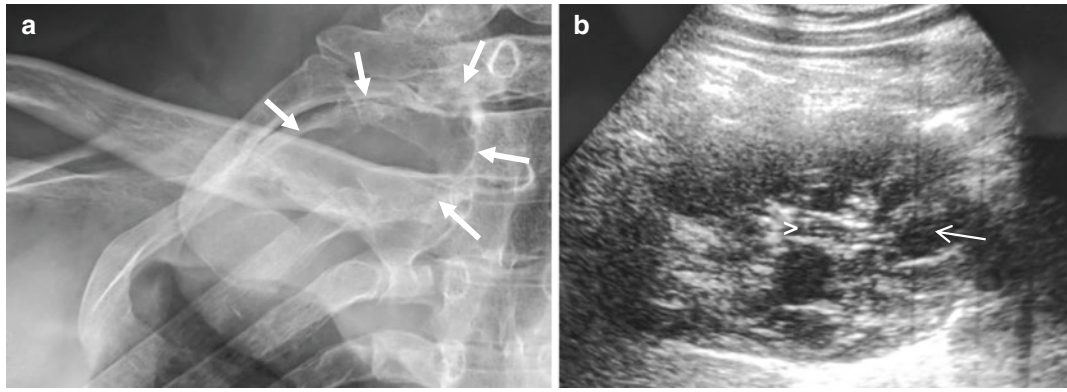

Fig. 5 Costovertebral hydatidosis. (**a**) Chest radiograph shows scalloping (arrows) of a right T2 vertebral body and transverse process and adjacent right 2nd rib. (**b**) Ultrasonographic image of the mass shows a multivesicular cyst, well-defined fluid collection with vesicles (arrows), calcifications, and small echoes corresponding to hydatid sand (arrowhead)

shows extension of cystic lesions to the spinal canal and to the foramen, causing enlargement of intervertebral foramina (Fig. 8). CT may also depict soft tissue involvement, which is characterized by multivesicular extraosseous cysts, outlined by an enhancing rim after intravenous contrast administration.

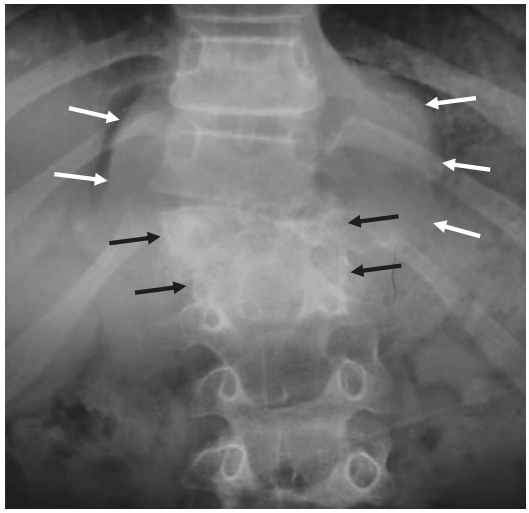

Fig. 6 Thoracolumbar spine hydatidosis. Frontal lumbar spine radiograph shows a destructive lesion involving T12 and L1 vertebrae (black arrows) with vertebral collapse and a paraspinal mass (white arrows)

MRI is the most helpful tool for diagnostic confirmation, evaluation of local extension, preoperative planning, and postoperative follow-up of bone hydatidosis (Braithwaite and Lees 1981). MRI is more reliable than CT in the assessment of bone and soft tissue involvement because it better depicts the characteristic multivesicular appearance and better assesses its local extension and relationship with the surrounding tissues (Fig. 9), especially the spinal cord (Braithwaite and Lees 1981; Singh et al. 1998). Bone hydatidosis shows signal hypointensity on T1-weighted images and signal hyperintensity on T2-weighted images with no enhancement after intravenous Gd-DTPA administration. Intralesional hypervascularization may be seen after surgery. The adjacent bone marrow typically has normal signal.

In spinal hydatidosis, MRI better depicts the parasite extension into the spinal canal, as well as its relationship with spinal cord and nerve roots (Fig. 10). In established bone hydatidosis, vesicles are rare. MRI shows T1-hypointense and T2-hyperintense collections that may contain T2-hypointense debris. Because of its high sensitivity, MRI is used to detect early postoperative recurrence. Postoperative MRI is useful to assess

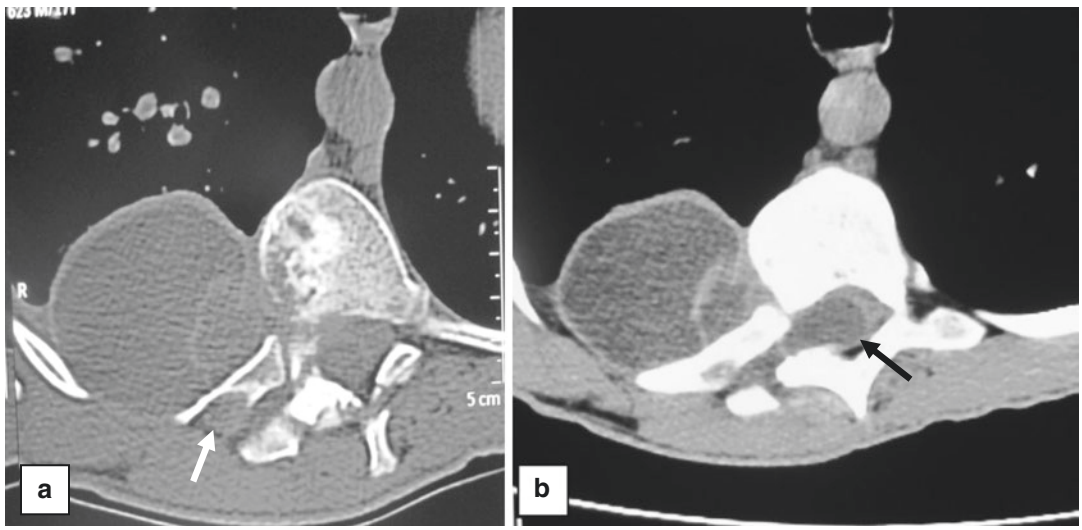

Fig. 7 Costovertebral hydatidosis. Axial CT images taken in (**a**) bone and (**b**) soft tissue window settings show a hypodense multiloculated lesion destroying the vertebral body, the right pedicle, and the adjacent rib (white arrow) with cysts protruding into the thoracic cavity and the spinal canal (black arrow)

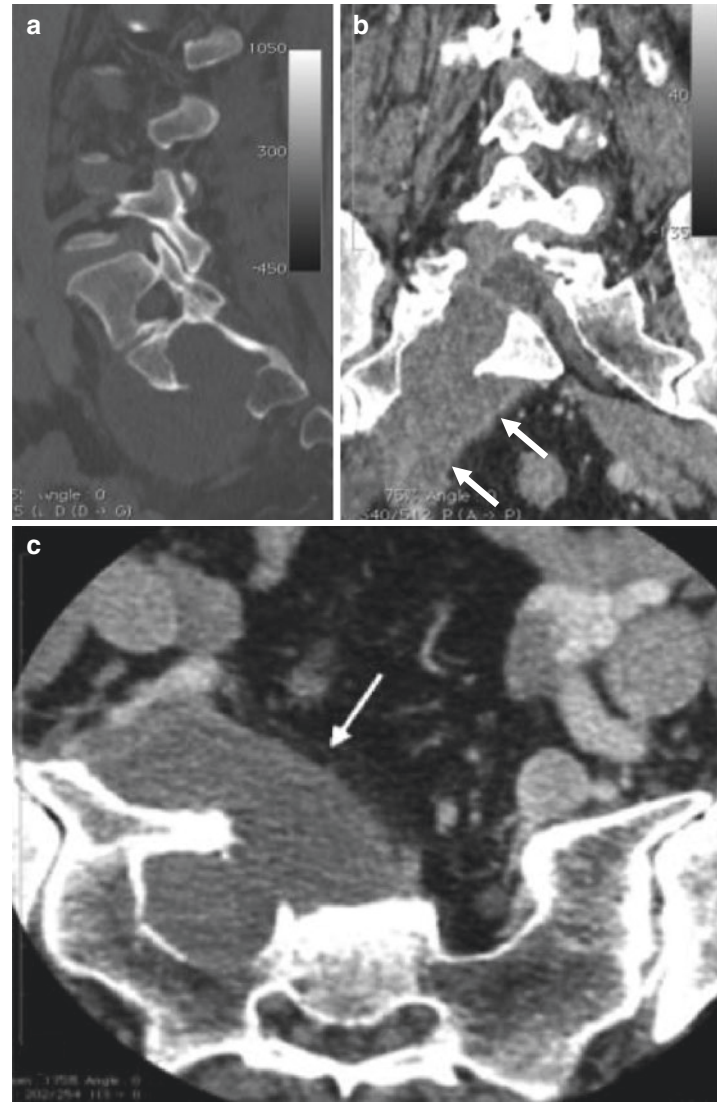

Fig. 8 Sacral hydatidosis. (**a**) Sagittal CT image taken in bone window setting and (**b**) coronal and (**c**) axial CT images taken in soft tissue window setting show sacral hydatidosis enlarging the first right sacral foramen and extending into the pelvis (arrows)

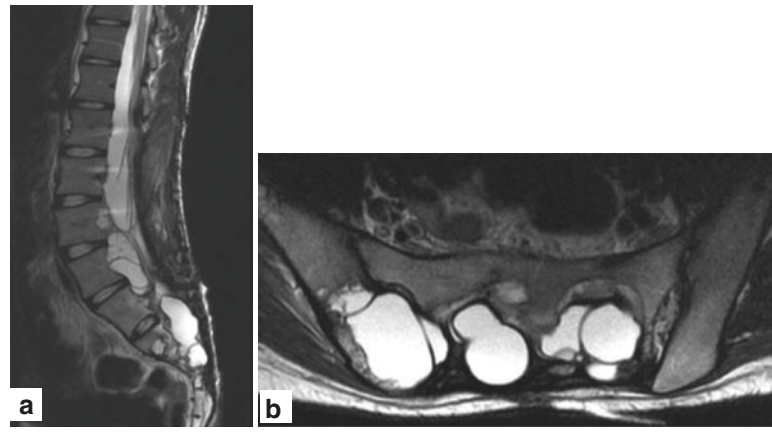

Fig. 9 Spinal hydatidosis. (**a**) Sagittal and (**b**) axial T2-W MR images of the lumbar spine show osseous and epidural extension of the characteristic multivesicular appearance of the disease, with no spinal cord involvement

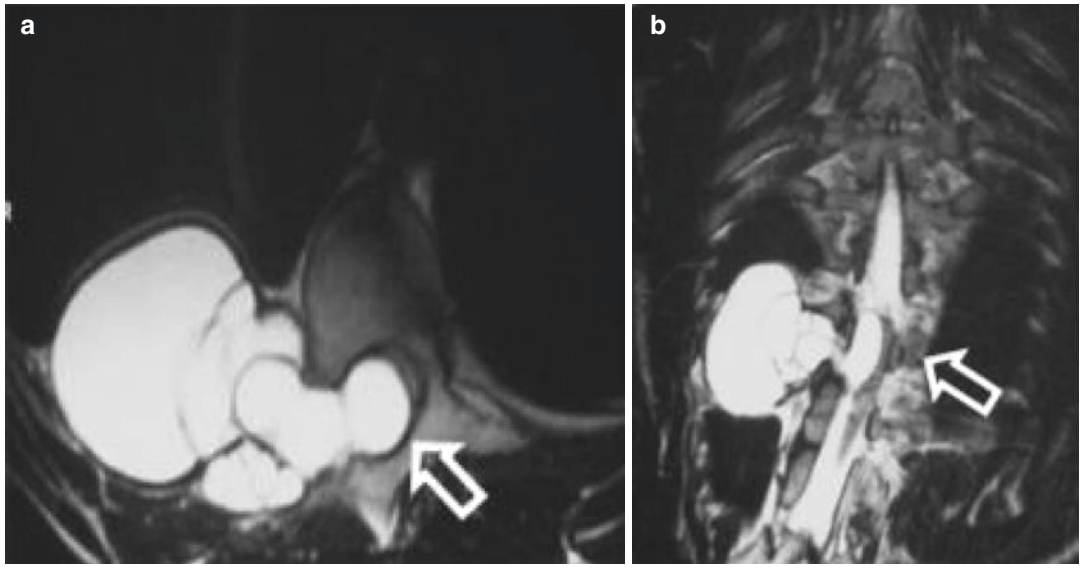

Fig. 10 Costovertebral hydatidosis. (**a**) Axial and (**b**) coronal T2-W MR images show intraspinal extension of large multivesicular cystic masses with cord compression (arrows)

the success of the excision and can be used as reference for future MRI exams. To the best of our knowledge, no consensus is available regarding imaging follow-up.

5.3 Differential Diagnosis

Spinal tuberculosis is the main differential diagnosis (Table 1). Some imaging characteristics have been described as being typical of spinal hydatidosis. These include a long-term preservation of vertebral body height despite prominent bone destruction, late disk narrowing, absence of edema, lack of osteoporosis and sclerosis (Engin et al. 2000; Thompson 2017), involvement of contiguous ribs or the iliac bone, and presence of paravertebral cystic mass (Braithwaite and Lees 1981). Differential diagnosis may also include brucellar pseudo-Pott disease with extensive bone destruction, multifocal involvement, and voluminous paravertebral abscess (Chelli Bouaziz et al. 2008).

Alveolar echinococcosis is a rare parasite infection mostly observed in some regions of China (Autonomous Region of Xinjiang), North America, Japan, and central Europe and usually affects the spine. Imaging features resemble those of bone hydatidosis (Fig. 11). MRI shows infiltration of the spine by cystic vesicles with paravertebral soft tissue extension surrounded by a thick and well-vascularized wall similar to an abscess, as a result of direct (per continuitatem) spread of the hepatic primary lesion. Calcifications are typical of the hepatic manifestations of the disease (Moro and Schantz 2009).

Table 1 Differences between tuberculous spondylitis and spinal hydatidosis

	Tuberculous spondylitis	Spinal hydatidosis
Disk	Narrow	Intact or late narrowing
Bone sclerosis	Late and mild	Absent
Bone marrow edema	Present	Absent
Soft tissue abscess	Frequent, large abscess with smooth margins	Constant, multivesicular collection
Extension to the ribs and iliac bone	Rare	Frequent

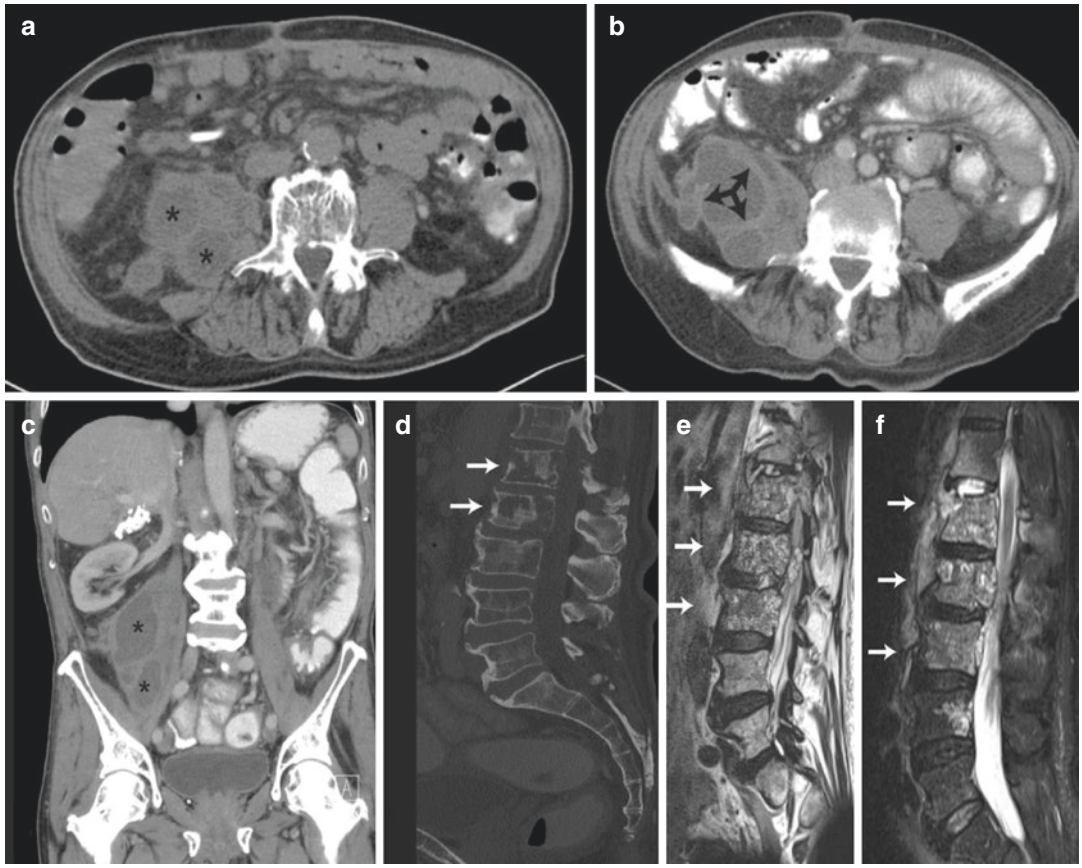

Fig. 11 Alveolar echinococcosis of the spine. (**a**, **b**) Axial, (**c**) coronal, and (**d**) sagittal CT images show osteolytic and sclerotic lesions of L1, L2 (arrows), and L3 vertebrae, with preserved L1/L2 and L2/L3 disk heights. Multiloculated fluid collection of the right psoas muscle is present (asterisks). Sagittal (**e**) T2-W and (**f**) fat-suppressed T2-W MR images show infiltration of multiple vertebrae by cystic vesicles with a prevertebral collection (arrows) (Courtesy of Dr. Manuel Nell)

5.4 Diagnosis

Serological tests are helpful in making the diagnosis of hydatidosis in humans, particularly when there is a differential diagnosis. There are two categories of serological examinations for the diagnosis of the hydatid cyst disease, namely, the detection of antibodies in the blood serum of patients (the current gold standard serodiagnosis) and the detection of antigens.

There are many immunological methods, such as (1) immunoprecipitation techniques used for the detection of arc-5, such as immunoelectrophoresis, double-diffusion test, and electrosyneresis; (2) indirect hemagglutination assay (IHA); (3) latex agglutination; (4) enzyme-linked immunosorbent assay (ELISA); (5) immunofluorescence (IF); and (6) immunoblotting (IB). The immunoreaction of the human body is related to the hydatid cyst integrity, growth vigor, and location. In fact, immunoreaction is higher in ruptured hydatid cysts, lower when intact, and negative when aged, calcified, or dead.

When bone hydatidosis is suspected, both screening and confirmatory tests should be done, as they are positive in only 30–40%. Only positive tests are helpful for confirming the diagnosis; that is why complete reliance on serology for definitive diagnosis is not recommended. However, they are particularly useful in postoperative monitoring when looking for a local or more remote recurrence (Steinmetz et al. 2014).

In the chronic phases of hydatidosis, the IgG1 and IgG4 IgG subclasses are predominant (Manzano-Román et al. 2015).

Complete surgical removal of the lesions induces a rapid decrease of the specific antibodies which subsequently become undetectable. However, the persistence of high levels of antibodies or their additional increase may suggest a residual disease or recurrence. This can be observed even when the cysts have been removed successfully, thus confusing experienced clinicians. Serum antibodies may persist for a prolonged period, reaching up to 10 years after the hydatid cyst removal, so their detection is likely to indicate previous exposure to *E. granulosus* and not necessarily the presence of an established and viable infection. Concerning circulating antigen detection tests, they are not very sensitive because of the low antigen released by the cyst or antigens bound by antibodies forming immune complexes.

DNA-based methods are used for the identification of species, genotypes, and haplotypes observed in *E. granulosus sensu stricto* and for the differential diagnosis of *E. granulosus sensu lato* from the other species (Mandal and Mandal 2012).

In cases of doubtful clinical, imaging, and serological diagnosis, there is a role for fine needle biopsy. However, certain precautions should be taken. The overall risk of anaphylaxis linked to percutaneous puncture of hydatidosis has been vastly exaggerated in the past. Analysis of the literature shows that lethal anaphylaxis related to percutaneous treatment of hydatidosis is an extremely rare event and is observed no more frequently than drug-related anaphylactic adverse effects (Khabiri et al. 2006). This minor risk may be avoided by standby emergency preparation and by establishing a peri-interventional preventative chemoprophylaxis as stated by the published recommendation of the World Health Organization (WHO) informal working group on hydatidosis, based on the excellent protoscolicidal activity of praziquantel (Mandal and Mandal 2012). Some centers advocate using albendazole plus praziquantel for peri-interventional spillage prophylaxis without any consensus on the dose and duration of treatment.

5.5 Treatment

5.5.1 Surgical Treatment

Currently, there is no effective drug to treat bone hydatid disease. For this reason, surgery is the most common option for treatment (Song et al. 2007; Xie et al. 2015). Because of the hardness of the bone, the parasite cannot grow into large spherical cysts as in soft tissues (e.g., liver, lungs) and does not have a fibrous capsule. The parasite grows in the direction of least resistance, infiltrating and damaging the bone like a tumor, with a risk of fracture (Pamir et al. 2002; Song et al. 2007; Vicidomini et al. 2007). During surgery, it is important to protect the surrounding tissue from further spread of the parasite. However, complete removal of the parasite is not guaranteed with surgery due to the infiltrative nature of this infection, with recurrence rates reported to be as high as 48% (Neumayr et al. 2013a, b). Furthermore, surgical treatment may also lead to complications such as disability and deformity (Ozdemir et al. 2004).

The radical resection of the infested long bones (especially the femur, humerus, and tibia) together with neighboring muscles is possible in some situations.

The treatment of vertebral hydatidosis is essentially surgical, although it is seldom curative and usually takes a chronic course with many recurrences (Bettaieb et al. 1978; Torricelli et al. 1990; Engin et al. 2000; Liu et al. 2004). All the forms of non-surgical treatment have not proved to be curative (Bouvier et al. 1974; Dorn et al. 1984). Thus, the ideal treatment is total vertebral resection; however, this is often impossible because of the lesion extent (Neumayr et al. 2013a, b; Neumayr 2015). Del Campo (1950) was the first to attempt this procedure in Uruguay, approaching the fifth lumbar vertebra transperitoneally, which permitted him to treat the anterior abscess and remove the entire body of the vertebra (Del Campo 1950). The operation may be completed by arthrodesis (Fig. 12).

In our practice, laminectomy is the common therapeutic method for decompression in paraplegic patients with spinal hydatidosis and is performed mainly in neurosurgical institutes. This

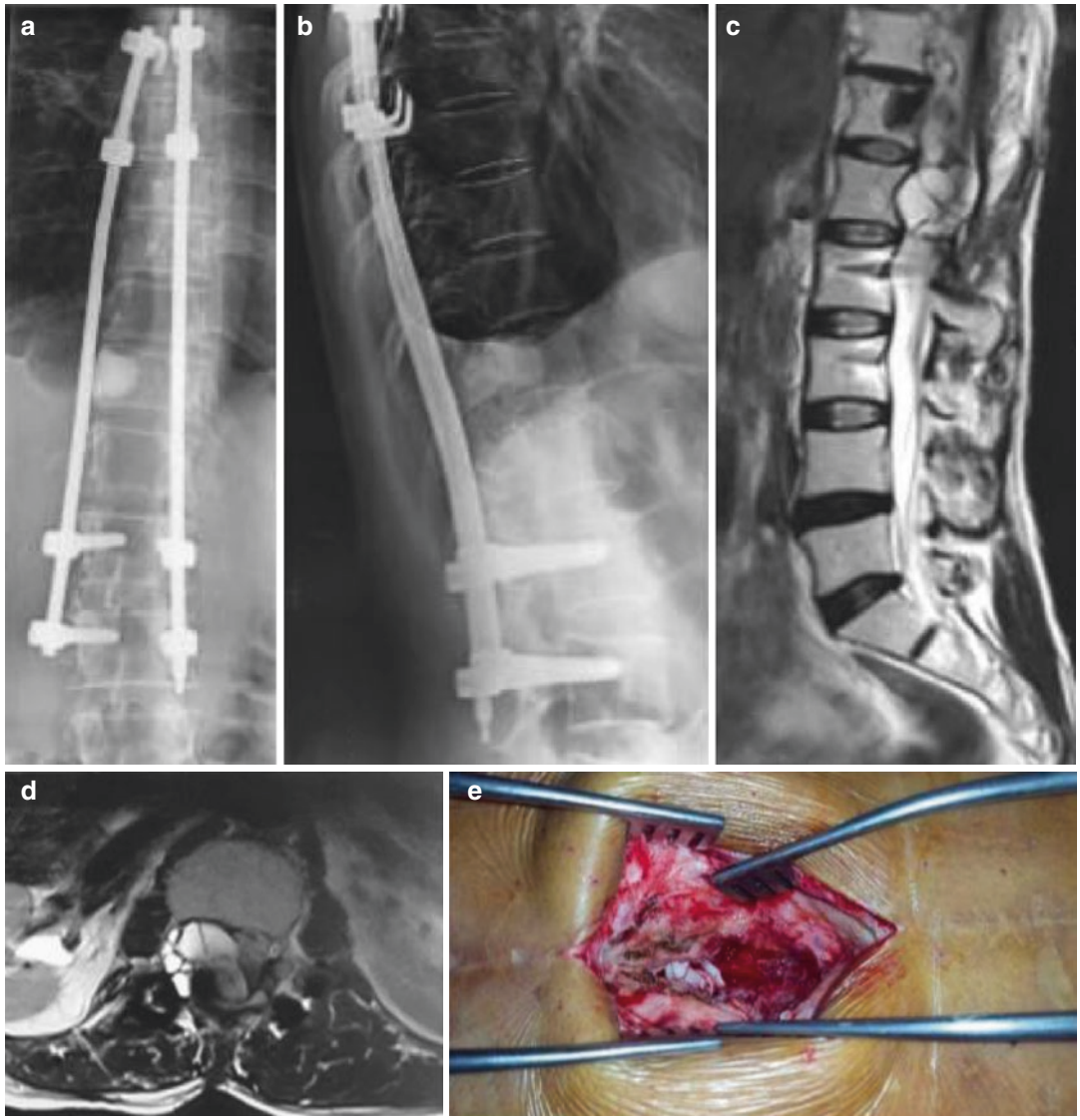

Fig. 12 A 29-year-old man surgically treated 4 years ago for T12 vertebral hydatidosis. (**a**) Frontal and (**b**) lateral radiographs show hemilaminectomy with acrylic cement placement. After the first recurrence at the L1 vertebra after 2 years, posterior fixation of the spine and evacuation of the cysts were performed. (**c**) Sagittal and (**d**) axial T2-W MR images show the second recurrence at the L1 vertebral level. (**e**) Operative photograph shows limited surgical evacuation of cysts and membranes

surgical technique is straightforward but does not ensure efficiency in the long term, and recurrence will occur. It preserves a great part of the posterior elements (transverse and articular process and pedicles) and vertebral body, which will explain disease recurrence. Over the past 30 years, we have aimed for complete removal of the focus, if possible, by a two-stage surgical procedure; this consists of posterior bone resection and instrumentation in first instance, followed 15 days later by vertebral body resection and drainage of ossifluent abscess (Fitzpatrick 1965). Because of the insidious evolution of bone hydatidosis, postoperative recurrence may be difficult to detect. Severe recurrence should be suspected in case of neurological complica-

tions or when there is a huge ossifluent paravertebral abscess.

5.5.2 Nonsurgical Treatment

The literature is sparse when it comes to recommendations for the choice or duration of antimicrobial chemotherapy for bone hydatidosis. Several protocols for nonsurgical treatment have been proposed since 1928 (Devé 1928; Beard et al. 1978; Bekhti et al. 1980; Pedrosa et al. 2000). International treatment guidelines exist for visceral organs such as the liver but not for the bone. Benzimidazoles (albendazole and mebendazole) may be used to treat some patients with bone hydatidosis (Herrera et al. 2005; Song et al. 2007). They may be effective when used in conjunction with surgical treatment to reduce the risk of recurrence. Perioperative chemoprophylaxis covers the inevitable spillage during surgery, as well as the use of protoscolicidal solutions during surgery. They can also be used alone for a long duration, in cases of inoperable bone hydatid disease sited at difficult or multiple locations.

Because of its higher level in blood plasma, albendazole is the first choice for treatment of bone hydatidosis. High doses are recommended, even if optimal dosage and optimal duration have never been formally assessed, as albendazole is less toxic. Albendazole is used at a dosage of 10–15 mg/kg body weight/day, in two divided doses, taken together with fat-rich meals. The reported duration of treatment varies, as there is no consensus established for the duration. Albendazole, 15 mg/kg/day, in monotherapy is the preferred regimen. It should be administered continuously, without the monthly treatment interruptions recommended in the 1980s to limit long-term toxicity data available in the early days of use. The median duration of therapy is 6 months. At least one course should be given preoperatively. Benzimidazoles are generally well tolerated, even over a course of 10 years of administration (Franchi et al. 1999; Song et al. 2007). Albendazole liposomes (L-Alb), which refer to the encapsulation of albendazole within liposomes (10 mg/kg daily for 3 months), may alter albendazole metabolism and increase the drug bioavailability. It was used postoperatively for 3 months to prevent recurrence (Liu et al. 2004).

Radiotherapy seems to be a potential alternative or adjunct treatment option to surgery in inoperable cases of bone hydatidosis. Larger-scale, prospective, randomized controlled trials with blinded outcome assessment are needed to reliably establish the efficacy of radiotherapy and to determine the optimal dose and regimen for irradiation (Neumayr 2015).

6 Conclusion

Cystic echinococcosis is a worldwide zoonosis. The clinical and radiographic features of spinal hydatidosis may be non-specific, although there are some suggestive imaging patterns of spinal involvement. CT and MRI are the best imaging tools for diagnostic confirmation, assessment of local extension, and postoperative follow-up. Results of surgical treatment of bone hydatidosis are not gratifying. Medical treatment may help to reduce the risk of recurrence.

References

Beard TC, Rickard MD, Goodman HT (1978) Medical treatment for hydatids. Med J Aust 17: 633–635

Bekhti A, Nizet M, Capron M et al (1980) Chemotherapy of human hydatid disease with mebendazole. Follow-up of 16 cases. Acta Gastroenterol Belg 43:48–65

Bettaieb A, Khaldi M, Ben Rhouma T et al (1978) Spinal echinococcosis; clinical study of 32 cases. Neurochirurgie 24:205–210

Bouvier M, Lejeune E, Jeanneret J et al (1974) The solitary epidural hydatid cyst. Rev Rhum Mal Osteoartic 41:173–177

Braithwaite PA, Lees RF (1981) Vertebral hydatid disease: radiological assessment. Radiology 140:763–766

Brunetti E, Kern P, Vuitton DA, Writing Panel for the WHO-IWGE (2010) Expert consensus for the diagnosis and treatment of cystic alveolar echinococcosis in humans. Acta Trop 114:1–16

Chelli Bouaziz M, Ladeb MF, Chakroun M et al (2008) Spinal brucellosis: a review. Skeletal Radiol 37:785–790

Del Campo JC (1950) Vertebral echinococcosis; total resection of the fifth lumbar vertebra. Arch Urug Med Cir Espec 36:337–335

Devé F (1928) L'échinococcose vertébrale. Son processus pathologique et ses lésions. Ann Anat Pathol 5:841–859

Dorn R, Kuesswetter W, Wuensch P (1984) Alveolar echinococcosis of the femur. Acta Orthop Scand 55:371–374

Engin G, Acunaş B, Rozanes I et al (2000) Hydatid disease with unusual localization. Eur Radiol 10: 1904–1912

Fitzpatrick SC (1965) Hydatid disease of the lumbar vertebrae; report of a case. J Bone Joint Surg Br 47:286–291

Franchi C, Di Vico B, Teggi A (1999) Long-term evaluation of patients with hydatidosis treated with benzimidazole carbamates. Clin Infect Dis 29:304–309

Herrera A, Martinez AA, Rodriguez J (2005) Spinal hydatidosis. Spine 30:2439–2444

Karantanas AH, Paterakis K, Karavelis A (2003) Intervertebral disk hydatid cysts: MR imaging findings. AJR Am J Roentgenol 180:1739–1740

Karray S, Zlitni M, Fowles JV et al (1990) Vertebral hydatidosis and paraplegia. J Bone Joint Surg Br 72:84–88

Khabiri AR, Bagheri F, Assmar M et al (2006) Analysis of specific IgE and IgG subclass antibodies for diagnosis of Echinococcus granulosus. Parasite Immunol 28:357–362

Liu D, Xie ZR, Zhang R et al (2004) Treatment and diagnosis of bone hydatid disease. Chin J Orthop 24:403–406

Mandal S, Mandal MD (2012) Human cystic echinococcosis: epidemiologic, zoonotic, clinical, diagnostic and therapeutic aspects. Asian Pac J Trop Med 5:253–260

Manzano-Román R, Sánchez-Ovejero C, Hernández-González A et al (2015) Serological diagnosis and follow-up of human cystic echinococcosis: a new hope for the future? Biomed Res Int 2015:428205. https://doi.org/10.1155/2015/428205

Moro P, Schantz PM (2009) Echinococcosis: a review. Int J Infect Dis 13:125–133

Neumayr A (2015) Radiotherapy of osseous echinococcosis: where is the evidence? Int J Infect Dis 33: 75–78

Neumayr A, Tamarozzi F, Goblirsch S et al (2013a) Spinal cystic echinococcosis—a systematic analysis and review of the literature: part 1. Epidemiology and anatomy. PLoS Negl Trop Dis 7:e2450

Neumayr A, Tamarozzi F, Goblirsch S et al (2013b) Spinal cystic echinococcosis—a systematic analysis and review of the literature: part 2. Treatment, follow-up and outcome. PLoS Negl Trop Dis 7:e2458

Ozdemir HM, Ogün TC, Tasbas B (2004) A lasting solution is hard to achieve in primary hydatid disease of the spine: long-term results and an overview. Spine 29:932–937

Pamir MN, Ozduman K, Elmaci I (2002) Spinal hydatid disease. Spinal Cord 40:153–160

Papakonstantinou O, Athanassopoulou A, Passomenos D et al (2011) Recurrent vertebral hydatid disease: spectrum of MR imaging features. Singapore Med 52:440–445

Pedrosa I, Saíz A, Arrazola J et al (2000) Hydatid disease: radiologic and pathologic features and complications. Radiographics 20:795–817

Savioli L, Abdykerimov K, Christofi G et al (2011) Report of the WHO Informal Working Group on cystic and alveolar echinococcosis surveillance, prevention and control, with the participation of the Food and Agriculture Organization of the United Nations and the World Organisation for Animal Health. WHO 1–26

Scarlata F, Giordano S, Saporito L et al (2011) Cystic hydatidosis: a rare case of spine localization. Infez Med 19:39–41

Singh S, Korah IP, Gibikote SV et al (1998) Sacral hydatidosis: value of MRI in the diagnosis. Skeletal Radiol 27:518–521

Song XH, Ding LW, Wen H (2007) Bone hydatid disease. Postgrad Med J 83:536–542

Steinmetz S, Racloz G, Stern R et al (2014) Treatment challenges associated with bone echinococcosis. J Antimicrob Chemother 69:821–826

Thompson RCA (2017) Biology and systematics of echinococcus. Adv Parasitol 95:65–109

Torricelli P, Martinelli C, Biagini R et al (1990) Radiographic and computed tomographic findings in hydatid disease of bone. Skeletal Radiol 19:435–439

Vicidomini S, Cancrini G, Gabrielli S et al (2007) Muscular cystic hydatidosis: case report. BMC Infect Dis 30:23

Xie Z, Chen L, Xie Q et al (2015) Surgery or radiotherapy for the treatment of bone hydatid disease: a retrospective case series. Int J Infect Dis 33:114–119

Zlitni M, Ezzaouia K, Lebib H et al (2001) Hydatid cyst of bone: diagnosis and treatment. World J Surg 25:75–82

Imaging of Fungal Spondylodiscitis

Hend Riahi, Mohamed Fethi Ladeb, Mouna Chelli Bouaziz, Lamia Ammari, and Soumaya Rammeh

Contents

H. Riahi (✉) · M. F. Ladeb · M. Chelli Bouaziz
Department of Radiology, MT Kassab Institute of Orthopaedics, Tunis, Tunisia

Faculty of Medicine of Tunis, Tunis-El Manar University, Tunis, Tunisia
e-mail: hend.riahi@gmail.com; fethiladeb@hotmail.fr; bouaziz_mouna@yahoo.fr

L. Ammari
Department of Infectious Diseases, Rabta Hospital, Tunis, Tunisia

Faculty of Medicine of Tunis, Tunis-El Manar University, Tunis, Tunisia
e-mail: lamia_ammarib@yahoo.fr

S. Rammeh
Department of Pathology, Charles Nicolle Hospital, Tunis, Tunisia

Faculty of Medicine of Tunis, Tunis-El Manar University, Tunis, Tunisia
e-mail: rammehs@yahoo.fr

Abstract

Fungal spondylodiscitis is most commonly encountered in immunocompromised patients. The incidence of fungal infections has increased in the past decade. *Candida* and *Aspergillus* are the most common causes of opportunistic fungal infection. The imaging findings are similar to that of pyogenic infection, with T1-hypointense signal at the infected vertebral end plates. However, abnormal T2-weighted signal change is relatively less commonly identified in patients with fungal spondylodiscitis. Even though fungal spondylodiscitis is less common than pyogenic or tuberculous involvement, it is important to consider fungal infection in the differential diagnosis and utilize the clinical history and the patient presentation to enable a more accurate imaging diagnosis.

© The Author(s), under exclusive license to Springer Nature Switzerland AG 2021

M. F. Ladeb, W. C. G. Peh (eds.), *Imaging of Spinal Infection*,
Medical Radiology Diagnostic Imaging, https://doi.org/10.1007/978-3-030-70459-9_14

Abbreviations

CT Computed tomography
MRI Magnetic resonance imaging
PCR Polymerase chain reaction

1 Introduction

Fungal spondylodiscitis is uncommon, but the immunocompromised population which is susceptible to fungal infections is ever increasing (Kim et al. 2006). A wide variety of fungal organisms can cause spinal infection. The most common fungal organisms causing spondylodiscitis include *Aspergillus* spp., *Candida* spp., and *Cryptococcus neoformans* (Kim et al. 2006). Whereas *Cryptococcus*, *Candida*, and *Aspergillus* have a worldwide distribution, other fungi such as *Coccidioides immitis* and *Blastomyces dermatitidis* are limited to specific geographical areas. Therefore, residence in or travel to endemic areas should be taken into consideration when evaluating patients with chronic spondylodiscitis. The common denominator in many cases appears to be an incompetent host defense mechanism secondary to conditions such as diabetes mellitus, corticosteroid use, chemotherapy, malnutrition, or intravenous drug use.

2 Pathogenesis and Clinical Features

Fungal spondylodiscitis can occur via one of two routes. The first is through hematogeneous spread. As the intervertebral disk does not have a direct blood supply in adults, most hematogeneous infections of the disk space are the result of dissemination from the adjacent bone. The spread from an initial pulmonary source has also been described. The second route of transmission is through contiguous spread or by direct inoculation of the organism during surgery (Kim et al. 2006).

Insidious back pain is the most frequent complaint. Neurological impairment appears to be relatively infrequent (Kim et al. 2006). Kyphosis can also be seen, due to the indolent nature of the infection. Involvement of the vertebral bodies can lead to vertebral compression fractures and deformity of the spine. In addition, the spread of infection along the anterior longitudinal ligament can lead to paravertebral or psoas muscle abscesses (Skaf et al. 2010).

3 Aspergillosis

Aspergillus is an opportunistic mycelial organism which is abundant in the environment. It lives as saprophyte, and its concentration in the air undergoes seasonal variation (higher in summer). Nosocomial aspergillosis is due to infiltration of conidia into ward air from outside. *Aspergillus* is the most common cause of infection and death in patients with chronic granulomatous disease (Heinrich et al. 1991). Aspergillosis is also the second most common invasive fungal infection in cancer patients, with most of them being or had previously been neutropenic. Bone marrow transplant recipients may be at risk of invasive aspergillosis, especially during profound neutropenia (Govender 2003). *Aspergillus* is the most common cause of skeletal mycosis, with the vertebrae being the most commonly involved structures in mycotic osteomyelitis. The most common causative species is *A. fumigatus*. Less frequently, *A. flavus*, *A. niger*, *A. nidulans*, and *A. terreus* have been isolated (Govender et al. 1991).

The radiological features of *Aspergillus* spondylodiscitis are nonspecific, and they may involve single or multiple bodies. The lumbar region is the main area (63%) of osseous involvement (Hummel et al. 1993). Spinal aspergillosis is often confused with tuberculous spondylodiscitis. As in tuberculous spondylodiscitis, *Aspergillus* infection may extend from an anterior lesion of the vertebral body beneath the anterior longitudinal ligament to the anterior parts of neighboring intervertebral disk and vertebral bodies or involve multiple vertebral segments with skip lesions. However, the shape of epidural or paravertebral abscesses may be helpful in differentiating between them. *Aspergillus* abscesses have a thick irregular wall, whereas tuberculous abscesses typically have a thin smooth wall (Jung et al. 2004) (Fig. 1).

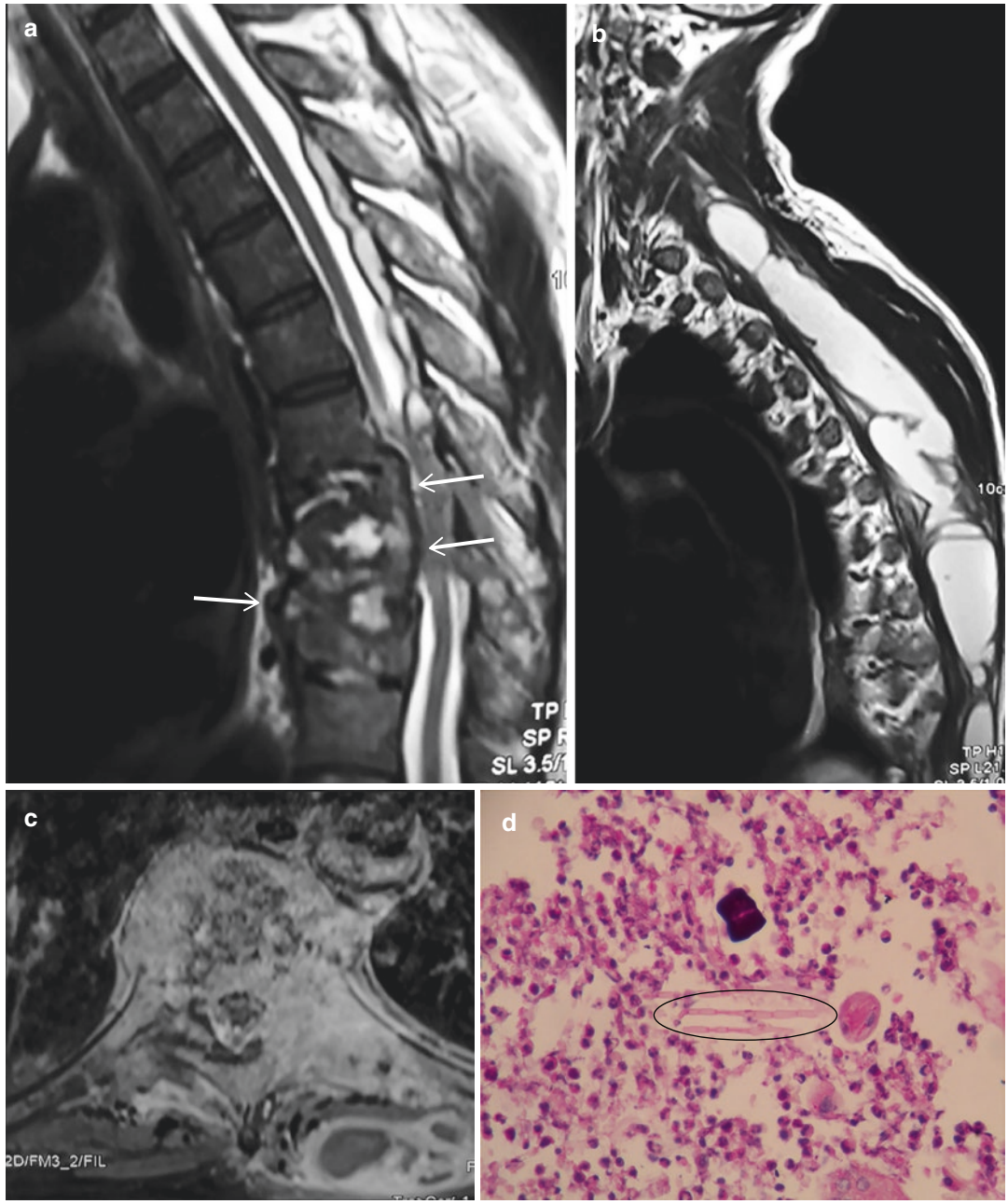

Fig. 1 A 55-year-old man with diabetes mellitus who presented with progressive back pain and fecal and urinary incontinence. (**a**, **b**) Sagittal T2-W MR images show multilevel disease with areas of hyperintensity in the T9, T10, T11, and T12 vertebrae and intervertebral disks. Large confluent paraspinal abscess and epidural disease are also present. Subligamentous spread of infection (arrows) is seen along anterior and posterior margins of the vertebral bodies. (**c**) Axial contrast-enhanced T1-W MR image shows infective arthritis of facet and costovertebral joints and paravertebral abscesses with thin peripheral rim enhancement. CT-guided percutaneous needle biopsy was performed and mycological examination revealed *Aspergillus flavus*. (**d**) Histopathological examination showed acute inflammation and necrosis with hyaline, branching septate hyphae (circled)

Additionally, in invasive aspergillosis, the lesion spreads more circumferentially than longitudinally. It destroys the vertebral body and the neural arches and then, extends into the chest wall and the thoracic cavity (Ur-Rahman et al. 2000). Moreover, the nuclear cleft in *Aspergillus*-induced spondylodiscitis may be preserved, and *Aspergillus* infection may show band-like signal hypointensity in the subchondral bone marrow on T2-weighted MR images. The subchondral T2-hypointense signal is attributed to the presence of paramagnetic and ferromagnetic elements within the fungi. This finding is similar to the proposed mechanism for T2 hypointensity in fungal sinusitis (Hong et al. 2009; Kwon et al. 2011).

The biological diagnosis is based on the detection of *Aspergillus* after Sabouraud agar culture of discovertebral biopsy fragments, associated with the observation of mycelial hyphae on the same samples on direct examination. Detection of fungal biomarkers is highly contributory. Serology is based on the detection of anti-*Aspergillus fumigatus* antibodies by different techniques (ELISA, Western Blot). The search for the galactomannan antigen is particularly recommended for neutropenic patients, while the (1-3)-β-D-glucan antigen has a negative predictive value. Molecular biology by RT-PCR also has a good negative predictive value (Nicolle et al. 2013).

The treatment of *Aspergillus* spondylodiscitis is multimodal, involving early antifungal therapy and surgical intervention (Korovessis et al. 2014). Various studies have demonstrated the superiority of voriconazole over amphotericin B in the treatment of invasive aspergillosis, with improved survival and lower toxicity (Herbrecht et al. 2002). Despite limited experience with voriconazole for the treatment of *Aspergillus* spondylodiscitis, it is currently recommended by the Infectious Diseases Society of America (IDSA) guidelines for a minimum of 6–8 weeks in immunocompromised patients (Walsh et al. 2008).

4 Candidosis

Candida spondylodiscitis accounts for approximately 1% of infectious spondylodiscitis (Richaud et al. 2017). It was previously considered a complication of intravenous drug use (Cornely et al. 2012; Pappas et al. 2016) but now is mostly a healthcare-associated infection, such as invasive *Candida* infection. With the increase in invasive *Candida* infection, *Candida* spondylodiscitis cases are increasing, and this trend will likely continue in the future. Although there are nearly ten species of *Candida* that are pathogenic to humans, 62% of cases of vertebral osteomyelitis are caused by *C. albicans*, 19% by *C. tropicalis*, and 14% by *C. glabrata* (Kim et al. 2006). Infection caused by *C. glabrata* is becoming more common. The lower thoracic or lumbar spine is most frequently involved, seen in 95% of patients. At presentation, 83% of patients complain of back pain for more than 1 month, and only 32% of patients have fever (Kim et al. 2006).

Radiographs frequently show erosive and destructive vertebral changes, but these may not be visible for weeks to months (Bonakdarpour and Gaines 1983). *Candida* spondylodiscitis looks like a pyogenic infection with areas of hypointensity on T1-weighted MR images and minimal hyperintensity or isointensity on T2-weighted MR images of the vertebral bodies. The clinical usefulness of minimal signal change on T2-weighted images may however be limited, since a recent review of MRI findings in spinal osteomyelitis showed T2 hyperintensity in the vertebral bodies in only 56% of cases (Dagirmanjian et al. 1996). In *Candida* spondylodiscitis, there is posterior element involvement, which is unusual in pyogenic spondylodiscitis and is more commonly seen in tuberculosis. In addition, paraspinal inflammation is usually minimal to moderate in extent and commensurate with the amount of bone destruction and disk space involvement. This is in contrast to tuberculosis, which is characteristically associated with a large paraspinal inflammatory component (Whelan et al. 1985) (Fig. 2).

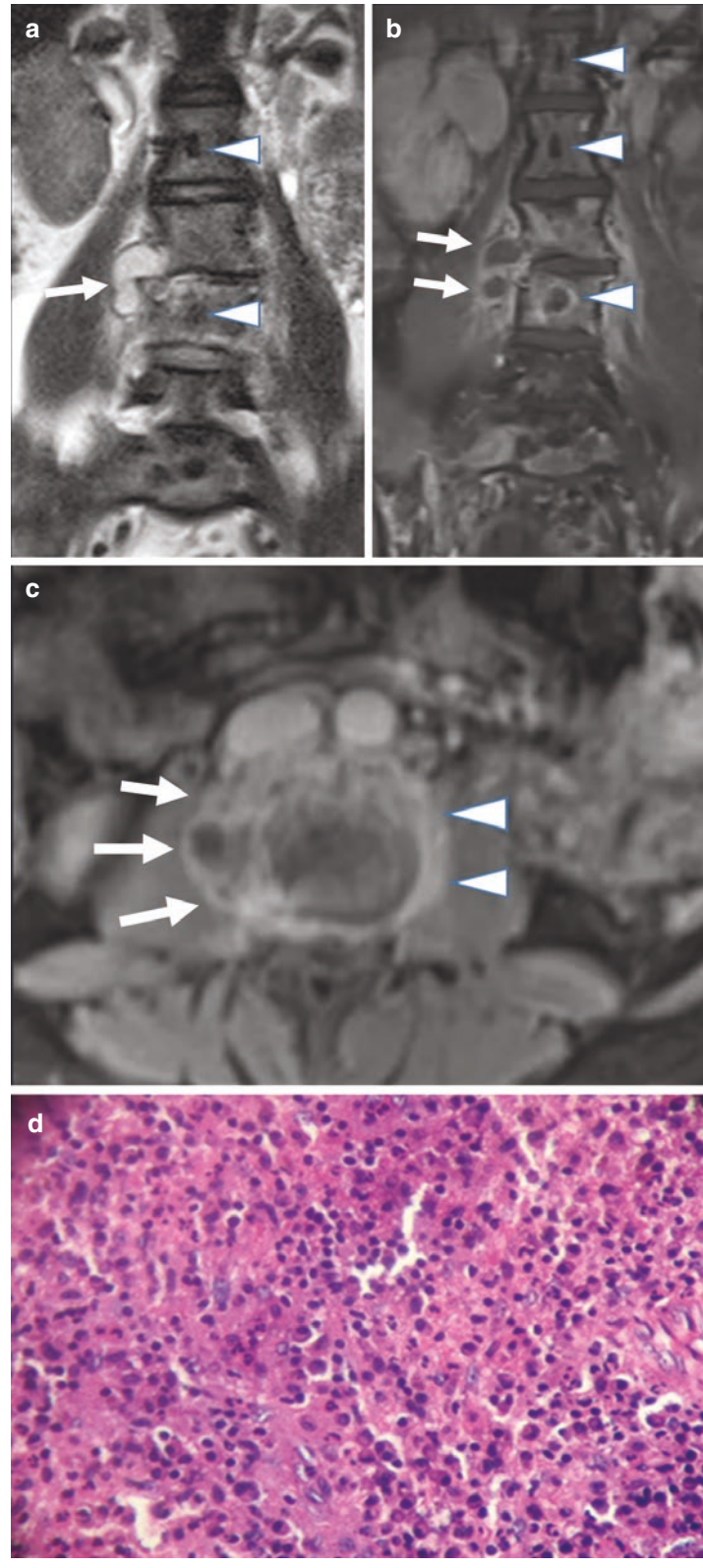

Fig. 2 A 27-year-old man with thalassemia and sickle cell anemia. Coronal (**a**) T2-W and (**b**) contrast-enhanced T1-W MR images show extensive signal abnormality involving the entire spine with irregular patchy areas of signal hypointensity due to hemopathy (arrowheads), destruction of L3/L4 disk, and paravertebral abscesses, more prominent on the right (arrows). (**c**) Axial contrast-enhanced T1-W MR image shows multiple small paraspinal abscesses (arrows) and diffusely enhancing left paraspinal inflammatory mass (arrowheads). CT-guided percutaneous needle biopsy was performed, and mycological examination revealed *Candida tropicalis*. (**d**) Histopathological examination showed foci of granulomatous inflammatory tissue and necrosis

Blood cultures are negative in 24–50% of cases (Arias et al. 2004). Antigen and antibody detection assays are useful in fungal infections, where they have a high positive predictive value for the diagnosis of *Candida albicans*. These tests are based on the detection of circulating cell wall fungal antigens. Molecular techniques have also been used with fungal infections and have enhanced the sensitivity of conventional methods used in diagnostic mycology (Skaf et al. 2010).

There are no treatment guidelines or evidence-based recommendations for *Candida* spondylodiscitis in immunocompetent or immunocompromised patients. In addition, the optimal medication and treatment duration for fungal spondylodiscitis are unknown. Antifungal drug resistance is considered less problematic in *Candida* species than in other pathogens. The preferred treatment is fluconazole for 6–12 months or amphotericin B for 6–10 weeks (Kim et al. 2006).

5 Cryptococcosis

Cryptococcosis is a systemic mycosis that often involves the lungs and the central nervous system. It is caused by *Cryptococcus neoformans*, which is found in fruit, milk, soil, and feces of some birds. The disease has a worldwide distribution. Immunosuppression related to altered T-cell function is the most common predisposing factor. In non-human immunodeficiency virus (HIV)-infected patients, predisposing factors for cryptococcosis include malignancy, solid organ transplantation, connective tissue diseases, and immunosuppressive therapy. Estimates of the annual incidence of cryptococcosis in non-HIV individuals are 1.3–8 per 100,000 (Legarth et al. 2014).

The disease is generally acquired by the respiratory route through inhalation of aerosolized spores. Pulmonary infection with *Cryptococcus* may be asymptomatic or symptomatic. It may regress, progress, or remain stable for years. Extrapulmonary infection usually results from hematogeneous spread and can involve any organ. There is a predilection for central nervous system involvement, which is the most common extrapulmonary manifestation (Kim et al. 2006). Osseous involvement is a manifestation of disseminated cryptococcosis in 5–10% of cases. The most commonly involved skeletal sites are the spine, pelvis, ribs, skull, tibia, and knee (Chhem et al. 2001).

The thoracic spine is the most frequently affected spinal segment. Radiological findings in spinal cryptococcosis are not specific and are usually similar to those of tuberculosis spondylodiscitis. There is involvement of the vertebral body and extensive involvement of the posterior elements and paraspinous and perivertebral soft tissues, with relative preservation of the disk (Andres et al. 2014). Radiographs may reveal a cystic lesion involving a single body or multiple vertebral bodies, which may mimic metastatic disease or multiple myeloma. In immunocompetent hosts, the lung fields may be normal, but in immunocompromised patients, chest radiographs may reveal pneumonia or a fungal ball in a preexisting cavity (Hoeprich et al. 1994) (Fig. 3).

The serum cryptococcal antigen test has been reported to have an accuracy of 66% in immunocompetent patients with cryptococcosis (Kiertiburanakul et al. 2006). The detection of fungal nucleic acid by PCR has promise as a diagnostic tool. Biopsy and histopathological assessments are critical in the diagnosis of fungal infection. Further identification can be aided by the phenol oxidase reaction for cryptococcus. It is crucial that microscopical appearances are correlated with microbiological findings and other tests for specific host antibodies, fungal antigens, and fungal nucleic acids (O'Shaughnessy et al. 2003). Amphotericin B in combination with oral flucytosine is the recommended medical therapy (Casadevall and Perfect 1998). Surgery helps in establishing the diagnosis, in reducing the burden of infection, and in the stabilization of the spine (Gupta et al. 2003).

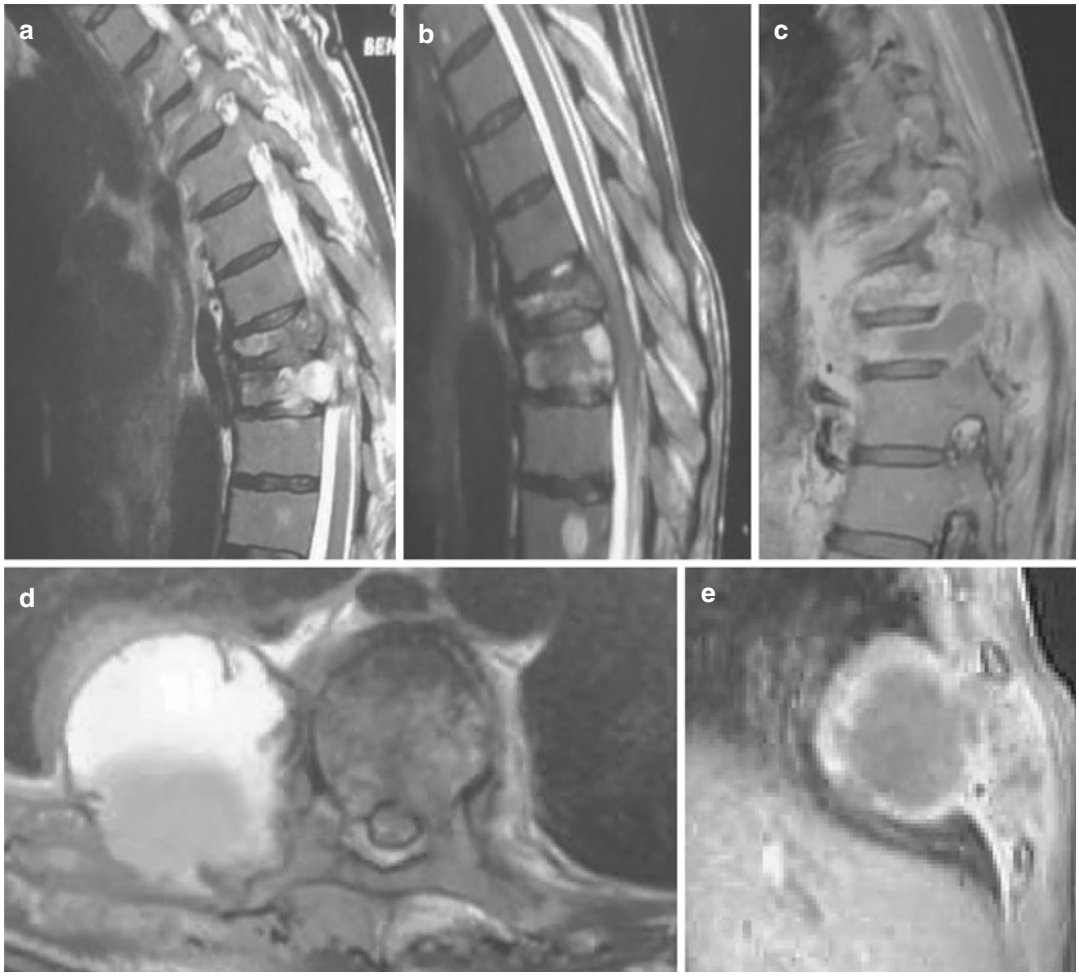

Fig. 3 (**a**, **b**) Sagittal T2-W and (**c**) right parasagittal contrast-enhanced fat-suppressed T1-W MR images show areas of T2 hyperintensity in the collapsed T8 and T9 vertebral bodies and spinous processes. Epidural abscess with compression of spinal cord and a large prevertebral abscess are also seen at the T8-T9 levels. There is also extension to the right pedicle and lamina of the T8 and T9 vertebrae. The vertebral bodies and right posterior elements show peripheral enhancement. Note normal height and signal intensity of the adjacent disks. (**d**) Axial and (**e**) coned right parasagittal contrast-enhanced fat-suppressed T1-W MR images show a large paravertebral abscess which protrudes into the pleural cavity and involves the adjacent posterior ribs. CT-guided percutaneous needle biopsy revealed cryptococcosis

6 Coccidioidomycosis

Coccidioidomycosis is endemic in South Africa, South America, and the United States (Dalinka et al. 1971). Coccidioidomycosis results from inhalation of spores of the fungus, which causes a variable pulmonary response in affected individuals. Extrapulmonary dissemination develops in approximately 0.5% of affected patients. Spinal involvement develops in approximately 25% of patients with disseminated disease (Huntington et al. 1967; Galgiani 1993).

In patients with coccidioidomycotic spondylodiscitis, radiographs usually show single or multiple osteolytic lesions with poorly defined borders. A rim of sclerosis may be present in patients under amphotericin treatment (Herron 2003). The MRI features of spinal coccidioidomycotic spondylodiscitis are nonspecific. An abnormal but minimally narrowed disk, extensive soft tissue

involvement, heterogeneous marrow signal intensity, and a lack of bony deformity are features that suggest coccidioidomycosis (Olson et al. 1998). The posterior elements alone may rarely be affected but are not uncommonly involved with advanced disease. One-third of patients have contiguous or noncontiguous multiple levels of disease (Olson et al. 1998). Extraosseous soft tissue involvement is typical and is usually extensive, with spread beneath the longitudinal ligaments and epidural disease (Fig. 4).

Serological testing and biopsy are the mainstays of diagnosis. Mature spherules with endospores on pathology indicate *Coccidioides immitis* infection (Herron 2003). The preferred medical treatment is amphotericin B and flucytosine for 2 weeks and then fluconazole for a minimum of 10 weeks (Kim et al. 2006). The indications for surgical treatment in coccidioidal spondylodiscitis are those of spinal surgery in general, namely, instability, neurological deficit, and/or deformity (Herron 2003).

7 Blastomycosis

Blastomyces dermatitidis is a dimorphic fungus endemic in the southeastern and south central states of the United States. It is considered to be an inhabitant of soil, and infection occurs by inhalation of conidia. Hematogeneous dissemination of infection to almost any organ can occur months to years after the initial pulmonary involvement (Kuzo and Goodman 1996). The skin is the most common extrapulmonary site, with a 40–80% incidence (Hadjipavlou et al. 1998). Skeletal blastomycosis is seen in 14–60% of disseminated cases (Riegler et al. 1974; Hadjipavlou et al. 1998). The spine is the most common site of skeletal involvement, followed by the skull, ribs, tibia, and the bones of the foot and wrist.

The lower thoracic and lumbar spines are most affected. The anterior aspect of the vertebral body is usually affected initially. Further bone destruction can lead to vertebral compression fractures, and spread to adjacent vertebral bodies is through the disk (Kim et al. 2006). Nonadjacent vertebral bodies also can be affected by spread of infection along the anterior longitudinal ligament. Infection can lead to psoas or paravertebral abscesses. With *Blastomyces*, collapse and gibbus deformity tends to be seen more commonly. As in tuberculosis, blastomycosis can form large paraspinal abscesses that occasionally extend into the groin and upper thigh with fistula formation.

The diagnosis can be made only by visualization of the yeast in pus, sputum, and secretions and on the basis of the histological examination (Hadjipavlou et al. 1998). The most sensitive test, and therefore the gold standard for diagnosis, remains fungal culture which may take several days or weeks. Antigen testing for blastomycosis antigens can be performed with urine and serum, using enzyme immunoassay (EIA). PCR testing of culture material and formalin-fixed paraffin-embedded tissue is also available (Emamian et al. 2019). The preferred treatment for blastomycosis is amphotericin B for life-threatening disease and itraconazole for 6–12 months for mild to moderate disease. Local debridement with abscess drainage may be necessary for spinal or skin involvement (Detrisac et al. 1980).

8 Mycetoma

Mycetoma is a neglected tropical disease that is endemic in many tropical and subtropical areas. Mycetoma is a chronic mutilating disease of the skin and the underlying tissues which is caused by fungi (eumycetoma) or bacteria (actinomycetoma). The most common pathogens reported in eumycetoma are *Madurella mycetomatis*, *Madurella grisea*, *Pseudallescheria boydii*, and *Leptosphaeria senegalensis*. It follows implantation of infectious organisms into subcutaneous tissue, from where infection spreads to the skin and bone. The organisms form small microcolonies that are discharged onto the skin surface via sinus tracts or can burrow into other adjacent tissues including the bone (Zijlstra et al. 2016).

Mycetoma occurs in all age groups but is rarely seen in children. It commonly occurs in field laborers and cultivators whose occupation

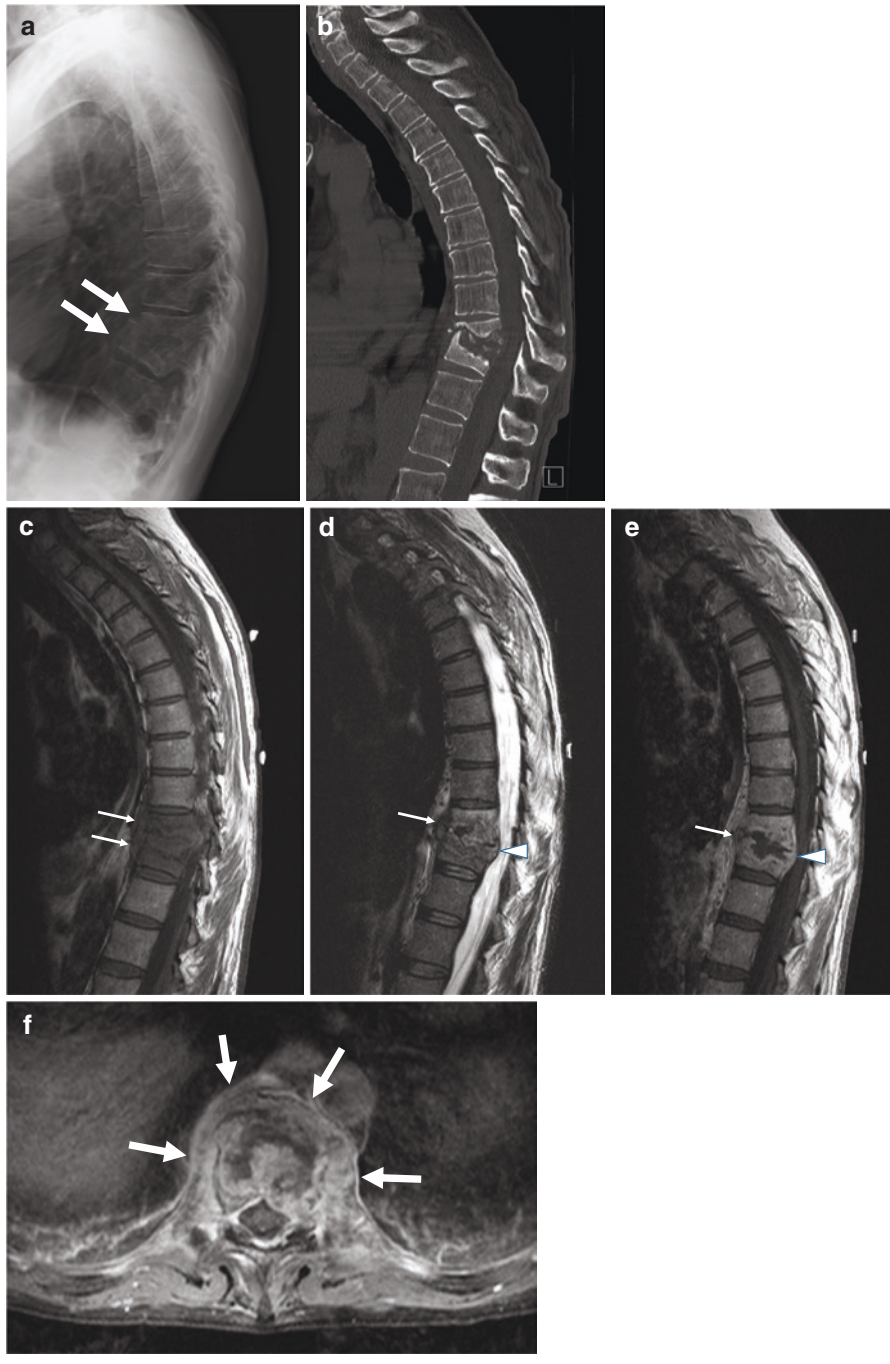

Fig. 4 A 59-year-old man with T10-11 coccidioidomycotic spondylodiscitis. (**a**) Lateral radiograph shows destruction and collapse of the T10 and T11 vertebral bodies and T10/11 disk (arrows), producing a kyphotic deformity. (**b**) Sagittal CT image shows the extent of discovertebral destruction in greater detail, including several small bony fragments. Sagittal (**c**) T1-W, (**d**) T2-W and (**e**) contrast-enhanced fat-suppressed T1-W MR images show T1-hypointense and heterogeneous T2-hyperintense signal alteration of the infected vertebral bodies with moderate enhancement, including rim enhancement around the T10/11 discovertebral fluid collection. Anterior subligamentous (small arrows) and epidural (arrowhead) extensions are present. (**f**) Axial contrast-enhanced fat-suppressed T1-W MR image shows involvement of the posterior elements bilaterally, as well as anterior and paravertebral soft tissue extension (arrows). [Courtesy of Prof. Mihra Taljanovic, University of New Mexico, Albuquerque, USA]

involves direct contact with the soil (Lichon and Khachemoune 2006). The foot is the commonest site affected by mycetoma (70%), followed by the hand (12%) (Fahal 2004). Spinal cord involvement is rare, and only a few cases have been reported (Cascio et al. 2011; Fahal 2011). In mycetoma, spread occurs locally and through the lymphatics. Hematological spread has also been described.

In early disease, radiographs are essentially normal. Eventually a soft tissue mass may be seen as a dense shadow or as multiple scattered soft tissue shadows. Later on, there may be bone scalloping, periosteal reaction, and multiple punched-out cavities. MRI is useful for determining the extent of the lesions and invasion of structures. It usually shows multiple small lesions (2–5 mm) of hyperintense signal, interspersed within a hypointense matrix. The "dot in circle" sign, which indicates the presence of grains, highly characteristic (Fahal 2017).

Different laboratory-based diagnostic techniques are available to determine and identify the causative agents. These include direct microscopy and cytological, histopathological, and immunohistochemical techniques in addition to the classical grain culture and molecular-based techniques (Fahal 2017). Treatment of mycetoma is still based on expert opinion, in the absence of WHO treatment guidelines. Varying antimicrobial treatment options for actinomycetoma exist. Eumycetoma treatment usually poses a challenge. Antifungals are used, and in many cases, a combination of surgery and antifungals is preferred (Emmanuel et al. 2018).

9 Conclusion

Fungal spondylodiscitis remains a rare pathology, although an increased incidence has been reported. Fungal infection should be considered in an immunodeficient patient with lumbar pain, progressive onset with atypical changes on the spine imaging, negative cultures, and persistent symptoms despite antibiotic treatment.

References

Andres A, Feliza R, Mauricio C (2014) Spinal infections: clinical and imaging features. Top Magn Reson Imaging 23:303–314

Arias F, Mata-Essayag S, Landaeta ME et al (2004) *Candida albicans* osteomyelitis: case report and literature review. Int J Infect Dis 8:307–314

Bonakdarpour A, Gaines VD (1983) The radiology of osteomyelitis. Orthop Clin North Am 14:21–33

Casadevall A, Perfect JR (1998) Cryptococcus neoformans. ASM Press, Washington, DC, pp 407–456

Cascio A, Mandraffino G, Cinquegrani M et al (2011) Actinomadura pelletieri mycetoma—an atypical case with spine and abdominal wall involvement. J Med Microbiol 60:673–676

Chhem RK, Wang S, Jaovisidha S et al (2001) Imaging of fungal, viral, and parasitic musculoskeletal and spinal diseases. Radiol Clin North Am 39:357–378

Cornely OA, Bassetti M, Calandra T et al (2012) ESCMID guideline for the diagnosis and management of Candida diseases 2012: non-neutropenic adult patients. Clin Microbiol Infect 18(Suppl 7): 19–37

Dagirmanjian A, Schils J, McHenry M et al (1996) MR imaging of vertebral osteomyelitis revisited. AJR Am J Roentgenol 167:1539–1543

Dalinka MK, Dinnenberg S, Greendyk WH et al (1971) Roentgenographic features of osseous coccidioidomycosis and differential diagnosis. J Bone Joint Surg Am 53:1157–1164

Detrisac DA, Harding WG, Greiner AL et al (1980) Vertebral North American blastomycosis. Surg Neurol 13:311–312

Emamian S, Fox MG, Boatman D et al (2019) Spinal blastomycosis: unusual musculoskeletal presentation with literature review. Skeletal Radiol 48:2021–2027

Emmanuel P, Dumre SP, John S et al (2018) Mycetoma: a clinical dilemma in resource limited settings. Ann Clin Microbiol Antimicrob 17:35. https://doi.org/10.1186/s12941-018-0287-4

Fahal AH (2004) Mycetoma: a thorn in the flesh (2006). Trans R Soc Trop Med Hyg 98:3–11

Fahal AH (2011) Mycetoma. Review article. Khartoum Med J 4:514–523

Fahal AH (2017) Mycetoma. In: Current progress in medical mycology. Springer Nature, pp 355–380

Galgiani JN (1993) Coccidioidomycosis. West J Med 159:154–171

Govender S (2003) Aspergillosis of the spine. In: Govender S, Leong JCY (eds) Inflammatory diseases of the spine. TTG Asia, Singapore, pp 13.1–13.8

Govender S, Rajoo R, Goga IE et al (1991) *Aspergillus* osteomyelitis of the spine. Spine 16:746–749

Gupta SK, Chhabra R, Sharma BS et al (2003) Vertebral cryptococcosis simulating tuberculosis. Br J Neurosurg 17:556–559

Hadjipavlou AG, Mader JT, Nauta HJ et al (1998) Blastomycosis of the lumbar spine: case report and review of the literature, with emphasis on diagnostic laboratory tools and management. Eur Spine J 7:416–421

Heinrich SD, Finney T, Craver R et al (1991) *Aspergillus* osteomyelitis in patients who have chronic granulomatous disease. J Bone Joint Surg Am 73: 456–460

Herbrecht R, Denning DW, Patterson TF et al (2002) Invasive Fungal Infections Group of the European Organisation for Research and Treatment of Cancer and the Global Aspergillus Study Group. Voriconazole versus amphotericin B for primary therapy of invasive aspergillosis. N Engl J Med 347:408–415

Herron L (2003) Coccidioidal spondylitis. In: Govender S, Leong JCY (eds) Inflammatory diseases of the spine. TTG Asia, Singapore, pp 14.1–14.9

Hoeprich PD, Hoeprich PD, Jordan C et al (1994) Cryptococcosis. In: Infectious diseases. Lippincott-Raven, Philadelphia, pp 1132–1140

Hong SH, Choi JY, Lee JW et al (2009) MR imaging assessment of the spine: infection or an imitation? Radiographics 29:599–612

Hummel M, Schuler S, Weber U et al (1993) Aspergillosis with *Aspergillus* osteomyelitis and diskitis after heart transplantation: surgical and medical management. J Heart Lung Transplant 12:599–603

Huntington RW, Waldmann WJ, Sargent JA et al (1967) Pathologic and clinical observations on 142 cases of fatal coccidioidomycosis. In: Ajello L (ed) Coccidioidomycosis. University of Arizona Press, Tucson, pp 221–222

Jung NY, Jee WH, Ha KY et al (2004) Discrimination of tuberculous spondylitis from pyogenic spondylitis on MRI. AJR Am J Roentgenol 182:1405–1410

Kiertiburanakul S, Wirojtananugoon S, Pracharktam R et al (2006) Cryptococcosis in human immunodeficiency virus-negative patients. Int J Infect Dis 10:72–78

Kim CW, Perry A, Currier B et al (2006) Fungal infections of the spine. Clin Orthop Relat Res 444:92–99

Korovessis P, Repanti M, Katsardis T et al (2014) Anterior decompression and fusion for aspergillus osteomyelitis of the lumbar spine associated with paraparesis. Spine 19:2715–2718

Kuzo RS, Goodman LR (1996) Blastomycosis. Semin Roentgenol 31:45–51

Kwon JW, Hong SH, Choi SH et al (2011) MRI findings of *Aspergillus* spondylitis. AJR Am J Roentgenol 197:W919–W923

Legarth RA, Christensen M, Calum H et al (2014) Cryptococcal rib osteomyelitis as primary and only symptom of idiopathic CD4 penia. Med Mycol Case Rep 4:16–18

Lichon V, Khachemoune A (2006) Mycetoma: a review. Am J Clin Dermatol 7:315–321

Nicolle A, De la Blanchardière A, Bonhomme J et al (2013) Aspergillus vertebral osteomyelitis in immunocompetent subjects: case report and review of the literature. Infection 41:833–840

O'Shaughnessy EM, Shea YM, Witebsky FG (2003) Laboratory diagnosis of invasive mycoses. Infect Dis Clin North Am 17:135–158

Olson EM, Duberg AC, Herron LD et al (1998) Coccidioidal spondylitis: MR findings in 15 patients. AJR Am J Roentgenol 171:785–789

Pappas PG, Kauffman CA, Andes DR et al (2016) Clinical Practice Guideline for the Management of Candidiasis: 2016 update by the Infectious Diseases Society of America. Clin Infect Dis 62:e1–e50

Richaud C, De Lastours V, Panhard X et al (2017) Candida vertebral osteomyelitis (CVO) 28 cases from a 10-year retrospective study in France. Medicine (Baltimore) 96:e7525

Riegler HF, Goldstein LA, Betts RF (1974) Blastomycosis osteomyelitis. Clin Orthop Relat Res 100: 225–231

Skaf GS, Kanafani ZA, Araj GF et al (2010) Non-pyogenic infections of the spine. Int J Antimicrob Agents 36:99–105

Ur-Rahman N, Jamjoom ZA, Jamjoom A (2000) Spinal aspergillosis in non-immunocompromised host mimicking Pott's paraplegia. Neurosurg Rev 23: 107–111

Walsh TJ, Anaissie EJ, Denning DW et al (2008) Infectious Diseases Society of America. Treatment of aspergillosis: clinical practice guidelines of the Infectious Diseases Society of America. Clin Infect Dis 46:327–360

Whelan MA, Schonfeld S, Post JD et al (1985) Computed tomography of nontuberculous spinal infection. J Comput Assist Tomogr 9:280–287

Zijlstra EE, Van de Sande WW, Welsh O et al (2016) Mycetoma: a unique neglected tropical disease. Lancet Infect Dis 16:100–112

Diagnostic Algorithm of Spinal Infection

Kheng Song Leow, Say Tat Ooi, and Wilfred C. G. Peh

Contents

Abstract

The clinical presentation of spinal infection is often nonspecific. Delayed diagnosis can result in devastating morbidities and mortality. MRI has become the preferred imaging modality of choice for detection and diagnosis of spinal infection. Biopsy, either open surgical or percutaneous image-guided, is recommended for pathogen identification and targeted treatment. Utilizing a diagnostic algorithm enables a systematic approach to effectively diagnose and manage patients with spinal infection.

K. S. Leow (✉)
Department of Diagnostic Radiology, Woodlands Health Campus, Singapore, Republic of Singapore
e-mail: leow_kheng_song@whc.sg

S. T. Ooi
Division of Infectious Diseases, Department of General Medicine, Khoo Teck Puat Hospital, Singapore, Republic of Singapore
e-mail: ooi.say.tat@ktph.com.sg

W. C. G. Peh
Department of Diagnostic Radiology, Khoo Teck Puat Hospital, Singapore, Republic of Singapore
e-mail: Wilfred.peh@gmail.com.sg

© The Author(s), under exclusive license to Springer Nature Switzerland AG 2021, corrected publication 2021

M. F. Ladeb, W. C. G. Peh (eds.), *Imaging of Spinal Infection*,
Medical Radiology Diagnostic Imaging, https://doi.org/10.1007/978-3-030-70459-9_15

Abbreviations

CT	Computed tomography
ESR	Erythrocyte sedimentation rate
MRI	Magnetic resonance imaging
WBC	White blood cell count

1 Introduction

Spinal infection can be caused by pathogenic agents such as bacteria (pyogenic infection), tuberculosis and fungi (granulomatous infection), and, less commonly, others such as parasites. At present, the majority of spinal infections are bacterial in etiology, commonly *Staphylococcus aureus*, with an incidence of 50–75% of all microorganisms (Jensen et al. 1997; Mackenzie et al. 1998). The routes of pathogen spread can be categorized into direct external inoculation (from surgery and lumbar puncture), contiguous adjacent spread (associated with retropharyngeal abscess and esophageal perforation), and distant hematogeneous spread (e.g., secondary to pneumonia and urinary tract infection). Patients who are susceptible to spinal infection include the elderly, intravenous drug users, and patients with diabetes mellitus, human immunodeficiency virus infection, and oncological and rheumatological conditions (Fantoni et al. 2012).

2 Diagnosis of Spinal Infection

The diagnosis of spinal infection is often delayed, due to its nonspecific clinical presentation and insidious nature of the disease. The diagnosis can be delayed up to 2–6 months, from the time of first clinical presentation (Frangen et al. 2006; Tsiodras and Falagas 2006). An accurate diagnosis of spinal infection often requires a combination of clinical, laboratory, imaging, and/or histopathological findings.

2.1 Clinical Presentation

The diagnosis of spinal infection begins from the attending doctor having a high level of clinical suspicion. Patients with spinal infection can present with nonspecific neck or back pain that is insidious in onset, constant in nature, and typically described as being worse at night. Up to 15% of patients with spinal infection do not experience pain (Fantoni et al. 2012). Other less common clinical symptoms include fever (occurring in approximately 48% of patients), neurological deficit, dysphagia, and torticollis, if the infection affects the cervical spine (Schimmer et al. 2002; Mylona et al. 2009; Kim et al. 2010). Physical examination often reveals no significant abnormality in early infection. In advanced infection, patients can present with back swelling, kyphotic deformity as result of pathological compression fractures, or neurological deficits secondary to cord or cauda equina compression (Duarte and Vaccaro 2013).

2.2 Laboratory Findings

Inflammatory markers are commonly raised when the patient mounts an immune response to the infection. The commonly ordered laboratory tests include white blood cell count (WBC), C-reactive protein (CRP), and erythrocyte sedimentation rate (ESR). Of these tests, WBC is the least useful marker, due to its low sensitivity (Beronius et al. 2001; Euba et al. 2008). ESR and CRP are relatively more sensitive, but they lack specificity. CRP is elevated in more than 90% of patients with spondylodiscitis (Beronius et al. 2001; Euba et al. 2008). ESR can be a useful marker to assess for therapeutic response. Reduction of the initial ESR value after antibiotic treatment has been found to be a good prognostic indicator (Carragee et al. 1997). Blood cultures are recommended when spinal infection is suspected. Specimens collected should be sent for gram smears, culture, acid-fast bacilli smears, and tuberculosis (TB) polymerase chain reaction

(PCR), depending on the clinical suspicion (Duarte and Vaccaro 2013). The specific causative microorganisms can be identified in up to 59% of positive blood cultures in patients with pyogenic spondylodiscitis (Sobottke et al. 2008; Duarte and Vaccaro 2013).

2.3 Imaging

Radiographs, the first-line imaging modality that is usually used to investigate suspected spinal infection, lack sensitivity and specificity in early stages of the disease. Radiographs are useful for the detection of compression fracture, gross anatomical deformity, or an area of bone destruction (Pineda et al. 2011). Compared to radiographs, computed tomography (CT) provides better delineation of cortical bone destruction and early periosteal reaction and is often used for image-guided percutaneous biopsy, particularly of small vertebral lesions. However, CT involves ionizing radiation and has inferior soft tissue resolution compared to magnetic resonance imaging (MRI) (Peh 2006; Chihara and Segreti 2010). MRI has become the preferred imaging modality of choice in the imaging assessment of spinal infection. Detailed discussion of the role of radiography, CT, and MRI in various infections of the spine can be found in the preceding chapters of this book.

3 Image-Guided Percutaneous Biopsy

Biopsy involves removal of infected body tissues with the goal of identifying the causative agent and establishing a definitive diagnosis. Biopsy can be performed by a surgical (open biopsy) or percutaneous (closed biopsy) approach. Compared to surgical biopsy, percutaneous needle biopsy is safer, cheaper, and more time-effective and cost-effective (with shorter hospital stay), allows avoidance of general anesthesia, and has lower complication rates (Peh 2006). Details of percutaneous biopsy can be found in the chapter entitled "Percutaneous Biopsy of Spinal Infection".

CT is currently the modality of choice for guiding percutaneous needle biopsy of spinal lesions, particularly those that are small or located in structures that are difficult to access surgically or by other imaging means. Correlation with prior MR images is required, particularly for areas of infection that are not clearly visible on CT. Ultrasound-guided biopsy can be attempted if the source of infection is superficial. There is no absolute contraindication to biopsy. Relative contraindications include bleeding diathesis, coagulopathy, and lack of a safe window for biopsy (Srinivasan and Peh 2011).

At least three specimens should be obtained during biopsy to confirm adequacy of biopsy specimens. In suspected spondylodiscitis, in addition to the intervertebral disk, the adjacent subchondral bone should be biopsied, as these are common sites of microorganism deposition from hematogeneous spread (Michel et al. 2006). For the thoracic and lumbar spine and posteriorly located cervical spine lesions, biopsy specimens can usually be obtained via transpedicular, transcostovertebral, or posterolateral paravertebral approaches. For anteriorly located lesions in the cervical spine, the anterolateral approach is usually adopted with protection of the carotid artery, internal jugular vein, and adjacent nerves (Peh 2006).

Aspiration and core biopsy specimens have a complementary role (Schweitzer et al. 1996). CT-guided needle aspiration has been found to be accurate in identifying active bacterial disk infection, but it is less reliable for fungal infection. Addition of cytopathologic to the microbiologic analysis can also improve the detection sensitivity of infective lesions (Peh 2006). Blood clots that are aspirated should be sent for analysis and not discarded, as they may contain microorganisms (Hewes et al. 1983; Peh 2006). Further details of percutaneous biopsy technique can be found in the chapter entitled "Percutaneous Biopsy of Spinal Infection".

Withholding empirical antibiotics prior to performing biopsy is a well-recognized practice. This approach is important to increase the chances of biopsy yields. The diagnostic rates of patients who had pre-procedural antibiotics can drop significantly to 23% versus 60% in patients without pre-procedural antibiotics (De Lucas et al. 2009). Kim et al. (2015) studied 58 patients with primary pyogenic vertebral osteomyelitis and found that patients who were exposed to pre-procedural antibiotics had significantly lower tissue culture positivity compared to the control group (12.7% versus 46.7%). Another recent study concluded that patients who had pre-procedural antibiotics of 4 or more days had lower positive blood cultures, compared to patients who were only exposed to antibiotics for 1–3 days (Agarwal et al. 2016). Nevertheless, empirical antibiotics should not be withheld in patients with severe sepsis or who are hemodynamically unstable and can be administered after blood cultures have been collected (Lazzeri et al. 2019).

4 Diagnostic Algorithm

Utilizing a diagnostic algorithm allows a systematic approach to effective diagnosis and prompt treatment in patients with a suspected spinal infection. The diagnostic algorithm is divided into two parts. Based on an extensive literature review, Duarte and Vaccaro (2013) formulated a useful two-part algorithm to aid diagnostic assessment and management of spinal infection. We have modified this algorithm, with incorporation of elements from the consensus statement by the European Association of Nuclear Medicine (EANM)/European Society of Neuroradiology (ESNR) and European Society of Clinical Microbiology and Infectious Diseases (ESCMID) and clinical practice guidelines (CPG) by the Infectious Diseases Society of America (IDSA) 2015, as well as from our own experience in diagnosing and managing patients with spine infection. The first part (Fig. 1) aims to confirm or exclude the diagnosis of spinal infection in clinically suspected cases, while the second part (Fig. 2) aims to enable the appropriate management pathway and identify the causative microorganism.

4.1 Part 1: Clinical Suspicion of Spinal Infection (Fig. 1)

When a patient's clinical presentation is suspicious of spinal infection, common laboratory tests such as CRP, ESR, WBC, and blood cultures as well as spine radiographs are reviewed. MRI with intravenous gadolinium-based contrast agent administration, the next preferred imaging modality, is performed. When characteristic MRI findings are present, the diagnosis of spinal infection is confirmed. However, in patients with contraindication(s) to MRI or who have MRI findings that are inconclusive, fluorine-18 fluoro-D-glucose positron emission tomography/computed tomography (^{18}F FDG-PET/CT) is recommended. A recent meta-analysis has concluded that ^{18}F FDG-PET/CT has a very good diagnostic performance in patients with spondylodiscitis, with reported sensitivity of 94.8% and specificity of 91.4% (Treglia et al. 2020). If ^{18}F FDG-PET/CT is not available, ^{99m}Tc-MDP bone scan or ^{67}Ga citrate scintigraphy can be performed (Lazzeri et al. 2019). The characteristic MRI and radionuclide imaging features of spinal infection are discussed in preceding chapters of this book.

4.2 Part 2: Management and Etiological Diagnosis of Spinal Infection (Fig. 2)

Following completion of diagnostic investigations for clinically suspected spinal infection, the two possible scenarios are (a) patient with MRI evidence of spinal infection or (b) patient with strong clinical suspicion of spinal infection but inconclusive imaging findings. Those with urgent indications, such as spine instability (with or without deformity), neurological deficit, and/or epidural/subdural collection with mass effect and cord compression, follow the surgical pathway.

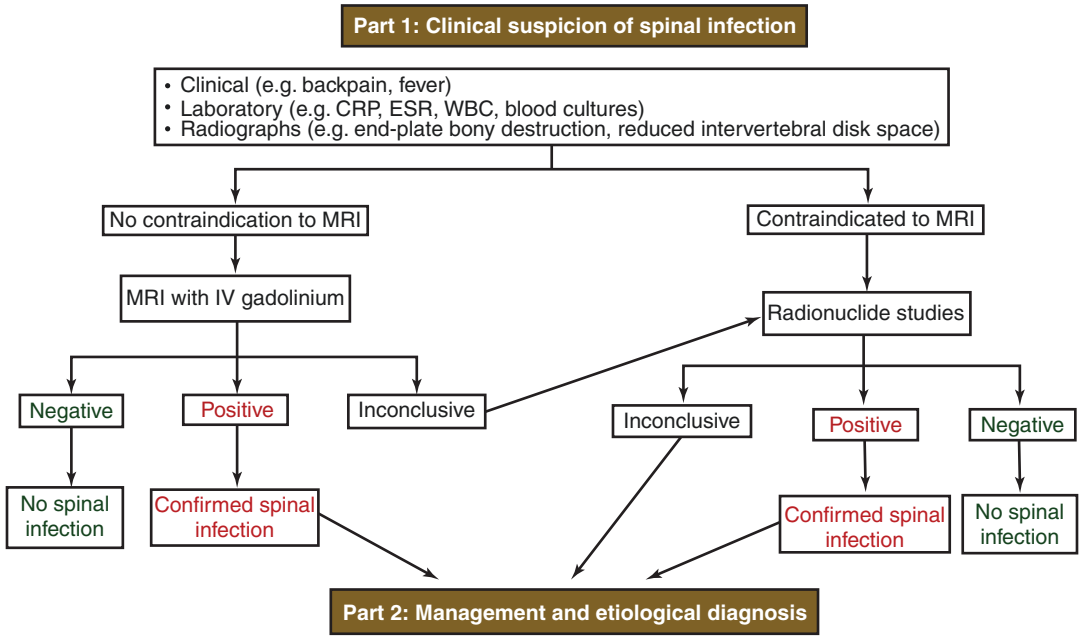

Fig. 1 Flow chart shows the diagnostic algorithm (part 1) approach to patients with clinical suspicion of spinal infection

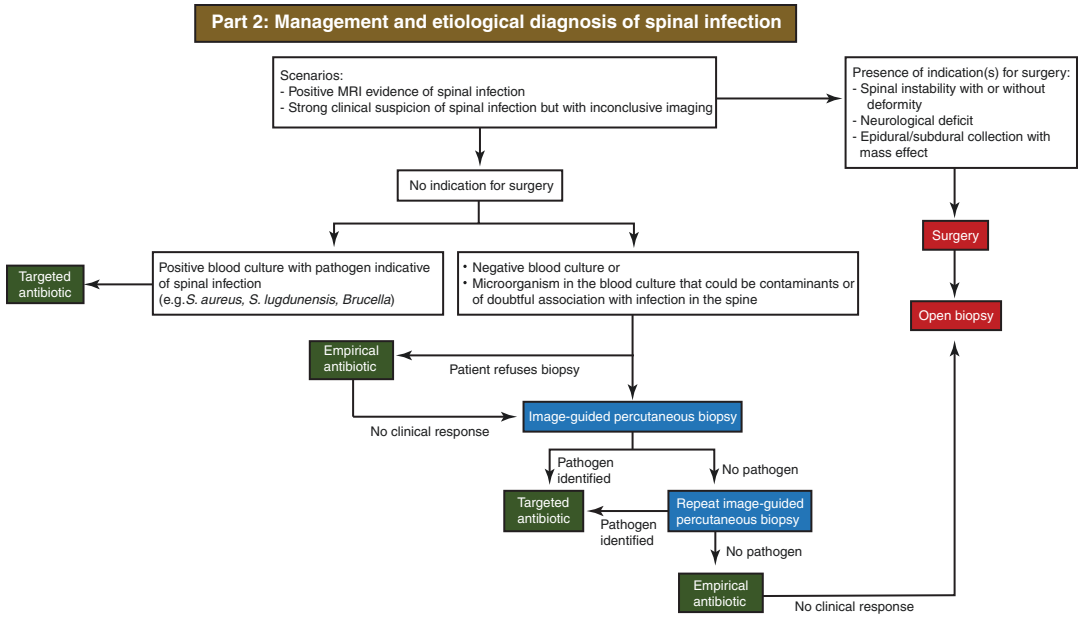

Fig. 2 Flow chart shows the diagnostic algorithm (part 2) dealing with the management and etiological diagnosis of patients with spinal infection

The objectives of surgery are to stabilize the spine, decompress the spinal canal, and relieve the source of neural compression, as well as drainage and debridement of infected tissue. During the operation, specimens via open biopsy should be obtained, as these usually produce higher tissue yields (Berbari et al. 2015; Lazzeri et al. 2019).

Approximately 50–60% of patients are expected to have positive blood culture or serology results (Duarte and Vaccaro 2013; Lazzeri et al. 2019). When specific microorganisms are present in the blood culture (e.g., *S. aureus*, *S. lugdunensis*) or serology (e.g., *Brucella* spp.), percutaneous biopsy may not be needed (Berbari et al. 2015). A retrospective study involving 125 patients with vertebral osteomyelitis showed that 24% of patients with vertebral osteomyelitis and who previously had *S. aureus* bacteremia was later shown to have the same microorganism from biopsy specimen as the previous blood cultures (Wang et al. 2012). Brucellosis is very common cause of spinal infection in endemic countries in the Mediterranean region, Middle East, and Central and South America. Bozgeyik et al. (2008) showed that all patients with brucellar spinal infection were found to have serum antibody titer of ≥1:160 on agglutination test. Thus, it is reasonable not to perform biopsy in patients with strong positive serology for *Brucella* spp. living in endemic areas (Berbari et al. 2015).

Approximately 50% of patients are expected to have negative blood cultures (Duarte and Vaccaro 2013; Berbari et al. 2015). For this group of patients and when there is a doubt about the association between the microorganisms identified from blood culture and spinal infection, image-guided percutaneous biopsy should be performed (Lazzeri et al. 2019). For the latter doubtful group, microorganisms detected in blood culture may be contaminants (e.g., from the skin) or may originate from another concurrent source of infection (e.g., pneumonia, urinary tract infection). Percutaneous biopsy is relatively safe and offers superior diagnostic yields. It is an extremely useful method to identify the specific pathogens, limit the unnecessary use of antibiotic, and reduce antimicrobial resistance (Hadjipavlou et al. 2000; Turunc et al. 2007; Euba et al. 2008; Karadimas et al. 2008; Duarte and Vaccaro 2013; Lazzeri et al. 2019). Targeted antibiotic can be commenced once a specific pathogen is identified. Repeat percutaneous biopsy may be required, if results of the first biopsy are negative. If the repeated biopsy is again negative, trial of empirical antibiotic is a reasonable approach. If there is no clinical response to the empirical antibiotic, open biopsy should be considered (Duarte and Vaccaro 2013; Berbari et al. 2015; Lazzeri et al. 2019). Details of the microbiological, histopathological, cytological, and molecular diagnosis of spinal infection are found in the chapter entitled "Percutaneous Biopsy of Spinal Infection".

4.3 Part 3: Patients with Unsuspected Spinal Infection

Occasionally, patients may incidentally be found to have typical features of spinal infection during imaging done for other clinical indications. These clinical scenarios where MRI of the spine are performed include: (a) child presenting with nonspecific back pain, fever, and tachycardia, (b) elderly patient with compression fracture (with initial purpose to differentiate between acute versus chronic or pathological versus osteoporotic vertebral fracture), and (c) adult patient presenting with persistent back pain without fever (Royal College of Radiologists 2017). If relevant laboratory tests have not yet been carried out, then WBC, CRP, ESR, and blood culture should be performed (Lazzeri et al. 2019). These groups of patients should then be managed according to the part 2 algorithm (Fig. 2).

5 Conclusion

The clinical presentation of spinal infection is often nonspecific and requires a high index of clinical suspicion. Utilizing a diagnostic algorithm enables a systematic approach to effectively diagnose and manage patients with spinal infection.

References

Agarwal V, Wo S, Lagemann GM et al (2016) Image-guided percutaneous disc sampling: impact of antecedent antibiotics on yield. Clin Radiol 71: 228–234

Berbari EF, Kanj SS, Kowalski TJ et al (2015) Infectious Diseases Society of America (IDSA) clinical practice guidelines for the diagnosis and treatment of native vertebral osteomyelitis in adults. Clin Infect Dis 61:e26–e46

Beronius M, Bergman B, Andersson R (2001) Vertebral osteomyelitis in Göteborg, Sweden: a retrospective study of patients during 1990-95. Scand J Infect Dis 33:527–532

Bozgeyik Z, Ozdemir H, Demirdag K et al (2008) Clinical and MRI findings of Brucellar spondylodiscitis. Eur J Radiol 67:153–158

Carragee EJ, Kim D, van der Vlugt T et al (1997) The clinical use of erythrocyte sedimentation rate in pyogenic vertebral osteomyelitis. Spine 22:2089–2093

Chihara S, Segreti J (2010) Osteomyelitis. Dis Mon 56:5–31

de Lucas EM, González MA, Gutiérrez A et al (2009) CT-guided fine-needle aspiration in vertebral osteomyelitis: true usefulness of a common practice. Clin Rheumatol 28:315–320

Duarte RM, Vaccaro AR (2013) Spinal infection: state of the art and management algorithm. Eur Spine J 22:2787–2799

Euba G, Narváez JA, Nolla JM et al (2008) Long-term clinical and radiological magnetic resonance imaging outcome of abscess-associated spontaneous pyogenic vertebral osteomyelitis under conservative management. Semin Arthritis Rheum 38:28–40

Fantoni M, Trecarichi EM, Rossi B et al (2012) Epidemiological and clinical features of pyogenic spondylodiscitis. Eur Rev Med Pharmacol Sci 16:2–7

Frangen TM, Kälicke T, Gottwald M et al (2006) Surgical management of spondylodiscitis. An analysis of 78 cases. Unfallchirurg 109:743–753

Hadjipavlou AG, Mader JT, Necessary JT et al (2000) Hematogenous pyogenic spinal infections and their surgical management. Spine 25:1668–1679

Hewes RC, Vigorita VJ, Freiberger RH (1983) Percutaneous bone biopsy: the importance of aspirated osseous blood. Radiology 148:69–72

Jensen AG, Espersen F, Skinhøj P et al (1997) Increasing frequency of vertebral osteomyelitis following Staphylococcus aureus bacteraemia in Denmark 1980-1990. J Infect 34:113–118

Karadimas EJ, Bunger C, Lindblad BE et al (2008) Spondylodiscitis. A retrospective study of 163 patients. Acta Orthop 79:650–659

Kim CJ, Song KH, Jeon JH et al (2010) A comparative study of pyogenic and tuberculous spondylodiscitis. Spine 35:1096–1100

Kim CJ, Kang SJ, Yoon D et al (2015) Factors influencing culture positivity in pyogenic vertebral osteomyelitis patients with prior antibiotic exposure. Antimicrob Agents Chemother 59:2470–2473

Lazzeri E, Bozzao A, Cataldo MA et al (2019) Joint EANM/ESNR and ESCMID-endorsed consensus document for the diagnosis of spine infection (spondylodiscitis) in adults. Eur J Nucl Med Mol Imaging 46:2464–2487

Mackenzie AR, Laing RBS, Smith CC et al (1998) Spinal epidural abscess: the importance of early diagnosis and treatment. J Neurol Neurosurg Psychiatry 65:209–212

Michel SCA, Pfirrmann CWA, Boos N et al (2006) CT-guided core biopsy of subchondral bone and intervertebral space in suspected spondylodiskitis. AJR Am J Roentgenol 186:977–980

Mylona E, Samarkos M, Kakalou E et al (2009) Pyogenic vertebral osteomyelitis: a systematic review of clinical characteristics. Semin Arthritis Rheum 39:10–17

Peh WCG (2006) CT-guided percutaneous biopsy of spinal lesions. Biomed Imaging Interv J 2:1–12

Pineda C, Pena A, Espinosa R et al (2011) Imaging of osteomyelitis: the key is in the combination. Int J Clin Rheumatol 6:25–33

Royal College of Radiologists (2017) iRefer: RCR imaging guidelines. In: Making the best use of clinical radiology, 8th edn. https://www.rcr.ac.uk/clinical-radiology/being-consultant/rcr-referral-guidelines/about-irefer

Schimmer RC, Jeanneret C, Nunley PD et al (2002) Osteomyelitis of the cervical spine: a potentially dramatic disease. J Spinal Disord Tech 15:110–117

Schweitzer ME, Gannon FH, Deely DM et al (1996) Percutaneous skeletal aspiration and core biopsy: complementary techniques. AJR Am J Roentgenol 166:415–418

Sobottke R, Seifert H, Fätkenheuer G et al (2008) Current diagnosis and treatment of spondylodiscitis. Dtsch Arztebl Int 105:181–187

Srinivasan S, Peh WCG (2011) Imaging-guided biopsy in musculoskeletal infections. Semin Musculoskelet Radiol 15:561–568

Treglia G, Pascale M, Lazzeri E et al (2020) Diagnostic performance of ^{18}F-FDG PET/CT in patients with spinal infection: a systematic review and a bivariate meta-analysis. Eur J Nucl Med Mol Imaging 47:1287–1301

Tsiodras S, Falagas ME (2006) Clinical assessment and medical treatment of spine infections. Clin Orthop Relat Res 444:38–50

Turunc T, Demiroglu YZ, Uncu H et al (2007) A comparative analysis of tuberculous, brucellar and pyogenic spontaneous spondylodiscitis patients. J Infect 55:158–163

Wang Z, Lenehan B, Itshayek E et al (2012) Primary pyogenic infection of the spine in intravenous drug users: a prospective observational study. Spine 37:685–692

Correction to: Imaging of Spinal Infection

Mohamed Fethi Ladeb and Wilfred C. G. Peh

Correction to: M. F. Ladeb, W. C. G. Peh (eds.), *Imaging of Spinal Infection*, Medical Radiology Diagnostic Imaging, https://doi.org/10.1007/978-3-030-70459-9

The book was inadvertently published with an incorrect affiliation for all the authors in the following chapters,

Radiography and Computed Tomography of Spinal Infection
Magnetic Resonance Imaging of Spinal Infection
Nuclear Medicine Imaging of Spinal Infection
Imaging of Hematogeneous Pyogenic Spondylodiscitis
Imaging of Iatrogenic Spinal Infection
Imaging of Pyogenic Epidural Abscess
Diagnostic Algorithm of Spinal Infection

The incorrect affiliation has been deleted now.

The updated version of the book can be found at https://doi.org/10.1007/978-3-030-70459-9

© The Author(s), under exclusive license to Springer Nature Switzerland AG 2021

M. F. Ladeb, W. C. G. Peh (eds.), *Imaging of Spinal Infection*,
Medical Radiology Diagnostic Imaging, https://doi.org/10.1007/978-3-030-70459-9_16